Extension Division

Proceedings
of the

International Symposium on Earthquake Structural Engineering

August 19-21, 1976

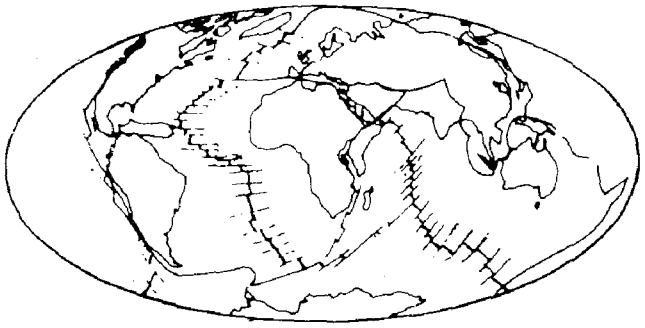

In Two Volumes

Vol. II

Second Edition
Edited by
FRANKLIN Y. CHENG

University of Missouri - Rolla

Proceedings of the

International Symposium on Earthquake Structural Engineering

In two volumes
Volume II

August 19-21, 1976
St. Louis, Missouri, U.S.A.

Edited by
Franklin Y. Cheng
Professor of Civil Engineering

Department of Civil Engineering
University of Missouri - Rolla

Presented by
Department of Civil Engineering
Extension Division
University of Missouri - Rolla

PLANNING COMMITTEE

F.Y. Cheng, Symposium Director, University of Missouri - Rolla
J.H. Senne, Symposium Co-director, University of Missouri - Rolla
G.E. Lorey, University of Missouri - Rolla
J.B. Heagler, University of Missouri - Rolla
W. Kratzer, University of Missouri - Rolla
E.C. Murphy, University of Missouri - Rolla

TECHNICAL COMMITTEE

A.H-S. Ang, University of Illinois at Urbana-Champaign
F.Y. Cheng, Coordinating Chairman, University of Missouri - Rolla
C.G. Culver, National Bureau of Standards, Washington, D.C.
T.V. Galambos, Washington University
J.E. Goldberg, Purdue University and University of Illinois - Chicago Circle
W.A. Nash, University of Massachusetts-Amherst
O.W. Nuttli, St. Louis University

PREFACE

The 89 papers contained in these two volumes constitute the proceedings of the International Symposium on Earthquake Structural Engineering, which was held in St. Louis, Missouri, and presented by the University of Missouri - Rolla. The symposium was endorsed by the American Society for Engineering Education; the St. Louis and Mid-Missouri sections of the American Society of Civil Engineers; and the Joint Committee on Tall Buildings established by the International Association for Bridge and Structural Engineering, the American Society of Civil Engineers, the American Institute of Architects, the American Institute of Planners, the International Federation for Housing and Planning, and the International Union of Architects.

A large quantity of effective research has been put forth in the various areas of destructive earthquakes, seismicity, ground motions, earthquake instrumentation, earthquake zoning, and disaster prevention. In each, a tremendous amount of world-wide information has been accumulated that should be discussed and disseminated in specialized conferences, such as the one held in St. Louis, to provide for interaction and cooperation among researchers, educators, practitioners, and civil authorities in the field of earthquake structural engineering and to focus attention on structural design so as to minimize the distructive and killing effects of earthquakes. It is hoped that the presentations and discussions contained herein will contribute significantly toward this end.

It is not possible here to thank each and every person who contributed toward the organization of the conference, but sincere appreciation is extended to the authors for their cooperation and contributions and to all the Technical Committee members and Session Chairmen for their untiring efforts.

Special appreciation is expressed to the NSF for its partial financial support in publishing these proceedings. We are grateful for the assistance of Drs. S.C. Liu and J.B. Scalzi, Program Managers of Earthquake Engineering, Division of Advanced Environmental Research and Technology of the National Science Foundation, and for the encouragement and support of Drs. D. Thompson, Vice Chancellor, G.E. Lorey, Dean of Extension, and J.S. Johnson, Dean of School of Engineering, Prof. J.K. Roberts, Assist. Dean of School of Engineering, of the University of Missouri - Rolla. Last, but not least, the cooperation of the Planning Committee and University staff is acknowledged with thanks, and the skilled assistance of Mrs. Ann Mitchell and Margot Lewis in typing portions of the proceedings deserves special mention.

Rolla, Missouri, August 1976

Franklin Y. Cheng
Joseph H. Senne

TABLE OF CONTENTS
Volume II

PROGRAM

Registration **Wednesday, August 18, 1976**

6:00 p.m. - 9:00 p.m., Mississippi Room

Thursday, August 19, 1976

7:30 a.m. - 5:00 p.m., Registration, Mississippi Room

8:15 a.m. **OPENING SESSION**, Mississippi Room
Presiding: J.H. SENNE, University of Missouri - Rolla
Welcome Remarks
J.H. POELKER, Mayor of St. Louis
Representative of Honorable J.W. SYMINGTON, U.S. Congressman
D. THOMPSON, Vice Chancellor, University of Missouri - Rolla

9:05 a.m. **INVITED LECTURE**, Mississippi Room
Presiding: T.V. GALAMBOS, Washington University
On the Specification of a Design Earthquake, by O.W. NUTTLI, St. Louis University

9:40 a.m. Coffee Break

10:00 **SESSION IA**, Mississippi Room
BUILDINGS AND BRIDGES
Chairman:
T.V. GALAMBOS, Washington, University
Co-Chairman:
W.A. ANDREWS, University of Missouri - Rolla

A Study of the Effect of the Frequency Characteristics of Ground Motions on Nonlinear Structural Response, by A.T. DERECHO, G.N. FRESKAKIS, and M. FINTEL, U.S.A.

Seismic Retrofitting for Highway Bridges, by A. LONGINOW, R.R. ROBINSON, K.H. CHU, and J.D. COOPER, U.S.A.

The Non-Linear Deformations in the Ground Base of Large-Panel Buildings Under Oscillation, by G.A. SHAPIRO and G.N. ASHKINADZE, U.S.S.R.

Dynamic Behavior of Cable Stayed Bridges, by E.A. EGESELI, and J.F. FLEMING, U.S.A.

Modal Analysis and Seismic Design of Tall Building Frames, by P. PARAMASIVAM, S. NASIM, and S.L. LEE, Singapore

Development in Structural Solutions of Multi-Storey Seismic-Proof Frameless Buildings of In-Situ Reinforced Concrete in USSR, by M.E. SOKOLOV and Y.V. GLINA, U.S.S.R.

The Inelastic Seismic Response of Bridge Structures, by R.D. SHARPE, and A.J. CARR, New Zealand

Effect of Coupling Earthquake Motions on Inelastic Structural Models, by F.Y. CHENG and K.B. OSTER, U.S.A.

10:00 **SESSION IB**, Illinois Room
FOUNDATION AND STRUCTURE INTERACTION
Chairman:
M. ALIZADEH, Shannon & Wilson, Inc.
Co-Chairman:
W.A. NASH, University of Massachussets - Amherst

The Effect of Foundation Compliance on the Fundamental Periods of Multi-Storey Buildings, by E. MENDELSON, and I. ALPAN, Israel

Inverted-Pendulum Effect on Seismic Response of Tall Buildings Considering Soil-Structure Interaction, by T.H. LEE, U.S.A.

On the Use of Precast Pile-Foundations in Construction of Earthquake-Proof Large-Panel Buildings, by L.D. MARTYNOVA, Y.A. SIMON, V.F. ZAKHAROV, and N.V. KONDRATYEV, U.S.S.R.

Some Seismic Response Solutions for Soil-Foundation-Building Systems, by J.K. MINAMI and J. SAKURAI, Japan

Response of Structures Embedded in the Ground to Traveling Seismic Waves, by E.G. PRATER and M. WIELAND, Switzerland

Some Comparisons of Dynamic Soil-Structure Analyses, by G.R. JOHNSON, H.I. EPSTEIN, and P. CHRISTIANO, U.S.A.

Gypsum Layer in Soil-Structure Systems, by Y.C. HUNG and M.D. SNYDER, U.S.A.

The Soil Foundation-Structure Interaction Under the Action of Earthquake Loads, by I. CIONGRADI and N. UNGUREANU, Romania

12:00 Lunch

1:30 - 2:10 **INVITED LECTURE**, Mississippi Room

Presiding: V.V. BERTERO, University of California-Berkeley

Protection of Communications Facilities in Earthquake Areas, by S.C. LIU, National Science Foundation

2:15 **SESSION 2A**, Mississippi Room ANALYSIS AND DESIGN

Chairman:
T.C. HUANG, University of Wisconsin-Madison

Co-Chairman:
V.B. VENKAYYA, U.S. Air Force Flight Dynamics Laboratory, Wright Patterson, Ohio

Critical Excitation and Response of Free Standing Chimneys, by P.C. WANG, W.WANG, R. DRENICK, and J. VELLOZZI, U.S.A.

Dynamic Analysis of Elastic-Plastic Space Frames, by N.F. MORRIS, U.S.A.

On the Limit Analysis of Box-Unit Buildings Under Static and Dynamic Effects, by T.I. NASSONOVA and M.J. FRAINT, U.S.S.R.

2:15 **SESSION 2B**, Illinois Room DYNAMIC TESTS ON STRUCTURES

Chairman:
M. FINTEL, Portland Cement Association

Co-Chairman:
V.V. BERTERO, University of California-Berkeley

Reversing Load Tests of Five Isolated Structural Walls, by A.E. FIORATO, R.G. OESTERLE, JR. and J.E. CARPENTER, U.S.A.

Dynamic Behavior of a Reinforced Concrete Spray Tower, by T.J. FOWLER and D.M. WILLIAMS, U.S.A.

Experimental Studies on Hysteretic Characteristics of Steel Reinforced Concrete Columns and Frames, by M. WAKABAYASHI, and K. MINAMI, Japan

3:00 Coffee Break

3:30

Dynamic Response of Cantilever Beam-Columns with Attached Masses Supported on a Flexible Foundation, by A.N. KOUNADIS, Greece

Vibrations and Interactions of Layered Beam Foundations, by V.N. SHAH and T.C. HUANG, U.S.A.

Generating Response Spectra from Displacement and Velocity Time History Input, by A. CHUANG, T.H. LEE, D.A. WESLEY and S. LU, U.S.A.

A Simplified Nonlinear Seismic Response Analysis of Structures Including Vertical Ground Motion, by D.R. BERVIG, U.S.A.

Response of an Elasto-Plastic Spherical Structure in a Fluid to Earthquake Motions, by D. SRIMAHACHOTA, T. HONGLADAROMP, Thailand and S.L. LEE, Singapore

Dynamic Response of Retaining Walls During Earthquake, by C.S. YEH, Republic of China

Dynamic Response of Bridge Grid Under Moving Force, by N. MUNIRUDRAPPA, India

Static and Dynamic Tests of a Large-Size Model of a Frameless In-Situ Reinforced Concrete Residential Building, by Y.V. BARKOV and Y.V. GLINA, U.S.S.R.

Experimental Study on Reinforced Concrete Truss Frames as Earthquake Resistance Elements, by T. SHIMAZU and Y. FUKUHARA, Japan

Ductile Behavior of Coupled Shear Walls Subjected to Reversed Cyclic Loading, by A.R. SANTHAKUMAR, India

Earthquake Response of Guyed Towers, by A.V. du BOUCHET, U.S.A.

Experimental Study on Reinforced Concrete Columns with Special Web-Reinforcements, by H. UMEMURA, T. SHIMAZU, S. TADEHARA, T. KONISHI and Y. ABE, Japan

Torsional Response at Large Eccentricities, by K. J. MEYER and I.J. OPPENHEIM, U.S.A.

A New Method for Numerical Integration of Equations of Motion by J.E. GOLDBERG, U.S.A.
Sheraton Hotel in Santo Domingo, Dem. Rep.: Analysis, Design, and Construction Techniques, by A.A. RICART NOVEL, Dom. Rep.

Friday, August 20, 1976

8:00 - 12:00 Registration, Mississippi Room

8:30 - 9:10 **INVITED LECTURE**, Mississippi Room
Presiding: J.B. SCALZI, National Science Foundation
Establishment of Design Earthquakes--Evaluation of Present Methods, by V.V. BERTERO, University of California-Berkeley

9:15 **SESSION 3A**, Mississippi Room ANALYSIS AND DESIGN
Chairman:
J.B. SCALZI, National Science Foundation
Co-Chairman:
R.E. DAVIS, McDonnell Douglas Automation Co.

A Unified Approach to Designing Structures for Three Components of Earthquake, by A.K. GUPTA and S.L. CHU, U.S.A.

Resizing of Frames Subjected to Ground Motion, by V.B. VENKAYYA and F.Y. CHENG, U.S.A.

Problems in Establishing and Predicting Ductility in Aseismic Design, by S.A. MAHIN and V. V. BERTERO, U.S.A.

10:00 Coffee Break

10:30

Shear Coefficient and Shear Force Distribution in Nuclear Power Plant Structures due to Seismic Loading, by N.C. CHOKSHI and J.P. LEE, U.S.A.

Evaluation of the Reservoir Effect on the Dynamics of Dams, by H.U. AKAY and P. GULKAN, Turkey

Dynamic Response Characteristics of an Elasto-Plastic Structure on a Random Soil Ground, by T. KOBORI, Y. INOUE and M. KAWANO, Japan

Some Design Considerations of Earthquake Resistant Reinforced Concrete Shear Walls, by T. PAULAY, New Zealand

Earthquake Resistance of Structures with Suspended Masses, by N.A. NIKOLAENKO and I.N. BURGMAN, U.S.S.R.

9:15 **SESSION 3B**, Illinois Room CODES AND REGULATIONS
Chairman:
J.E. GOLDBERG, Purdue University and University of Illinois-Chicago
Co-Chairman:
V.R. BUSH, International Conference of Building Officials

On Specifications for Earthquake-Resistant Design of the Honshu-Shikoku Bridges [JSCE-1974], by I. KAWASAKI and E. KURIBAYASHI, Japan

Comparison of Aseismic Steel Building Design Practice in Japan and USA, by P.H. CHENG, U.S.A.

Comparative Study of the New Turkish Earthquake Resistant Design Code, by M. CELEBI, Turkey

Application of Structural, Mechanical and Electrical Codes and Standards in the Design of Safety Related Structures, Components, and Systems for Nuclear Power Plants, by D.S. MEHTA and B.L. MEYERS, U.S.A.

On Specifications for Earthquake-Resistant Design of Highway Bridges [Jan. 1971], by K. KAWAKAMI, E. KURIBAYASHI, T. IWASAKI and Y. IIDA, Japan

The New Turkish Aseismic Code: A Critical Evaluation with Emphasis on Soil Amplification Considerations, by A. GURPINAR, Turkey

Earthquake Dynamic Environment **within Buildings**, by K.L. MERZ, U.S.A.

Earthquake Response of a Tall Multi-Flue Stack, by P. KARASUDHI, Y.C. TSAI and K.P. CHAU, Thailand

On Earthquake Resistant Design of a Submerged Tunnel, by C. TAMURA and S. OKAMOTO, Japan

Seismic Design of the Veteran's Administration Hospital at Loma Linda, California, by W.T. HOLMES, U.S.A.

12:00 Lunch

1:30 - 2:10 **INVITED LECTURE**, Mississippi Room
Presiding: S.C. LIU, National Science Foundation
Risk and Safety Analysis in Earthquake-Resistant Design, by A. H-S. ANG, University of Illinois at Urbana-Champaign

2:15 **SESSION 4A**, Mississippi Room SAFETY, RELIABILITY, AND POWER PLANT STRUCTURES
Chairman:
S.C. LIU, National Science Foundation
Co-Chairman:
J.T.P. YAO, Purdue University

Structural Damage and Risk in Earthquake Engineering, by D.S. HSU, J.T. GAUNT and J.T.P. YAO, U.S.A.

On Non-Stationary Spectrum and Mean Square Response of a Simple Structural System to Earthquake Excitation, by T. KOBORI and Y. TAKEUCHI, Japan

Dynamic Earthquake Analysis of a Bottom Supported Industrial Boiler, by N. J. MONROE and N. DASA, U.S.A.

2:15 **SESSION 4B**, Illinois Room GROUND MOTIONS, CONSTRUCTION AND REPAIR OF STRUCTURES
Chairman:
O.W. NUTTLI, St. Louis University
Co-Chairman:
J.L. BEST, University of Missouri - Rolla

Methodology for Incorporating Parameter Uncertainties into Seismic Hazard Analysis for Low Risk Design Intensities, by R.K. mcguire, U.S.A.

Epoxy Repair of Structures, by J.M. PLECNIK, J.E. AMRHEIN, W.H. JAY, and J. WARNER, U.S.A.

A California Structural Engineer Shares Three Years of On-Site Experiences in the Design of Reparations for Buildings in Managua, by P.J. CREEGAN, Nicaragua

3:00 Coffee Break

3:30

Effects of Earthquake Input in Seismic Responses of Nuclear Power Plant Sites, by B.T.D. LU, J.A. FISCHER and J. Peir, U.S.A.

Discrete Modeling of Containment Structures, by Y.J. LIN and A.H. HADJIAN, U.S.A.

Seismic Risk Analysis of Nuclear Power Plant Sites Including Power Spectrum Simulation of Future Earthquake Motion, by A. GURPINAR, Turkey

Safety of Seismic Protective Systems with Reserve Elements, by I.M. EISENBERG, U.S.S.R.

Seismic Dynamic Parametric Study on Finite Element Model of Nuclear Power Plant Facility, by J.S. TERASZKIEWICZ, U.S.A.

Troika for Earthquake-Resistant Building Design, by J.R. TISSELL, U.S.A.

Safety of Cities During Severe Earthquakes, by O.C. MANN, U.S.A.

Evaluation of Greek Strong Motion Records, by P.G. CARYDIS and J.G. SBOKOS, Greece

Behavior of Reinforced Concrete Structures During the Managua Earthquake, by G. ESTRADA-URIBE, Columbia

Site Response Analysis for Earthquake Loading, by Y.S. LOU, S.J. DIXON and C.R. MacFADYEN, U.S.A.

Approximate Random Vibration Analysis of Elastoplastic Multi-Degree-of-Freedom Structures, by G. GAZETAS and E.H. VANMARCKE, U.S.A.
Probabilistic Approach to Ultimate Aseismic Safety of Structures, by M. YAMADA and H. KAWAMURA, Japan
Seismic Analysis of Hyperbolic Cooling Towers by the Response Spectrum Method, by P.L. GOULD, S.K. SEN and H. SURYOUTOMO, U.S.A.

6:20 p.m. Social Hour, Illinois Room
7:20 p.m. Banquet
Presiding: J.K. ROBERTS, University of Missouri - Rolla
SUBJECT: **Structural Damage Caused by Guatemala Earthquakes of 4 and 6 February 1976**, by J. ROESSET, Massachusetts Institute of Technology

Saturday, August 21, 1976

8:30 a.m. **INVITED LECTURE**, Mississippi Room
Presiding: P.L. GOULD, Washington University
Observational Studies on Earthquake Response of Buildings in Japan, Y. OSAWA, M. MURAKAMI, and T. MINAMI, University of Tokyo, Japan
9:15 a.m. **SESSION 5**, Mississippi Room STRUCTURAL ELEMENTS AND SPECIAL STRUCTURES
Chairman:
P.L. GOULD, Washington University
Co-Chairman:
A.H. HADJIAN, Bechtel Power Corporation
Discrete Modeling of Symmetric Box-Type Structures, by A.H. HADJIAN, and T.S. ATALIK, U.S.A.
Inelastic Seismic Response of Isolated Structural Walls, by G.N. FRESKAKIS, A.T. DERECHO and M. FINTEL, U.S.A.
Effects of Sectional Shape on the Strength and Ductility of Slender Structural Walls in Earthquake-Resistant Multistory Buildings, by S.K. GHOSH and M. FINTEL, U.S.A.

10:00 Coffee Break

10:20
On the Shear Pinched Hysteresis Loops, by M. CELEBI, Turkey
Confined Concrete in Compression Zones of Structural Walls Designed to Resist Lateral Loads Due to Earthquakes, by P.H. KAAR, A.E. FIORATO, J.E. CARPENTER, and W.G. CORLEY, U.S.A.
Response of an Empty Cylindrical Ground Supported Liquid Storage Tank to Base Excitation, by S.H. SHAABAN and W.A. NASH, U.S.A.
Seismic Design of Liquid Storage Tanks to Earthquakes, by P.C. CHEN and R.B. BARBER, U.S.A.
Analysis of Non-Uniform Coupled Shear Walls With Two Rows of Openings, by A.R. SANTHAKUMAR, India
Aseismic Design Examples of Prestressed Concrete Water Tank, by A. SAKURAI, C. KURIHARA and T. IWATATE, Japan
A New Structural Model for Shear Walls Analysis, by N. UNGUREANU, Romania
Response of Reinforced Concrete Chimneys to Earthquake Forces, by C.K. RAMESH and P.V. FADNIS, India

12:20 Closing Remarks
F.Y. CHENG, University of Missouri - Rolla

12:30 Adjourn

INTERNATIONAL SYMPOSIUM ON
EARTHQUAKE STRUCTURAL ENGINEERING
St. Louis, Missouri, USA, August, 1976

DYNAMIC RESPONSE CHARACTERISTICS OF AN ELASTO-PLASTIC STRUCTURE ON A RANDOM SOIL GROUND

TAKUJI KOBORI*, YUTAKA INOUE**, and MASAHIRO KAWANO***

* Professor, Department of Architectural Engineering, Kyoto University, Kyoto, Japan

** Associate Professor, Department of Architectural Engineering, Osaka University, Suita, Japan

*** Lecturer, Department of Architectural Engineering, Osaka University, Suita, Japan

Summary

The dynamic ground compliance of a random soil ground represented by the two-dimensional finite element model is, first, presented analytically, and evaluated numerically through the Monte Carlo simulation method. Using this random ground compliance, some discussions on the response characteristics of the soil-structure system to a white random excitation are developed.

1. Introduction

It has been recognized that the dynamic behavior of a building structure during earthquake is considerably affected by the formation and the property of the soil ground under the structure. In particular, the geological and topographical irregularities or random inhomogeneities in the soil ground seem to have a tremendous effect on the characteristics of the earthquake ground motion and also on the associated structural damage of the building. The objective of this paper is to investigate the effect of the soil ground with such random inhomogeneities on the earthquake response of the elasto-plastic structure, concerning with the modeling method problem of the soil-structure interaction system to derive the reasonable results.

First of all, the ensembles of the two dimensional finite element model are provided for the analysis of a random soil ground, an elastic modulus of which is presented as random variable with the prescribed spectral density in the space coordinate and simulated numerically by the Monte Carlo method, because it is difficult to obtain the analytical solution of dynamic responses of a random medium without employing perturbation theory on the assumption that the fluctuation of random variables is to be very small.

Secondly, the dynamic response characteristics of such an irregular visco-elastic medium with random properties are evaluated, in terms of the dynamic ground compliance. For the evaluation of the dynamic responses of a structure on such a random soil ground, it assumes that the mathematical model of a soil structure interaction system consists of a random visco-elastic medium, an elasto-plastic boundary soil layer underneath the above structure and a main structure with bi-linear hysteresis characteristics.

Finally, the statistical response characteristics of the system sub-

jected to a white random ground motion are investigated for the corresponding ensemble of the dynamic ground compliance.

2. Dynamic Response of a Random Soil Ground

If elastic moduli of a soil ground vary randomly in the space coordinates, the equation of wave motion seems to be a kind of nonlinear equation and it's solution may not be obtained through an analytical procedure except the case of a weakly random medium, where the parameters contained in the equation of wave motion are approved to deviate only slightly from their mean values. Then, the finite element method is provided for the analyses of soil medium with an any elastic random property in this paper. An each element of a finite element model consists of homogeneous, isotropic solid, in which the stress vector σ is related to the strain vector ε based on the elastic theory in the form:

$$\sigma = \mu D \varepsilon \tag{1}$$

where matrix D involves Young's modulus E and poisson's ratio $\nu = \lambda/2(\lambda+\mu)$. λ and μ are Lamé's elastic constants. Assembling the stiffness matrices of each element derived from eq. (1) to the whole stiffness matrix of a medium, the following fundamental equation of motion of the medium with the boundary conditions at the bottom divided into finite element is expressed by

$$m \ddot{U} + C \dot{U} + K U = P \tag{2}$$

in which m, C and K are mass-, damping- and stiffness-matrix of a random medium, respectively; U and P denote the nodal displacement vector and the nodal force vector. Applying the Fourier transform to both sides of eq. (2), this equation yields to

$$[-a_0^2 m + (j\eta a_0 + 1) K] \tilde{U} = \tilde{P} \tag{3}$$

where, $\tilde{U}(j a_0) \subset U(t)$, $\tilde{P}(j a_0) \subset P(t)$

$$a_0 = \frac{b\omega}{V_s} \quad , \quad V_s = \sqrt{\frac{\mu}{\rho}} \quad , \quad \eta = \frac{V_s}{b}\frac{\mu'}{\mu} \quad , \quad j = \sqrt{-1}$$

and ω denotes circular frequency; V_s is shear wave velocity; a_0 means a nondimensional frequency parameter; η is a nondimensional viscous damping coefficent and μ' denotes the damping coefficent corresponding to shear modulus μ , respectively. Supposing that only the stiffness matrix varies randomly, the matrix K may be expressed by

$$K = {}_0K + {}_1K \quad , \quad {}_1K_{ij} < {}_0K_{ij} \tag{4}$$

where, ${}_1K$ denotes the deviation matrix from its mean matrix ${}_0K$ Reordering the double summation over i and j of each element in K to i or j , the matrix K is transformed to the vector K'

$$K' = {}_0K' + {}_1K' \quad , \quad {}_1K'_i < {}_0K'_i \tag{5}$$

Normalizing the mean vector ${}_0K'$ in eq. (5), the following equation is

$$K'_N = \mathbb{1} + {}_E K' \quad , \quad {}_E K'_i < 1 \tag{6}$$

in which ${}_E K'$ denotes the refractive index vector of a soil medium. Since the spatial variations of the refractive index in a soil medium lead to the amplitude and phase fluctuations of the resultant wave field, the wave motion $\tilde{U}$ in eq. (3) may be expressed by

$$\tilde{U} = {}_0\tilde{U} + {}_1\tilde{U} \quad , \quad {}_1\tilde{U}_i \ll {}_0\tilde{U}_i \tag{7}$$

Eq. (7) means the each element of the inhomogeneous medium becomes to be a source of the secondary scattered wave motion $_1\tilde{U}_l$ under the primary wave motion $_0\tilde{U}_l$. From eqs. (3), (4) and (7), $_0\tilde{U}_l$ and $_1\tilde{U}_l$ may be approximately represented as follows:

$$\begin{aligned} {}_0\tilde{U}_l &= {}_0\tilde{U}_{lR} + j\,{}_0\tilde{U}_{lI} = \mathbb{L}^{-1}\tilde{P} \\ {}_1\tilde{U}_l &= {}_1\tilde{U}_{lR} + j\,{}_1\tilde{U}_{lI} = -q_0\mathbb{L}^{-2}{}_1k\tilde{P} \end{aligned} \tag{8}$$

where, $\mathbb{L} = [-a_0^2 m_l + q_{0\,0}k)$, $q_0 = j\eta a_0 + 1$

and eqs. (7) and (8) lead to the following equations

$$\begin{aligned} \tilde{U}_l &= \tilde{U}_{lR} + j\tilde{U}_{lI} = ({}_0\tilde{U}_{lR} + {}_1\tilde{U}_{lR}) + j({}_0\tilde{U}_{lI} + {}_1\tilde{U}_{lI}) \\ &= \mathbb{L}^{-1}(\mathbb{I} - q_0\mathbb{L}^{-1}{}_1k)\tilde{P} \end{aligned} \tag{9}$$

From eq. (9), it is noted that the random inhomogeneity of a medium affects on both of the real and imaginary parts of the complex response vector $\tilde{U}_l$. By making use of eq. (8), the dynamic ground compliance, defined as a ratio of the complex displacement amplitude of a rigid foundation on a medium to the harmonic force acting on the foundation is shown as:

$$f_{1H} + j f_{2H} = \frac{[{}_0\tilde{U}_{R,H}(0,0)]}{\sum_k g^k} + \frac{[{}_0\tilde{U}_{I,H}(0,0)]}{\sum_k g^k} \tag{10}$$

for a deterministic component in eq. (8), where $_0\tilde{U}_R$ and $_0\tilde{U}_I$ are each element of the vector $_0\tilde{U}_l$ respectively and

$$f'_{1H} + j f'_{2H} = \frac{[{}_1\tilde{U}_{R,H}(0,0)]}{\sum_k g^k} + \frac{[{}_1\tilde{U}_{I,H}(0,0)]}{\sum_k g^k} \tag{11}$$

for a random component in eq. (8), where $_1\tilde{U}_R$ and $_1\tilde{U}_I$ denote each element of the vector $_1\tilde{U}_l$ and suffix H means the direction of the force acting on the foundation. Under the boundary stress condition, it is assumed that the exciting force acts uniformly upon the surface nodal points being into contact with a foundation mass, and the resultant force of the excitation is expressed as $\sum_k g^k$ in eqs. (10) and (11).

3. Solution of Linear Differential Equation with Random Coefficients

The statistical analysis of the dynamic responses of a random soil medium represented by eq. (7) or (9) may be reduced to one of some problems interested to solve linear differential equations with random coefficients recently. The probability density function of the output involving the random variable is obtained from the fact that the equation of the state variable in the differential equations is satisfied with the Liouville's equation. The solution may be written as an analytical expression because the probability density function concerning with both of the initial conditions and the coefficents in the equation is given by the arbitrary form. Eq. (2) may be transformed into the equation of the state variables

$$U_l = h(U_l(t), k(t), t), \quad U_l(0) = U_{l0} \tag{12}$$

where,

$$k = k(E, t) \tag{13}$$

means a random coefficients process characterized by a random vector E. When the elastic properties of a soil medium are random variables only in space, eq. (13) is rewritten as $k = k(E)$. Assuming that the joint probability

density function $P(u, \dot{u}; t)$ of $u(t)$ and $\dot{u}(t)$ exists with the known joint probability density funciton $P_0(u_0, \dot{u})$, $P(u, \dot{u}; t)$ satisfies the Liouville's equation

$$\frac{\partial P(u, \dot{u}; t)}{\partial t} + \sum_i \frac{\partial [P(u, \dot{u}; t) h_i]}{\partial u_i} = 0 \qquad (14)$$

$$P(u, \dot{u}; 0) = P_0(u_0, \dot{u})$$

where u_j and h_j are the j-th element of u and h , respectively.

From eq. (14), the following equation is

$$\frac{\partial P}{\partial t} + P \nabla \cdot h + \sum_i h_i \frac{\partial P}{\partial u_i} = 0 \qquad (15)$$

where $\nabla \cdot h$ means the divergence of vector h . Consequently, the associated Lagrange system of eq. (14) is

$$\frac{dt}{1} = -\frac{dP}{P \nabla \cdot h} = \frac{du_1}{h_1} = \cdots\cdots = \frac{du_n}{h_n} \qquad (16)$$

When the harmonic excitation $P = A_0 e^{i\omega t}$ acts on this system under the initial condition $t = 0$, the general transient solution may be written in the following expression

$$u(j a_0; t) = f(u_0, \dot{u}, j a_0; t) \qquad (17)$$

Then, the probability density function of the general solution $u(t)$ is derived from the first equality of eq. (16) as following:

$$P(u, \dot{u}; t) = P_0(u_0, \dot{u}) \exp\left\{-\int_0^t \nabla \cdot h \, [u = f(u_0, \dot{u}, j a_0; \tau)] d\tau\right\} \qquad (18)$$

where, $u_0 = f^{-1}(u, \dot{u}, j a_0; t)$ means the inverse function corresponding to eq. (17). Thus the mean value and the mean square value of the dynamic ground compliance are expressed by eq. (18). However, the probability density function may be solved in a few particular case, since the general solution $u(t)$ can not be generally obtained in a explicit form.

4. Dynamic Response of an Elasto-Plastic Structural System on a Random Soil Medium

The dynamic ground compliance of a random soil medium is simulated by the following approximate transfer function derived from numerical values, $f_{1H}(\omega') + j f_{2H}(\omega')$, for the case of horizontal excitation acting upon a rectangular foundation

$$K_H(s') = \frac{c}{b} \cdot \frac{s'^2 + a_4 s' + a_3}{a_2 s' + a_1} \simeq \frac{c}{b} \cdot \frac{1}{f_{1H}(a_0') + j f_{2H}(a_0')} \qquad (19)$$

where $s' = j a_0'$, $a_0' = b\sqrt{\frac{\rho}{\mu}}\omega'$

ω' is the angular frequency; ρ is the density of a soil medium: b and c denote the half length of the rectangular foundation in the direction of excitation and that in the other direction, respectively: s' is complex parameter of Laplace transform. Then, the dynamic responses of a random medium are characterized by the random coefficents a_1 , a_2 , a_3 , and a_4 substituted in eq. (19). In this paper, the above-ground structure has the bi-linear hysteretic restoring characteristics represented by the equivalent stiffness K_e and the eqivalent damping d_e through a statistical linearization technique.

$$K_e(t) = \frac{\int_0^\infty \left\{ \frac{2}{\pi}(1-r_1)(2-x)\sqrt{x-1} + \frac{(1-r_1)}{\pi}x^2\cos^{-1}\left(1-\frac{2}{x}\right) + r_1 \right\} P_x(x;t)\,dx}{\int_0^\infty x^2 P(x;t)\,dx}$$

$$d_e(t) = \frac{\int_0^\infty \frac{4}{\pi\bar{\omega}}(1-r_1)(x-1)P_x(x;t)\,dx}{\int_0^\infty x^2 P_x(x;t)\,dx} \qquad (20)$$

where $P_x(x;t)$ denotes the probability density function of peak amplitude x ; r_1 is the stiffness ratio of the second stiffness to the first one in the bi-linear restoring characteristics. Then, the dimensionless fundamental equation of the soil-structural system with respect to the moving coordinate is expressed in the Laplace transform

$$\left([m']S^2 - [K(S)] \right)\{\tilde{x}_i\} = \{m'\}f \qquad (21)$$

$$[m'] = \begin{bmatrix} 0 & \cdots & 0 \\ \vdots & m_0' & \\ & & \ddots \\ 0 & & m_n' \end{bmatrix}, \quad [K(S)] = \begin{bmatrix} K_g K_H(\beta S) + K_0(d_e + K_e), & -K_0(d_e S + K_e), & \cdots \\ -K_0(d_e S + K_e), & & \\ & \ddots & \\ & & -K_n \\ & -K_n, & K_n \end{bmatrix} \qquad (22)$$

$$\{\tilde{x}_i\} = \{\tilde{x}_g, \tilde{x}_0, \tilde{x}_1, \cdots, \tilde{x}_n\}^T$$

where S is the complex parameter of the Laplace transform associated with a dimensionless time τ. The independent and dependent variables and the inhomogeneous terms in the dimensionless fundamental equations with respect to S and τ are related to the original physical equations as follows:

$$\tau = \sqrt{\frac{\bar{K}}{\bar{M}}}\,T \quad , \quad \omega = \sqrt{\frac{\bar{M}}{\bar{K}}}\,\Omega \quad , \quad \beta = b\sqrt{\frac{\rho}{\mu}}\sqrt{\frac{\bar{K}}{\bar{M}}}$$

$$\{\tilde{x}_i\} = \{\tilde{x}_i - F_H\} \subset \{x_i\} = \left\{\frac{x_i - x_H}{\bar{\Delta}}\right\} \quad , \quad \{\tilde{x}_i\} \subset \left\{\frac{x_i}{\bar{\Delta}}\right\}$$

$$F_H \subset \frac{x_H}{\bar{\Delta}} \quad , \quad f = S^2 F_H \subset \alpha\alpha(\tau) \qquad (23)$$

$$\alpha = \frac{A\bar{M}}{\bar{K}\bar{\Delta}} = \frac{A\bar{M}}{\bar{B}} \quad , \quad \alpha(\tau) = \frac{d^2}{dT^2}\left(\frac{x_H}{A}\right)_{T=\sqrt{\frac{\bar{M}}{\bar{K}}}\tau}$$

where, T is time; x_i , x_0, and x_g are the displacements of the i-th mass of the above-ground structure, of the foundation mass and of the elastic ground in the absolute coordinate, respectively; x_H is the displacement of an earthquake excitation; A is the maximum amplitude of acceleration of excitation; $\bar{M}$, $\bar{K}$, $\bar{\Delta}$ and $\bar{B}$ are the reference values of mass, stiffness, displacement and strength. And the mass ratio, m_g , of the foundation to the elastic ground and the equivalent stiffness, K_g , of elastic ground are defined as follows:

$$m_g = \frac{M_0}{\rho b^3} \quad , \quad K_g = \frac{\mu b}{\bar{K}} \qquad (24)$$

For the representation of response of the interaction system in the frequency domain, replacing $S = j\omega$ in eq. (21), the spectral density matrix of the displacement response with respect to the relative coordinate is expressed by

$$[_0S_v(\omega)] = \{v(j\omega)\}\{v(j\omega)\}^* = S_0[I]\{G(j\omega)\}\{G(j\omega)\}^*[I]^T \qquad (25)$$

where $\{G(j\omega)\} = \left(-\omega^2[m'] + [K(j\omega)]\right)^{-1}\{m_i'\}$

and $$[T] = \begin{bmatrix} 1 & \cdots & \cdots & 0 \\ -1 & 1 & & \\ \vdots & -1 & \ddots & \\ \vdots & & \ddots & 1 \\ 0 & & & \end{bmatrix} \qquad (26)$$

$\{G(j\omega)\}^*$ denotes the transposed conjugate vector of $\{G(j\omega)\}$. S_o is the level of the power spectral density of a white random excitation. And the covariance matrix of relative displacement is represented by

$$[\sigma_v^2] = [R_v(\tau)]_{\tau=0} = \frac{1}{2\pi}\int_{-\infty}^{\infty} [_o S_v(\omega)]\, d\omega \qquad (27)$$

in which $[R_v(\tau)]$ is the auto-correlation function matrix of the relative displacement of the system. From eq. (27), the standard deviations of the relative displacement of an elasto-plastic structure on a random soil medium can be evaluated corresponding to the random dynamic ground compliance.

5. Numerical Results

Since the solution of eq. (2) with random coefficients can not be determined analytically, the Monte Carlo simulation method is used to evaluate the response of the random system. The method used here to generate random coefficents has been repressented by Shinozuka, which can make a stochastic process with any spectral density function. In this paper, the stiffness matrix is characterized by stochastic property, because Young's moduli of soil elements are treated as random variables with the mean values of Poisson's ratio $\nu = 0.25$. It may be more desirable to treat a two-demensional random process in itself, for a soil medium is represented as to two-dimensional finite element model. For simplicity, the random process with one-dimensional spectral density function is assumed here along either one horizontal or vertical direction as follows:

$$E(z) = \sqrt{2}\sum_{k=1}^{N} [\mathcal{J}(\xi_k)\Delta\xi]^{\frac{1}{2}} \cos(\xi_k' z + \Phi_k), \quad z = x, y \qquad (28)$$

where Φ_k is a random phase angle distribution uniformly between 0 to 2π. ξ_k' denotes the wave number with the upper bound ξ_u and the lower bound ξ_ℓ. $\mathcal{J}(\xi)$ is the prescribed spectral density function of Young's modulus along either direction in the form,

$$\mathcal{J}(\xi) = \frac{\xi_o^4 + 4h^2\xi_o^2\xi^2}{(\xi_o^2 - \xi^2)^2 + 4h^2\xi_o^2\xi^2} \cdot \frac{\sigma_E^2}{I_o} \qquad (29)$$

In eq. (29), σ_E^2 means the variance derived from the spectral density and ξ_o is the wave number corresponding to the variation of modulus along the direction considered. h and I_o are a parameter describing the shape of the spectral density function and a normalizing factor. Thus, Table 1 shows the combination of the parameter σ_E^2 and ξ_o to characterize the random variable $E(z)$ of Young's modulus. An ensemble with thirty samples is generated by eq. (28) to ensure good convergence to the mean response.

In Fig. 1, the mean values of the dynamic ground compliance $E\{f_{1H} + f_{1H}'\}$ and $E\{f_{2H} + f_{2H}'\}$ to the horizontal excitation acting on the foundation are presented for the variance $\sigma_E^2 = 0.05$ with other parameters characterizing the random inhomogeneity of soil ground. The deviations from the compliance of a deterministic homogeneous medium are, at most, several percents, according to the variations of Young's modulus. To investigate the difference between the compliance of a random soil medium and that of a deterministic homogeneous medium, the fluctuations $E\{f_{1H}'/f_{1H}\}$ and $E\{f_{2H}'/f_{2H}\}$ represented by eqs.

(10) and (11) are shown in Figs. 2 to 5 according to the parameters of the spectral density of eq. (29). Figs. 2 and 3 indicate the fluctuations of the real and imaginary parts of the compliance for the Young's modulus process with variance $\sigma_E^2 = 0.01$ and 0.05 simulated to the horizontal direction. In these figures, the mean values of the compliance for the case $\xi_0 = 20$ are greater than for the case $\xi_0 = 2.5$ Then, it may be pointed out that there exists a relationship between the size of the random inhomogeneity and the length of wave scattered in a random soil medium.

Figs. 4 and 5 show the fluctuations of the compliance $E\{t_{1H}'/t_{1H}\}$ and $E\{t_{2H}'/t_{2H}\}$ for Young's modulus process with the variance $\sigma_E^2 = 0.01$ and 0.05 simulated to the vertical direction. Comparing with Figs. 3 and 5, the wave motion is apt to be scattered if the direction of the excitation coincides with that of the simulation of Young's modulus process. The wave motion is varied by the spatial variation of the stiffness in a random medium and the scattering of the wave motion grows up with the increase of path length in traveling wave, so that the energy itself supplied by the excitation acting on the foundation is not dispersed away from the exciting point where the dynamic ground compliance is evaluated. Therefore, the scattering effect on the dynamic ground compliance is mainly governed with the amount of energy back scattered to the foundation due to the random inhomogeneity. Then, it is necessary to explain the dependence between the fluctuation of the dynamic ground compliance and the variation of the refractive index. To find such the dependence theoretically, it is convenient to introduce the wave parameter

$$D = \frac{4\ell}{\xi a^2} \tag{30}$$

defined as the ratio of the size of the first Fresnel zone to the scale of the inhomogeneity, where ℓ is the wave transmission distance. The scattering depends essentially on the value of the parameter D . In eq. (30), ξ and a denote the wave number and the correlation length of the refractive index $_E k'$. To explain the amplitude and phase fluctuations due to the random inhomogeneity, the following two cases are considered, which correspond to the limiting values of the wave parameter; $D \gg 1$ and $D \ll 1$. The wave parameter $D|_{\xi_0=20} = (42 \sim 21)\ell$ belongs obviously to the small-scale scattering region $(D \gg 1)$ in which the isotropic scattering occurs. As the wave length in this case is large compared with the scale of the inhomogeneity, the deviation of the refractive index $_E k'$ from its mean value has the different signs at the different points of the random medium. Therefore, all of the elementary scattered waves do not arrive in phase at the foundation. They are partially interfared, and as a result the fluctuation grows up slowly with the increase of the distance ℓ . Then, the dynamic ground compliance seems to be large as compared with that of non-random medium. On the other hand, the wave parameter $D|_{\xi_0=2.5} = (0.65 \sim 0.32)\ell$ belongs to the large-scale scattering region $(D \ll 1)$ in the small distance. Since the dimension of the first Fresnel zone in this case is small compared with the scale of the random inhomogeneity, the deviation of the refractive index $_E k'$ from it's mean value has the same sign within the medium. Therefore, all waves scattered by the different elements of the medium arrive at the foundation in phase, and the fluctuation increases rapidly with distance. A remarkable effect will be only produced by inhomogeneity which is concentrated within a cone with it's vertex at the foundation and with an aperture angle of the order $1/\xi a$. The scattering in this case has a sharply directed character and most of the scattered energy is concentrated within a small angle $1/\xi a$, so that the dynamic ground compliance seems to be small as compared with

that of the non-random medium.

Figs. 6 shows the amplitude fluctuations of the compliance for Young's modulus process simulated to the horizontal and vertical directions. Since the wave length becomes relatively small as compared with the correlation length of inhomogeneity with the increase of non-dimensional frequency parameter a_0, it is apt to induce the large-scale scattering for a large value of a_0.

Fig. 7 shows the coefficients of variation for the compliance corresponding to Fig. 6. In this figure the coefficients for $\xi_0 = 2.5$ are greater than those for $\xi_0 = 20$.

Figs. 8(a)~8(d) show the probability density distribution for the natural frequencies of a random medium excited to the horizontal direction. The variational character presented in Fig. 7 is also pointed out in these figures. In Fig. 1, the effect of the variation of the natural frequency of a soil medium can be found in the part about $a_0 = 1.6$

Furthermore, to evaluate the dynamic response of an elasto-plastic structure on a random soil ground, the following parameter is introduced.

$$\bar{\lambda} = \frac{{}_1\Omega_s}{{}_1\Omega_g} = \frac{{}_1\omega_s}{{}_1\omega_g} \tag{31}$$

in which ${}_1\Omega_s$ is the fundamental natural frequency of the above-ground structure with rigid base, and ${}_1\Omega_g$ is that of a substructure consisting of a foundation and soil medium. The parameter $\bar{\lambda}$ means the interaction effect of the substructure on the dynamic response of the above-ground structure. The fluctuations of the standard deviation of relative displacement of whole interaction system with simplified structure of a single-degree-of-freedom system, boundary soil layer and random elastic medium are shown with respect to the parameters σ_E^2 and $\bar{\lambda}$.

In Fig. 9(a), the response of simplified structure decreases for a large value of ξ_0, where the isotropic scattering is induced. For a small value of ξ_0, however, the effect of the large-scale scattering makes the response increase. Fig. 9(b) shows the fluctuations of the standard deviation of the relative displacement of the soil-structure system with bi-linear hysteretic characteristics. The effect of the nonlinear characteristics, especially of the stiffness ratio of the second stiffness to the first one in restoring force upon the structural responses can be found in these figures. The fluctuations of elasto-plastic response of a main structure for $\bar{\lambda} = 0.4$ are similar to those for $\bar{\lambda} = 1.2$ because the degrading stiffness and the hysteresis damping of the structure decrease the fundamental frequency of a whole system. In the case of $\bar{\lambda} = 1.2$, the energy dissipation has little effect on the interaction so that the fluctuations of the structure seem to be almost flat along the parameter ξ_0. Thus the fluctuations of elastic and elasto-plastic responses of a main structure are scarcely affected by the direction of Young's modulus process simulated herein.

5. Concluding Remarks

In order to estimate earthquake responses of a building structure, one should not only take the dynamic properties of the structure but also those of the subsoil ground close to the structure into account. The vibrational characteristics of the structural system may be affected by the additional damping due to the energy radiated into the ground, the elongation of the fundamental natural period of a whole system, the resonant vibration of the structure surrounding the surface soil layer, and so forth. The dynamic

ground compliance may be considered as the suitable concept to explain the dynamics of the soil-structure interaction. In most of investigations related to the dynamic ground compliance, the soil medium has been supposed to be a homogeneous, isotropic solid. On the other hand, it is necessary to consider the earthquake structural response as a random process and to evaluate the anti-seismic safety of a structure from the stochastic point of view, since the earthquake response of a structural system may extremely involve irregular features. The influences of the randomness in the dynamic interaction of a soil-structure system on the earthquake response characteristics have not been tried to make clean yet.

Then, in this paper, the dynamic responses of a random soil medium are analyzed by the two-dimensional finite element model and also the elasto-plastic response characteristics of the random soil-structure interaction system are evaluated. From the results of these analyses, the following physical significances concerning with the scattering effect are derived:

(1) The wave parameter D is very important to explain the relation between the random inhomogeneity of a soil medium and the property of elastic waves generated in such a medium.

(2) The dependence of the variation of the refractive index characterizing a random soil medium on the fluctuation of the dynamic ground compliance is explained by virtue of the two limiting cases of the wave parameter $D \gg 1$ and $D \ll 1$. In the case of a large value of wave parameter ($D \gg 1$) , where the isotropic scattering is induced, the equivalent damping property due to the energy radiated into a random soil ground increases and the equivalent stiffness of a random soil medium decreases. On the other hand, in the case of small value of wave parameter ($D \ll 1$) , where the scattering has a sharply directed character, the equivalent damping property of random medium decreases and its equivalent stiffness increases.

(3) Since the wave length scattered in a soil medium becomes large as compared with the correlation length of the random inhomogeneity for a large value of ξ_0 , the low-path filtering characteristics are emphasized with decreasing the elastic response of an above-ground main structure. On the contrary, in the region of a small value of ξ_0 , the elastic response characteristics of displacement have a trend to increase.

(4) The hysteresis damping and the degrading stiffness of a main structure in the plastic deformation decrease considerably the fluctuations of the range of a small value of $\bar{\lambda}$

References

[1] Still, C. J., Nosserir, S. B. and Shinozuka, M. ; Impact Loading on Structures with Random Properties, Journal of Structure Mechanics, Vol. 1, No. 1, 1972, pp. 63-77.

[2] Chernov, L. A. ; Wave Propagation in a Random Medium, McGraw Hill, New York, 1960.

[3] Collins, J. D. and Thomson, W. T. ; The Eigenvalue Problem for Structural Systems with Statistical Properties, American Institute of Aeronatuics and Astronautics Journal, Vol. 7, No. 4, 1969, pp. 642-648.

[4] Kobori, T., Minai, R. and Inoue, Y. ; On Earthquake Response of Elasto-Plastic Structure Considering Ground Characteristics, Proceedings of the Fourth World Conference on Earthquake Engineering, Chile, 1969, A-6, pp. 117-132.

[5] Kozin, F. ; On the Probability Densities of the Output of Some Random Systems, Journal of Applied Mechanics, Vol. 28, No. 2, 1961, pp. 161-164.

[6] Shinozuka, M. and Jan, C. M. ; Digital Simulation of Random Process and its Applications, Journal of Sound and Vibration, Vol. 25, No. 1, 1972, pp. 111-128.

[7] Soong, T. T. and Chuang, S. N. ; Solutions of a Class of Random Differential Equation, SIAM Journal of Applied Mathematics, Vol. 24, No. 4, 1973, pp. 449-538.

Table 1 Combination of parameters σ_E^2 and ξ_0 and direction of random process simulated

Variance of random process, σ_E^2	Dominant wave number of random process, ξ_0	Direction of random process simulated
0.01	2.5	vertical
0.01	2.5	horizontal
0.01	20.0	vertical
0.01	20.0	horizontal
0.05	2.5	vertical
0.05	2.5	horizontal
0.05	20.0	vertical
0.05	20.0	horizontal

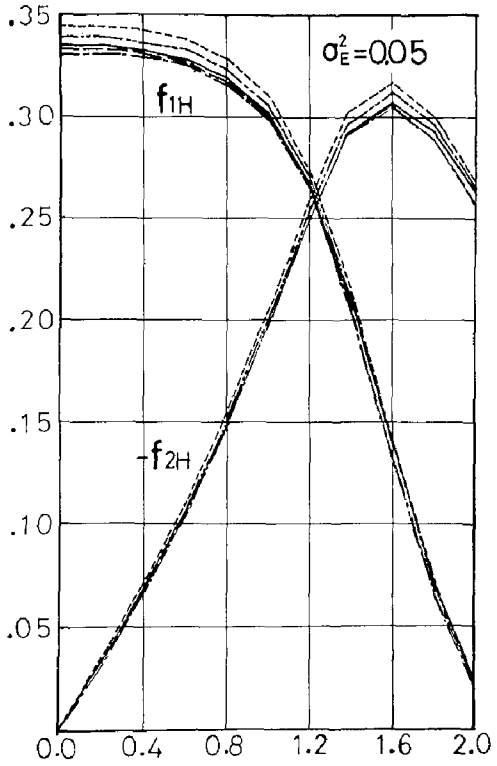

Fig. 1 Mean values of dynamic ground compliance

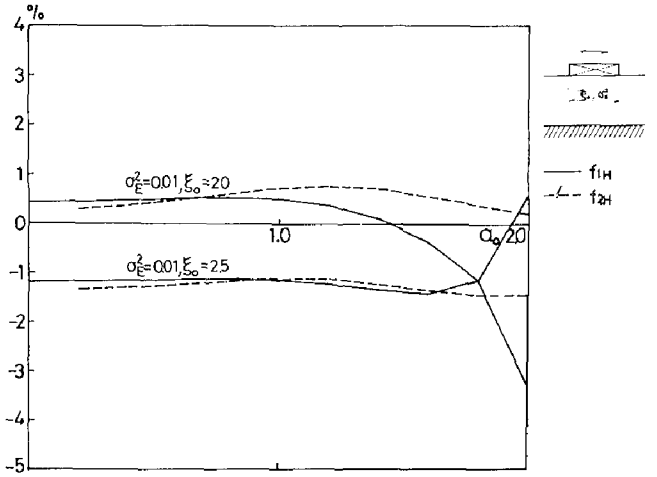

Fig. 2 Fluctuations of dynamic ground compliance

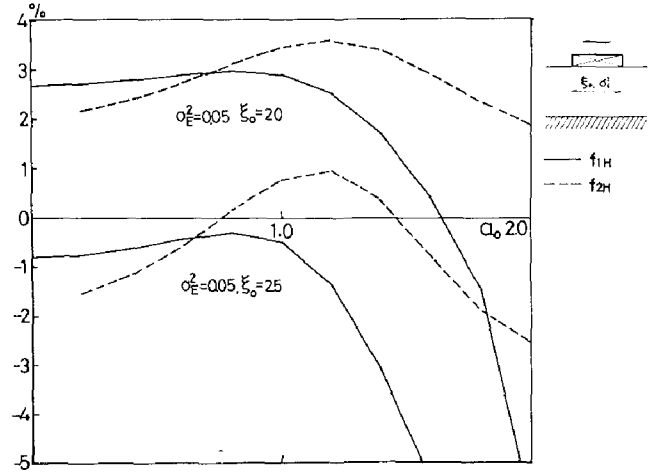

Fig. 3 Fluctuations of dynamic ground compliance

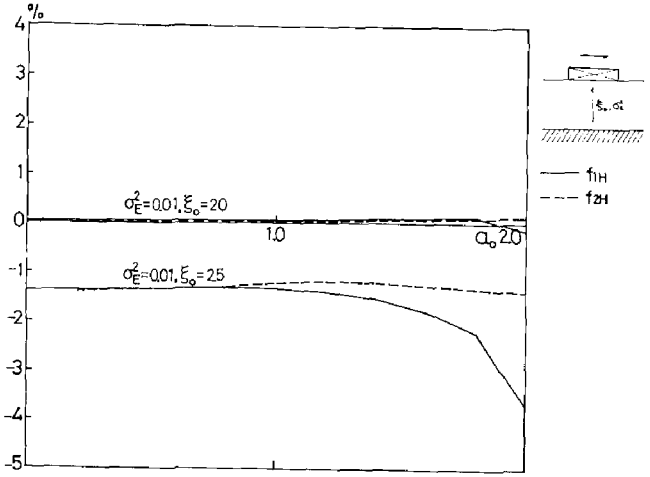

Fig. 4 Fluctuations of dynamic ground compliance

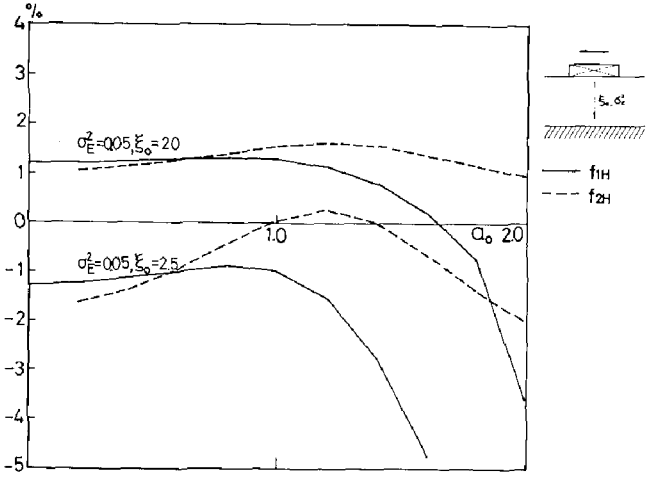

Fig. 5 Fluctuations of dynamic ground compliance

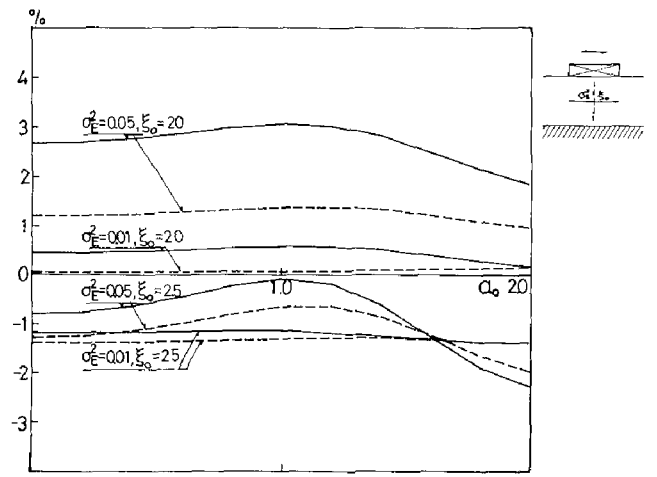

Fig. 6 Fluctuations of amplitude characteristics of dynamic ground compliance

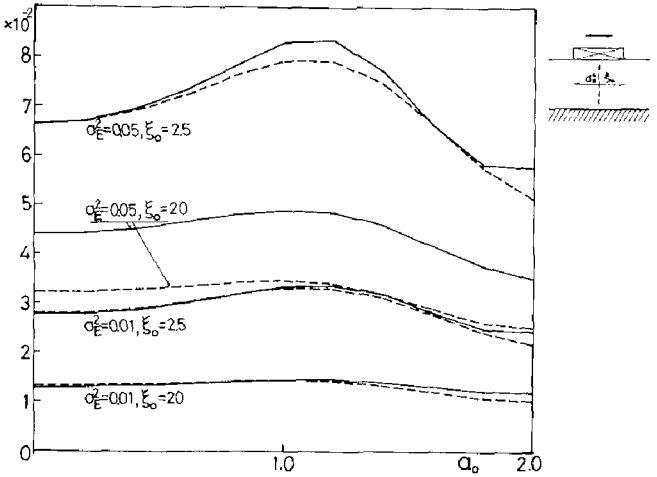

Fig. 7 Coefficients of variation for amplitude characteristics of dynamic ground compliance

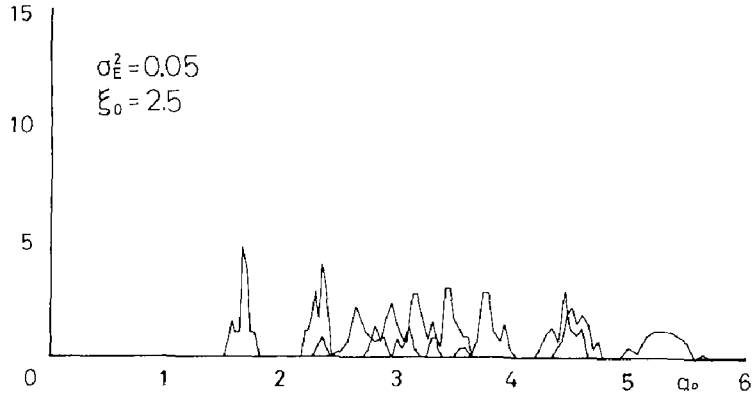

Fig. 8(a) Probability density distribution natural frequencies (direction of Young's modulus process is horizontal)

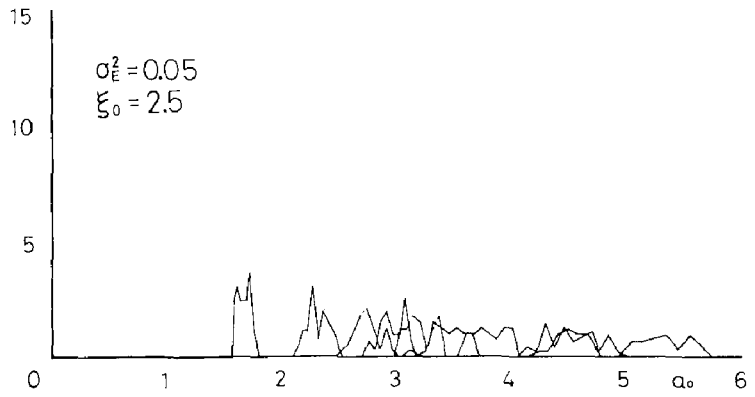

Fig. 8(b) Probability density distribution of natural frequencies (direction of Young's modulus process is vertical)

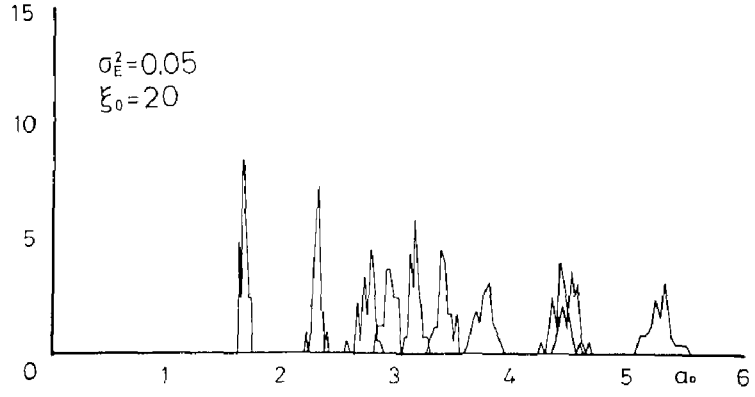

Fig. 8(c) Probability density distribution of natural frequencies (direction of Young's modulus process is horizontal)

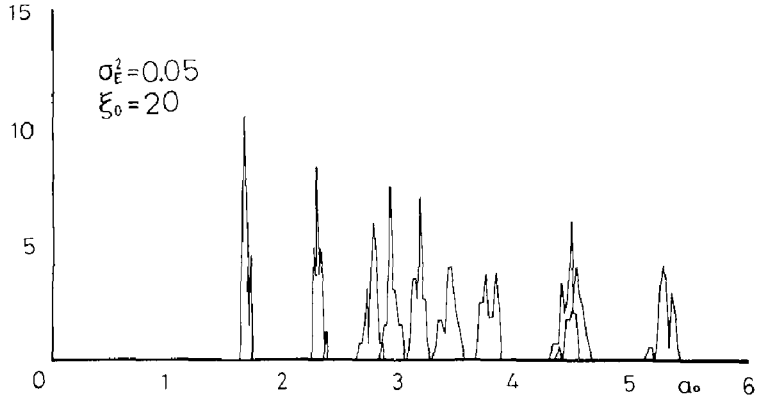

Fig. 8(d) Probability density distribution of natural frequencies (direction of Young's modulus process is vertical)

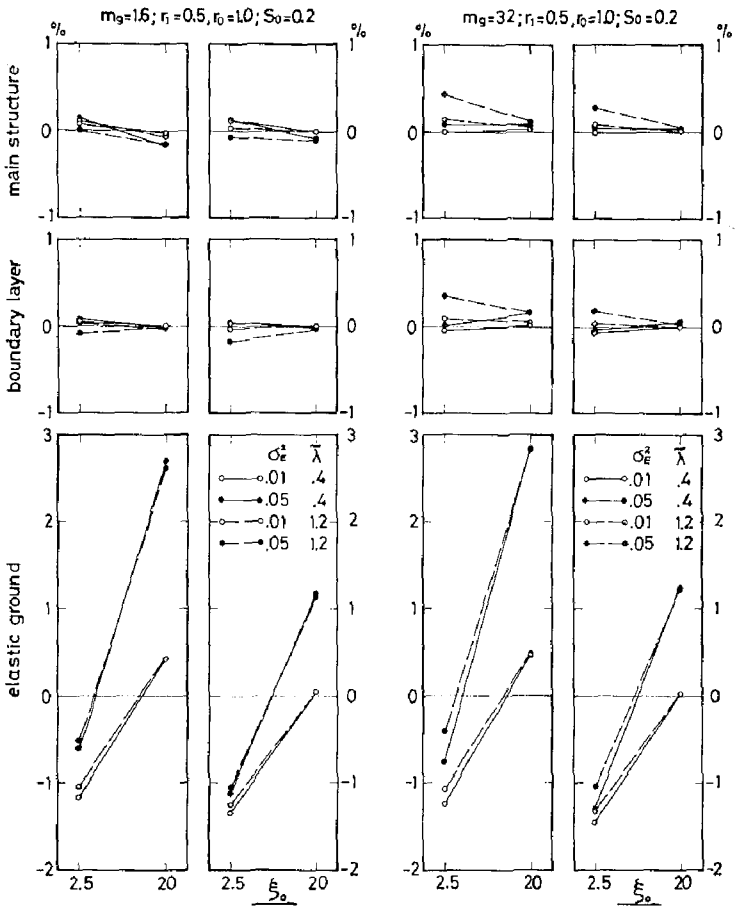

(horizontal)(vertical) (horizontal)(vertical)

Fig. 9(a) Fluctuations of elastic responses of soil-structure system

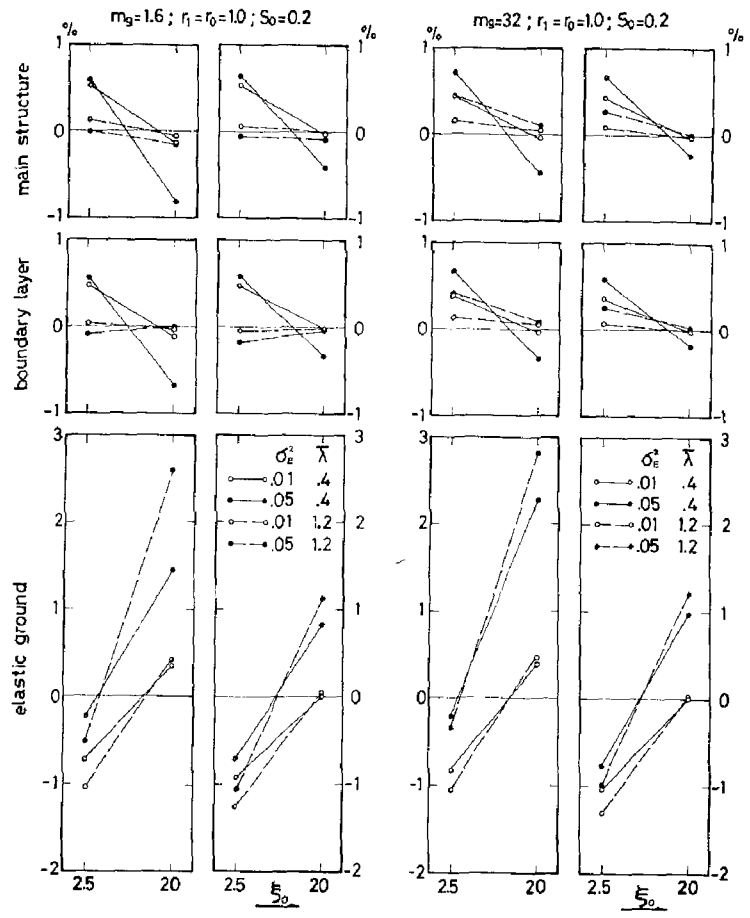

(horizontal)(vertical) (horizontal)(vertical)

Fig. 9(b) Fluctuations of elasto-plastic responses of soil-structure system

INTERNATIONAL SYMPOSIUM ON
EARTHQUAKE STRUCTURAL ENGINEERING
St. Louis, Missouri, USA, August, 1976

SOME DESIGN CONSIDERATIONS OF EARTHQUAKE RESISTANT REINFORCED CONCRETE SHEAR WALLS

THOMAS PAULAY

Professor of Civil Engineering

University of Canterbury

Christchurch, New Zealand

SUMMARY

The possible failure modes in cantilever shear walls are examined, particularly from the point of view of energy dissipation capacity and the suitability of the mechanisms involved in earthquake resistant buildings. Design recommendations with respect to flexure, instability, diagonal tension and sliding shear are made. The introduction of concepts of energy dissipation by shear along a vertical fibre of a cantilever shear wall, leads to the examination of coupled shear walls. Using the evidence obtained from extensive tests it is shown that with the dispersal of and intelligent hierarchy in suitable energy dissipating mechanisms, achieved with relative ease in practice, coupled shear walls can be made to possess all the desirable features of an efficient earthquake resistant structure. To illustrate this a comparison between two coupled shear wall models, one with conventionally the other with diagonally reinforced coupling beams, is made in terms of strength degradation and cumulative energy absorption during progressive reversed cyclic loading.

INTRODUCTION

The protection against damage, that reinforced concrete shear walls can offer in earthquake resistant buildings, is now well appreciated. The good performance of well designed shear walls was also evidenced during recent earthquakes. For lack of quantitative evidence many codes require, however, that shear wall structures be designed for larger strength against lateral loads than ductile rigid jointed reinforced concrete frames with similar dynamic characteristics. This caution seems to stem from the belief that shear walls are inherently less ductile than frames and hence they can absorb only limited energy in the post-elastic range of behaviour. The fact that, because of their greater stiffness, they give superior protection against damage of the non-structural components of a building, is beyond dispute. It is generally accepted that ductility with limited

degradation of strength and stiffness are essential prerequisites in structures, including shear walls, that are expected to survive large intensity reversed cyclic loading, such as would occur during severe seismic disturbances.

In the following failure modes of reinforced concrete cantilever and coupled shear wall structures are discussed, particularly from the point of view of energy dissipation capacity. It is hoped that this qualitative rather than analytical examination of some seismic aspects of structural behaviour will assist designers in conceiving, proportioning and detailing shear walls that would have the promise of a desirable performance during large earthquakes.

CANTILEVER SHEAR WALLS WITHOUT OPENINGS

Most cantilever shear walls in multistorey buildings are slender enough to be treated as ordinary beams. There is no reason to suspect that in their behaviour such walls would disobey the familiar principles of reinforced concrete theory. Therefore the analogy to beams or beam-columns is appropriate. The performance of squat shear walls, which is not examined here, may be dominated by shear and hence they require special treatment.

It is a prerequisite for any ductile structure that its strength shall not be limited by insufficient anchorage of the reinforcement or by the instability of any of its components, including reinforcing bars subjected to extensive compressive yield strain.

Fig. 1.a shows a prototype cantilever shear wall in a multistorey building, subjected to gravity and lateral loading, and the corresponding critical actions at the base. In the following, the possible failure modes of this structure together with critical aspects of its behaviour are examined briefly.

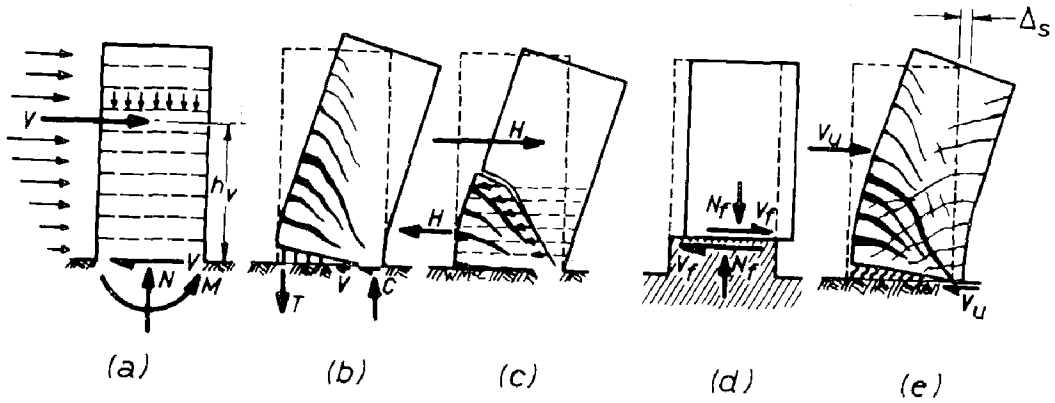

Fig. 1. Failure modes in a laterally loaded reinforced concrete cantilever shear wall

Flexure

Because of load reversals shear wall sections necessarily contain substantial compression reinforcement. Gravity loads commonly produce

only small axial stresses. Consequently the available curvature ductility at the critical section, shown in Fig. 1.b, is usually ample. The ductility of the section is affected by the distribution of the reinforcement within the section.[4] Curvature ductility increases when the flanged shear wall sections are used.[4] If and when required, the concrete in the vicinity of maximum concrete strains may be confined and thus the ductility of a section may be further increased. Because the flexural failure mode in a cantilever shear wall, illustrated in Fig. 1.b, is usually associated with adequate ductility every attempt must be made by the designer to force upon the structure this energy dissipating failure mechanism.

Because of the repeated and reversed nature of the loading the flexural (vertical) reinforcement at the extreme fibres of wall section may be subjected to large tensile yielding. This implies that after load reversal considerable compression yielding must occur before a previously formed large crack can close and the concrete can again contribute to carrying compression. It is essential therefore that compression bars that could possibly yield be restrained against buckling. Near the extreme fibres of the section, where concrete strains may well be in excess of 0.003, it is advisable to disregard the contribution of the cover concrete, and to rely entirely on transverse ties to give lateral support to the compression bars. The spacing of such ties over the potential plastic hinge length should not exceed $6d_b$, where d_b is the diameter of the principal bar to be laterally supported.[3]

Instability of Shear Wall Sections

The instability of a cantilever shear wall, as a structural member, will seldom need be considered in practice because the floors, which introduce the lateral load to the wall, will normally provide ample lateral support. However, because in shear wall structures relatively thin walled sections are common, some precaution must be taken to ensure that in the potential plastic hinge region the repeated and reversed full load can be sustained within the horizontal diaphragms (floors) that provide lateral support.

A theoretical or experimental study of the "compactness" of shear wall sections has not been reported to the writer's knowledge. However, using existing code[1] requirements for slender columns some crude but conservative guides can be established to limit slenderness in shear walls. It may be conservatively stipulated that any part of a thin wall element, which may be subjected to large compression and which does not receive lateral support between floors, should be considered as an isolated column. Hence it is suggested that the thickness, b , of any part of a shear wall, two storeys or higher, in which the combination of flexure and

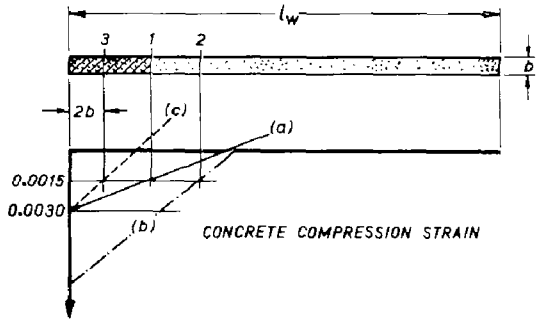

Fig. 2. Strain profiles affecting the lateral stability of thin wall sections.

axial load can produce a compression strain of 0.0015 or more, should not be less than $l_u/10$, where l_u is the clear vertical distance between floors or other effective horizontal lines of lateral support. For a rectangular wall section Fig. 2 indicates that for the strain profile (a) the shaded portion of the section would have to comply with the above requirements. Where the ductility of the section is to be enhanced by larger concrete strains, as shown by strain profile (b), the section extending to line 2 would need to comply. In this case substantial confining reinforcement would need to be provided between the extreme compression fibre and line 2.

When the compressed area is relatively small, as is the case in an underreinforced wall section subjected to flexure, one may assume that adequate lateral support is provided by the adjacent lowly stressed parts of the section. Hence it is suggested that the above limitation need not apply to shear walls with rectangular cross sections if the compression strain specified (0.0015) occurs within a distance of $2b$ or $0.2\,l_w$, whichever is less, from the extreme compression edge, where b is the thickness and l_w is the horizontal length of the wall. Strain profile (c) in Fig. 2 illustrates this situation.

In articulated wall sections one part of the wall may provide some support to other parts and this benefit should be made use of. Consequently it is suggested that in shear walls with other than a rectangular cross section the above limitations on the thickness, b, need not apply to fibres which are within a distance of $3b$ from any vertical line of continuous lateral support, such as the inside of a corner formed by a wall return or a flange. Fig. 3 shows for two strain profiles parts of a flanged shear wall section where, according to these suggestions, the wall thickness could be less than $l_u/10$. The shaded area of the flange is considered to be too far from the vertical line of lateral support and hence its width b' should be at least $l_u/10$. The bottom diagram in Fig. 3 shows for the strain profile (1) the extent over which the wall thickness would need to be increased, so as to form a boundary element, if the wide flanges shown above cannot be provided.

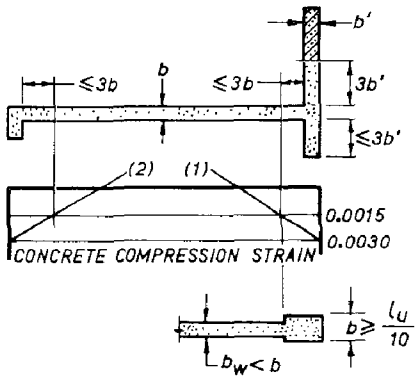

Fig. 3. Parts of articulated wall sections to be considered for instability.

Shear Strength

It is now more generally recognized that the shear strength of tall shear walls can be assessed the same way as that of beams. The behaviour of short shear walls requires special considerations.[6] Shear failures are generally associated with limited ductility. When shear dominates the response of a shear wall the undesirable features of degrading stiffness and strength become distinct consequences of simulated seismic cyclic loading. Therefore every attempt must be made to suppress a shear

failure.

In a cantilever shear wall a distinction must be made between the potential plastic hinge area and the remainder of the structure which, even though extensively cracked, is likely to remain in the elastic domain of response. Diagonal cracks are usually extensions of flexural cracks, as illustrated in Fig. 1.b. Therefore the yielding of the flexural (vertical) reinforcement affects also the widening of the diagonal cracks. It is advisable therefore that over the length of the potential plastic hinge the contribution of all mechanisms to the shear strength, except that of the web reinforcement, be neglected. This implies that in order to ensure a ductile flexural response the plastic hinge region must have sufficient (horizontal) stirrup reinforcement to carry below its yield strength level the entire shear force, shown as H in Fig. 1.c, associated with the maximum possible flexural strength of the shear wall. In the remainder of the cantilever shear wall the shear strength may be assumed to be the sum of the contributions of the concrete, V_c, and that of the web reinforcement, V_s.

It is to be noted that for cantilever shear walls the code specified equivalent lateral static load does not necessarily give satisfactory protection against a shear failure when during a severe excitation the maximum flexural strength at the base is being developed. During certain combinations of the different modes of vibrations the centre of the lateral inertia forces, located with h_v in Fig. 1.a, may be lower than that indicated by customary code prescribed load patterns, such as an inverted triangular load. Consequently considerably larger shear forces may be generated when the moment capacity at the base is attained. It has been shown in case studies that for a number of standard ground motion inputs the ratio of shear forces induced during the combined higher mode responses to the shear force derived from statics and the base moment capacity increases with the fundamental period of the cantilever structure.[2] To guard against a shear failure under such circumstances the design shear envelope for the cantilever wall could be the shear force diagram, corresponding with a code specified static load, magnified by a factor, which will depend on the class of the building and the fundamental period of the structure. Values of 1.0 to 1.8 for this factor have been suggested[2] for shear wall structures from one to 20 storeys.

Sliding Shear

There are two potential locations in cantilever shear walls where a failure by sliding shear could occur. One is a horizontal construction joint which is sensitive to the quality and nature of surface preparation. The other is the plastic hinge zone, usually immediately above foundation level, where, because of the yielding of the flexural reinforcement in both faces and consequent residual strains, continuous cracks across the full depth of the shear wall section will occur.

The sliding along construction joints, illustrated in Fig. 1.d, often observed in shear walls damaged by earthquakes[5], can be suppressed if, in accordance with the concepts of shear friction, adequate distributed vertical reinforcement is provided over the length of the wall to supply, together with the available gravity load, the necessary clamping force, N_f.[7] The inelastic response of the mechanisms associated with sliding

shear indicates drastic loss of stiffness and strength with reversed cyclic loading.[6] Therefore sliding shear must be considered as being an unsuitable energy dissipating mechanism in earthquake resistant structures. It is relatively easy to provide the necessary clamping force across construction joints below yield strength level of the vertical wall reinforcement. The increased shear forces due to higher mode responses, as outlined in the previous section should , however, be considered.

The possibility of sliding shear is much more serious in the plastic hinge zone where, as a result of reversed cyclic load and the ensuing residual plastic strains in the flexural reinforcement of the wall, large continuous cracks may form as shown in Fig. 1.e. The interlock between two serrated faces of such a full depth crack is greatly diminished and if the axial compression across the section due to gravity loads is small, a sliding shear failure may occur across the precracked compression zone (see Fig. 1.e) at nominal shear stresses well below values permitted by codes.[1] Shear transfer by dowel action of the vertical reinforcement is mobilized only after a substantial slip, shown by Δ_s in Fig. 1.e, has occurred. A particularly severe situation can arise in wide flanged shear walls when the neutral axis of the section, at the development of the full flexural capacity, is in or near the flange. Under such circumstances the previously cracked compression area, over which the major part of the shear force must be transmitted, is very small and consequently the interface shear stress can become excessive. Extensive related experimental work, currently carried out at the laboratories of the Portland Cement Association at Skokie, is likely to contribute significantly to the understanding of the phenomenon.

COUPLED SHEAR WALLS

Concepts of Behaviour

In a homogeneous, isotropic cantilever beam the maximum shear stresses, which may be critical, will be induced along the fibre of the neutral axis. If this critical shear fibre, or some other fibres nearby, are potentially weak, as may be the case in precast panel construction, a sliding shear failure along the fibre, as illustrated in Fig. 4.a, is a possibility.

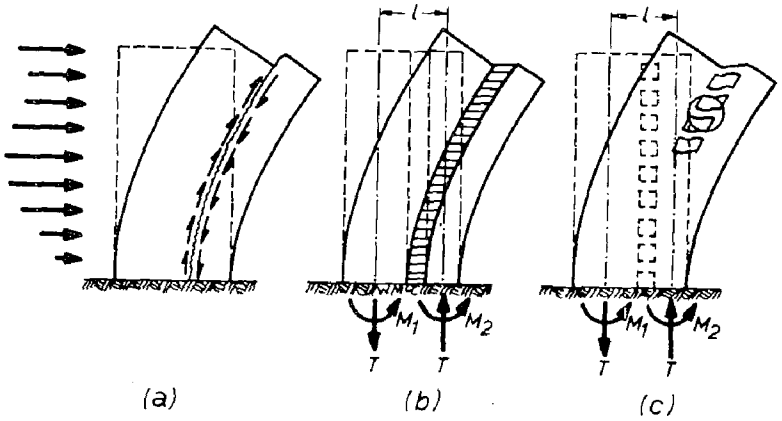

Fig. 4. Laterally loaded coupled shear walls.

However, if this failure mechanism could be made to be ductile and also to possess good energy dissipating properties under reversed cyclic loading, then it could be used as a viable component of the total load resisting system when shaking of extreme intensity is to be survived. By assuming that such a ductile shear transfer mechanism can be constructed, the previously discussed cantilever shear walls could be transformed into coupled shear walls, illustrated in Fig. 4.b. It is seen that the total over-turning moment, produced by the external lateral load, is now resisted by flexure in each of the two cantilever walls, M_1 and M_2, and by the axial force, T, in each of the walls, which operates on an internal lever arm l. The axial force, T, is simply the sum of the shearing forces across the continuous coupling system. The elastic analysis of this model structure has been the subject of numerous studies over the last two decades.

The potential of this structure, as an efficient earthquake resistant construction, would stem from its ability to dissipate energy, when required, within this shear transfer (coupling) system over its full height. This would be in addition to the energy dissipated in the plastic hinge that would be expected to form eventually at the base of each wall. The behaviour of the coupled walls would be similar to that of cantilevers, discussed in the previous sections, except that the effect of the axial force, T, would have to be also considered.

With an intelligent selection of relative stiffness and strength properties it is possible to reinforce the various components in such a way that under continuously increasing lateral static loading the strength of the coupling system is developed before the onset of yielding at the base of the walls. This would imply that considerable energy could be dissipated by the coupling system, involving yielding and consequent damage, before damage and permanent misalignment of the coupled walls would occur. Under catastrophic conditions the major part of the total energy to be dissipated could be derived from the coupling system, thus reducing the ductility demand at the wall hinges.

In comparison with cantilever walls coupled shear walls offer more than one line of defence when energy dissipation is required. The wider dispersal of energy dissipating devices is likely to result in improved structural damage control. When a coupling system with a reasonable stiffness is chosen, which is relatively easy to achieve in practice, the reduction of the stiffness of the coupled shear wall structure, in comparison with a cantilever wall with the same overall dimensions, is insignificant. Consequently the protection against damage of the non-structural components of the building within the elastic response of the coupled shear walls can still be assured.

It appears that a deliberate introduction of a weakness to a cantilever shear wall in the form of a ductile shear fibre, as shown in Fig. 4.a, or its equivalent, illustrated in Fig. 4.b, may result in a structure which possesses the features that are so desirable in earthquake resistant construction, i.e. adequate stiffness to give overall damage control during moderate disturbances and ample ductility and energy dissipating ability for the catastrophic situation. For obvious reasons, the coupling system, which normally is an insignificant component when gravity loads are considered, lends itself much better for repair than cantilever

walls.

Observed Behaviour

In real coupled shear wall structures the shear transfer from one wall to another is afforded by discrete beams, formed between window or door openings, arranged in one or more rows as shown in Fig. 4.c. In some cases functional requirements will determine the depth of these coupling beams, in others some freedom of choice will exist. Naturally the stiffer the coupling system becomes the more efficient will shear transfer be. Sensitivity studies indicated[11] that it is pointless to increase deliberately the beam depth beyond a certain limit because very little additional overall stiffness is gained. However, for efficient coupling it is suggested that at the development of full strength of the coupled shear wall structure, such as shown in Fig. 4.c, at least two thirds of the overturning moment at the base be resisted by the 1T component of the internal moment of resistance. This will ensure that energy dissipation in the coupling system, when required, will be very substantial. It is therefore advantageous to utilize the full depth allowed by architectural requirements.

When the coupling is efficient relatively deep beams with large potential flexural capacity will be used. However, the development of the flexural strength is often associated with shear forces that could be large enough to destroy the beam in a brittle manner. Extensive tests, carried out at the University of Canterbury, have shown that adequate ductility can not be extracted from such beams unless the maximum nominal shear stress developed is small. It is always possible to suppress diagonal tension failures, which have been repeatedly observed in buildings damaged by earthquakes. However, under reversed cyclic loading, involving desirable member ductilities for coupling beams, a sliding shear, similar to that previously described for cantilever walls, will normally occur.[8] As stirrups are not involved in the sliding mechanisms increased amounts of stirrup reinforcement will not prevent a sliding failure.

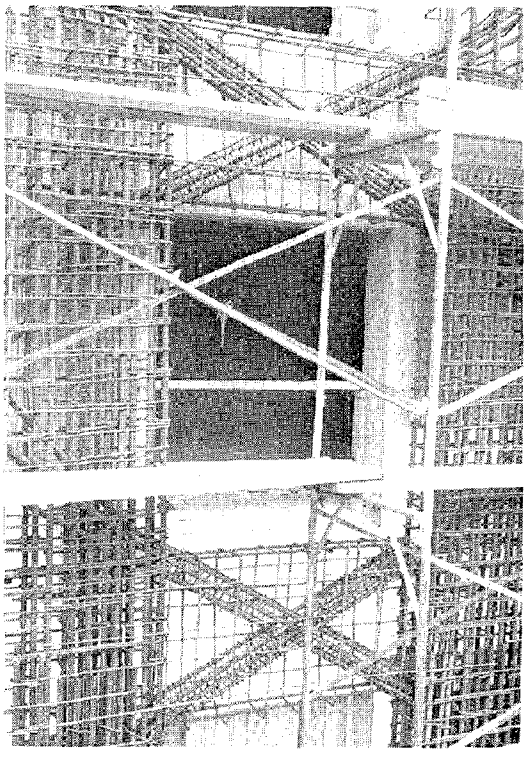

Fig. 5. Diagonally reinforced coupling beams.

To overcome this difficulty beams were studied in which the conventional flexural reinforcement, consisting of horizontal bars running continuously in the top and the bottom of the beam, were omitted. Instead two bundles of diagonal bars of the type shown in Fig. 5 were used.[9] All other reinforcement placed in these beams serves only

secondary purposes. It may be shown from first principles that this system satisfies the requirements of statics simultaneously for moments and shear imposed on the beam by lateral load on the structure. With cyclic loading, involving yielding of the diagonal steel, the internal forces are gradually transferred entirely to the reinforcement. It is therefore not surprising that very large ductilities, similar to those observed in steel beams, could be obtained in tests. Secondary design considerations of such beams have been reported elsewhere.[6,9]

To verify the contribution of conventionally and diagonally reinforced coupling beams to the overall elasto-plastic response of coupled shear walls, two one quarter full size seven storey reinforced concrete coupled shear wall models were constructed, instrumented and tested under simulated cyclic loading. The current code requirements in New Zealand are such that a shear wall structure of this type is expected to be able to sustain a load which would cause a lateral displacement, usually measured at roof level, at least 4 times as much as the displacement at yield. Moreover, the load, when applied in this manner at least four times in each direction, must not diminish by more than 20%. Briefly, a displacement ductility of 4 must be sustained at least 4 times in each direction with a strength loss not exceeding 20%. The tests were carried out in such a way that the cumulative ductility, imposed during progressive and increasingly severe loadings, was at least 16 (i.e. 4 x 4) in each direction of the load application. Only the highlights of the results, most relevant to the design of coupled shear walls, are presented here. Details of the study may be obtained from other reports.[6,9,10,11]

The reinforcing details for Shear Wall A, with conventionally reinforced coupling beams and the corresponding details for Shear Wall B, with diagonally reinforced beams, together with the crack pattern of both specimens at the completion of the tests, are presented in Fig. 6. The massive base block enabled the shear wall models to be attached to a steel frame in order to develop the overturning moments generated by three approximately equal lateral point loads applied at the 3rd, 5th and 7th floor levels. Floor slabs were not simulated but provision was made for both, the prevention of lateral instability and the introduction of an equivalent gravity load.

It is evident from Fig. 6 that at the end of the test all coupling beams of Shear Wall A failed at one or both ends by sliding shear. The crack pattern in the beams of Shear Wall B on the other hand show considerably less distress in spite of large imposed lateral displacements which corresponded with a displacement ductility factor, μ , of more than 10.

Because of strain hardening of the Grade 40 reinforcement both walls developed a total lateral load capacity, P_u , which exceeded by up to 20% the theoretical load capacity, P_u^* , based on the observed strength properties of the steel and the concrete. Fig. 7 shows that with progressive loading, as measured by the cumulative displacement ductility, the strength, P_u , of Wall A was gradually reducing. However, no significant strength loss was observed in Wall B in spite of the severe loading sequence which imposed a cumulative ductility of approximately 32 (i.e. 2 x 16) in both directions. Fig. 7 thus shows the excellent performance of the coupled shear wall model with diagonally reinforced beams in terms of the repeatedly sustained ultimate load, P_u .

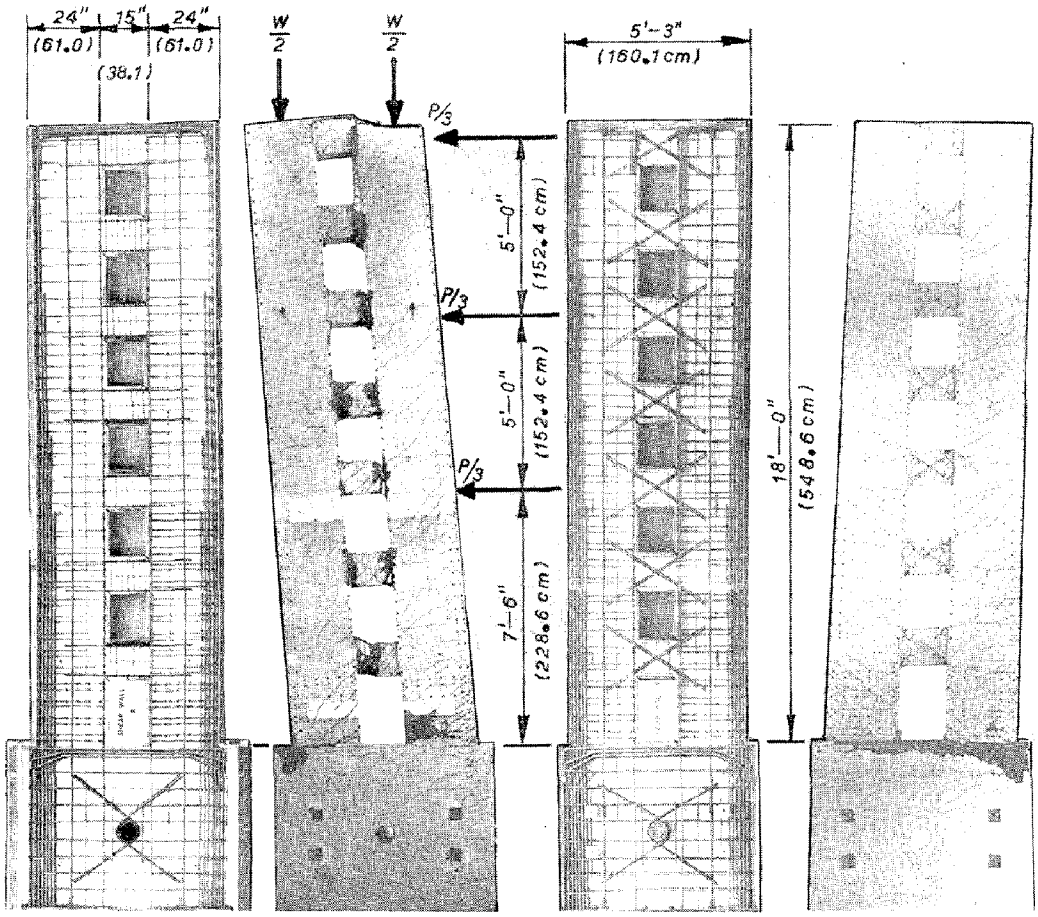

Fig. 6. Reinforcing details and crack patterns of two model coupled shear walls subjected to simulated seismic loading.

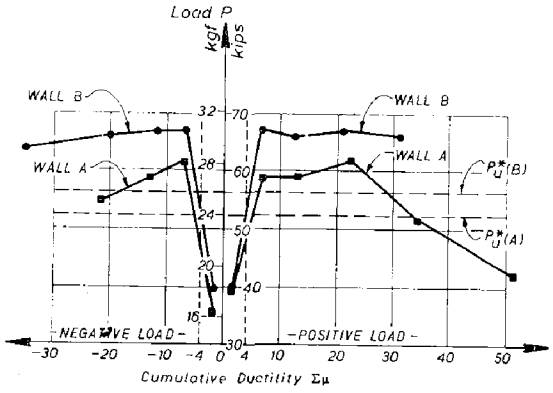

Fig. 7. A comparison of the load sustained with imposed cumulative ductility in two coupled shear walls.

From the load-displacement relationship observed for each of the two models the energy absorbed in each half load cycle, i.e. the area of each hysterisis loop, was determined. The total energy absorbed during the test, as the cyclic loading progressed was then plotted against the cumulative displacement ductility. Fig. 8, which presents these results, shows the superior performance of Wall B. For the same imposed cumulative ductility during the similar load history Wall B absorbed about twice as much energy as Wall A.

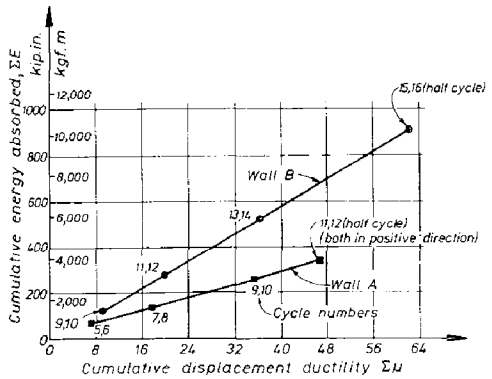

Fig. 8. A comparison of the cumulative energy absorbed with imposed cumulative ductility in two coupled shear walls.

Fig. 5 shows the reinforcing details of the coupling beams of a coupled shear wall structure which has been designed in accordance with the above principles, and which has been completed recently in New Zealand.

CONCLUSIONS

The most likely failure modes of reinforced concrete cantilever shear walls, that could occur during very severe seismic disturbance, were discussed. It was emphasized that in order to obtain sufficient ductility and ability to dissipate energy during postelastic deformation in shear walls all failure modes but flexure must be suppressed by the designer.

Suggestions were made for dimensional limitations of shear wall sections in order to ensure that instability will not intervene with the repeated development of the full flexural capacity. Further research is required to substantiate and to improve on these intuitive guides.

No special treatment is proposed for the assessment of the shear (diagonal tension) strength of tall shear walls. However, it is suggested that in the potential plastic hinge zone the full base shear, associated with the maximum possible flexural capacity of the wall, be resisted by shear reinforcement only. Some account should be made for shear forces generated during the higher modes of dynamic response.

Attention must be paid to horizontal construction joints to prevent premature sliding shear failures, which do not possess adequate energy dissipating capacity.

When the nominal shear stress across the critical base section is large and the axial compression of the cantilever shear wall is relatively small a sliding shear failure after cyclic reversed load along a full depth crack is a distinct possibility.

By discussing the features of the behaviour of coupled shear walls it is shown that energy dissipation can be dispersed in such structures.

Moreover, with a suitable selection of stiffness and strength properties it is possible to ensure that the coupling system will yield before the coupled walls, and that a considerable part of the total energy could be dissipated in the coupling beams. These are advantages which cantilever shear walls do not possess.

The strength degradation and the energy absorption capacity of two quarter full size reinforced concrete model shear walls, subjected to reversed cyclic loading, are compared. It is shown that coupled shear walls with diagonally reinforced coupling beams, when suitably proportioned and detailed, can be made to possess all the desirable features of an efficient earthquake resistant structure.

REFERENCES

1. ACI Committee 318, "Building Code Requirements for Reinforced Concrete (ACI 318-71)", American Concrete Institute, Detroit, 1971, 78 pp.

2. Blakeley, R.W.G., Cooney, R.C., and Megget, L.M., "Seismic Shear Loading at Flexural Capacity in Cantilever Wall Structures", Bulletin of the New Zealand National Society for Earthquake Engineering, Vol.8, No.4, Dec. 1975, pp.278-290.

3. Bresler, B. and Gilbert, P.H., "Tie Requirements for Reinforced Concrete Columns", ACI Journal, Proceedings, V.58, No.5, November 1961, pp.555-570.

4. Fintel, Mark, "Ductile Shear Walls in Earthquake Resistant Multi-story Buildings", ACI Journal, Proceedings, V.71, No.6, June 1974, pp.296-305.

5. Jennings, P.C., "Engineering Features of the San Fernando Earthquake, February 9, 1971", California Institute of Technology, Report EERL 71-02, Pasadena, June 1971, 512 pp.

6. Park, R. and Paulay, T., "Reinforced Concrete Structures", John Wiley & Sons, 1975, 769 pp.

7. Paulay, T., Park, R. and Phillips, M.H., "Horizontal Construction Joints in Cast in Place Reinforced Concrete", Shear in Reinforced Concrete, ACI Special Publication 42, Vol.2, Detroit, 1974, pp.599-616.

8. Paulay, T., "Simulated Seismic Loading of Spandrel Beams", Journal of the Structural Division, ASCE, Vol.97, ST9, September 1971, pp.2407-2419.

9. Paulay, T. and Binney, J.R., "Diagonally Reinforced Coupling Beams of Shear Walls", Shear in Reinforced Concrete, ACI Special Publication 42, Detroit, 1974, pp.579-598.

10. Paulay, T. and Santhakumar, A.R., "Ductile Behaviour of Coupled Shear Walls", Journal of the Structural Division, ASCE, Scheduled for

publication in the January 1976 issue.

11. Santhakumar, A.R., "The Ductility of Coupled Shear Walls", Ph.D. Thesis, 1974, University of Canterbury, Christchurch, New Zealand, 412 pp.

INTERNATIONAL SYMPOSIUM ON
EARTHQUAKE STRUCTURAL ENGINEERING
St. Louis, Missouri, USA, August, 1976

EARTHQUAKE RESISTANCE OF STRUCTURES WITH SUSPENDED MASSES.

NIKOLAENKO N.A.[x], BURGMAN I.N.[xx]

[x] Senior scientific worker, Department of Structural Earthquake Resistance, Doctor of Engineering, Professor.

xx) Senior Scientific worker, Department of Structural Earthquake Resistance, Cand. of Engineering.

Central Research Institute of Building Structures,
Gosstroi of the USSR.
Moscow, the USSR.

SUMMARY

The paper deals with some problems of earthquake resistance of structures with suspended masses. It provides the results obtained in studies of linear and nonlinear vibrations of structures with suspended masses under a horizontal seismic effect which is assumed in a form of a random process. In a linear analysis of the dynamic response of the systems the energy dissipation process is considered according to the com plex hypothesis of damping. Studies of steady and transfer sta tes of vibrations of frameworks with suspension masses are given with the application of the correlation theory. The statistical analysis is done according to the characteristics of the dynamic factor obtained by a computer for different versions of constructive designs. When considering nonlinear problems of the system vibrations, there were studied equations with viscous damping and with a nonlinear-elastic diagram of a soft type approximated by a cubic parabola. Differential equations are solved by means of the statistical linearization method.

INTRODUCTION

The idea of developing a principally new system of a construction with suspended storeys was first put forward for civil buildings in the 20^{ies} this century in the USA and Germany, but it has not been used widely in practice. Over recent ten years the attention has again beendrawn to it and nowadays in many countries dozens of such buildings are being designed and built. Similar constructive designs of apartment blocks have been developed at a number of institutes of our country.

Structures with suspended storeys and suspended technological equipment for industrial buildings was first proposed here in the 60^{ies}. The suggestion was to transfer some technological loads located in upper floors to suspensions or suspended floors. Indeed, multi-storey industrial buildings are, as a rule, subjected to significant loads due to equipment and

weights.During an earthquake these weights set up additional seismic forces to withstand which the structures should be de signed.If to transfer these loads to suspensions or suspended floors,then horizontal seismic forces can be significantly re duced.

The applocation of structures with suspended masses in industrial construction is manyfold.At present suspended heat aggregates are widely used.In framed buildings of a height up to 120m on a multitude of suspensions geat aggregates of 10 to 100 thousand tons are located.Structures of such buildings can be resolved to a diagram shown in Fig.1.In cellulose-paper industry on top floors of buildings heavy equipment is si tuated which can be placed on suspended floors(Fig.2).In some branches of non-ferrous metallurgy the placing of heavy masses on elastic hangers in necessitated technologically.E.g.,in constructions for mechanical treatment of minerals bins for ore and hoppers with heavy masses are placed on elastic hangers.Adiagram of such a construction is given in Fig.3.Constructions in which equipment and loads can be placed on separate suspended plat forms can be resolved to the diagram in Fig.4.To simelar diagrams some constructive designs of residential and public buildings are resolved.As an example of such a constructive design can serve the design of a hostel for students devised in France.Three steel frames connected by longitudinal rafters to which living blocks are suspended(Fig.5)form the load bearing structure of that building.Diagrams in Fig.1-5 can also be used for dif ferent constructive solutions of suspended roofs in industrial buildings and ev en of suspended buildings,which designs are suggested by some countries.

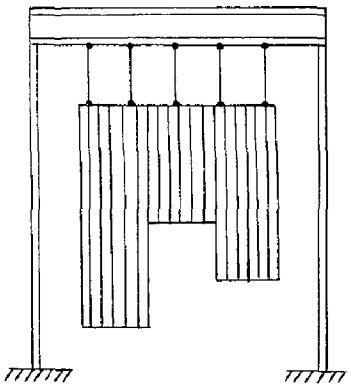

Fig.1

The present paper discusses some problems of studying structures with suspended masses under horizontal seismic seismic effects.

The seismic effect is of a random nature,making,in fact impossible the presente tion of exciting vibrations in a for m of a determinate function.Due to the heterogeneity of star ting seismological date and difficulties in reflecting the diversity of the seismic process in a single universal model various realization exist.In many works the model of the sei smic motion pf the ground was presented as a succession of uncorrelated impulses.To evaluate maximum values of the seis mic response "white noise" is often used as a model of the seismic effect.There have been developed methods to design structures for seismic effects presented in the form of an unsteady random process.

Design of structures can be rather less laborous if to present the ground acceleration as a steady random process. In /1/ Barstein M.F. proposed to consider the ground acceleration $\ddot{x}_0(t)$ as a steady random process $F(t)$, and to consider the process of an elastic system in a transit state at zero initial conditi ons.

$$\ddot{x}_0(t) = \begin{cases} F(t) & \text{at } t=0 \\ 0 & \text{at } t<0 \end{cases}$$

With such a presentation the output of the system will be an unsteady process The suggestion was then termed in lite rature as a "hypothesis of steadiness of the seismic effect".The author of the hypothesis of steadiness of the seismic process selected for statistical processing a series of accelograms of strong earthquakes regarding that such accelograms provide larger seismic forces as compared to rapidly attenuating ones.For them were built up normalized correlated functions which are well ap proximated by typical analytical expressions of correlation functions.

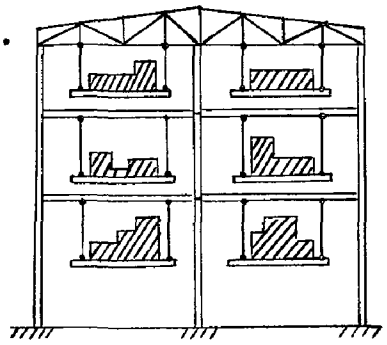

Fig.2

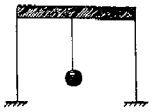

Fig.3

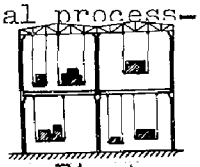

Fig.4

$$k_н(\tau) = e^{-\alpha|\tau|} \cdot \cos\beta\tau$$

The parameters of this function α and β characterize respectively the correlation time and prevaili ng frequencies of seismic ground motions.

In studying the problems of ear thquake resistanse of frameworks with suspended masses there was used the model of a steady seismic effect with the normal distribution law with probabilistic characteristics α =7 I/s β =18 I/s

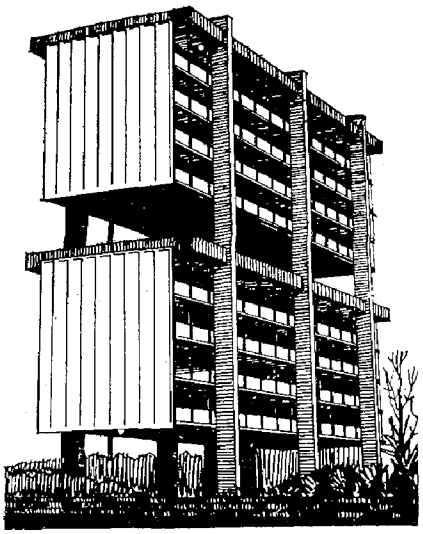

Fig.5

It is assumed that dynamic design models of constructions corres pond to discrete systems with masses concentrated at the floor levels. Vibrations of systemswith suspended masses are regarded on the example of a single-storey framework with one or a few loads.Here the simplest dynamic model is a system with two degrees of freedom.It is supposed that the suspended loads perform translatory motion and they can be regarded as pendulums.The diagram of such a construction is shown in Fig.6 and Fig.7gives its dynamic design scheme.It is supposed that vib. ration amplitudes of the frameworks are low and those of sus-

pendedloads are finite.The structure under consideration is taken in a moving system of coordinates (x,y), that moves progressively as regards the inertial axis (X,Y). This motion is determined by the horizontal component of the seismic effect $x_0(t)$.

The process of energy dissipation influences considerably the pattern of the system motion. When analysing linearly the dynamic response of frameworks E.S.Sorokin's complex hypothesis is used in the paper. According to this hypothesis damping intensity depends linearly up on the value of deformation and elastic restoring force, and as for the phase it is shifted with respect of the vector of deformation by 90^0 $(u+iv)k_1x_1$. For resistance forces in hinges of suspensions Kelvin-Voigt's hypothesis of viscous friction is used, according to which the moment of resistance forces is proportional to the angular velocity of the pendulum movement $(M_c = b_k\dot{\theta}_k)$.

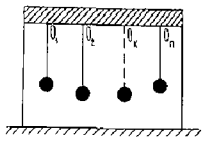

Fig.6

Equations for the system motion are obtained with the help of Lagrange equations

$$\begin{aligned} &\ddot{x}_1 + (u+iv)\Omega_1^2 x_1 = -\ddot{x}_0 + \sum_{k=1}^{n} d_k(-\ddot{\theta}_k\cos\theta_k + \dot{\theta}_k^2\sin\theta_k) \\ &\ddot{\theta}_k + 2\beta_k\dot{\theta}_k + \omega_k^2\sin\theta_k = -c_k(\ddot{x}_1+\ddot{x}_0)\cos\theta_k, \end{aligned} \qquad (1)$$

where

$$\Omega_1^2 = \frac{k_1}{M_1+\sum_{k=1}^{n} m_k} = \frac{k_1}{M_{tot}};$$

$M_{tot} = M_1 + \sum_{k=1}^{n} m_k$ – is the total mass of the whole system

$$d_k = \frac{m_k\ell_k}{M_{tot}};\quad 2\beta_k = \frac{b_k}{J_{ok}};\quad J_{ok} = \ell_k^2 m_k;\quad \omega_k^2 = \frac{g}{\ell_k};\quad c_k = \frac{1}{\ell_k}. \qquad (2)$$

If to replace the variable $\theta_k = c_k\varphi_k$ then in a linear approximation these equations will have the form;

$$\begin{aligned} &\ddot{x}_1 + (u+iv)\Omega_1^2 x_1 = -\ddot{x}_0 - \sum_{k=1}^{n} r_k\ddot{\varphi}_k; \\ &\ddot{\varphi}_k + 2\beta\dot{\varphi}_k + \omega_k^2\varphi_k = -\ddot{x}_0 - \ddot{x}_1 \quad (k=1,2,\dots n), \end{aligned} \qquad (3)$$

where

$$r_k = c_k d_k = \frac{\omega_k^2 m_k \ell_k}{g\cdot M_{tot}} = \frac{m_k}{M_{tot}}. \qquad (4)$$

The values u and v are related to the coefficient of non-elastic resistance $\gamma = \frac{\delta}{\pi}$ by the relationships $u = \frac{4-\gamma^2}{4+\gamma^2}$, $v = \frac{4\gamma}{4+\gamma^2}$ where δ is the logarithmic decrement of vibrations.

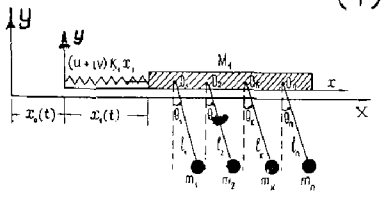

Fig.7

Investigations of vibrations of framed systemsare started with the determination of the spectrum of natural frequencies of vibrations of a structure with one and " " suspended loads. Equations of free vibrations are solved by analytical and graphical methods. Expressions are obtained for determining exact (formula 5) and approximate (formula 6) values of coupled frequencies of the system vibrations

$$\bar{\omega}_{1,2}^2 = \frac{(\Omega_1^2+\omega_1^2) \pm \sqrt{(\Omega_1^2+\omega_1^2)^2 - 4(1-r_1)\Omega_1^2\omega_1^2}}{2(1-r_1)}; \qquad (5)$$

$$\bar{\omega}^2 = \frac{\Omega_1^2}{1-r_1} = \frac{k_1}{M_{tot}(1-r_1)}. \qquad (6)$$

If the framework carries a few suspended loads, the approximate value of the highest frequency of coupled vibrations can be determined by the following expression

$$\bar{\omega}^2 = \frac{\Omega_1^2}{1 - \sum_{k=1}^{n} \tau_k} = \frac{k_1}{M_{tot}\,(1 - \sum_{k=1}^{n} \tau_k)} \qquad (7)$$

By means of expression (7) approximate values of coupled frequencies of the system vibration further required for obtaining the values of seismic loads can be found.

Fig.8 shows the graphical solution of equations of free vibrations of a system with four suspended loads. The abscissas of points of intersection of the straight lines y_1 with the curves y_2 determine the values of roots of coupled frequencies of vibration ($\bar{\omega}$) of the whole system. It follows from the graph that the highest frequency of the system vibration with suspended loads, e.g. ($\bar{\omega}_4$) is always greater than the vibration frequency of the framework (Ω_1) with loads resting on the floors.

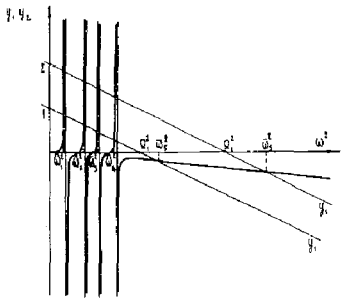

Fig.8

Steady and transit states of induced vibrations of a single-storey framework with one suspended load have been studied. To find the variance of the output (σ_x^2) of the steady process of vibrations of the dynamic system in question the known formulas of the correlation theory were used. Omitting elementary calculations, the expression for determining the variance of the system output is given

$$\sigma_x^2 = \frac{2\alpha B(0)}{2\pi} \int_{-\infty}^{\infty} \frac{\left[1 - \sum_{k=1}^{n} \tau_k \frac{\omega^2}{\omega^2 - \omega_k^2}\right]^2 \cdot (\omega^2 + m^2)\, d\omega}{\left\{\left[-\omega^2 + \mu\Omega_1^2 + \sum_{k=1}^{n} \tau_k \frac{\omega^4}{\omega^2 - \omega_k^2}\right]^2 + (\nu\Omega_1^2)^2\right\}(\omega^4 + 2a\omega^2 + m^4)} \qquad (8)$$

where $B(0)$ is the variance of the acceleration $\ddot{x}_0(t)$

$2\alpha = \frac{\omega^2 - m^2}{\omega^4 + 2a\omega^2 + m^4}$ is the spectral density $\ddot{x}_0(t)$

$\alpha = 7$ I/s, $\beta = 18$ I/s, $m^2 = \alpha^2 + \beta^2$; $a = \alpha^2 - \beta^2$. (9)

Let's ascertain the values ω_k and τ_k entering formula (8) and determining the dynamic parameters of suspended loads which can be encountered in practice.

From formula (2) it follows that $\omega_k^2 = \frac{g}{l_k}$. Following the constructive opportunities for design of suspensions, their length should evidently be $l_k \geq 1$ m what corresponds to the upper bound of frequencies $\omega_k = 3{,}12$ 1/s.

The value τ_k is determined by expression (4). If the suspended load is regarded as concentrated, then it is always $\tau_k = \frac{m_k}{M_{tot}} < 1$. The mentioned restrictions were used in the selection of design versions of dynamic systems.

One of the main characteristics of vibration of structures is the dynamic factor which is the ratio of the dynamic deflection to the static one. The root mean square value of the dynamic factor $\xi(t)$ is equal to

$$\langle \xi^2(t) \rangle = \frac{\sigma_x^2(t)}{\sigma_{st}^2} \qquad (10)$$

where $\sigma_{st}^2 = \frac{B(0)}{\Omega_1^4}$ is the root mean square value of the static deflection.

For the steady process the values σ_x^2 and $\langle \xi^2 \rangle$ do not depend upon time

$$\langle \xi^2 \rangle = \frac{\sigma_x^2 \Omega_1^4}{B(0)} \qquad (11)$$

If the framework bears one suspended load then

$$\langle \xi^2 \rangle = \frac{2\alpha}{2\pi} \Omega_1^4 \int_{-\infty}^{\infty} \frac{\left[1 - \tau_1 \frac{\omega^2 - \omega_2^2}{\omega^2 - \omega_1^2}\right]^2 (\omega^2 + m^2)\, d\omega}{\left\{\left[-\omega^2 + u\Omega_1^2 + \tau_1 \frac{\omega^2 - \omega_2^2}{\omega^2 - \omega_1^2}\right]^2 + (v\Omega_1^2)^2\right\} (\omega^4 + 2a\omega^2 + m^4)} \qquad (12)$$

the complex integrand is written in the form of complex-conjugate expressions and after transformations it resolves itself to the table integral

$$\langle \xi^2 \rangle = \frac{2\alpha \Omega_1^4}{2\pi i} \int_{-\infty}^{\infty} \frac{g_6(\omega)\, d\omega}{F_6(\omega)\, F_H(-\omega)} \qquad (13)$$

where

$$g_6(\omega) = i\left[(\omega^2 - \omega_1^2)^2 + \tau_1 \omega^4 - 2(\omega^2 - \omega_1^2)\tau_1 \omega^2\right](\omega^2 + m^2)$$

The integral $\langle \xi^2 \rangle$ is a table one and is equal to the expression

$$\langle \xi^2 \rangle = \alpha \Omega_1^4 \frac{M_6}{a_0 \Delta_6} \qquad (14)$$

Where

$$M_6 = b_2\left[a_5^2 + a_1 a_3 a_6 - a_1 a_4 a_5\right] + b_3\left[a_3 a_5 + a_1^2 a_6 - a_1 a_2 a_5\right] +$$
$$+ b_4\left[-a_1 a_5 + a_3^2 + a_1^2 a_4 - a_1 a_5 a_3\right] + \frac{b_5}{a_6}\left[a_5^2 + a_1 a_3 a_6 - 2a_1 a_4 a_5 -\right.$$
$$\left. - a_2 a_3 a_5 + a_3^2 a_4 - a_1^2 a_2 a_6 + a_1^2 a_4^2 + a_1 a_2^2 a_5 - a_1 a_2 a_3 a_4\right];$$

$$\Delta_6 = a_5^3 + 3a_1 a_3 a_5 a_6 - 2a_1 a_4 a_5^2 - a_2 a_3 a_5^2 - a_3^3 a_6 +$$
$$+ a_3^2 a_4 a_5 + a_1^3 a_6^2 - 2a_1^2 a_2 a_5 a_6 - a_1^2 a_3 a_4 a_6 +$$
$$+ a_1^2 a_4^2 a_5 + a_1 a_2^2 a_5^2 + a_1 a_2 a_3^2 a_6 - a_1 a_2 a_3 a_4 a_5;$$

$$a_0 = 1;\quad a_1 = (2\alpha + \bar{\omega}_1);\quad a_2 = m^2 + 2\alpha\bar{\omega}_1 + \bar{\omega}_2;\quad a_3 = m^2\bar{\omega}_1 + 2\alpha\bar{\omega}_2 + \bar{\omega}_3;$$
$$a_4 = m^2\bar{\omega}_2 + 2\alpha\bar{\omega}_3 + \omega_4;\quad a_5 = m^2\bar{\omega}_3 + 2\alpha\bar{\omega}_4;\quad a_6 = \bar{\omega}_4 m^2;$$
$$b_2 = (1 - \tau_1)^2;\quad b_3 = 2\tau_1\omega_1^2 - 2\omega_1^2 + (1 - \tau_1)^2 m^2;$$
$$b_4 = (2\tau_1\omega_1^2 - 2\omega_1^2)m^2 + \omega_1^4;\quad b_5 = \omega_1^4 m^2;$$

$$u_2 = \sqrt{\frac{1}{2}\left[\left(\frac{a}{2} + u_1\right) + \sqrt{\left(\frac{a}{2} + u_1\right)^2 - \left(\frac{b}{2} + v_1\right)^2}\right]};$$

$$v_2 = \sqrt{\frac{1}{2}\left[-\left(\frac{a}{2} + u_1\right) + \sqrt{\left(\frac{a}{2} + u_1\right)^2 + \left(\frac{b}{2} + v_1\right)^2}\right]};$$

$$u_3 = \sqrt{\frac{1}{2}\left[\left(\frac{a}{2} - u_1\right) + \sqrt{\left(\frac{a}{2} - u_1\right)^2 + \left(\frac{b}{2} - v_1\right)^2}\right]};$$

$$v_3 = \sqrt{\frac{1}{2}\left[-\left(\frac{a}{2} - u_1\right) + \sqrt{\left(\frac{a}{2} - u_1\right)^2 + \left(\frac{b}{2} - v_1\right)^2}\right]};$$

$$u_1=\sqrt{\frac{1}{2}\left(\bar{a}_1+\sqrt{\bar{a}_1^2+\bar{b}_1^2}\right)}\;;\qquad v_1=\sqrt{\frac{1}{2}\left(-\bar{a}_1+\sqrt{\bar{a}_1^2+\bar{b}_1^2}\right)}\;;$$

$$\bar{a}_1=\frac{a^2}{4}-\frac{b^2}{4}-c\;;\qquad \bar{b}_1=\frac{ab}{2}-d\;;\qquad a=\left(\frac{\omega_1^2}{\Omega_1^2}+u\right)\frac{\Omega_1^2}{1-\tau_1}\;;$$

$$c=u\,\frac{\Omega_1^2\,\omega_1^2}{1-\tau_1}\;;\qquad b=v\,\frac{\Omega_1^2}{1-\tau_1}\;;\qquad d=v\,\frac{\Omega_1^2\,\omega_1^2}{1-\tau_1}\,.$$

From the above formulas by means of a computer values of the dynamic factor ξ were calculated which areplotted in diagrams of Fig.9 and 10 for different values of τ_1, ω_1, ν depending on Ω_1. The value $\nu=0{,}1$ is for reinforced concrete structures, and $\nu=0{,}05$ is for steel ones.

Theprocessingof the results of calculations has shown that the values of the dynamic factor for frequency magnitudes $0.1<\omega,<2.5$ and $10<\omega\lesssim 15$ I/s change very little. Therefore in figure 9 and 10 values ξ for these frequencies are combined

For the convenience of use the calculation results in the determination of values of seismic loads Fig.9 and 10 present corrected diagrams of the dynamic factor for characteristic frequencies ω_1, of practical value. The shaded-dotted line shows the plots of the dynamic factor adopted in the Code, and the dotted line gives the same for cases when suspended loads are rigidly connected with the floor of the framework. As the estimations have shown tne standard of the dynamic factor depends very little upon the value ω_1 within the interval of frequencies $0{,}1\leqslant\omega_1\leqslant 2{,}5\ 1/s$, i.e. for cases corresponding to feasible constructive designs of suspensions.

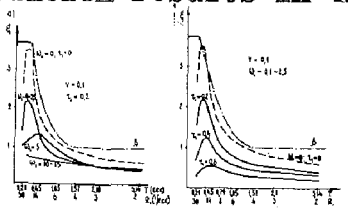

Fig.9

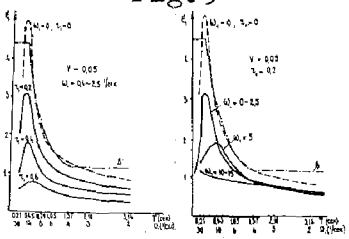

Fig.10

When considering the transit process of vibrations the system of equations was reduced to one integral-differential equation. To fulfill this the solution of the second equation (3)

$$\varphi_k(t)=-\frac{1}{2i\omega_k}\int_0^t[\ddot{x}_0(\tau)+\ddot{x}_1(\tau)]\cdot\left[e^{(-\beta_k+i\omega_k)(t-\tau)}-e^{(-\beta_k-i\omega_k)(t-\tau)}\right]d\tau \qquad (15)$$

was differentiated twice and the value $\ddot{\varphi}_k(t)$ was put into the first equation. All the calculations done, equation (3) becomes

$$\bar{c}\ddot{x}_1(t)+(u+iv)\Omega_1^2x_1-\sum_{k=1}^{n}\tau_k\frac{\omega_k^2+\beta_k^2}{2i\omega_k}\int_0^t e^{-\beta_k(t-\tau)}\left\{e^{i[\omega_k(t-\tau)-2\psi_k]}-\right.$$

$$\left.-e^{-i[\omega_k(t-\tau)-2\psi_k]}\right\}\ddot{x}_1(t)\,d\tau=-\bar{c}x(t)+ \qquad (16)$$

$$+\sum_{k=1}^{n}\tau_k\frac{(\omega_k^2+\beta_k^2)}{2i\omega_k}\int_0^t e^{-\beta_k(t-\tau)}\left\{e^{i[\omega_k(t-\tau)-2\psi_k]}-e^{-i[\omega_k(t-\tau)-2\psi_k]}\right\}\ddot{x}_0(\tau)\,d\tau,$$

where

$$\psi_k=\operatorname{arctg}\frac{\omega_k}{\beta_k};\qquad \bar{c}=1-\sum_{k=1}^{\infty}\tau_k \qquad (17)$$

Equations (16) were solved with the help of Laplace trans-

formations.

Omitting transformations and some mathematical calculations, the expression for mean root square value of the dynamic coefficient, by which the calculations on the computer were done for different magnitudes of the system's parameters can be written as:

$$\xi^2(t)=\frac{2\alpha\Omega_1^4}{2\pi}\int_{-\infty}^{\infty}\left|\sum_{s=1}^{n+1}\frac{F_1(p_s)}{p_s F_2(p_s)}e^{p_s t}\right|^2\frac{(\omega^2+m^2)\,d\omega}{(\omega^4+2a\omega^2+m^4)}. \quad (18)$$

Integral (18) was calculated with a time step of 0.2 and 0.1 s. Fig 11 provides plots of the dynamic factor for different values of Ω_1 and ω_1 ($\tau_1=0.2$ and $\gamma=0.1$). For comparison are given also the plots of the dynamic factor in case the suspended loads are considered to be rigidly connected with the framework ($\tau_1=0, \omega_1=0$).

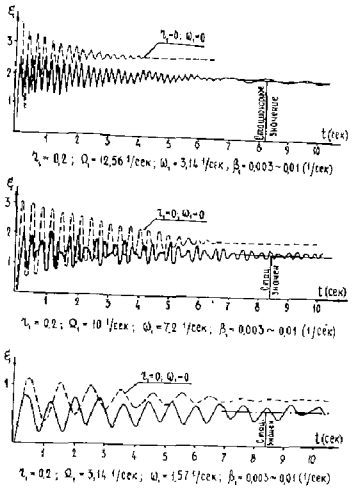

Fig.11

DESIGN VALUE OF SEISMIC LOAD FOR THE FRAMEWORK. VIBRATION AMPLITUDES OF SUSPENDED LOADS.

The design value of the seismic load for a single-storey framework with one suspended load

$$S=\xi(t)\,M_{tot}\,j_{des} \quad (19)$$

Here $\xi(t)$ –the dynamic factor in the transit state;

M_{tot} –the full mass of the system;

j_{des} –the design value of seismic acceleration for the given region.

$$j_{des}=K_{\ddot{x}_0}\sqrt{B(0)}$$

$K_{\ddot{x}_0}$ is the number of standards.

The design value of seismic acceleration is expressed through the seismic factor K_c

$$j_{des}=\frac{K_{\ddot{x}_0}\sqrt{B(0)}}{g}\,g=K_c g, \quad B(0)=K_c^2 g^2. \quad (20)$$

The values $B(0)$ assumed for calculations are close to the variance of the ground acceleration obtained in the processing of accelelograms of earthquakes of different intensity/6/.

The maximum value of the standard of the dynamic factor $[\xi(t)]$ in the transit state is 1.4 times as large as ξ for the steady process (see plots in Fig.9,10,11).

$$\xi(t)=1{,}4\xi.$$

Then the seismic force for a single-storey framework will be defined by

$$S=1{,}4\,Q\,K_c\,\xi, \quad (21)$$

where Q –the total weight (the weight of all structures and

suspended load); ξ - the standard of the dynamic factor which is found from the plots in Fig.9 and 10 in terms of the period of natural vibrations "T" and the fabric of load-bearing structures.

If to take into account that the dynamic factor ξ does not depend on the value ω_1 within the range of $0.1<\omega_1\leqslant 2.5$ I/s. then, following the procedure of standard documents the following formula can be obtained for the seismic force

$$S=\frac{M_{tot}}{g}(1-\tau_1)K_c 1,4\xi=(P_1+Q_1)(1-\tau_1)K_c 1,4\xi=P_1 K_c 1,4\xi \qquad (22)$$

where P_1 -the weight of the construction(without the suspended load);

Q_1 -the weight of the suspended load;

ξ -the dynamic factor calculated by formula (12).

The value ξ is determined in terms of the frequency of natural vibration Ω_1^* which is equal to

$$\Omega_1^{*2}=\frac{\Omega_1^2}{1-\tau_1}=\frac{K_1 g}{(P_1+Q_1)(1-\tau_1)}=\frac{K_1 g}{P_1} \qquad (23)$$

where K_1 -the total rigidity of posts of the framework.

If the framework carries n suspended loads and $0,1<\omega_k\leqslant 2.5$ I/s($K=1,2,\ldots n$), then the seismic force will be equal to

$$S=\frac{M_{tot}}{g}(1-\sum_{k=1}^{n}\tau_k)K_c\cdot 1,4\xi=(P_1+\sum_{k=1}^{n}Q_k)(1-\sum_{k=1}^{n}\tau_k)K_c 1,4\xi=P_1 K_c 1,4\xi \qquad (24)$$

The frequency Ω_1^* is determined by the expression

$$\Omega_1^{*2}=\frac{K_1 g}{(P_1+\sum_{k=1}^{n}Q_k)(1-\sum_{k=1}^{n}\tau_k)}=\frac{K_1 g}{P_1} \qquad (25)$$

As can be seen from formulas (22) and (24) in the indicated frequency range the value of the seismic force does not depend upon the weight of the suspended load.

When designing constructions with suspended loads it is also necessary to know the amplitudes of their deviations in order to avoid damages of outside and inside structures and equipment. Therefore gaps should be left providing for free swinging of suspended loads. This task can be solved only in case the maximum amplitudes of their vibrations are known beforehand.

The variance of the deviation angle is found from the known formulas of the correlation theory

$$\langle\varphi_k^2\rangle=\frac{2\alpha B(0)}{2\pi}u^2\Omega_1^{*4}\int_{-\infty}^{\infty}\frac{g_6(\omega)d\omega}{H_6(\omega)H_6(-\omega)}, \qquad (26)$$

where

$$g_6(\omega)=\omega^2+m^2$$

$$H_6(\omega)=(\omega^2+i\cdot 2\beta_k\omega+\omega_k^2)(\omega^2-i2\bar{\tau}\Omega_1^*\omega-\Omega_1^{*2})(\omega^2-i2\alpha\omega-m^2)$$

where

$$H_6(-\omega)=(-\omega^2-i2\beta_k\omega+\omega_k^2)(\omega^2+i2\bar{\tau}\Omega_1^*\omega-\Omega_1^{*2})(\omega^2+i2\alpha\omega-m^2),$$

$$\bar{\tau}\approx\frac{\gamma}{2}.$$

The roots $H(i\omega)$ are in the upper half-plane, and $H(-i\omega)$ are in the lower one.

Using tables of integrals/2,5/ and performing simple calculations, one arrives at: $\langle \varphi_k^2 \rangle = B(0)\, u^2 \Omega_1^{*4} \mathcal{J}_6$

where $$\mathcal{J}_6 = \frac{\alpha M_6}{a_0 \Delta_6} \tag{27}$$

If to assume the length of the arc over which the centre of the suspended load moves, being equal to the amplitude, and for small angles θ_1 it can always be done, then the vibration amplitude of the load K

$$A_k = \theta_k l_k = l_k c_k \varphi_k \tag{28}$$

and the variance

$$\langle A_k^2 \rangle = l_k^2 c_k^2 \cdot \langle \varphi_k^2 \rangle \tag{29}$$

Taking into account (27) the design value of the vibration amplitude of the suspended load is

$$A_{k\,des} = l_k c_k k_{\ddot{x}_0} \sqrt{\langle \varphi^2 \rangle} = l_k c_k k_c g u \Omega_1^{*2} \sqrt{\mathcal{J}_6} \tag{30}$$

Using the relationship $C_k = I/l_k$ and condition $u=1$, the final formula for determining the design value of the vibration amplitude of the suspended load or suspended roof becomes

$$A_{k\,des} = g \Omega_1^{*2} k_c \sqrt{\mathcal{J}_6} \tag{31}$$

NONLINEAR VIBRATIONS WITH SUSPENDED MASSES.

Under intensive seismic loads load-bearing structures of buildings are subject to significant displacements accompanied by absorption of energy of the outer effect and occurrence of residual deformations. At this stage of the behaviour the linear relationship between stresses and deformations (loads and displacements) is broken.

Vibrations of the suspended load can be regarded as simple harmonic ones only when $\sin\theta \approx \theta$. If this condition is not satisfied, then more complex motion takes place. In this case the restoring force is not proportional to the displacement and the vibration frequency will decrease with the increase of the amplitude.

To ascertain the influence of nonlinear factors on the parameters of the dynamic response, the coupled system (the framework with the suspended mass) is studied under the assumption that final deformations develop. The relationship of the restoring force and displacement for the framework and suspended load is taken in the form of nonlinear-elastic diagram of a soft type approximated by a cubic parabola.

To describe nonlinear vibrations of the framework and suspended loads the first equation (1) is supplemented by the term $\bar{\Omega}_1^2 x_1^3$, characterizing the nonlinearity of the restoring force of the framework. The dissip ative forces of the framework are taken according to Voigt's hypothesis with further correction according to Schlippe-Bock.

After transforming nonlinear terms into an exponential series and retaining the two first terms of the series, equati

ons for motion of a single-storey framework with a suspended mass will be:

$$\ddot{x}_1 + 2\beta_0\dot{x}_1 + \Omega_1^2 x_1 - \bar{\Omega}_1^2 x_1^3 = -\ddot{x}_0 - d_1\ddot{\theta}_1\left(1-\frac{\theta_1^2}{2!}\right) + d_1\dot{\theta}_1^2\left(\theta_1 - \frac{\theta_1^3}{3!}\right)$$

$$\ddot{\theta}_1 + 2\beta_1\dot{\theta}_1 + \omega_1^2\left(\theta_1 - \frac{\theta_1^3}{3!}\right) = -c_1(\ddot{x}_1 + \ddot{x}_0) + c_1(\ddot{x}_1 + \ddot{x}_0)\cdot\left(\frac{\theta_1^2}{2!}\right) \qquad (32)$$

where

$$\Omega_1^2 = \frac{K_1}{M_{tot}}; \qquad \bar{\Omega}_1^2 = \frac{\bar{K}_1}{M_{tot}}$$

K_1-the coefficient of the linear component of the framework rigidity;

$\bar{K}_1$-the coefficient of the nonlinear component of the framework rigidity;

β_0 and β_1 -the damping coefficients in the structure and suspension hinge respectively.

Other symbols are similar to those adopted earlier.

Equations(32) are true for final deviations of frameworks and suspended masses.It is supposed that the magnitudes of the deviation angle θ_1 for actual building structures are less than one radian.In equations (32) the addends $d_1\dot{\theta}_1\frac{\theta_1^2}{2!}$; $d_1\dot{\theta}_1^2\theta_1$ and $d_1\theta_1^2\frac{\theta_1^3}{3!}$ can be neglected since the value $d_1\ddot{\theta}_1\frac{\theta_1^2}{2!}$ is almost by one order less than $d_1\ddot{\theta}_1$,the equation terms $d_1\dot{\theta}_1^2\theta_1$ and $d_1\theta_1^2\frac{\theta_1^3}{3!}$ are respectively values of second and third order of amallness as compared to the angular acceleration $\ddot{\theta}_1$ .For the same reason the addends $c_1\ddot{x}_1\frac{\theta_1^2}{2!} \ll c_1\ddot{x}_1$ can be neglected;let it be $G_{\ddot{x}}(\omega,p)\approx 0(\theta_1)$ where $p_1=1,2,4$ .With account of the above assumptions the equations for motion(32) become

$$\ddot{x}_1 + 2\beta_0\dot{x}_1 + \Omega_1^2 x_1 - \bar{\Omega}_1^2 x_1^3 = -\ddot{x}_0 - d_1\ddot{\theta}_1$$

$$\ddot{\theta}_1 + 2\beta_1\dot{\theta}_1 + \omega_1^2\theta_1 - \omega^2\frac{\theta_1^3}{3!} = -c_1(\ddot{x}_1 + \ddot{x}_0) \qquad (33)$$

The problem of vibrations of the nonlinear-elastic system in question under a steady random excitation can be solved conveniently by the method of statistical linearization permitting the correlation theory to be used.

Nonlinear functions in (33) are approximated by linear ones statistically equivalent to the starting ones.It is known that functions are statistically equivalent if moments of the first and second order are equal.

We assume that the process at the input is steady following the normal distribution law and the first order moment is equal to zero.Then the statistical transfer factor of the non linear element will be the function only of the second order moment.For nonlinear terms $\Omega_1^2 x_1^3$ and $\omega_1^2\frac{\theta_1^3}{3!}$ this factor is $3{,}436\bar{K}_1\sigma_x^2$ and $3{,}436c_1^2\sigma_{\varphi_1}^2/6$ /4/respectively.

After the linearization of the system and replacement of the variables $\varphi_1 = \frac{\theta_1}{c_1}$ and $\tau_1 = d_1c_1$ we obtain

$$\ddot{x}_1 + 2\beta_0\dot{x}_1 + \nu_1^2(\sigma_{x_1}^2)x_1 = -\ddot{x}_0 - \tau_1\ddot{\varphi}_1 \qquad (34)$$

$$\ddot{\varphi}_1 + 2\beta_1\dot{\varphi}_1 + \alpha_1^2(\sigma_{\varphi_1}^2)\varphi_1 = -\ddot{x}_0 - \ddot{x}_1$$

where $\nu_1^2(\sigma_{x_1}^2) = \Omega_1^2(1-3{,}436\sigma_{x_1}^2\bar{R}_1/R_1)$

$x_1^2(\sigma_{\varphi_1}^2) = \omega_1^2(1-3{,}436\, c_1\sigma_{\varphi_1}^2/6)$

The system of linearized equations(6)is investigated by the correlation theory methods. Expressions for complex transfer factors and the variance of the output of the system are determined following the standard procedure, earlier described in detail. Here the values of the variance of the framework displacement $\sigma_{x_1}^2$ and the deviation angle of the suspended mass become

$$\sigma_p^2 = (-M_p/\Delta_p)\alpha B(0)/a_0, \qquad p = x_1, \varphi_1 \tag{35}$$

$$M_{6x_1} = \begin{vmatrix} 0 & 0 & b_2 & b_3 & b_4 & b_5 \\ a_0 & a_2 & a_4 & a_6 & 0 & 0 \\ 0 & a_1 & a_3 & a_5 & 0 & 0 \\ 0 & a_0 & a_2 & a_4 & a_6 & 0 \\ 0 & 0 & a_1 & a_3 & a_5 & 0 \\ 0 & 0 & a_0 & a_2 & a_4 & a_6 \end{vmatrix}; \quad M_{6\varphi_1} = \begin{vmatrix} 0 & 0 & 0 & 0 & b_6 & b_7 \\ a_0 & a_2 & a_4 & a_6 & 0 & 0 \\ 0 & a_1 & a_3 & a_5 & 0 & 0 \\ 0 & a_0 & a_2 & a_4 & a_6 & 0 \\ 0 & 0 & a_1 & a_3 & a_5 & 0 \\ 0 & 0 & a_0 & a_2 & a_4 & a_6 \end{vmatrix} \quad \Delta_{6x_1} \equiv \Delta_{6\varphi_1} \equiv \begin{vmatrix} a_1 & a_3 & a_5 & 0 & 0 & 0 \\ a_0 & a_2 & a_4 & a_6 & 0 & 0 \\ 0 & a_1 & a_3 & a_5 & 0 & 0 \\ 0 & a_0 & a_2 & a_4 & a_6 & 0 \\ 0 & 0 & a_1 & a_3 & a_5 & 0 \\ 0 & 0 & a_0 & a_2 & a_4 & a_6 \end{vmatrix}$$

$a_0 = 1$; $a_1 = (2\alpha + \bar{\omega}_1^*)$; $a_2 = -(m^2 + 2\alpha\bar{\omega}_1^* + \bar{\omega}_2)$; $a_3 = m^2\bar{\omega}_1^* + 2\alpha\bar{\omega}_2^* + \bar{\omega}_3^*$;

$a_4 = m^2\bar{\omega}_2^* + 2\alpha\bar{\omega}_3^* + \bar{\omega}_4^*$; $a_5 = -(m_2\bar{\omega}_3^* + 2\alpha\bar{\omega}_4^*)$; $a_6 = -\bar{\omega}_4^* m^2$;

$b_2 = 1 - 2z_1 + z_1^2$; $b_3 = (z_1-1)2x_1^2 + (1-z_1)^2 m^2$; $b_4 = x_1^4 + \nu_1^2\omega_1^4 + (z_1-1)2x_1^2 m^2$;

$b_5 = x_1^4 m^2 + \nu_1^2\omega_1^4 m^2$; $b_6 = \nu_1^4 + \nu_0^2\Omega_1^4$; $b_7 = m^2 b^6$

$\bar{\omega}_1^* - \bar{\omega}_4^*$ -roots of the denominator of the integrands for the variance of the framework displacement and deviation angles of the suspended load.

Let's consider a numerical example. In equations(35)it is taken $\alpha = 7$, $\beta = 18$; $a_0 = 1$; $B(0)$ is the variance of seismic acceleration. In the numerical solution of equations(35) the design value is taken $B(0) = k_c^2 g^2$ where k_c is the seismic factor.

The problem was solved on the M-220 computer by means of the iteration method. In realization of the programme to determine the variance of the system output($\sigma_{x_1 n.\ell}^2$ and $\sigma_{\varphi_1 n.\ell}^2$) the results of solving the linear problem were taken as a first approximation. The degree of accuracy in the iteration process was taken abs($\sigma_{x_1 n.\ell}^2 - \sigma_{x_1 \ell}^2$) $< \sigma_{x_1 n.\ell}^2 10^{-3}$.

In choosing versions of estimation it was forseen that it could be varied in a wide range of initial variables of numerical parameters: the mass ratio $0 \leqslant z_1 \leqslant 0{,}6$; the framework frequency $0{,}3 \leqslant \Omega \leqslant 5$ гц.; frequency of the suspended mass $0{,}15 \leqslant \omega_1 \leqslant 0{,}8$ гц. Constant parameters are assumed as follows: damping in the suspension hinge $\beta_1 = 0{,}03$; damping in the structure of the steel framework is 0.05 ; the design value of the variance of the outer effect $B(0) = 625 \text{kg/cm}^2$, that corresponds to $k_c = 0.025$; the ratio of stiffness coefficients of the nonlinear and linear

components $k = \bar{k}_1/k_1 = 0.005$.

The influence of the nonlinearity of the system on the values of the variance of displacement of the framework and deviation angle of the suspended load is determined by ratios

$$\Pi_{x_1} = \sigma^2_{x_1 n.l.} / \sigma^2_{x_1 l.}; \quad \Pi_{\varphi_1} = \sigma^2_{\varphi_1 n.l.} / \sigma^2_{\varphi_1 l.}.$$

As the analysis of theestimation results show, the effect of the geometric nonlinearity of the system can almost be neglected for the values of the variance at the magnitudes of natural frequencies of the framework of 6 to 30 1/s. Π_{x_1} and Π_{φ_1} undergo significant changes within the range of low frequencies of 2 to 4 1/s and particularly at the frequency of the framework of 2 1/s. It is characteristic of this frequency that the ratio Π_{x_1} increases and Π_{φ_1} decreases, i.e. at larger deviations of the framework the vibration amplitude of the suspended load is less than the respective values of amplitudes for linear systems (Fig.12). Fig.13 shows the diagram of change of Π_{x_1} and Π_{φ_1} for flexible frameworks $\Omega_1 = 2 \div 4$ 1/s depending on the vibration frequency of the suspended load ω_1 (the suspension length l_1) at various ratios of the mass γ_1. The analysis of the diagram (Fig.13) indicates that the system response (displacement of the framework and rotation angles of the suspended loads) difers from responses of linear systems mostly when partial frequencies of two connected oscillators become equal.

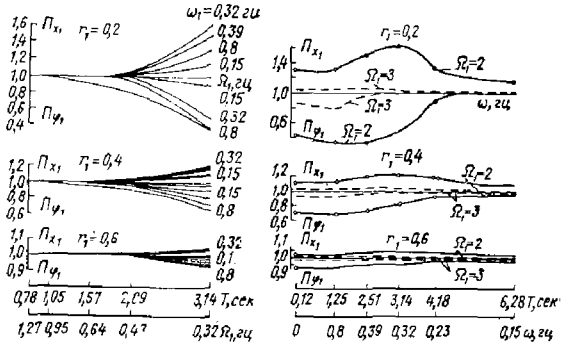

Fig.12

Fig.13

One more characteristic feature of the system under consideration should be mentioned. With the increase of the ratio γ_1, i.e. with the increase of the mass of the suspended load the magnitudes of the variance of the framework and suspendedload displacements approximate the values obtained for linear systems (Fig.12).

The results mentioned refer to the case when the parameter characterizing the nonlinearity of the framework is $k = 0.005$. In addition there were investigated parameters of the system response at $k = 0.0005; 0.002; 0.006$ and constant value of β (0) corresponding to $k_c = 0.025$.

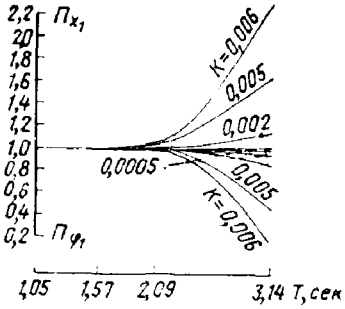

Fig.14

The analysis of estimations carried out by a computer has shown, that the pat-

tern of change of Π_x and Π_φ is similar to the above indicated but their absolute values for flexible frameworks increase abruptly with the increase of the factor k .Fig.14 provides as an example calculation results at τ_i =0.2 and ω_1 = 2 1/s for a wide frequency range of the framework and factors k .

At frequencies of the framework of 6 to 30 1/s seismic loads can be determined with reasonable accuracy as for a linear system.For frameworks with a frequency of 2 to 4 1/s at all investigated frequences of the suspended load it is recommended that the stipulated value of the seismic forces should be multiplied by the correction factor $\bar{\xi}_{n\ell}$ .Table 1 provides the values of $\bar{\xi}_{n\ell}$ estimated by the authors for different frequency characteristics of the framework,suspended load and ratios of masses.

ω_1	Ω_1 / τ_1	30–6	4	3	2	Ω_1 / τ_1	30–6	4	3	2	Ω_1 / τ_1	30–6	4	3	2
1		1	0,97	0,94	0,81		1	0,99	0,98	0,93		1	0,99	0,99	0,98
1,5		1	0,97	0,94	0,85		1	0,99	0,98	0,95		1	0,99	0,99	0,97
2	0,2	1	0,96	0,95	0,82	0,4	1	0,99	0,98	0,92	0,6	1	0,99	0,99	0,97
2,5		1	0,97	0,96	0,73		1	0,99	0,98	0,90		1	0,99	0,99	0,95
5		1	0,97	0,93	0,66		1	0,98	0,95	0,85		1	0,99	0,97	0,93

As the analysis of the table shows,for flexible frameworks the account of geometric nonlinearity of the so called soft type loads to the reduction of seismic loads(up to 30 per cent).

CONCLUSIONS.

Basing on the investigation carried out the following main inferences can be drawn:

1.A procedure for a statistical analysis of vibrations of linear and nonlinear framework systems with suspended masses under horizontal seismic effects has been devised.

There have been obtained and solved differential equations of coupled vibrations under the supposition of elastic and nonlinear-elastic structural behaviour and at translatory displacements of suspended masses.

2.Basing on the solution of the respective differential equations of vibration with account of transfer states numerical values of dynamic factors,magnitudes of displacements of frameworks and deviation angles of suspended loads for various initial parameters of structures have been obtained.

The analysis of the results shows that
a)the values of the standard of the dynamic factor for

structures with loads located on floors are 2 to 3.5 times as large as the respective values of the standard for structures with suspended loads.

b)maximum values of the standard of the dynamic factor in the transfer state are 1.3 to 1.4 times as large as those in the steady state;

c)the increase of the ratio of the suspended load mass to the whole structure mass leads to the decrease of absolute values of the dynamic factor standard;

d)magnitudes of seismic forces effecting the structural framework do not depend upon the weight of suspended loads if frequencesof the latter are less than 2.5 1/s.

3.Nonlinear horizontal vibrations of frameworks with sus pended masses have been studied.

Nonlinear equations of the system motion have been solved by the method of statistical linearization and linearized equations of motion have been investigated by methods of the correlation theory.

A programme for solving nonlinear differential equations have been worked out.Systems with different coefficients of elastic nonlinearity have beenconsidered,characteristics of the response of nonlinear-elastic system are determined at va rious levels of the effect.

The analysis of the calculation results allows conclusions to be drawn regarding the consideration of the influence of nonlinear factorson the parameters of structural response:

a)magnitudes of seismic forces for frequences of the framework of 6 to 30 1/s and of suspended loads of 1 to 2.5 1/s at effects of 7-9 degrees intensity can be determined with a sufficient degree of accuracy as for linear systems;

b)for flexible frameworks with frequencies of 2-4 1/s and those of suspended masses of 1 to 5 1/s it is recommended that the stipulated value of the seismic force arrived at in the linear analysis should be multiplied by the correction factor $\mu_{n.l.}$,which values are given in Table 1.

REFERENCES

1.Barstein M.F.Prilozhenie veroyatnostnykh metodov k raschetu sooruzhenii na seismicheskie vozdeistviya.J."Stroitelnaya mekhanika i raschet sooruzhenii", №2,1960.

2.Grandstein I.S.,Ryzhik I.M.Tablitsy integralov summ,ryadov i proizvedenii.4-th edition,revised.M.,Fizmatgiz Publishing House,1962.

3.Kazakov I.E.,Dostupov B.G.Statisticheskaya dinamika nelineinykh avtomaticheskikh sistem.Gosstroiizdat,1962.

4.Nikolaenko N.A.Veroyatnostnye metody dinamicheskogo rascheta mashinostroitelnykh konstruktsii."Mashinostroenie" Publishing House, M.,1967.

5.Pugachev V.S.Teoriya sluchainykh funktsii i eyo primenenie k zadacham avtomaticheskogo upravleniya.Fizmatgiz Publishing House, 1960.

6.Zharov A.M.Shkala i sistema izmereniya seismicheskoi ballnosti (instead of GOST 6249-52), TsNIISK,1972.

INTERNATIONAL SYMPOSIUM ON
EARTHQUAKE STRUCTURAL ENGINEERING
St. Louis, Missouri, USA, August, 1976

EARTHQUAKE RESPONSE OF A TALL MULTI-FLUE STACK

P. KARASUDHI
Associate Professor

Y.C. TSAI
Graduate Student

K.P. CHAU
Graduate Student

Division of Structural Engineering and Materials
Asian Institute of Technology
P.O. Box 2754, Bangkok, Thailand

SUMMARY

The response of a tall multi-flue stack to earthquake was investigated in this study. Each flue consists of a number of equal lengths supported on platforms. The platforms are connected to rubber bearings which are in turn supported by the outer shell. The outer shell mass was idealized into the same number of elements as the flue lengths. The system was therefore represented by a number of masses with associated springs and damping elements. The equation of motion was derived by means of Lagrange equation incorporating the rotational effects of all masses. The stiffness of the outer shell and the flues were computed on the assumption that they behave as slender beams. The damping matrix in the system was assumed to be proportional to the stiffness matrix of the system. The equations of motion were solved by the method of classical normal modes.

The reinforced concrete stack chosen for illustrating the analysis is 242 m high. The outer shell with a 26 m diameter encloses three elliptical flues. Comparing the responses of the cases of rubber bearing and rigid bearing, the rubber bearings reduce the fundamental frequency, maximum shear force and bending moment in the outer shell by approximately fifty percent.

INTRODUCTION

The ever-increasing demand for air pollution control in the last decade or two has led to the construction of tall stacks. Many stacks higher than 800 ft have already been built. With the increase of their height, their response to lateral forces such as wind and earthquakes becomes more important.

In 1956, Isada (3)* presented a paper on reinforced concrete chimneys subjected to earthquakes. Rumman (5), in 1964, presented a paper on the

---

* Numbers in parentheses designate References at end of paper.

earthquake forces in a reinforced concrete single stack. Later, Maugh and Rumman (4) presented a paper on the seismic design of a reinforced concrete chimney with a single stack.

In the recent years, due to the necessity of large boilers in industry, there appear multi-flue stacks. The idea of a multi-flue stack is that the outer shell is primarily for the lateral loads and the inner flues for thermal stresses due to the hot gas flowing inside them. Veeraraghavachary (6) accorded to a formula to show the benefit of a big multi-flue stack. For dispersing the same amount of gas, the height of the multi-flue stack could be lower than two third of the length of each of single stacks needed with the same number as the flues. In 1970 and 1971, Waller (7,8) presented the design of a tall multi-flue stack subjected to wind loads.

The purpose of this study is to formulate a lumped-mass mathematical model which represents the actual structure in a dynamic analysis and to calculate the response of the model due to an earthquake. The multi-flue stack of the Drax Power Station, England (7,8) is adopted for illustration.

FORMULATION OF PROBLEM

As described by Waller (7,8), the outer shell of a multi-flue stack is made of reinforced concrete, the inner structure is composed of three or four flues, which are made of reinforced concrete or steel with circular or elliptical cross section. The interior of each flue is coated with protective linings. Each flue is divided into a number of equal lengths. The flue lengths are rigidly connected at their mid-lengths by platforms which in turn are connected to the outer shell by means of rubber bearings (Fig.1). The joints between the flue lengths are sealed by a flexible material to prevent the flue gas from attacking the unprotected surface. In the dynamic analysis of this structure, the outer shell is idealized into the same number of elements as the flue length.

Equations of Motion

The idealized model of the structure is shown in Fig. 2. The flues are represented as n masses. The shell is broken up into a number of n elements to correspond with the flue lengths. The rotational inertia of each mass is considered in this study. The complete system is therefore represented by 2n masses with associated spring and damping systems. The lumped outer shell masses are $M_1, M_2, \ldots, M_n$; and the lumped flue masses are $m_1, m_2, \ldots, m_n$. The relations between the rotational angles θ_i of the outer shell masses M_i and their absolute displacements X_i in terms of finite differences are as following.

$$2\ell\theta_1 = X_2 - X_1 \tag{1}$$

$$2\ell\theta_i = X_{i+1} - X_{i-1} \quad ; \quad i = 2,3,\ldots, n-1 \tag{2}$$

$$\ell\theta_n = X_n - X_{n-1} \tag{3}$$

in which ℓ is the distance between two consecutive lumped masses.

This computational model is governed by Lagrange equation of the form

$$\frac{d}{dt}\begin{Bmatrix} \frac{\partial L}{\partial \dot{X}_i} \\ \hline \frac{\partial L}{\partial \dot{q}_i} \end{Bmatrix} - \begin{Bmatrix} \frac{\partial L}{\partial X_i} \\ \hline \frac{\partial L}{\partial q_i} \end{Bmatrix} = \begin{Bmatrix} Q_{xi} \\ \hline Q_{qi} \end{Bmatrix} ; \quad i = 1,2,\ldots, n \tag{4}$$

where $L = T - \bar{U}$, T = kinetic energy of the system, $\bar{U}$ = strain energy of the system Q_i = non-conservative force of the system at point i, q_i = displacement of lumped flue mass m_i relative to M_i and a dot ($\dot{}$) denotes a time derivative. Neglecting the higher order terms in the displacement functions, T can be written as

$$T = \frac{1}{2}\sum_{i=1}^{n} M_i \dot{X}_i^2 + \frac{1}{2}\sum_{i=1}^{n} m_i(\dot{X}_i+\dot{q}_i)^2 + \frac{1}{2}\sum_{i=1}^{n} I_i^s(\dot{\theta}_i)^2 + \frac{1}{2}\sum_{i=1}^{n} I_i^f(\dot{\theta}_i)^2 \tag{5}$$

in which the first term is the translational kinetic energy of the outer shell, the second term is the translational kinetic energy of the flues, the last two terms are the rotational kinetic energy of the outer shell and inner flue respectively; I_i^s and I_i^f are rotational moments of inertia of the outer shell mass M_i and the flue mass m_i respectively. The strain energy $\bar{U}$ is in the form

$$\bar{U} = \frac{1}{2}\sum_{i=1}^{n}\sum_{j=1}^{n} K_{ij}(X_i-G)(X_j-G) + \frac{1}{2}\sum_{i=1}^{n} k_i^f q_i^2 + \frac{36EI}{\ell^3}(X_1 - G + q_1)^2$$
$$+ \frac{18EI}{\ell^3}\sum_{i=1}^{n-1}(X_{i+1}-X_i+q_{i+1}-q_i)^2 + \frac{9EI}{\ell}(\theta_1)^2 + \frac{9EI}{2\ell}\sum_{i=1}^{n-1}(\theta_{i+1}-\theta_i)^2 \tag{6}$$

in which the first term is the strain energy of the outer shell, the second term the strain energy of the rubber bearings, and the rest the strain energy of the inner flues assumed to behave as slender beams built-in at the platforms and hinged at the ends of each flue length. In addition, K_{ij} = stiffness coefficient of outer shell assumed to behave as a slender beam, k_i^f = translational stiffness of the rubber bearing which is supporting m_i, G = foundation displacement, E = Young's modulus of the flues, I = area moments of inertia of inner flues, and non-conservative forces are

$$\begin{Bmatrix} Q_{xi} \\ \hline Q_{qi} \end{Bmatrix} = - [C]\begin{Bmatrix} \dot{X}_i - \dot{G} \\ \hline \dot{q}_i \end{Bmatrix} \tag{7}$$

where [C] = damping coefficient matrix to be described later. Substituting Eqs. 5, 6 and 7 in Eq. 4, in view of Eqs. 1, 2 and 3, leads to

$$[M]\{\ddot{y}\} + [C]\{\dot{y}\} + [H]\{y\} = \{F\} \tag{8}$$

where

$$\{y\} = \begin{Bmatrix} U_i \\ \hline q_i \end{Bmatrix} \quad ; \quad i = 1,2,\ldots, n \tag{9}$$

$$U_i = X_i - G \tag{10}$$

$$\{F\} = -\left\{\begin{array}{c}\{M_i+m_i\}\\ \hline \{m_i\}\end{array}\right\} \ddot{G} \qquad ; \quad i = 1,2,\ldots, n \tag{11}$$

[M] and [H] are symmetrical matrices of mass, and stiffness respectively. The elements in these matrices are the followings. In [M];

$$M_{11} = \frac{1}{48}[48(M_1+m_1) + M_2 + m_2] \tag{12}$$

$$M_{12} = -\frac{1}{48}(M_1 + m_1) \tag{13}$$

$$M_{13} = -\frac{1}{48}(M_2 + m_2) \tag{14}$$

$$M_{22} = [M_2+m_2+\frac{1}{48}(M_3+M_1+m_3+m_1)] \tag{15}$$

$$M_{24} = -\frac{1}{48}(M_3 + m_3) \tag{16}$$

$$M_{ii} = [M_i+m_i+\frac{1}{48}(M_{i+1}+M_{i-1}+m_{i+1}+m_{i-1})] \; ; \quad i = 3 \text{ to } n-2 \tag{17}$$

$$M_{i,i+2} = -\frac{1}{48}(M_{i+1} + m_{i+1}) \qquad ; \quad i = 3 \text{ to } n-2 \tag{18}$$

$$M_{n-1,n-1} = [M_{n-1}+m_{n-1}+\frac{1}{48}(M_{n-2}+4M_n+m_{n-2}+4m_n)] \tag{19}$$

$$M_{n-1,n} = -\frac{1}{48}(4M_n + 4m_n) \tag{20}$$

$$M_{nn} = \frac{1}{48}[52(M_n+m_n) + (M_{n-1}+m_{n-1})] \tag{21}$$

$$M_{i,i+n} = m_i \qquad ; \quad i = 1 \text{ to } n \tag{22}$$

$$M_{n+i,n+i} = m_i \qquad ; \quad i = 1 \text{ to } n \tag{23}$$

and other elements are zero. In [H];

$$[H] = \left[\begin{array}{c|c}[A] & [B]\\ \hline [B] & [D]\end{array}\right] \tag{24}$$

where [A], [B] and [D] are symmetrical matrices, in which

$$B_{11} = \frac{108EI}{\ell^3} \tag{25}$$

$$B_{ij} = -\frac{36EI}{\ell^3} \quad ; \quad i = 1 \text{ to } n-1 \text{ , } j = 2 \text{ to } n \tag{26}$$

$$B_{ii} = \frac{72EI}{\ell^3} \quad ; \quad i = 2 \text{ to } n-1 \tag{27}$$

$$B_{nn} = \frac{36EI}{\ell^3} \tag{28}$$

$$A_{ij} = K_{ij} + E_{ij} \quad ; \quad i,j = 1 \text{ to } n \tag{29}$$

In Eq. 29, E_{ij} is equal to E_{ji} and defined as follows.

$$E_{11} = \frac{459EI}{4\ell^3} \tag{30}$$

$$E_{12} = -\frac{171EI}{4\ell^3} \tag{31}$$

$$E_{13} = -\frac{9EI}{4\ell^3} \tag{32}$$

$$E_{22} = \frac{333EI}{4\ell^3} \tag{33}$$

$$E_{ij} = -\frac{153EI}{4\ell^3} \quad ; \quad i = 2 \text{ to } n-3 \text{ , } j = 3 \text{ to } n-2 \tag{34}$$

$$= -\frac{9EI}{2\ell^3} \quad ; \quad i = 1 \text{ to } n-3 \text{ , } j = 4 \text{ to } n-1 \tag{35}$$

$$= \frac{9EI}{4\ell^3} \quad ; \quad i = 2 \text{ to } n-3 \text{ , } j = 5 \text{ to } n \tag{36}$$

$$E_{ii} = \frac{81EI}{\ell^3} \quad ; \quad i = 3 \text{ to } n-2 \tag{37}$$

$$E_{n-2,n-1} = -\frac{81EI}{2\ell^3} \tag{38}$$

$$E_{n-1,n-1} = \frac{171EI}{2\ell^3} \tag{39}$$

$$E_{n,n-1} = -\frac{171EI}{4\ell^3} \tag{40}$$

$$E_{nn} = \frac{81EI}{2\ell^3} \tag{41}$$

$$D_{ij} = B_{ij} \quad ; \quad i \neq j \tag{42}$$

$$D_{ii} = k_i^f + B_{ii} \tag{43}$$

Elements of matrices [A], [B] and [D] which are not defined in Eqs. 25 to 43 are zero.

In practice, the value of the bearing stiffness k_i^f is very small in comparison with B_{ii} and will be neglected in Eq. 43. It is also a common

practice to assume a damping coefficient to be proportional to its corresponding stiffness. Neglecting the damping stiffness C_i^f of the rubber bearing, there remains only "structural damping" in matrix [C] which can be written in the form

$$[C] = \beta[H] \tag{44}$$

where β is a constant, in this study, to be equivalent to 1.5% of the critical damping of the vibration of the system in the fundamental mode.

Solution of the Equations of Motion

In view of Eq. 44, the solution of Eq. 8 can be solved by the method of classical normal modes (1) in which y_i is related to the normal coordinates η_m by

$$\{y_i\} = [\varphi]\{\eta_m\} \tag{45a}$$

or

$$y_i = \sum_{m=1}^{2n} \varphi_{im}\eta_m \quad ; \quad i = 1 \text{ to } 2n \tag{45b}$$

where

$$[\varphi] = [\{\varphi^{(1)}\}\{\varphi^{(2)}\} \ldots \{\varphi^{(2n)}\}] \tag{46a}$$

in which $\{\varphi^{(m)}\}$ = eigenvector corresponding to the m^{th} eigenvalue of the following system

$$[[H] - \omega^2[M]]\{y_i\} = \{0\} \tag{46b}$$

These eigenvalues, arranged in an ascending order, i.e., $\omega_1^2 < \omega_2^2 < \ldots < \omega_{2n}^2$, and their corresponding eigenvectors can be obtained by means of a standard computer program, e.g., NROOT of IBM. Substituting Eq. 45a into Eq. 8 and premultiplying the result by the transpose of $[\varphi]$ leads to

$$\ddot{\eta}_m + 2\xi_m\omega_m\dot{\eta}_m + \omega_m^2\eta_m = f_m \quad ; \; m = 1,2,\ldots, 2n \tag{47}$$

where

$$f_m = \{\varphi^{(m)}\}^T\{F\} \tag{48}$$

and ξ_m is the critical damping ratio, i.e.,

$$\xi_m = \frac{\beta\omega_m}{2} \tag{49}$$

In Eq. 48, T denotes the transpose of a matrix. The solution of Eq. 47 is given by

$$\eta_m = \frac{1}{p_m}\int_0^t f(\tau)e^{-\xi_m\omega_m(t-\tau)}\sin p_m(t-\tau)d\tau \; ; \; m = 1,2,\ldots, 2n \tag{50}$$

where

$$p_m = \omega_m\sqrt{1-\xi_m^2} \tag{51}$$

It has been shown that the seismic response of a system having classical normal modes is primarily due to the first few of these modes (2).

Expecting this phenomenon to exist in the multi-flue stack system, the response of the structure can be obtained, in place of Eq. 45, by the following equation

$$y_i = \sum_{m=1}^{N} \varphi_{im} \eta_m \quad ; \quad i = 1 \text{ to } 2n \tag{52}$$

where N is much smaller than 2n. This leads to a considerable reduction of computing time.

Shear Forces and Bending Moments

The equivalent external forces applied on the outer shell are given by

$$\{P\} = [A]\{U\} \tag{53}$$

where P_i is the equivalent external force on M_i. The shear forces S_i and the bending moments M_{bi} of the outer shell are the following:

$$\begin{Bmatrix} S_1 \\ S_2 \\ \vdots \\ S_i \\ \vdots \\ S_n \end{Bmatrix} = \begin{bmatrix} 1 & 1 & 1 & . & . & 1 \\ & 1 & 1 & . & . & 1 \\ & & 1 & . & . & 1 \\ & & & & . & 1 \\ & 0 & & & . & 1 \\ & & & & & 1 \end{bmatrix} \begin{Bmatrix} P_1 \\ P_2 \\ \vdots \\ P_i \\ \vdots \\ P_n \end{Bmatrix} \tag{54}$$

$$\begin{Bmatrix} M_{b1} \\ M_{b2} \\ \vdots \\ M_{bi} \\ \vdots \\ M_{bn-1} \end{Bmatrix} = \begin{bmatrix} \ell & \ell & \ell & . & . & \ell \\ & \ell & \ell & . & . & \ell \\ & & \ell & . & . & \ell \\ & & & & . & \ell \\ & 0 & & & . & \ell \\ & & & & & \ell \end{bmatrix} \begin{Bmatrix} S_2 \\ S_3 \\ \vdots \\ S_i \\ \vdots \\ S_n \end{Bmatrix} \tag{55}$$

The bending moment at the base of the outer shell is

$$M_{bo} = M_{b1} + S_1 \frac{\ell}{2} \tag{56}$$

The shear forces μ_i in the rubber bearing are

$$\mu_i = k_i^f q_i \quad ; \quad i = 1 \text{ to } n \tag{57}$$

Effect of Rubber Bearings

It is a practical interest to learn about the effect of the rubber bearing by comparing the solution obtained in the previous sections with

the one with rigid bearing. For the latter case, the displacements of the flues relative to the outer shell vanish, i.e., q and $\dot{q}$ in Eqs. 5 and 6 are zero. The equations of motion are reduced in number into n and contain only outer shell displacements U_i, i = 1 to n. The solution of these equations can be obtained by the method of classical normal modes as described previously.

NUMERICAL EXAMPLE AND CONCLUSIONS

Numerical Example

The multi-flue stack of the Drax Power Station, England (7,8) is adopted in this study. It has a height of 242 m and a constant outside diameter of 26 m. The reinforced concrete outer shell is made of a thickness varying from 0.61 m just above the plinth to 0.23 m at the top. The outer shell mass alone is 31,000 ton, and the unit weight and Young's modulus of concrete are assumed to be 2.4 ton/m^3 and 2.0 x 10^6 ton/m^2 respectively. There are three flues, of reinforced concrete and elliptical section, having major and minor axes of 13.7 m and 9.2 m respectively and a thickness of 0.13 m with a protective lining. Each flue has eleven 22 m-lengths supported on platforms which in turn are supported on laminated neoprene and steel expansion bearings with a total dynamic stiffness horizontally of 1,000 ton/m. The biggest bearings are 0.58 m square and 0.61 m thick. The outer shell was idealized into the same number of elements as the flue lengths. Each length of the flue has a mass of 1,300 ton and the total mass of the stack as a whole is thus 45,000 ton. The complete system is therefore represented by 22 masses with associated spring and damping systems (Fig.2).

Numerical Results

For the cases of rubber bearings and rigid bearings, the fundamental frequency ω_1 was found to be 3.4 and 6.8 rad/sec respectively, and the damping factor β corresponding to ξ_1 = 0.015 was determined from Eq. 49 as 0.0088 and 0.0044 sec respectively. The N-S component of El Centro 1940 earthquake was used in this numerical example. The displacements, bearing force, shear force and bending moment in the outer shell are plotted in Figs. 3 and 4. The results were obtained accurately by summation of solution of the first five natural modes of vibration.

Conclusions

A rational analysis of a tall multi-flue stack subjected to an earthquake is presented in this study. Neglecting in the equations of motion the terms k_i^f and C_i^f, which are very small in comparison with their corresponding elements of the total system, makes possible the application of the method of classical normal modes. Comparing the responses for the cases of rubber bearings and rigid bearings, the rubber bearings reduce the fundamental frequency, shear force and bending moment in the outer shell by approximately fifty percent. The reduction in maximum deflection of the outer shell is, however, not achieved.

REFERENCES

1. Caughey, T.K., "Classical Normal Modes in Damped Linear Dynamic Systems", Journal of Applied Mechanics, ASME, Vol. 27, No. 2, June 1960, pp. 269-271.

2. Clough, R.W., "Earthquake Analysis by Response Spectrum Superposition", Bulletin of Seismological Society of America, Vol. 52, No. 3, July 1962, pp. 647-660.

3. Isada, N.M., "Design and Analysis of Tall Tapered Reinforced Concrete Chimneys Subjected to Earthquake", Proceedings of the First World Conference on Earthquake Engineering, Berkeley, California, 1956, pp. 14-1 to 14-21.

4. Maugh, L.C. and Rumman, W.S., "Dynamic Design of Reinforced Concrete Chimneys", Journal of the American Concrete Institute, Vol. 64, September 1967, pp. 558-567.

5. Rumman, W.S., "Earthquake Forces in Reinforced Concrete Chimneys", Journal of the Structural Division, ASCE, Vol. 93, No. ST6, Proc. Paper 5650, December 1967, pp. 55-70.

6. Veeraraghavachary, K., "New Trend in Design of Chimneys", Indian Journal of Power and River Valley Development, Vol. 21, May 1971, pp. 163-166.

7. Waller, R.A., "Design Techniques for Practical Wind Problems", Proceedings of Conference on Dynamic Wave in Civil Engineering, edited by Howells, D.A., Haigh, I.P., and Taylor, C., University College of Swansea, Swansea, Wales, 1970, pp. 57-71.

8. Waller, R.A., "The Design of Tall Structures with Particular Reference to Vibration", The Institution of Civil Engineers, Vol. 48, February 1971, pp. 303-323.

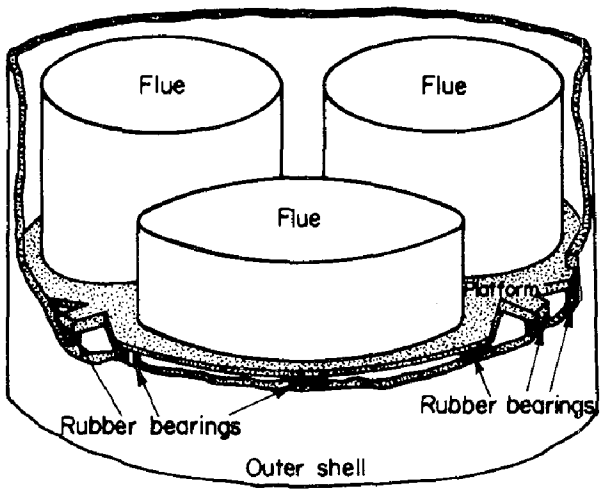

Fig. 1 General Arrangement of Flue Supports

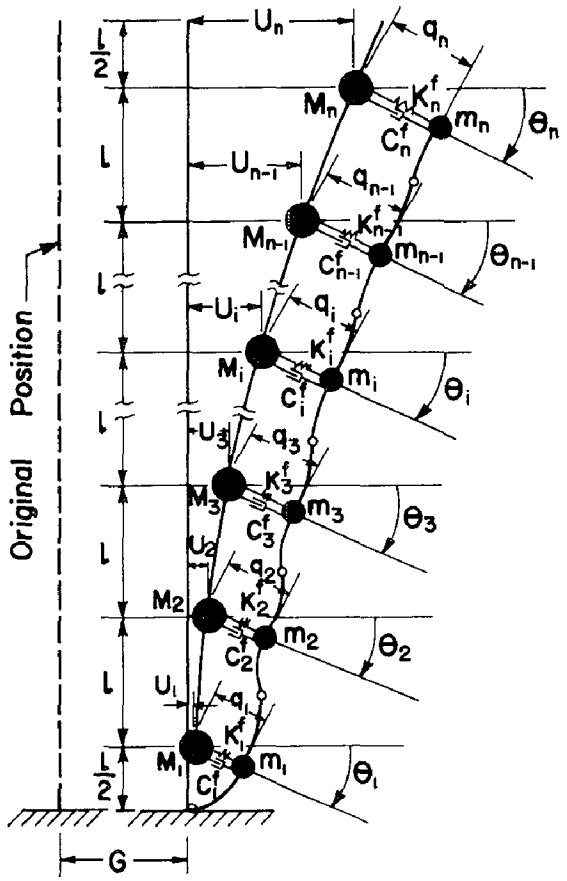

Fig. 2 Computational Model

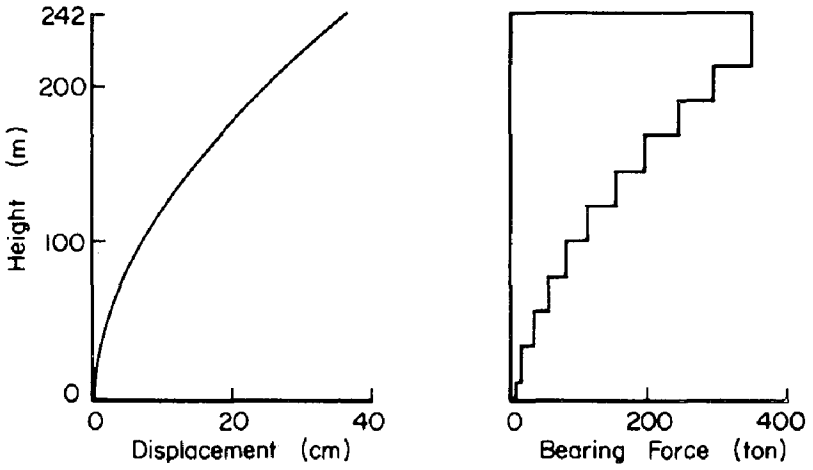

Fig. 3 Maximum Flue Displacement Relative to the Outer Shell and Force in Rubber Bearings

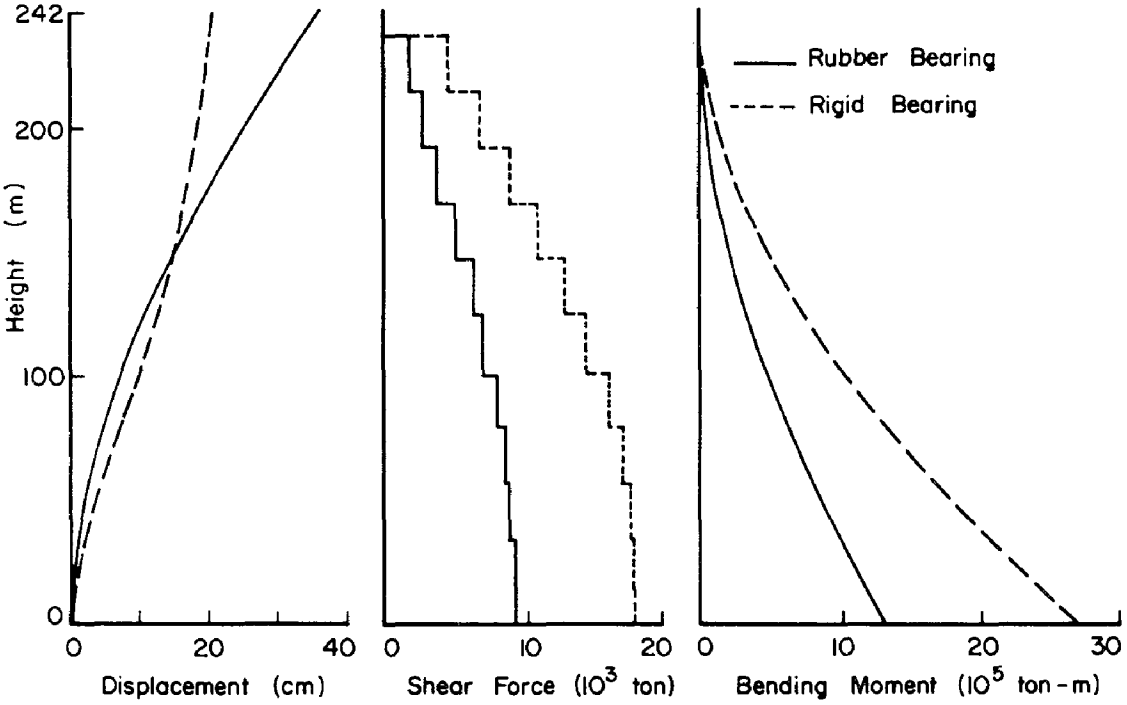

Fig. 4 Maximum Displacement Relative to Ground, Shear Force and Bending Moment of the Outer Shell

INTERNATIONAL SYMPOSIUM ON
EARTHQUAKE STRUCTURAL ENGINEERING
St. Louis, Missouri, USA, August, 1976

ON SPECIFICATIONS FOR EARTHQUAKE-RESISTANT DESIGN OF THE HONSHU-SHIKOKU BRIDGES (JSCE-1974)

by
ISHIO KAWASAKI
Director, Honshu-Shikoku Bridge Authority
and
EIICHI KURIBAYASHI
Chief, Earthquake Engineering Section
Public Works Research Institute
Ministy of Construction

JAPAN

I. INTRODUCTION

The Japan Society of Civil Engineers firstly issued "Specifications for Earthquake-Resistant Design of the Honshu-Shikoku Bridges"[1] in May, 1967. The Specifications were drawn up by a JSCE's Sub-Committee (Chairman: Professor Shunzo Okamoto), which existed for five years starting at 1962 with a commission jointly from the Ministry of Construction and the Japanese National Railways (the Japan Railways Construction Public Corporation took over the work of JNR after March, 1964). In May, 1970 three years after the completion of the above Specifications (1967), the Earthquake Engineering Committee (Standing Committee) of the JSCE set up a Joint Meeting for Studying Earthquake-Resistant Design of the Honshu-Shikoku Bridges (Chairman: Professor Shunzo Okamoto), in consideration of the needs of further investigations. The Joint Meeting was organized with a joint participation of the regular members of the Earthquake Engineering Committee, staff members of the Japan Highway Public Corporation, the Japan Railways Construction Public Corporation and the Honshu-

Shikoku Bridge Authority (the Authority was established in July, 1970), and experts from various organizations. It attempted to improve the Specifications (1967) in view of recent progresses in the relevant fields, and presented in June, 1971 a report[2] summarizing the results of its research activity.

Furthermore, with a commission from the Honshu-Shikoku Bridge Authority the JSCE established a Research Sub-Committee on Earthquake-Resistant Design of the Honshu-Shikoku Bridges (Chairman: Professor Keizaburo Kubo) in June, 1971. The Research Sub-Committee was primarily intended to amend the Specifications for Earthquake-Resistant Design of the Honshu-Shikoku Bridges (1967) and also to clarify the design procedure in details. For the purposes the Research Sub-Committee picked up the following three subjects to be investigated extensively.

1) Evaluation of seismic fources -- Effects of near earthquakes on structures, effects of long-period ground motions and their measuring systems, factors to be considered in determining the magnitude of seismic forces, etc.

2) Evaluation of dynamic characteristics of soils and foundations -- Dynamic characteristics of multi-column foundations and caisson foundations with an emphasis of obtaining a design procedure based on dynamic analysis for foundations, investigations on earthquake-resistant design practices for foundations, etc.

3) Earthquake-resistant design practices for bridges with span length of 200 m or more (such as suspension bridges, truss bridges, etc.)

The Research Sub-Committee performed investigations mainly on those subjects by March, 1974, and recently published the final report[3] The report proposes the revised Specifications for Earthquake-Resistant Design of the Honshu-Shikoku Bridges (1974). Although the new Specifications (1974) include the commentary which gives additional explanations necessitated for design practices, the main body of the Specifications will be introduced hereinafter.

II. SPECIFICATIONS FOR EARTHQUAKE-RESISTANT DESIGN OF THE HONSHU-SHIKOKU BRIDGES (JSCE-1974)

CONTENTS

1. General

1.1 Scope

The provisions in the Specifications apply to earthquake-resistant design of the Honshu-Shikoku bridges.

1.2 Notations

The following notations are used in the Specifications.

Notation	Definition	Unit
A	Lateral cross-sectional area of a structure	m^2
a	Length of cross-section of a structure in the parallel direction to that of seismic motion considered	m
b	Width of cross-section of a structure in the perpendicular direction to that of seismic motion considered	m
d	Depth of water	m
h	Damping ratio	m
K_D	Design seismic coefficient	
K_R	Response seismic coefficient	
S_a	Response acceleration spectrum	cm/sec^2
S_v	Response velocity spectrum	cm/sec
T	Natural period of a structure	sec
x	Any depth below the surface of water or ground	m
α	Coefficient dependent on vibrational modes of a structure	
β	Coefficient dependent on shape of a foundation	
γ_w	Unit weight of sea water	t/m^3

Notation	Definition	Unit
μ	Modification factors necessitated in obtaining design seismic coefficient from response seismic coefficient	

2. Earthquake to be Considered in Design

2.1 Earthquake to be Considered in Design

An earthquake with the following characteristics shall be considered in design:

1) Magnitude: Large-scale (Namely around 8 on the Richter scale)

2) Location: Comparatively far from the bridge sites (Namely off Kii Peninsula, or off Tosa)

3) Frequency: Once or twice per one hundred years

2.2 Design Ground Acceleration

The maximum value of the design ground acceleration shall be 180 gals at the level of the surface of ground lagers which support foundations at the bridge sites.

3. Basic Principle for Earthquake-Resistant Design

3.1 Method of Design Calculation

1) For structures whose principal dimensions are determined by some requirements other than those by earthquake resistant design, the modified seismic coefficient method considering structural response shall be adopted. The results shall generally be examined through a dynamic analysis.

2) For structures whose principal dimensions can be determined by requirements by earthquake-resistant design, structural dimensions shall be determined by the response spectrum method of dynamic analysis. In the case the results are required to be examined through the numerical integration method of dynamic analysis.

4. Design by the Modified Seismic Coefficient Method Considering Structural Response

4.1 Design Procedure

In design based on the modified seismic coefficient method considering structural response, seismic forces specified in 4.2 and additional effects specified in 4.4 shall be taken into account simultaneously.

4.2 Seismic Forces

Seismic forces shall be determined by the product of structural dead weight and the design seismic coefficient. The design seismic coefficient is provided in "4.3 Design Seismic Coefficient Considering Structural Response."

4.3 Design Seismic Coefficient Considering Structual Response

4.3.1 Horizontal Response Seismic Coefficient

The horizontal response seismic coefficient (K_R) shall be determined by Fig. 1. This figure was obtained by assuming the following conditions:

1) Foundations are constructed directly on the Tertiary layer (or older) at the site where the surfare Quaternary layer is shallow or none.

2) The maximum ground acceleration for design is expected around 180 gals.

4.3.2 Vertical Response Seismic Coefficient

The vertical response seismic coefficient shall be generally the half of the horizontal response seismic coefficient.

4.3.3 Design Seismic Coefficient Considering Structural Response

The design seismic coefficient considering structural response shall be determind by the following formula:

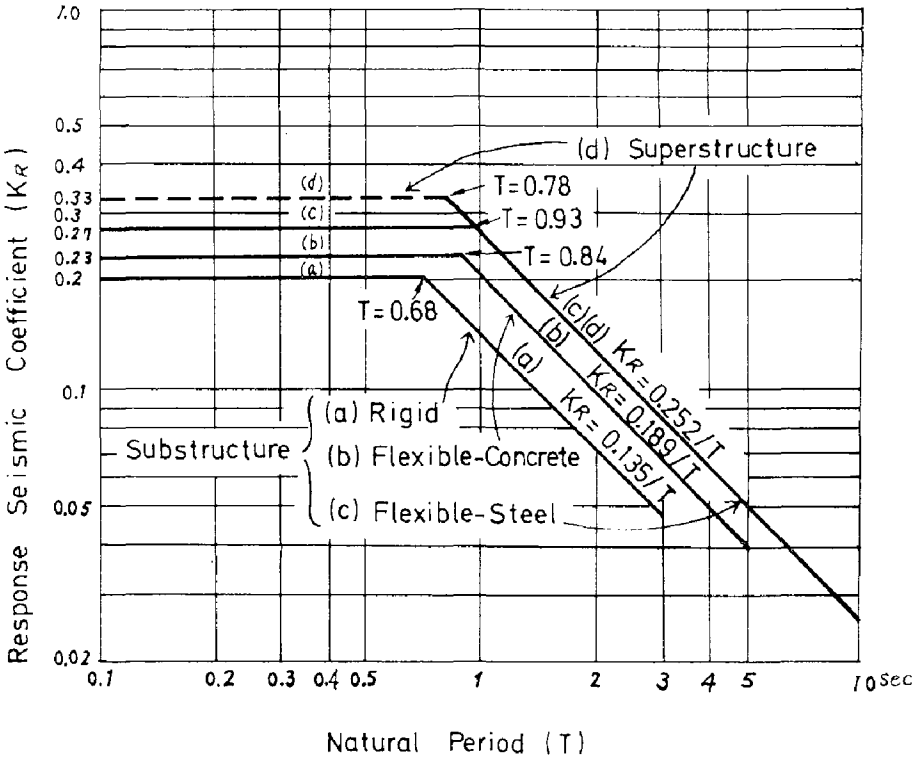

Fig. 1. Response Seismic Coefficient Used in Design

$$K_D = \mu_1 \cdot \mu_2 \cdot \mu_3 \cdot \mu_4 \cdot \mu_5 \cdot K_R$$

where K_D : Design seismic coefficient considering structural response,

K_R : Response seismic coefficient (see Fig. 1) dependent on structural type and the predominant natural period,

μ_1 : Modification factor dependent on the maximum ground acceleration for design ($\mu_1 = 1.0$ for the case of 180 gals)

μ_2 : Modification factor to cover the influences of the higher modes

μ_3 : Modification factor to apply equivalent uniform seismic loads

μ_4 : Modification factor to cover the case where the direction of structural response is perpendicular to that of seismic motion applied

μ_5 : Modification factor to be adjusted by engineering judgement

The predominant natural period here indicated the natural period corresponding to a vibration mode whose response (stress or displacement) is the most predominant in respective structural members. This predominant natural period does not necessarily coincide with the fundamental period.

4.4 Additional Effects to be Considered in Design

4.4.1 Effects of Ground Reactions on Structural Response and Stresses

In evaluating the effects of the surrounding soil on structural response and stresses, ground reactions shall be taken into account as the product of the structural displacement relative to the ground and the spring constant of the ground.

4.4.2 Effects of Surrounding Soil and Water on Structural Response

1) As the effects of surrounding soil on structural response, the spring and damping effects shall be taken into account. The mass effect of the soil, however, may generally be neglected.

2) The effects of water shall be taken into account by applying the virtual or added mass, as described in "5.5 Effects of Surrounding Water on Structural Response."

5. Dynamic Analysis

5.1 Methods of Analysis

The following methods shall be employed in the dynamic analysis to obtain structural response.

1) Response spectrum method: To calculate the meximum values of structural earthquake response on the basis of the response acceleration spectra specified in 5.3.

2) Numerical integration method: To calculate the time history of structural earthquake response to the specific seismic motions specified in 5.4.

5.2 Application of Dynamic Analysis

In performing earthquake-resistant design of structures the dynamic analysis shall be employed in the following ways:

1) The results of designing by the modified seismic coefficient method considering structural response or the seismic coefficient method are examined by the dynamic analysis.

2) The response spectrum method of dynamic analysis is employed for structures whose dimension can be assumed by the loads for normal time. Structural dimensions determined by the procedure are examined though the numerical integration method of dynamic analysis.

5.3 Response Acceleration Spectrum for Dynamic Analysis

The response acceleration spectral curves shown in Fig. 2 shall apply in the response spectrum method of dynamic analysis specified in 5.1 1).

5.4 Seismic Ground Motion for Dynamic Analysis

Seismic ground motions for the numerical integration method of dynamic analysis specified in 5.1 2) shall be either of the following two. The maximum acceleration shall be adjusted to 180 gals by

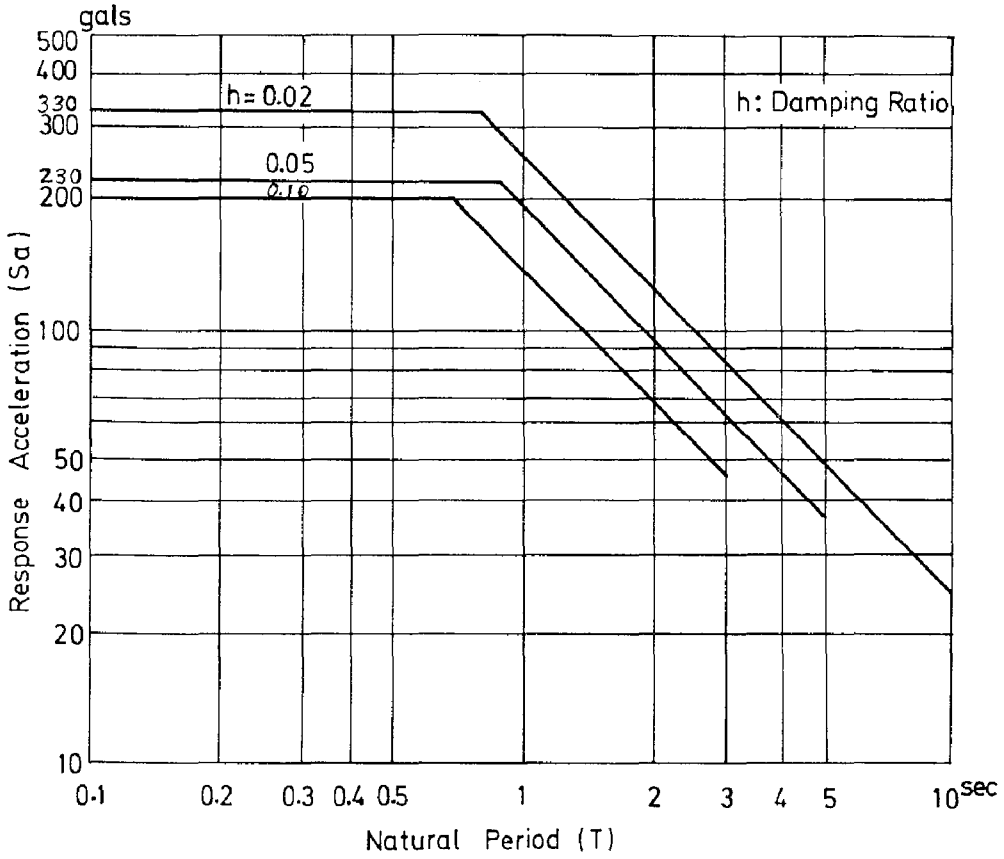

Fig. 2. Response Acceleration Spectral Curves (for maximum acceleration of 180 gals)

proportionally varying the original acceleration records.

1) Typical seismic records obtained near the bridge sites.

2) Strong motion record obtained at El Centro in 1940

5.5 Effects of Mass of Surrounding Soil on Structural Response

For dynamic analysis on substructures the effects of mass of soil on the response may be generrally neglected.

5.6 Effects of Surrounding Water on Structural Response

For the portion of the structure in water the virtual mass of water converted from the hydrodynamic pressure shall be considered by the following formula.

$$M_{wx} = \alpha \beta \frac{\gamma_w}{g} A \sqrt{\frac{x}{d}}$$

where

M_{wx} : Virtual mass (or added mass) per unit width at the depth of x below the water surface (t sec^2/m^2)

α : Coefficient dependent on ribrational mode of the struc structure

β : Cofficient dependent on shape of the foundation

1) $\beta = \frac{b}{a}(1-\frac{b}{4d})$ for the case of $\frac{b}{d} \leqq 2$

2) $\beta = \frac{b}{a}(0.7-\frac{b}{10d})$ for the case of $2 \leqq \frac{b}{d} \leqq 4$

γ_w : Unit weight of the sea water (t/m^3)

A : Lateral cross-sectional area of the foundation

g : Gravity of acceleration (= 9.8 m/sec^2)

a : Length of cross-section of the foundation in the parallel direction to that of the seismic motion considered (m)

b : Width of cross-section of the foundation in the perpendicular direction to that of the seismic motion considered (m)

d : Depth of water at the site (m)

5.7 Dynamic Characteristics of Structures

1) Directions of Seismic Motion to be Considered:

Directions of seismic motion to be considered in dynamic analysis shall be longitudinal, transverse, and vertical.

2) Natural Frequencies and Mode Shapes:

The structural earthquake response shall be analyzed taking into account the orders of natural frequencies and corresponding mode shapes which are necessary to obtain the precise maximum response, in consideration for erection stages needed and completed stage.

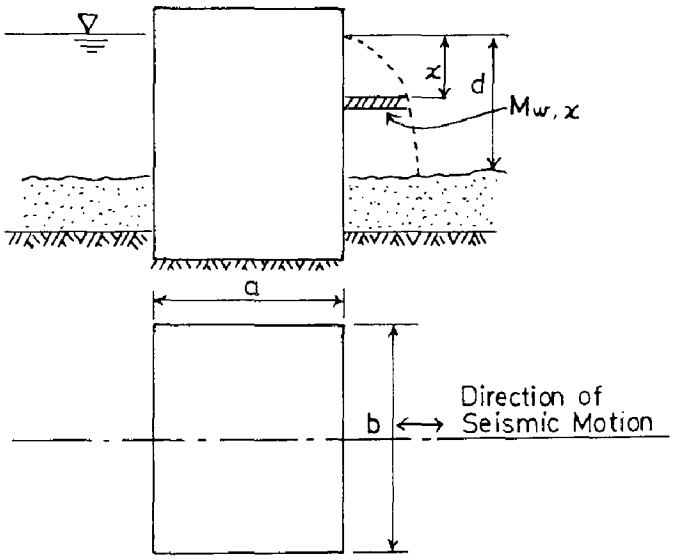

Fig. 3. Virtual mass of water

3) Damping ratios:

The damping ratios used for dynamic analysis shall be determined in view of the results of appropriate investigations.

6. Safety Considerations in Earthquake-Resistant Design

6.1 Factors of Safety in the Modified Seismic Coefficient Method Considering Structural Response

6.1.1 Combination of Loads

For Superstructure: Dead lood + live lood during earthquake + effects of temperature change + seismic effects + effects of movements of supports + effectes of erection errors

For Substructure: Loads from superstructure + dead load + soil pressure + water pressure + buoyancy or uplift + seismic effects

6.1.2 Increase in Allowable Stresses for Steel Superstructure

Increase in allowable stresses for steel superstructure in earthquake-resistant design shall be as follows:

For suspension bridges and long-span bridge: 1.5

For bridges other than the above: 1.7

6.1.3 Stability of Substructures

(1) Allowable bearing capacities of ground: The ultimate bearing capacities of ground shall be evaluated in accordance with the Specifications for Design of Substructures of Highway Bridges—Volume for Design of Spread Foundations (issued by the Japan Rood Association). The minimum values of the allowable bearing capacities shall be obtained by dividing the ultimate bearing capacities by the factors of sefety specified in Table 1.

Table 1. Factors of Safety for Bearing Capacities

	Construction Manner of Foundation Base	
	Dry	Under Water
Normal Design	3.0	4.5
Earthquake-Resistant Design	2.0	3.0

(2) Stability for Overturning

For normal design the position of the resultant force acting on the foundation base shall be located within the middle third of the base. For earthquake-resistant design that shall be generally located within the middle two thirds of the base. When the position of the resultant force for the earthquake-resistant design is slightly out of the middle two thirds, stability and deformation of ground and structures shall be fully examined.

(3) Stability for Sliding

The sliding resistance at the foundation base shall be evalu-

ated in accordence with the Specifications for Design of substructures of Highway Bridges—Volume for Spread Foundation (issued by the Japan Road Association).

The factures of safety for sliding shall be provided is Table 2.

Table 2. Factors of Safety for Sliding

	Construction Manner of Foundation Base	
	Dry	Under Water
Normal Design	2.0	2.5
Earthquake-Resistant Design	1.2	1.5

(4) Displacement Standards for Substructures

Displacements of substructures shall be generally less than the displacement standards provided in Table 3.

Table 3. Displacement Standards for Substructures

Suspension Bridges		Other Bridges
Abutments	Tower Foundations	Horizontal displacement at the level of ground surface (cm)
Horizontal displacement at the Saddle Position (cm)	Rotation at the tower base	
$\delta = 0.017\ell$	$\theta = 0.0055\ell + 2$	$\delta = 1$

ℓ : central span length (m)

6.2 Factors of Safety in the Design Based on Dynamic Analysis

Factors of Safety in the design based on dynamic analysis shall be principally in accordance with the provisions in 6.1.

III. REFERENCES

1) Japan Society of Civil Engineers, "Technical Report of Investigations on the Honshu-Shikoku Bridges," July, 1967. (in Japanese).

2) Japan Society of Civil Engineers, "Report of Research for Improving the Earthquake-Resistant Design Criteria for the Honshu-Shikoku Bridges," June, 1971. (in Japanese).

3) Japan Society of Civil Engineers, "Technical Report of Investigations on Earthquake-Resistance of the Honshu-Shikoku Bridges," September, 1974. (in Japanese).

INTERNATIONAL SYMPOSIUM ON
EARTHQUAKE STRUCTURAL ENGINEERING
St. Louis, Missouri, USA, August, 1976

COMPARISON OF ASEISMATIC STEEL BUILDING DESIGN PRACTICE IN JAPAN AND USA

PAUL H. CHENG

Chief Structural Engineer, Material Handling/Storage Division

Interlake, Inc. - Chicago, Illinois USA

Consultant, Kawatetsu-Interlake Ltd., Tokyo, Japan

Summary

Current official aseismatic building codes, steel structural design specifications, practice of steel building structural designs, as well as seismology and geology of both countries (Japan and West Coast of USA) were reviewed to provide a comparative reference for practical engineers. A sample building design was calculated in accordance with the building codes of both countries and is presented for comparison in detail. The calculated result indicated that the degree of safety, which was provided by codified safety regulations of Japan and USA for aseismatic steel structural design, is reasonably agreeing with the earthquake magnitude Richter scale.

A research study to correlate the earthquake magnitude Richter scale with codified safety regulations as the base for an international aseismatic building code is recommended.

I. Introduction

By an odd coincidence, the two parts of the world that are best known from the point of view of earthquakes, Japan and the west coast of the United States, lie symmetrically on either side of the Pacific between the same parallels, 32°N and 45°N. A long time ago, engineers and scientists noticed that different official building code requirements for earthquake engineering were developed independently in both countries (17); however, report on detailed comparative studies still cannot be found in the literature.

Regardless, the modern technology, such as computer dynamic analysis and shaking table test study are popular and officially accepted for the design of high rise buildings and special structures in both countries, but quantitatively, most structures which have been built still belong to the low or medium rise building and have been predominately designed by the long established simple building code design method. Therefore, the dual purposes of this paper are:

(1) To provide a comparative reference to practical engineers on current aseismatic design codes and specifications on steel structures in both countries.

(2) To promote the international understanding and cooperation for an international aseismatic design building code.

II. Geology and Seismology

(A) Japan

For the seismologist, Japan has the advantage of a long record history, a high density of population, and an urban culture with active research centers. It is reported that from 1596 and onwards, the earthquake records for the whole country can be regarded as fairly complete (20).

Japan is located in the circum-Pacific belt just where an important branching occurs. The Japanese sea coast of Honshu is a region of block tectonic. Two belts of deep-focus earthquakes, named the transverse and the söya zones, take courses which appear, at first, unrelated to the surface structures. The principal features of Pacific arcs, including deep oceanic trenches (fore-deeps) and belts of negative gravity anomalies, are all represented. Seismicity of this region is so high that lists, even of large earthquakes, grow lengthy as shown in Table 1. In this table, only earthquakes with magnitude of 8 and over in Japan and with magnitude of 7 and over along the West Coast of the USA in a period of 50 years (1901 - 1952) were listed (20).

(B) West Coast of USA

It has been estimated that earthquakes in California and western Nevada represent approximately 90 percent of the seismic activity of the contiguous United States (21). The earliest recorded earthquake in that region was in July 28, 1769. Actually, it was not until after the gold rush of 1849 that anyone began to trouble about the earthquakes in that area due to the area having been scarcely inhabited at all until then.

In California, the majority of these shocks occur at a relatively shallow focal depth of 10 to 15 miles, and along known faults. The principal fault in this area - the San Andreas - extends over 600 miles through California, from near the Salton Sea in Southern California northwest to Point Arena, which is roughly parallel to the coast. California is one of the few coasts in the fiery girdle not to be bordered by a deep submarine trench. Therefore, this region is not subjected to seismic conditions comparable with those of Japan. This fact is clearly shown out in the statistics in Table 1.

Earthquake magnitude is evidently related to energy which is radiated from the earthquake source in the form of elastic waves. The energy can be estimated by Gutenberg-Richter formula (20).

$$\text{Log } E = 11.5 + 1.5M$$

For example, the radiated energy of a magnitude 8 earthquake is $10^{23.4}$ ergs and a magnitude 7 earthquake is $10^{21.9}$ ergs.

The relationship between the observed magnitude scale of earthquake and the equivalent static lateral force to be used for aseismatic structural design has not been established yet; however, the statistics in Table 1 definitely indicated that quantitatively and qualitatively, the magnitude of earthquake damage to structures in Japan is more severe than on the West Coast of the USA.

III. Official Building Codes

As the seismic engineering is still in the state of art, undoubtedly, the building codes of each country are the collection of the most reliable knowledge and experience about the subject in that country at present time.

In the USA, the current building code which is discussed here is the Uniform Building Code 1973 edition (16). The historical and theoretical background of this code can be found in Ref. (11,22). It is acknowledged that the UBCI-ICBO convention in Monterey, California in September 1975 adopted a few major revisions on aseismatic design provisions for the 1976 edition UBC. However, the official copy of the convention minutes was unavailable at the deadline date of submission of this paper. In order to avoid confusion and mistakes, the discussion in this paper is limited to the 1973 edition only.

In Japan, the current building codes which are discussed here are:

(a) Building Standards Law No. Han-67 1974 (18)

(b) Building Standards Law Enforcement Order No. SEI-242 1973 (18)

(c) Ministry of Construction Notifications, 1950 and onward (3)

Generally speaking, there are four major fundamental areas of aseismatic design provisions being treated differently in both building codes; namely, equivalent static seismic force, live load, increment of allowable stress for temporary load and special structural designs.

(A) Equivalent static seismic force

In both building codes, the basic design approach is the same to use the equivalent static seismic force for aseismatic design, but the derivation of the formulae is different. In Japan, the derivation was based on the assumption of a simple rigid body moving together with the ground (3). The formulae of the UBC were cognizent of the principal factors which influence the dynamic response of a structure to earthquake ground motion (11,14, 22)

For a clear expression for comparison, formulae for the equivalent static seismic force in both codes is restated in one common form by four variables as:

$$F = ZABW$$

The variables are tabulated comparatively in Table 2.

(B) Live Load

There are significant differences in the treatment of live load for structural design in both codes. The difference existed in three areas; namely, (a) intensity of load for various occupancy, (b) reduction of floor live load to beam, column and foundation, and (c) contribution to the equivalent static seismac force. The details are summarized in Table 6.

(C) Increment of allowable stress for temporary loading

In both codes, the seismic load is considered as a temporary load, and

the allowable stress in the member is permitted to increase for the combined loading condition of dead, live and seismic loads. The multiplier for increment of allowable stress is 1.5 in Japan, but 1.33 in UBC.

(D) Special structure designs

The volume and cases covered in the UBC are much more than in Japanese laws, especially for the following cases, which cannot be found in Japanese laws. However, this does not mean that those practices are prohibited in Japan.

Generally, in Japan, all the structural calculations and design drawings must be submitted to local administrative offices for examination and approval which is the same as in the USA. However, the projects for the following cases shall be approved by the Ministry of Construction. The design calculation and drawings shall be reviewed by the Construction Building Center of Japan, which is a chartered agent under the Ministry of Construction (15). Specifications and standards which provided by AIJ, as discussed in the next chapter, can be used as reference for technical guides to such projects.

(a) High rise building which height is more than 148 ft. (45 m).

(b) The plastic design and analysis method for steel structures.

(c) Dynamic analysis method based on earthquake response spectra for aseismatic structural design.

(d) Any special design or construction method which is not covered in the building code.

IV. Steel Structural Design Specifications

It is almost universally true that a design engineer's work must depend on two kinds of local documents. The first one is the official building code. The code gives fundamental regulations for building design and construction that must be observed in every building design. The second one is the design specifications and standards recommended by local professional societies and industries. The specifications offer the basic design concepts, stress de termination, detailed designing of structural members, etc. to comply and to complement the official building code.

In Japan, the name of this important document for steel structural design is "Specifications for Steel Construction" 1970 edition (2), sponsored by the Architectural Institute of Japan, hereafter briefed as AIJ.

In the USA, the name of the aforementioned document is "Specifications for the Design, Fabrication and Erection of Structural Steel for Buildings, adopted February 1969" (1), sponsored by the American Institute of Steel Construction, hereafter briefed as AISC.

Each specification offers a hundred pages of information. It is impossible for the author to make a detailed comparison between them in this limited length paper. Therefore, only a general review and brief comparison of some special interesting points are given here.

(A) AISC covered more and a wider range of topics in one single volume of specifications than the AIJ. However, the AIJ issued separate standards to handle the following cases which were not included in Ref. (2).

(i) Ref. (4) for plastic analysis and design method
(ii) Ref. (5) for composite construction
(iii) Ref. (6) for simple and continuous span
(iv) Ref. (7) and (8) for fabrication, erection, quality control

(B) AISC offers more information for the application of new high-strength steel and more kinds of high-strength steel. However, the policy of the AISC is to issue individual volumnes of a supplement yearly based to keep the specification up to date and this causes a lot of difficulty for users to handle them properly without confusion or ignorance. However, the new issue of the AISC specification supplement is not automatically to be a part of the UBC. Generally, the new technical data must be reviewed and adopted by both code change committees and the General Assembly of the International Building Officials Conference for adoption into the UBC

(C) The base of formulae to calculate various allowable stresses is close to each other in both specifications except different factors of safety are used.

	Tension	Shear	Compression	Bearing
AISC	1.67	2.5	1.92	0.90
AIJ	1.5	1.5	2.17	0.91

(D) Regarding the interaction equation for combined bending and compression, AIJ recommended the simple form to ignore the amplification factor which must be considered in AISC.

(E) For the calculation of column effect length, AIJ provided more information than AISC, especially for the cases of built-up columns.

(F) AISC gives more information on design of plate girder, ponding problem of the roof system, and design of connections for various restraints of members.

V. Sample Calculations

A sample design calculation by both codes is presented for the purpose of a detailed comparison. The sample building, which was selected from pp. 247-286 of Ref. (9), was a three story steel office building. The dimensions and layout are shown in Fig. 3.

Due to limited space of this paper, only the calculated results for columns of interior bent (column line B) and the selected section of the interior column at the first floor are presented in Table 7. The design assumptions, procedures, reference, results, and the final selected section for the critical column section are summarized as follows:

(1) Results of calculations for both codes (i.e., Japan and UBC) are presented in CGS system.

(2) Dead load and snow load on the roof are the same in both calculations

as used in Ref. (9).

(3) The listed live loads for office buildings in Table 6 were used here. The calculated percentage of live load reduction for the UBC was 38.89%.

(4) The frame analysis for the vertical loads only (dead and live loads) was calculated by the Moment Distribution Method for the case of Japan as used in Ref. (9). But the Stiffness Analysis Method of the STRUDL computer program (19) and analytical procedure in Ref. (10) were used for the case of UBC. The results are reported in columns (4), (5) and (6) of Table 7.

The member stiffness for input of both preliminary analysis is the same as used in Ref. (9).

(5) The coefficients for equivalent static seismic force as listed in Table 2 were calculated as follows:

	Z	A	B	F
Japan	1.0	0.2	1.0	0.2 W-Japan
UBC	1.0	0.078	0.67	0.0523 W-UBC

W-Japan and W-UBC are W as defined in Table 2.

The distributed shear force at each level of columns of interior bent (column line B) are reported in column 7 of Table 7. This force in the case of Japan was calculated by the "MUTO D-Method". The details of this method can be found in Ref. (9). The detailed calculation procedure for the distribution of shear force for the case of UBC can be found in Ref. (12).

(6) Usually the manual calculation of the frame analysis for combined vertical and lateral load (dead, live and seismic loads) is very tedious. In Japan, the "MUTO D-Method" offered a very easy, simple and reliable calculation procedure for rigid frames under 6 stories high. This method is very popular in Japan, not only for steel structural frames, but also for reinforced concrete structural frames. The details of this method can be found in Ref. (9),(3).

The frame analysis for the UBC case was calculated by the Stiffness Analysis Method of STRUDL computer program (19) and by the analytical procedure explained in Ref. (12), which includes the additional effects of overturning moment and accidental horizontal torsion. Due to the building is a low rise and regular in shape, the additional effect of overturning moment and accidental torsion is very small. The results of the analyses are recorded in column (8), (9) and (10) of Table 7.

(7) The "Net Combined" of column (14)(15) and (16) of Table 7 is the figures of column (11),(12) and (13) divided by the permitted increment of allowable stress by both codes, which is 1.5 by Japan and 1.33 by UBC. The figures of columns (14),(15) and (16) are the net different results by both codes for combined dead, live and seismic loadings.

(8) Based on the steel column design procedures in Ref. (9) and (10) or Ref. (2) and (1), the most critical column section of the bent-B, the interior column at first floor was calculated. The results are:

Japan Japanese H-section 250x250x9x14 at 72.4 $^{kg}/_{m}$

UBC Japanese H-section 200x200x8x12 at 49.9 $^{kg}/_{m}$

The Japan SS41 steel was used. The Fy is 2.4 t/sq. cm.

The calculated column K-factor for UBC case was 1.17 which was based on the assumption that the structure possesses the same properly designed footing as used in Ref. (9) for both cases.

(9) After a close examination on the results in Table 7, the following facts can be summarized:

In the case of structural design for normal loading conditions; i.e., under dead and live load only, regardless the different unit live load, rules of reduction of live load and analytical methods, the end results in terms of axial load and moments for the critical sections of the whole structure are very close to each other.

The difference of effect of seismic load to the structural design by both codes is significant. However, the difference became smaller as the design progresses to the completion, which can be illustrated as follows for the critical section of interior column at first floor.

	Seismic Shear Force	Combined End Moment	Weight Of Column Section
	Col. (7)	Col. (16)	
Japan / UBC	$\frac{5.4}{1.38} = 4.75$	$\frac{7.47}{2.19} = 3.41$	$\frac{72.4}{49.9} = 1.45$

The decrease of difference is logical which reflects the role of the seismic force in each stage of design. It is obvious the difference will be reduced more when the comparison is at the stage of total cost of the building if the costs for both cases can be calculated on the same base.

VI. Conclusions and Recommendations

Official building codes, as well as structural design specifications and practices of Japan and the USA, were briefed and compared through a sample calculation. The result of the calculation showed the codified safety regulation in Japan provided significantly higher degree of safety than UBC. However, on the other hand, the geology and seismological statistics informed us that the frequency and magnitude of earthquakes are also more severe in Japan than in the USA.

The comparison work of this paper accidentally indicated that there is a great possibility that the codified seismic safety regulations can be correlated with the earthquake magnitude Richter scale.

For years, it was criticized that the codified seismic safety regulations do not provide any guide as to the safety levels that they imply (13); therefore, the following research work is recommended to meet the urgent needs of an international aseismatic building code.

(1) Based on the seismology and engineering data of developed countries such as Japan and the USA, to develop an international aseismatic building code, the codified safety regulations must be correlated to the recorded earthquake magnitude Richter scale and using the modified Mercalli intensity scale as a local modification which can be assigned as desired to locations without intensity records.

(2) The developers of this new international code must keep in mind that the application of this new code is not only to the developed countries, but more important and helpful to those developing countries where they are crowded by new construction projects, but lack local seismological records except the historical data of earthquake magnitude on the Richter scale recorded by remote seismological stations.

TABLE 1

STATISTICS OF LARGE EARTHQUAKES IN JAPAN AND WEST COAST U.S.A.

Date	California Lat. N	California Long. W	Japan Long. E	Magnitude In Richter Scale
1901 Apr. 5	45		148	8
1901 Jun. 24	27		130	8
1901 Aug. 9	40		144	8
1903 Jan. 24	31-1/2	115		7+
1904 Jun. 7	40		134	8
1904 Aug. 24	30		130	8
1905 Jun. 2	34		132	8
1905 July 6	39-1/2		142-1/2	8
1906 Jan. 21	34		138	8.4
1906 Apr. 18	38	123		8.3
1909 Mar. 13	31-1/2		142-1/2	8-1/4
1909 Nov. 10	32		131	8
1911 Jun. 15	29		129	8.7
1915 Oct. 3	40-1/2	117-1/2		7.6
1915 Nov. 21	32	115		7.1
1918 Nov. 8	44-1/2		151-1/2	8
1920 Jun. 5	23-1/2		122	8-1/4
1922 Jan. 31	41	125-1/2		7.6
1923 Jan. 22	40-1/2	124-1/2		7.3
1923 Sept. 1	35-1/4		139-1/2	8.3
1927 Mar. 7	35-3/4		134-3/4	8
1927 Nov. 4	34-1/2	121-1/2		7.5
1932 Dec. 21	38-3/4	118		7.3
1933 Mar. 2	39-1/4		144-1/2	8-3/4
1934 Dec. 31	32	114-3/4		7.1
1940 May 19	32.7	115.5		7.1
1941 Nov. 18	32		132	8
1944 Dec. 7	33-3/4		136	8-1/4
1946 Dec. 20	32-1/2		134-1/2	8.5
1952 Mar. 4	42-1/2		143	8.6
1952 July 12	35.0	119		7.7

TABLE 2 - COMPARISON OF EQUIVALENT STATIC SEISMIC FORCE

	Japan	UBC*
F	Lateral force at each floor level	Total lateral force or shear at base to be distributed to each floor level by $f_i = \frac{(F - f_t)w_i h_i}{w_x h_x}$ $f_t = 0.004F(\frac{h_n}{D_s})^2$
W	Dead load and specified live load as in Table 6.	Dead load and snow load only, except for storage occupancy plus 25% of the floor live load.
Z	3 zone coefficient 1.0, 0.9 and 0.8 as shown in Fig. 1.	3 zone coefficient 1.0, 0.5 and 0.25 as shown in Fig. 2
A	0.2 for height $\leq$16M 0.2 + D for height > 16M D = 0.01 for every 4M over 16M. 0.3 for water tank, chimney project from roof.	Dynamic factor $C = \frac{0.05}{\sqrt[3]{T}}$
B	Modification factor for the ground conditions as shown in Table 3.	Structural stiffness factor as shown in Table 4.
Remarks	(1) "A" can be reduced to 50% by the Minister of Construction	(1) The product of AB shall be simplified to one single factor C_p for part or portion of building or other structures as shown in Table 5.
	(2) The product of AB shall not be less than 0.5.	(2) The effects of 5% accident horizontal torsion and overturning moment should be included.

* Symbols and notations please refer to p. 127 of Ref. (16) due to shortage of space in this paper.

TABLE 3 - MODIFICATION FACTOR OF THE SEISMIC COEFFICIENT ACCORDING TO THE GROUND CONDITIONS FOR THE STEEL FRAMED CONSTRUCTION IN JAPAN

I. Ground consisting of rock, hard sandy gravel, etc. classified as tertiary or older strata over a considerable area around the structure.	0.6
II. Ground consisting of sandy gravel, sandy hard clay, loam, etc. classified as diluvial, or gravelly alluvium, about 5 meters or more in thickness, over a considerable area around the structure.	0.8

TABLE 3 - (Cont'd.)	
III. Standard ground except Kind II, consisting of sand, sandy clay, clay, classified as alluvium.	1.0
IV. Bad and soft ground which falls in one of the following categories: 1) Alluvium consisting of soft delta deposits, topsoil, mud or the like (including heaping up, if any), whose depth is about 30 meters or more. 2) Filled ground which falls in one of the following items. A. Land obtained by reclamation of a marsh, muddy sea bottom, etc. B. Earth filling is bad and soft such as topsoil and mud. C. The depth of earth filling is about 3 meters or more. D. Thirty years have not yet elapsed since the time of reclamation.	1.0

TABLE 4 - UBC STRUCTURAL STIFFNESS K

Type of Arrangement of Resisting Elements	Value of K
All building framing systems except as hereinafter classified	1.00
Buildings with a box system	1.33
Buildings with a dual bracing system consisting of a ductile moment resisting space frame and shear walls using the following design criteria: (1) The frames and shear walls shall resist the total lateral force in accordance with their relative rigidities considering the interaction of the shear walls and frames (2) The shear walls acting independently of the ductile moment resisting portions of the space frame shall resist the total required lateral forces. (3) The ductile moment resisting space frame shall have the capacity to resist not less than 25 percent of the required lateral force.	0.80
Buildings with a ductile moment resisting space frame designed in accordance with the following criteria: The ductile moment resisting space frame shall have the capacity to resist the total required lateral force.	0.67
Elevated tanks plus full contents, on four or more cross-braced legs and not supported by a building	3.00
Structures other than buildings and other than those set forth in Table 5.	2.00

TABLE 5 - UBC HORIZONTAL FORCE FACTOR "C_p" FOR PARTS OR PORTIONS OF BUILDINGS OR OTHER STRUCTURES

Part or Portion of Building*	Direction Of Force	Value Of C_p
Exterior bearing and nonbearing walls, interior bearing walls and partitions, interior nonbearing walls and partitions over 10 feet in height, masonry or concrete fences over 6 feet in height .	Normal to flat surface	0.20
Cantilever parapet and other cantilever walls, except retaining walls.	Normal to flat surface	1.00
Exterior and interior ornamentations and appendages	Any direction	1.00
When connected to, part of, or housed within a building: towers, tanks, towers and tanks plus contents, storage racks over 6 feet in height plus contents, chimneys, smokestacks and penthouses.	Any direction	0.20
When resting on the ground, tank plus effective mass of its contents	Any direction	0.10
Floors and roofs acting as diaphragms	Any direction	0.10
Connections for prefabricated structural elements other than walls, with force applied at center of gravity of assembly.	Any horizontal direction	0.30

* Only portion of the table of UBC was present here for the purpose of comparison

TABLE 6 - COMPARISON OF LIVE LOAD

Unit: Lbs. per Sq. Ft. (kg per sq. ft.)

	For Floor Slab		For Girder, Column, Foundation		For (W) of Seismic Force (F) Calculations	
	Japan	UBC	Japan*	UBC**	Japan	UBC
1. Residential	36.9 (180)	40.0 (195)	26.6 (130)	40.0 (195)	12.3 (60)	None "
Hospital Wards	36.9	40.0	26.6	40.0	12.3	"

TABLE 6 - Cont'd.

	For Floor Slab		For Girder, Column, Foundation		For (W) of Seismic Force (F) Calculations	
	Japan	UBC	Japan*	UBC**	Japan	UBC
	(180)	(195) or 1000 lb (454) kg	(130)	(195)	(60)	None
2. Office Room	61.5 (300)	50.0 (244) or 2000 lb (909) kg	36.9 (180)	50.0 (244)	16.4 (80)	None
3. Class Room	47.1 (230)	40.0 (195) or 1000 lb (454) kg	43.0 (210)	40.0 (195)	22.5 (110)	None
4. Sales room in Department Store or Shop	61.5 (300)	75.0 (365) or 2000 lb (909) kg	49.2 (240)	75.0 (365)	26.6 (130)	None
5. Assembly Hall						
Fixed Seat Area	61.5 (300)	50.0 (244)	55.3 (270)	50.0 (244)	32.8 (160)	None
Other Area	73.8 (300)	100.0 (488)	67.6 (330)	100.0 (488)	43.0 (210)	
6. Garage						
General Storage	112.7 (550)	100.0 (488) or ***	82.0 (400)	100.0 (488)	41.0 (200)	None
Private Storage	112.7 (550)	50 (244) or 2000 lb	82.0 (400)	50.0 (244)	41.0 (200)	None
7. Storage						
Light	82.0 (400)	125 (610)	82.0 (400)	125.0 (610)	82.0 (400)	31.3 (152)
Heavy	Actual	250 (1220)	Actual	250.0 (1220)	Actual	62.5 (305)

* In Japan, live load reduction for calculation of axial stress in column and foundation shall be as follows:

Number of Floors Supported	1	2	3	More than 4
Value to be multiplied for reduced live load	100%	95%	90%	5% additional reduction for each floor, but not less than 60%.

** In UBC, the unit live load reduction shall be the smaller one of the following two formulae:

A. 8% per sq. ft. of area supported by the member for live load less than

100 lb/sq. ft. and support area by the member more than 150 sq. ft. The maximum reduction is 40% for horizontal member and 60% for vertical member.

B. Reduction in percent = 23.1 (1 + deal load/live load). For storage live load exceeding 100 lb/sq. ft., 20% reduction for column, but none for girder.

*** 2 or 3 concentrated loads shall be spaced 5 feet in center. Each of them shall be 40% of the gross weight of the maximum size vehicle to be accommodated.

TABLE 7 - FORCES IN INTERIOR BENT AT COLUMN LINE B

			Dead & Live Loads			Seismic Load				D+L+S Combined			Net Combined		
			Axial	Moment		Force at	Axial	Moment		Axial	Moment		Axial	Moment	
Fl	Col	Spc.	Load	Top	Bot	Ea. Lev.	Load	Top	Bot	Load	Top	Bot	Load	Top	Bot
3	Int	Japan	4.09	0.2	0.2	0.9	0	1.8	1.3	4.09	2.0	1.5	2.73	1.33	1.0
		UBC	6.03	0.24	0.24	0.477	0.04	0.99	0.99	6.07	1.23	1.23	4.56	0.92	0.92
	Ext	Japan	5.39	1.4	2.2	0.6	0.3	1.3	0.8	5.69	2.7	3.0	3.79	1.8	2.0
		UBC	2.93	2.09	2.11	0.477	0.15	0.71	0.74	3.08	2.80	2.85	2.32	2.11	2.14
2	Int	Japan	24.98	0.7	0.4	3.4	0.1	6.0	5.0	25.08	6.7	5.4	16.72	4.47	3.6
		UBC	25.89	0.75	0.71	0.9	0.12	1.93	1.82	26.01	2.68	2.53	19.56	2.02	1.90
	Ext	Japan	18.45	7.4	6.8	2.1	1.4	3.7	3.1	19.85	11.1	9.9	13.23	7.4	6.6
		UBC	11.93	5.42	5.05	0.9	0.59	1.26	1.09	12.51	6.68	6.14	9.41	5.02	4.62
1	Int	Japan	45.87	0.4	0.2	5.4	0.3	7.3	11.0	46.17	7.7	11.2	30.78	5.13	7.47
		UBC	46.06	0.24	0.41	1.138	0.23	2.04	2.50	46.29	2.28	2.91	34.80	1.71	2.19
	Ext	Japan	31.51	3.4	1.7	4.3	3.2	4.4	10.2	34.71	7.8	11.9	23.14	5.2	7.93
		UBC	21.33	3.38	1.76	1.138	1.15	1.62	2.30	22.48	5.0	4.06	16.90	6.65	3.05
(1)	(2)	(3)	(4)	(5)	(6)	(7)	(8)	(9)	(10)	(11)	(12)	(13)	(14)	(15)	(16)

NOTE: Axial load in ton, Moment in ton-meter.

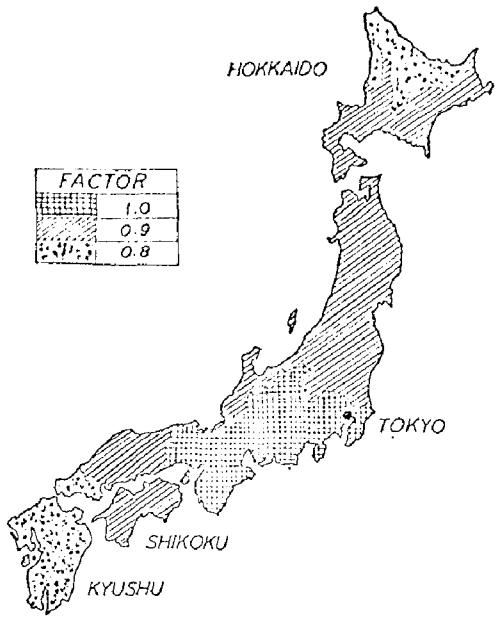

REDUCTION FACTORS FOR SEISMIC FORCES

Fig. 1 Japan

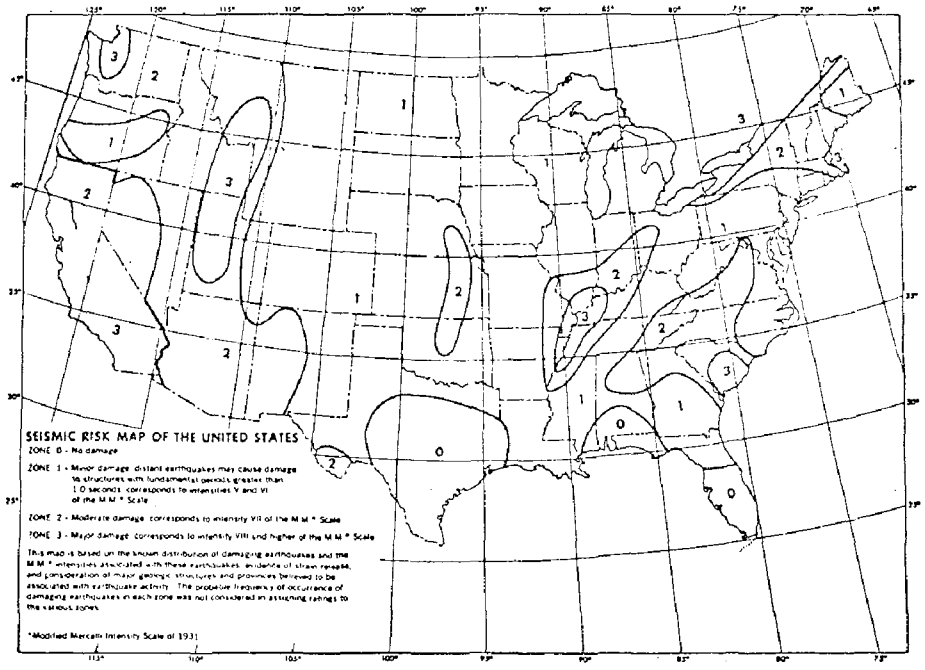

Fig. 2 USA

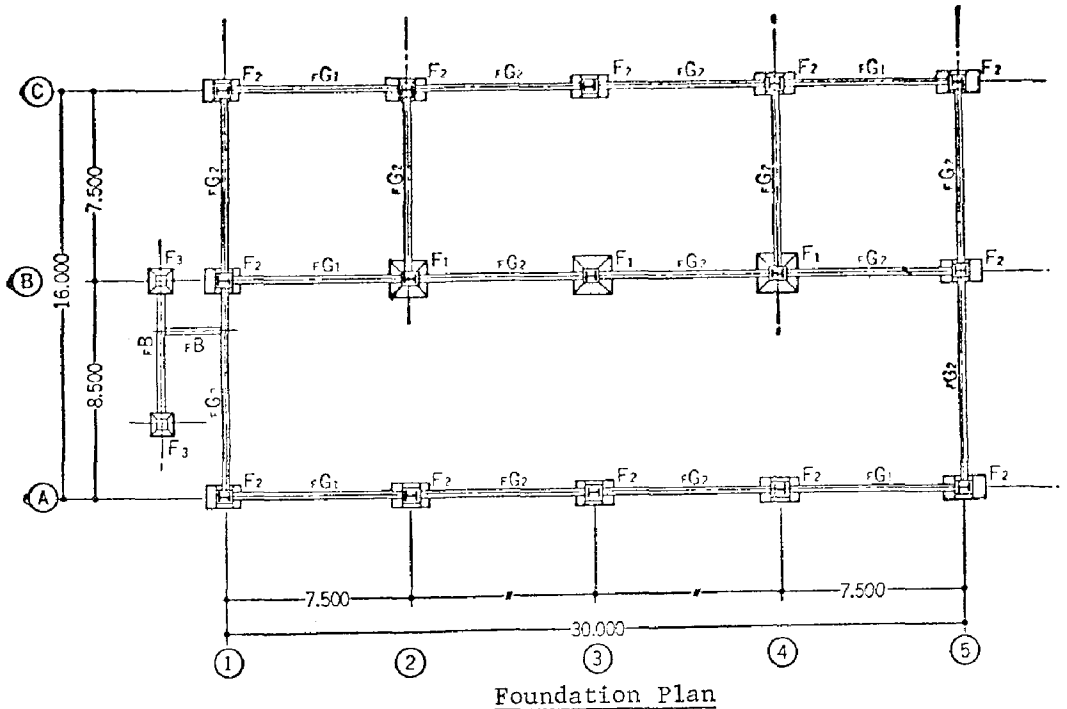

Foundation Plan

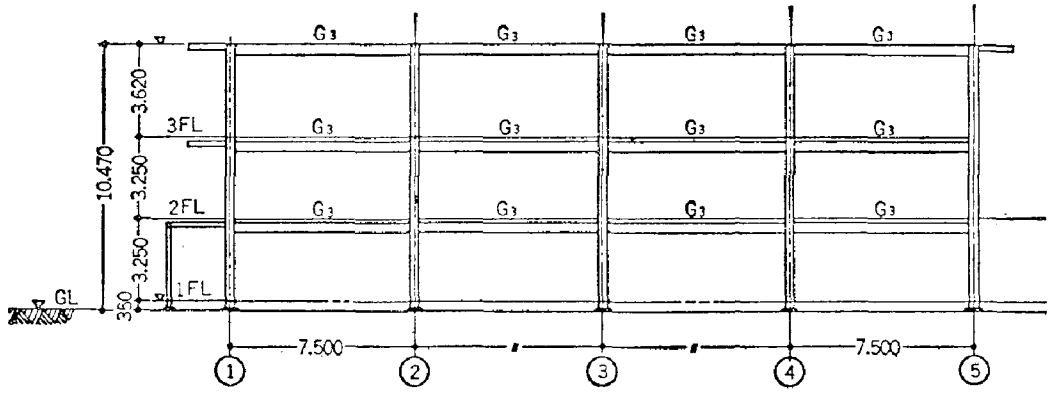

Section at Col. Line B

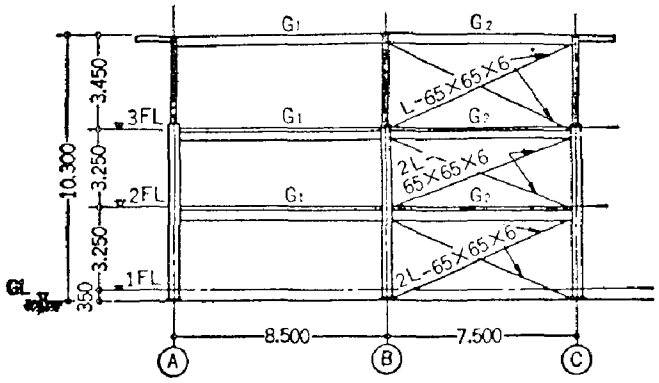

Sections at Col. Line 1 & 5
Sections at Col. Line 2 & 4
Except No X-Brace at 3rd Fl.

Fig. 3

REFERENCES

(1)
American Institute of Steel Construction "SPECIFICATION FOR THE DESIGN, FABRICATION AND ERECTION OF STRUCTURAL STEEL FOR BUILDINGS" Feb. 1969.
Supplement No. 1 Nov. 1970
No. 2 Dec. 1971
No. 3 Jun. 1974

(2)
Architectural Institute of Japan "SPECIFICATION FOR STEEL CONSTRUCTION 1970 EDITION". 1973 2nd Print. (In Japanese) Tokyo, Japan

(3)
Architectural Institute of Japan "DESIGN ESSENTIALS IN EARTHQUAKE RESISTANT BUILDINGS" 1970, Tokyo, Japan

(4)
Architectural Institute of Japan "STANDARD FOR PLASTIC DESIGN OF STEEL STRUCTURES" (In Japanese) Tokyo, Japan

(5)
Architectural Institute of Japan "STANDARD FOR STRUCTURAL CALCULATION OF MIXED STEEL-CONCRETE STRUCTURE" (In Japanese)

(6)
Architectural Institute of Japan "STANDARD FOR STRUCTURAL CALCULATION OF STEEL STRUCTURE" (In Japanese)

(7)
Architectural Institute of Japan "TOLERANCE STANDARD FOR STEEL CONSTRUCTION" (In Japanese)

(8)
Architectural Institute of Japan "STANDARD FOR WELDING PROCEDURE" (in Japanese)

(9)
Architectural Insitute of Japan, Kanto District "DESIGN OF STEEL STRUCTURE", 4th edition 1973 (In Japanese)

(10)
Beedle, L.S. "STRUCTURAL STEEL DESIGN" The Ronald Press Company 1964

(11)
Binder, R.W. & Wheeler, W.T. "BUILDING CODE PROVISIONS FOR ASEISMIC DESIGN" Proceedings of the 2nd World Conference on Earthquake Engineering, 1960, Japan

(12)
Blume, Newmark, Corning "DESIGN OF MULTI-STORY REINFORCED CONCRETE BUILDING FOR EARTHQUAKE MOTIONS" Portland Cement Assoc.

(13)
Blume, J.A. 'ANALYSIS OF DYNAMIC EARTHQUAKE RESPONSE" Proceeding Vol. 1b International Conference on Planning and Design of Tall Buildings, Lehigh University, Bethlehem, Pa. Aug. 1972

(14)
Committee of Structural Steel Producers of American Iron & Steel Institute "THE AGADIR MOROCCO EARTHQUAKE FEB. 29, 1960" 1962

(15)
Fujimoto and Funahashi "CURRENT JAPANESE STANDARDS FOR TALL STEEL BUILDINGS" Proceedings, International Conference on Planning and Design of Tall Buildings, Lehigh University, Bethlehem, Pa. 1972

(16)
International Conference of Building Officials "UNIFORM BUILDING CODE, 1973 EDITION"

(17)
International Association for Earthquake Engineering "PROCEEDINGS OF THE FIRST WORLD CONFERENCE ON EARTHQUAKE ENGINEERING" California USA 1956

(18)
Kamatani Giyou, "COLLECTION OF LAWS & ORDERS RELATED TO CURRENT BUILDING STANDARD LAWS, 1975 EDITION" Seven Stars Publisher, Tokyo, Japan 1975 (In Japanese)

(19)
Massachusetts Institute of Technology "ICES STRUDL-II THE STRUCTURAL DESIGN LANGUAGE ENGINEERING USER'S MANUAL" Cambridge, Massachusetts

(20)
Richter, C.F. "ELEMENTARY SEISMOLOGY" W. H. Freeman Co. 1958

(21)
U. S. Department of Commerce "EARTHQUAKE HISTORY OF THE UNITED STATES" Publicztion 41-1 Revised Edition 1973

(22)
Seismology Committee "RECOMMENDED LATERAL FORCE REQUIREMENTS AND COMMENTARY" Structural Engineers Assoc. of California 1973

INTERNATIONAL SYMPOSIUM ON
EARTHQUAKE STRUCTURAL ENGINEERING
St. Louis, Missouri, USA, August, 1976

COMPARATIVE STUDY OF THE NEW TURKISH EARTHQUAKE RESISTANT DESIGN CODE

MEHMET ÇELEBİ
Associate Professor
Department of Civil Engineering
Middle East Technical University
Ankara, Turkey

SUMMARY

Some highlights of the new 1975 Turkish Earthquake Resistant Design Code are presented in comparison with other major codes. The seismic zoning factors are increased in the new code; therefore, the resultant seismic coefficients are higher than the 1968 Code and the UBC 1970.

A new spectrum factor of the seismic coefficient is formulated in the new code. The spectrum factor is given as a function of the natural periods of vibration of both the structure and the underlying soil layer. The inclusion of the natural period of vibration of soil into the spectrum factor is discussed in light of recent research results and investigations of the causes of past earthquake damages.

The methods of determination of the natural period of structure are reviewed.

Conclusions are drawn as a result of the comparisons made.

INTRODUCTION

Turkey is a natural laboratory for earthquake engineering.

During the last 50 years, destructive earthquakes have claimed their toll both in life and property (over 60 000 deaths and 360 000 structures destroyed). In the last five years, five destructive earthquakes occurred (Gediz-1970, Burdur-1971, Bingöl-1971, İzmir-1974, Lice-1975). 91.4% of Turkey is within the four seismically active zones of the five zone seismic risk map (9). Therefore, an extensive number of rural housing most of which is built without engineering assistance (approximately $4x10^6$), modern high-rise structures as well as numerous industrial plants and dams are prone to earthquake danger.

Turkey is within the family of countries which has had an earthquake resistant design code for many years. Both public and private organizations are aware of the gigantic material losses as well as the dangers to lives caused by earthquakes and realize that only through earthquake resistant design and construction can the earthquake hazard be minimized. In light of the damages that occurred during the above cited recent earthquakes and changes made in the new seismic risk map which went into effect in 1973, the 1968 Turkish Earthquake Resistant Design Code (TERDC) is changed with a new one that went into effect on June 9, 1975 (4).

The highlights of the new code are to be examined herein. The various parameters of the equations for the seismic coefficient of major earthquake resistant design codes of other countries are compared with the new code.

SEISMIC COEFFICIENTS OF THE CODES

All codes listed in the World List advocate the seismic coefficient concept for earthquake resistant design of structures (5). This is done with the understanding that unless other reliable methods of determination of earthquake forces and dynamic analysis of structures due to these forces can be applied, then the structures will be designed for the minimum equivalent lateral static load expressed in terms of the percentage of the weight of the structure :

$$V = C\,W \qquad (1)$$

where C is the seismic coefficient, W is the weight of the structure plus some percentage of live loads and V is generally termed as the base shear force. The percentage given by C is considered to be equal to the force created by that acceleration (expressed in terms of percentage of the acceleration of gravity) the building experiences laterally during an earthquake.

It used to be the simpler the terms of the seismic coefficient, the easier the calculations and the earthquake resistant design. However with vast amount of theoretical and experimental research on dynamic elastic and inelastic behavior of structures and components, on soil-structure interaction and post-earthquake investigations of the causes of damages of

structures during earthquakes, the determination of the seismic coefficients is constantly being revised and improved. Rinne suggests that while perhaps a unified code is not necessary for all countries, more uniform expressions of the principles needed to be applied to resist earthquake motions in man-made structures is desirable (5).

Summary of Seismic Coefficients of Various Codes

The expressions for seismic coefficients of both the 1968 and 1975 TERDC as well as of various other codes are tabulated in Table I.

Most codes listed in Table I advocate a seismic risk zoning factor and a spectrum factor. The other factors are : factor for type of structure and structure importance factor. There is also a soil factor which in some codes is included in the spectrum factor. However, the seismic zoning and the spectrum factors are the dominant factors of the seismic coefficient.

The seismic zoning factor is based on the seismic risk zoning maps of each country. The seismic risk zoning map of Turkey is shown in Figure 1. The spectrum factor is related to the acceleration response of the structure; therefore also commonly is called as the response or dynamic factor. The spectrum factor in most codes is expressed as a function of the natural period of vibration of the structure and other parameters if applicable.

The spectrum factor of the 1968 TERDC was equal to unity for structures whose periods are less than 0.5 seconds and equal to $0.5T^{-1}$ for structures whose periods are greater than 0.5 seconds. This spectrum factor is typically similar to the first seismic coefficient (put forward by the Joint Committee of the San Francisco Section of ASCE and SEAOC) which adopted the period of the structure as an important parameter. The code of the Architectural Institute of Japan (AIJ) still retains similar expressions for buildings with heights, $h > 45$ meters (6). Another widely used version of spectrum factor is the originally 1957 SEAOC factor which is still in the 1970 UBC (11) as $C_o = 0.05T^{-1/3}$ with modification by a factor of 10 in the 1970 revision of the Indian Code, $0.5T^{-1/3}$ (2). The factor of 10 is taken care of by adjusting the seismic zoning factor accordingly.

More up to date expressions of the spectrum factors incorporate the local soil conditions. The Chilean Code uses :

$$C_o = 0.1 \frac{2TT_o}{T^2 + T_o^2} \qquad (2)$$

equation where T and T_o are the natural period of vibration of the structure and of vibration of $_o$ the underlying soil layer respectively. The 1975 TERDC uses the expression (5) :

$$S = \frac{1}{|0.8 + T - T_o|} \qquad (3)$$

with limitation that maximum value of $S = 1.0$. The proposed Japanese Building Research Institute Code (6) which is put forward to unify all codes in Japan

uses

$$C_o = \frac{0.35S'}{T-G} \qquad (4)$$

where S' (0.9 or 1.0) is the construction factor and G (-0.75, 0, 0.5, 0.75) is the soil factor.

The above cited seismic coefficients of the codes listed in Table I are shown in Figures 2 and 3. In both figures, only the highest severity seismic zones are considered and the factors for the type of structure and importance of the structure are both taken as unity. In Figure 2 the 1968 TERDC, UBC 1970 and 1975 TERDC seismic coefficients are compared. It is seen that the 1968 TERDC yields seismic coefficients that are lower than the UBC 1970. For building periods T>1, the seismic coefficients of the 1968 TERDC is approximately half those by the UBC 1970.

The investigations by Bertero and Collins following the 1971 San Fernando Earthquake resulted in criticisms of the 1970 UBC seismic coefficients which especially for T<2 seconds (particularly for 0.1<T<1 seconds) yielded base shear forces that were too low (1). Therefore, in Turkey with less advanced construction technology and not so adequate quality control, the 1968 TERDC had to be changed in a way so that higher and adequate seismic coefficients could be used in design. The resulting 1975 TERDC yields for T<2 seconds, seismic coefficients higher than UBC 1970 for all soil conditions. However, still,the main reason for the increases in the seismic coefficients of the 1975 TERDC is due to the increase of seismic zoning factors.

In Figure 3, the seismic coefficients of the 1975 TERDC are compared with those of the Chilean Code and AIJ Code of Japan. In Table I, the spectrum factor S for the 1975 TERDC is shown to have a maximum value of unity. Therefore, accordingly, with the highest seismic zoning factor of 0.1, the seismic coefficient of the 1975 TERDC is kept at 0.1 provided that K and I factors (Table I) are taken as unity. Plots of the seismic coefficients for the 1975 TERDC and the Chilean Code have been made both for the lowest (hard rock) and highest (soft soil) T_o . Both codes still yield seismic coefficients that are lower than the AIJ Code of Japan.

In the 1975 TERDC, the applicability of the seismic coefficient equation is limited to those structures with continuous load carrying elements such as columns and shear walls. The use of the equation is also limited to structures with less than 75 meters height. For higher structures reliable dynamic analysis methods are recommended. However, the base shear force determined by dynamic analysis is not permitted to be less than 70% of the base shear force determined by the seismic coefficient equation. In Japan different seismic coefficient equations are recommended for structures of different heights (Table I).

Soil Related Factors

To incorporate local soil conditions, some codes simply provide a factor. The Indian Code (2) uses a soil factor between 1.0 and 1.5. The 1968 TERDC provided soil factors 0.8, 1.0 and 1.2.The Chilean Code and the 1975 TERDC take care of the local soil conditions by incorporating the natural period of vibration of the underlying soil layer, T_o within the spectrum factor.

The Caracas Earthquake of 1967, the San Fernando Earthquake of 1971, the Gediz (Turkey) Earthquake of 1970 and several other earthquakes caused damages to structures that were attributed to the lack of consideration of local soil conditions. Seed as well as other researchers pointed out the influence of local soil conditions on the characteristics of ground surface motions and therefore the response of structures (7). If T and T_o are close figures, the response of the structure is amplified (resonance phenomenon). Seed even suggests a factor to change the base shear force by a factor of 1 to 5 according to the characteristics of the underlying soil layer (8). No provision in any code is given for $T \tilde{\sim} T_o$.

In the 1975 TERDC, if the thickness of the soil layer is less than 50 meters, then the natural period of the underlying soil can be taken from a provided table which is detailed enough for the designer to use. Should the underlying soil layer thickness, H, exceed 50 meters, then the shear wave velocity, v_s (meters/second) which can be obtained from a detailed table in the Code unless other methods are not applicable is used in the equation for the natural period of vibration of the soil :

$$T_o = 4H\ v_s^{-1} \tag{5}$$

Natural Period Calculation for Structures

The natural period of vibration of a structure within a spectrum type of factor appears in most codes discussed herein. In the 1975 TERDC as in the 1968 TERDC, the SEAOC empirical formula

$$T = 0.09h\ D^{-0.5} \tag{6}$$

is retained. In this formula, h (in meters) is the height of the structure and D (in meters) is the width of the structure in the direction that vibration is considered. A second formula that depends on the number of storeys (N) of framed structures

$$T = 0.1\ N \tag{7}$$

that appeared both in UBC 1970 and 1968 TERDC is revised in the 1975 TERDC as

$$T = (0.07 \sim 0.10)N \quad . \tag{8}$$

Use of these equations is limited to structures with $h<35$ meters. Also, use of the lower value of either equation is recommended.

Degenkolb suggests further research in use of equation 6 in order to estimate the value of natural period better (3). More recently, Bertero and Collins (7) indicated that more realistic methods of estimation of the natural period of vibration are necessary.

A more rational equation that is widely used in Japan (10) and based on Rayleigh's method is :

$$T = (0.16 \sim 0.20) \quad \delta \tag{9}$$

where δ is the static uppermost story deflection (in centimeters) calculated by loading the structure as a flagpole at every floor by the lateral force equivalent to the weight of that floor. The rationality of the equation is that the structure stiffness is more realistically idealized and considered in calculation of δ.

Distribution of the Base Shear Force

UBC 1970 equation for distribution of the base shear force is adopted in the 1975 TERDC.

TORSIONAL MOMENTS IN THE 1975 TERDC

To the eccentricity between the center of rigidity and mass, 5% of the width which is perpendicular to the direction of the earthquake force under consideration is to be added and the sections of members are to be checked for the torsional moments created by such eccentricity.

ALLOWABLE STRESSES

The factor of safety for earthquake resistant design of structures is increased by reduction of the increment of the allowable stresses of both concrete and reinforcing steel from 50% in the 1968 TERDC to 33% in the 1975 TERDC.

DUCTILITY CONSIDERATIONS

In the 1975 TERDC, the recommendations for detailing the members and joints are such that ductile characteristics are provided. In general, ACI 318-71 seismic design provisions and suggestions are adopted for detailing lateral reinforcements of columns, girders and shear walls and anchorage lengths.

As in UBC 1970, the seismic coefficient is reduced by a factor (K) of 0.6 for ductile framed structures. For non-ductile structures, the factor K can be as high as 1.60.

CONCLUSIONS

The new 1975 TERDC yields seismic coefficients that are higher than those by both the 1968 TERDC and UBC 1970. This is mainly due to increases in the seismic zoning factors.

In the new code, as in the Chilean Code, incorporation of the natural period of underlying soil layer into the spectrum factor is an improvement and reflects the suggestions of current researches as well as the principles of structural dynamics. It is expected that more rational evaluation of the probable base shear force that the structure is to be designed for will be possible with the new spectrum factor. However it is believed that some restrictions must be brought for cases when the period of structure is approximately same as that of the underlying soil layer.

Certain limitations as to the applicability of the seismic coefficient equation has been introduced. For structures higher than 75 meters, dynamic analysis is recommended in the new code. For structures higher than 35 meters, methods other than formulas are recommended for determination of the natural period. This is in accordance with the availability of digital methods for the designer.

Criticisms of the UBC 1970 are summarized to be in its lacking a soil factor as well as in its yielding low base shear forces.

For determination of the natural period of the structure, methods that depend on stiffness of the structure are more reliable. Although not discouraged dependence on simplified formulas, is cautioned.

Further improvements and revisions of all codes will take place with time. It is believed that the 1975 TERDC brings with it up to date concepts and higher factors of safety for earthquake structural engineering in Turkey.

Acknowledgement

The 1975 TERDC was prepared with joint efforts of staff members of Technical University of Istanbul, Middle East Technical University in Ankara, Boğaziçi University in Istanbul, Earthquake Research Institute of the Ministry of Reconstruction and Resettlement and private practicing engineers.

REFERENCES

1. Bertero, V.V., and Collins, R.G., "Investigation of the Failures of the Olive View Stairtowers During the San Fernando Earthquake and Their Implications on Seismic Design," EERC Report 73-26, Univ. of California, Berkeley, 1973, p.164.

2. Criteria for Earthquake Resistant Design of Structures, (draft second revision IS 1893-1970), Indian Standards Institution, New Delhi, 1970.

3. Degenkolb, H.J., "Earthquake Forces on Tall Structures," Bethlehem Steel Publication (lecture delivered to Engineering Institute of Canada, Montreal, 1962).

4. Earthquake Resistant Code (in Turkish), Ministry of Reconstruction and Resettlement, Ankara, 1975.

5. Earthquake Resistant Regulations - A World List, International Assoc. of Earthquake Engineering, 1966 (also 1970 and 1973).

6. Muto, K., Aseismic Design Analysis of Buildings, Maruzen Co., Tokyo, 1974.

7. Seed, H.B., "Dynamic Characteristics of Soil Structure Systems," Conference on Planning and Design of Tall Buildings, Lehigh University, August 1972.

8. Seed, H.B., lecture notes on Short Course on Earthquake Engineering, Univ. of Calif., Berkeley, June 1972.

9. Tabban, A., Türkiye Deprem Bölgeleri ve Nüfus ve Alan Araştırmaları (Earthquake Zonning in Turkey and Demographic Studies), ERI Publication No. 8, Ministry of Reconstruction and Resettlement, Ankara, 1973.

10. Umemura, H., Earthquake Resistant Design of Structures, Univ. of Tokyo, 1972.

11. Uniform Building Code, International Conference of Building Officials, 1970 ed., Whittier, Calif.

TABLE I (continued)

Country	Code Designation	Seismic Coefficient	Factors of Seismic Coefficient
CHILE	CEC 1967 (5)	$C = C_o k_1 k_2$	C_o = spectrum factor = $0.1 \frac{2TT_o}{T^2 + T_o^2}$ for $T > T_o$ $= 0.1$ for $T < T_o$ T_o = 0.3 seconds for hard soil T_o = 0.9 seconds for soft soil k_1 = structure importance factor (0.8 - 1.2) k_2 = type of structure factor (0.8 - 1.2)
JAPAN	Conventional (6)	$C = K_o Z S' C_1$ h < 45 m	K_o = 0.2 for h < 16 m = 0.2 + i for h > 16 m (i = 0.01/4 m over 16 m) Z = seismic zoning factor (1.0, 0.9, 0.8) $S'C_1$=soil and construction factor (0.6 - 1.5)
	AIJ (6)	h > 45 m	$(0.18/T) \lesssim C \lesssim (0.36/T)$, $0.05 \lesssim C \lesssim 0.2$
	Building Research Institute (6)	$C = C_o Z I$	C_o = 0.2S' for T < G + 1.75 seconds $= \frac{0.35S'}{(T-G)}$ for T > G + 1.75 seconds S' = construction factor (0.9, 1.0) G = soil factor (-0.75, 0.05, 0.75) I =structure importance factor

TABLE I. SEISMIC COEFFICIENTS OF VARIOUS CODES

Country	Code Designation	Seismic Coefficient	Factors of Seismic Coefficient
Turkey	TERDC 1968	$C = Z\alpha\beta\gamma$	Z = seismic zoning factor (0.06, 0.04, 0.02) α = soil factor (0.8, 1.0, 1.2) β = structure importance factor (1, 1.5) γ = spectrum factor = 1 for $T < 0.5$ secs. = 0.5/T for $T > 0.5$ secs.
	TERDC 1975 (4)	$C = ZKSI$	Z = seismic zoning factor (0.1, 0.08, 0.06, 0.03) K = factor for type of structure (0.6 - 1.6) I = structure importance factor (1.0, 1.5) S = spectrum factor = $\frac{1}{\lvert 0.8 + T - T_o \rvert}$, $S_{max} = 1.0$ T = natural period of vibration of structure T_o = natural period of vibration of soil layer
USA	UBC 1970 (11)	$C = ZKC_o$	Z = seismic zoning factor (0, 0.25, 0.5, 1.0) K = factor for type of structure (0.67 - 1.33) C_o = spectrum factor = $0.05\ T^{-1/3}$
INDIA	ISI-1970 (2)	$C = C_o\ \alpha\beta$	C_o = spectrum factor = $0.5\ T^{-1/3}$ α = seismic zoning factor (0.01, 0.02, 0.04, 0.05, 0.08) β = soil factor (1.0 - 1.5)

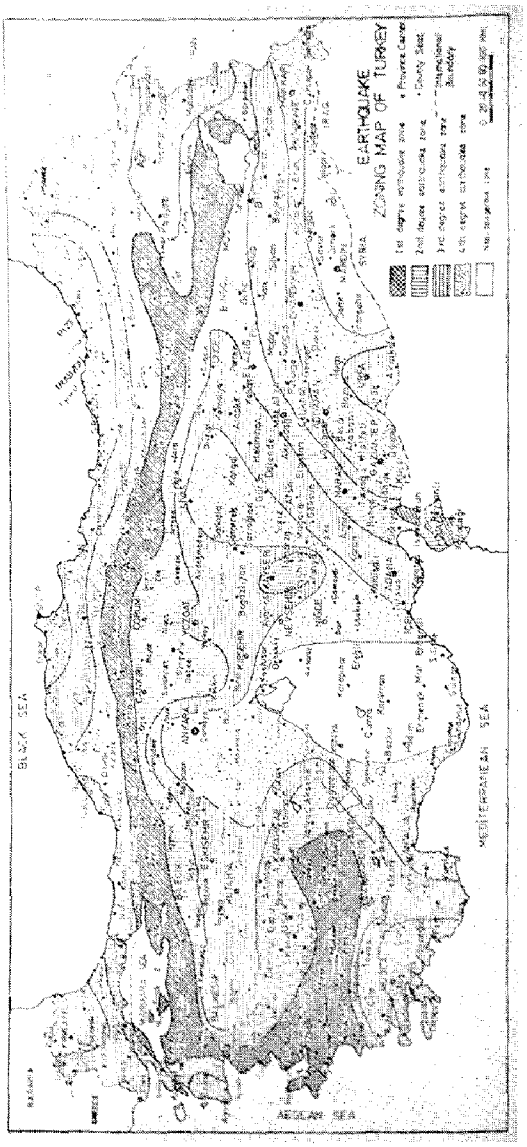

FIGURE 1. EARTHQUAKE ZONING MAP OF TURKEY

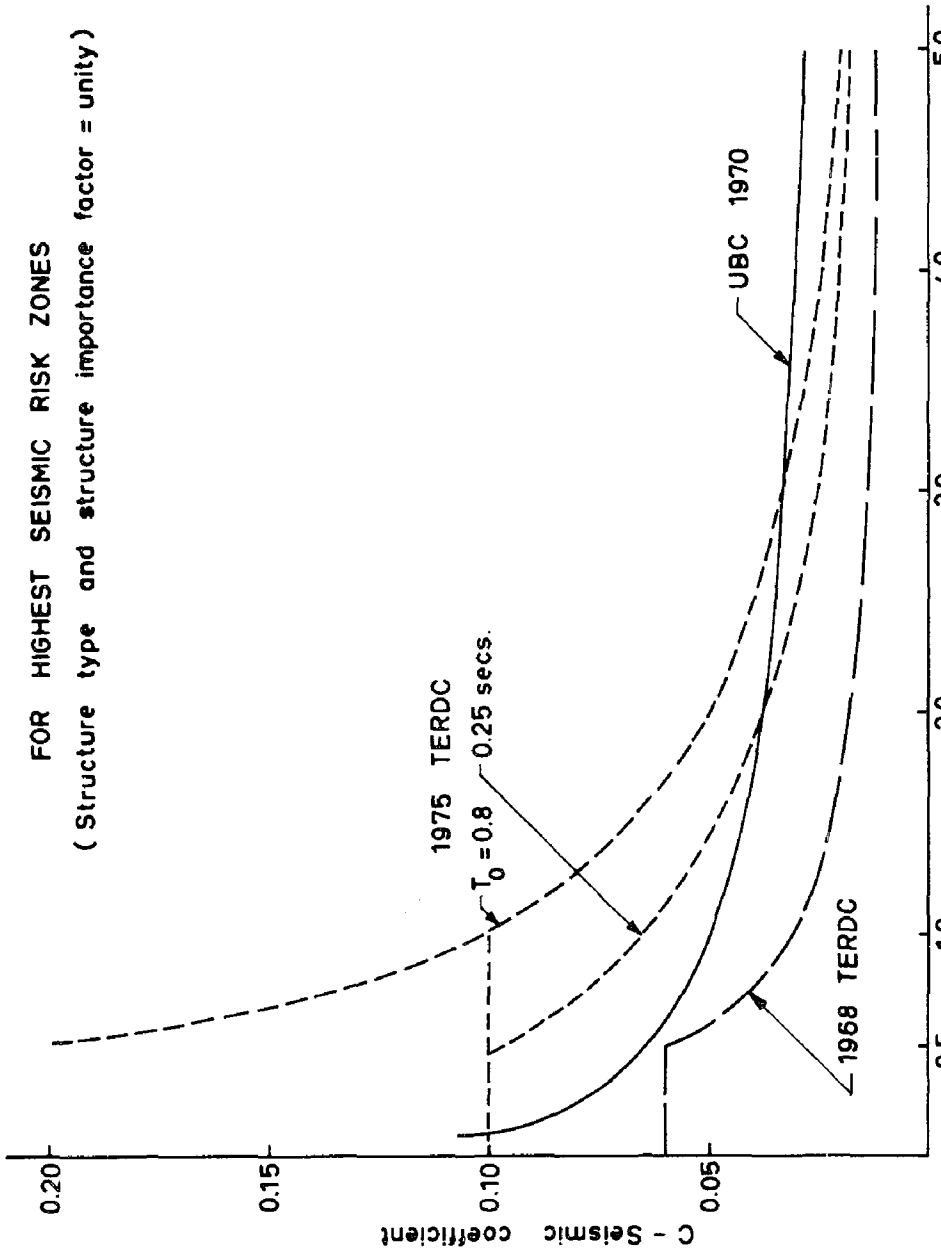

FIGURE 2. COMPARISON OF SEISMIC COEFFICIENT (1968 AND 1975 TERDC AND UBC 1970)

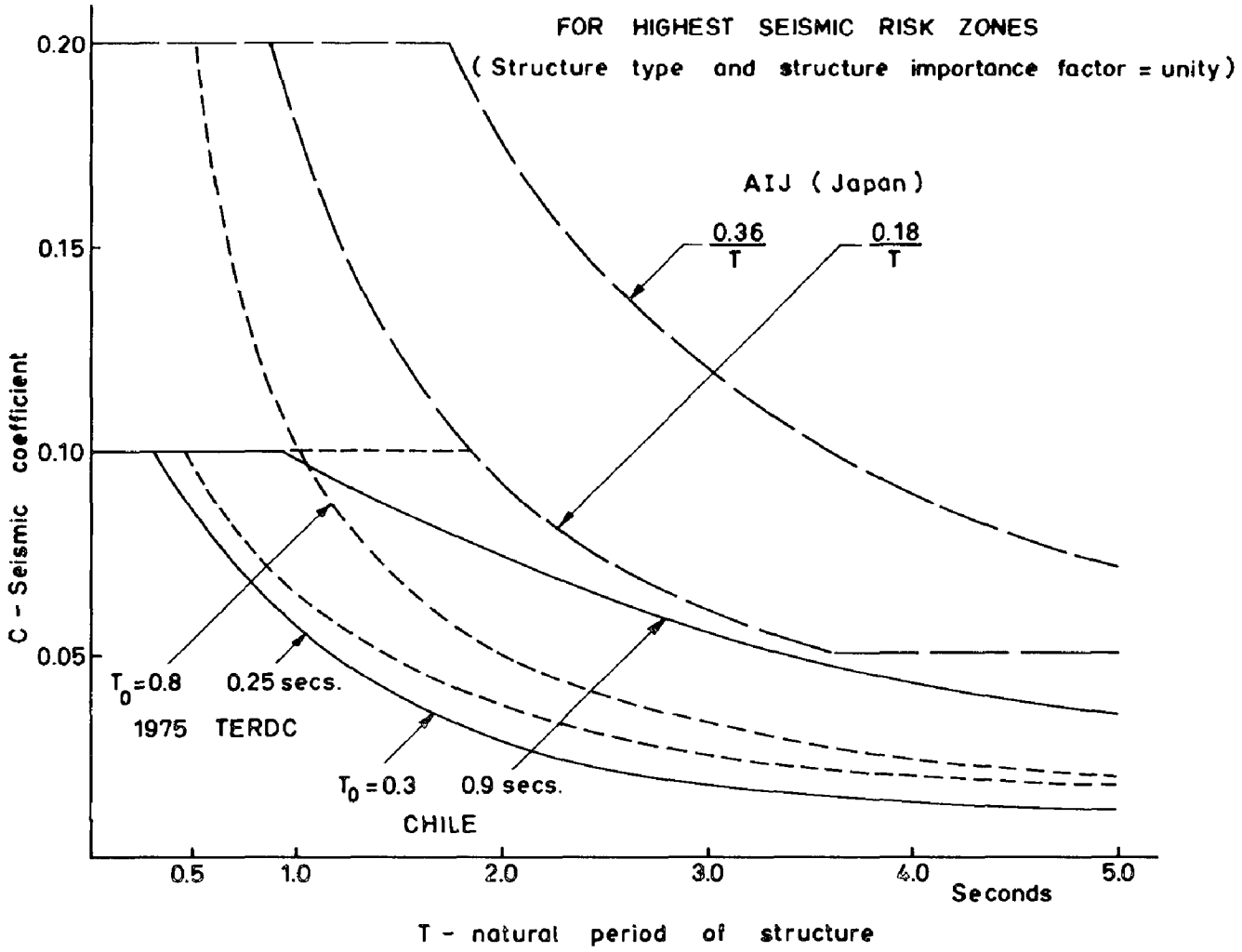

FIGURE 3. COMPARISON OF 1975 TERDC SEISMIC COEFFICIENT WITH AIJ AND CHILE

INTERNATIONAL SYMPOSIUM ON
EARTHQUAKE STRUCTURAL ENGINEERING
St. Louis, Missouri, USA, August, 1976

APPLICATION OF STRUCTURAL, MECHANICAL AND ELECTRICAL CODES AND STANDARDS IN THE DESIGN OF SAFETY RELATED STRUCTURES, COMPONENTS AND SYSTEMS FOR NUCLEAR POWER PLANTS

by

D. S. MEHTA*, and B. L. MEYERS**

BECHTEL POWER CORPORATION

GAITHERSBURG, MARYLAND, USA

SUMMARY

This paper identifies and provides a brief summary of the codes, standards, and code of federal regulations corrently being used in the design of safety related structures, components and systems for Nuclear Power Plants. Also discussed are the current requirements that must be applied prior to issuance of a construction permit and operating license for nuclear power plants. The current status and brief summaries of the codes and standards are presented in this paper.

INTRODUCTION

The basic requirements for the seismic and analysis of safety related structures, components, and systems important to public safety are given in mandatory and nonmandatory Regulatory Standards, Regulations, Regulatory Guides and Industry Standards. During the last decade, various aspects of these requirements have been standardized for the many nuclear plants under design or construction. At present, approximately 56 nuclear power plants are in commercial operation while applications for construction and operating permits are under review by the Nuclear Regulatory Commission for approximately 85 additional nuclear power plants. In all cases, safety related structures, systems and components are designed in accordance with NRC Regulations, Regulatory Guides and various standards prepared by the American National Standards Institute (ANSI). ANSI standards are developed by members of the working groups from the American Nuclear Society (ANS), the Institute of Electrical and Electronics Engineers (IEEE), the American Society of Mechanical Engineers (ASME), and other national engineering organizations.

* Engineering Specialist
** Engineering Supervisor

In addition to ANSI Standards, organizations like the American Concrete Institute, the American Society of Civil Engineers, the Uniform Building Code and the Structural Engineers Association of California (SEAOC) have also prepared some requirements for the seismic design and analysis of the structures.

NRC Regulatory Guides are issued to describe and make available the public methods acceptable to the NRC staff of implementing specific parts of the Commission's regulations and to delineate techniques used by the staff in evaluating specific problems or postulated accidents or to provide guidance to applicants. These Regulatory Guides are not substitutes for regulations and compliance with them is not required. The methods and solutions different from those set out in the guides are acceptable if they provide a basis for the findings requisite to the issuance or continuance of a permit or license by the Commission. In addition to Regulatory Guides, standard review plans are prepared for the guidance of the Office of Nuclear Reactor Regulations staff responsible for review of applications to construct and operate nuclear power plants.

Table I shows the list of various mandatory and nonmandatory regulations and standards issued by the NRC. Table II shows the list of various standards from the industry. Both types of standards are discussed below.

CODE OF FEDERAL REGULATION

o 10 CFR Part 50, Appendix A "General Design Criteria for Nuclear Power Plants"

General Design Criteria 2 of 10 CFR Part 50 of Appendix A requires that structures, systems, and components important to safety shall be designed to withstand the effects of natural phenomena such as earthquakes without loss of capability to perform their safety functions. The design bases for these structures, systems, and components should include,

(a) Appropriate consideration of the most severe of the natural phenomena that have been historically reported for the site and surrounding area, with sufficient margin for the limited accuracy, quantity, and period of time in which the historical data have been accumulated.

(b) Appropriate combinations of the effects of normal and accident conditions with the effects of the natural phenomena, and

(c) The importance of the safety functions to be performed.

o 10 CFR Part 100 "Reactor Site Criteria" and Appendix A "Seismic and Geologic Siting Criteria"

Regulation 10 CFR 100 describes the basic criteria in evaluating license applications for either construction or operating permit for

nuclear power plants required by 10 CFR Part 50. This regulation also describes the radiation dose limit to the population which must not be exceeded during a major hypothetical accident. The purpose of the Appendix A to 10 CFR 100 is to set forth the principal seismic and geologic considerations which guide the Commission in its evaluation of the suitability of proposed sites for nuclear power plants and the suitability of the plant design bases established in consideration of the seismic and geologic characteristics of the proposed sites in order to provide reasonable assurance that the nuclear power plant can be constructed and operated at a proposed site without undue risk to the health and safety of the public.

This appendix also defines the Safe Shutdown Earthquake for which safety related systems must be designed to remain functional. The Safe Shutdown Earthquake (SSE) is that earthquake which is based upon an evaluation of the maximum earthquake potential considering the regional and local geology and seismology and the specific characteristics of local subsurface material. This appendix further defines an Operating Basis Earthquake (OBE) as an earthquake which produces vibrating ground motion for which those features of the nuclear power plant necessary for continued operation without undue risk to the health and safety of the public are designed to remain functional, and considering the regional and local geology and seismology and specific characteristics of local subsurface material, which could reasonably be expected to affect earthquake vibratory motion at the plant site during the operating life of the plant.

USNRC REGULATORY GUIDES AND STANDARD REVIEW PLANS

o Regulatory Guide 1.60(1) provides the NRC requirements for the shape of the horizontal and vertical design response spectra. The horizontal-component ground-design response spectra of the SSE or the OBE on sites underlain by rock or soil, without soil-structure interaction effects, should be linearly scaled from Figure 1 of this guide, in proportion to the maximum horizontal ground acceleration specified for the earthquake.

The design basis for maximum vibratory ground motion and acceleration is determined by evaluation of the detailed geology and seismic history of the site and its nearby region. Minimum required value of the horizontal ground acceleration for any site is 0.1 g for the SSE.

The maximum vertical ground acceleration of the SSE is equal to the maximum horizontal ground acceleration of the SSE specified forthe site. The vertical component ground-design response spectra of the SSE or OBE on sites underlain by rock or soil, without soil-structure interaction effects, should be linearly scaled from Figure 2 of this guide, in proportion to the maximum horizontal ground acceleration specified for the earthquake.

Based on the study by Newmark and Blume (2, 3 & 4), the NRC regulatory staff has determined the above-mentioned design response spectra. These design spectra are based on a statistical evaluation of the actual response spectra of sixteen strong-motion earthquakes recorded at sites underlain by various geologic materials.

o Regulatory Guide 1.61(5) states the regulatory position for the damping values for seismic design of nuclear power plants. Acceptable modal damping values, expressed as a percentage of critical damping, are shown in Table IV of this guide.

o Regulatory Guide 1.12 specifies the regulatory position for the instrumentation required for earthquakes. It requires the installation of triaxial time-history accelerographs, triaxial peak accelerographs, and triaxial response-spectrum recorders at appropriate locations on the seismic Category I structures, systems, and components to provide data on the seismic input to containment and on the frequency, amplitude, and phase relationship of the seismic response of the containment structures and other seismic Category I structures, systems, and components. This guide refers to ANSI N18.5 with certain exceptions.

o Regulatory Guide 1.29 provides a method for use in identifying and classifying nuclear plant structures, systems and components to remain functional and withstand the effects of safe shutdown earthquake.

o Regulatory Guide 1.48 provides the regulatory position for seismic Category I fluid system components to withstand loading combinations within the design limits specified in the appropriate ASME Code, depending on code classification for vessels, piping, pumps, acting valves, and nonacting valves.

o Regulatory Guide 4.7 discusses the major site characteristics related to public health and safety which the NRC staff considers in determining the suitability of sites for light-water cooled and high temperature gas-cooled nuclear power stations. Review plans listed in Table I provide useful guidance for NRC's position for seismic design and soil-structure interaction analysis for safety related structures whose foundations are deeply embedded in soil.

INDUSTRY STANDARDS

o ANSI N18.5: "Earthquake Instrumentation Criteria for Nuclear Power Plants Revision 0, January 1974

This standard defines the minimum requirements for an earthquake instrumentation system to be installed at nuclear power plants in order to provide information on the input vibratory ground motion and resultant vibratory response of representative Category I structures, equipment and piping should an earthquake occur. By comparing this information with the vibratory motions used in the seismic design of the facility, an evaluation can be made as to whether or not the design vibratory motions have been exceeded. This standard was developed by working group 2.2.

o ANSI N643: "Guideline for Retrieval, Review, Processing and Evaluations for Records Obtained from Seismic Instrumentation

This standard will cover general philosophy associated with the use of data obtained from seismic instrumentation for nuclear power plants. Specifically, the standard will present overall philosophy, guidelines for retrieval, guidelines for preliminary design, specifications for data reduction, specification for analysis and guidelines for interpretation of results. No specific operator decisions will be defined. This standard is under development by working group ANS 2.10.

o IEEE 344: Recommended Practices for Seismic Qualification of Class IE Equipment for Nuclear Power Generating Stations (IEEE Std. 344-1975)

These recommended practices provide direction for establishing procedures to verify that the Class IE equipment can meet its performance requirements during and following one SSE (Safe Shutdown Earthquake) preceded by a number of OBEs (Operating Basis Earthquakes).

This standard also provides guidance for the seismic qualifications of Category I electrical equipment which must demonstrate the ability to perform its required function during and after forces resulting from the SSE either by mathematical and/or testing of equipment under simulated seismic conditions. However, following topics are under consideration for future revision to this standard:

(a) Simplified methods for multiaxis testing

(b) Expanding the guidance on combined testing and analysis

(c) Expanding the guidance for power spectral density testing

o ANSI N635: Guidelines for Combining Severe Environmental Phenomena to Determine Design Basis (Under Development)

This standard will provide guidelines for selecting:

Combinations of natural hazards

Combinations of manmade hazards, and

Combinations of natural and manmade hazards to be used in the design of power reactor structures, systems, and components.

Probability level acceptance criteria will be provided for selecting combinations of hazardous events at a particular site. Methods for calculating probabilities of combinations will be presented.

o ANSI N174: Guidelines for Evaluating Site-Related Geotechnical Parameters at Power Reactor Sites (Under Development)

This standard will develop guidelines for evaluating site-related geotechnical parameters for nuclear power facilities. Aspects which will be considered include: geology, groundwater, foundation engineering, earthwork engineering, and earthquake engineering. These guidelines will identify the basic geotechnical parameters to be considered in the evaluation and design for nuclear power facilities, and will outline the investigative and analytical procedures necessary to evaluate them. They will also include the identification of those parameters which require observation during the construction and post-construction phases. Those areas where interrelationships with other standards may exist, will be indicated.

o ANSI N180: Guidelines for Assessing Capability for Surface Faulting at Nuclear Power Reactor Sites (Under Development)

This standard will present guidelines for performing exploratory investigations to assess the capability for surface faulting at power reactor sites.

o ANSI N690: Design and Analysis of Steel Safety Class Structures Other than Pressure Retaining Components and Their Supports

This standard will present the design and analysis requirements for steel safety class structures other than pressure retaining components and their supports. It will include identification of margins of safety. This standard will include requirements on materials, fabrication, erection, inspection and quality assurance procedures consistent with the use of structural steel in Safety Class Nuclear Structures. The design providions of the existing AISC building code, which are essentially the same as those defined for the ASME Boiler and Pressure Vessel Code, Section III, Appendix XVII Linear Supports will be used in this standard.

o ANSI N18.4: Vibratory Ground Motion for the Design Earthquake (Under Development)

This stand will provide guidance for the determination of seismic ground accelerations for design earthquake.

o ACI Standard: Proposed ACI Standard Code Requirements for Nuclear Safety Related Concrete Structures (Feb. 1975)

This proposed standard covers the design and construction of concrete structures which form a part of a nuclear plant and which have nuclear safety related functions, but does not cover concrete reactor vessels and concrete containment structures.

o ASME Code: ASME Boiler and Pressure Vessel Code, Section III, Division 2 Code for Concrete Reactor Vessels and Containments (ACI Standard 359-74)

This code establishes rules for the design, construction, inspection, and testing of composite concrete and steel components for reactor vessels and containments for nuclear power plants.

Table II lists many other standards which are currently under development such as ANSI N166, ANSI N167, ANSI N168, ANSI N175 and ANSI N690.

o American Society of Civil Engineers

In 1973 the Nuclear Structures and Materials Committee of the Structural Division of ASCE, initiated an effort to prepare a manual for the design of nuclear power plants. As of this writing the manual has not been issued. However, in December of 1975 (6)an Ad Hoc Group of the same committee presented the draft report "Analyses for Soil-Structure Interaction Effects for Nuclear Power Plants". The efforts of the Ad Hoc Group and other similar groups are extremely important to the designer of nuclear safety related structures. The response of the structures and the surrounding soil medium must be first accurately and then conservatively modeled. The above report deals with both of these important areas.

CONCLUSIONS

The basic seismic design and analysis requirements for safety related structures, components and systems important to public safety have been established by USNRC Regulatory Guides, Code of Federal Regulations and Industry Standards. Completion of the various industry standards and close coordination with Nuclear Regulatory Commission to establish standardized criteria will be a signficant achievement for the Nuclear Standardization Program.

BIBLIOGRAPHY

1. Directorate of Standards, USAEC Regulatory Guide 1.60, Design Response Spectra for Seismic Design Response Spectra for Seismic Design of Nuclear Power Plants (Revision 1, 1973).

2. Newmark, N. M., John A. Blume and Kanwar K. Kapur, "Design Response Spectra for Nuclear Power Plants" ASCE Structural Engineering Meeting, San Francisco, April 1973.

3. Newmark, N. M., Consulting Services, "A Study of Vertical and Horizontal Earthquake Spectra," San Francisco, USAEC Contract AT (49-5)-2667, WASH-1255, April 1973.

4. Blume, John A. & Associates, "Recommendations for Shape of Earthquake Response Spectra," San Francisco, USAEC Contract AT(49-5)-3011, WASH-1254, February 1973.

5. Directorate of Standards, USAEC Regulatory Guide 1.61, Damping Values for Seismic Design of Nuclear Power Plants,(October 1973).

6. P. K. Agrawal, et al, "Analyses for Soil-Structure Interaction Effects for Nuclear Power Plants,"Ad Hoc Group on Soi-Structure Interaction, Nuclear Structures and Materials Committee of the Structural Division of ASCE, Draft, December 5, 1975.

TABLE I

MANDATORY REGULATIONS

10 CFR Part 50 General Design Criteria 2
10 CFR Part 100 "Reactor Site Criteria"
10 CFR Part 100 Appendix A "Seismic and Geologic Siting Criteria

USNRC REGULATORY GUIDES

Regulatory Guide 1.60 Revision 1, December 1973, Design Response Spectra for Seismic Design of Nuclear Power Plants

Regulatory Guide 1.61, October 1973, Damping Values for Seismic Design of Nuclear Power Plants

Regulatory Guide 1.92, December 1974, Combination of Modes and Spatial Components in Nuclear Power Plants

Regulatory Guide 1.70 Revision 2, September 1975, "Standard Format and Content of Safety Analysis for Nuclear Power Plants"

Regulatory Guide 1.12 Revision 1, April 1974, Instrumentation for Earthquakes

Regulatory Guide 1.29 Revision 1, August 1973, Seismic Design Classification

Regulatory Guide 1.48, May 1973, Design Limits and Loading Combinations for Seismic Category I Fluid System Components

Regulatory Guide 1.XXX Seismic Qualifications of Class I Electric Equipment (Under Development)

Regulatory Guide 4.7, Revision 1, November 1975, General Site Suitability Criteria for Nuclear Power Stations

USNRC STANDARD REVIEW PLANS, NOVEMBER 1975

Section 3.7.1	Seismic Input
Section 3.7.2	Seismic System Analysis
Section 3.7.3	Seismic Subsystem Analysis
Section 3.7.4	Seismic Instrumentation Program
Section 3.10	Seismic Qualification of Category I Instrumentation and Electrical Equipment
Section 2.5.1	Basic Geologic and Seismic Information
Section 2.5.2	Vibratory Ground Motion
Section 2.5.3	Surface Faulting

TABLE II

INDUSTRY STANDARDS

ANSI NUMBER	TITLE	WORKING GROUP	STATUS
ANSI N18.4	Vibratory Ground Motion for the Design Earthquake	ANS 2.1	Under Development
ANSI N 18.5	Earthquake Instrumentation Criteria for Nuclear Power Plants	ANS 2.2	Issued on Jan. 1974
ANSI N180	Guidelines for Assessing Likelihood of Surface Faulting at Power Reactor Sites	ANS 2.7	Under Development
ANSI N643	Guidelines for Retrieval, Review and Processing and Evaluations of Records Obtained from Seismic Instrumentation	ANS 2.10	Under Development
ANSI N174	Guidelines for Determining Foundation Soil and Geological Characteristics at Power Reactor Sites	ANS 2.11	Under Development
ANSI N166	Seismic Qualifications for Nuclear Power Plant Structures and Mechanical Equipment	ASME Section III	Under Development
ANSI N167	Seismic Analysis of Category I Structures, Systems and Components	ASME Section III	Under Development
IEEE Std. 344-1975	IEEE Recommended Practices for Seismic Qualifications of Class IE Electric Equipment for Nuclear Power Generating Stations	IEEE 344	Issued on Jan. 1975 (Rev. of ANSI N41.7, IEEE Std. 344)
ASME Section III Div. 2 Code	Code for Concrete Reactor Vessels and Containments	ACI-ASME Joint Committee	1975 Edition, January 1, 1975

TABLE II (continued)

INDUSTRY STANDARDS

ANSI NUMBER	TITLE	WORKING GROUPS	STATUS
Proposed ACI Standard	Code Requirements for Nuclear Safety Related Concrete Structures	ACI-349 Committee	Under Development
ANSI N168	Design and Analysis of Concrete Seismic Category I Structures Other Than Containment	ASCE	Under Development
ANSI N175	Geologic Design Criteria	ASCE	Under Development
ANSI N690	Design and Analysis of steel safety class structures other than Pressure Retaining Components and Their Support	——	Under Development
ANSI N689	Requirements for Qualifications of Nuclear Power Plant Safety Related Equipment	——	Under Development
ANSI N635	Guidelines for Combining Severe Environmental Phenomena to Determine Design Basis	——	Under Development

INTERNATIONAL SYMPOSIUM ON
EARTHQUAKE STRUCTURAL ENGINEERING
St. Louis, Missouri, USA, August, 1976

ON SPECIFICATIONS FOR EARTHQUAKE–RESISTANT DESIGN OF HIGHWAY BRIDGES (JANUARY 1971)

by
KENJI KAWAKAMI
Ex-Director, Public Workks Research Institute

EIICHI KURIBAYASHI
Chief, Earthquake Engineering Section
Public Works Research Institute

TOSHIO IWASAKI
Chief, Ground Vibration Section
Public Works Research Institute

YUTAKA IIDA
Chief, Survey Section Road Construction Office in Yokohama
Kanto Regional Construction Bureau

Ministry of Construction

JAPAN

I. INTRODUCTION

In the event of a major seismic disaster, highway networks should perform their duties to facilitate the conduct of evacuation, rescue and recovery operations with consequent reductions of life and property losses. In such a case, bridges, viaducts and so forth, which constitute important parts of highways, would decide the fate of each route of highway networks. Therefore structural safety of these structures against earthquakes are extremely significant.

In 1966 the Ministry of Construction commissioned the Japan Road Association to draw up new comprehensive specifications for earthquake-resistant design of highway bridges in order to rationalize earthquake-resistant design criteria for bridges and accordingly to afford maximum protection against earthquakes at minimum cost. In response to the commission, the Japan Road Association established a special committee and the committee had seriously attempted to draw up new specifications through every means available. The committee finished its task in January 1971. The Japan Road Association immediately reported to the Ministry of Construction. The Ministry of Construction notisfied highway administerial organizations of the specifications as ministerial technical standards for bridges, viaducts and so forth in the names of the Directors of Road Bureau and City Bureau in March 1971.

The nortifications of the Directors are supplements to Article 5 of the Ministry of Construction Ordinance for the enforcement of the Road Structure Ordinance which is a governmental ordinance. The legal ground is as follows. The Road Structure Ordinance is in force in conformity with the Road Law. Article 30 of the Road Law provides that technical standards of bridges and other principal structures, which are definitely designated by a governmental ordinance, may be provided by a governmental ordinance. Paragraph 1 of Article 35 of the Road Structure Ordinance provides that bridges, viaducts and so forth shall be steel or concrete structures or similar ones. Paragraph 2 of Article 35 provides the total weights of design live loads, i. e. 20 tons or 14 tons, for bridges and so forth. Paragraph 3 provides that necessary matters concerned

with structural standards of bridges and so forth shall be provided by a Ministry of Construction ordinance. Article 5 of the Ministry of Construction Ordinance for the enforcement of the Road Structure Ordinance provides that bridges, viaducts and so forth shall be sufficiently safe against dead loads, live loads, wind loads, seismic effects and other loads which are expected to act on bridges and so forth and combinations of loads, considering structural types, traffic situations, topographical, geological, meteorological and other conditions.

II. OUTLINES OF SPECIFICATIONS FOR EARTHQUAKE-RESISTANT DESIGN OF HIGHWAY BRIDGES (JANUARY 1971)

Since 1956, the earthquake-resistant design of highway bridges had been conducted in accordance with the provisions of Section 13 (Section 2.9 in the English version) of "Specifications for Design of Steel Highway Bridges," which were issued in 1956 by the Japan Road Association originally and revised in 1964 (the English version were issued in 1968) and displaced by "Specifications for Highway Bridges" in 1972. The Section provided the followings.

(1) The horizontal design seismic coefficient shall be determined by Table 1.

Table 1. Horizontal Design Seismic Coefficient (Out of Date)

Ground Conditions* / Regions*	Weak	Ordinary	Firm
Where severe earthquakes have been frequently experienced	0.35~0.30	0.30~0.20	0.20~0.15
Where severe earthquakes have been occurred	0.30~0.20	0.20~0.15	0.15~0.10
Other regions	0.20	0.15	0.10

*no further discription on regions and ground conditions.

(2) The vertical design seismic coefficient shall be assumed as 0.10.

(3) Increases in allowable stresses for seismic forces alone or for dead loads plus seismic loads shall be taken as

70% for steel structures,

50% for concrete structures and reinforced concrete structures.

Since the provisions in the Section 13 were not comprehensive, it was necessary to draw up new detailed specifications exclusively for aseismic design of highway bridges. Current "Specifications for Earthquake-

Resistant Design of Highway Bridges" were issued in January 1971, by the Japan Road Association, which apply to the design of highway bridges with spans not longer than 200 meters, to be constructed on expressways, national highways, prefectural highways and principal municipal highways.

The specifications basically stipulate to employ seismic coefficient methods and provide two methods in determining design seismic coefficients. One is the conventional seismic coefficient method that applies to the design of relatively rigid structures. The other is the modified seismic coefficient method considering structural response that applies to the design of relatively flexible structures. The followings are the principal points of the specifications.

(1) The horizontal design seismic coefficient for a rigid structure is determined systematically, depending on the geographical location of the bridge site, the ground conditions at each sub-structure site, and the importance of the bridge. The horizontal design coefficient for a flexible structure is determined depending on the fundamental natural period of each structural system.

(a) In the seismic coefficient method that is employed for relatively rigid structures, the horizontal design seismic coefficient (k_h) shall be determined by

$$k_h = \nu_1 \ \nu_2 \ \nu_3 k_o \quad \cdots\cdots\cdots\cdots\cdots\cdots\cdots\cdots\cdots\cdots (1)$$

where

k_h : horizontal design seismic coefficient,

k_o : standard horizontal design seismic coefficient (= 0.2),

ν_1 : seismic zone factor,

ν_2 : ground condition factor,

ν_3 : importance factor.

The values of ν_1, ν_2 and ν_3 are shown in Tables 2, 3 and 4 respectively. The definitions of classification are specified in the provisions. The minimum value of k_h shall be considered as 0.10.

Table 2. Seismic Zone Factor ν_1 for General Highway Bridges

Zone	Value of ν_1
A	1.00
B	0.85
C	0.70

Note: Refer to Fig. 1.

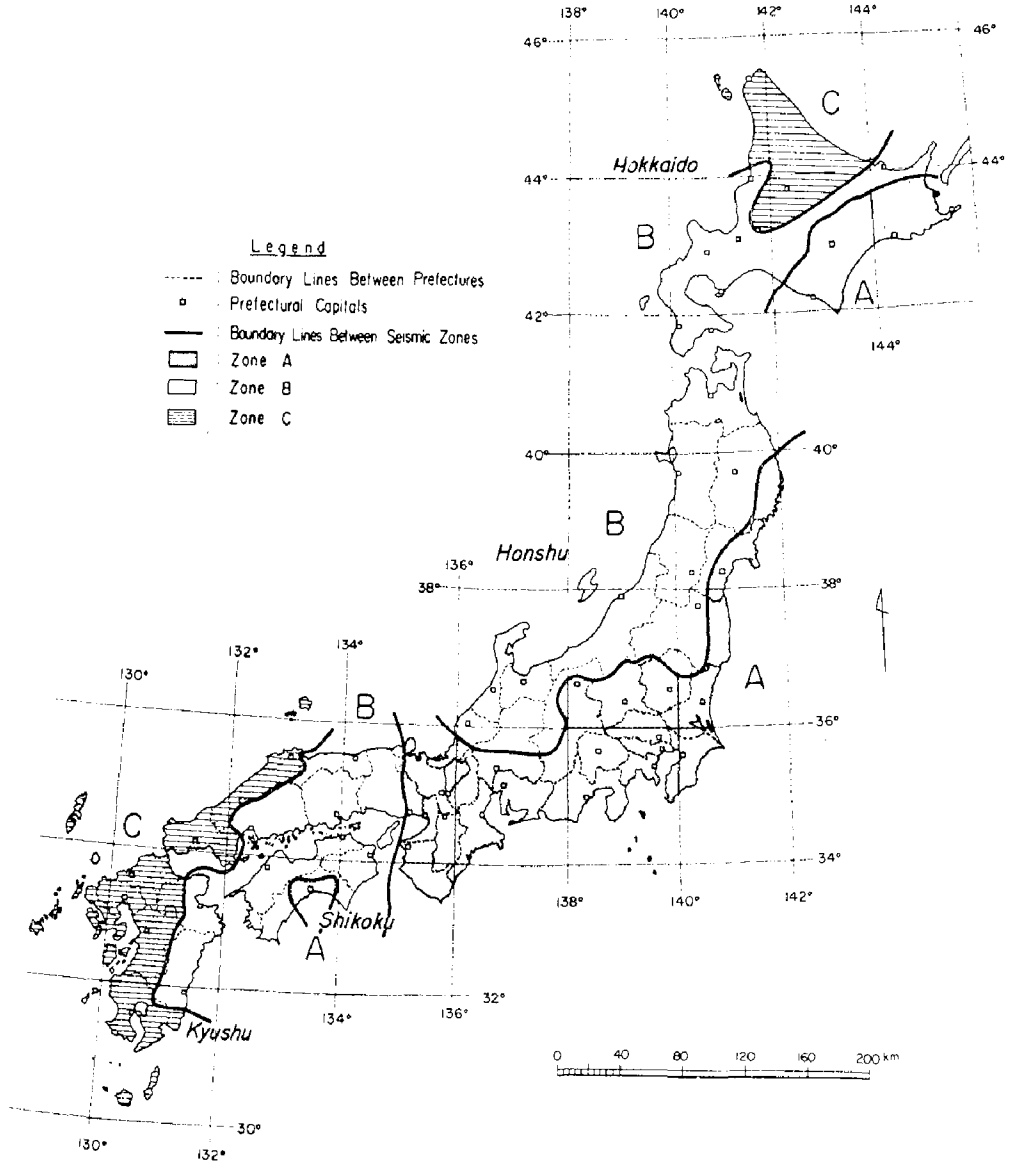

Fig. 1. Seismic Zoning Map

Table 3. Ground Condition Factor ν_2 for General Highway Bridges

Group	Definitions[1]	Value of ν_2
1	(1) Ground of the Tertiary era or older (defined as bedrock hereafter) (2) Diluvial layer[2] with depth less than 10 meters above bedrock	0.9
2	(1) Diluvial layer[2] with depth greater than 10 meters above bedrock (2) Alluvial layer[3] with depth less than 10 meters above bedrock	1.0
3	Alluvial layer[3] with depth less than 25 meters, which has soft layer[4] with depth less than 5 meters	1.1
4	Other than the above	1.2

(Notes) 1) Since these definitions are not very comprehensive, the classification of ground conditions shall be made with adequate consideration of the bridge site.
Depth of layer indicated here shall be measured from the actual ground surface.

2) Diluvial layer implies a dense alluvial layer such as a dense sandy layer, gravel layer, or cobble layer.

3) Alluvial layer implies a new sedimentary layer made by a landslide.

4) Soft layer is defined in Section 3.7 "Soil Layer Whose Bearing Capacities are Neglected in Earthquake Resistant Design".

Table 4. Importance Factor ν_3 for General Highway Bridges

Group	Definitions	Value of ν_3
1	Bridges on expressways (limited-access highways), general national highways and principal prefectural highways. Important Bridges on general prefectural highways and municipal highways.	1.0
2	Other than the above	0.8

Note: The value of ν_3 may be increased up to 1.25 for special cases in Group 1.

(b) In the modified seismic coefficient method considering structural response that is employed for relatively flexible structures such as a bridge with highrise piers higher than 25 m or a bridge with a fundamental period longer than 0.5 seconds, the horizontal design seismic coefficient (k_{hm}) shall be determined by

$$k_{hm} = \beta k_h \quad \cdots\cdots (2)$$

where

k_{hm} : horizontal design seismic coefficient in the modified seismic coefficient method considering structural response,

k_h : coefficient given by eq. (1),

β : a factor dependent on the fundamental period of the bridge, and obtained by Fig. 2.
For structures whose fundamental periods are shorter than 0.5 seconds, β may be considered as 1.0.

The minimum value of k_{hm} shall be 0.05.

(2) The vertical design seismic coefficient may generally be considered as zero, except for special portions such as bearing supports.

(3) The horizontal design seismic coefficient for structural parts, soils and water below the ground surface may be considered as zero.

(4) Hydrodynamic pressure during earthquakes are specified in the specifications. Earth pressures during earthquakes, however, are

specified in the related specifications.

(5) A specific attention is paid to very soft soil layers and soil layers vulnerable to liquefaction during earthquakes. The bearing capacities of these layers are neglected in the design, in order to assure high earthquake-resistance for structures that are built in these layers.

(6) A special attention is also paid to the design of structural details, in consideration of the damage previously experienced to bridge structures. To this aim provisions are specified for bearing supports and devices for preventing bridge girders from falling.

(7) Increases in allowable stresses of materials may be considered in the earthquake-resistant design, magnitudes of increases for various materials are specified in the several related specifications. The increasing rates are as follows:

concrete in reinforced concrete structures:	50%
reinforcements in reinforced concrete structures:	50%
structural steel for superstructures:	70%
structural steel for substructures:	50%
concrete in prestressed concrete structures against compressive forces:	65%
foundation soils:	50%

Detailed descriptions on the specifications are provided in Appendix of this paper.

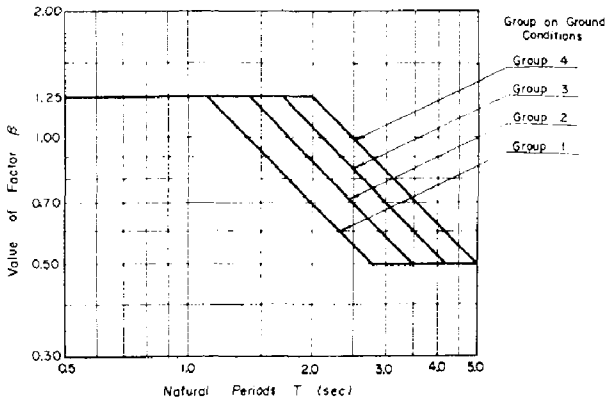

Fig. 2. Factor

III. ACKNOWLEDGEMENT

Specifications for Earthquake-Resistant Design of Highway Bridges (January 1971) are the fruit of efforts of the Earthquake-Resistant Design Branch-Committee of the Specifications Subcommittee under the Highway Bridge Committee, the Japan Road Association. Special thanks are extended to the Branch-Committee headed by Mr. Yasuo Tada for its energetic efforts.

APPENDIX
CONTENTS
OF
SPECIFICATIONS FOR EARTHQUAKE-RESISTANT DESIGN OF HIGHWAY BRIDGES (JANUARY 1971)

INTERNATIONAL SYMPOSIUM ON
EARTHQUAKE STRUCTURAL ENGINEERING
St. Louis, Missouri, USA, August, 1976

THE NEW TURKISH ASEISMIC CODE : A CRITICAL EVALUATION WITH EMPHASIS ON SOIL AMPLIFICATION CONSIDERATIONS

AYBARS GÜRPINAR

Assistant Professor of Engineering Sciences

Middle East Technical University

Ankara, Turkey

SUMMARY

The new Turkish aseismic code is evaluated with respect to its soil amplification regulations. The major critique is directed to the computation of T_o, predominant soil period.

A brief outline of the code in general and a more detailed outline of soil considerations in the code is first presented. Then the results from an earlier two dimensional modal study are given. These results include several relationships between modal periods, thicknesses and P and S wave velocities of soil layers. A comparison between these and code formulas, as well as several recommendations are included.

INTRODUCTION

The new Turkish Aseismic Code[A] went into effect in June 1975[1]. In 1973, the Earthquake Research Institute of the Ministry of Reconstruction and Resettlement who is responsible for the preparation of the code, had asked concerned institutions for their opinions on the subject which led to a cooperative effort by engineers and researches from İstanbul Technical University, Middle East Technical University and Boğaziçi University. After two years of constant meetings a code was drafted which is technically far ahead of the previous 1968 code. Probably the most important and radical concept that was incorporated in the code concerns soil amplification considerations. This article will aim at evaluating these newly introduced concepts from a point of view of theoretical soundness as well as practically. A general presentation of the new Turkish Aseismic Code will be made by a different speaker in this Symposium (2) and for this reason the general outline of the code will be kept at a minimum.

[A] The actual name of the code is "Code Concerning Buildings in Disaster Areas"

CODE: A BRIEF OUTLINE

The code is made up of two principal parts: (a) regulations for construction, (b) regulations for the determination of lateral forces. Regulations for construction includes reinforced concrete buildings as well as non-engineered structures such as adobe, masonry, wood frame and stone dwellings. Regulations for the determination of lateral forces are applicable only for engineer designed structures. The total lateral force F is taken proportional to the weight of the structure W with C as the proportionality constant.

$$F = C\,W \tag{1}$$

$$C = C_o \times K \times S \times I \tag{2}$$

In Equation (2), C_o, K and I denote coefficients concerning zoning, building type and importance respectively. S, on the other hand is the "spectrum coefficient" and is determined by the relationship between the natural period of the structure and the predominant period of the soil upon which the structure is located.

$$S = \frac{1}{|0.8 + T - T_o|} \tag{3a}$$

$$S \leq 1 \tag{3b}$$

where T is the natural period of the structure and T_o is the predominant period of the soil, (both in seconds). Figure 1 is a plot of Equation (3) for four values of T_o indicated in Table (2).

CODE: SOIL CONSIDERATIONS

For the determination of T_o, the code is rather elaborate. Below is a paraphrased translation of the related section of the code. Unless determined by experimental, empirical or theoretical means based on reliable essumptions and field observations, the predominant soil period T_o will be taken from Table 1. The values in the table, however, are usable for soil formations up to around 50 meters thick overlying bedrock or formations with characteristics equivalent to bedrock. If the soil thickness is greater than 50 meters shear wave velocity v_s and the soil thickness H_z should be determined experimentally, or theoretically with greater accuracy and predominant soil period should be calculated using

$$T_o = \frac{4H_z}{v_s} \tag{4}$$

In case where it is not possible to determine v_s more accurately by experimental, empirical or theoretical means values for v_s given in Table 2 may be used.

If the soil formation is made up of several layers with different v_s values, then a different T_o should be calculated for each layer.

Formations for which the shear wave velocity exceeds 700 m/sec. may be considered to be very firm, and equivalent to bedrock

A TWO - DIMENSIONAL STUDY

In two previous studies, the problem of random wave propagation in two dimensional layered media was investigated (3,4,5). The method employed in these studies, briefly, was to modify the transfer matrix approach which is used in analyzing layered media, so that the transferred matrix is the frequency response matrix of each layer. After imposing the appropriate boundary conditions; assumed velocity (acceleration, or displacement) power spectra at the bedrock level was "filtered through" the soil layers and thus simulated power spectra (for both P and S waves) were obtained on the ground surface. The following can be expressed as the strong points of the outlined method; (a) ease of handling of any number of soil layers (it should be remembered that in transfer matrix methods the order of matrix stays the same for variable number of layers), (b) consideration of both P and S waves and their comparison, (c) θ (angle of incidence) dependency of the solution. The effects of some of these have been discussed elsewhere with respect to concrete problems (6,7, 8).

In this article, modal periods of a layered soil medium will be discussed and compared with Equation (4). The term "modal" frequency is used here rather than "predominant" as the periods that are considered correspond to vibrational modes of the soil medium. The term "predominant" period, on the other hand, refers to the "average" or expected period which may easily be computed using the power spectra but which may not correspond to a peak value at all if there are more than one mode.

Figure 2 shows three soil layers with indicated Lamé parameters, P and S wave velocities (v_1 and v_2) and angle of incidence $\theta = 45^{\circ}$. These parameters were chosen to represent a soft alluvial soil deposit. d, which is the thickness of each layer, was allowed to take values varying from 1 meter to 70 meters. For each value of d, power spectra were calculated and the periods corresponding to the first three peaks were plotted against d. Figure 3 shows this plot for $0 \leq d \leq 100$ m. It should be pointed out that all the computed points lay almost exactly on the three straight lines and that the regression equations went through theorigin without any forcing. Regression equations for these tree modes are as follows:

$$T = \frac{d}{8.28} \quad \text{(first mode)} \tag{5a}$$

$$T = \frac{d}{11.15} \quad \text{(second mode)} \tag{5b}$$

$$T = \frac{d}{19.11} \quad \text{(third mode)} \tag{5c}$$

Unexpectedly, first mode was not always the most critical

(highest peak). In fact in most cases third mode seemed to govern as d increased. Two of the velocity power spectra (for d = 16 m, and d = 40 m) may be seen in Figures 4 and 5 respectively. In Figure 5, for example it is clear that second mode is more critical than the first.

Now, going back to the regression equations (Equations 5a, 5b, 5c), it may be seen that it is possible by trial and error to investigate the nature of the coefficients (given as denominators) and their velocity dependency. This was done in the following two ways: (a) Instead of d, using H 3d and also using the average of the three velocity values get a relationship between T, H and $\bar{v}$ (either P or S); (b) using d and the velocity of the upper most layer (lowest velocity) get a relationship between T, d and v(either P or S). The results are as follows:

First Mode:

$$T = 2.03 \frac{H}{\bar{v}_2} \quad (6a)$$

$$T = 10.3 \frac{H}{\bar{v}_2} \quad (6b)$$

$$T = 3.9 \frac{d}{v_2} \quad (6c)$$

$$T = 20.0 \frac{d}{v_1} \quad (6d)$$

Second Mode:

$$T = 1.5 \frac{H}{\bar{v}_2} \quad (7a)$$

$$T = 7.7 \frac{H}{\bar{v}_1} \quad (7b)$$

$$T = 2.9 \frac{d}{v_2} \quad (7c)$$

$$T = 14.8 \frac{d}{v_1} \quad (7d)$$

Third Mode:

$$T = 0.88 \frac{H}{\bar{v}_2} \quad (8a)$$

$$T = 4.5 \frac{H}{\bar{v}_2} \quad (8b)$$

$$T = 1.7 \frac{d}{v_2} \quad (8c)$$

$$T = 8.7 \frac{d}{v_1} \quad (8d)$$

As was mentioned before v_1 and v_2 in the above equations denote the P and S wave velocities, respectively, of the upper most layer.

COMPARISON WITH THE CODE

The code recommends Equation (4) for the calculation of T_o if the soil thickness exceeds 50 meters. This seems to be in good agreement with Equation (6c) which was calculated for the upper most layer and the first mode. Furthermore, the code suggests to calculate different T_o values in case of layering and add these up to find the "predominant" period. This is an application of Zeevaert's work (9) where

$$T_n = 4 \sum_{i}^{i} \frac{d_i}{(v_s)_i} \qquad (9)$$

is given. Zeevaert also states that; "The largest resonant periods are obtained by addition of all the soft soil strata confined between the firm base and the ground surface.", but fails to mention that this is true for only the very special case of uncoupled dynamic systems. Soil layers, on the other hand, must be modeled as heavily coupled as idealizations in layering are frequently very arbitrary.

To see the size of the difference between Equations (6) and (9), take, for example, $d = 40$ meters ($H = 120$ meters). Using Equation (6a), $T = 4.83$ sec, and using Equation (9), $T = 10.60$ sec. which is more than twice the value computed using Equation (6a). This difference is easy to explain, however, as an uncoupled system is a "softer" system and therefore has higher predominant periods of vibration.

CONCLUSION

The code formula (Equation 4) should be used with caution and only for soils which may be modeled with a single layer. For the multiple layer case, direct superposition of single layer periods should be avoided as it will invariably yield very high periods.

Equations (6-8) may be used for layered soil in the context of a code if formulae involving P wave velocities are excluded. Two points must be remembered, however, when using these formulae: (a) As the model is linear, the predominant periods for nonlinear behavior will be somewhat larger than given in these equations; (b) These equations are good for "normal" layering, that is to say lowest velocity layer on top, then the next lowest velocity and so on. In case of a sandwiching situation of either a soft or a hard layer, results will be different and a full analysis of the problemshould be undertaken. The results of such a study may be seen in Reference (7).

ACKNOWLEDGEMENT

The author wishes to gratefully acknowledge contributions of Prof. Çetin Soydemir, co-author of Reference (5) from which some results are taken.

REFERENCES

1) Code Concerning Buildings in Disaster Areas , Ministry of Reconstruction and Resettlement of Turkey, July 1975 (in Turkish)

2) Çelebi, M. "Comperative Study of the New Turkish Earthquake Resistant Design Code", Int. Sym. on Earthquake Engineering, University of Missouri, 1976.

3) Özgür, D. and Gürpınar, A. Simulation of Earthquake Acceleration Spectra , TBTAK MAG-302, 1973 (in Turkish)

4) Özgür, D. and Gürpınar A. "A Theoretical Simulation of Earthquake Acceleration Spectra", Proc. Fifth World Conference on Earthquake Engineering, Rome, 1973.

5) Gürpınar, A., Özgür, D. and Soydemir, C., Influence of Soil Conditions on Earthquake Acceleration Spectra, TBTAK MAG-339 1974 (in Turkish)

6) Soydemir, C. Gürpınar, A. and Özkan, Y. "A Geodynamical Study of the Central Ankara Region", Proc. CENTO Symposium on Earthquake Engineering and Engineering Seismology, METU, Ankara, November 1974.

7) Soydemir, Ç. and Gürpınar, A. "A Geodynamical Evaluation of the Elbistan Power Plant Site", Proc. Fifth European Conference on Earthquake Engineering, İstanbul, September 1975

8) Gürpınar, A. et.al. Local Earthquake Study for Nuclear Power Plant Sites, Pro. No. 75-04-09-01, Middle East Technical University, 1975 (in Turkish).

9) Zeevaert, L., Foundation Engineering for Difficult Subsoil Conditions, Van Nostrand Reinhold Co., 1973.

Table 1. Soil Classification for Period Determination

Soil Type	Description	N_{sp} Standard Penetration no.	D_r Relative Density %	q_u Unconfined Compressive Strength kg/cm^2	V_s Shear Wave Velocity m/sec
I	a) Massive volcanic formations, unde - composed metamorphic formations and sedimentary rocks with very hard cement	-	-	-	700
	b) Very firm sand, pebbles,	50	85-100	-	
	c) Very hard clay	32	-	4.0	
II	a) Loose magmatic rocks such as tüff and aglomerates, decomposed sedimentary rocks with planes of discontinuity	-	-	-	400-700
	b) Firm sand, pebbles	30-50	65-85	-	
	c) Hard clay	16-32	-	20-4.0	
III	a) Heavily decomposed metamorphic and sedimentary rocks with soft planes of discondinuity	-	-	-	200-400
	b) Medium firm sand, pebbles	10-30	35-65	-	
	c) Hard Silty clay	8-16	-	1.0-2.0	
	a) Soft and thick alluvium with high water table, marsh or ocean fill	-	-	-	200
	b) Loose sand	0-10	35	-	
	c) Soft silty clay	0-8	-	1.0	

Table 2. Predominant Soil Period

Soil Type		T_o (sec) Predominant Soil Period	T_o (sec) Average
I	a	0.20	0.25
	b	0.25	
	c	0.30	
II	a	0.35	0.42
	b	0.40	
	c	0.50	
III	a	0.55	0.60
	b	0.60	
	c	0.65	
IV	d	0.70	0.80
	b	0.80	
	c	0.90	

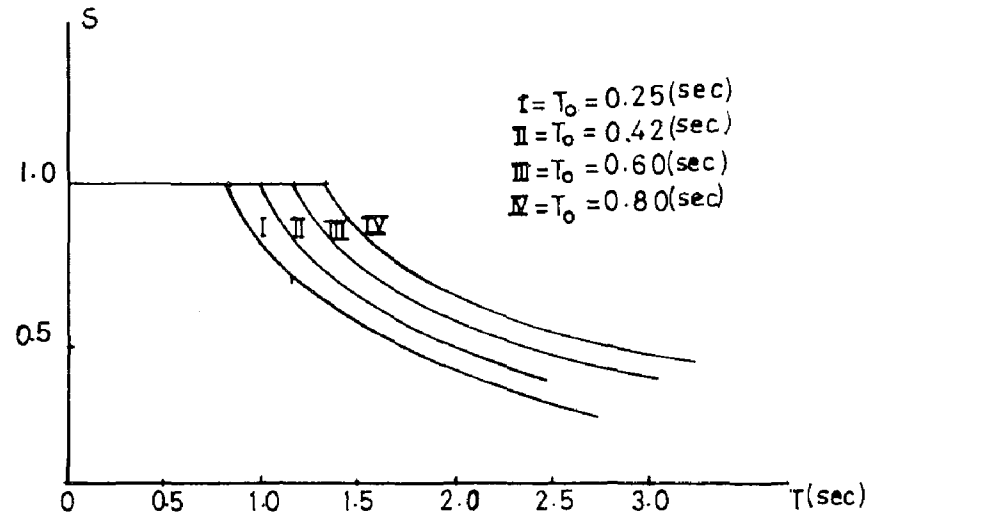

Figure: 1. Spectrum Coefficient for Four Different Soil Predominant Periods (T_o)

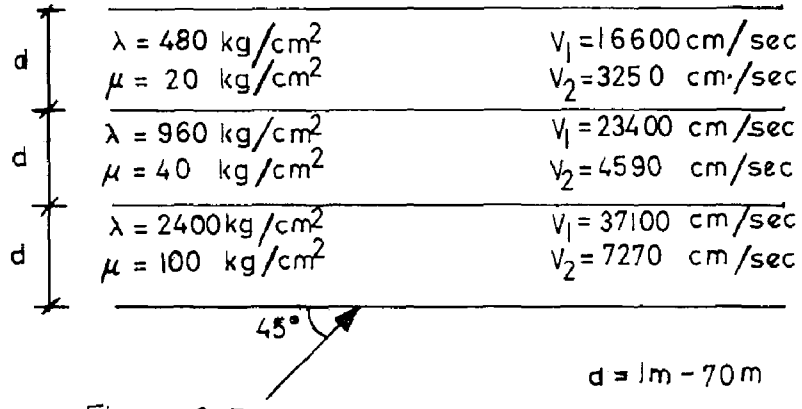

Figure 2. Parameters for Alluvial Soil Deposit

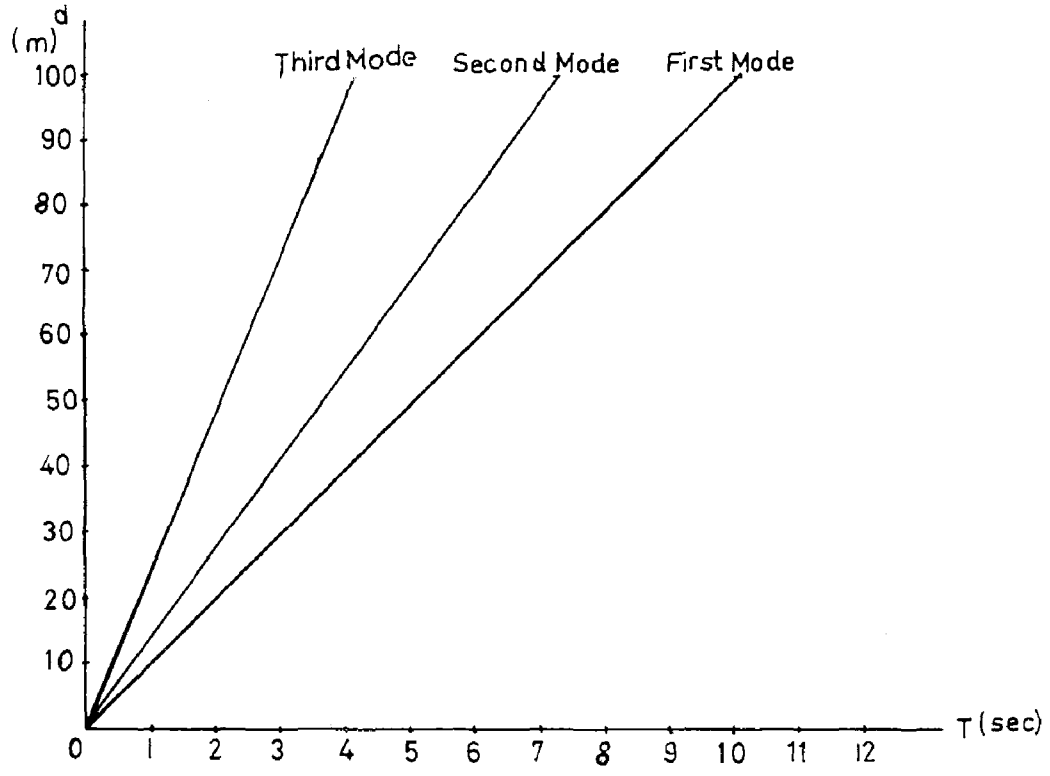

Figure 3. Modal Periods v.s Layer Thickness

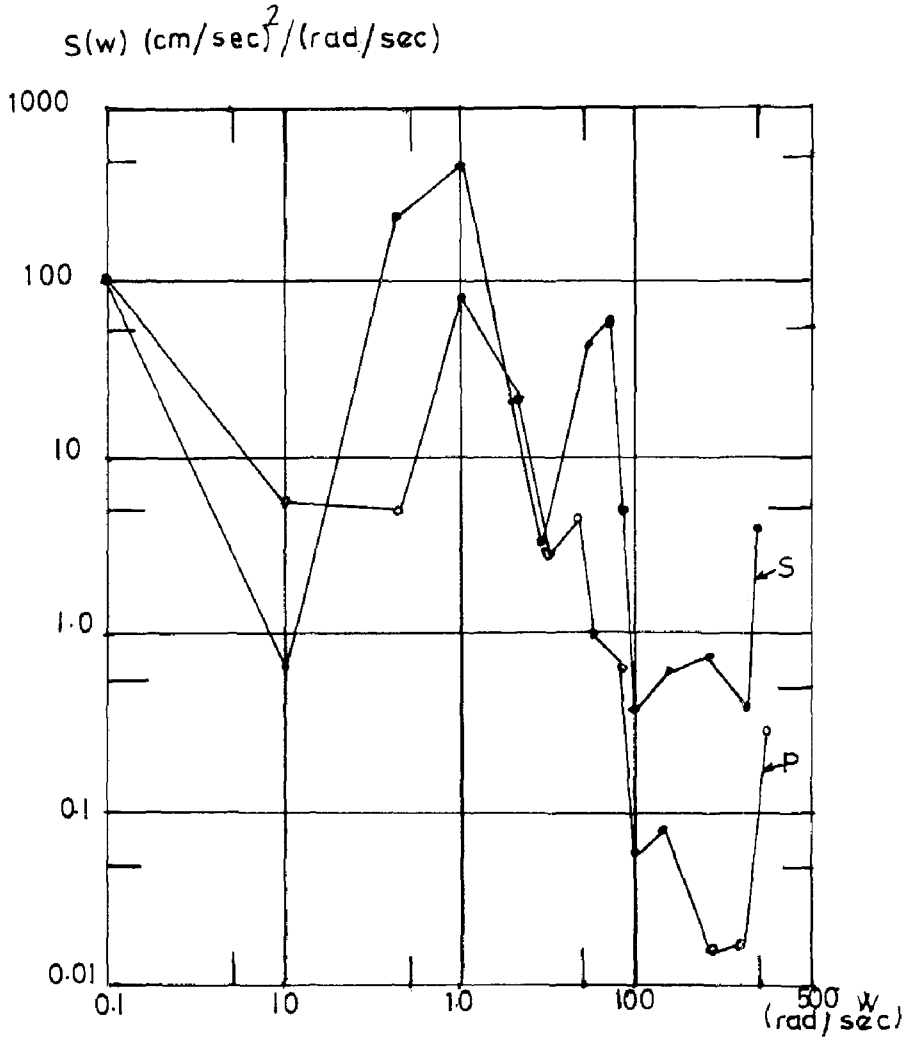

Figure 4. Velocity Spectral Density Function, d=16m

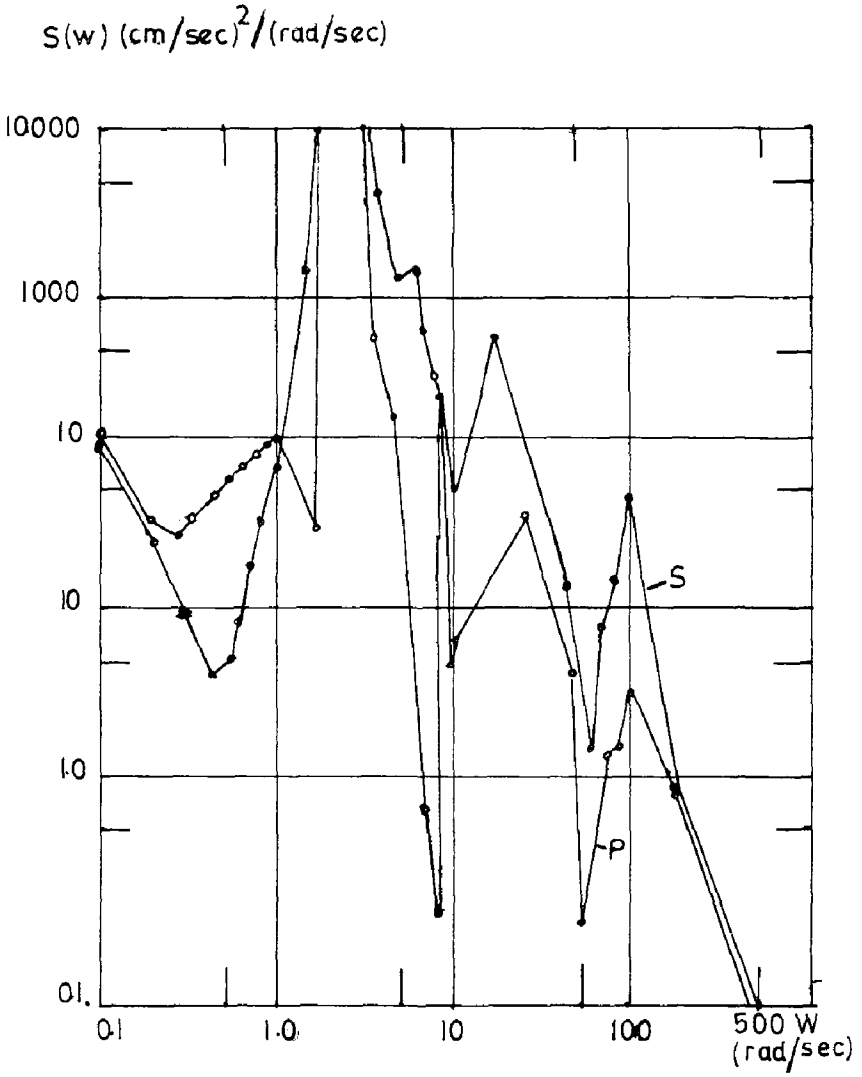

Figure 5. Velocity Spectral Density Function, d=40m

INTERNATIONAL SYMPOSIUM ON
EARTHQUAKE STRUCTURAL ENGINEERING
St. Louis, Missouri, USA, August, 1976

EARTHQUAKE DYNAMIC ENVIRONMENT WITHIN BUILDINGS

K. L. MERZ

Earthquake Research Engineer

Ayres & Hayakawa Energy Management

Los Angeles, California, USA

SUMMARY

An understanding of building response to earthquake ground motion is necessary for nonstructural designers to prepare specifications for equipment manufacturers and suppliers. The proper design of equipment anchorage and the interconnection of nonstructural components within a building requires knowledge of the magnitude of the forces induced in equipment and the deformations imposed upon the components. The present paper provides a review of the actual building motions recorded during the 1971 San Fernando Earthquake to allow realistic estimation of the distribution of floor acceleration and building drifts over a building height. Peak Floor Amplification Factors (FAF) are presented for a sample of 49 high-rise buildings. The statistics of floor acceleration peaks over the time duration of motion are also examined for an example building to provide some information about the probability of exceeding a given value of peak acceleration. The analysis of the records recorded during the 1971 San Fernando earthquake provide data in the form of floor response spectra. This data is reviewed to provide guidance for the design of typical spring mounted (vibration isolated) building service equipment. The relative deflection between floors of a building, or story drift, is a critical parameter. The drift response determined from a recorded building motion is examined to provide guidance for the realistic estimation of building drifts, which are the result of the nonlinear response behavior of buildings.

INTRODUCTION

The nonstructural components of a building include facades, curtain walls, ceilings, partitions, elevators, lights, electrical power systems, plumbing, ventilation and air conditioning systems, heating systems, fire protection systems, telephone and communication systems, storage racks, and even large pieces of owner-supplied furniture or portable equipment. In the past, the usual structural design procedure has been based on the philosophy that to design a building to avoid all damage during a major earthquake is not economically justifiable; the structural system of the building

is intended to be deformed by strong ground motion, and damage to some of the nonstructural elements is expected. However, recent major earthquakes (Alaska 1964, San Fernando 1971, and Managua 1972) have caused considerable damage to the nonstructural elements and electrical/mechanical equipment of buildings sustaining only moderate structural damage. The investigation (1-6)* of the damage caused by these earthquakes has indicated the need for architects and designers of nonstructural building systems to acquire background and additional skills in the analysis and design (7) of these systems for the building dynamic environment caused by the structural response to earthquake ground motion. An even greater emphasis is provided by the fact that approximately 70 percent of the construction cost of a building is for equipment and nonstructural elements. An increasing concern over the life-safety aspects of building design is also apparent. Thus, not only must the substantial monetary investment in nonstructural elements and equipment be protected, but also the systems concerned with insuring life-safety must be made seismic resistant. A building is not safe if, during an earthquake, light fixtures and ceilings fall, elevators do not operate, emergency generators do not come on, loose objects block exits, and broken glass falls into the street. A building is not properly designed if an owner sustains huge losses due to nonstructural damage. The lessons learned by detailed studies of damage sustained by earthquake-tested buildings must be carefully reviewed by both architects and engineers. One lesson from past earthquakes is clear: The amount of damage sustained by nonstructural building components could have been greatly reduced by relatively inexpensive corrective measures.

The development of plans and specifications for a modern building is a team effort, coordinated and managed by an architect. The primary outside consultants on the design team are the structural, mechanical, and electrical engineers. An additional outside consultant is usually retained to design the elevators and the structural engineer and the architect require the services of foundation and soil engineers. Usually, the structural engineer is the only member of the design team to analyze the effect of dynamics forces induced by earthquakes. All members of the design team, however, must inform themselves of the nature of earthquake-induced forces in buildings and of the manner in which the stress paths occur between the structural and nonstructural elements of a building. The structural frame may absorb the earthquake forces without significant damage, but the movement of the building induces significant secondary damage to nonstructural elements. The resulting damage to nonstructural components shows a lack of knowledge among nonstructural designers of building response characteristics due to an earthquake. Since the majority of building service equipment is located both on the ground floor and roof, the nonstructural designer must understand the characteristics and response effects of both ground motion and floor motion.

Since 1965, the City of Los Angeles has required placement of three strong-motion accelergraphs in all new structures greater than six stories in height. Subsequently, adjacent municipalities have adopted similar requirements. These instruments are placed in the basement (base level), mid-portion (intermediate level) and

* Numbers in parenthesis designate references at end of paper.

near the top (upper level) of buildings. The 1971 San Fernando earthquake may be viewed as a full-scale experimental test of a wide variety of building types to strong ground motion. Forty-nine buildings, ranging in height from 7 stories to 43 stories, recorded motion in three component directions at the base level and at least one higher level. These buildings were located at distances from the epicenter ranging from 20km to 83 km and were exposed to peak horizontal base (ground) accelerations ranging from 0.030G to 0.255G and peak vertical base accelerations ranging from 0.019G to 0.171G (1G = 980.6 cm/sec/sec). These recorded accelerograms were uniformly processed, digitized, corrected, and analyzed by the Earthquake Engineering Research Laboratory of the California Institute of Technology. The published (8, 9, 10) data set forms the basis of this paper.

BUILDING AMPLIFICATION

A structural system acts as a mechanical narrow-band filter for earthquake ground motion, amplifying and filtering at approximately the fundamental frequency of the building. The resulting floor motion becomes the input base motion for anchored (and unanchored) equipment. The severity of floor motion is usually measured by the peak or maximum floor acceleration. While the use of peak acceleration as measure of damage is often unsatisfactory, the maximum acceleration parameter is physically understood as a measure of the inertial force that must be resisted by a rigid, anchored object. Figure 1 shows an example of the recorded and processed acceleration data from the 1971 San Fernando earthquake for a horizontal component of building response. For the present discussion the base level is assumed to be the building foundation, the intermediate level is assumed to be at mid-height of the building, and the upper level is assumed to be the building roof. The recorded data (9) is absolute (sum of ground and building motion) acceleration and the absolute displacement is obtained by double integration (9). The spring-mass systems indicated in Figure 1 represent spring-mounted equipment. The occurrence of peak horizontal (largest of two horizontal components) floor acceleration for the recorded building data set is given in Table 1. The occurrence of peak vertical floor acceleration is given in Table 2.

The Floor Amplification Factor is defined:

$$FAF = \frac{\text{Maximum Floor Acceleration of } i^{\text{th}} \text{ Recorded Component}}{\text{Maximum Ground Acceleration of } i^{\text{th}} \text{ Recorded Component}}$$

The horizontal amplification characteristics of the buildings are given in Figure 2 which compares the computed FAF (largest of two component directions) over the range of story heights (11) of the buildings with recorded motion. Figure 3 compares the vertical FAF over the range of story heights. As can be noted from both Figures 2 and 3, the amplification behavior of the buildings is relatively independent of story height with an average horizontal FAF value of 2.3 and an average vertical FAF value of 2.6 for the group of buildings with recorded motion.

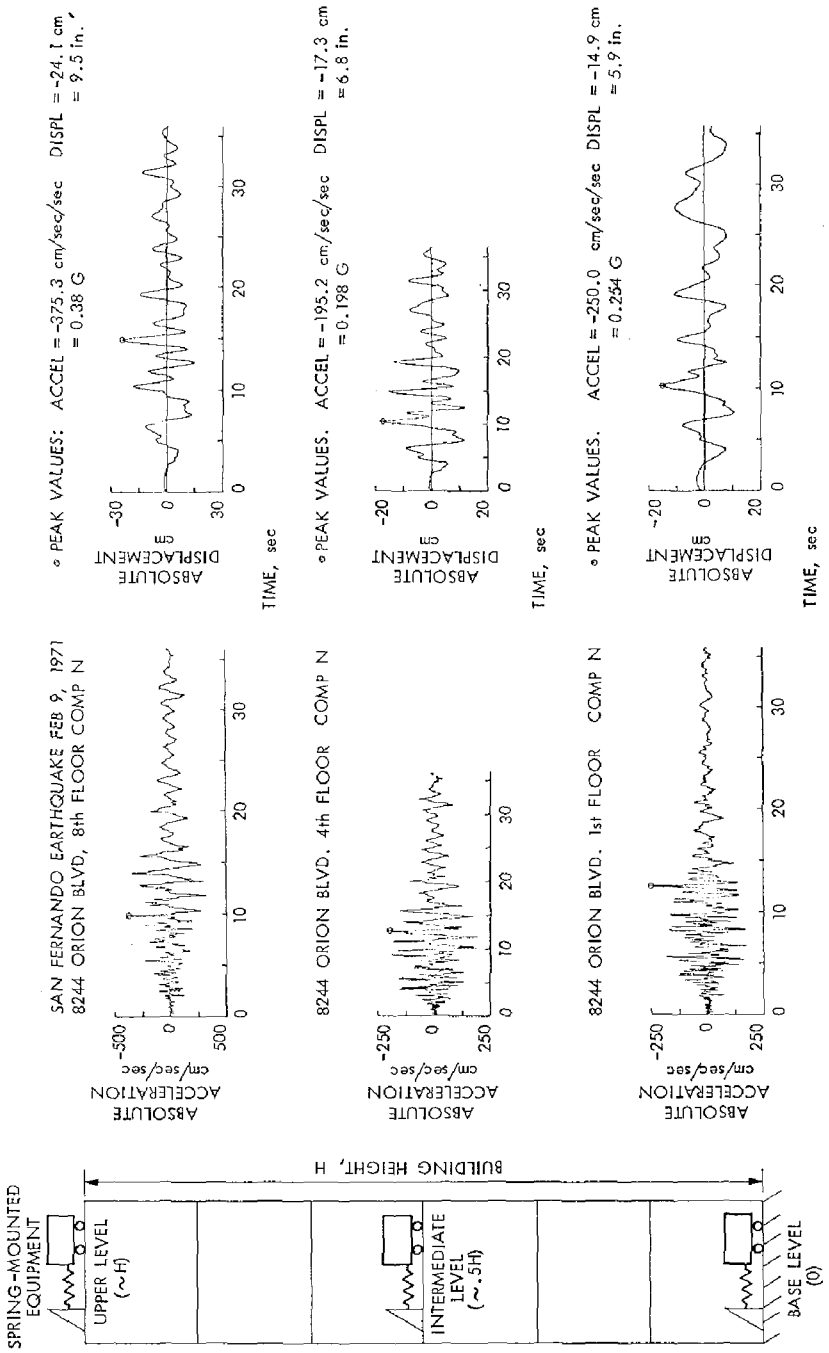

FIGURE 1. EXAMPLE OF RECORDED BUILDING RESPONSE, 1971 SAN FERNANDO EARTHQUAKE.

Floor Level	Total No. of Buildings with Recorded Motion	Horizontal Floor Acceleration Range									
		$\ddot{X} < 0.05G$	$0.05G \leq \ddot{X} < 0.10G$	$0.10G \leq \ddot{X} < 0.15G$	$0.15G \leq \ddot{X} < 0.20G$	$0.20G \leq \ddot{X} < 0.25G$	$0.25G \leq \ddot{X} < 0.30G$	$0.30G \leq \ddot{X} < 0.35G$	$0.35G \leq \ddot{X} < 0.40G$	$0.40G \leq \ddot{X} < 0.45G$	$0.45G \leq \ddot{X} < 0.50G$
Base Level (Ground)	49	4	9	16	13	6	1	-	-	-	-
Intermediate Level (~0.5H)	39	2	2	10	10	8	5	1	1	-	-
Upper Level (~H)	47	-	4	6	6	7	11	4	6	2	1

TABLE 1. OCCURRENCE OF PEAK HORIZONTAL FLOOR ACCELERATION FOR RECORDED BUILDING MOTIONS, 1971 SAN FERNANDO EARTHQUAKE.

Floor Level	Total No. of Buildings with Recorded Motion	Vertical Floor Acceleration Range							
		$\ddot{X} < 0.05G$	$0.05G \leq \ddot{X} < 0.10G$	$0.10G \leq \ddot{X} < 0.15G$	$0.15G \leq \ddot{X} < 0.20G$	$0.20G \leq \ddot{X} < 0.25G$	$0.25G \leq \ddot{X} < 0.30G$	$0.30G \leq \ddot{X} < 0.35G$	$0.35G \leq \ddot{X} < 0.40G$
Base Level (Ground)	49	16	27	4	2	-	-	-	-
Intermediate Level (~0.5H)	38	5	18	8	5	1	1	-	-
Upper Level (~H)	47	3	8	13	11	7	4	-	1

TABLE 2. OCCURRENCE OF PEAK VERTICAL FLOOR ACCELERATION FOR RECORDED BUILDING MOTIONS, 1971 SAN FERNANDO EARTHQUAKE.

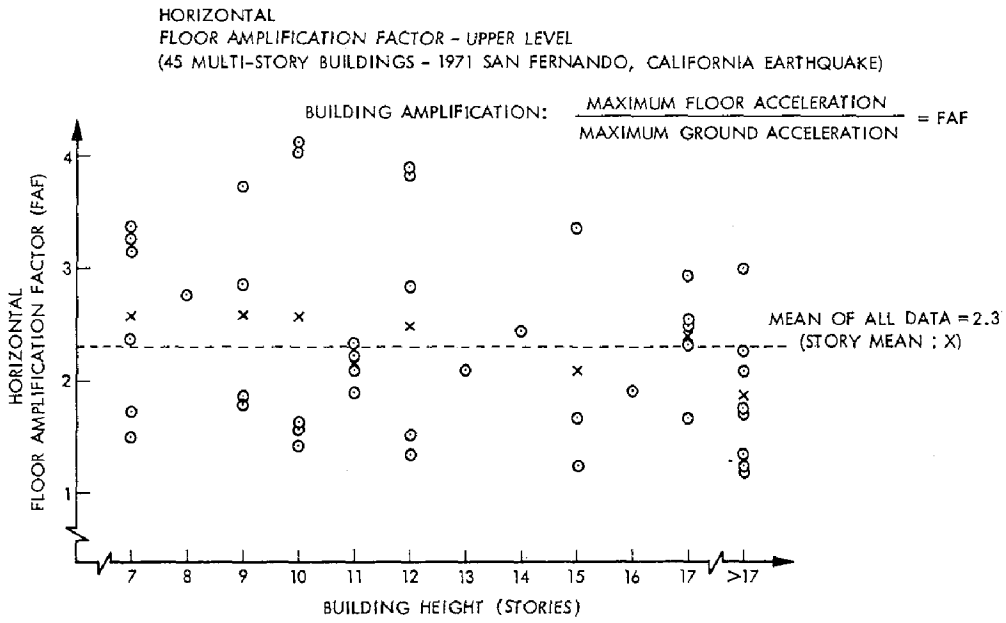

FIGURE 2. HORIZONTAL UPPER LEVEL BUILDING AMPLIFICATION.

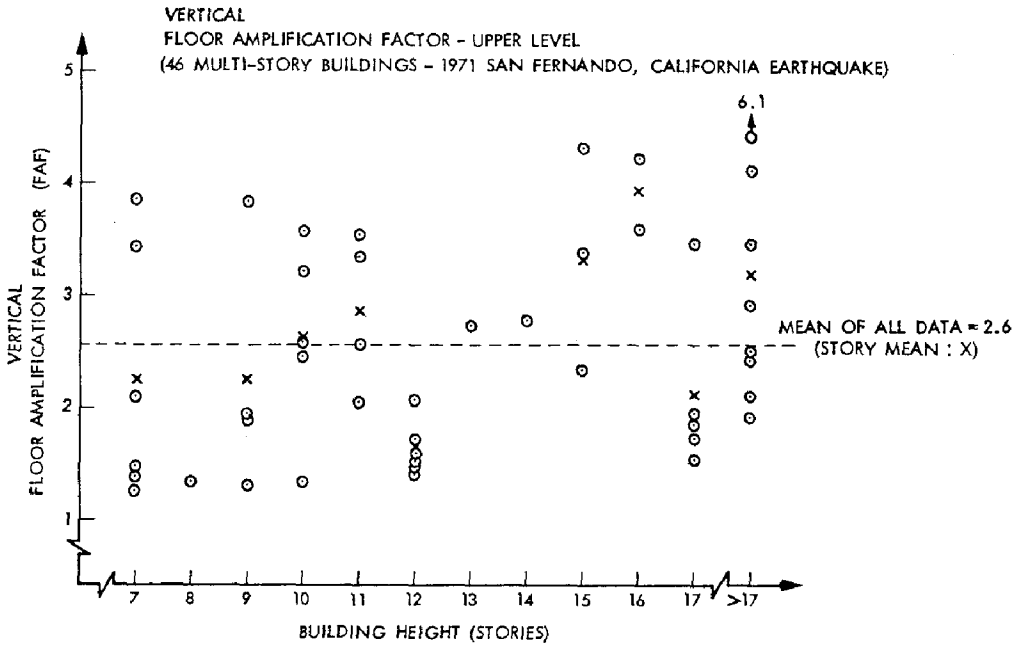

FIGURE 3. VERTICAL UPPER LEVEL BUILDING AMPLIFICATION.

Figures 4 and 5 compare the horizontal and vertical FAF to the maximum recorded ground (base) acceleration. In Figure 4, the largest horizontal FAF is compared to the largest peak ground acceleration, disregarding component direction. This comparison indicates a trend of decreasing building amplification with increasing peak ground acceleration. Assuming that peak recorded base acceleration is a measure of the overall strength or intensity of ground motion, we observe that the amplification decline may be attributed to the increased equivalent damping level caused by accumulated structural damage. However, any use of the data to indicate a definite trend should be avoided due to the few data points greater than 0.20G horizontal and 0.10G vertical. The distribution of amplification over a building height is shown in Figures 6 and 7. Both horizontal and vertical components have the same average amplification, FAF = 1.8, for the intermediate levels.

RESPONSE STATISTICS

The previous discussion characterized the amplification of building motion by the ratio of peak output (floor) acceleration to peak input (base) acceleration. This comparison yielded average values for a large sample of building types, heights, and construction of recent design. The understanding of the response behavior of a building subjected to ground motion is complicated by the effects of three dimensional motion, coupled torsional-lateral response, and non-linear behavior. A great many parameters influence the response of a particular structure including the frequency content of the ground motion at the building site, soil-structure interaction, discontinuities in structural framing, the detailing of the structural connections, and even the stiffness of the non-structural components. In addition, the recorded motion represents the response of a singular point within the structure, thus a wide range of values should be expected when using the extreme or maximum peak values as a measure of response severity.

An example of a recorded building response is shown in Figure 8 for a duration of 35 seconds. The nonlinear filtering behavior of the building is easily noted by the comparison of the base level accelerograph record with the upper level record. The frequency of response during the first 10.7 sec. has considerably higher frequency content than the latter 24.3 sec. of record. If the maxima occurring for each zero crossing are treated as a statistical sample and the mean and standard deviation of the sample computed, the distribution of floor acceleration maxima (12) is closely modeled by an exponential distribution with the computed mean and standard deviation as shown in Figure 9. However, the a priori knowledge of the sample size (i.e. the number of zero crossings) is, in general, not predicable. A more detailed evaluation of the recorded floor motion reveals that the average period of response during the first portion of the record is approximately 0.6 sec. and then lengthens to 1.5 sec. for the remainder of the record. For this presentation, the record was filtered by eye to remove the higher frequencies present in the recorded accelerogram (the larger scale plot contained in (8) was used as a guide; of course the record could also be numerically filtered). If the maxima of this "filtered" record are treated as a separate statistical sample, then the distribution of acceleration maxima is reasonably modeled by a log-normal distribution with the computed sample mean and standard deviation as shown in Figure 9. Now, given that the number of cycles of the fundamental response can be predicted (including nonlinear period lengthening), a procedure for estimating the probability of exceeding a given

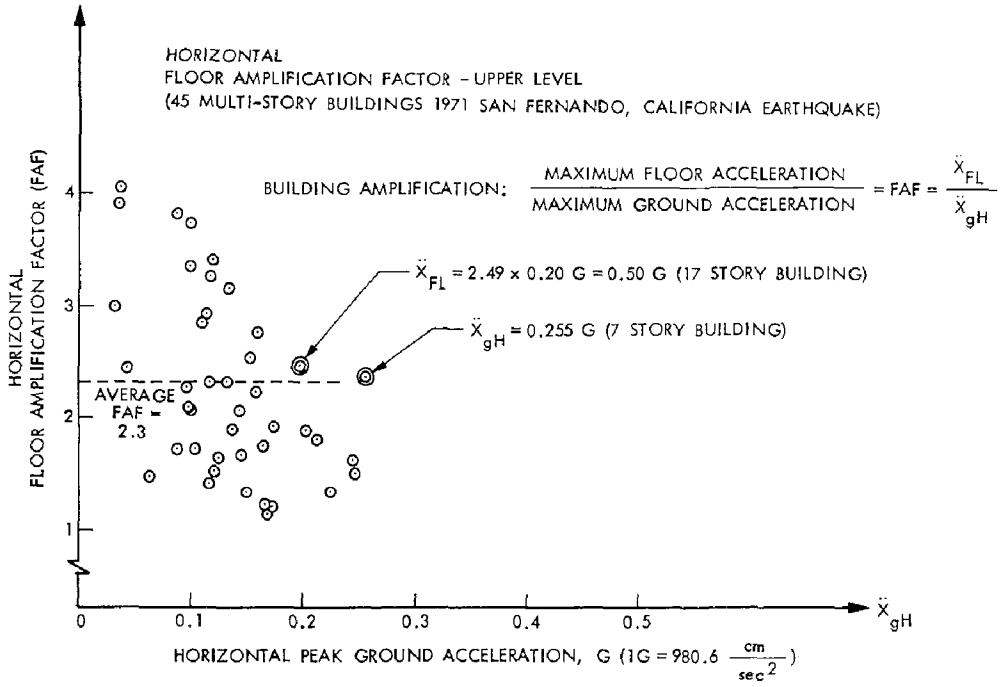

FIGURE 4. HORIZONTAL BUILDING AMPLIFICATION COMPARED TO PEAK GROUND MOTION.

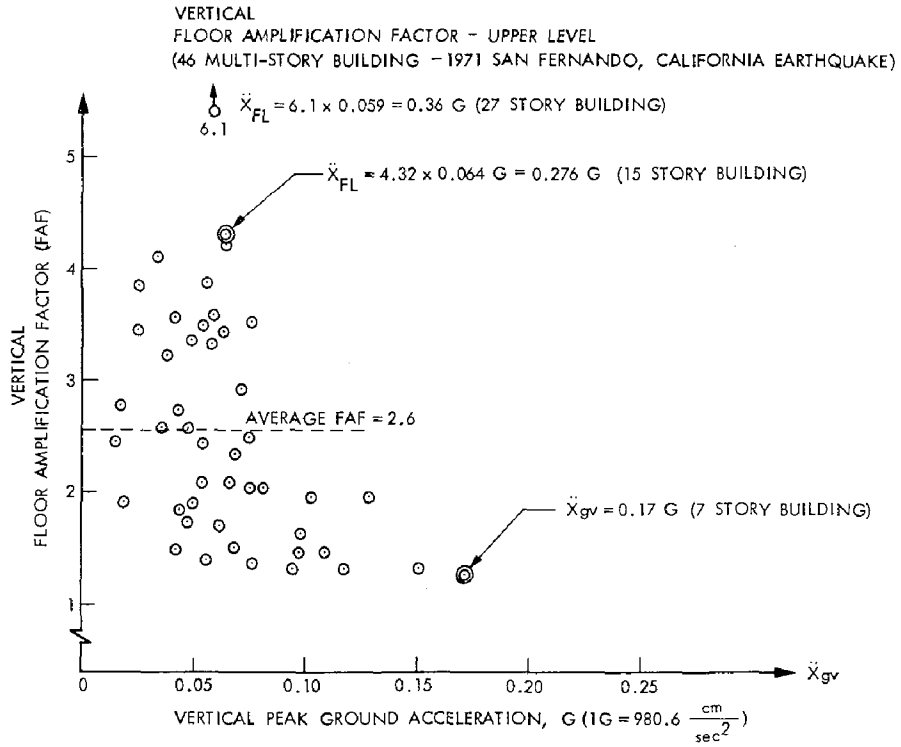

FIGURE 5. VERTICAL BUILDING AMPLIFICATION COMPARED TO PEAK GROUND MOTION.

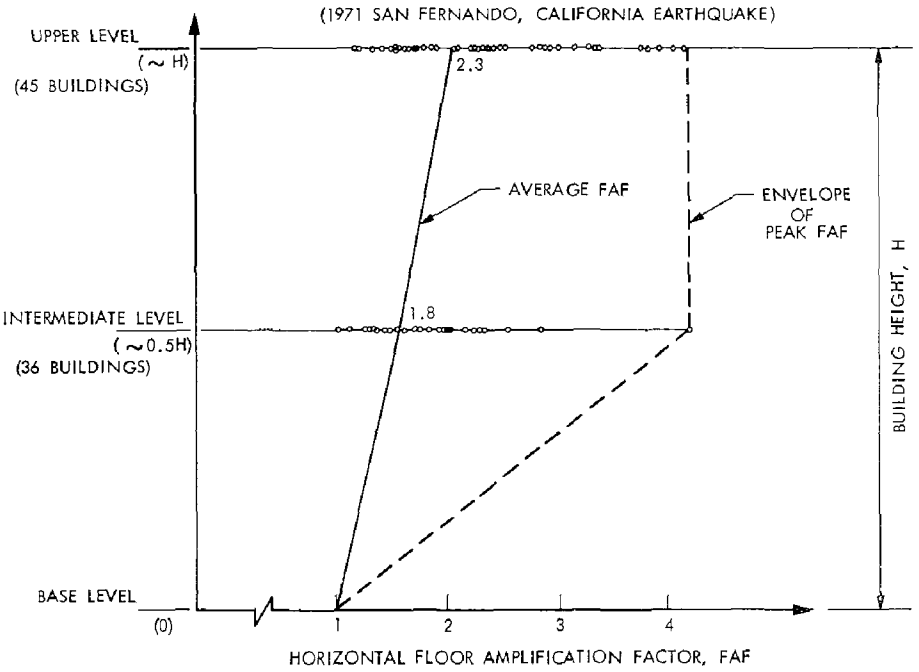

FIGURE 6. DISTRIBUTION OF HORIZONTAL BUILDING AMPLIFICATION OVER BUILDING HEIGHT.

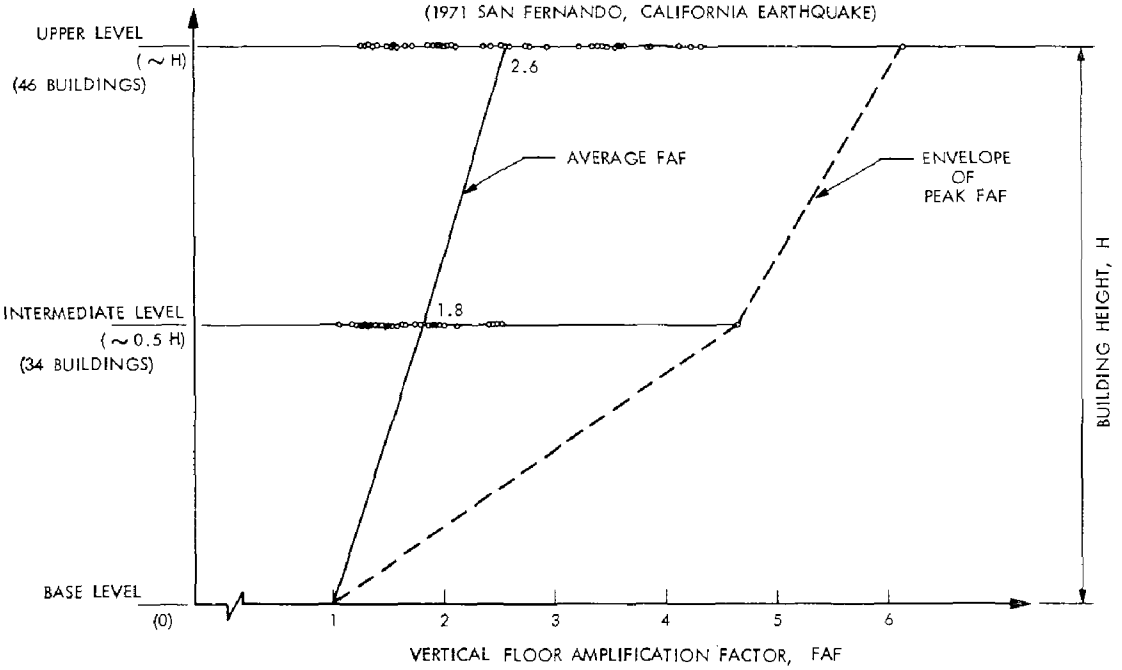

FIGURE 7. DISTRIBUTION OF VERTICAL BUILDING AMPLIFICATION OVER BUILDING HEIGHT.

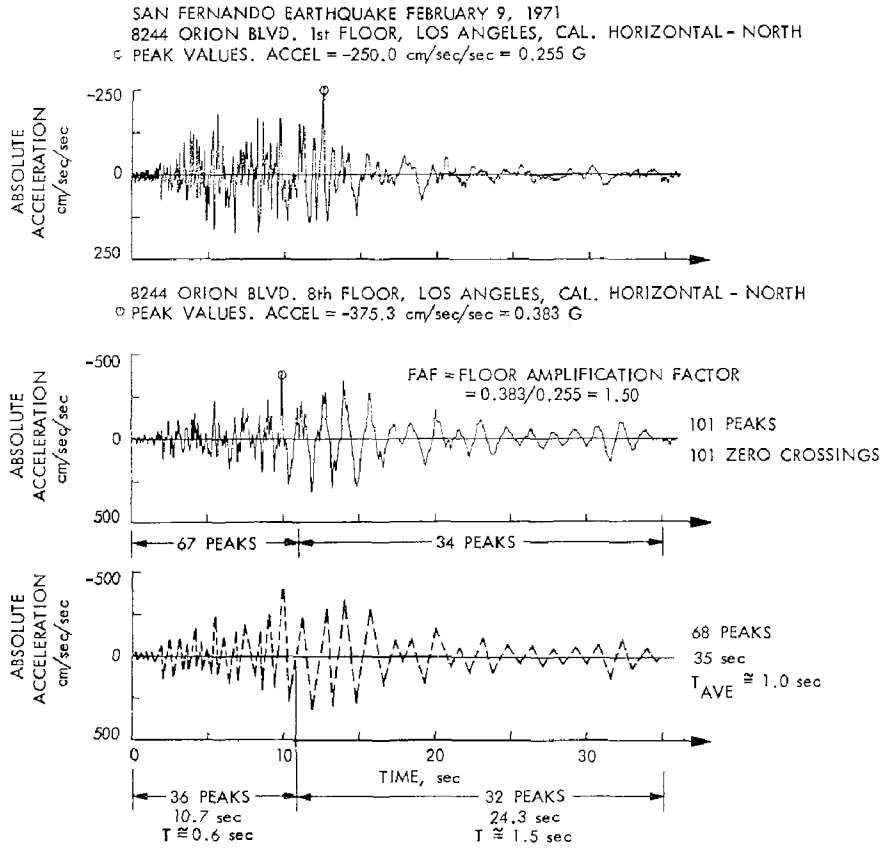

FIGURE 8. EVALUATION OF RECORDED BUILDING MOTION.

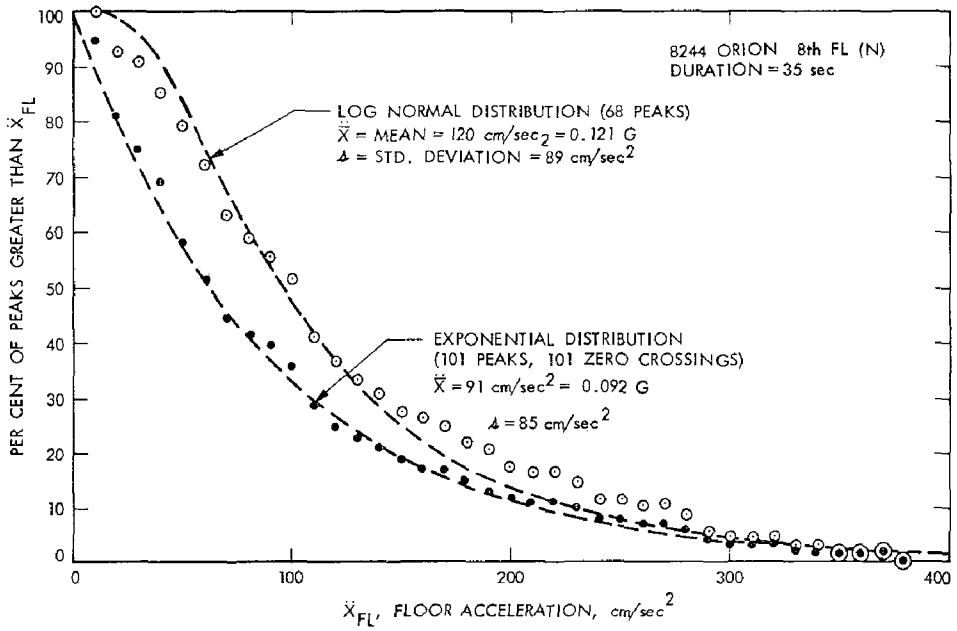

FIGURE 9. DISTRIBUTION OF FLOOR ACCELERATION MAXIMA.

value of floor acceleration is suggested. No definite conclusions should be drawn from the present discussion, since the evaluation of additional recorded building motions is required.

SPRING MOUNTED EQUIPMENT RESPONSE

Building service equipment is often placed on spring mounts, or vibration isolators, to reduce the transmission of equipment vibration to the structure (and tenants). The failure of vibration mounts and the resulting overstress of connecting pipe and conduit is a frequent observation during post-earthquake damage surveys. The specification of spring mounts with 1.0 in.(2.54 cm) static deflection and equal vertical and lateral stiffness is a common practice (13) for building service equipment, resulting in equal vertical and horizontal natural frequencies of 3.1 cps (Hz) (ignoring for the present discussion the effect of rotatory inertia due to a base mount configuration). The response of flexible equipment within a building is best evaluated using floor response spectra. The analysis (10) of the recorded building motions provides computed floor response spectra for each component of building motion recorded.

The Response Spectrum Amplification Factor is defined for a specified range of system frequency and damping:

$$\text{RSAF} = \frac{\text{Response Spectrum Ordinate of } i^{\text{th}} \text{ component}}{\text{Maximum Ground Acceleration of } i^{\text{th}} \text{ component}}$$

The computed RSAF for the lateral response of spring isolated equipment with 1.0 in.static deflection mounts and equal vertical and horizontal stiffness are compared in Figure 10 for equipment located at the base, intermediate, and upper levels of a building. The largest computed (10) response spectrum ordinate (acceleration) within a frequency band, $f = 3.1 \pm 0.4$ cps, for a system with 5% critical damping was used in computing the RSAF of each component of motion. The range of upper level horizontal response spectrum ordinates was 1.85G to 0.123G. The largest RSAF of the two horizontal component directions for each building level is compared in Figure 10. The average amplification for a spring mounted equipment item ($f = 3.1$ cps, 5% damping) was 3.3 at the base level, 5.0 at the intermediate level, and 6.2 at the upper level of the buildings with recorded motion.

BUILDING DRIFT

The response of structures (in terms of structural element stress) at earthquake levels which exceed the design capacity are mitigated by nonlinear behavior but at the expense of large yielding displacements or drifts. Often, drift is the cause of the majority of damage sustained by buildings during an earthquake, since story drift determines the deformation or state of stress that nonstructural elements with floor-to-floor connection such as slab-to-slab partitions (fire-walls), curtain walls, and stairs must accommodate or be damaged by the imposed forces. Exterior and interior glazing, doors, and hung ceilings, while normally not directly connected between floors must accommodate the deformation imposed by the exterior panels or interior partitions. The cost of repairing plaster, drywall, glass, and other drift damage is often

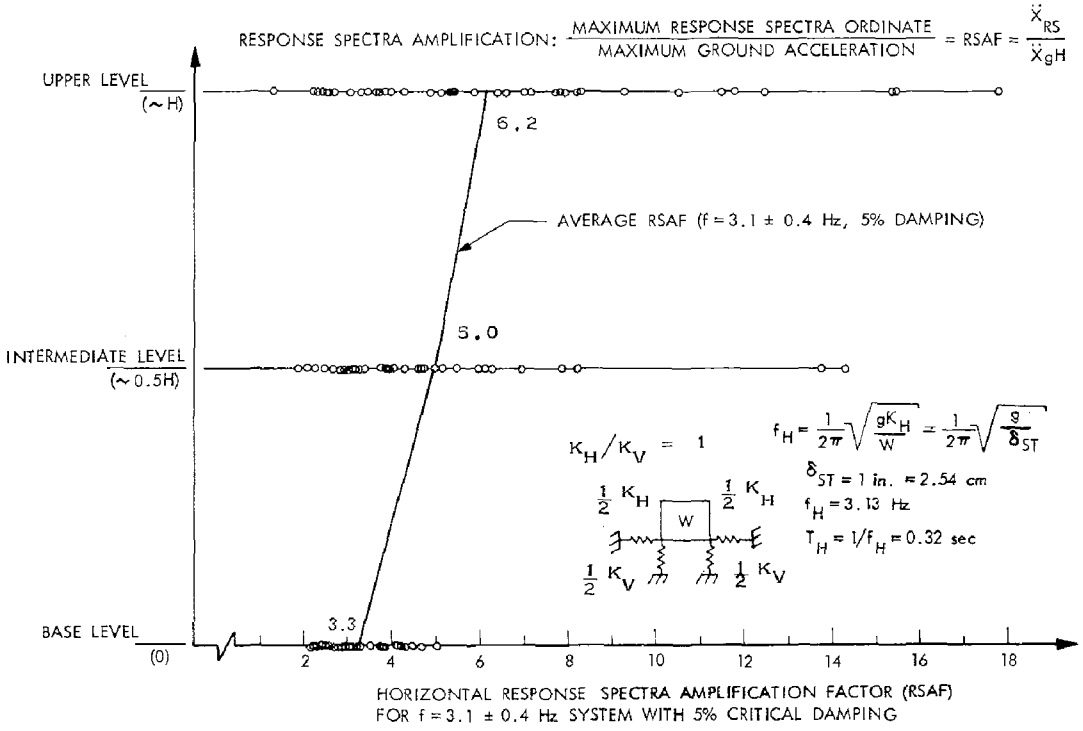

FIGURE 10. SPRING MOUNTED EQUIPMENT RESPONSE AMPLIFICATION.

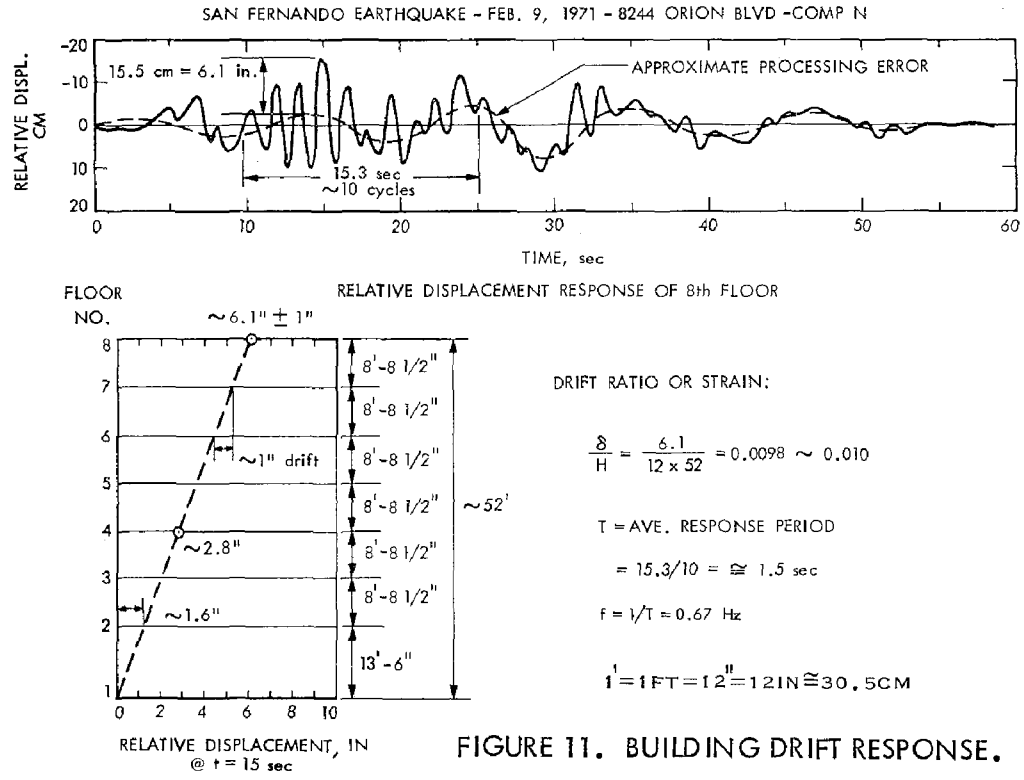

FIGURE 11. BUILDING DRIFT RESPONSE.

the most costly post-earthquake repair item due to the labor manhours required.

The review of actual recorded building motion provides a realistic estimation of building drifts which are the result of the ductile behavior of buildings during moderate earthquakes. Figure 11 gives the drift determined from recorded data (9) obtained from an instrumented multi-story building. The relative displacement response of the building upper level was obtained by graphically subtracting the plotted (9) absolute displacement of the base level from the absolute displacement of the upper level (assuming that both instruments were trigered at the same time). The long period (11 sec) fluctuation is due a processing error caused by misalignment of sectional enlargements of the record during the digitization process (15; see also 9, Part G). Since the relative displacement response is dominated by the fundamental mode, the response of the floors are in phase thus the peak story drift distribution over the building may be estimated by plotting the upper and intermediate peak relative displacements as shown in Figure 11. The peak story drift for this example building was of the order of one inch or 0.01 foot drift per foot of building height which is in accordance with the observed (14) nonstructural damage resulting from the 1971 San Fernando earthquake.

CONCLUSIONS

Recent changes to seismic building code provisions and other organization requirements (16 - 19) have upgraded the lateral force factors for nonstructural elements and equipment, particularly for "critical" facilities. These lateral force factors for essential facilities and building life safety systems range from 0.50 to 1.00. Additional "footnote" provisions to the code lateral force tables suggest the consideration of larger force factors for flexible equipment and equipment located in the upper levels of multistory buildings. The consideration of the amplification experienced in instrumented buildings during the 1971 San Fernando earthquake will, hopefully, allow for realistic and cost-effective seismic nonstructural requirements being included in future construction. Realistic story drifts which range between 0.010 and 0.005 times the story height should be considered in the detailing of nonstructural components.

REFERENCES

1. Ayres, J.M., Sun, T.Y., and Brown, F.R., "Nonstructural Damage to Buildings", The Great Alaska Earthquake of 1964: Engineering, National Academy of Sciences, Washington, D.C., 1973, p. 346.
2. Ayres, J.M. and Sun, T.Y., "Nonstructural Damage", The San Fernando California Earthquake of February 9, 1971, National Oceanic & Atmospheric Administration, Washington, D.C., 1973, p. 735 (Vol.1B).
3. Earthquake Engineering Research Institute, "Managua, Nicaragua Earthquake of December 23, 1972", Conference Proceedings, Vol. I & II, November 1973, San Francisco.
4. Lew, H.S., Leyendecker, E.V., Dikkers, R.D., Engineering Aspects of the 1971 San Fernando Earthquake, National Bureau of Standards, BSS 40, December 1971.

5. Jephcott, D.K. and Hudson, D.E., The Performance of Public School Plants During the San Fernando Earthquake, Earthquake Engineering Research Laboratory, California Institute of Technology, September 1974.
6. Jennings, P.C., "Engineering Features of the San Fernando Earthquake of February 9, 1971", Report EERL 71-02, Earthquake Engineering Research Laboratory, California Institute of Technology, June 1971.
7. Ayres, J.M. and Sun, T.Y., "Criteria for Building Services and Fumishings", Building Practices for Disaster Mitigation, Building Science Series 46, U.S. Department of Commerce, National Bureau of Standards, February 1973, p. 253.
8. Trifunac, M.D., et al, Strong Motion Earthquake Accelerograms Digitized and Plotted Data, Vol. I: Uncorrected Accelerograms, Parts C-S, Earthquake Engineering Research Laboratory, California Institute of Technology, Pasadena, California, 1971-1974.
9. Trifunac, M.D., et al, Strong Motion Earthquake Accelerograms Digitized and Plotted Data, Vol. II: Corrected Accelerograms and Integrated Ground Velocity and Displacement Curves, Parts C-S, Earthquake Engineering Research Laboratory, California Institute of Technology, Pasadena, California, 1971-1974.
10. Trifunac, M.D., et al, Analysis of Strong Motion Earthquake Accelerograms, Vol. III: Response Spectra, Parts C-S, Earthquake Engineering Research Laboratory, California Institute of Technology, Pasadena, California, 1971-1974.
11. Hudson, D.E., Strong-Motion Instrumental Data on the San Fernando Earthquake of Feb. 9, 1971, Earthquake Engineering Research Laboratory, California Institute of Technology, September, 1971.
12. Hart, G.C., et al, "Ambient, Aftershock, and Mainshock Response of Two High Rise Buildings", Proceedings of the International Conference on Microzonation for Safer Construction, Research & Application, Seattle, Washington, October 30 - November 3, 1972.
13. ASHRAE Handbook & Product Directory, 1973 Systems Volume, Chapter 35, "Sound and Vibration Control", American Society of Heating, Refrigerating & Air Conditioning Engineers, New York, New York, 1973.
14. John A. Blume & Associates, Engineers, "Holiday Inn - Orion Avenue", The San Fernando California Earthquake of February 9, 1971, National Oceanic & Atmospheric Administration, Washington, D.C., 1973, p. 359 (Vol. IA).
15. Iemura, H. and Jennings, P.C., "Hysteretic Response of a Nine-Story Reinforced Concrete Building", Earthquake Engineering and Structural Dynamics, Vol. 3, p.p. (183-201), 1974.
16. International Conference of Building Officials, "Annual Report of the Code Changes Committee, Fiscal Year 1974-1975", Building Standards, Part III, May-June 1975.
17. Departments of the Army, the Navy, and the Air Force, Seismic Design for Buildings, Army TM 5-809-10, Navy NAV FAC P-355, Air Force AFM 88-3, Chapter 13, April 1973.
18. Veterans Administration, Earthquake Resistant Design Requirements for VA Hospital Facilities, Handbook H-08-8, Office of Construction, Washington, D.C., June 1973 (Revised March 1974).
19. State of California, California Administrative Code, Title 17. Chapter 8. Safety of Construction of Hospitals, 1974.

INTERNATIONAL SYMPOSIUM ON
EARTHQUAKE STRUCTURAL ENGINEERING
St. Louis, Missouri, USA, August, 1976

ON EARTHQUAKE RESISTANT DESIGN OF A SUBMERGED TUNNEL

by

CHOSHIRO TAMURA* and SHUNZO OKAMOTO**

* Professor, Institute of Industrial Science,
University of Tokyo, J a p a n
** President of The University of Saitama
Professor emeritus of University
of Tokyo, J a p a n

S u m m a r y

For the purpose of earthquake resistant designing of a submerged tunnel, mathematical model of the tunnel for dynamic analysis on it's behavior during earthquakes is shown. Earthquake resistant design data obtained from dynamic response analysis of the tunnels to typical earthquake motions in various ground conditions are presented,comparison between result from the earthquake observation on the real tunnel and that from numerical analysis using the presented data is shown and practical method to estimate the stresses in the tunnel during earthquakes is presented.

§.1 Mathematical Model for Dynamic Analysis

Authors presented the mathematical model of the submerged tunnel for dynamic analysis,synthesizing the results from vibration tests on the model and that from the earthquake observation on real submerged tunnel.(1) The basic conceptions to formation of the mathematical model were as follows, assuming that the ground was composed of a simple surface layer on the hard base layer for an idealized ground condition.

(1) It is assumed that the vibration characteristics of the ground is not affected by the presence of a submerged tunnel. The fundamental mode of shear vibration of the surface layer is ordinarily most predominant in the displacement of the ground in time of severe earthquakes,which is considered to give the greatest influence on the strain generated in the submerged tunnel during earthquakes, therefore only this fundamental mode of the vibration is considered in this case.

(2) The effect of inertia force of the tunnel itself upon the behavior of the tunnel is not considered since it is very small.

---

(1) C.TAMURA,S.OKAMOTO and M.HAMADA; DYNAMIC BEHAVIOR OF A SUBMERGED TUNNEL DURING EARTHQUAKE, Report of the Institute of Industrial Science, University of Tokyo, Vol. 24,No. 5, March, 1975

(3) The deformation of the tunnel is calculated from the deformation of the ground along the tunnel, by assuming that the tunnel is a beam on the elastic foundation (the characteristics of the foundation is not necessarily limited to a linear type).

(4) Horizontal vibrations in two directions, along the tunnel axis and perpendicular to it, are analyzed.

According to the assumptions(1),(2) and (3) above,the deformation of the submerged tunnel is calculated from the deformation of the ground along the tunnel axis. The mathematical model of the ground used here is a multiple mass-spring model,as shown in Fig. 1, composed of mass M_e ,spring K_3 , K_{zx}(in the direction of the tunnel axis) and K_{zy}(in the direction perpendicular to the tunnel axis).

The ground along the tunnel axis is divided into a number of segments, and each segment of the ground is replaced with one mass-spring model having the same period with the fundamental natural period of the ground segment. The mass M_{ei} is the equivalent mass of the fundamental vibration mode of the ground segment i. The K_{3i} is the spring of one mass-one spring system which represents the ground segment i . The adjacent masses of point i and i-1 are connected by spring K_{zx}(i~i-1)and K_{zy}(i~i-1). Spring $K_{zx}$is related to the resistance to the axial relative displacement between adjacent ground segment, while spring $K_{zy}$is related to the shear resistance to the relative displacement between adjacent segments.

If the fundamental vibration mode of the ground along vertical axis at mass point i is taken as $\Phi_i(z)$(z denotes the depth from the ground surface) and the mass of the ground segment i is denoted by $m_i(z)$, the equivalent mass M_{ei} will be expressed as

$$M_{ei}=\frac{\{\int_0^{h_i} m_i(z)\phi_i(z)dz\}^2}{\int_0^{h_i} m_i(z)\phi_i^2(z)\,dz} \qquad \cdots (1)$$

where h_i : the thickness of the surface layer at the ground segment i ; and

$m_i(z)$: the soil mass of the ground segment i per unit depth at the depth z

The spring K_{3i} is obtained as follows.

$$K_{3i} = M_{ei}\cdot(\frac{2\pi}{T_i})^2 \qquad \cdots (2)$$

where T_i : fundamental natural period of the ground segment i

When mass point i has caused unit displacement, the displacement $f_i(z)$ at the depth z can be expressed as

$$f_i(z) = \frac{\int_0^{h_i} m_i(z)\,dz}{\int_0^{h_i} m_i(z)\phi_i(z)dz}\,\phi_i(z) \qquad \cdots (3)$$

The displacement of mass points can be obtained from the following equation.

$$[M]\{\ddot{D}\} + [C]\{\dot{D}\} + [K]\{D\} = -[\bar{M}]\{\ddot{z}\} \qquad \text{.....(4)}$$

where

$[M]$: Mass matrix of equivalent mass Me_i;
$[C]$: Damping matrix ;
$[K]$: Stiffness matrix composed of spring constants K_{3i} and $K_{2x,i}$or $K_{2Y,i}$;
$\{D\}$: Displacement vector of mass points ;
$[\bar{M}]$: Mass matrix of $\bar{M}e$which is a product of Me and participation factor which is the ratio of Me to the mass of the ground ; and
$\{\ddot{z}\}$: Vector representing seismic acceleration on base layer.

Since the tunnel is assumed as a beam upon an elastic ground, the displacement of the tunnel can be determined by the following equations, neglecting the inertia force of the tunnel by assumption (2).

In the direction perpendicular to the tunnel axis,

$$EI\frac{d^4V}{dx^4} + K_y(V-V_g) = 0 \qquad \text{..... (5)}$$

where

V ,V_g : Displacement of the tunnel in the direction perpendicular to the tunnel axis and that of the ground calculated by equations(3) and (4),respectively;
K_y : Coefficient of subgrade reaction in the direction perpendicular to the tunnel axis;
EI : Bending rigidity of the tunnel.

In the direction of the tunnel axis,

$$EA\frac{d^2U}{dx^2} - K_x(U-U_g) = 0 \qquad \text{..... (6)}$$

where

U ,U_g : Displacement of the tunnel in the axial direction and that of the ground calculated by equations (3) and (4),respectively;
K_x : Coefficient of subgrade reaction in the axial direction;
EA : Rigidity of axial direction of the tunnel.

For the purpose of examination the propriety of the model above mentioned ,comparisons were made between the result of the response analysis by the method and that of the model test on a tunnel. Reasonably good agreements are found between these results.

§.2 Earthquake Resistant Design Data for Submerged Tunnel

To investigate the dynamic behaviors of submerged tunnel by numerical analysis and to develope the practical earthquake resistant design, typical ground conditions,typical submerged tunnels and seismic waves were selected and the linear earthquake response including the stress and strain response were calculated for more 260 cases by the method described above. About fundamental elements which were seemed to have great effect on the behavior of the tunnel during earthquake, that is, period of the ground,length and shape of slope, dimension of cross-section of the tunnel and coeffi-

cient of subgrade reaction and input seismic waves, their influences were studied on the behavior of the tunnel. Typical profile of the ground and the tunnel for analysis were shown in Fig.3. In this ground model, it is assumed that the land part and the sea-bottom part have fundamental natural periods T_1 and T_2, respectively,and that the transitional ground condition between both parts changes linearly or bi-linearly.

For the input seismic waves, the following three earthquakes records were used.

A) Hachinohe EW (Off-Tokachi Earthquake,1968,M=7.8,Δ=170km)
B) Taft EW (Tehachapi Earthquke,1952,M=7.7,Δ=40km)
C) El Centro NS (Imperial Valley Earthquake,1940,M=7.0,Δ=6km)

Fig.4 shows the displacement response spectra for the three records of which maximum accelerations were modified as 100 gals. Damping factor was 0.1 to critical damping. The response spectra show that three earthquake records have the different characteristics, especially the response displacement of Hachinohe EW within the periods of 0.8 sec to 2.0 sec are two to three times larger than for the other two records.(Fig.4)

The maximum response axial stress (σ_t) in the tunnel due to axial deformation and the maximum response fiber stress (σ_B) in the tunnel due to bending deformation varied greatly owing to the input seismic waves of which maximum accelerations were modified to 100 gals. So that, to decrease the deviation of these stresses due to the input seismic waves, they were normalized as follows,taking the relative displacement of the ground of land part and the sea-bottom part into account.

$$\bar{\sigma}_t = \frac{\sigma_t}{D_L + D_s}(\mathrm{kg/cm^2/cm}) \qquad \bar{\sigma}_B = \frac{\sigma_B}{D_L + D_s}(\mathrm{kg/cm^2/cm})$$

where D_L is the value of the response displacement corresponding to the period of the land part obtained by the response spectrum, while D_s is that of the sea-bottom part.

In this analysis, Young's modulus of the reinforced concrete of the tunnel was assumed to be 3×10^6 ton/m^2 referred to the data of the real structures.

Results of the numerical analysis were as followings:

1) Influence of natural period of the ground on stresses

σ_t and σ_B were calculated assuming that the area of the tunnel section of 90 m^2, the moment inertia of 7000 m^4, the length of the slope of 150 m, the uniform gradient slope, $\beta_x(=\sqrt{K_x/EA})$ of 0.55×10^{-2}(1/m) and $\beta_Y(=\sqrt[4]{K_Y/EI})$ of 0.275×10^{-1}(1/m). By selecting only the maximum values of $\bar{\sigma}_t$ and $\bar{\sigma}_B$ from the results regardless of input seismic waves to every combination of T_1 and T_2, relations between $\bar{\sigma}_t$ or $\bar{\sigma}_B$, T_1 and T_2 were obtained as shown in Figs. 5 and 6. It is observed that $\bar{\sigma}_t$ and $\bar{\sigma}_B$ increase as the difference between T_1 and T_2 increase. If fundamental period of the ground of the land part and that of the sea-bottom part are known, it will be possible to obtain the approximate value of stress that will be developed in the tunnel during earthquakes by using Figs.5 and 6 for ordinal ground condition.

However, the appropriate modification should be done for the different condition as described in the following section, and only the shear vibration of the ground is considered on idealized ground condition assuming that the propagation velocity of the seismic wave in the base layer is within the range of infinity. Therefore, stresses will be nil if the natural period of the ground of the land part is equall to that of the sea-bottom part. Considering the assumption in the analysis and the actual behaviors of the ground observed from the field observations, when the difference of periods is small the values on the lines of $T_2 = 0.9 \times T_1$ in the Figs.5 and 6 is recommended for the minimum value of the stresses in the design of submerged tunnels.

The values of $\bar{\sigma}_t$ and $\bar{\sigma}_B$ in Figs.5 and 6 are hereinafter referred to standard values of $\bar{\sigma}_t$ and $\bar{\sigma}_B$, respectively.

2) Influence of length of slope on stresses

The influence of the horizontal length of the slope (herein after refered to L) on stresses on the tunnel was studied by using seven combinations of T_1 and T_2. It was assumed that the gradient of the slope was uniform and $\beta_x = 0.55 \times 10^{-2}$ (1/m) and $\beta_Y = 0.275 \times 10^{-2}$ (1/m).

Fig.7 shows the ratio of $\bar{\sigma}_t$ on condition of various length of the slope to the standard value of $\bar{\sigma}_t$ in Fig.5 and also Fig.8 for $\bar{\sigma}_B$. And the distributions of maximum response axial force and maximum response bending moment on the tunnel axis were shown in Figs.9 and 18. From the results, it is observed that the effect of L on $\bar{\sigma}_t$ is comparatively small and the differece of $\bar{\sigma}_t$ by L is within about 10%. On the contrary, L has a great influence over the distribution of bending stress $\bar{\sigma}_B$.

3) Influence of coefficient of subgrade reaction and rigidity of tunnel on stresses

The deformation of the tunnel caused by the deformation of the ground depend on greatly on the rigidity of the tunnel (EA or EI) and the coefficient of subgrade reaction. Fig.10 shows the ratio of $\bar{\sigma}_t$ on condition of various β_x to the standard value of $\bar{\sigma}_t$ shown in Fig.5. Fig.11 shows the values of $\bar{\sigma}_B$ on condition of various β_Y. As to $\bar{\sigma}_t$, increase of the $\bar{\sigma}_t$ to the increase of the β_x is shown aproximatly in bi-linear relation and the influence of β_x on $\bar{\sigma}_t$ is almost independent on L. The increasing rate of $\bar{\sigma}_B$ with an increase of β_Y varied a little corresponding to the relation between T_1 and T_2.

4) Influence of shape of slope on stresses

The influence of the shape of the slope on $\bar{\sigma}_t$ and $\bar{\sigma}_B$ was studied. Fig. 12 and 13 show the ratios of $\bar{\sigma}_t$ and $\bar{\sigma}_B$ on condition of the slope of bi-linear type to those in Figs.5 and 6, respectively. From Figs.12 and 13, it is observed that the slope has a great influence on the magnitude and distribution of the bending stresses, whereas it has comparatively small influence on those of axial stress.

§.3 Application of design data to analysis of earthquake record

1) Outline of ground condition and tunnel

Earthquake observation has been continued at the Haneda submerged tunnel (railway) since 1970. Geological condition of the site of the tunnel

is shown in Fig. 15. The soft alluvial layer consisted of mainly silty clay covers the hard diluvial sand gravel layer of N-value 50 or more. The thickness of the alluvial layer is 35 m to 40 m in the center of the river and gradually becomes thinner in the right bank of the river.

The submerged tunnel is composed of 6 elements having an oval shape section (about 8 m in height and 13 m in width and the wall is reinforced concrete of about 1 m in thickness covered by corrosion-proof steel plate), each measuring 80 m in length. The mechanical values of the tunnel and the ground used for analysis are as follows;

Cross sectional area A = 30 m^2, moment inertia I = 650 m^4, section modulus 1/100(1/m^3), Young's modulus of the tunnel materials E = 3×10^6 ton/m^2, K_Y= 8000 ton/m^2, $\beta_x=\sqrt{K_x/EA}$ = 0.0082 (1/m), K_x= 6000 ton/m^2, and $\beta_Y=\sqrt[4]{K_Y/EI}$ = 0.045 (1/m).

2) Earthquake record analysed

Fig. 16 is a portion of the record of earthquake which occured at 280 km south of Tokyo near the Hachijo Island, Dec. 4, 1972. The magnitude is 7.3, the depth of origin is 50 km and the epicentral distance to the tunnel is about 280 km. In Fig.16, No.4 TSA is acceleration perpendicular to the tunnel axis and No.5 ~ No.8 are axial strains at the both side of the tunnel wall at two points set 50 m apart. In this record, maximum acceleration is 14.7 gals and the maximum strain is 20.4×10^{-6}.

As shown in the figure, main portions of the acceleration and of the strain were not coincide, and frequency characteristics of these records were nonstational, so that, the records were divided into the following four sections: (1) The section which includes the major portions of the records, of acceleration and strain (0 to 107.8 sec), (2) The succeeding section where there is low frequency component having strain waveforms of more than 1 Hz and all waveforms are stationary (108 to 139.8 sec.), (3) The section which corresponds to the last part of the records where vibrations of around 0.14 Hz are predominant in strain waveforms (171 to 203.4 sec.) and (4) the section where the strain shows the maximum value (56 to 80 sec.). (a),(b),(c) and (d) in Fig. 17 show the power spectra of acceleration corresponding to the mentioned above sections (1),(2),(3) and (4), respectively, and (a),(b), (c) and (d) in Fig. 18 also show those of strain corresponding to the sections, respectively.

3) Ground motion

The ground motion of the tunnel site during earthquakes is essential to investigate the behavior of the tunnel, but in the observation the ground motion was not observed owing to inconviniences of the instrumentation. So that, for the purpose of estimation of the ground motion at the site in time of the earthquake , Dec.4, 1972, results of the earthquake observation performed by the Public Work Research Institute, Ministry of Construction, at the Ukishima Park which located 4 km from the tunnel along the right embankment to the estuary of the Tama river, were referred. From the results of boring at the park, well compacted sand layer of N-value 60 or more was covered by soft silty clay of 50 m in thickness. This geological condition is similar to that of the tunnel site. About 7 gals and about 60 gals of maximum acceleration in the earthquake were recorded at the depth of 127 m and on the ground surface, respectively. The former maximum acceleration was appreciated to be valuable to estimation of the acceleration in the gravel sand layer of the site, because this value was not so affected by the soft alluvial layer on

the ground surface.

Fig. 22 shows the predominant periods obtained from the micro-tremor observation along the axis of the tunnel. The abscissa denotes the tunnel axis, and numbers correspond to the number of the elements. The predominant period of the micro-tremor were in accordance well with those of acceleration records and strain records of the earthquake.

The model ground conditions of the right side and of the center part of the Tama river were constructed refering these data and the data obtained at Ukishima Park. In Fig. 23, frequency response of the models calculated by wave propagation theory are shown. For the three-layer system (center part of the river) frequency components of 0.30 Hz. 0.577 Hz and 1.09 Hz are magnified in 7.0, 11.7 and 4.1 times and for the two-layer system, (right side of the river) frequency components of 0.3 Hz, 0.743 Hz and 1.19 Hz are magnified to 5.6, 10.0 and 5.7 times, respectively. The ratio of the standard deviation for the ground surface to that for the ground at the depth of 127 m which were calculated from the frequency response curve, is 2.35. From this ratio, the acceleration on the ground surface was estimated to be 2.35 times of 7 gals, that is, 16.5 gals, although this is not completely the maximum acceleration.

Fig.25 shows the ratio of the amplitude of the tunnel to that of the ground of which displacement curves are assumed to be sine wave. Fig.26 shows strains in the tunnel wall due to axial deformation and due to bending deformation. In these figures, $(K_Y/EI)=4.1\times10^{-6}$, $(K_X/EA)=6.67\times10^{-5}$ are correspond to the tunnel considered. Amplitude of the sine wave is 1 m.

From these figures, it is clarified that the wave length of the ground motion gives an influence on these values in this case, especially in the case of comparatively short wave length and that the acceleration of the ground at the level of the tunnel may become greater than that of the tunnel.

From the facts above mentioned, in this case, maximum acceleration of the ground was assumed to be 1.2 times of that of the tunnel independently from frequency, maximum acceleration becomes about 17 gals.

In (d) in Fig. 18, frequency components of 0.27 Hz, 0.56 Hz, 0.87 Hz and 1.28 Hz were predominant. Acceleration calculated from the power of the power spectra were 1.0 gal, 3.2 gals, 3.8 gals and 2.4 gals for 0.27 Hz, 0.56 Hz 0.87 Hz and 1.28 Hz, respectively. After multiplying these values by 1.2 and dividing by square of each circular frequency, displacement amplitude of the ground were obtained as 0.42 cm, 0.3 cm, 0.15 cm and 0.05 cm in order of lower frequency.

4) Estimation of stress in tunnel

Since the surface ground was expected to be consisted of three layer in case of this site, the ground condition is not so simple as the ground condition assumed in § 2. During severe earthquakes, each natural vibration of the surface ground may be generated indivisually. So, in this case, strains produced in the tunnel during the earthquake must be treated separately in each frequency component.

Using the ground displacement determined previously, the maximum stress in the tunnel during the earthquake was calculated to each frequency as follows;

$$\sigma = \delta_t \times \bar{\sigma} \times C_L \times C_\beta \times C_s$$

where

δ_t: Response displacement of the ground at the depth of the tunnel;
$\bar{\sigma}$: Standard value for T_1 and T_2;
C_L: Compensation factor for the length of slope;
C_β: Compensation factor for the value of β ;
C_s: Compensation factor for the shape of slope.

$\bar{\sigma}$, C_L, C_β and C_s were determined by Fig.5 or Fig.6, Fig.7 or Fig.8, Fig.10 or Fig.11 and Fig.12 or Fig.13, respectively. In this case, value of $\bar{\sigma}$ for 0.27 Hz and 1.28 Hz were selected from the values on the line of $T_2 = 0.9\ T_1$, because there are predominant vibration with frequency nearly equall to this frequency in both part of the right side and the center of the river. $\bar{\sigma}$ for 0.27 Hz was estimated by extrapolation of the line. The length of the slope was considered about 150 m, then $C_L = 1.0$ and $C_s = 1.0$ was assumed. C_β was expected by Fig.10 to be 1.4 and also 1.3 from the line of case 5 in Fig.11.

σ for each frequency was calculated as follows;

	Hz	δ_t(cm)	$\bar{\sigma}$(kg/cm^3)	C_β	C_L	C_s	σ(kg/cm^2)
σ_t	0.27	0.42	2.5	1.4	1.0	1.0	1.5
	0.56	0.30	6.0	1.4	1.0	1.0	2.5
	0.87	0.15	6.0	1.4	1.0	1.0	1.3
	1.28	0.05	6.0	1.4	1.0	1.0	0.4
σ_B	0.27	0.42	0.0	1.3	1.0	1.0	0.0
	0.56	0.30	4.0	1.3	1.0	1.0	1.6
	0.87	0.15	4.0	1.3	1.0	1.0	0.8
	1.28	0.05	2.5	1.3	1.0	1.0	0.2

Using these values, $\sqrt{\Sigma\sigma^2}$ and $\Sigma|\sigma|$ were determined as 3.7 kg/cm^2 and 8.3 kg/cm^2. So that, it was known that maximum strain observed in the tunnel during the earthquake (maximum strain x Young's modulus), 6.4 kg/cm lies between these values.

Another analysis of this type was carried in case of the earthquake of M = 6.2 and a similar result was obtained.

The results mentioned above show that this proposed method is capable of estimating of the stress (strain) in the tunnel during earthquakes, if the ground displacement in time of the earthquakes is given.

Using a response velocity spectrum to the hard ground presented by the Public Work Research Institute, Ministry of Construction, Japan, as shown in Fig.14, an estimation of the stress in the tunnel in time of the earthquake was carried out in the same process described above. Surface layer of 210 m in thickness of the site was converted to two- or three- layer linear vibration system. The damping factors were decided only taking the energy dissipation of the vibration system into the base layer. Because the energy loss of the

surface layer due to nonlinear characteristics of the soil during the earthquake was estimated to be comparatively small. Dynamic characteristics of the model ground is shown as follows;

	Hz	Me/M (%)	δ_s	δ_c	h(%)	S(cm/sec)
3-layer	0.28	75	7.0	3.80	13.3	10.5
	0.58	6	11.7	2.33	22.0	7.5
	1.09	12	4.1	1.66	31.8	5.9
2-layer	0.29	79	5.6	2.85	17.8	8.9
	0.75	8	10.0	1.30	42.5	4.5
	1.19	5	5.7	1.24	45.2	4.5

where

Me : equivalent mass;

δ_s : response magnification of the ground surface to unit input;

δ_c : response magnification of the center of the gravity of each mode to unit input;

h : damping factor (ratio to critical damping)

$$h^2 = (1-\sqrt{1-(1/\delta_c)^2})/2 \ ;$$

S : response velocity to the input of 100 gals.

From Fig.14, response velocity of the center of gravity for each mode was determined and the displacements of the ground at the level of the tunnel to maximum input acceleration of 6 gals which derived from the standard deviation of the frequency response curve of the ground at 127 m in depth, were decided. The maximum stresses obtained were as follows,

$$\sqrt{\Sigma\sigma^2} = 8.7 \ (kg/cm^2) \qquad \Sigma|\sigma| = 19.8 \ (kg/cm^2)$$

These valued were somewhat larger comparing with those values calculated previously.

§ 4 Consideration on input earthquake motion

In this paper, a practical method to estimate the stresses generated in the tunnel during earthquakes was shown and appreciated. In this method, it is fundamental to get information of the dynamic characteristics of the ground and of the frequency characteristics of the earthquake motion of the base layer.

Figs. 20 and 21 are results of the earthquake observation at the Haneda Submerged Tunnel (Railway). The similar figures in reference (I) were revised and added by new data and replaced by these figures. Fig. 20 shows the relation between the maximum strain and the maximum acceleration in the tunnel during earthquakes. From this figure, it is clear that, although the maximum strain increases as the maximum acceleration increases, the one value deviates considerably corresponding to the other. By investigation on the earthquake records in detail, it is found out that the deviation of these values depends greatly upon the frequency characteristics of the earthquake motion, that is, magnitude of frequency component corresponding to the lower natural frequency of the ground. Fig. 21 shows the relation between the maximum strain and the epicentral distance taking the magnitude of the earthquakes as a parameter. From this figure, it is noted that the maximum strain does not so vary by the epicentral distance when the magnitude of the earthquakes is constant, compared with the variation of the maximum acceleration by the epicentral distance. These facts show that a careful selection of the input earthquake motion taking the frequency characteristics and the magnitude into account in dynamic analysis on the tunnel is just necessary.

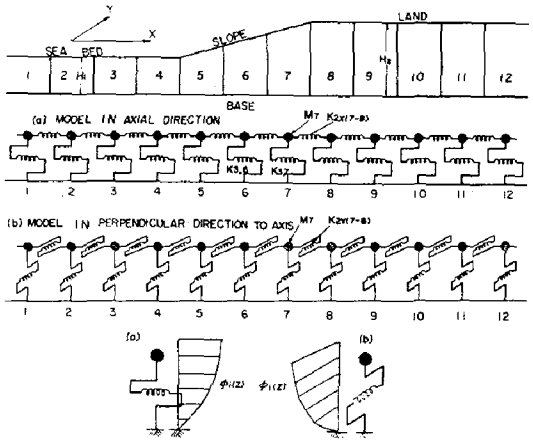

Fig. 1 Mathematical model of tunnel

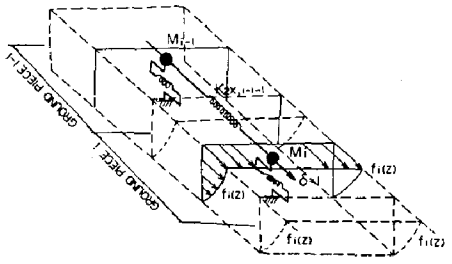

Fig. 2 Illustration of spring K2X

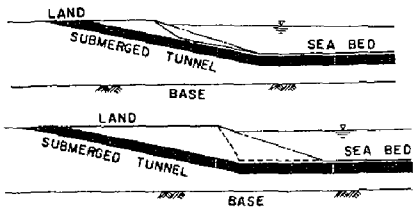

Fig. 3 Typical profile of ground and tunnel for analysis

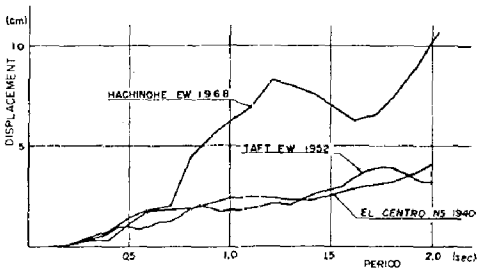

Fig. 4 Displacement response spectra of modified earthquakes with max. accelerations of 100 gal

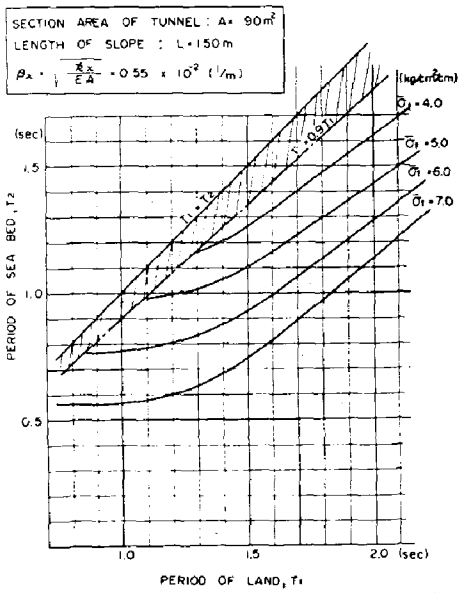

Fig. 5 Max. response axial stresses of tunnel

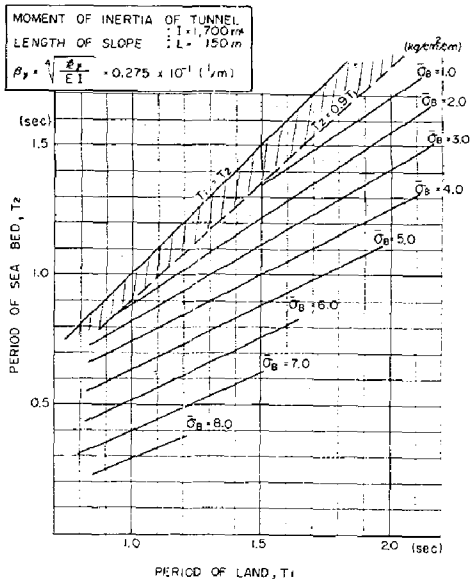

Fig. 6 Max. response fiber stresses of tunnel due to bending deformation

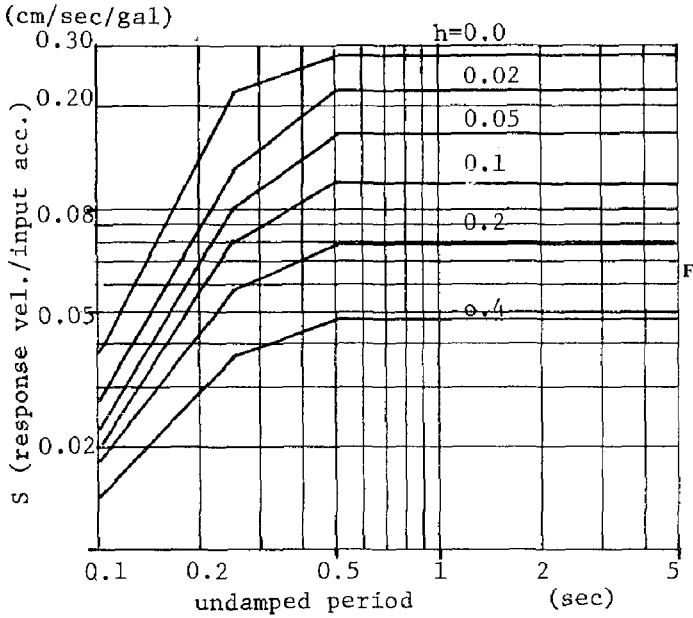

Fig. 14 Response vel. to input acc. of 1 gal

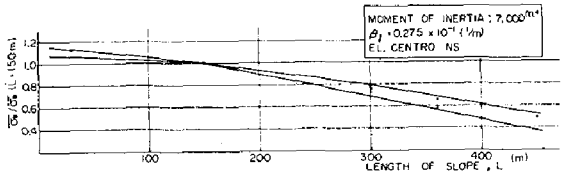

Fig. 8 Relation between σ_B/σ_B (L=150m) and L

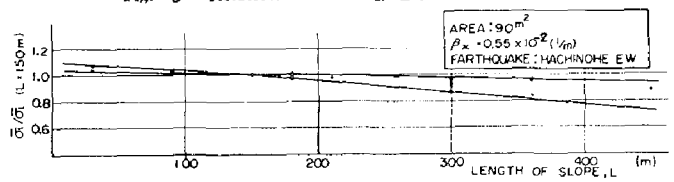

Fig. 7 Relation between $\bar{\sigma}_t/\bar{\sigma}_t$(L=150m) and l

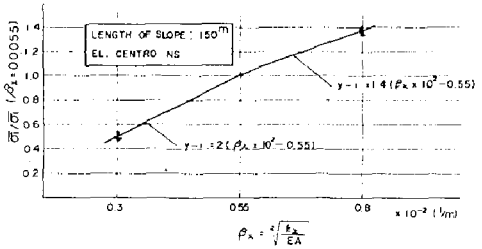

Fig. 10 Influence of β_B on $\bar{\sigma}_t/\bar{\sigma}_l$ (β = 0.0055) (L = 150m)

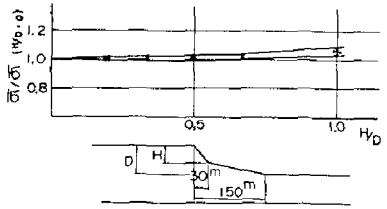

Fig. 12 Influence of shape of slope on $\bar{\sigma}_t/\bar{\sigma}_t(H/D=0)$

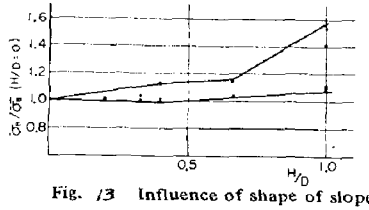

Fig. 13 Influence of shape of slope on $\bar{\sigma}_B/\bar{\sigma}_B$(H/D = 0)

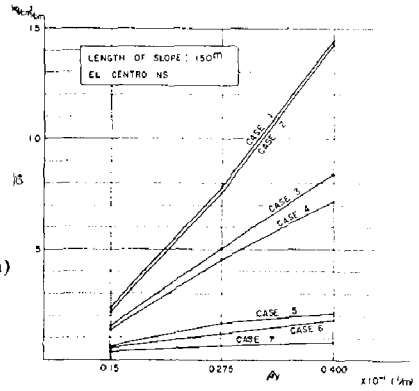

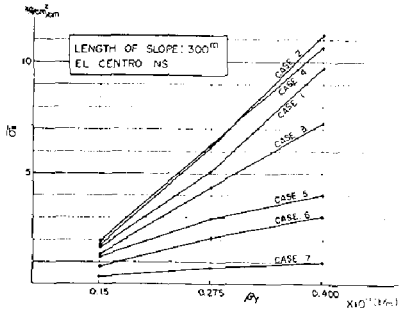

CASE	T_1 (sec)	T_2 (sec)	CASE	T_1 (sec)	T_2 (sec)
1	0.80	0.371	5	1.60	1.171
2	1.20	0.485	6	2.00	1.286
3	1.20	0.771	7	2.00	1.571
4	1.60	0.886		—	—

Fig. 11 Influence of β_y on $\bar{\sigma}_B$ (L-300m)

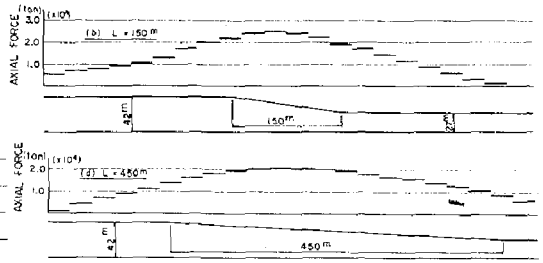

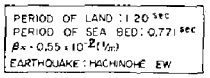

Fig. 9 Distrubution of max. response axial force of Tunnel

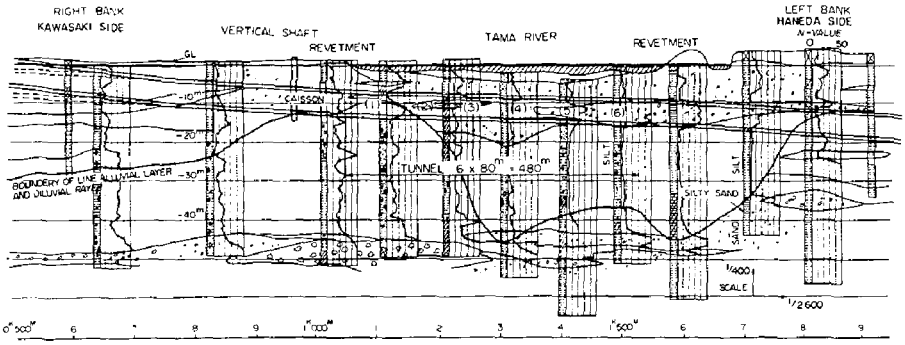

Fig. 15 Geological map of the site of the Haneda Submerged Tunnel (Railway)

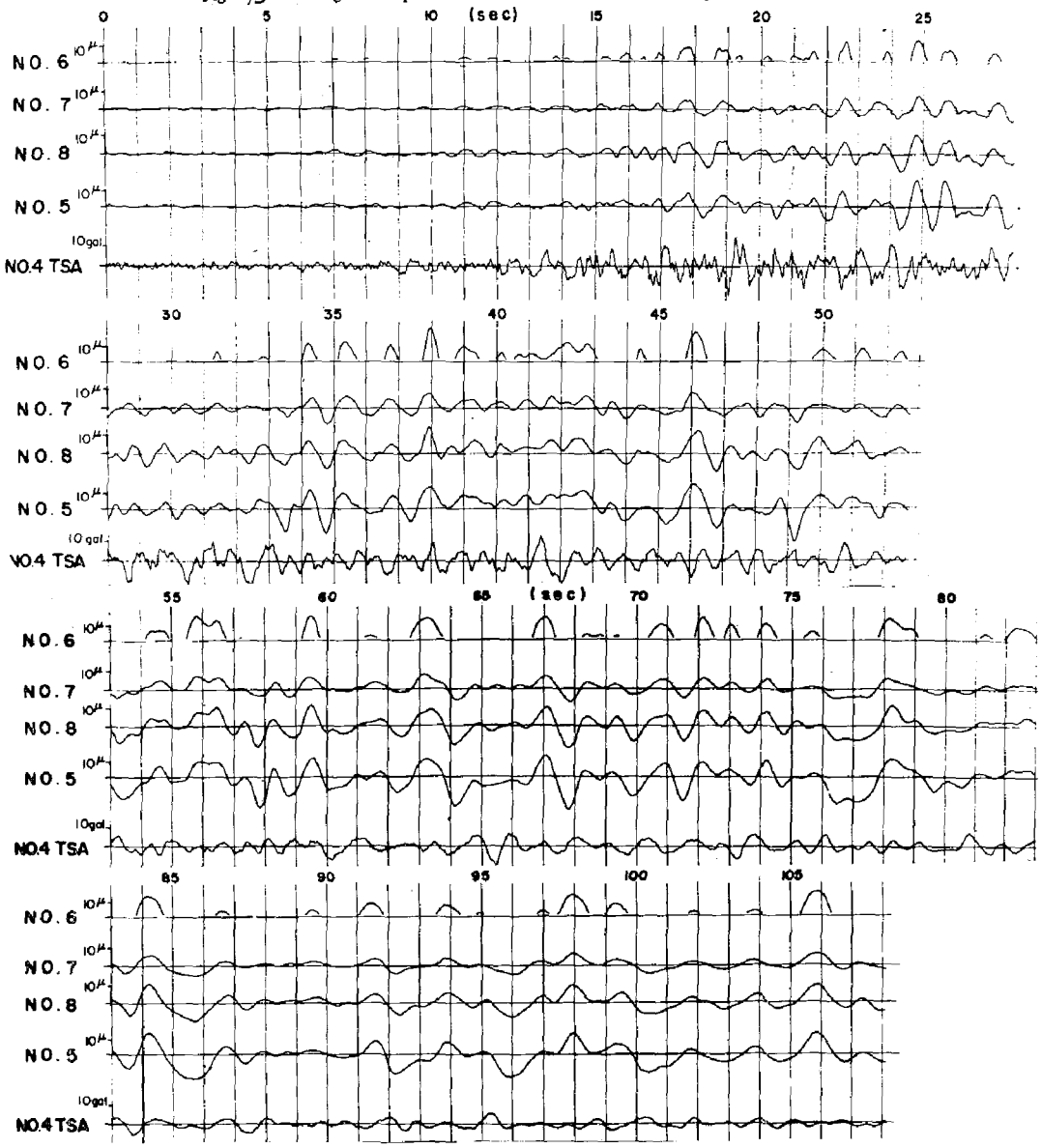

Fig.16 Earthquake record(Dec. 4, 1972)

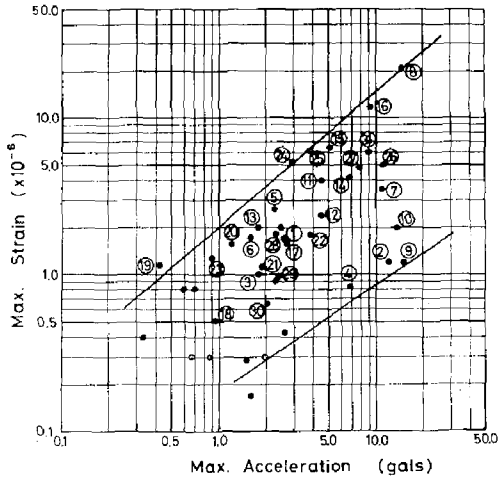

Fig. 20 Relation between max. acceleration and max. strain

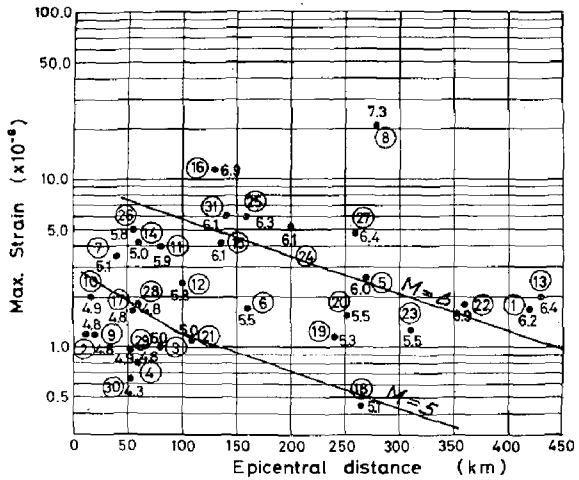

Fig. 21 Relation between max. strain of tunnel, epicentral distance and magnitude of earthquake

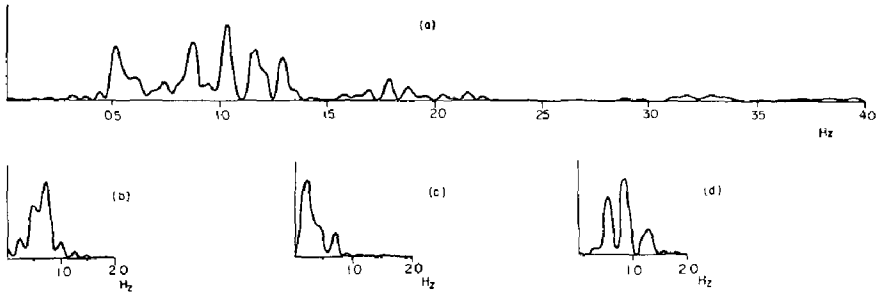

Fig. 17 Power spectra of No.4 TSA of earthquake (December 4, 1972)

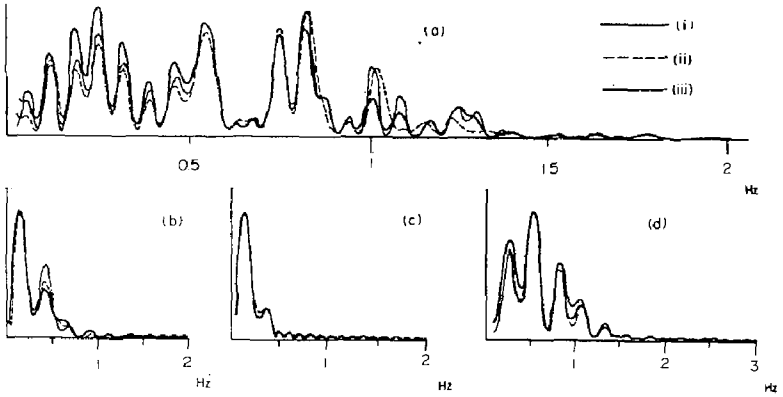

Fig. 18 Power spectra of strains of earthquake (December 4, 1972)

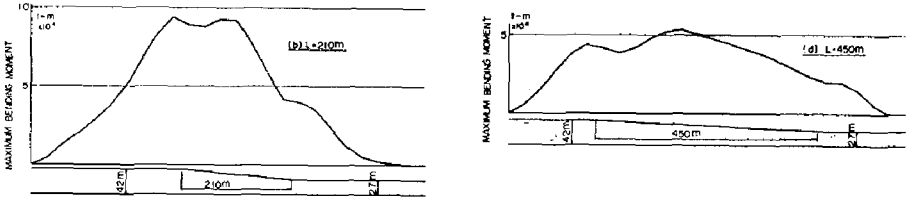

Fig. 19 Distribution of max. response bending moment of tunnel

Fig. 22 Predominant period of the ground at the tunnel site

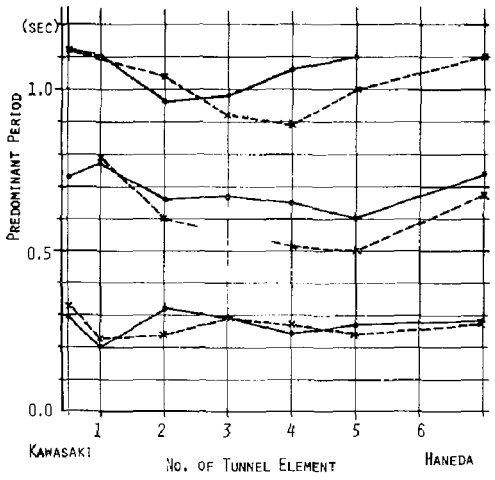

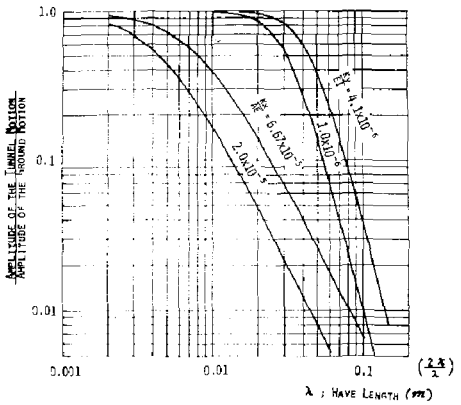

Fig.25 Wave lenghth and ratio of of amplitude of tunnel motion to that of ground motion

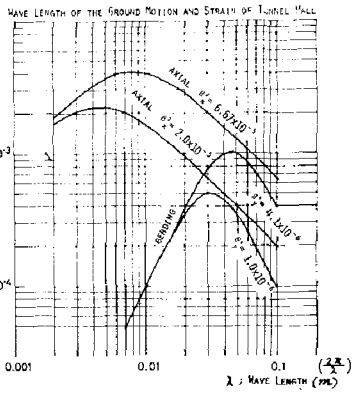

Strain due to axial deformation
Strain due to bending deformation (x 6.5)

Fig. 26 Wave length and strain in tunnel

Fig.23 Frequency characteristics of model ground

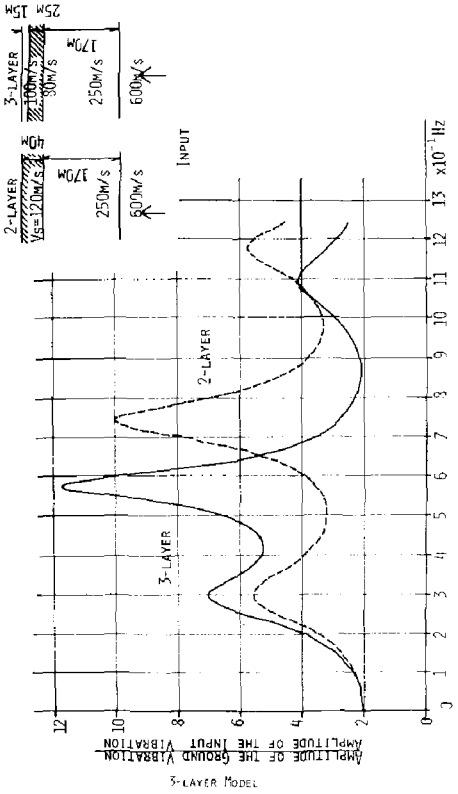

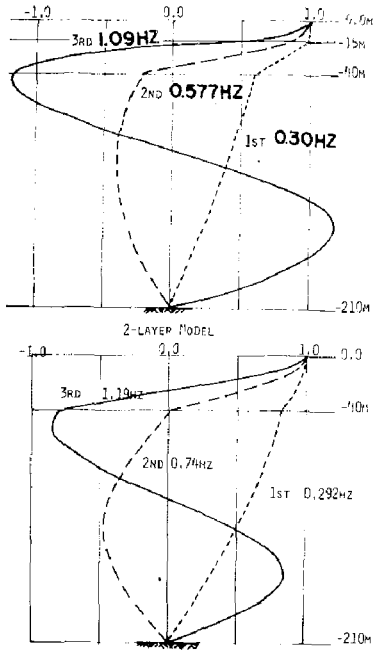

Fig. 24 Predominant mode of model ground

INTERNATIONAL SYMPOSIUM ON
EARTHQUAKE STRUCTURAL ENGINEERING
St. Louis, Missouri, USA, August, 1976

SEISMIC DESIGN OF THE VETERAN'S ADMINISTRATION HOSPITAL AT LOMA LINDA, CALIFORNIA

WILLIAM T. HOLMES

STRUCTURAL ENGINEER

RUTHERFORD & CHEKENE

SAN FRANCISCO, CALIFORNIA, U.S.A.

SUMMARY

The 500 bed Veteran's Administration Hospital in Loma Linda, California, now under construction, lies in a region of high seismicity and was designed for the new VA criteria of remaining operational after a major earthquake. Extensive studies were performed to determine site characteristics and, as a result, design lateral forces on the structure were significantly larger than required by conventional codes.

This paper summarizes the design procedure used and describes the resulting structure.

INTRODUCTION

Early in 1973, design began on a 500 bed Veteran's Administration Hospital in Loma Linda, California. The new facility was to replace beds lost due to the San Fernando Earthquake of 1971, to add needed beds in the San Bernardino area, and to serve as a prototype for a new building system developed for the VA. The timing of the project was such that the severe damage to hospitals in the San Fernando Earthquake was still fresh in mind but sufficient time had not elapsed to allow full development of data and conclusions. As a result, the VA required that their new hospitals be designed to "remain operational after a major earthquake", although no code had been developed for their new design philosophy. Since that time both the VA and the State of California have codified design criteria intended to meet that requirement for hospitals in their jurisdiction.[4,8]

The building system to be used in this facility was an open system developed for the VA by the joint venture of Stone, Marraccini & Patterson and Building Systems Development, that primarily organizes and integrates the many complex subsystems required in modern hospitals.[1,2,5,10]

Structural requirements of the system were an intermediate span shallow floor system, large story to story heights, with lateral force resisting elements concentrated in "permanent" mechanical and vertical transportation towers to keep the functional hospital space as open as possible. In terms of planning, the hospital is considered as an assembly of large scale service modules of approximately 10,000 sq. ft. (930 m^2), having variable content and organization. These modules have certain common characteristics which permit their assembly into hospitals of widely different size, program, siting and aesthetic treatment. The common characteristics of these service modules include their essential mechanical and electrical independence, interstitial space which separates functional and service activities, and common subsystem characteristics and disciplines.

Varying structural demands had been a requirement of the system and different site and environmental conditions had been considered in its development. However, conditions such as extreme seismicity coupled with changes in seismic design philosophy had not been contemplated. The San Bernardino Valley is seismically very active and the final site selected had 11 known active faults within a 65 mile (105 km) radius including the San Jacinto and two segments of the San Andreas. Fortunately the flexibility of the open system allowed satisfaction of these severe structural requirements within the system framework.

Considering the size, importance, and nature of the project, and the new design philosophy for hospitals as a result of San Fernando, extensive efforts were necessary to assure an appropriate seismic design.

SITE STUDIES

In January 1972 a Site Evaluation Report was done to determine the feasibility of building the proposed facility on two sites in Loma Linda considering the high seismicity in the area. The conclusions of that report, in part, were "the proposed hospital can be so designed and constructed at either of the two potential sites as to remain operational during the occurrence of a major earthquake". However, the trace of the Loma Linda fault was believed to be located near the Southeast corner of the site most desirable to the VA and a considerable setback from the inferred trace was recommended. Further recommendations included use of a structural system consisting of a ductile moment resisting space frame and properly designed shear walls, a design force level approximately twice that of the Uniform Building Code, and a comprehensive investigation of the site finally selected to develop further data for design.

The final Site Seismic Hazard Report on the selected site was completed in January 1973. Significant conclusions of that report included the following:

1 - Based on extensive trenching, the surface trace of the Loma Linda fault does not pass through the site. The report said, "Conclusive evidence indicated that no surface faults exist on the Loma Linda site; therefore, the probability of surface faulting through the site is essentially zero". The most likely location of the Loma Linda fault was said to be 200 to 400 feet (61 m to 122 m) Southwest of the site and no specific setback dimensions were recommended.

2 - Although some ten fault zones within 65 miles of the site were studied, the San Andreas and the San Jacinto were identified as being most significant in terms of site ground shaking.

3 - Because of a deep groundwater table, there was no liquefaction potential at the site.

4 - Preliminary ground response analysis indicated acceleration amplification factors of 0.9 to 1.1 from rock-like material to the ground surface. Surface accelerations were estimated to be 0.6 to 0.7g (g = gravitational acceleration) from large events on the San Jacinto and 0.5 to 0.55g from large events on the San Andreas.

To determine response spectra for design, it was necessary to determine the appropriate size and source of specific events to be studied, and the characteristics of those events. The following considerations were discussed for this determination:

1 - The VA criteria that the hospital should be operational after a major earthquake indicated that the events studied in detail should be large.

2 - Maximum credible events postulated in the Site Seismic Hazard Report had recurrence intervals of 100 to 300 years; therefore, the events to be studied should be slightly smaller than these maximums.

3 - Earthquakes emanating from the San Andreas and San Jacinto faults undoubtedly would produce the most intense ground motions. Because of the different distances from the site, the predominant frequencies produced by these sources would be slightly different and, in fact, would probably bracket the range of periods of structures proposed for the site.

It was concluded that the effect on the proposed structures of events with the characteristics as shown in TABLE 1 should be studied in detail to determine appropriate design parameters. Also listed in TABLE 1 are time histories used to represent the chosen events in the subsequent Site Response Studies and response spectra development.

SOURCE	DISTANCE FROM SITE	MAGNI-TUDE	MAXIMUM ROCK ACCELE-RATION	AVERAGE COMPUTED SURFACE ACCELER.	TIME HISTORIES
San Andreas (SA1)	7 Mi.	8+	0.53 g	0.59 g	Synth 8+(CAL) A-1 (Caltech)
San Jacinto (SJ1)	1¾ Mi.	7-7½	0.65 g	0.56 g	Lake Hughes Taft

TABLE 1 - DESIGN EARTHQUAKE CHARACTERISTICS

The time histories were projected through the site soils using varying depths to rock and varying soil properties by procedures developed by Seed and Idriss at the University of California. The average of the

maximum calculated surface accelerations are also listed above. Response Spectra were calculated at the surface for structural damping of 5% and 10% of critical. The smooth spectra shown in FIGURE 1 represent the upper average of the computed spectra for events SA1 and SJ1. These smoothed spectra were used in the structural pseudo-dynamic analysis to determine their effects on the proposed structures. Also shown in these figures are the 1959 Housner generalized spectra and the 1969 Newmark Hall suggested generalized spectra.

DESIGN PHILOSOPHY

The predominant feature of the Loma Linda lateral design philosophy is the phrase, "operational after a major earthquake". Early discussions revealed difficulty in specifically identifying a design level consistent with this criteria. However, in general terms, it was agreed that structural drift should be kept small to prevent damage to contents and that ductility requirements should be kept low to minimize structural damage.

A dual lateral force resisting system of concrete shear walls and a ductile moment resisting "back up" frame was chosen for the following reasons:

1 - Concrete shear walls as primary elements provide lateral deflection control essential to minimizing non-structural damage and internal disruption.

2 - At high lateral force levels it would be difficult, if not impossible, to prevent the vertical-load-carrying frame from taking some part in lateral resistance. This participation suggests a need for ductility considering the uncertainties that must be dealt with in earthquake resistant design. The ductility of steel makes its use logical.

3 - In the event of the unpredictable truly catastrophic earthquake the participation of the frame becomes more significant and its use is mandatory to insure structural stability.

4 - The cost of this system is competitive with alternatives and in most cases proves most economical.

Therefore, the stiff primary shear wall system would be designed for a high force level that is capable of withstanding at low lateral deflections the design events previously described. The back up frame will be designed to carry all vertical loads, including the shear walls, and to maintain stability laterally for some smaller force level. The reduced force level on the frame has been embodied in the Structural Engineers Association of California Blue Book[6] for some time and is based upon the following rationale:

1 - The shear walls will provide large damping and energy absorption for the frame.

2 - The frame will have a much larger period than the primary system.

3 - The most intense shaking will probably be over by the time the frame is forced to act.

The chances of the back up frame being forced to work to its full capacity were small, but considering the extent and importance of the facility, they could not be ignored. The uncertainties in earthquake characteristic prediction and construction quality makes mandatory the uses of a frame capable of redistributing forces and preventing collapse.

CONFIGURATION STUDIES

It has long been acknowledged that the configuration, and the simplicity and directness of the seismic resistant system of a structure is just as important, if not more important, than the actual lateral design forces. For this reason, it is necessary for the Structural Engineer to work closely with the Project Architect in early configuration studies. The architect, therefore, balanced VA program requirements, project cost, and inherent seismic resistance in his configuration determination.

For planning and aesthetic reasons a low building was required, so it was decided to point toward as low and stiff a building as possible to minimize drifts and possibly lower response from the projected response spectra peaks (Period = 0.3 sec. for SJ1 and Period = 0.8 sec. for SA1). Solutions using multiple and single buildings of four and five stories, with full basement, half basement and no basement combinations were studied for optimization of the above three parameters. Symmetry, shear wall availability, separation joint requirements, and continuity of vertical stiffnesses were considered in evaluating seismic resistance.

All solutions studied utilizing basements produced vertical stiffness discontinuity at the first level. Multi-building solutions were difficult to make symmetrical and all required several separation joints. It was finally decided that a single block configuration, almost square in plan, with no basement, provided the best characteristics considering the generalized three parameters studied.

After the shape was determined, various combinations of shear wall locations were tested for sufficiency in extent, symmetry and distribution. Because of the large plan area, it was necessary to balance shear wall rigidities throughout the plan to maintain low diaphragm stresses.

The final configuration is shown in FIGURES 2 and 3. The structure is four floors and is built up of service modules as defined by the building system previously discussed. The plan is essentially symmetrical, has an even distribution of shear walls throughout and, because of the regular framing layout, has direct distribution members to all walls.

DESIGN FORCE DETERMINATION

Given a response spectrum shape (normalized to surface acceleration equal to 1), in our case tailored to the site by a Site Response Study, there are still many variable parameters that must be studied and estimated before actual design lateral forces can be obtained. A compilation of these parameters is listed below as they are used. In parentheses are shown the values studied for this project.

1 - Approximate the structural damping of the proposed structure and adjust the spectrum accordingly.	(5%, 10%)
2 - Proportion the response spectrum shape to the extimated maximum ground surface acceleration.	(SJ1 - 0.55g to 0.65g; SA1 - 0.6g to 0.65g)
3 - Linearly reduce the spectrum to take into account the following effects that are difficult to account for numerically in dynamic analysis of the structure using modal analysis:	
a. Reduction of high singular acceleration spikes.	
b. High repetitive accelerations producing small displacement responses not causing damage proportional to the computed forces.	
c. Duration effects.	
d. Out of phase input motions due to large building size.	
It has been suggested that this reduction could be as high as 50 percent if all effects were present.	(0.7 to 1.0)
4 - Assign a ductility to the structure for determination of yield level forces from the adjusted spectrum. The ductility can also be calculated as a demand, after a force level has been set and the structure designed.	(2 to 3)
5 - The analysis and design of the structure is then dependent upon the determination of the periods of the building; or the modeling assumptions made for both the structure and its base if a computer is used for calculation of all mode shapes and periods.	(T = 0.2 to 0.3 sec.)
6 - Combine the modal responses for a total response.	(Root mean square, Sum of Modes 1 and 2)

All of the above steps were performed and the effects of varying all of the listed parameters were studied. For the configuration proposed for Loma Linda, the SJ1 spectrum was used because its peak (0.25 to 0.35 sec.) approximately coincides with the building period. It was not considered reasonable to assume that the building period could lengthen to the peak of SA1 spectrum (0.8 sec.) especially considering the spectral value of SA1 in the critical period range is approximately 60% of SJ1.

Based upon the above described studies, particularly the uncertainties involved, it was decided to set the base shear for the structure at 0.5 W (W = Building Mass), design elements at yield level, and calculate an approximate ductility demand under various conditions.

The peak of the SJ1 response spectrum was set at the first mode period in the following calculations, thereby eliminating the period as a variable. An infinite array of ductility demands still can be generated by varying other parameters, but the most reasonable combinations are listed in TABLE 2.

STRUCTURAL DAMPING	INPUT ACCELERATION	RESPONSE SPECTRUM REDUCTION	CALCULATED DUCTILITY DEMAND
10%	0.55	0.7	1.3
5%	0.55	0.7	1.7
5%	0.65	0.7	2.0
5%	0.60	0.8	2.1*
10%	0.65	1.0	2.2
5%	0.55	1.0	2.4
5%	0.65	1.0	2.9

*Considered most probable combination

TABLE 2 - DUCTILITY DEMANDS

Since the ductilities calculated are well within the accepted range for properly reinforced shear walls with steel column edge members, especially with the stress and reinforcing criteria that were used, and since shear wall design is practical both economically and architecturally at this level, 0.5W was set as the design lateral force. Actual member forces were determined by normalizing the full spectrum RMS computer solution to 0.5W base shear.

Using this criteria for shear wall design, the calculated maximum story drift-to-story height ratios under full spectral input loadings was approximately 0.004, well within presently accepted standards for hospitals.

DESIGN

Basic framing for the structure can be seen in FIGURE 4. Three steel girders, placed at 40'-6" o.c. (12.35 m) run longitudinally spanning the 22'-6" (6.86 m) column spacing. Eight such bays make up the service module which is the structure's basic building block. Steel beams, composite with the steel deck and concrete floor, span transversely at 11'-3" o.c. (3.43 m). The 22'-6" x 40'-6" column spacing is consistent throughout except for 54' (16.47 m) inside bays at the courts. Shear

walls are always placed at the perimeter of service modules to minimize planning interferences. Interior girders are dropped below the beams to minimize interference with services running between the beams; this also allows beam continuity across the module. All of the above framing characteristics are features of the systems integration for which Loma Linda is the prototype.

The design of the structure can be split into three basic areas: the steel moment resisting space frame, the concrete shear walls, and the foundations. Each will be discussed separately.

STEEL FRAME

The steel frame was designed for a lateral force of 0.05W or 10% of the total design lateral force. This is less than the usual 25% used for back up frames, but it was not felt that this large lateral design force was necessary for the back up frame to perform its function. A force of 0.05W is still more than three times that required by the Uniform Building Code for a back up frame and about equal to the total lateral force required if the frame was the structure's primary lateral system. Final design of elements was based upon the greater values obtained considering the frame acting in conjunction with the shear walls for 0.5W or the frame acting alone for 0.05W. Lateral drift was not considered critical in the design of the frame and yield level stresses were allowed in conjunction with lateral forces.

Since the force level in the frame was of a conventional order of magnitude, few special problems were encountered. The large collector forces created by the overall 0.5W level increased the steel weight of the members affected 10 to 20 percent. The criteria that the frame vertically support the weight of the shear walls required addition of intermediate columns between shear wall columns greater than 22'-6" apart. The final frame steel weight was 16.5 lb/sq. ft. (80 kg/m^2).

SHEAR WALLS

Although shear walls in the project were used in lengths of 40'-6", 45', 54', and 91' (12.35, 13.72, 16.47, 24.7 m), with a variety of penetration configurations for architectural use (functional zone) and mechanical use (service zone), a typical wall is represented in FIGURE 5. The exclusive use of "infill" walls that simply enclose portions of the overall steel framing pattern has several advantages:

1 - There are always beams or girders parallel and on line with the walls to serve as lateral force collectors.

2 - The continuation of these members through the wall allows direct transfer of forces from the diaphragm to the wall.

3 - The columns at the end of walls form the required ductile flange members for wall bending.

4 - Frame members are in correct position to provide vertical support for shear wall dead load.

Thickness of walls varied from a minimum of 12" (30.5 cm) to a maximum of 24" (71 cm). Minimum reinforcing to concrete ratio was 0.25% in each direction. Heaviest wall steel used was 1.2 in^2/ft (2540 mm^2/m) each way on each face of a 24" wall.

The predominantly first period response of the stiff shear walls coupled with the high force level created large bending moments at the base of the shear walls. Net tension forces in the wall flanges were as high as 3,800,000 lb. (16,910 KN). This required use of a concrete "tension block" to transfer these forces to the foundation system (see FIGURE 6). The tension block is cast ober the steel column base plate and the tensile forces are transferred to the concrete through upward bearing. The block is anchored to a heavily reinforced pier cap which spans between the cast-in-place reinforced concrete pier foundations.

The steel column flanges of the walls are made composite with the concrete by shear friction, utilizing welded transfer dowels (FIGURE 7). The floor to wall and beam to wall connection is shown in FIGURE 8. Shear is transferred through the beam from the wall above to the wall below (or from the beam to the wall in the case of beam collectors) also by shear friction but using dowels placed through holes pre-punched in the beam flanges. The lightweight floor concrete, weaker in shear than the hardrock wall concrete, is not cast through the wall. The steel decking was temporarily supported independently of the main beams at the wall to further prevent a shear weakness at the floors and to allow the contractor freedom to cast slabs and walls independently. The contractor, in fact, used this to full advantage by casting slabs continuously and letting the more complicated wall construction progress at its own rate.

FOUNDATIONS

The use of drilled cast in place concrete friction piers was determined by an early economic analysis. Technically, their characteristics of small settlement and high uplift resistance were mandatory.

As with the shear wall design, axial overturning forces at walls required careful consideration of the foundation response to high force levels. The piers were designed to transfer 90% of the calculated wall overturning moment into the soil. The 10% reduction in calculated forces was arbitrary and probably should have been larger. It stems from the fact that although the shear wall flexure exists, the actual tendency to overturn does not, especially in a short period building. The rapid reversals in direction do not allow time for significant overturning action to take place. Field observation of earthquake damage indicates that designing foundations for full overturning is overly conservative. It was decided that small vertical slippage between pier and soil at responses over 0.5W was acceptable as long as vertical load carrying capacity was maintained by insuring pier ductility.

The treatment of lateral forces at the foundations was a much more difficult problem. Coupling the structure to the soil for the structural

design level of 0.5W was a consistent design approach, but the interaction between soil and foundations at higher force levels had to be investigated. Plastic hinging of the piers at the top and at the point of centraflexure, as well as soil yielding was involved and the order in which these occurred was critical.

Initially it was determined that the piers under walls placed for vertical load and overturning were totally insufficient to transfer the distributed lateral forces, wall by wall, into the ground. In some walls, it would have been impossible from a physical standpoint to provide the required capacity without reverting to battered piers. Battered piers were undesirable unless they were used throughout because of their incompatibility with the rest of the building, and battered piers throughout were uneconomical and would provide no allowance for desirable minor movements and energy absorption. The greatest concern was to prevent different responses of individual walls due to different soil coupling stiffnesses. Such action would negate any dynamic analysis which assumes a single response to a single input and would have severely damaging effects on the structure.

For these reasons, it was decided to make all piers, including the piers away from shear walls, capable of resisting lateral forces, and tie the building together at the ground level sufficiently to force unified action of the building base. Although foundation tie beams between individual pier locations were already contemplated, it was necessary to have diaphragm action in the slab on grade to distribute the concentrated loads at walls throughout the building. In order to then properly design this system for overall ductility, it was necessary to determine pier stiffness under a wide variety of conditions. The most difficult portion of overall pier stiffness to determine was the basic pier-soil interaction, but varying top fixity conditions as well as group action also had to be considered. Exhaustive computer studies were done to determine the affects of these parameters and pier rigidities were calculated. A lateral load of 0.5W was distributed to the piers according to these rigidities and bending moments calculated at that load level. It was discovered that the rotation of the top of piers at free-standing columns was causing certain columns to hinge between the first and second floor. Tie beams, originally designed for axial loads only, were increased in size and properly reinforced so that the combined stiffness of column and tie beams always exceeded the pier stiffness, thus forcing the hinge into the pier. The piers were designed at the 0.5W moment at the point of first yield, which, as discussed above, always occurred at the pier-cap intersection. However, the pier could continue to take additional load until a second hinge formed at the point of centraflexure or until the soil itself yielded. To insure ductility, shear reinforcing was provided on a pier by pier basis for this limiting condition. This design procedure will insure consistent elastic response up to 0.5W load and will prevent loss of vertical load carrying capacity at greater loads caused by sudden shear failure in the piers or column hinging.

COSTS

The additional cost of the design at Loma Linda is difficult to estimate without a total parallel code design because such a large increase in design parameters changes the scope of the lateral systems. However, costs of designs at other force levels were estimated in connection with final establishment of the design forces used. By extension of this information, the difference in construction cost between Loma Linda and a conventional code (1973 UBC) design can be estimated. These additional costs are summarized in TABLE 3.

ELEMENT	ADDITIONAL STRUCTURAL COST OVER CONVENTIONAL DESIGN
Shear Walls	$ 800,000 - $1,200,000
Steel Frame	300,000 - 400,000
Foundations	350,000 - 400,000
Slab on Grade	100,000 - 200,000
TOTAL	$1,550,000 - $2,350,000

Percentage increase of structural cost ($15,850,000) - 10-15%

Percentage increase of total cost ($55,100,000) - 2.8-4.3%

TABLE 3 - INCREASE IN CONSTRUCTION COSTS

The costs are consistent with those reported by the Applied Technology Council in a recent report[3] done to investigate the problems of general use of the response spectrum approach in design.

Additional cost and general information, along with project acknowledgements, are contained in TABLE 4.

OWNER: Veteran's Administration, Washington, D.C.

LOCATION: Loma Linda, CA, approximately 60 miles east of Los Angeles

AREA: 724,063 square feet

BASIS OF DESIGN: Development Study, VA Hospital System by SMP/BSD, a Joint Venture, for the VA Office of Construction Research Staff

DESCRIPTION: Four floors made up of 15,000 S.F. planning modules each mechanically independent. All services distributed through interstitial spaces between floors. Exterior of concrete and stucco. Structure consists of a steel frame with 40'-6" span steel composite beams. Basic lateral system is concrete shear walls. Interstitial spaces formed with hung steel purlins and poured gypsum concrete.

SCHEDULE: Design 1973-1975; Construction 1974-1977

CONTRACTORS: PHASE 1 - Structural and Site Grading:
Robert McKee, Inc.

PHASE 2 - Architectural, Mechanical, Landscape:
J.W. Bateson Co., Inc.

APPROXIMATE COSTS:

Site and Landscape	$ 3,000,000	
Structural	15,850,000	($21.90 psf)
Architectural, Transport. Equipment	25,900,000	($25.90 psf)
H V C	6,500,000	($ 9.00 psf)
Plumbing	6,500,000	($ 9.00 psf)
Electrical	4,500,000	($ 6.20 psf)
	$ 55,100,000	

DESIGN TEAM:

Architect: Stone, Marraccini & Patterson and Building Systems Development, A Joint Venture

Site Selection Analysis: LeRoy Crandall and Associates
(Consultants: James E. Slosson & Associates
J.H. Wiggins Co., Brandow & Johnston Associates,
and Clarence R. Allen)

Site Seismic Hazard, Site Response and Soil Reports:
Woodward Lundgren and Associates

Structural Engineers: Rutherford & Chekene
(Consultants: Henry J. Degenkolb, H. Bolton Seed,
Ray Clough, Ed Wilson, and Ben Lennert)

Civil Engineers: Rutherford & Chekene

Mechanical Engineers: Ayres & Hayakawa

Electrical Engineers: Cohen, Lebovich and Pascoe

Landscape Architect: Arutunian/Kinney Associates

TABLE 4 - LOMA LINDA HOSPITAL
PROJECT SUMMARY AND ACKNOWLEDGMENTS

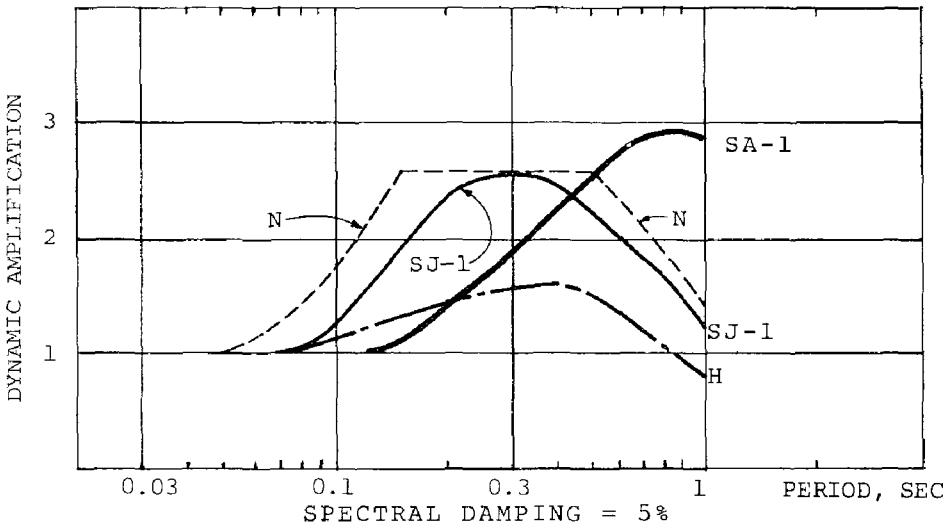

NOTE: SPECTRA FOR SA-1 AND SJ-1 REPRESENT UPPER AVERAGES OF THE COMPUTED SPECTRA

N = NEWMARK HALL (1969), H = HOUSNER (1959)

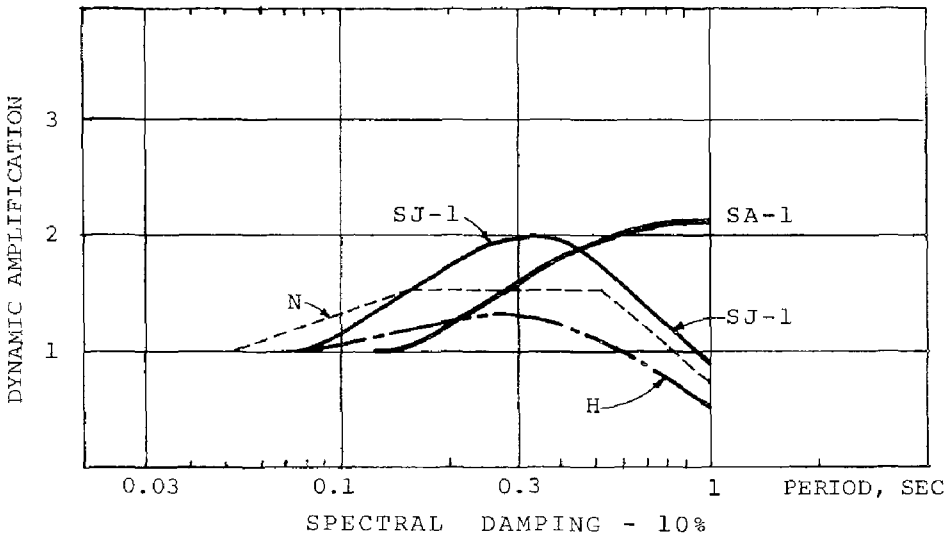

FIGURE 1 - SITE RESPONSE SPECTRA

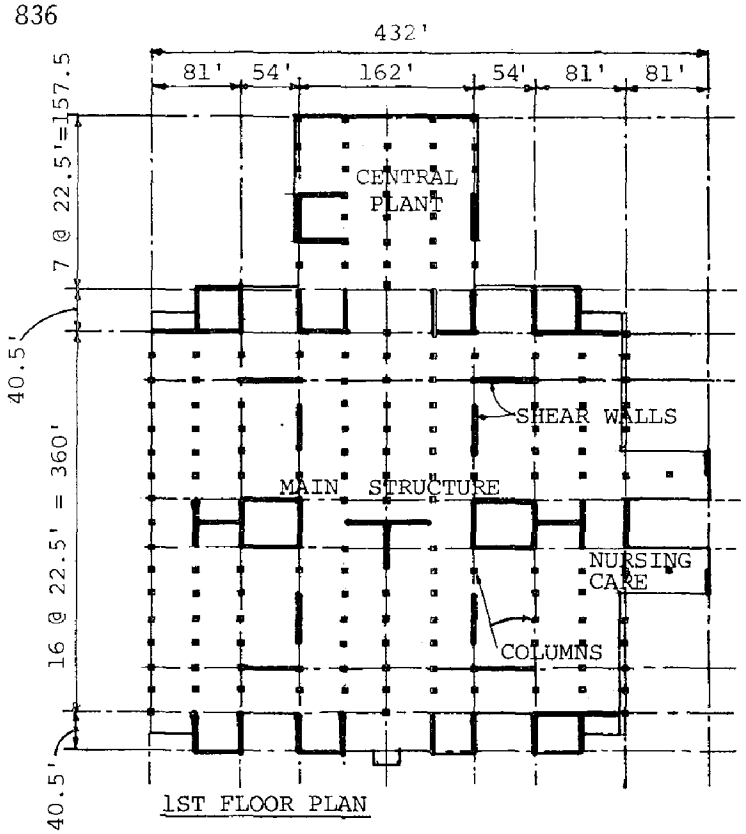

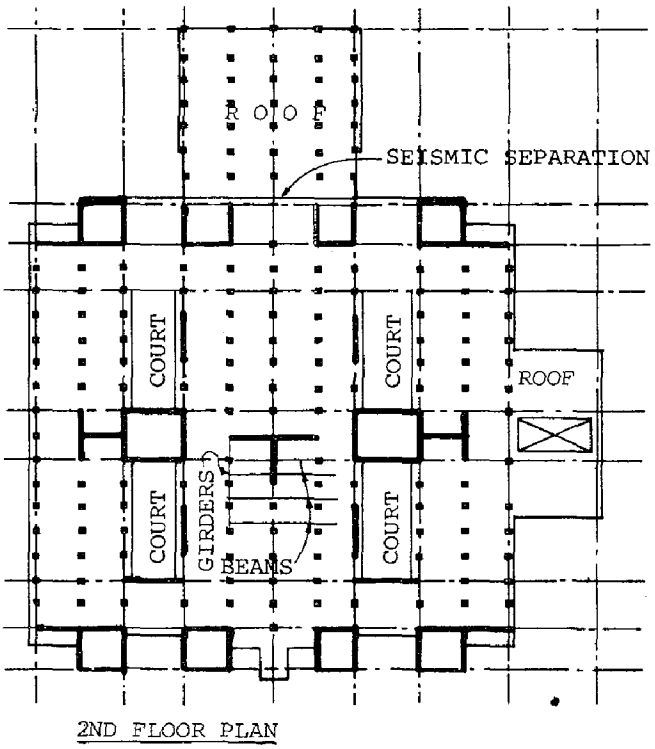

FIGURE 2 - FLOOR PLANS

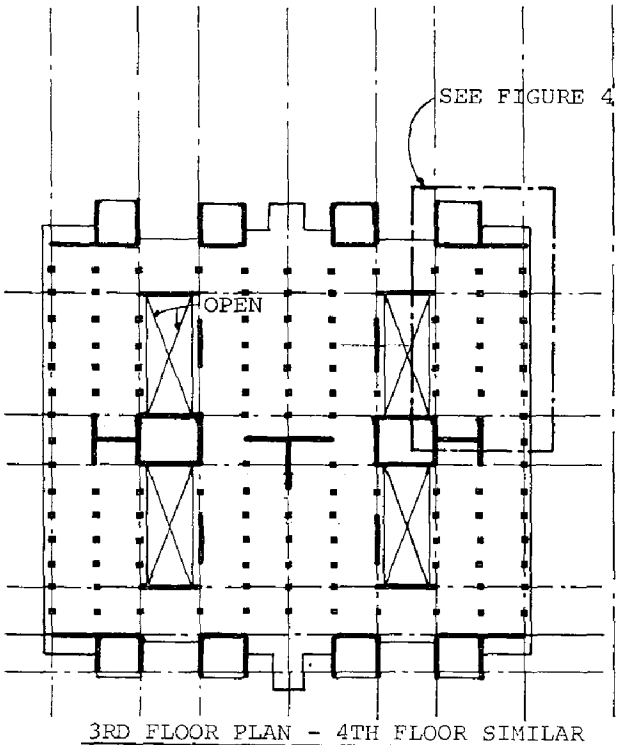

3RD FLOOR PLAN - 4TH FLOOR SIMILAR

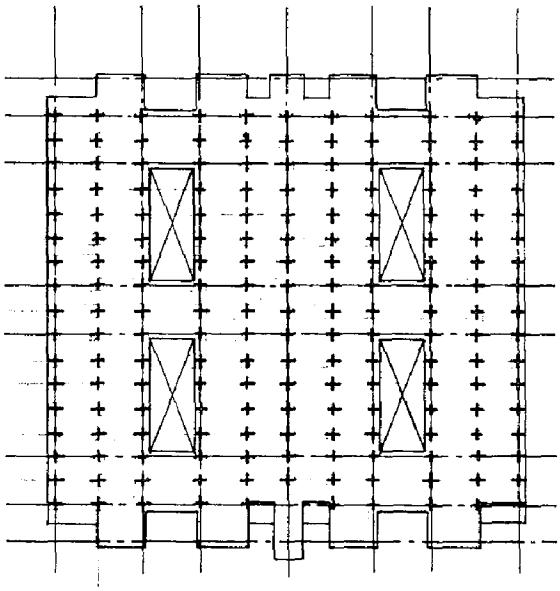

ROOF PLAN

FIGURE 3 - FLOOR PLANS

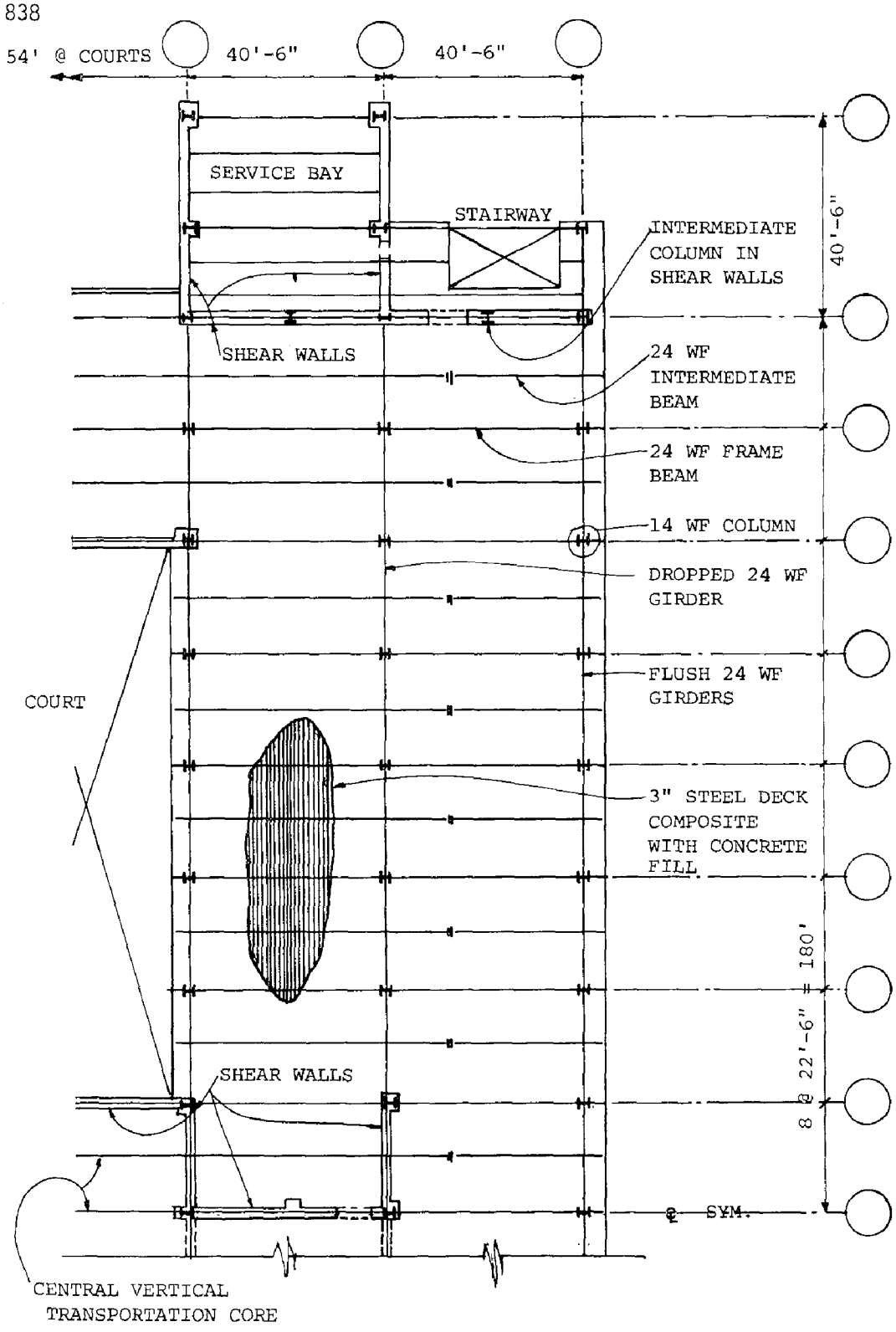

FIGURE 4 - TYPICAL SERVICE MODULE FRAMING

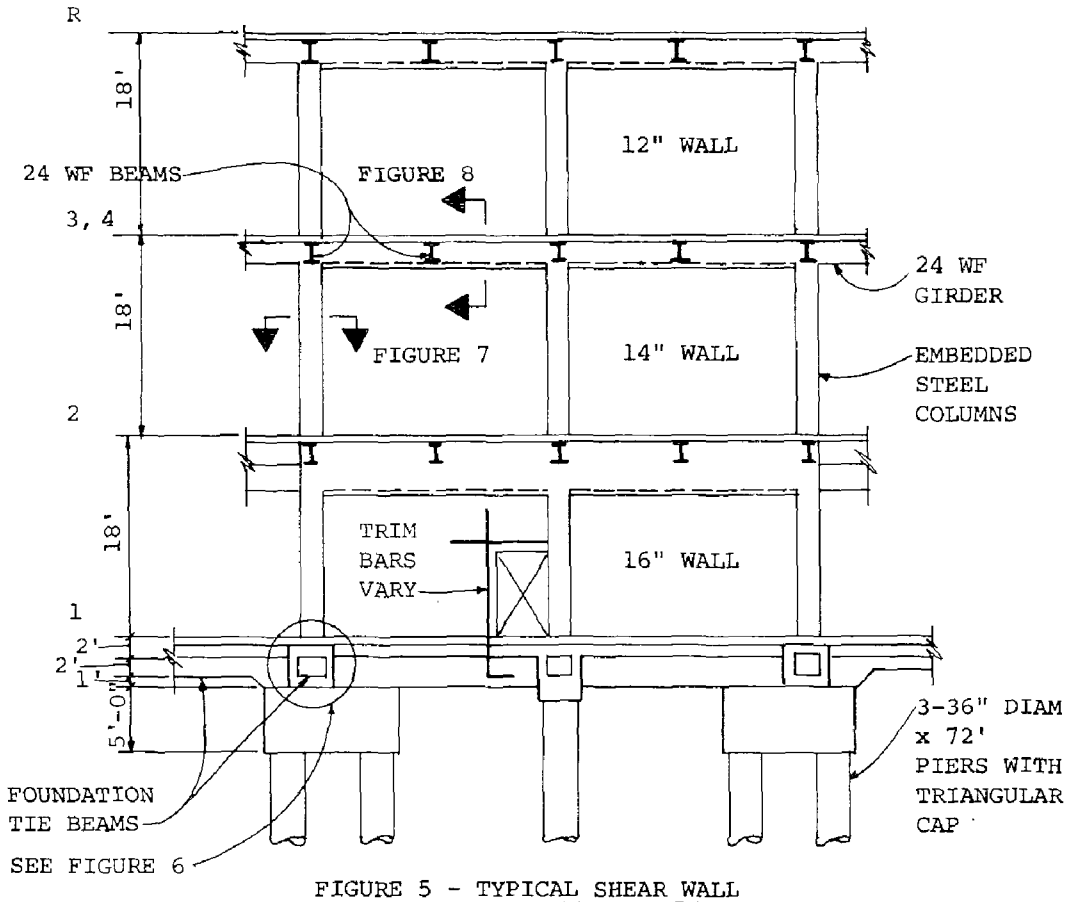

FIGURE 5 - TYPICAL SHEAR WALL

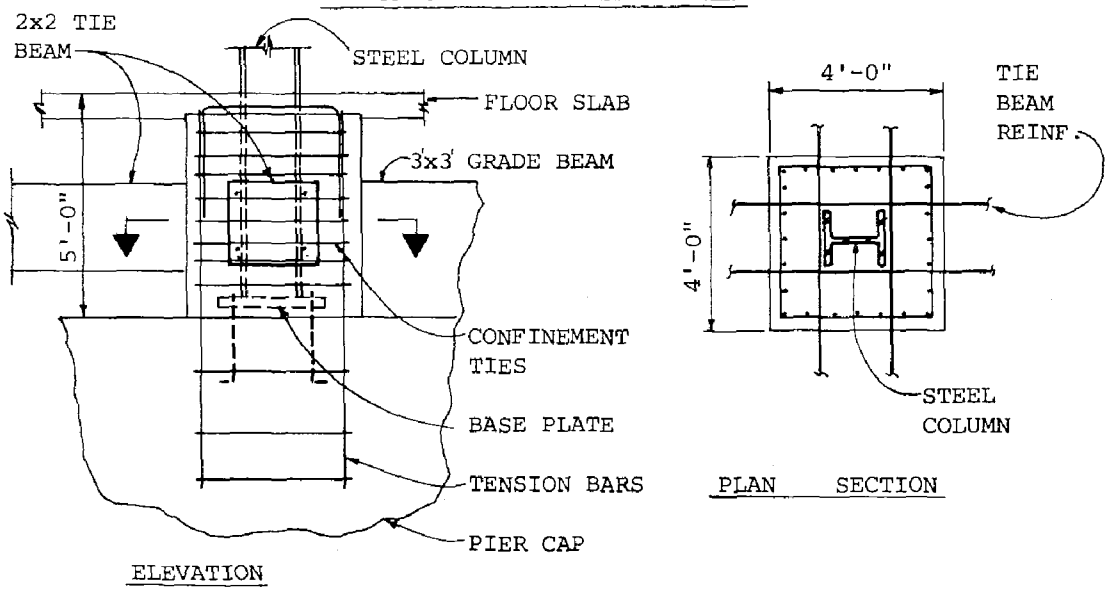

FIGURE 6 - TYPICAL TENSION BLOCK

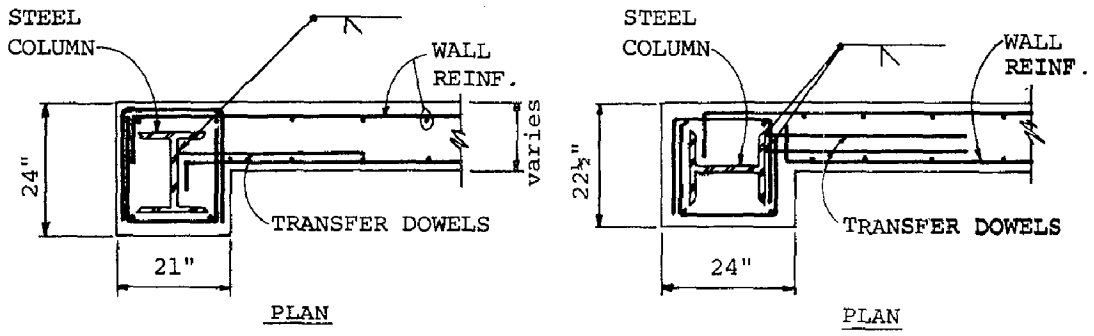

FIGURE 7 - TYPICAL COLUMNS AT SHEAR WALL

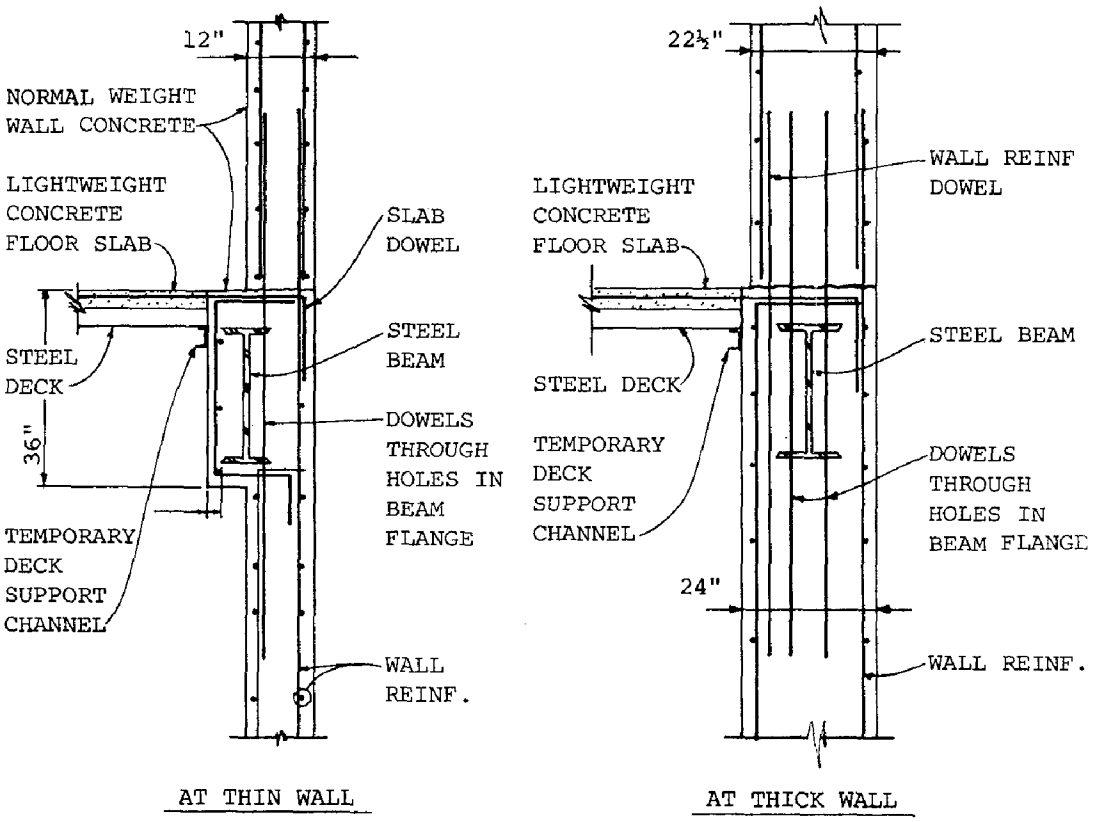

FIGURE 8 - TYPICAL FLOOR/SHEAR WALL DETAIL

BIBLIOGRAPHY

1 - Agron, George, "Application of the VA Hospital Building System to the Design of Loma Linda VA Hospital", Architectural Record, September 1973.

2 - Agron and Borthwick, "Hospital Planning Research", Architectural Record, June, 1972.

3 - Applied Technology Council, An Evaluation of a Response Spectrum Approach to Seismic Design of Buildings, ATC2, San Francisco, CA, September, 1974.

4 - California, State of, California Administrative Code, Title 17 Public Health, available from State Office of Procurement, Publications Section, P.O. Box 20191, Sacramento, CA 95820.

5 - Schmidt, William A., "The VA Hospital Building System", Heating, Piping, Air Conditioning, March, 1975.

6 - Structural Engineers Association of California, Recommended Lateral Force Requirements and Commentary, San Francisco, 1973.

7 - Veterans Administration, Office of Construction, Earthquake Resistive Design of Non-Structural Elements of Buildings, VA Construction Standard CD-55, 1973.

8 - Veterans Administration, Office of Construction, Earthquake Resistant Design Requirements for VA Hospital Facilities, Handbook H-08-8, March, 1974.

9 - Veterans Administration, Office of Construction, Post-Earthquake Engineering Utility Services and Access Facilities, VA Construction Standard CD-54, 1972.

10 - Veterans Administration, Development Study - VA Hospital Building System, U.S. Government Printing Office, Washington, D.C. 20402

INTERNATIONAL SYMPOSIUM ON
EARTHQUAKE STRUCTURAL ENGINEERING
St. Louis, Missouri, USA, August, 1976

STRUCTURAL DAMAGE AND RISK IN EARTHQUAKE ENGINEERING

D. S. Hsu
Research Assistant

J. T. GAUNT
Associate Professor

J. T. P. YAO
Professor

School of Civil Engineering

Purdue University

W. Lafayette, Indiana U.S.A.

Summary

A methodology is presented herein for the evaluation of structural damage and risk in earthquake engineering. For the purpose of illustration, three types of structures and five levels of damage (including no damage) are considered. Results of this study indicate that it is possible to assess the seismic risk of a certain type of structure in a given region with past earthquake records.

Introduction

During these last two decades, risk analysis has become an important tool for making rational decisions in structural engineering [10,17]. It is desirable to describe structural risk in such a way that (a) it can be used for design purposes to minimize the total cost for different types of structures, and (b) the structures will remain functional during the intended life span [5,15,18]. There are various definitions and interpretations for seismic risk such as encounter probability, distribution of waiting time, distribution of total damage, mean total damage, probability of failure, seismic intensity, and reward-risk-ratio [2,3,5,9,20].

A methodology to deal with structural risk in earthquake engineering is introduced herein. To-date, seismic risk has been considered in several different ways, and various factors are involved in it. Those factors which might be considered in seismic risk analysis include disease, transportation accidents, natural hazards, loss of life [10,18], material properties, structural arrangement, actual loadings [15], damage control, and life safety [20]. Generally speaking, the environmental risk including earthquake probability and the risk for a given building structure should be considered.

The owner of a structure is primarily concerned with costs related to the structural risk such as repairing cost, re-construction cost, cost-benefit, and reward ratio [3]. Since these cost factors are easy to understand, the damage of structures can be represented in terms of

these costs to aid the owner in making a decision such as whether or not a damaged structure should be repaired. Some of the statistical methods as applied to the repairing cost data for a certain earthquake region have been reported [18,19]. In these studies the damage was classified into several damage states without clear definitions.

Formulation

In this study, the following levels of damage are considered:

D_0 = no damage occurred
D_1 = non-structural damage only
D_2 = minor and repairable structural damage
D_3 = major structural damage
D_4 = total collapse of the structure

Furthermore, define events E_j by using the MMI scale [14] as follows:

E_0 = the occurrence of earthquake(s) with MMI V or less
E_j = the occurrence of earthquake(s) with j^{th} intensity

j	MMI
1	VI
2	VII
3	VIII
4	IX
5	X
6	XI
7	XII

For a given type of structure, the risk of resulting in i^{th} level damage with the occurrence of j^{th} intensity earthquake can be found by using the following equation:

$$r_{ij} = P(D_i|E_j)P(E_j) \tag{1}$$

For a given earthquake intensity j, the frequency of the earthquakes can be assumed to follow the Bayesian distribution [1] as given by

$$P(X_J = x|J = j) = P_{x_j}(x) = \frac{t^x t_0^{r_0+1}}{(t_0 + t)^{r_0+x+1}} \quad \frac{(x + r_0)!}{x!\Gamma(r_0 + 1)} \quad , x = 0,1,2,\ldots \tag{2}$$

where

X_J = random variable denoting the number of earthquakes with intensity J during the intended life of the structure
J = random variable denoting the intensity of future earthquakes
t_0 = past period (years)
r_0 = number of earthquakes occurred in t_0

t = future period (years)

Then,

$$P(E_j) = P(X_J \geq 1, J = j)$$
$$= [1 - p_{X_j}(0)]P(J = j) \quad (3)$$

Using Equations (2) and (3), the risk as given in Equation (1) can be evaluated. The probability of having i^{th} level damage for a given type of structure is then given by

$$P[D_i] = \sum_{j=1}^{7} r_{ij} \quad (4)$$

Numerical Examples

Three regions, assigned by R1, R2, R3, in California have been selected. They are located at:

R1: N.lat. 37°20'00" ∿ 38°10'00"
W.long. 121°30'00" ∿ 122°30'00"

R2: N.lat. 36°45'00" ∿ 37°00'00"
W.long. 121°20'00" ∿ 121°50'00"

R3: N.lat. 33°30'00" ∿ 34"00'00"
W.long. 118°00'00" ∿ 118°30'00"

The earthquake data in these regions have been collected during a two-hundred-year period [6,21] as shown in Table 1.

Twenty and fifty years are chosen as the intended life-time of structures, and the occurrences in the future period are calculated up to twenty times. There are two different ways to use the data in estimating the parameters of $p_{X_j}(x)$, and both results are plotted in Figures 1 through 4. These results show that there does not appear to be any significant difference.

Assume there are three types of structures, namely, A, B, and C. Type A structures refer to those which are designed with the state-of-the-art methodology and well-built. Type B structures are designed according to current codes and specifications. Type C structures refer to the so-called "non-engineered" structures. For the purposes of illustration, the values $P[D_i^I|E_j]$ in Table 2 are assigned subjectively.

Substituting the values of $p_{X_j}(0)$ and P(J=j) into Equation 3, we obtain values of $P(E_j)$, which are then used in computing r_{ij} and $P[D_i]$ according to Equation (4). These results for an intended life-time of 50 years are plotted in Figures 5 through 7.

Discussion and Conclusions

1. The risk analysis presented herein depends on both the chance of the occurrence of certain intensities of earthquakes and the type of structures.

2. For the purpose of illustration, certain values such as the elements of the damage matrix, $P[D_i^I|E_j]$ are assigned subjectively herein. It will be desirable to determine these values more rationally later. If this methodology were adopted further improvements can be made in this regard.

3. Past earthquake records are used here for the evaluation of environmental risk. It is known that there exists a certain degree of uncertainty in such data. Such uncertainties should also be considered in any further developments.

4. The intensity for each earthquake is recorded by the intensity at the epicenter. Since the propagation of seismic motion from the epicenter to the site which we are dealing with is a very important consideration, a proper propagation formula is needed in order to make this metholology more efficient. The empirical equation [7,8,13]

$$y = b_1 e^{b_2 m} [f(R)]^{-b_3} \varepsilon \tag{5}$$

can be used for this purpose.

5. As a result, a seismic risk map according to the damage and risk with certain types of structures can be constructed. It could provide very useful information for the decision making in the structural design.

6. In this investigation, the effect of combined occurrences of earthquakes with different intensities was not considered. In future studies, it will be desirable to account for such combinations.

Acknowledgement

This study was conducted in the School of Civil Engineering, Purdue University. The excellent typing of Connie Maurina is appreciated.

Table 1

Number of Earthquakes (MMI > VI) in given regions through 1769-1970 [7,13]

	37°20'00" 121°30'00" 38°10'00" 122°30'00"	36°45'00" 121°20'00" 37°00'00" 121°50'00"	33°30'00" 118°00'00" 34°00'00" 118°30'00"
XII	0	0	0
XI	0	0	0
X	3	0	0
IX	0	0	1
VIII	2	2	2
VII	12	7	3
VI	20	14	11
Total	37	23	17
	Region 1	Region 2	Region 3

Table 2

Earthquake Level		Damage Level				
		D_0	D_1	D_2	D_3	D_4
	E_6	1.0	---	---	---	---
		0.9	0.1	---	---	---
		0.8	0.2	0.1	---	---
	E_7	0.9	0.1	---	---	---
		0.8	0.1	0.1	---	---
		0.5	0.3	0.1	0.1	---
	E_8	0.7	0.2	0.1	---	---
		0.5	0.3	0.1	0.1	---
		0.1	0.3	0.3	0.2	0.1
	E_9	0.4	0.3	0.2	0.1	---
		0.1	0.2	0.3	0.2	0.2
		---	0.1	0.3	0.3	0.3
	E_{10}	0.2	0.3	0.3	0.1	0.1
		---	0.1	0.3	0.3	0.3
		---	0.1	0.1	0.3	0.5
	E_{11}	0.1	0.1	0.2	0.3	0.3
		---	0.1	0.1	0.3	0.5
		---	---	0.1	0.2	0.7
	E_{12}	---	---	0.1	0.2	0.7
		---	---	---	0.1	0.9
		---	---	---	---	1.0

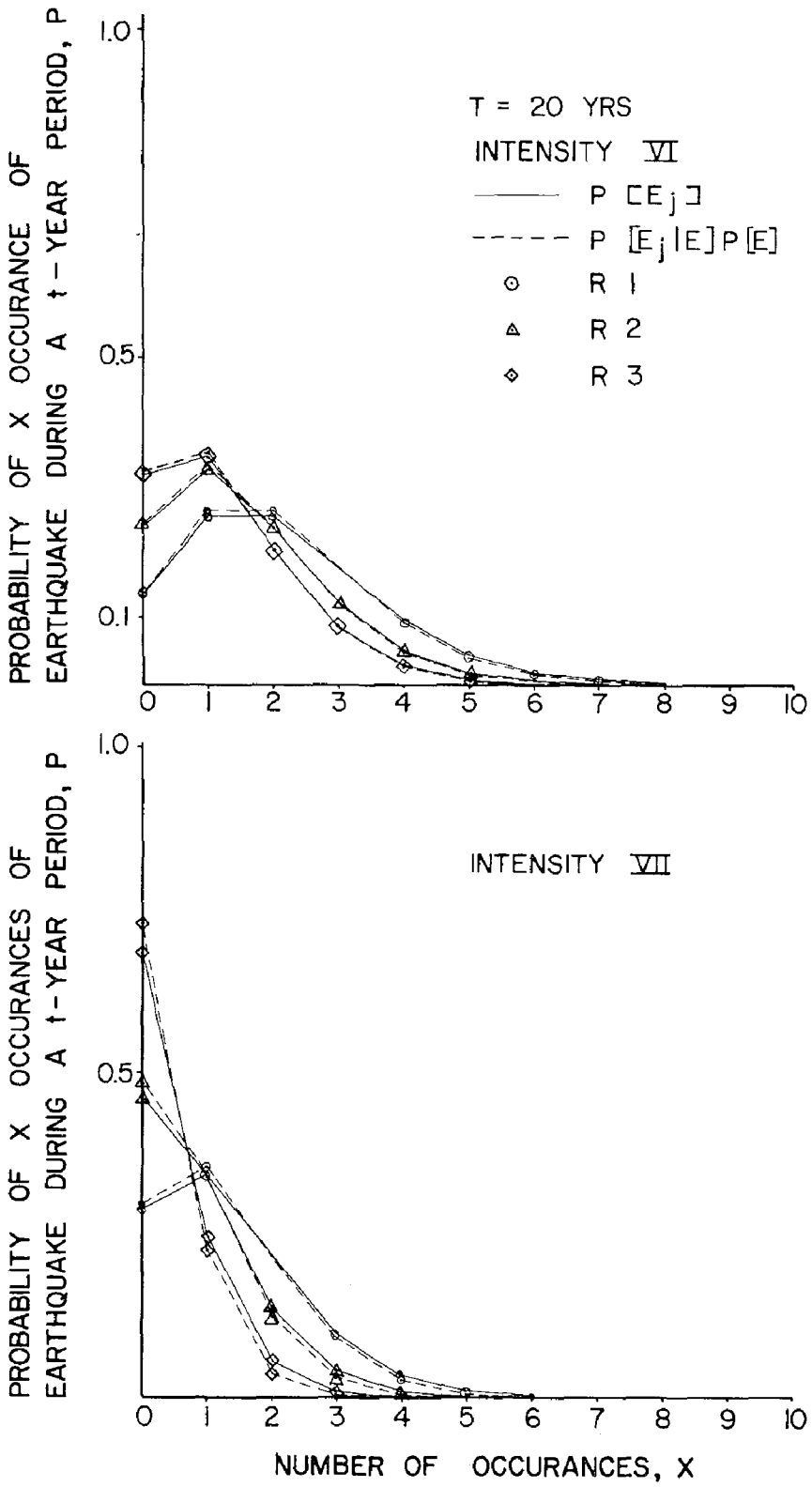
PROBABILITY OF X OCCURANCE OF EARTHQUAKE DURING A t-YEAR PERIOD, P
1.0
0.5
0.1
T = 20 YRS
INTENSITY VI
P [E_j]
P [E_j|E]P[E]
R 1
R 2
R 3
0 1 2 3 4 5 6 7 8 9 10
PROBABILITY OF X OCCURANCES OF EARTHQUAKE DURING A t-YEAR PERIOD, P
1.0
0.5
INTENSITY VII
0 1 2 3 4 5 6 7 8 9 10
NUMBER OF OCCURANCES, X

FIGURE 1

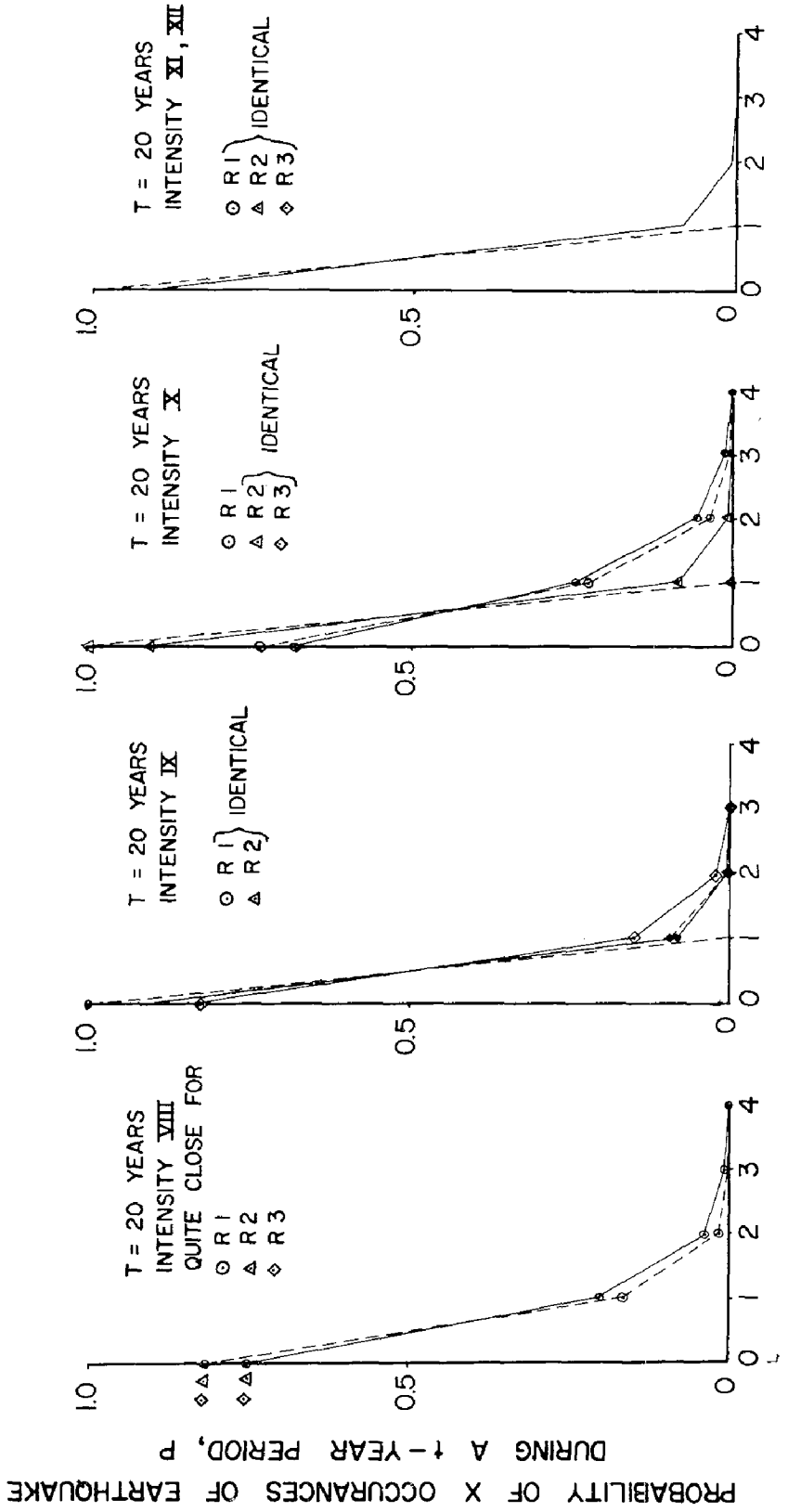
T = 20 YEARS
INTENSITY VIII
QUITE CLOSE FOR
R 1
R 2
R 3
T = 20 YEARS
INTENSITY IX
R 1
R 2
IDENTICAL
T = 20 YEARS
INTENSITY X
R 1
R 2
R 3
IDENTICAL
T = 20 YEARS
INTENSITY XI, XII
R 1
R 2
R 3
IDENTICAL
1.0
0.5
0
0
1
2
3
4
NUMBER OF OCCURANCES, X
PROBABILITY OF X OCCURANCES OF EARTHQUAKE
DURING A 1-YEAR PERIOD, P

FIGURE 2

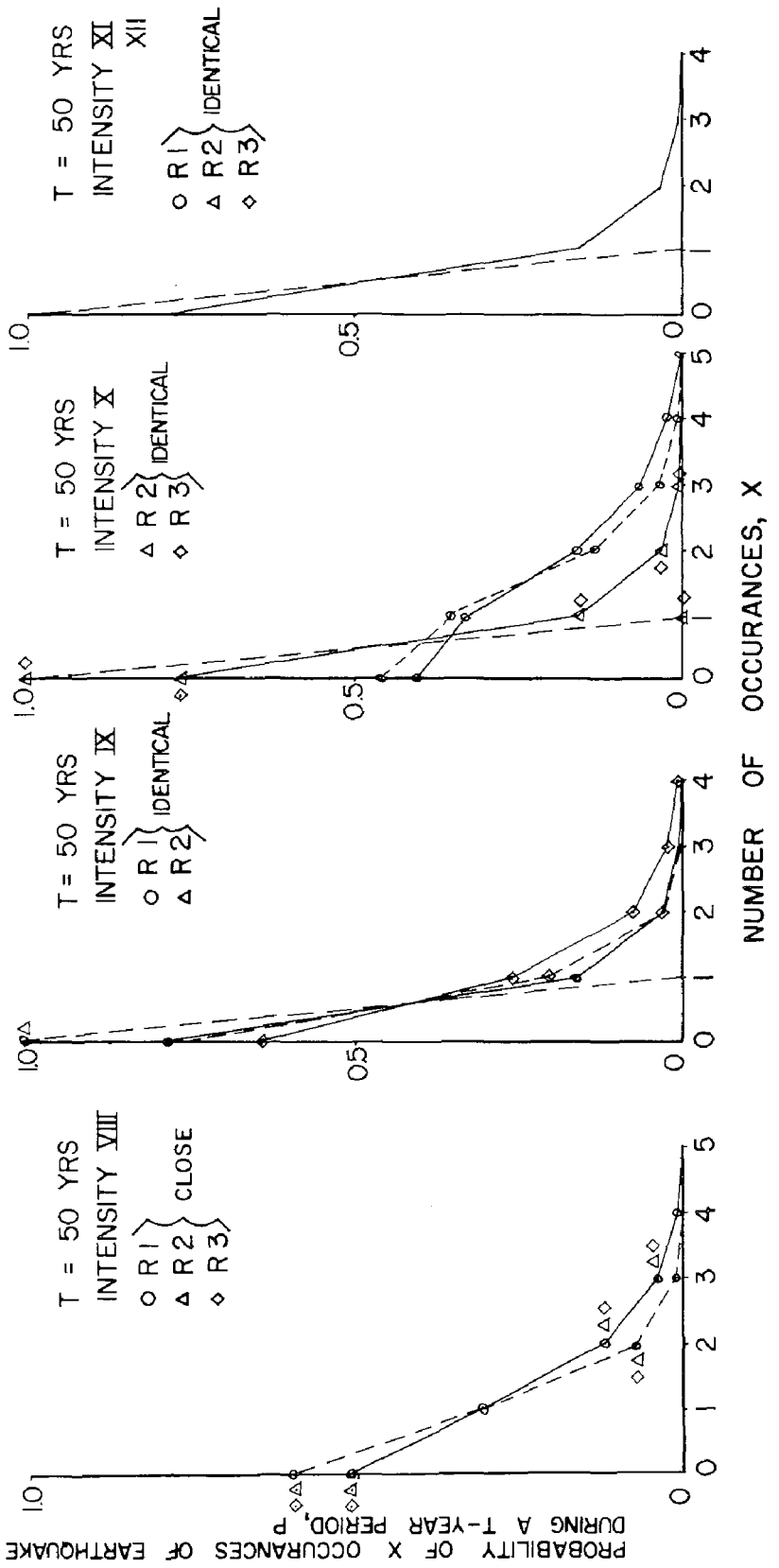
T = 50 YRS
INTENSITY VIII
R1
R2
R3
CLOSE
T = 50 YRS
INTENSITY IX
R1
R2
IDENTICAL
T = 50 YRS
INTENSITY X
R2
R3
IDENTICAL
T = 50 YRS
INTENSITY XI
XII
R1
R2
R3
IDENTICAL
PROBABILITY OF X OCCURANCES OF EARTHQUAKE DURING A T-YEAR PERIOD, P
NUMBER OF OCCURANCES, X

FIGURE 3

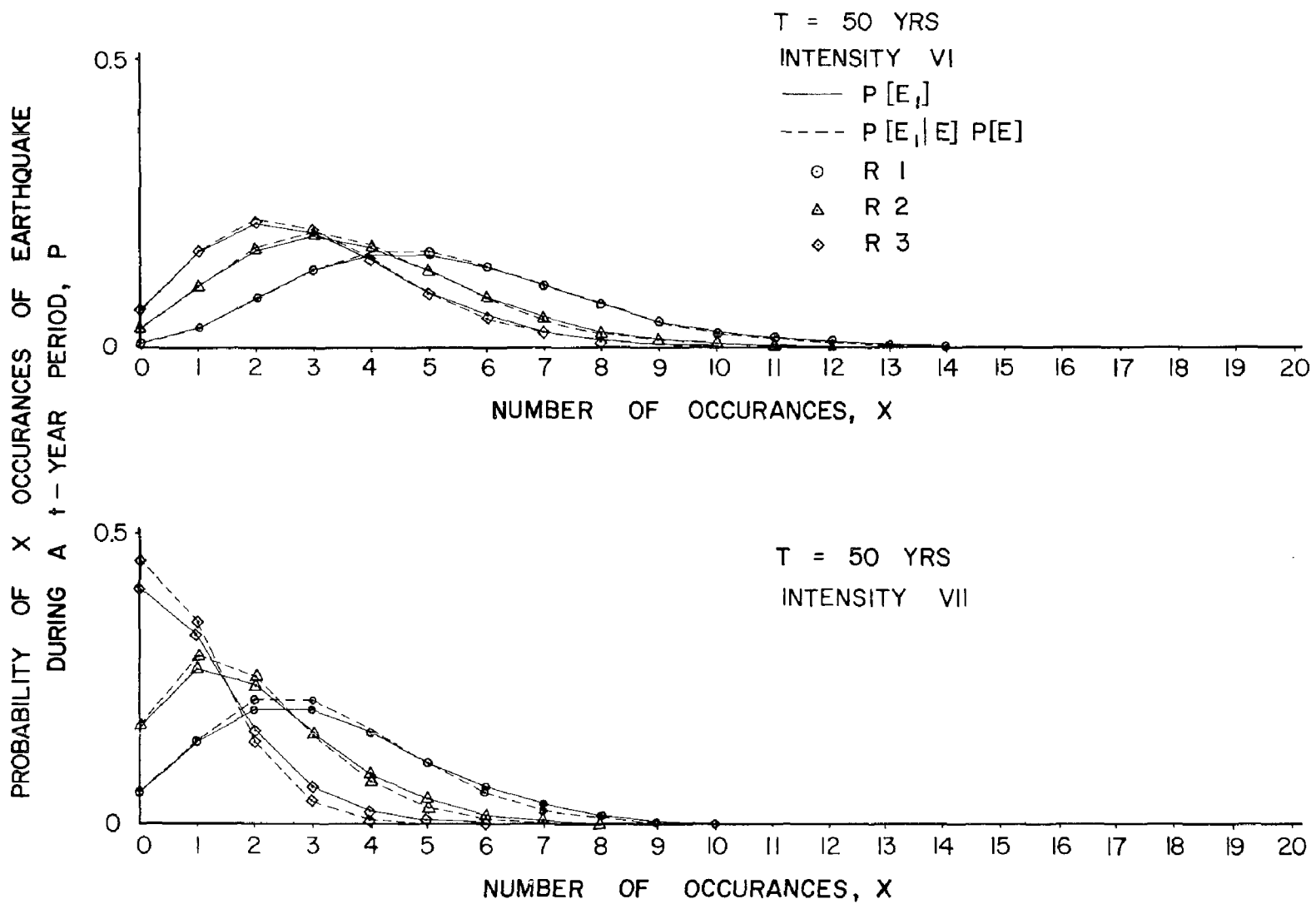
T = 50 YRS
INTENSITY VI
P [E,]
P [E, | E] P[E]
R 1
R 2
R 3
0.5
0
0 1 2 3 4 5 6 7 8 9 10 11 12 13 14 15 16 17 18 19 20
NUMBER OF OCCURANCES, X
PROBABILITY OF X OCCURANCES OF EARTHQUAKE DURING A t - YEAR PERIOD, P
T = 50 YRS
INTENSITY VII
0.5
0
0 1 2 3 4 5 6 7 8 9 10 11 12 13 14 15 16 17 18 19 20
NUMBER OF OCCURANCES, X

FIGURE 4

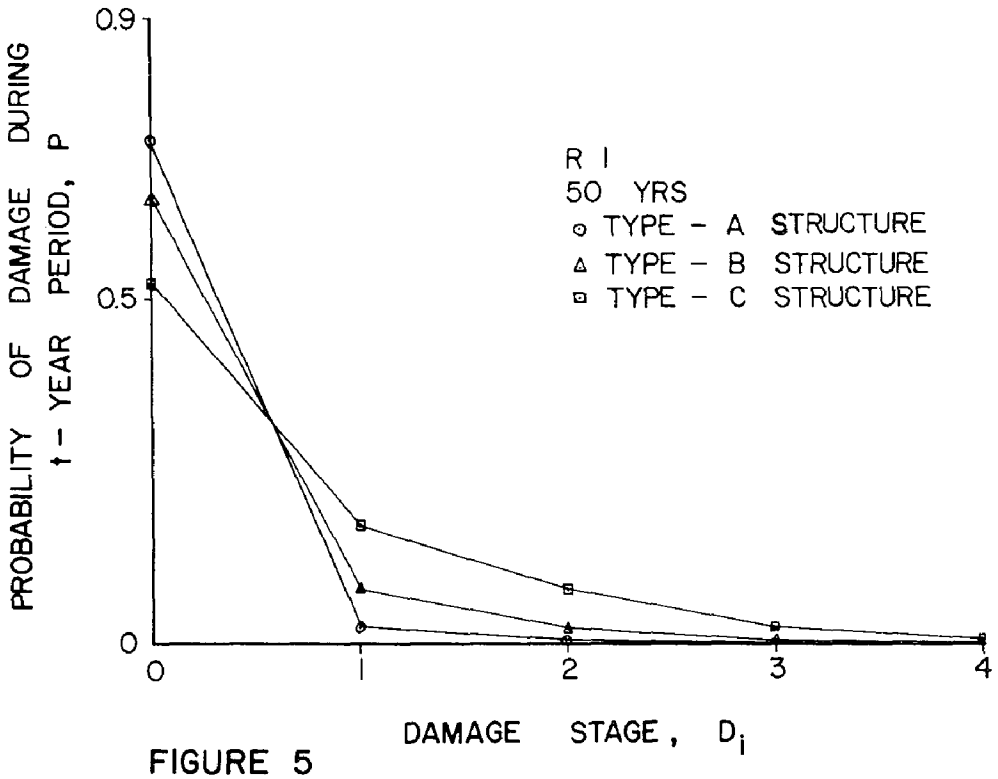

FIGURE 5

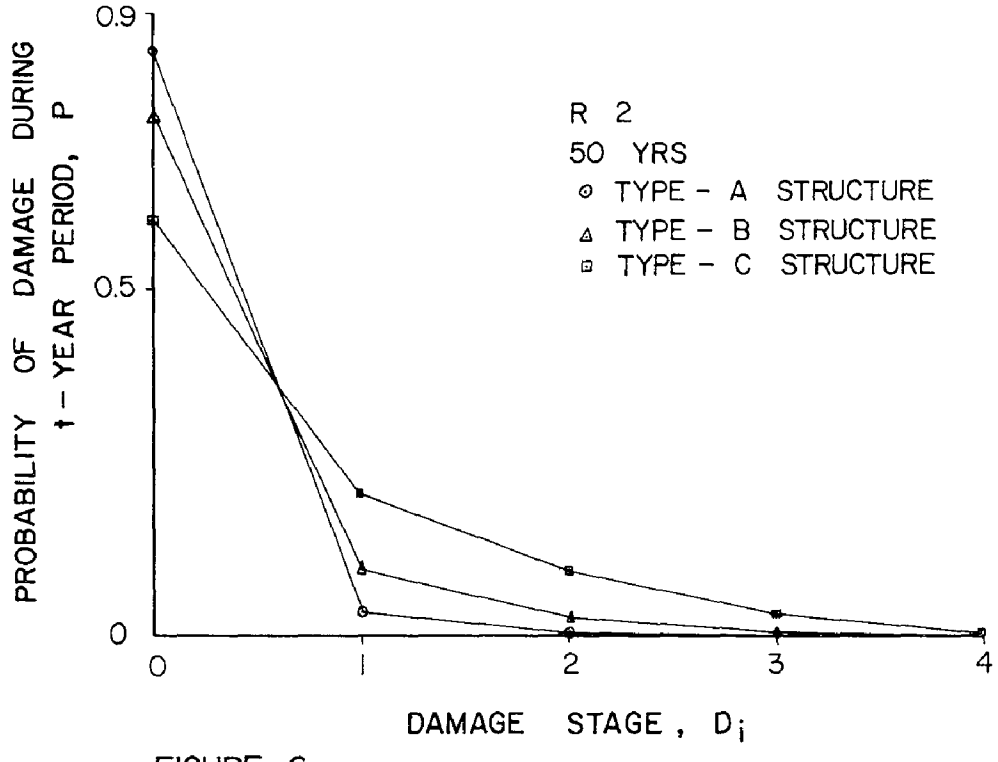

FIGURE 6

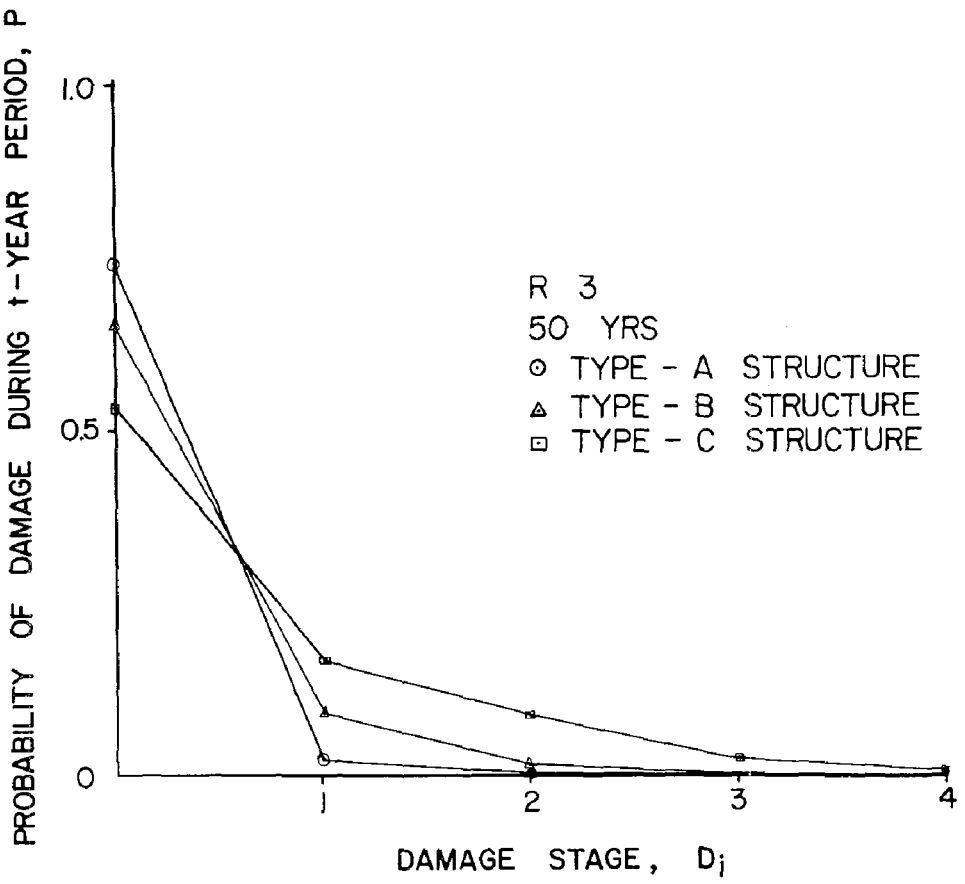
PROBABILITY OF DAMAGE DURING t-YEAR PERIOD, P
1.0
0.5
0
1
2
3
4
DAMAGE STAGE, D_j
R 3
50 YRS
TYPE - A STRUCTURE
TYPE - B STRUCTURE
TYPE - C STRUCTURE

FIGURE 7

References

1. Benjamin, J. R., and Cornell, C. A., Probability, Statistics, and Decision for Civil Engineers, McGraw-Hill, 1970, Chap. 6.

2. Borges, J. F., "Quantification of Design Rules Based on the Assessment of Earthquake Risk", Proceedings, 5th WCEE, Rome, Italy, June 25-29, 1973, Vol. 2, pp. 2502-2511.

3. Borgman, L. E., "Risk Criteria", Journal of the Waterways and Harbors Division, ASCE, Vol. 89, No. WW3, Proceeding Paper 3607, August, 1963, pp. 1-35.

4. Carlos, S. O., "Seismic Risk Analysis for a Site and a Metropolitan Area", Report to the NSF, University of California, Berkeley California, Report No. EERC 75-3, August, 1975.

5. Carmona, J. S., and Castano, J. E., "Analysis of Seismic Risk on the Site of Special Constructions in Argentina", Microzonation Conference, Seattle, Washington, October 30-November 3, 1972, Vol. 1, pp. 249-266.

6. Coffman, J. L., and von Hake, C. A., Editors, Earthquake History of the United States, Publication 41-1, Revised Edition (Through 1970), U.S. Department of Commerce, National Oceanic and Atmospheric Administration, 1973.

7. Cornell, C. A., Dynamic Waves in Civil Engineering, John Wiley and Sons, Lon., N.Y., 1971, Chap. 27.

8. Esteva, L., "Bases para la Formulacion de Deciones de Diseno Sismico", Instituto de Ingenieria, No. 182, University Nacional Autonoma de Mexico, 1968.

9. Gates, M., and Scarpa, A., "Reward-Risk-Ratio", Journal of the Construction Division, ASCE, December, 1974, pp. 521-531.

10. Grandori, G., and Benedetti, D., "On the Choice of the Acceptable Seismic Risk", Proceedings of the 4th European Symposium on Earthquake Engineering, London, September 5-7, 1972.

11. Key, D., "The Development of a Seismic Design Code for the Caribbean", Proceedings of 4th European Symposium on Earthquake Engineering, London, September 5-7, 1972.

12. Medveder, S. V., "Fundamental Principles of Seismic Risk Estimation", Proceedings of 4th European Symposium on Earthquake Engineering, London, September 5-7, 1972.

13. Newmark, N. M., and Rosenblueth, E., Fundamentals of Earthquake Engineering, Prentice Hall, 1971, Chap. 7.

14. Richter, C. F., Elementary Seismology, W. H. Freeman and Company, San Francisco, 1958.

15. Rowe, R. E., "Current European Views on Structural Safety", Journal of the Structural Division, ASCE, Vol. 96, No. ST3, Proc. Paper 7132, March, 1970, pp. 461-467.

16. Vanmarcke, E. H., Cornell, C. A., Whitman, R. V., and Reed, J. W., "Methodology for Optimum Seismic Design", Proc. 5th WCEE, Rome, Italy, June, 1973, Vol. 2, pp. 2521-2530.

17. Wagy, W. E., "Earthquake Damage", Abstract Journal of Earthquake Engineering, Vol. 1, September, 1972, University of California, Berkeley.

18. Whitman, R. V., "Risk-Based Seismic Design Criteria for Lifelines", ASCE, National Meeting on Water Resources Engineering, January 21-25, 1974, Los Angeles, California.

19. Whitman, R. V., Reed, J. W., and Hong, S. T., "Earthquake Damage Probability Matrices", Proceedings, 5th WCEE, Rome, Italy, Vol. 2, June, 1973, pp. 2531-2540.

20. Wiegel, R. L., (Coordinating Editor), Earthquake Engineering, Prentice-Hall, Inc., England Cliffs, N. J., 1970.

21. Wood, H. O., and Heck, N. H., Revised Edition (Through 1963) by Eppley, R. A., Earthquake History of the United States, Part II, U.S. Department of Commerce, Environmental Science Services Administration and Coast and Geodetic Survey, 1966.

INTERNATIONAL SYMPOSIUM ON
EARTHQUAKE STRUCTURAL ENGINEERING
St. Louis, Missouri, USA, August, 1976

ON NON-STATIONARY SPECTRUM AND MEAN SQUARE RESPONSE OF A SIMPLE STRUCTURAL SYSTEM TO EARTHQUAKE EXCITATION

TAKUJI KOBORI* and YOSHIHIRO TAKEUCHI**

* Professor, Department of Architectural Engineering, Kyoto University, Kyoto, Japan

** Associate Professor, Department of Architectural Engineering, Fukui University, Fukui, Japan

Summary

A method of evaluating the non-stationary spectral characteristics of the earthquake excitation is presented, by using the concept of the non-stationary spectral density under the assumption that the earthquake excitation may be considered as a non-stationary stochastic process. In this paper, the non-stationary spectral density is defined by the finite time averaged variance of output process of the narrow band filter taking account of the resolution in the frequency and time domains. As to the characteristics of the narrow band filter, the transfer characteristics of one-mass-system can be available. Some discussions on the physical interpretation of this non-stationary spectral density are shown and the numerical calculations are carried out for several recorded accelerograms. Through these discussions, the evaluation of mean square response of the lumped mass system for the non-stationary spectral density is examined, relating to the procedure of evaluating the maximum structural response from the response spectrum, and the numerical results with regard to the lumped mass type structural models are presented.

1. Introduction

It is one of the most important problems for anti-seismic design of the building structure to evaluate the non-stationary spectral characteristics of an earthquake excitation, concerning with the procedure of assessing such some significant statistical quantities as mean square response, threshold crossing probability and cumulative fatigue damage. A number of recent papers have provided various mathematical representations and the physical interpretation for the non-stationary spectra of an earthquake excitation.

In this paper, the non-stationary spectra for an earthquake excitation are defined as the finite time averaged variance of output process through a narrow band filter. The characteristics of a narrow band filter can be adopted for those of an ideal rectangular filter or one-mass-system with

an appropriate damping value. This spectral representation for a non-stationary process implies an approximate description of a non-stationary spectral density under the restriction on the resolution either in the frequency domain or in the time domain. Furthermore, adopting the transfer characteristics of one-mass-system as a narrow band filter, it can be considered that the procedure of evaluating the mean square response of the lumped mass system is same, in the physical concept, as the evaluation procedure for the maximum structural response from the response spectrum of an earthquake excitation.

We discuss, first of all, on the theoretical background and the physical meaning of non-stationary spectral density, associating with the spectral resolution of the filter band-width in the frequency domain and the averaging time interval in the time domain. And then, the non-stationary spectral densities are evaluated for several actual recorded accelerograms and the numerical results are presented graphically. From these analytical results of the non-stationary spectral characteristics, the predominant frequencies detected at any instant of time are discussed in comparison with the results from the stationary spectral analysis. Finally, by using the non-stationary spectral density, the numerical evaluations are shown with regard to the mean square response of two types of three degrees of freedom systems on the basis of the similar technique as the ordinary approach of the so-called response spectrum.

2. Non-stationary spectral density of earthquake excitation

An earthquake excitation can be considered as the non-stationary stochastic process with duration time from about ten seconds to several minutes. The non-stationary characteristics of an earthquake excitation depend upon two physical quantities in the time and frequency domains. One of the physical quantities in the time domain is a time variation of energy level of an excitation and the other in the frequency domain is a spectral distribution of energy at each instant time. As to the examination of the time variation of energy level of an earthquake excitation, it seems to be suitable to use an envelope function of waveform, which is equivalent to the local variance evaluated by the weighting function with finite time interval. By using the evaluation of the local variance of an excitation, the facts have been investigated that the envelope functions of the recorded accelerograms are slowly varying time function and that the characteristics of envelope functions vary with epicentral distance and magnitude of earthquake. On the other hand, there are various approaches to the procedure of the non-stationary spectral analysis for an earthquake excitation based on the concept of the generalized spectral density for the non-stationary process. In this section, the definition of the non-stationary spectral density is discussed from the viewpoint of spectral distribution of energy in the frequency domain.

The non-stationary spectral density is defined, in the following equation (1), as the time averaged variance within the time interval t_o of output process $x(t)$ through a narrow band filter $g(t)$ with band-width Δf.

$$\phi(f, t) = \frac{1}{t_o} \int_{t-\frac{t_o}{2}}^{t+\frac{t_o}{2}} dt' \frac{1}{\Delta f} \int_{-\infty}^{\infty} \int_{-\infty}^{\infty} g(\xi_1) g(\xi_2) K_x(t'-\xi_1, t'-\xi_2) d\xi_1 d\xi_2 \qquad (1)$$

where Kx(t, t') is the covariance function of output process x(t) with regard to the time t and t'. It is, therefore, clear that this spectral density function is the positive real valued function with respect of two variables ,frequency f and time t. In equation (1), the filter characteristics g(t) is adopted to the ideal rectangular filter with center frequency f and narrow band-width Δf.

$$\left.\begin{aligned} g(t) &= \frac{2}{\pi t}\sin\pi\Delta f t\cos 2\pi f t \\ G(f) &= U\{|f'|-(f-\frac{f}{2})\} - U\{|f'|-(f+\frac{f}{2})\} \end{aligned}\right\} \qquad (2)$$

where U represents a unit step function. Substituting equation (2) into equation (1), then we have

$$\phi(f,t) = \frac{1}{t_o}\int_{t-\frac{t_o}{2}}^{t+\frac{t_o}{2}} dt' \frac{1}{\Delta f}\int_{-\infty}^{\infty}\int_{-\infty}^{\infty} K_x(t'-\xi_1, t'-\xi_2)\frac{1}{\pi^2\xi_1\xi_2}\sin\pi\Delta f\xi_1 \sin\pi\Delta f\xi_2 \times \frac{1}{2}\{\cos 2\pi f(\xi_1-\xi_2) + \cos 2\pi f(\xi_1+\xi_2)\}\, d\xi_1 d\xi_2 \qquad (3)$$

Taking the integral of the above equation $\phi(f, t)$ over the area of total frequency domain $(-\infty, \infty)$ with respect to f, we have

$$Q(t) = \int_{-\infty}^{\infty}\phi(f,t)df = \frac{1}{2t_o}\int_{t-\frac{t_o}{2}}^{t+\frac{t_o}{2}} dt' \frac{1}{\Delta f}\int_{-\infty}^{\infty}\{K_x(t'-\xi_1, t'-\xi_1) + K_x(t'-\xi_1, t'+\xi_1)\}\left(\frac{\sin\pi\Delta f\xi_1}{\pi\xi_1}\right)^2 d\xi_1 \qquad (4)$$

In (4), it is necessary to determine the averaging time interval t_o and narrow band-width Δf appropriately under the consideration for the total time duration of an earthquake excitation and the natural period of building structure. Because of slowly varing properties, within the time interval t_o, both of the envelope function and spectral characteristics of an earthquake excitation, the covariance function Kx(t, t') might be assumed to be locally-stationary, and so eq.(4) reduces approximately to eq.(7) by using eqs.(5) and (6).

$$K_x(t'-\xi, t'+\xi) \simeq I(t')\,\bar{K}_x(2\xi) \qquad (5)$$

$$\left.\begin{aligned} \bar{S}_x(p) &= \int_{-\infty}^{\infty}\bar{K}_x(\xi)\, e^{-j2\pi p\xi}\, d\xi \quad , \quad \bar{K}_x(\xi) = \int_{-\infty}^{\infty}\bar{S}_x(p)\, e^{j2\pi p\xi}\, dp \\ L(g) &= \int_{-\infty}^{\infty} I(t')\, e^{-j2\pi gt'}\, dt' \quad , \quad I(t') = \int_{-\infty}^{\infty} L(g)\, e^{j2\pi gt}\, dg \end{aligned}\right\} \qquad (6)$$

$$Q(t) \simeq \frac{1}{2t_o}\int_{t-\frac{t_o}{2}}^{t+\frac{t_o}{2}} dt' \int_{-\infty}^{\infty}(I(t'-\xi_1) + I(t')\,\bar{K}_x(2\xi_1))\frac{\sin^2\pi\Delta f\xi_1}{\pi^2\xi_1^2\Delta f}d\xi_1 = \frac{1}{2t_o}\int_{t-\frac{t_o}{2}}^{t+\frac{t_o}{2}} dt' \int_{-\infty}^{\infty} d\xi_1 \int_{-\infty}^{\infty} L(p)\{e^{j2\pi(t'-\xi_1)p} + \bar{K}_x(2\xi_1)e^{j2\pi pt'}\}\left(\frac{4\sin\pi\Delta f\xi_1}{\pi^2\xi_1^2\Delta f}\right)dp \qquad (7)$$

In these equations, I(t) is an envelope function which represents the variation of energy level of x(t) and $K_x(\xi)$ is a covariance function with unit mean square value. Considering the following relationship,

$$\left.\begin{aligned} &\frac{\sin^2\pi\Delta f\xi}{\pi^2\xi^2\Delta f} = \int_{-\infty}^{\infty} D(p)e^{-j2\pi\xi p}dp \\ &D(p) = 1 - \frac{|p|}{\Delta f} \quad |p| \leqq \Delta f, \qquad D(p) = 0 \quad |p| > \Delta f \end{aligned}\right\} \tag{8}$$

then, eq.(7) becomes

$$\begin{aligned} Q(t) &= \frac{1}{2t_o}\int_{t-\frac{t_o}{2}}^{t+\frac{t_o}{2}} dt' \int_{-\infty}^{\infty} L(p)\{D(p)+\int_{-\Delta f}^{\Delta f} S_x(\tfrac{\nu}{2})D(\nu)d\nu\}e^{j2\pi pt'}dp \\ &= \int_{-\infty}^{\infty} L(p)\frac{\sin\pi pt_o}{\pi pt_o}e^{j2\pi pt}dp \end{aligned} \tag{9}$$

in which, $Sx(\nu)$ is constant within the interval Δf. Taking the restriction of band-width Δf and averaging time t_o as $\Delta f t_o \gg 1$ in eq.(9), we have

$$Q(t) = \frac{1}{t_o}\int_{t-\frac{t_o}{2}}^{t+\frac{t_o}{2}} I(t')dt' = \frac{1}{t_o}\int_{t-\frac{t_o}{2}}^{t+\frac{t_o}{2}} K_x(t', t')dt' \tag{10}$$

From this, it is pointed out that the function $\phi(f,t)$ may be an approximate representation of spectral density in the neighbourhood of instant of time t.

The filter characteristics in eq.(2) are available for the transfer characteristics of one-mass-system which are so-called narrow band filter by an appropriate value of damping coefficient.

$$\left.\begin{aligned} g(t) &= \Delta f e^{-\pi\Delta f t}\sin 2\pi f t\ U(t) \\ G(f) &= \frac{2\pi\Delta f f}{(f^2-f'^2)+j\Delta f f'} \end{aligned}\right\} \tag{11}$$

Making use of this filter characteristics, the concept of the non-stationary spectral density can be applied in the same way as the case of obtaining eq.(10). Then, corresponding to eqs.(3) and (4), we have

$$\begin{aligned} \phi(f, t) = \frac{1}{t_o}\int_{t-\frac{t_o}{2}}^{t+\frac{t_o}{2}} dt' \frac{1}{\Delta f}\int_{-\infty}^{\infty}\int_{-\infty}^{\infty} K_x(t'-\xi_1, t'-\xi_2)\ e^{-j\pi\Delta f(\xi_1+\xi_2)} \\ \times \Delta f^2 \sin 2\pi f\xi_1 \sin 2\pi f\xi_2\ d\xi_1 d\xi_2 \end{aligned} \tag{12}$$

$$Q(t) = \frac{1}{t_o}\int_{t-\frac{t_o}{2}}^{t+\frac{t_o}{2}} dt' \frac{\Delta f}{2}\int_{o}^{\infty} K_x(t'-\xi_1, t'-\xi_1)\ e^{-2\pi\Delta f\xi_1}\ d\xi_1 \tag{13}$$

Assuming the same conditions in eqs.(5), (6) and $\Delta f t_o \gg 1$, we obtain the following result similar to eq.(10),

$$Q(t) = \int_{-\infty}^{\infty}\phi(f, t)df \simeq \frac{1}{4\pi}\int_{-\infty}^{\infty} dp \frac{1}{t_o}\int_{t-\frac{t_o}{2}}^{t+\frac{t_o}{2}} L(p)e^{j2\pi pt'}dt' = \frac{1}{t_o}\int_{t-\frac{t_o}{2}}^{t+\frac{t_o}{2}} I(t')dt' \tag{14}$$

3. Spectral characteristics of the recorded accelerograms

In this section, the numerical evaluations of the non-stationary spectral density defined in eq.(1) are carried out for the cases of five kinds

of the recorded accelerograms; El Centro (1940), Taft (1952), Vernon (1933), Olympia (1949) and Tokachi-oki (1968). As mentioned in the previous section, the evaluation of the non-stationary spectral density for an earthquake excitation corresponds to that of the spectral distribution of the input energy, the time variation of which is described by the envelope function of the waveform of an excitation. For the recorded accelerograms, the spectral distribution at any instant time and/or the time variation of the spectrum at any frequency can be evaluated from the non-stationary spectral density. So that the numerical results of the spectral distribution at each instant time is represented graphically in comparison with the spectral characteristics by the application of the quasi-stationary analysis.

The restriction with respect to $\Delta f t_o$, as shown in the previous section, suggests in itself the restriction for the resolution either in the frequency or time domain. For the usual building structure with its natural frequency of 1 - 2 Hz and the strong ground motion of 1 - 2 minutes duration time, their resolutions are required in the frequency domain where the frequency resolution Δf is less than about 1/2 Hz and also in the time domain where the averaging time t_o is less than about ten seconds. On carrying out the numerical analysis, the values of $\Delta f t_o$ are chosen within the range from 1.25 to 20.0 under the consideration for the resolution as above mentioned.

The analytical results by the definition in eq.(1) are shown in figures, from Fig. 1 to Fig. 5. The frequency range in the numerical analysis is from 0.1 Hz to 5.0 Hz and a number of the instants of time are located at three points within the duration time of the excitation. Some of the parameters peculiar to the filter characteristics of one-mass-system are determined so as to maintain the unit area for the total energy of the output process. The ordinate in Figs. 1 and 2 is scaled, with reference to the case that the maximum acceleration amplitude of the excitation is unity. On the other hand, in order to illustrate clearly the difference of the spectral characteristics at each instant time, the scale of the ordinate in Figs. 3 - 5 is determined under the condition that the energy level of the excitation at the corresponding instant time is unity.

Figs. 1-(a), 1-(b), 2-(a), and 2-(b) show that the degree of the resolution decreases according to the values of $\Delta f t_o$, for the case of El Centro and Taft accelerograms. From these results, it seems to be necessary to take a comparably small value of $\Delta f t_o$ so as to assure the resolution for these accelerograms with about half a minute duration time. Figs. 3 - 5 reveal the analytical results of the spectral analysis for Vernon, Olympia and Tokachi-oki accelerograms in the case of two kinds of the values of $\Delta f t_o$. The time variation of the spectral characteristics can be estimated from the feature of the variations for the predominant frequency and its peak value, so that the tendency of the time-dependent spectral characteristics for the recorded accelerograms are apparently pointed out in these figures. It is, therefore, necessary to consider sufficiently the influence of the time variation of the spectral distribution for the problems of evaluating the structural responses as statistical quantities.

As shown in Fig. 6, the spectral density of El Centro accelerogram is provided from the application of the stationary analysis, with regard to stationary part of quasi-stationary process whose deterministic function is given by the envelope function of an excitation. In this figure, there exist some predominant frequencies of the recorded accelerogram at the frequency about 1 Hz, 1.5 Hz, 2 Hz and 3 Hz. These predominant frequencies

is found to coincide with several frequencies, which are obtained from the total sum of the spectral characteristics at each instant time in Fig. 1(c). From this fact, we find that the spectral distribution in the stationary analysis, which seems to indicate the smoothing results averaged over the total duration of the excitation, is decomposed into the non-stationary spectral characteristics at each instant time.

4. Mean square response of lumped mass system

The mean square response of linear structural system subjected to non-stationary random excitation has been studied on the basis of random pulse sequense, quasi-stationary process and locally-stationary process. In general, the evaluation of the mean square response of multi-degree of freedom system is included in the determination of covariance matrix of output response of structural system. In order to determine this output covariance matrix, it is necessary to evaluate impulsive response function matrix and input covariance matrix. By using eigen value matrix and eigen vector matrix of the structural system, the representation of output covariance matrix can be reduced to simple form, concerning to the structural systems with the modal uncoupling characteristics. For usual building structures with some small damping values, it is reasonable to suppose the modal uncoupling characteristics of structural system and so the maximum value of the structural response can be evaluated by response spectrum technique on the application of modal analysis. In the problem of calculating mean square response by non-stationary spectral density, the transfer characteristics of one-mass-system should be adopted as narrow band filter, and its band-width Δf, which gives the resolution in frequency domain, is determined by the value of damping coefficient of one-mass-system. Considering the fact that a value of damping coefficient in usual building structure is small, it seems to be valid to adopt the transfer characteristics of one-mass-system as a narrow band filter. On the other hand, it is unable to adopt large averaging time interval on account of the natural frequency of the structural system and the duration of an earthquake excitation, although the averaging time interval t_o is desirable to be sufficiently large under the condition such as $\Delta f t_o \gg 1$. This condition is, in particular, important for the response analysis of structural system with the long period. From this restriction for $\Delta f t_o$, it is advisable to take the value of $\Delta f t_o$ as comparably small value at the sacrifice of the strict characteristics as spectral density, in order to preserve the resolution in the frequency and time domains. On evaluating the mean square response by making use of the evaluation procedure as mentioned in this section, it is pointed out that the influence of cross-correlation among different vibration modes is considered to be small in contract with the value of its variance in vibration modes, and so the influence of cross-correlation can be neglected in the evaluation of mean square response. Then, it is permissible to calculate the mean square value of displacement response at any point as the sum of each mean square response at the corresponding point with regard to normal coordinate. The mean square response of lumped mass system is, as a result, evaluated from the figures obtained in the previous section on the basis of similar evaluation procedure as that of response spectrum.

In this section, we investigate two types of three degrees of freedom systems, in which mass distribution {m} and stiffness distribution {k} are

as follows;

CASE I; $\{ m \} = \{ 1.0, 1.0, 1.0 \}$, $\{ k \} = \{ 1.0, 1.0, 1.0 \}$

CASE II; $\{ m \} = \{ 1.0, 1.0, 1.0 \}$, $\{ k \} = \{ 0.5, 0.823, 1.0 \}$

The natural circular frequencies and the vibration modes of the structural systems are shown in Fig. 7, taking the standard quantities of mass and stiffness as M and K respectively. Fig. 8 shows the numerical results of the mean square response of displacement, which are obtained from Figs.1-(a) and 2-(a) for the case that the fundamental natural frequencies of both structural systems of CASE I and CASE II is 2 Hz and the values of $\Delta f t_o$ for the El Centro and Taft accelerograms are taken as 1.25 and 1.5 respectively. It is found that the influence of first vibration mode is predominant in the results of the mean square value of displacement response in both cases. As the filter band width is related directly to the damping ratio of one-mass-system, the value of damping coefficient can be represented by the filter band-width Δf. For an example, by expressing the filter band-width Δf as the frequency interval at the height of half a its peak value, Δf becomes to be equivalent to $2hf_o$, where h and f_o represent values of damping ratio and fundamental natural frequency respectively, and then, corresponding to $\Delta f t_o$ of 1.25 and 1.5, the damping ratios of 5.5 and 6.2 percents are obtained with respect to fundamental natural frequency. The dotted lines shown in Fig. 8 present the mean square responses, by the earthquake response analysis, that are evaluated at each instant time as the time averaged variance of the structural system within finite time interval. The averaging time intervals are 5.6 seconds for the El Centro accelerogram and 6.0 seconds for Taft accelerogram. It is found, in this figure, that these results correspond successfully to the results evaluated by the non-stationary spectral density. The differences between both results are about from ten to twenty percents and this arises from the reason why the influence of correlation among the vibration modes is neglected.

5. Concluding remark

In this paper, some discussions on the non-stationary spectral density are presented, in which the non-stationary spectral density is defined by the finite time averaged variance of output process through narrow band filter taking account of resolution of the frequency and time domains. By using this, the non-stationary characteristics of the recorded accelerograms are evaluated numerically. It is, moreover, shown that the mean square response of the lumped mass system can be evaluated from the non-stationary spectral density by adopting the transfer characteristics of one-mass-system as a narrow band filter.

In order to maintain strictly the characteristics as spectral density, it is required to satisfy the condition $\Delta f t_o \gg 1$. Concerning to an usual earthquake excitation, duration of which is less than one minute, the resolution in the frequency and time domains is restricted by this condition. It is, therefore, necessary to use comparably small value of $\Delta f t_o$ in order to preserve the characteristics as spectral density.

From the analytical results of the recorded accelerograms, it is found that the spectral characteristics evaluated from the application of the theory of quasi-stationary analysis are decomposed into the non-stationary spectral characteristics at each instant time. The time-dependent spectral characteristics of an earthquake excitation are detected from these analyses

for the recorded accelerograms, and then the statistical evaluation of the structural response analysis is suggested to be necessary for the aseismic design of a structure taking account of this time-dependent characteristics.

The method of evaluating the mean square response of the lumped mass system is examined and the numerical analyses are presented for two types of the structural system. Through this investigation, the evaluation procedure of the mean square structural response seems to be developed by using the non-stationary spectral density.

Reference

[1] Amin, M. and Ang, A. H. -S. ; Nonstationary Stochastic Model of Earthquake Motion, Proc. of ASCE, Vol. 94, EM2, 1968, pp. 559-583

[2] Hasselman, T. ; Linear Response to Nonstationary Random Excitation, Proc. of ASCE, Vol. 98, No. EM3, 1972, pp. 519-529

[3] Holman, R. E. and Hart, G. C. ; Nonstationary response of Structural Systems, Proc. of ASCE, Vol. 100, No. EM2, 1973, pp. 415-431

[4] Jennings, P. C., Housner, G. W. and Tsai, N. C. ; Simulated Earthquake Motions for Design Purposes, Proc. of the 4th WCEE, 1969, pp. 145-160

[5] Kobori, T. and Minai, R. ; Nonstationary Response of the Linear Systems to Random Excitation, Bulletin of the Disaster Prevention Research Institute of Kyoto Univ., Vol. 16, part 2, No. 111, 1967, pp. 37-80

[6] Kobori, T. ; Some Topics on Anti-Seismic Safety of Building Structures, Reliability Approach in Structural Engineering, Maruzen Co., Inc., 1975, pp. 275-295

[7] Liu, S. C. ; Evolutionary Power Spectral Density of Strong-Motion Earthquake, Bulletin of the Seismological Society of America, Vol. 60, No. 3, 1970, pp. 891-900

[8] Mark, W. D. ; Spectral Analysis of the Convolution and Filtering of Non-Stationary Stochastic Processes, Journal of Sound and Vibration, 1970, 11(11), pp. 19-63

[9] Priestley, M. B. ; Evolutionary Spectra and Non-Stationary Processes, Journal of Royal Statistical Society, B27, 1965, pp. 204-236

[10] Takeuchi, Y. ; Non-Stationary Mean Square Response of Structural Systems to Quasi-Stationary and Locally-Stationary Random Excitation, Memoirs of the Faculty of Engineering, Fukui University, Vol. 23, No. 2, 1975, pp. 237-251 (in Japanese)

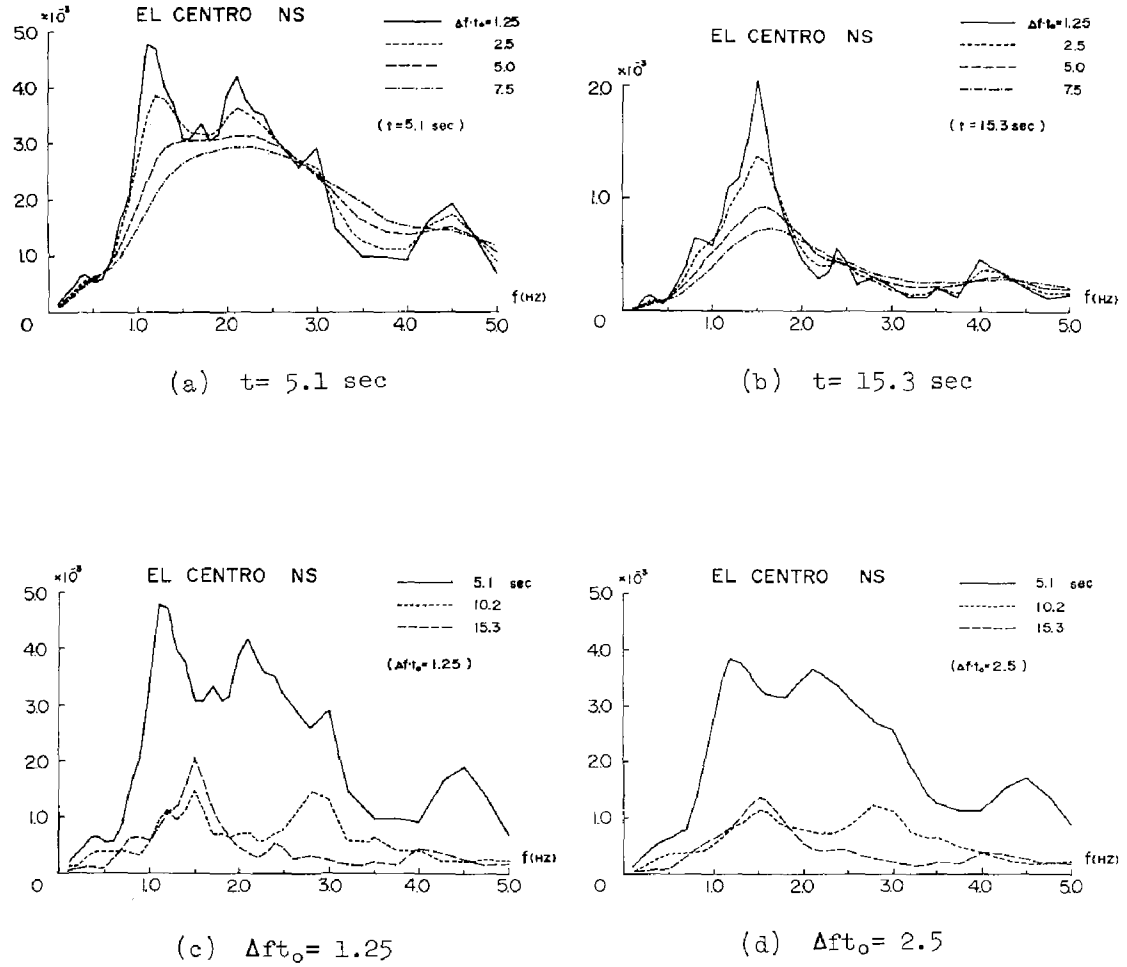

(a) t= 5.1 sec

(b) t= 15.3 sec

(c) $\Delta f t_o$= 1.25

(d) $\Delta f t_o$= 2.5

Fig. 1 Non-stationary spectra of El Centro accelerogram, NS component (1940)

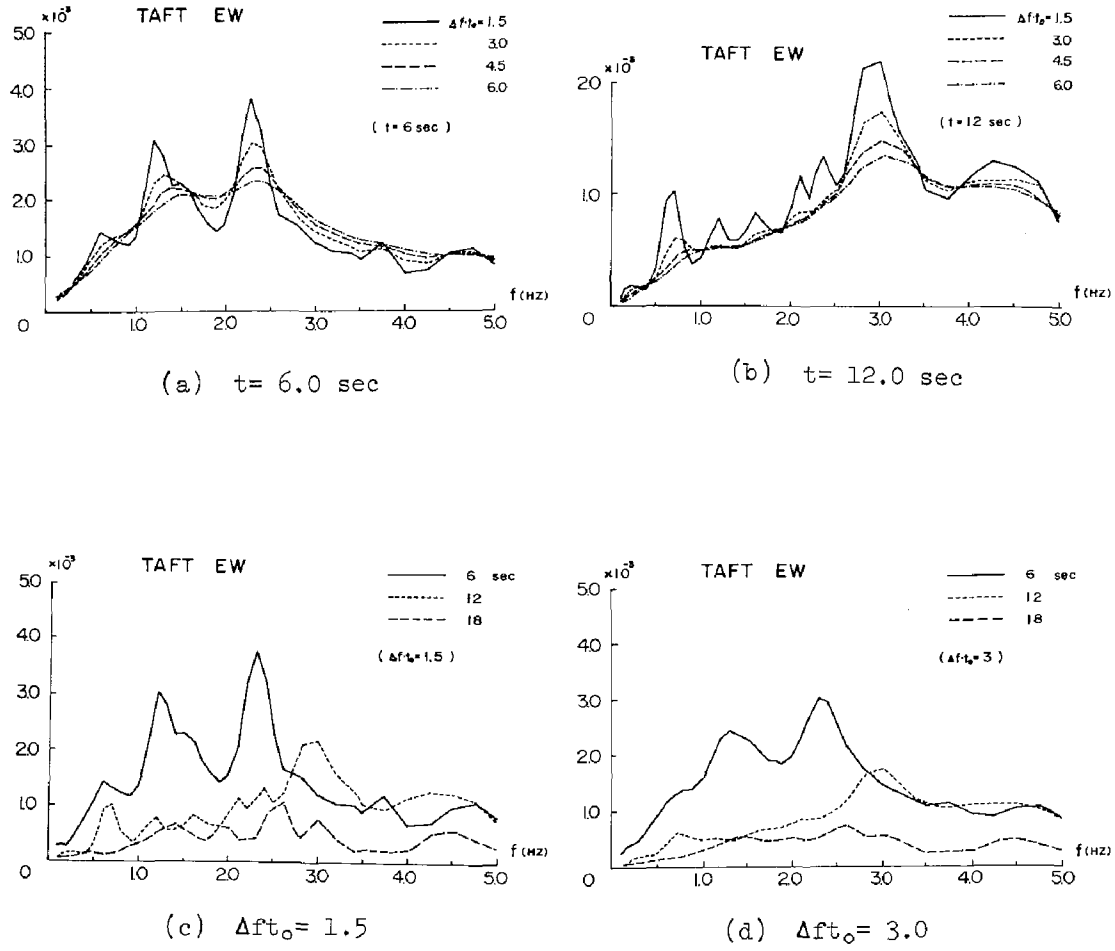

Fig. 2 Non-stationary spectra of Taft accelerogram, EW component (1952)

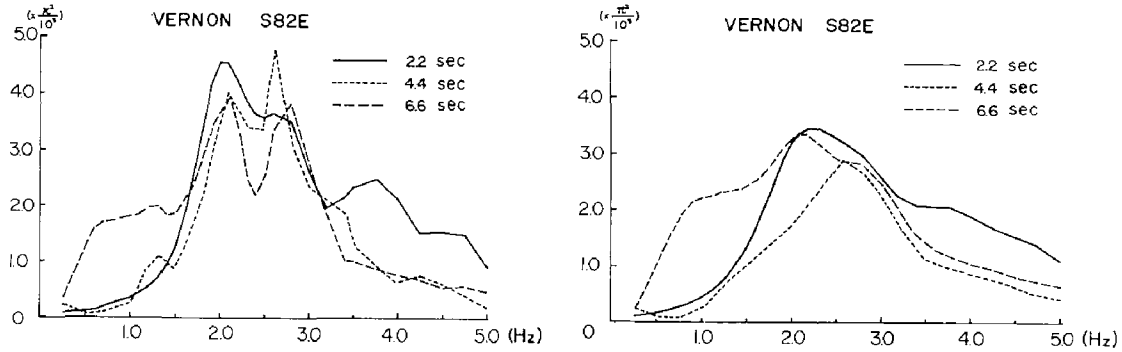

(a) Δft_o=1.0 (b) Δft_o= 2.0

Fig. 3 Non-stationary spectra of Vernon accelerogram, S82°E component (1933)

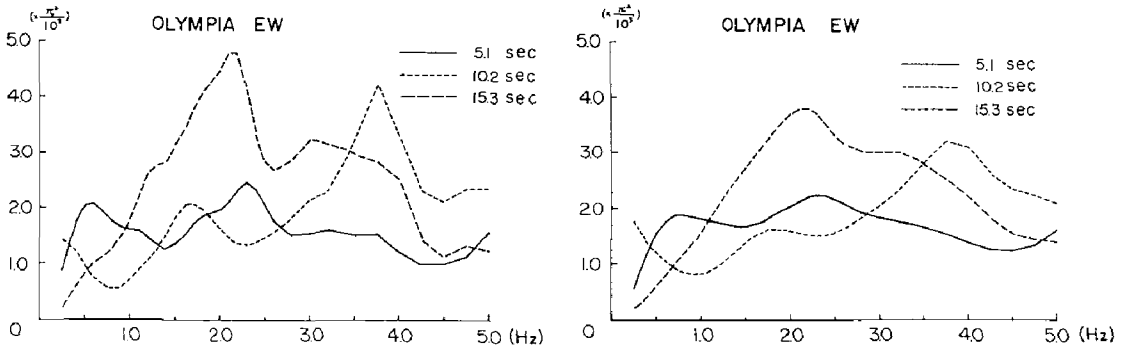

(a) Δft_o=5.6 (b) Δft_o= 11.2

Fig. 4 Non-stationary spectra of Olympia accelerogram, EW component (1949)

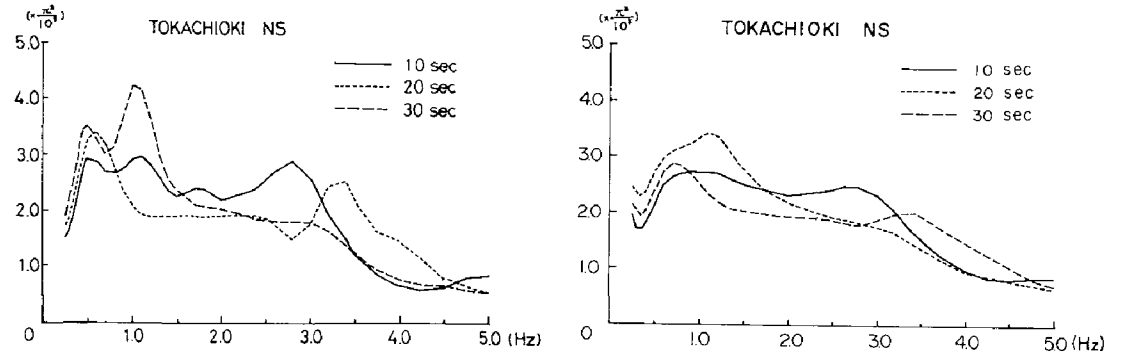

(a) Δft_o= 10.0 (b) Δft_o= 20.0

Fig. 5 Non-stationary spectra of Tokachi-oki accelerogram, NS component (1968)

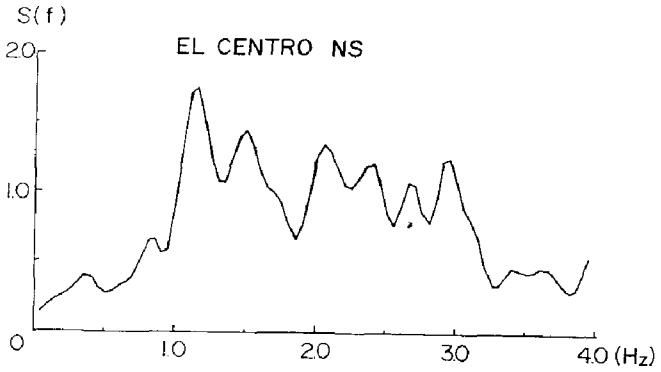

Fig. 6 Stationary spectrum of El Centro accelerogram, NS component (1940), by quasi-stationary analysis

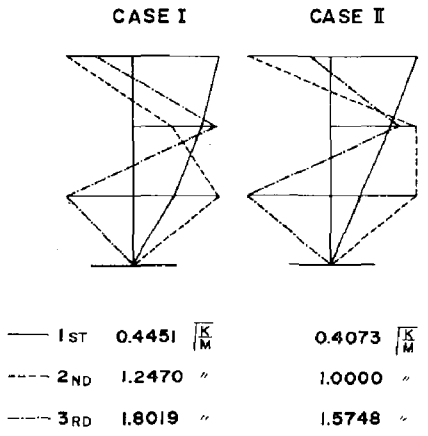

Fig. 7 Natural frequencies and vibration modes of two kinds of structral systems

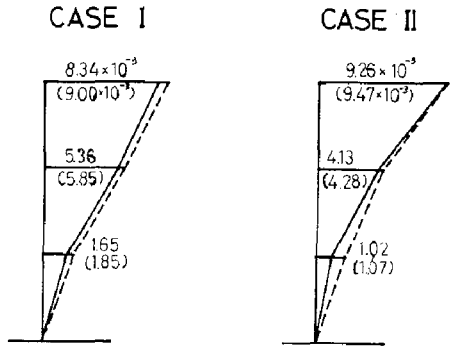

(a) El Centro accelerogram, t= 5.1 sec

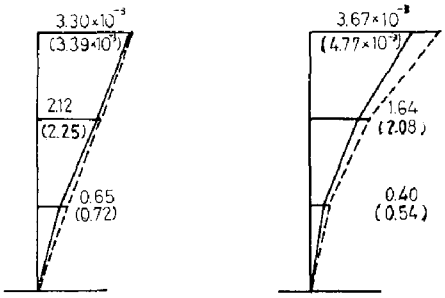

(b) Taft accelerogram, t= 6.0 sec

Fig. 8 Transient variances of two kinds of structural systems,
solid line; by non-stationary spectra
dotted line; by earthquake responses analysis

INTERNATIONAL SYMPOSIUM ON
EARTHQUAKE STRUCTURAL ENGINEERING
St. Louis, Missouri, USA, August, 1976

DYNAMIC EARTHQUAKE ANALYSIS OF A BOTTOM SUPPORTED INDUSTRIAL BOILER

N. J. MONROE N. DASA

Section Manager Senior Engineer

The Babcock & Wilcox Company
Power Generation Group
North Canton, Ohio, U.S.A.

ABSTRACT

In this paper a dynamic earthquake analysis of a large bottom supported boiler is presented. The assumptions and modeling techniques necessary to developing the mathematical model are stated and the dynamic response of the structure and the resultant stresses are tabulated. The results of the dynamic analysis are compared to the results of the static earthquake analysis which is presently required by the various nationally accepted building codes. In addition, results are presented of a dynamic analysis of the same boiler using a more detailed mathematical model. The advantages of both models are discussed and recommendations are made based on a comparison of the results presented.

INTRODUCTION

Most building codes require that a structure be designed to resist earthquakes. The method of analysis usually specified is based on static analysis procedures. An equation, which is a function of the total weight of the structure, is used to determine the total horizontal earthquake force to be resisted by the supports of the structure. This force is then divided into increments acting along the height of the structure. The method used in distributing the horizontal force results in having more force near the top of the structure. The structure is then analyzed, treating the earthquake loads as constant static forces and without considering the structure's response to the dynamic nature of this earthquake loading. A static method of earthquake analysis was a good practical method to use prior to the development of the high speed computers and the various sophisticated programs capable of analyzing very large and complex structures. A better analysis and design can result by using a dynamic earthquake input at the base of a structure and then determine the earthquake loads resulting from the actual response of structure to the dynamic load. Using such a method the load distribution becomes a function of the structures flexibility and it changes if the flexibility of certain members is revised. This type of approach is more realistic and it identifies more

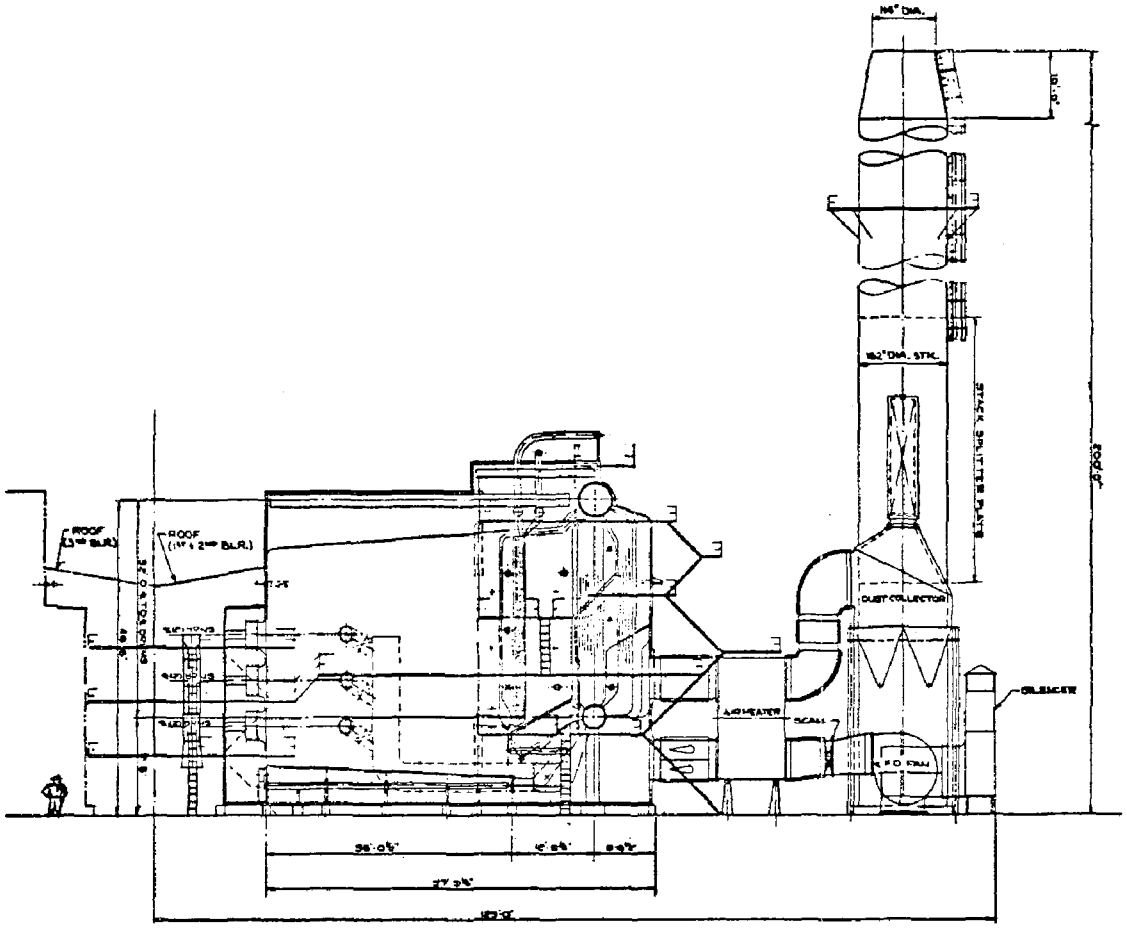

FIG. 1 Typical Arrangement of Boiler and Auxiliary Equipment

adequately the structure's behavior during an earthquake. In addition, the designer develops more confidence in the adequacy of the structure to resist an earthquake when he observes its response and understands its behavior when subjected to a dynamic force.

The actual structure is represented in the computer by a mathematical model. The accuracy of the results will depend on the accuracy of the model. However, in large complex structures it is impossible to model all structural details. When time and economics allow, the designer can develop more confidence in the mathematical model by observing the changes in its response when certain key members are modeled differently. This way, he can determine the sensitivity of certain members and how detailed their modeling has to be. For this reason the mathematical model used in this paper is compared to a similar but a more detailed model. The results of the analysis using two models are tabulated and compared. Recommendations are made as to the need of such an effort in designing a structure.

PROCEDURE

In the writer's opinion, the development of the mathematical model is the most important phase to performing a dynamic analysis. Upon the accuracy of the model depend the results of the analysis and how close they represent the actual structure. The computer can do an excellent job in analyzing a model. The designer needs to assure himself that his model truly represents the actual structure. This is easier said than done. Experience coupled with a good understanding of structural dynamics are the best guides.

A boiler is composed of numerous components. It is not possible to include all the components in the mathematical model. In developing the model used in this paper the boiler components were combined and represented as follows:

1 Drums
These are large and thick pressure vessels which are modeled as structural members and are represented by their actual geometric properties.

2. Generating Tubes
There are more than a thousand tubes connecting the upper (steam) drum and the lower (water) drum. Since they are too numerous to individually represent in the model they are combined into equivalent members whose properties represent their total actual flexibility.

3. Superheater Tubes
These tubes, due to their large number, are also represented by equivalent members as is the case with the generating tubes.

4. Screen Tubes
These tubes are also modeled using equivalent members.

5. Wall Tubes
These tubes are membraned together. Their properties are best represented modeling them as orthotropic plates.

6. Supports
Careful consideration should be given to modeling the boiler supports to reflect their true behavior during operation. This is necessary since most supports provide resistance in only specific directions while accommodating the thermal expansion of the structure.

7. Pipes and Structural Members
All these members are modeled using their actual geometry and properties.

Having developed the geometrical configuration and proper ties of all members and establishing their space coordinates, one has fully described the mathematical model to be used in the analysis. The earthquake spectrum required as input is the next step. For the structure analyzed in this

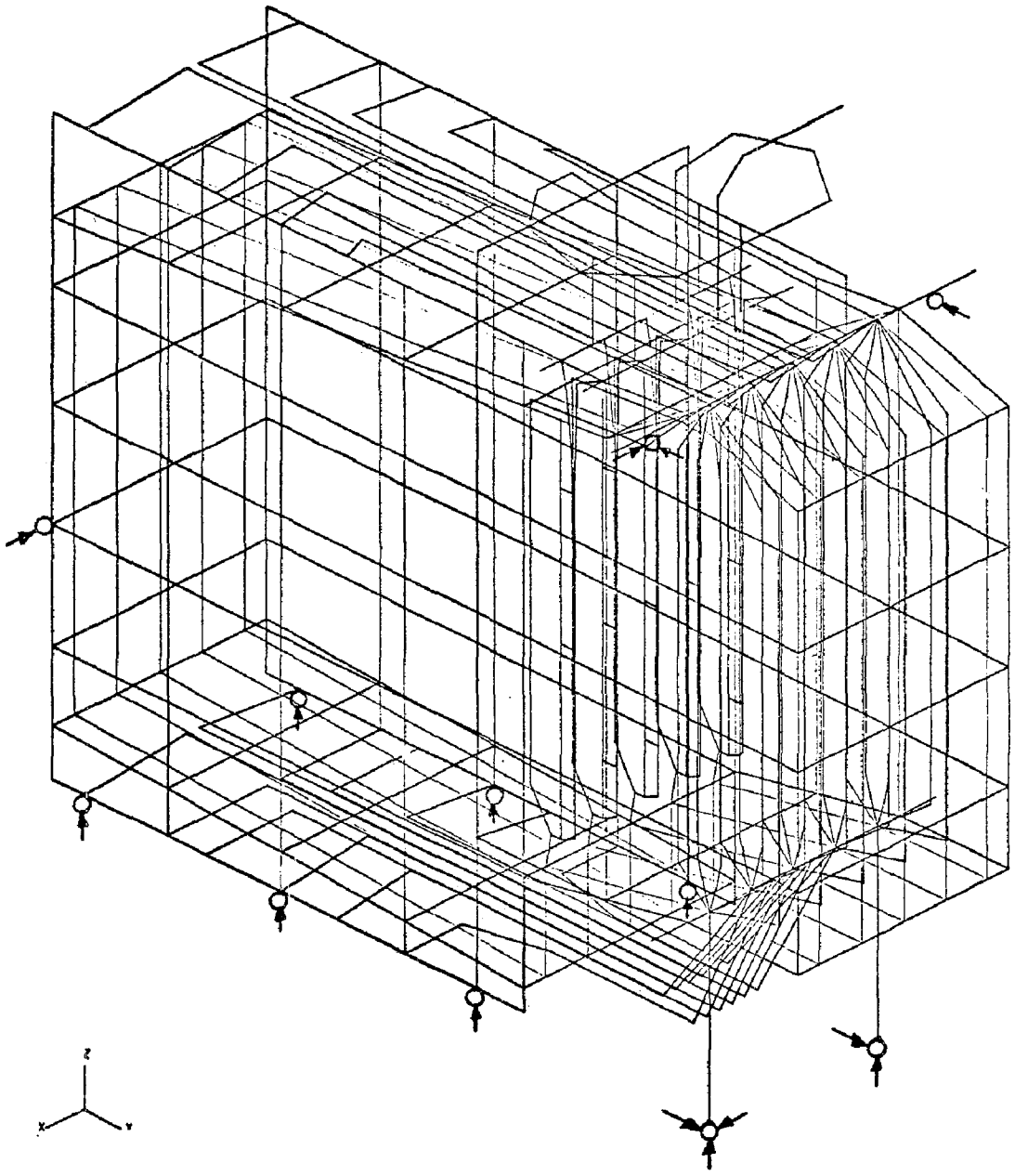

FIG. 2 Mathematical Model of Bottom Supported Boiler
5 Rows of Equivalent Tubes

paper a typical spectrum representing a Zone 2 earthquake with a 2% damping has been used. The same input has been used in all three directions. The computer program used to analyze the model is titled FESAP. This program is a modified version of the SAP program developed by Dr. E. L. Wilson of the University of California, which has been revised for our

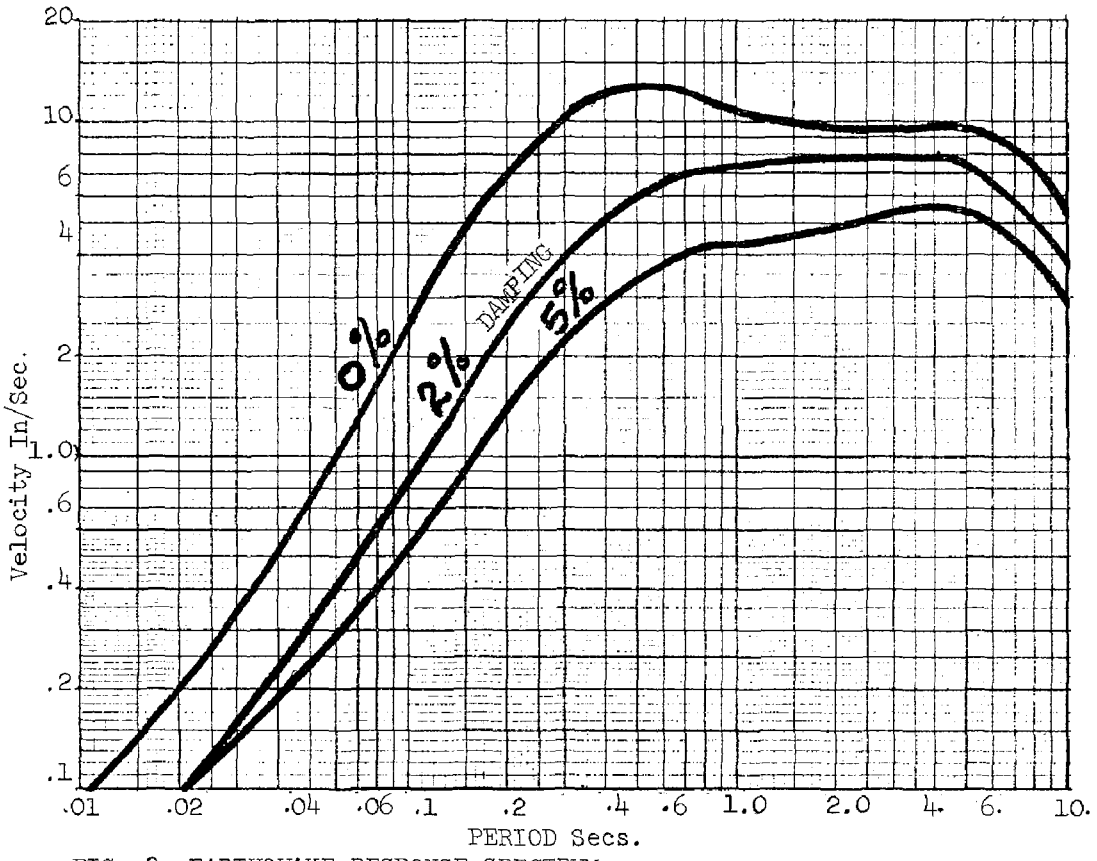

FIG. 3 EARTHQUAKE RESPONSE SPECTRUM

Company's own use. The figures 2 and 3 contain the mathematical model and a diagram of the earthquake input used in this study.

The work performed may be divided in the following three phases:

1. Dynamic earthquake analysis of a five row of equivalent tube model.

   The mathematical model used has lumped the generating screen and superheater tubes in five rows.

2. Static earthquake analysis of boiler.

   The model used is the same as above and a static earthquake input is applied on its members.

3. Dynamic earthquake analysis of a seven row of equivalent tube model.

   The mathematical model has been revised to represent the generating screen and superheater tubes by seven rows. The effects of that to the structure's response are reviewed and compared with the original model.

RESULTS

Phase 1

The boiler structure has many components of identical geometry and stiffeners. When analyzed, this results in many closely spaced model frequencies. As anticipated, the structure's participation in most of these modes is insignificant. Only the dominant modes have large participation factors which results in forces and moments critical to the design of the structure. These are the modes of importance to the designer since they identify the members responding to these modes and the predominant direction of response which is very important in understanding the structure's behavior. The Table 1 on the following page indicates the predominant frequencies, participation factors and direction of response for the bottom supported boiler being analyzed. The mode shapes corresponding to the three predominant frequencies are indicated on the Figures 4, 5, and 6.

By observing the response of each member and the resulting model stresses the designer can ascertain what, if any, changes are required to make it earthquake resistant. In other words, he can readily determine which members are the "weak links" of the design. This cannot be done by a static analysis because it is the response of the member to a dynamic load that produces a large displacement or a high stress condition. If changes are made to the critical members of the model and as a result, their flexibility or boundary conditions are changed, then another analysis should be made because the overall flexibility of the structure may have been altered. This process should be repeated until all components respond and are stressed within the acceptable limits.

In combining modal accelerations, displacements, and stresses the method of summation commonly used is the square root of the sum of the squares which has been identified herein as RSS. A table showing the results of this summation is shown on Table 2. The stresses shown on this table are the maximum dynamic stresses resulting from the earthquake analysis. In addition, the total effects of the analysis on the supports and the total stresses on all the members of the boiler structure, including normal operating stresses have been tabulated in order to obtain the total stress of each member. The total stresses obtained using this method are conservative since all maximum stress values are not always at the same location. The results are shown on Tables 3 and 4. The allowable stress used is the minimum yield stress for each member. This is an acceptable allowable used in various codes and it appears to be a good practical limitation.

The results of this analysis indicate that this type of boiler can adequately resist an earthquake of a Zone 2 severity. The earthquake spectrum used is one of many established for use in a nuclear installation and in the writer's opinion it is typical for a Zone 2 intensity.

TABLE 1 DYNAMIC CHARACTERISTICS OF THE MODEL

FREQUENCY CPS	1.6	1.9	2.6	3.	3.3	3.7	4.3	4.8	5.2	5.5	5.6	9.9	12.5	13.3	26.2
PARTICIPATION FACTOR	10.	5.7	21.	43.	23.	8.8	19.	3.5	6.2	6.2	8.7	6.2	7.1	8.2	3.0
DIRECTION	X	X	X	Y	X	X	X	Y	Y	X	Y	Z	Z	X	Z

TABLE: 2 Results of Dynamic Analysis on Boiler Components
Square Root of the Sum of the Squares - RSS

Component	Acceleration -G			Displacement - In. (cm)			Stresses - KSI (MPa)				
	X	Y	Z	X	Y	Z	X Bend	Y Bend	Axial	Max Princ	Min Princ
Generating Tubes	2.00	0.89	0.06	2.24 (5.7)	0.70 (1.8)	004 (.10)	13.7 (94.5)	0.3 (2.1)	0.1 (.7)	--	--
Screen Tubes	0.66	0.77	0.14	2.36 (6.0)	0.75 (1.9)	0.82 (2.1)	0.8 (5.5)	16.6 (114.)	0.6 (4.1)	--	--
Roof Tubes	0.09	0.19	0.14	0.84 (2.1)	0.20 (.51)	0.01 (.03)	--	--	--	3.8 (26.2)	0.2 (1.4)
Floor Tubes	0.09	0.20	0.17	0.08 (0.2)	0.20 (.51)	0.02 (.05)	--	--	--	9.3 (64.1)	0.3 (2.1)
Front Wall Tubes	0.01	0.21	0	0.01 (.03)	0.20 (.51)	0	--	--	--	1.1 (7.6)	0.9 (6.2)
Rear Wall Tubes	0.12	0.21	0	0.11 (.28)	0.20 (.51)	0	--	--	--	3.6 (24.8)	0.1 (.7)
Sidewall Tubes	0.37	0.20	0	0.23 (.58)	0.20 (.51)	0	--	--	--	5.2 (35.9)	0.1 (.7)
Superheater Tubes	0.30	0.30	0.03	1.09 (2.8)	0.30 (.67)	0.02 (.05)	7.0 (48.3)	0.4 (2.8)	0.1 (.7)	--	--
Supply Tubes	0.09	0.19	0.14	0.09 (.23)	0.19 (.48)	0.02 (.05)	1.2 (8.3)	0.6 (4.1)	0.1 (.7)	--	--
Riser Tubes	0.10	0.19	0.08	0.07 (.18)	0.20 (.51)	0.01 (.03)	0.6 (4.1)	0.4 (2.8)	0.1 (.7)	--	--
Drum Supports	0.11	0	0	0.10 (.25)	0	0	1.9 (13.1)	4.0 (27.6)	1.0 (6.9)	--	--

TABLE 3 Results of Dynamic Analysis on Boiler Supports

Support Points		Accelerations G			Displacements In. (cm)			Reactions KIPS (kN)		
		X	Y	Z	X	Y	Z	X	Y	Z
Water Drum	Right	0	0	0	0	0	0	22.9 (101.9)	11.0 (48.9)	33.7 (149.9)
	Left	0.11	0	0	0.10 (.25)	0	0	--	6.5 (28.9)	27.3 (121.4)
Steam Drum	Right	0.10	0.19	0	0.10 (.25)	0.20 (.51)	0.002 (.005)	7.3 (32.5)	38.9 (173.0)	--
	Left	0.10	0.19	0	0.10 (.25)	0.20 (.51)	0.002 (.005)	--	38.8 (72.6)	--
Right Side Wall	Rear	0.07	0.20	0	0.06 (.15)	0.20 (.51)	0	--	--	5.3 (23.6)
	Middle	0.06	0.20	0	0.03 (.08)	0.20 (.51)	0	--	--	38.4 (170.8)
	Front	0.04	0.20	0	0.01 (.03)	0.20 (.51)	0	--	--	0.8 (3.6)
Left Side Wall	Rear	0.07	0.20	0	0.06 (.15)	0.20 (.51)	0	--	--	5.3 (23.6)
	Middle	0.08	0.20	0	0.04 (.10)	0.20 (.51)	0	--	--	37.5 (166.8)
	Front	0.05	0.20	0	0.01 (.03)	0.20 (.51)	0	--	--	1.1 (4.9)
Front Wall	Right	0.01	0.20	0	0.01 (.03)	0.20 (.51)	0	15.2 (67.6)	--	--

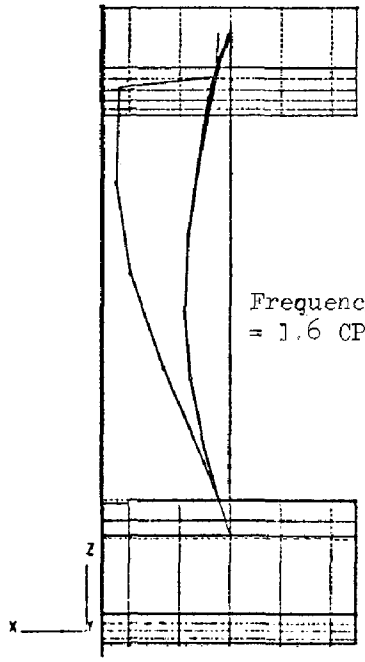

FIG. 4

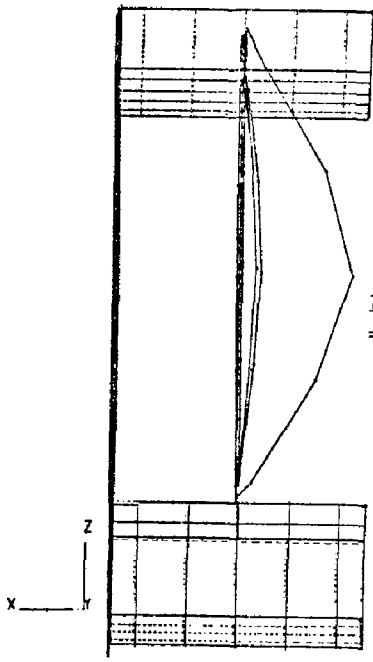

FIG. 5

TABLE 4 Summation of Stresses KSI (MPa)
Design Pressure = 1500 PSI (10.34 MPa)

Component	Pressure (Circ)	Pressure (Long)	Earth quake	Dead Load	Total	Allowable	Material & Temp °F(°C)
Generating Tubes	9.2 (63.4)	4.6 (31.7)	13.7 (94.5)	3.8 (26.2)	22.1 (152.4)	27.7 (191.0)	SA-178C 600 (316)
Screen Tubes	9.2 (63.4)	4.6 (31.7)	16.6 (114.5)	6.3 (43.4)	27.5 (189.6)	27.7 (191.0)	SA-178C 600 (316)
Roof Tubes	10.9 (75.2)	5.5 (37.6)	3.8 (26.2)	1.8 (12.4)	11.1 (76.5)	19.4 (133.8)	SA-178A 600 (316)
Floor Tubes	10.9 (75.2)	5.5 (37.6)	9.3 (64.1)	11.1 (76.5)	25.9 (178.6)	27.7 (191.0)	SA-178C 600 (316)
Front Wall Tubes	10.9 (75.2)	5.5 (37.6)	1.1 (7.6)	3.5 (24.1)	10.1 (69.6)	19.4 (133.8)	SA-178A 600 (316)
Rear Wall Tubes	10.9 (75.2)	5.5 (37.6)	3.6 (24.8)	1.5 (10.3)	10.6 (73.1)	19.4 (133.8)	SA-178A 600 (316)
Sidewall Tubes	10.9 (75.2)	5.5 (37.6)	5.2 (35.8)	7.1 (48.9)	17.8 (122.7)	19.4 (133.8)	SA-178A 600 (316)
Superheater Tubes	8.5 (58.6)	4.3 (29.3)	7.0 (48.3)	7.1 (48.9)	18.4 (126.9)	23.5 (162.0)	SA-210A 900 (482)
Supply Tubes	13.2 (91.0)	6.6 (45.5)	1.3 (9.0)	9.6 (66.2)	17.5 (120.7)	22.4 (154.4)	SA-106A 600 (316)
Riser Tubes	13.2 (91.0)	6.6 (45.5)	0.7 (4.8)	10.3 (71.0)	17.6 (121.3)	22.4 (154.4)	SA-106A 600 (316)
Drum Supports	—	--	4.4 (30.3)	2.3 (15.9)	6.7 (46.2)	32.9 (226.8)	A-36 200 (93)

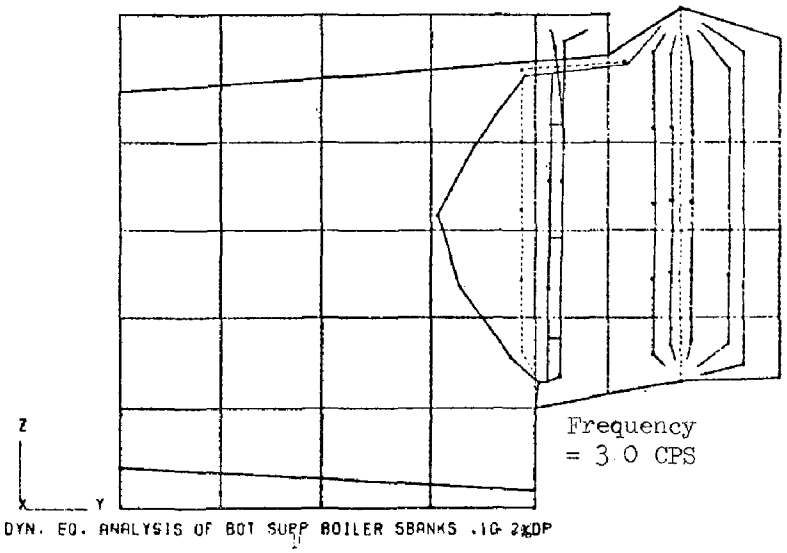

FIG. 6

Phase 2

The results of the static earthquake analysis have been tabulated and appear on tables 5 and 6 They are compared with the results from the dynamic analysis. One can clearly see that the two types of analysis yield different results. The displacements of the dynamic analysis are considerably larger than the displacements of the static analysis for the generating and screen tubes. Large differences are also observed in the resultant stresses for several members. In most cases the dynamic analysi yields higher stresses.

TABLE 5 LOADS ON BOILER SUPPORTS - KIPS (kN)

SUPPORT POINTS		DYNAMIC ANALYSIS			STATIC ANALYSIS		
		X	Y	Z	X	Y	Z
Water Drum	Right	22.9 (101.9)	11.0 (48.9)	33.7 (149.9)	40.6 (180.6)	9.2 (40.9)	26.2 (116.5)
	Left	--	6.5 (28.9)	27.3 (121.4)	--	5.2 (23.1)	22.3 (99.2)
Steam Drum	Right	7.3 (32.5)	38.9 (173.0)	--	12.7 56.5	35.5 (157.0)	--
	Left	--	38.8 172.6	--	--	35.3 (157.0)	--
Right Side Wall	Rear	--	--	5.3 (23.6)	--	--	4.6 (20.5)
	Middle	--	--	38.4 (170.8)	--	--	63.7 (283.4)
	Front	--	--	0.8 (3.6)	--	--	0.3 (1.3)
Left Side Wall	Rear	--	--	5.3 (23.6)	--	--	4.3 (19.1)
	Middle	--	--	37.5 (166.8)	--	--	62.8 (279.3)
	Front	--	--	1.1 (4.9)	--	--	1.1 (4.9)
Front Wall	Right	15.2 (67.6)	--	--	25.6 (113.9)	--	--

TABLE 6 COMPARISON OF RESULTS - DYNAMIC AND STATIC ANALYSES

COMPONENT	DYNAMIC ANALYSIS								STATIC ANALYSIS							
	Displacement In. (cm)			Stresses KSI (MPa)					Displacement In. (cm.)			Stresses KSI (MPa)				
	X	Y	Z	(X) Bend.	(Y) Bend.	Axial	Max Princ.	Min. Princ.	X	Y	Z	(X) Bend.	(Y) Bend.	Axial	Max Princ.	Min. Princ.
Generating Tubes	2 24 (5.7)	.70 (1.8)	04 (.10)	13.7 (94.5)	0.3 (2.1)	0.1 (.7)	--	--	.33 (.84)	.20 (.51)	.02 (.05)	.87 (6.0)	2.2 (15.2)	0 1 (.7)	--	--
Screen Tubes	2.36 (6 0)	75 (1.9)	.08 (21)	0.8 (5.5)	16.6 (114.)	0 6 (4.1)	--	--	.64 (1.63)	.83 (2.11)	.13 (.33)	2.9 (20.)	12.4 (85 5)	.5 (3.4)	--	--
Roof Tubes	08 (2 1)	.21 (51)	01 (03)	--	--	--	3.8 (26.2)	0.2 (1.4)	.15 (.38)	.14 (.36)	.008 (.02)	--	--	--	1.5 (10.3)	.1 (.7)
Floor Tubes	.08 (0 2)	.20 (51)	.02 (.05)	--	--	--	9 3 (64.1)	0.3 (2.1)	.14 (.36)	.14 (.36)	.025 (.06)	--	--	--	11.7 (80.7)	0.2 (1.4)
Front Wall Tubes	.01 (03)	20 (51)	0	--	--	--	1.1 (7.6)	0.9 (6.2)	.008 (.02)	.15 (.38)	0	--	--	--	0.8 (5.5)	0.4 (2.8)
Rear Wall Tubes	.11 (.28)	.20 (.51)	0	--	--	--	3.6 (24.8)	0.1 (.7)	.19 (.48)	.15 (.38)	0	--	--	--	2.2 (15.2)	0
Sidewall Tubes	.23 (.58)	.20 (.51)	0	--	--	--	5.2 (35.9)	0.1 (.7)	.18 (.46)	.14 (.36)	0	--	--	--	2.0 (13.8)	.1 (.7)
Superheater Tubes	1.09 (2 8)	.30 (.67)	.02 (.05)	7.0 (48.3)	0.4 (2.8)	0.1 (.7)	--	--	.20 (.51)	.32 (.81)	.04 (.10)	9.6 (66.2)	3.9 (26.9)	.5 (3.4)	--	--
Supply Tubes	.09 (.23)	.19 (.48)	.02 (.05)	1.2 (8.3)	0.6 (4.1)	0.1 (.7)	--	--	.31 (.79)	.17 (.43)	.19 (.48)	1.1 (7.6)	1.2 (8.3)	0.1 (.7)	--	--
Riser Tubes	.07 (.18)	.20 (.51)	.01 (.03)	0.6 (4.1)	0.4 (2.8)	0.1 (.7)	--	--	.27 (.69)	.14 (.36)	.22 (.56)	1.0 (6.9)	0.9 (6.2)	0.1 (.7)	--	--

Phase 3

In order to develop confidence in the modeling techniques used to represent the boiler, the mathematical model was revised by increasing the number of equivalent members representing the boiler tubes. This model has 200 more joints than the one originally used on FIG. 2. The results of a dynamic analysis performed on this model are compared to the original model on table 7 and 8. It can be observed that the two analyses yield very similar results in most areas. However, they differ considerably on the stresses produced on the screen and superheater tubes. These tubes are the most flexible tubes and participate the most at the lower modes In order to reduce the total stresses on the screen tubes additional internal supports will be installed tying them to the roof tubes. For the rest of the boiler components, plus the support end reactions, the original results are considered adequate.

TABLE 7 LOADS ON BOILER SUPPORTS KIPS (kN)

Support Points		DYNAMIC ANALYSIS Original Model			DYNAMIC ANALYSIS Revised Model		
		X	Y	Z	X	Y	Z
Water Drum	Right	22.9 (101.9)	11.0 (48.9)	33.7 (149.9)	22.2 (98.7)	6.6 (29.4)	29.2 (130.)
	Left	--	6.5 (28.9)	27.3 (121.4)	--	4.1 (18.2)	23.3 (103.6)
Steam Drum	Right	7.3 (32.5)	38.9 (173.0)	--	7.2 (32.0)	30.0 (133.4)	--
	Left	--	38.8 (172.6)	--	--	30.0 (133.4)	--
Right Side Wall	Rear	--	--	5.3 (23.6)	--	--	2.9 (12.9)
	Middle	--	--	38.4 (170.8)	--	--	36.5 (162.4)
	Front	--	--	0.8 (3.6)	--	--	0.5 (2.2)
Left Side Wall	Rear	--	--	5.3 (23.6)	--	--	3.1 (13.8)
	Middle	--	--	37.5 (166.8)	--	--	34.2 (166.8)
	Front	--	--	1.1 (4.9)	--	--	0.8 (3.6)
Front Wall	Right	15.2 (67.6)	--	--	16.1 (71.6)	--	--

TABLE 8 COMPARISON OF RESULTS

COMPONENT	DYNAMIC ANALYSIS-5 ROW OF TUBES								DYNAMIC ANALYSIS-7 ROW OF TUBES							
	Displacement In (cm)			Stresses KSI (MPa)					Displacement In (cm)			Stresses KSI (MPa)				
	X	Y	Z	(X) Bend.	(Y) Bend	Axial	Max. Princ	Min. Princ.	X	Y	Z	(X) Bend.	(Y) Bend	Axial	Max. Princ.	Min. Princ
Generating Tubes	2.24 (5.7)	.70 (1.8)	.04 (.10)	13.7 (94.5)	.3 (2.1)	10 (.7)	--	--	2.41 (6.1)	1.14 (2.9)	.04 (.10)	14.9 (102.7)	.2 (1.4)	.1 (.7)	--	--
Screen Tubes	2.36 (6.0)	.75 (1.9)	.08 (.21)	.8 (5.5)	16.6 (114.)	.6 (4.1)	--	--	2.46 (6.2)	1.09 (2.8)	.09 (.24)	1.3 (9.0)	23.9 (164.8)	2.8 (19.3)	--	--
Roof Tubes	.08 (2.1)	.20 (.51)	.01 (.03)	--	--	--	3.8 (26.2)	.2 (1.4)	.08 (.20)	.12 (.3)	.01 (.03)	--	--	--	3.0 (20.7)	.9 (6.2)
Floor Tubes	.08 (.2)	.20 (.51)	.02 (.05)	--	--	--	9.3 (64.1)	.3 (2.1)	.08 (.20)	.13 (.33)	.02 (.05)	--	--	--	8.8 (60.7)	1.3 (9.0)
Front Wall Tubes	.01 (.03)	.20 (.51)	0	--	--	--	1.1 (7.6)	.9 (6.2)	.01 (.03)	.12 (.3)	0	--	--	--	1.3 (9.0)	.9 (6.2)
Rear Wall Tubes	.11 (.28)	.2 (.51)	0	--	--	--	3.6 (24.8)	.1 (.7)	.11 (.28)	.12 (.3)	0	--	--	--	2.6 (17.9)	.1 (.7)
Sidewall Tubes	.23 (.58)	.2 (.51)	0	--	--	--	5.2 (35.9)	.1 (.7)	.24 (.61)	.12 (.3)	0	--	--	--	4.5 (31.0)	.1 (.7)
Superheater Tubes	1.09 (2.8)	.3 (.67)	.02 (.05)	7.0 (48.3)	.4 (2.8)	.1 (.7)	--	--	1.04 (2.6)	.58 (1.47)	.04 (.10)	10.8 (74.5)	.6 (4.1)	.4 (2.8)	--	--
Supply Tubes	.09 (.23)	.09 (.48)	.02 (.05)	1.2 (8.3)	.6 (4.1)	.1 (.7)	--	--	.07 (.18)	.12 (.30)	.01 (.03)	.8 (5.5)	.2 (1.4)	0.1 (.7)	--	--
Riser Tubes	.07 (.18)	.20 (.18)	.01 (.51)	.6 (.03)	.4 (4.1)	.1 (2.8)	--	--	.09 (.23)	.12 (.30)	.02 (.05)	.8 (5.5)	.4 (2.8)	0.1 (.7)	--	--

COMMENTS & RECOMMENDATIONS

The effect of this type of earthquake input on the boiler structure was relatively moderate. The reason for this is the fact that most of the important components, generating tubes, screen tubes, and superheater tubes are very flexible. This reduces the shock input into the structure during an earthquake. Therefore, even though numerous modes were considered, the resultant total stresses were not very high.

In comparing a conventional static earthquake analysis with a dynamic earthquake analysis the results of the support end reactions vary considerably. The stresses on most boiler components are similar except for the most flexible members for which the dynamic analysis yields much higher stresses. It is the writer's opinion that a dynamic analysis procedure should be used in designing most structures and especially those of high human occupancy and of critical nature. In a dynamic analysis, by observing mode shapes and modal stresses, the designer has a more realistic picture of the structure's behavior during the earthquake. This strengthens his confidence in the structural integrity of his structure to resist earthquake.

In establishing a mathematical model of a boiler structure, numerous assumptions and approximations are required in order to reduce the structure to within practical limitations. The most important task in simplifying or reducing the various components is to first understand their actual behavior and its effect on the total model. This is easy to say and extremely difficult to accomplish. Individual members could be analyzed to determine their natural frequency and compared to the frequencies of the total model. The sensitivity of the model can be checked by modeling important members using more than one modeling technique. This way, it can be determined how sensitive the overall structure is to their modeling. With this type of information available to him, the designer can then finalize the mathematical model and proceed to design the structure.

In testing the modeling techniques used, another mathematical model was developed which yielded higher stresses in two of the most flexible members. These stresses were discovered only because of the additional effort to evaluate and substantiate the adequacy of the original model to represent the boiler structure. Of course, this approach cannot always be followed because of time and economic considerations. However, it should be practiced whenever possible in order to establish the sensitivity of a mathematical model to several of its components and determine the best method of representing them.

The writer recommends that a dynamic analysis design procedure be developed and incorporated in the present building codes. The procedure will have to be comprehensive in order to safeguard against user's oversimplifying the mathematical model. All users should be required to perform certain basic steps in modeling to assure them of the adequacy of their model to represent the actual structure. The analysis is an approximation, but with good guidelines and judgment it can be a good approximation. The thing to remember is, if a structure affects people every possible precaution should be taken to assure their safety. As engineers, we are responsible to give our best engineering effort in all of our designs.

INTERNATIONAL SYMPOSIUM ON
EARTHQUAKE STRUCTURAL ENGINEERING
St. Louis, Missouri, USA, August, 1976

EFFECTS OF EARTHQUAKE INPUT IN SEISMIC RESPONSES OF NUCLEAR POWER PLANT SITES

BILL T.D. LU, Senior Project Engineer
Dames & Moore, Cranford, New Jersey

JOSEPH A. FISCHER, Partner
Dames & Moore, Cranford, New Jersey

JONG PEIR, Project Engineer
Formerly with Dames & Moore
Cranford, New Jersey

SUMMARY

In order to demonstrate the site-dependency effect in a seismic response evaluation and to develop an understanding of the degree of conservatism inherent in utilizing seismic input based only upon NRC's Regulatory Guide 1.60, a series of one-dimensional seismic response evaluations were performed for the soil conditions at a nuclear power plant site, using a one-dimensional strain compatible shear wave propagation theory. Thirty-three (33) earthquake records, as well as the artificial time history generated in accordance with Regulatory Guide 1.60,were used as input in the response analyses.

The results of this study indicate that the use of seismic input obtained from Regulatory Guide 1.60 can be overly conservative in defining the seismic design parameter evaluation for a nuclear power plant site. In the seismic evaluation of a specific site, it is more appropriate to utilize various earthquake time histories, recorded at similar site conditions, as input.

INTRODUCTION

The dynamic response of a site from incoming earthquake excitation is influenced by a number of factors, including (but not limited to) the characteristics of the seismic input and the geological condition at the site. Commonly, in evaluating the seismic response and liquefaction potential of a nuclear power plant site, the seismic input is artificially generated in order to yield response spectra enveloping the design response spectra outlined in the Nuclear Regulatory Commission's (NRC) Regulatory Guide 1.60 (USAEC, 1973).

The earthquake time history so generated is generally considered conservative, particularly when used to define response characteristics and liquefaction potential of soils. The conservatism inherent in this type of seismic input can result from:

1. The generated earthquake time history which combines a wide range of earthquake frequencies that cannot be developed in any single real site condition. This, in turn, may impose artificially high responses and stresses in any analytical model of a soil deposit; and

2. This artificial time history will have to contain several high spikes having magnitudes near the maximum site acceleration value in order to yield response spectra enveloping those specified in the NRC's Regulatory Guide 1.60. This also, in effect, will vastly overestimate the seismic response effect upon a real site soil.

It is also worthwhile to point out that the seismic input so generated does not differentiate between the possible site response that may result from a variety of site soil and geologic conditions that obviously will occur at different plant locations.

In view of the above shortcomings, it may be desirable, in appropriate situations, to use actual soil and earthquake time histories recorded upon soil and geologic conditions similar to those at the selected nuclear power plant site. In the study reported herein, thirty-three (33) earthquake records, as well as the artificial time history generated as outlined in NRC's Regulatory Guide 1.60, were used as seismic input for the seismic response evaluation of a nuclear power plant site.

The purposes of this study were to demonstrate the site-dependency effect in a seismic response evaluation and to develop an understanding of the degree of conservatism inherent in utilizing seismic input, based only upon Regulatory Guide 1.60. In order to accomplish these purposes, a series of one-dimensional seismic response evaluations were performed for the soil conditions at the plant site, using a one-dimensional strain-compatible shear wave propagation theory (Schnabel, et al, 1972). The results of these seismic response analyses were grouped into two basic categories for evaluation. The first category included those earthquakes recorded at site conditions similar to those at the plant site; the second included all 33 earthquake records irrespective of site geological conditions. The effect of seismic responses within the soil column resulting from these actually recorded earthquakes were then compared with those generated from the artificial time history derived from the Regulatory Guide 1.60.

The details presented in this paper were developed as part of the parametric study of the affect of various seismic inputs upon the response of a nuclear power plant site. The soil profile and associated material properties used in this study were specifically developed for this site. However, it is the writers' consensus that the concepts, results and conclusion of this study are generally applicable to other possible nuclear power plant sites, particularly for those with a deeper soil column.

ANALYSIS PROCEDURES

As in any analysis, various degrees of approximation and sophistication can be implemented in a one-dimensional seismic response evaluation. The basic requirements for a high-quality, one-dimensional seismic response evaluation should take the following factors into consideration.

1. The variation of soil characteristics with depth;
2. The non-linear and energy-absorbing (damping) characteristics of the soils;
3. The degree of conservatism inherent in the seismic input; and
4. The effect of seismic responses on the stability (liquefaction and cyclic straining) of the site soil column.

Consequently, the state-of-the-art procedures for a one-dimensional seismic response evaluation are as follows:

1. Determine the strain-dependent shear moduli and damping ratios for the soils within the profile;
2. Determine seismic input (time history and elevation of application);
3. Evaluate the seismic response; and
4. Evaluate the effect of seismic responses on the stability of the site soils.

For this study the earthquake motion was input at the free field deconvoluted to a depth (160 ft.) where no significant changes in response were noted.

SOIL PROFILE AND PROPERTIES USED IN THE ANALYSIS

A seismic response evaluation of a power plant site should be based on a subsurface profile and soil properties developed from extensive field investigation and laboratory testing programs. The methods and details of field and laboratory investigations for a typical site are presented by Hall et al (1974) and SW-AJA (1972), and are not included in this paper.

As previously mentioned, this study was developed as a portion of the parametric study to determine the effect of specific earthquake motion upon a nuclear power plant site. The associated soil profile used in this study consists of alternate layers of sands and clays of variable thickness. The strain-dependent shear moduli and damping ratios used in this study were determined from extensive field and laboratory testing programs. The soil profile and strain-dependent properties used in this study are summarized in Table 1.

SEISMIC INPUT

In this study, 33 earthquake time histories physically recorded upon various soil conditions and used by Blume et al (1973) formed the basis of the one-dimensional seismic response evaluation. It was these 33 earthquake records that were the basis of the response spectra specified in Regulatory Guide 1.60 presented herein. The pertinent facts concerning these 33 earthquake records are summarized in Table 2. For this study, all time histories were normalized with respect to a maximum ground acceleration level of 20 percent of gravity corresponding to the Safe Shutdown Earthquake (SSE) level specified for the nuclear power plant site studied in this paper.

An artificially generated earthquake time history with a maximum acceleration level of 20 percent of gravity was also developed to yield response spectra closely enveloping those specified in Regulatory Guide 1.60. This artificially generated earthquake time history input is shown in Figure 1 and is also used as seismic input in the one-dimensional seismic response evaluation. For simplicity, the artificial earthquake time history shown in Figure 1 will be referred to as the Regulatory Guide 1.60 time history in this study.

In this study, each seismic input was specified at the top of the surface of the soil profile in accordance with the current practice in soil dynamics. This location of seismic input is in agreement with the NRC requirement (USNRC, 1975).

SEISMIC RESPONSES ANALYSES - 33 EARTHQUAKE RECORDS

A series of one-dimensional seismic responses analyses, using each normalized earthquake time history as input at the top of site soil profile, were performed. The seismic responses in terms of induced shear stresses within the site soil profile were first evaluated utilizing a one-dimensional strain-compatible shear wave propagation computer program developed by Schnabel, Seed and Lysmer (1972). This computer program is capable of incorporating strain-dependent material properties using iterative equivalent linear properties which account for non-linear shear moduli and damping characteristics of the soils.

The induced stress levels from the excitation of the 33 earthquake records were then analyzed statistically obtaining the mean and the mean plus one standard deviation values of response. The statistical process of selecting the mean plus one standard deviation value is commonly used to determine a near upper bound value, and also formed the basis for the Regulatory Guide 1.60 response spectra criteria.

The mean and mean plus one standard deviation values of the seismic induced maximum shear stresses within the soil profile under the excitations of the 33 earthquake records are shown in Table 3. For comparison purposes, the maximum shear stresses within the same soil profile, using the Regulatory Guide 1.60 time history as seismic input, are also shown in Table 3.

The ratios of the mean and mean plus one standard deviation values of maximum induced shear stresses under the excitation of the 33 earthquake records to the maximum induced shear stresses due to the Regulatory Guide 1.60 time history, are plotted in Figure 2.

The results shown in Table 3 and Figure 2 indicate that:

1. The mean values of the maximum induced shear stresses within the soil profile caused by the 33 actually recorded earthquake time history excitations are smaller than the maximum shear stresses from the Regulatory Guide 1.60 time history;

2. The mean plus one standard deviation values of the maximum induced shear stress due to the excitations the 33 earthquake time histories are smaller than those from the Regulatory Guide 1.60 time history everywhere within the soil profile, except for a few feet near the top of the soil profile where they are approximately on the same order of magnitude; and

3. The use of the Regulatory Guide 1.60 time history as seismic input in the seismic response evaluation for a nuclear power plant site is conservative for the type of soil column investigated.

SEISMIC RESPONSE - SIX EARTHQUAKE RECORDS

The soil profile described in Table 1 can be categorized as a deep soil deposit site. It would appear reasonable to study the effect of several earthquake records obtained at similar deep soil deposit sites on the seismic response of the soil in question. Table 2 indicates six earthquake records which were recorded at deep soil deposit sites.

The mean and mean plus one standard deviation values of the sesimic induced maximum shear stresses within the soil profile, based on the six earthquake records obtained at deep soil deposit sites, are shown in Table 4. Again, the results of the seismic response using the Regulatory Guide 1.60 time history as sesimic input are also shown in Table 4 for comparison purposes.

The ratios of the mean and mean plus one standard deviation values of the maximum induced shear stresses under the excitations of these six earthquake records to the maximum induced shear stresses within the same soil profile from the Regulatory Guide 1.60 time history are compared on Figure 3.

Based on the results shown in Table 4 and Figure 3, the following remarks can be made:

1. The mean and mean plus one standard deviation values of the maximum induced shear stresses within the soil profile from the excitations of six earthquake records obtained at deep soil deposit sites are much smaller than the maximum shear stresses

induced by the Regulatory Guide 1.60 time history. Thus, the use of Regulatory Guide 1.60 time history as seismic input will yield unduly conservative results in the seismic responses evaluation of a nuclear power plant site on a deep soil site.

2. Comparison of the seismic response results shown in Table 3 with those shown in Table 4 clearly indicate the site-dependent effect in the seismic responses analysis of a nuclear power plant site. In aseismic response evaluation of a nuclear power plant site, it would appear more appropriate to utilize several earthquake time histories recorded at similar site geological conditions or artificially generated earthquake time histories in accordance with site-dependent response spectra, such as those recommended by Seed et al (1974) as seismic input. An obligatory use of the Regulatory Guide 1.60 time history as seismic input may yield unduly conservative results in evaluating the seismic response of soil solumns.

SEISMIC RESPONSE EFFECT ON SOIL STABILITY

The effect of variations in the duration, frequency content and acceleration level of an input earthquake is reflected in the induced shear stress time histories within the soil profile. The induced shear stress time history, like the seismic input, is cyclic in nature and has erratic magnitude. The duration and amplitude of the induced shear stress is of great significance in present day state-of-the-art analyses of soil stability under earthquake loading.

To assess the seismic response effect on a site soil, the irregular shapes of the induced shear stress time histories within the soil profile can readily be converted to an equivalent series of uniform stress cycles on an energy basis. This equivalent series may be compared directly with cyclic shear strength data obtained from physical laboratory tests, under uniform cyclic stress conditions, upon the site soils. This conversion is accomplished by appropriately weighting the ordinates of the stress time history based on a standard weighting curve representative of laboratory test data (DeAlba et al, 1975). Details of conversion procedures have been presented by Lee and Chan (1972) and Seed, et al (1975).

The usual practice in present-day soil dynamics analyses is to convert the induced shear stress time history to an equivalent uniform stress value, τ, corresponding to a suitable number of cycles of application. This equivalent stress value, τ, is usually taken to be a certain fraction of the maximum induced shear stress computed from the mathematical model. Therefore, the maximum induced shear stress and the equivalent number of cycles of application are the two important parameters to indicate the possible level of seismic response effect on the stability of the site soil column.

The effect of various earthquake records as well as the Regulatory Guide 1.60 time history on the magnitudes of the induced shear stress within the soil profile are already illustrated by the results shown in Tables 3 and 4, and Figures 2 and 3. In attempting to define the level of conservatism in a standard Regulatory Guide 1.60 analysis, the remaining task thus is to investigate the effect upon the determination of the equivalent number of cycles from the 33 actual earthquake records as well as from the Regulatory Guide 1.60 time history.

The results of calculating the equivalent number of cycles of stress application based on the seismic input of the 33 earthquake records and the Regulatory Guide 1.60 time history (in accordance with the procedure of Seed, et al 1975) indicate:

1. The calculated equivalent number of cycles based on the induced shear stress time histories from the 33 individual earthquakes in soils near the top of soil profile is on the same order of magnitudes as those calculated from the original time history input;

2. The calculated equivalent number of stress cycles from the induced shear stress time for soils located more than a few feet below the top of the soil profile is slightly less than those calculated for soils near the ground surface; and

3. The calculated equivalent number of stress applications, based upon each of 33 individual earthquake records, are much less than those calculated using the Regulatory Guide 1.60 time history as seismic input.

In other words, the use of the Regulatory Guide 1.60 time history as seismic input will result in an over-estimate of the seismic response effect upon a site soil column as concern the number of calculated stress cycle applications. This over-estimate will, in turn, lead to an over-conservative evaluation of site soil stability under earthquake excitation.

To further emphasize the degree of conservatism, it is worthwhile to note that the most important factor influencing the results of equivalent number of cycles calculation is the earthquake "magnitude", not the absolute value of acceleration level (Seed, et al 1975), nor by the convenience of enveloping a broad spectrum of recorded site motions (Regulatory Guide 1.60).

For the site analyzed in this study, the earthquake input with maximum ground acceleration of 20 percent gravity was determined on the basis of the regional and site geologic and seismic history in accordance with 10CFR100, Appendix A criteria. The SSE was determined to have a Richter magnitude less than 6. According to the results of a study by Seed, et al (1975), it would be reasonable to assume that the effect of each induced shear stress time history is approximately equivalent to 5 cycles of a uniform stress having an amplitude on the order of 0.65 of the maximum induced stress. However, the calculated effect from the shear stress time history specified by Regulatory Guide 1.60 can be found to be roughly equivalent to 15 cycles of a uniform stress application

with a magnitude being equal to 0.65 of the maximum induced stress. Thus, the conservatism of blindly using the Regulatory Guide 1.60 time history as seismic input is even more apparent.

CONCLUSION AND REMARKS

The results of this study indicate that the use of seismic input obtained from Regulatory Guide 1.60 is overly conservative in the seismic response evaluation of a nuclear power plant site. The extent of conservatism depends on the characteristics of the specific site geological conditions. While there is little doubt that the use of NRC Regulatory Guide 1.60 is extremely useful in providing a "first pass" evaluation of site seismic response, its use without a full understanding of its inherent conservatism may needlessly penalize sites otherwise suitable for nuclear facility construction. The designer must also understand the different degrees of conservatism which result when using Regulatory Guide 1.60 time histories for evaluating structural response in contrast to site response. In the seismic evaluation of a specific site, it is more appropriate to utilize various earthquake time histories, recorded at similar site conditions, as seismic input. These more realistic earthquakes can better represent the seismic input that the site may actually experience during the "design life" of the plant.

REFERENCES

Blume, J.A., and Associates, "Recommendations for Shape of Earthquake Response Spectra", Prepared for U.S. Atomic Energy Commission, Report No. WASH-1254, San Francisco, California, February, 1973.

DeAlba, P., Chan, C.and Seed, H.B., "Determination of Soil Liquefaction Characteristics by Large-Scale Laboratory Tests", Report No. EERC 75-14, Earthquake Engineering Research Center, University of California, Berkeley, May, 1975.

Hall, W.J., Newmark, N.M. and Hendron, A.J., "Classification, Engineering Properties and Field Exploration of Soils, Intack Rock and In Situ Rock Masses", Prepared for U.S. Atomic Energy Commission, Report No. WASH-1301, May, 1974.

Lee, K.L. and Chan, K., "Number of Equivalent Significant Cycles in Strong Motion Earthquakes", Proc. International Conf. on Microzonation, Vol. II, Seattle, Washington, Oct., 1972.

Schnabel, P.B., Lysmer, J., and Seed, H.B., "SHAKE-A Computer Program for Earthquake Response Analysis of Horizontally Layered Sites," Report No. EERC-72-12, Earthquake Engineering Research Center, University of California, Berkeley, 1972.

Seed, H. B., Idriss, I.M., Makdisi, F., and Banerjee, N., "Representation of Irregular Stress Time Histories by Equivalent Uniform Stress Series in Liquefaction Analyses", Report No. 75-29, Earthquake Engineering Research Center, University of California, Berkeley, October, 1975.

Seed, H. B., Ugas, C. and Lysmer, J., "Site-Dependent Spectra for Earthquake Resistant Design", Report No. EERC 74-12, Earthquake Engineering Research Center, University of California, Berkeley, November, 1974.

Shannon and Wilson, Inc., and Agbabian-Jaconsen Associates (SW-AJA) "Soil Behavior Under Earthquake Loading Conditions", Report Prepared Under Subcontract No. 3354 of Union Carbide Corp., Oak Ridge National Laboratory and Under Contract No. W-7405-eng-26, for U. S. Atomic Energy Commission, Jan., 1972.

U.S. Atomic Energy Commission (USAEC), Directorate of Regulatory Standards, Regulatory Guide No. 1.60, "Design Response Spectra for Nuclear Power Plant", Revision 1, Washington D.C., December, 1973.

U. S. Nuclear Regulatory Commission (USNRC), Office of Nuclear Reactor Regulation," Standard Review Plan - Section 3.7.1", Washington, D.C., June, 1975.

TABLE 1

SOIL PROFILE AND MATERIAL PROPERTIES USED IN THIS STUDY

SOIL TYPE	H	U	Max. G @ $\gamma = 10^{-4}\%$	Ratio of G to Gmax					Damping Ratio (%)				
				$\gamma=10^{-4}\%$	$\gamma=10^{-3}\%$	$\gamma=10^{-2}\%$	$\gamma=10^{-1}\%$	$\gamma=1\%$	$\gamma\ 10^{-4}\%$	$\gamma=10^{-3}\%$	$\gamma=10^{-2}\%$	$\gamma=10^{-1}\%$	$\gamma=1\%$
Fine Sand	7	125	Equ. (1) with $K_2 = 48$	1	0.98	0.87	0.42	0.05	1	1	1.7	10.5	21.2
Silty Clay	5	122	564000	1	1	0.75	0.37	0.09	4	4	4.7	8.6	18.0
Silty Sand	4	126	Equ. (1) with $K_2 = 38$	1	0.97	0.79	0.37	0.05	2.3	2.5	4	12.1	19.3
Plastic Clay	7	104	441000	1	1	0.85	0.5	0.15	2	2	2.6	5.8	15.3
Plastic Clay	7	104	462000	1	1	0.85	0.5	0.15	2	2	2.6	5.8	15.3
Silty Sand	13	131	Equ. (1) with $K_2 = 44$	1	0.96	0.84	0.37	0.05	1	1	2	10.4	21.5
Coarse to Fine Sand	1000	131	Equ. (1) with $K_2 = 54$	1	0.99	0.89	0.39	0.04	1.5	1.6	2	7.0	19.5

Notation: Equation (1): $G = 1000\ K_2\ \sigma_m^{0.5}$

G = Shear Modulus in psf (1 psf=0.489 g/cm^2)
σ_m = Mean Confining Stress in psf (1 psf - 0.489 g/cm^2)
H = Thickness of soil layer in ft. (1 ft.= 30.48 cm)
U = Unit Weight of soil in pcf (1 pcf= 0.016 g/cm^3)
g = shear strain

Remark: Soil type is listed in order of depths, as it appeared in the plant site.

TABLE 2

LIST OF 33 EARTHQUAKE RECORDS

	Earthquake Accelerogram	Maximum Acceleration (g)	Total Duration (Seconds)
1940	El Centro, St. 1 South	0.359	53.73
1940	El Centro, St. 1 West	0.224	53.47
1968	Hachinohe, Japan EW	0.187	119.92
1968	Hachinohe, Japan NS	0.230	119.92
1971	San Fernando St. 241 NS	0.258	59.50
1971	San Fernando St. 241 EW	0.140	59.60
1954	Eureka N11°W*	0.175	77.95
1954	Eureka N79°E*	0.283	79.56
1934	El Centro St. 24 South	0.169	90.32
1934	El Centro St. 24 West	0.184	90.26
1949	Olympia N4°W*	0.183	89.16
1949	Olympia S86°W*	0.306	89.15
1971	San Fernando St. 110 S69°E	0.289	61.87
1971	San Fernando St. 110 N21°E	0.335	61.82
1966	Cholame-Shandon St. 33 N65E	0.509	43.78
1965	Olympia S4°E*	0.161	82.14
1965	Olympia S86°W*	0.229	82.13
1971	San Fernando St. 446 N79°W	0.152	40.26
1971	San Fernando St. 446 N11°E	0.225	40.31
1971	San Fernando St. 220 S90°W	0.154	65.15
1971	San Fernando St. 220 N00°E	0.181	65.34
1935	Helena EW	0.156	51.04
1935	Helena NS	0.141	50.94
1966	Cholame-Shandon St. 34 N05W	0.403	44.01
1966	Cholame-Shandon St. 34 N85E	0.467	44.03
1966	Lima N8°E	0.369	65.68
1966	Lima N82°W	0.269	65.68
1957	Golden Gate N10°E	0.106	39.86
1957	Golden Gate N80°W	0.127	39.86
1966	Temblor N65W	0.282	30.41
1966	Temblor S25W	0.411	30.42
1952	Taft N21E	0.177	54.40
1952	Taft S69E	0.189	54.40

*Records obtained at Deep Soil Deposit Sites

TABLE 3

STATISTICAL RESULTS OF MAXIMUM INDUCED SHEAR STRESSES -
33 EARTHQUAKE RECORDS AND REGULATORY GUIDE 1.60 TIME HISTORY

Depth Below Top of Profile (ft)	Maximum Induced Shear Stress, τ_{max}, psf		
	Results from 33 Earthquake Records		Regulatory Guide 1.60 Time History
	Mean	Mean & Sta. Dev.	
3.5	83	88	88
9.5	203	225	224
14.5	267	313	312
19.5	325	392	414
26.5	356	448	502
36.5	392	519	600
51.0	516	679	772
67.0	644	868	970
83.0	730	1010	1167
99.0	786	1101	1313
115.0	820	1157	1473

TABLE 4

STATISTICAL RESULTS OF MAXIMUM INDUCED SHEAR STRESSES
EARTHQUAKE RECORDS ON DEEP SOIL SITE AND REGULATORY GUIDE 1.60 TIME HISTORY

Depth Below Top of Profile (ft)	Maximum Induced Shear Stress, τ_{max}, psf		
	Results from 6 Earthquake Records on Deep Soil Site		
	Mean	Mean & Sta. Dev. (PSF)	AGS/1.60 Earthquake (PSF)
3.5	82	84	88
9.5	204	216	224
14.5	270	301	312
19.5	328	381	414
26.5	359	435	502
36.5	423	494	600
51.0	546	602	772
67.0	671	841	970
83.0	781	1024	1167
99.0	859	1169	1313
115.0	911	1241	1473

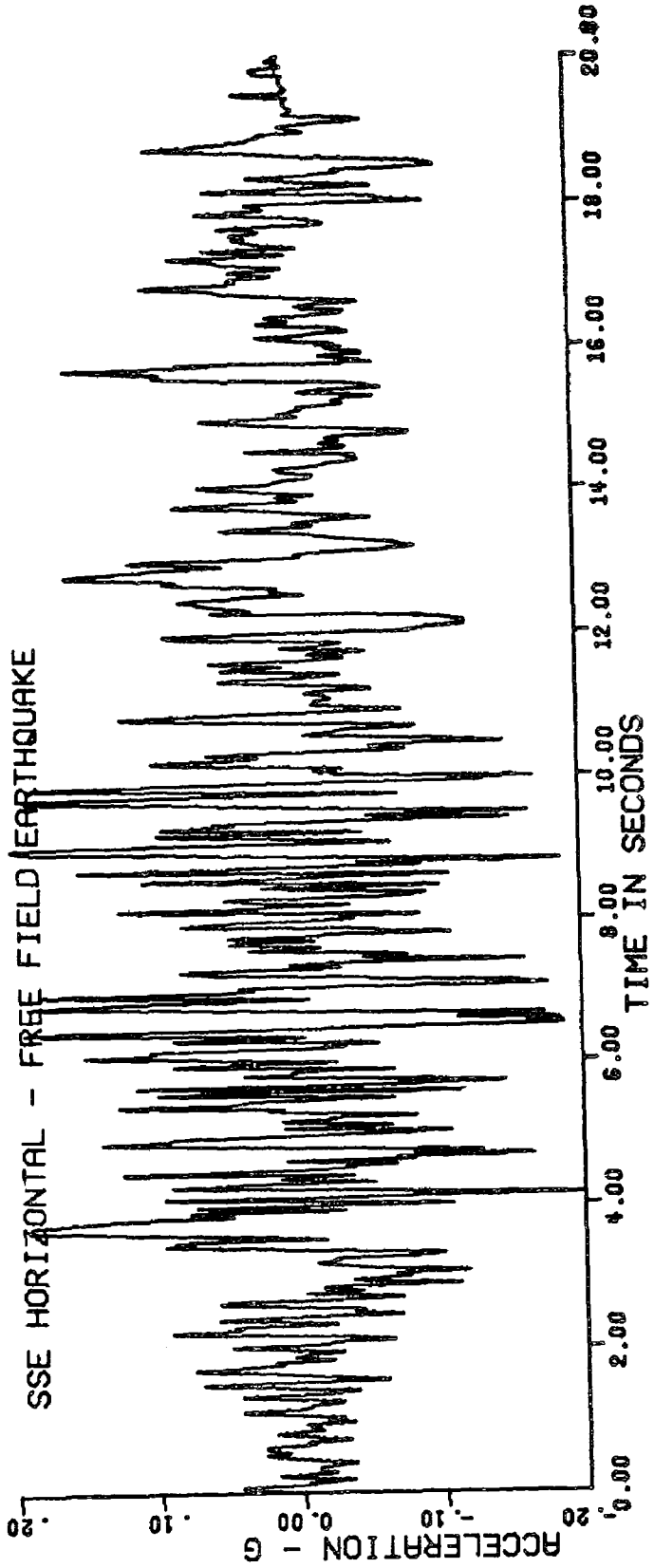

FIGURE 1 REGULATORY GUIDE 1.60 TIME HISTORY

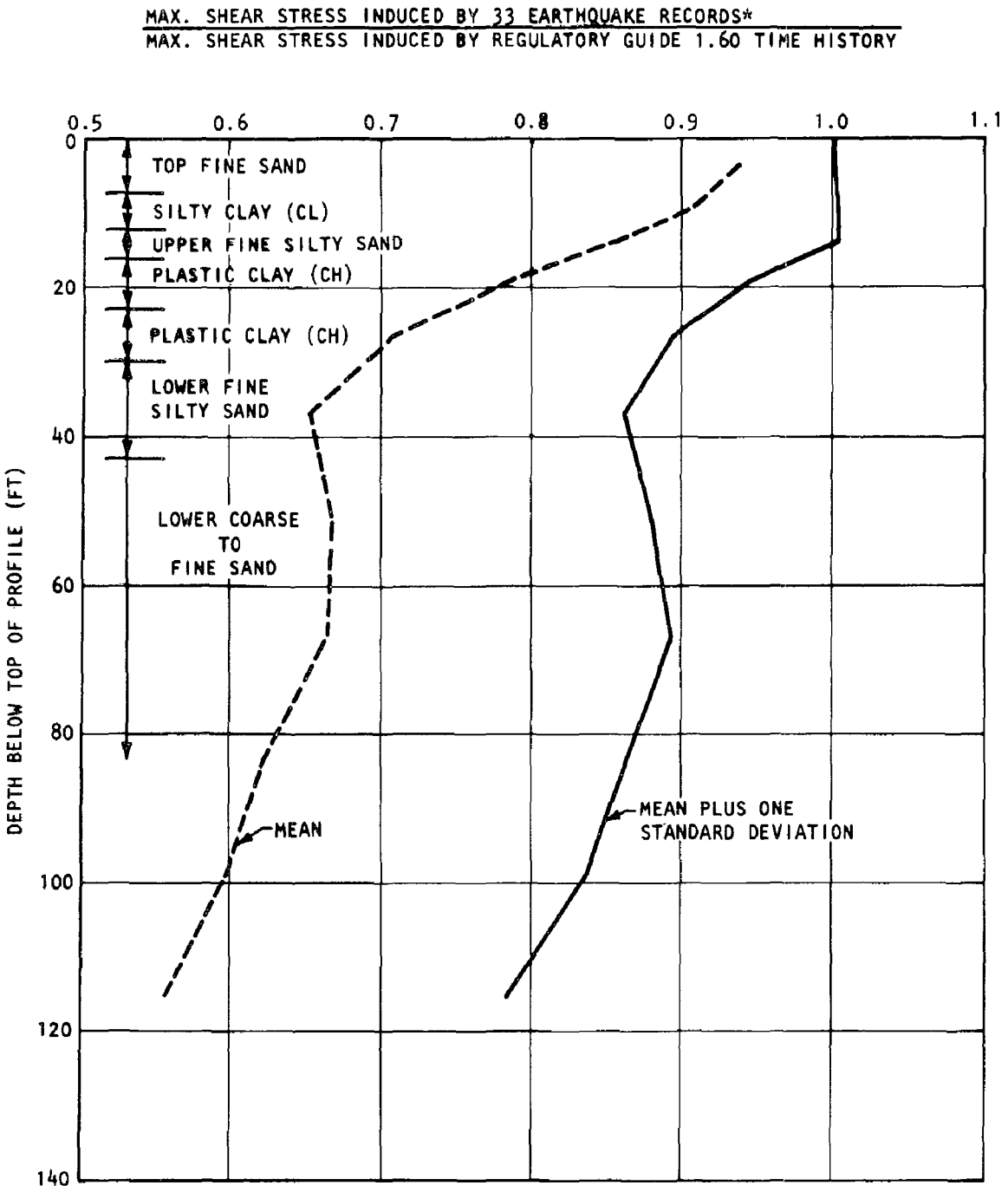

FIGURE 2 COMPARISON OF SEISMIC RESPONSES 33 EARTHQUAKE RECORDS AND REGULATORY GUIDE 1.60 TIME HISTORY

*SEE TEXT FOR EXPLANATION OF 33 EARTHQUAKE RECORDS REGULATORY GUIDE 1.60 TIME HISTORY

MAX. SHEAR STRESS INDUCED BY 6 EARTHQUAKE RECORDS OBTAINED AT DEEP SOIL SITES*
MAX. SHEAR STRESS INDUCED BY REGULATORY GUIDE 1.60 TIME HISTORY

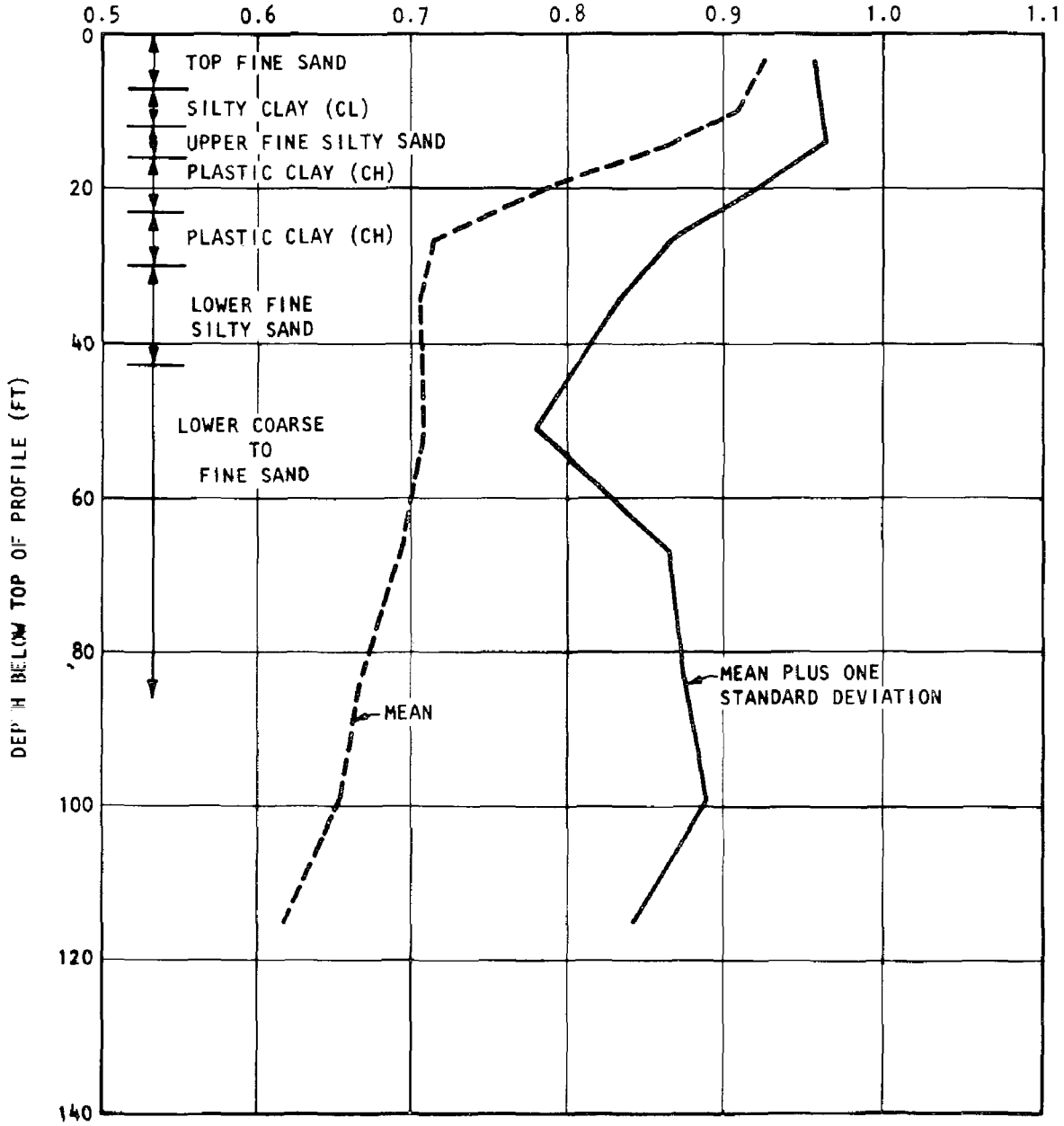

FIGURE 3 COMPARISON OF SEISMIC RESPONSES
6 EARTHQUAKE RECORDS AND REGULATORY
GUIDE 1.60 TIME HISTORY

*SEE TEXT FOR EXPLANATION OF 6 EARTHQUAKE RECORDS AND REGULATORY GUIDE 1.60 TIME HISTORY

INTERNATIONAL SYMPOSIUM ON
EARTHQUAKE STRUCTURAL ENGINEERING
St. Louis, Missouri, USA, August, 1976

DISCRETE MODELING OF CONTAINMENT STRUCTURES

Y. J. LIN and A. H. HADJIAN

Senior Engineer and Engineering Specialist

Bechtel Power Corp., Los Angeles Division

Norwalk, California, U.S.A.

SUMMARY

In practice the dynamic response of nuclear power plant containment structures is generally obtained by modeling the structures as either a lumped mass or a finite element model. The choice of model depends on the object of the analysis. This paper investigates the validity of the choice of a model to represent the actual shell structure. Cylindrical, hemispherical and containment vessel shapes are considered. The criteria for a minimum number of nodal points is also determined for both methods of analysis.

Treating the containment structure as a hollow cantilever beam of a length measured to the top of the dome, the Timoshenko beam equation predicts the structure frequencies with reasonable accuracy for a beam type mode (n = 1) up to the 3rd mode, while the bar theory predicts the fundamental frequency of the axisymmetric mode (n = 0) with equally acceptable accuracy. The simplicity of this approach is highly recommended since standard published curves and simple equations may be used as a means for a reliable prediction of containment natural frequencies.

INTRODUCTION

Nuclear power plant containment structures generally consist of cylindrical shells with domes. Although the combination of torus and spherical segment domes have been used in the past, hemispherical domes are more commonly used at the present time. Both prestressed concrete and reinforced concrete have been used in the construction of containment vessels. In the dynamic analysis of seismic response of the structures, it is assumed that the material is linear, elastic isotropic and homogenous. Furthermore, the effects of hatches, prestressing tendons, buttresses, etc. are assumed to be negligible and hence the containment vessel is considered to be axisymmetric.

Closed-form analytical solutions of thin shells are limited to special cases only. In practical analyses, the containments are generally modeled as discrete systems and analyzed by means of numerical methods. Two different numerical methods are generally used: the lumped-mass model and the finite element method. The method utilized depends on the purpose of the analysis: the lumped-mass model is used to generate in-structure response spectra and gross forces on the structure, and the finite element method is used mainly in stress analysis for structural design.

In applying the lumped mass method, shells are modeled as discrete systems in which masses are concentrated at nodal points and nodes are connected to each other by beam elements of uniform cross-sectional area. The general equation of motion of such a model is

$$[M]\{\ddot{X}\} + [C]\{\dot{X}\} + [K]\{X\} = -[M]\{\ddot{U}\} + \{F\} \qquad (1)$$

where [M], [C] and [K] are mass, damping and stiffness matrices, respectively, {F} represents an external force vector, and $\{\ddot{U}\}$ a ground acceleration vector. In the present study, the stiffness matrix is generated based on beam element model including shear deformation and rotary inertia effects [5], and the mass matrix is a consistent mass matrix which accounts for the actual distribution of mass throughout the structure. The computation of the consistent mass matrix is similar to the Rayleigh-Ritz formulation [1]. Thus the natural frequencies obtained by the use of the consistent mass matrix are an upper bound to the exact solution.

The finite element computer program used in the present study is a refinement of ASHSD code developed at the University of California, Berkeley [3]. The program discretizes the axisymmetric shell as a series of frustrum of cones, and the solid of revolution as triangular or quadrilateral toroids connected at their nodal point circles.

In the present presentation the studies of the convergency and accuracy of the structural modeling techniques are primarily based on the comparison of their natural frequencies.

DYNAMICS OF CYLINDRICAL SHELLS

The ratios of radius to wall thickness and length to radius of the cylindrical shells used in nuclear power plant containment structures are relatively low in terms of thin shell structures. The following values will be used as representative of most structures: 133.5 ft (40.72 m) diameter, 180 ft (69.26 m) height and 3.75 ft (1.23 m) wall thickness, Poisson's ratio of 0.27 and shear area coefficient of 0.5. It is believed that variations of these values would not invalidate the conclusions reached in this paper.

Horizontal excitation

It has been shown by Lin [4] that, based on a linear thin shell theory, a fixed-free cylindrical shell (fixed at one end and free at the other end), subjected to horizontal base excitations, can only be excited in a beam-type mode. Thus, only a beam type mode ($n = 1$; n is the circumferential mode number) is considered here.

Based on the finite element solution, the natural frequencies vs. total number of elements used are plotted in Fig. 1. It is found that the refinement of element sizes next to the boundary will not improve the results at all. Since the frequencies appear to be convergent when the calculations are based on 48 elements, these frequencies will be assumed to be the "exact" solutions.

In the beam-type mode vibration, the cross-sectional shape of the cylindrical shell is not distorted, thus the cylinder can be treated as a cantilever beam. Timoshenko's beam equation, which takes into account the effects of shear deformation and rotary inertia, is used to calculate the natural frequencies of a cantilever beam vs. ratios of radius of gyration to beam length. The results are plotted in Fig. 2.

The effects of shear deformations and rotary inertia become predominant for $r/\ell \geq 0.05$. It must be pointed out that similar curves published in texts have been erroneously presented, implying that these effects become important only for much larger values of r/ℓ. The frequencies for the sample problem considering the shell as a Timoshenko beam are shown in Fig. 1. The first two modes show excellent correlation to the finite element solution. Similar conclusions have been made by Forsberg [2] that indicate that the Timoshenko's beam theory can be used for long shells of ℓ/a ratios greater than 7. In the present study $\ell/a = 2.7$.

The results shown in Fig. 1 can be better visualized if the frequencies obtained for all models are normalized to the corresponding frequencies of the "exact" model, i.e. the model with 48 elements. These results are plotted in Fig. 3. It is seen that the 8 element model yields results with less than 10% error. This suggests that for proper modeling radius to element length ratios should be greater than 3.

In using a lumped mass model, the cylinder is divided into segments (nodes) of equal length, and the normalized frequencies based on various node numbers are shown in Fig. 4. The normalization is made

to the frequencies of the Timoshenko beam, on the premise that, as shown in Fig. 1, the Timoshenko beam equation accurately predicts the first two frequencies of the shell. It is seen that the lumped mass solution always gives an upper bound to the exact solution, as expected, when using the consistent mass formulation. For a maximum 10% error the number of nodes to be used is one higher than the mode number. Thus, if the 3rd mode is of interest, a 4 node model would be sufficient.

Vertical excitation

When a cylindrical shell is subjected to a vertical motion, an axisymmetrix mode of vibration (n = o) will be excited. In this case, the dynamic equation of a thin cylindrical shell can be reduced to a sixth order differential equation. For any fixed number of axial wave of free vibration, the shell will have three modes having three separate eigenvalues which involve (i) a pure torsional motion, (ii) a pure longitudinal motion, and (iii) a primary radial motion. For axial motion the shell can be considered to be a bar, and for radial motion, it can be considered to be a ring. Bar theory can only predict the longitudinal displacement components and the axial forces. For the case of $a/h = 20$, $\ell/a = 5$, and $\nu = 0.3$, the frequency obtained from a bar theory is approximately 2.5% higher than that from shell theory, and the axial force is approximately 5.5% higher [2].

By using the finite element method, the natural frequencies of the axisymmetric vibration of a cylindrical shell based on the model of 48 elements are assumed to be the convergent values. Similar to the horizontal case the normalized frequencies are plotted in Fig. 5.

Based on a bar theory, the frequency equation of longitudinal vibration of the fixed-free bar is given by

$$\omega_n = \frac{n}{4\ell}\sqrt{\frac{E}{\rho}} \quad \text{(in cps)} \qquad n = 1, 3, 5 \ldots \tag{2}$$

where E, ρ, and ℓ are modulus of elasticity, density and bar length, respectively. The equation gives a very good prediction of the fundamental frequency of axisymmetric vibration of a cylindrical shell.

The lumped mass model can only represent the vibration of a cylindrical shell in the longitudinal (axial) displacement component. The natural frequencies computed from the lumped mass model are normalized by those from eq. (2) and plotted in Fig. 6. Again the lumped mass model gives an upper bound to the exact value.

Within a 10% error the proper model should have twice as many mass points as the mode number of interest. However, for earthquake engineering purposes the fundamental node is sufficient since the higher nodes of containment structures are larger than 30 cps. Results from this study indicate that the fundamental frequency obtained even from a two mass model is very close to that obtained from the 48 element finite element model.

DYNAMICS OF HEMISPHERICAL SHELLS

In the finite element method, the spherical shell is treated as a series of conical frustrums. In the lumped mass modeling of spherical shell, the beam element between two adjacent nodes are assumed to be uniform. The average values of moment of inertias and the cross-sectional areas at the nodal points are used to calculate the mass and stiffness matrices.

In the present study, a hemispherical shell is divided into segments of equal meridional angles. There is one exception, however. For the 10-element model, the meridional angle of the first two elements is 5 degrees, and those of remaining elements are 10 degrees.

Horizontal excitation

Fig. 7 shows the natural frequencies of a hemispherical shell computed from the lumped mass model and the finite element method. Unlike the case of a cylindrical shell, the frequencies do not monotonically approach the convergent value as the number of elements used is increased. Nevertheless, the frequencies computed from 18 elements are assumed to be convergent. It is shown that at least 6 elements are required for an acceptable model.

The frequencies obtained from lumped mass solution are much higher than those of corresponding modes computed from finite element solution; the lumped mass modeling of hemispherical shells as described above is not adequate. Since by itself the modeling of the hemispherical shells is not of practical importance, other methods were not explored. The more important problem is the modeling of the complete containment structure.

Vertical excitation

When a hemispherical shell is subjected to a vertical excitation at the base, an axisymmetric vibration will be excited. The natural frequencies of axisymmetric modes computed from the finite element method are plotted in Fig. 8 for two different edge conditions.

Similar comments as for the horizontal excitation also apply for the lumped mass model.

DYNAMICS OF CYLINDRICAL SHELLS WITH HEMISPHERICAL DOMES

The modeling techniques discussed previously for the cylindrical and hemispherical shells are utilized to predict the response of containment structures assumed to be fixed at their base.

Horizontal excitation

When a cylindrical shell with a hemispherical cap is subjected to a horizontal excitation at its base, the beam-type mode (n = 1) is the predominant mode [6]. Thus, only the beam-type mode will be examined in the present study.

Natural frequencies of a cylindrical shell with a hemispherical cap at one end and clamped at other end are tabulated in Table 1. The above studies indicate that the model with 48 elements produces convergent value for a cylindrical shell and the model with 18 elements for a hemispherical shell. Thus, the frequencies calculated from the model with 48 elements in the cylinder and 18 elements in the dome are assumed to be convergent. These values are used to study the percentage of error of the frequencies computed from various models shown in parentheses in Table 1. The combination of 8 elements in the cylindrical shell and 3 elements in the cap produces relatively good results. The combination of 12 elements in the cylinder and 6 elements in the cap produces very good results with the error being less than 1%.

The frequencies computed from the lumped mass model are tabulated in Table 2. The results show that for the first and third modes the frequency calculation is insensitive to the number of nodes used; and an average error of 10% is indicated for the first mode and 15% for the third mode. Some effects of increasing the number of nodes in the second mode is indicated.

The frequencies were computed by treating the cylindrical shell with a hemispherical cap as a fixed-free Timoshenko beam of a length measured up to the top of the dome. The results are listed in the last column of Table 1. For this case the total volume of the dome remains unchanged. The results show that this type of modeling gives satisfactory results, and could therefore extremely simplify the calculation of frequencies using published curves as shown in Fig. 2.

Vertical excitation

Based on the finite element solution, the natural frequencies of axisymmetric vibration of a cylindrical shell with a hemispherical dome are tabulated in Table 3. Assuming that the frequencies computed from the model with 48 elements in the cylinder and 18 elements in the cap are convergent, the results indicate that at least 6 elements are required in the dome. The model with 8 elements in the cylinder and 6 elements in the dome produces satisfactory results for even the higher modes.

The natural frequencies computed from the lumped mass model are tabulated in Table 2. It is shown that only the fundamental frequency can be adequately predicted by the lumped mass method as in the case of axisymmetric vibration of a cylindrical shell.

The cylindrical shell with a hemispherical cap may be approximately modeled 1) as a bar of length measured up the spring line with a concentrated mass at the end, or 2) as a uniform bar of length measured up to the

top of the dome. The results tabulated in Table 3 (last two columns) indicate that both models give a very good prediction for the fundamental frequency, thus reducing the calculations to the solution of Eq. 2.

Conclusions

A typical containment structure was investigated using a finite element and lumped mass models. The results indicate that for practical applications either method gives adequate results provided that sufficient discretization is considered. Guidelines are provided in the text. In fact an extremely simplified model is suggested that would replace the containment structure with a uniform Timoshenko beam of height equal to the apex of the dome.

REFERENCES

1. Archer, J. S., "Consistent Mass Matrix for Distributed Mass System," Journal of Structural Division, ASCE, ST4, August 1963.

2. Forsberg, K., "Axisymmetric and Beam-Type Vibration of Thin Cylindrical Shell," AIAA Journal, Vol. 7, No. 2, February 1969.

3. Ghosh, S. and Wilson, E., "Dynamic Stress Analysis of Axisymmetric Structures under Arbitrary Loading," Report No. EERC 69-10 College of Engineering, University of California Berkeley, California, September 1969.

4. Lin, C. W., "Seismic Response of Nuclear Reactor Containment Vessels," Nuclear Engineering and Design 9, 1969, pp. 234-238.

5. Przemieniecki, J. S., Theory of Matrix Structural Analysis, McGraw-Hill Book Co., 1968.

6. Tsai, N. C., et al, "Seismic Analysis of Structures and Equipment for Nuclear Power Plants," Topical Report, BC-TOP-4, Revision 4-A, 1975.

Table 1

NATURAL FREQUENCIES (CPS) OF CYLINDRICAL SHELL WITH HEMISPHERICAL CAP (n=1)

(Finite Element Model)

No. of Elem.	Cyl.	8	8	8	12	12	12	24	24	24	48	Timoshenko Beam
	Dome	3	6	9	3	6	9	3	6	9	18	
1st Mode		3.15 (1.013)	3.12 (1.003)	3.11 (1.00)	3.15 (1.013)	3.12 (1.003)	3.11 (1.00)	3.15 (1.013)	3.12 (1.003)	3.11 (1.00)	3.11	3.10
2nd Mode		9.99 (1.004)	9.97 (1.002)	9.97 (1.002)	9.98 (1.003)	9.96 (1.001)	9.96 (1.001)	9.97 (1.002)	9.96 (1.001)	9.95 (1.00)	9.95	9.74
3rd Mode		17.61 (1.002)	17.62 (1.002)	17.61 (1.002)	17.60 (1.001)	17.61 (1.002)	17.61 (1.002)	17.58 (1.00)	17.59 (1.001)	17.59 (1.001)	17.59	18.69
4th Mode		18.92 (1.007)	18.89 (1.005)	18.85 (1.003)	18.91 (1.006)	18.88 (1.005)	18.84 (1.003)	18.90 (1.006)	18.84 (1.004)	18.82 (1.002)	18.79	22.52
5th Mode		21.28 (0.986)	21.59 (1.00)	21.54 (0.998)	21.26 0.985)	21.64 (1.002)	21.62 (1.001)	21.17 (0.981)	21.60 (1.001)	21.61 (1.001)	21.59	29.79
6th Mode		21.69 (0.952)	22.70 (0.997)	22.54 (0.990)	21.69 (0.932)	22.98 (1.009)	22.82 (1.002)	21.69 (0.952)	23.04 (1.011)	22.89 (1.005)	22.78	

Note: Numbers in ( ) are the ratio to the 48/18 elements model

Table 2

NATURAL FREQUENCIES (CPS) OF A CYLINDRICAL SHELL WITH HEMISPHERICAL CAP (Lumped Mass Model)

	No. of Nodes	Cyl.	8	8	8	12	12	12	FEM	Uniform Beam No. of Nodes	
		Dome	3	6	9	3	6	9		6	8
Horizontal	1st Mode		3.47 (1.116)	3.41 (1.096)	3.40 (1.093)	3.46 (1.113)	3.40 (1.093)	3.40 (1.093)	3.11	3.12	3.12
	2nd Mode		10.51 (1.056)	10.42 (1.047)	10.41 (1.046)	10.25 (1.030)	10.40 (1.005)	10.40 (1.005)	9.95	9.75	9.71
	3rd Mode		20.39 (1.159)	20.17 (1.147)	20.16 (1.146)	18.77 (1.067)	20.07 (1.141)	20.07 (1.141)	17.59	18.96	18.73
Vertical	1st Mode		11.14 (1.120)	10.89 (1.094)	10.87 (1.092)	11.06 (1.112)	10.89 (1.094)	10.87 (1.092)	9.95	10.27	10.26
	2nd Mode		33.25	32.62	32.56	32.89	32.51	32.46	19.74	31.53	31.18
	3rd Mode		55.06	54.38	54.33	54.19	53.85	53.79	23.21	54.90	53.29

Note: Numbers in ( ) are the ratios to the solution by the Finite Element method.

Table 3

NATURAL FREQUENCIES (CPS) OF AXISYMMETRIC VIBRATION OF CYLINDRICAL SHELL WITH HEMISPHERICAL CAP (n=0)
(Finite Element Model)

No. of Elem.	Cyl.	8	8	8	12	12	12	24	24	24	48	Bar Theory	
	Dome	3	6	9	3	6	9	3	6	9	18	Model 1	Model 2
1st Mode		10.46 (1.051)	9.97 (1.002)	9.95 (1.00)	10.05 (1.010)	9.98 (1.002)	9.96 (1.001)	10.05 (1.010)	9.98 (1.002)	9.96 (1.001)	9.95	10.24	10.04
2nd Mode		18.99 (0.962)	19.71 (0.998)	19.65 (0.995)	18.98 (0.982)	19.78 (1.002)	19.74 (1.00)	18.98 (0.962)	19.82 (1.004)	19.79 (1.003)	19.74	30.72	33.36
3rd Mode		20.62 (0.888)	23.08 (0.994)	23.17 (0.998)	20.62 (0.888)	23.08 (0.994)	23.20 (1.00)	20.62 (0.888)	23.03 (0.992)	23.17 (0.998)	23.21		
4th Mode		21.55 (0.897)	23.84 (0.942)	23.80 (0.990)	21.44 (0.892)	24.01 (0.999)	24.01 (0.999)	21.32 (0.887)	24.04 (1.00)	24.04 (1.00)	24.03		
5th Mode		23.82 (0.968)	24.28 (0.986)	24.28 (0.986)	23.96 (0.960)	24.58 (0.998)	24.58 (0.998)	23.96 (0.973)	24.62 (1.00)	24.63 (1.00)	24.62		
6th Mode		24.37 (0.970)	24.90 (0.991)	24.92 (0.992)	24.69 (0.983)	25.07 (0.998)	25.18 (1.002)	24.71 (0.994)	25.02 (0.996)	25.09 (0.999)	25.12		

Note: Numbers in ( ) are the ratios to the 48/18 elements model.

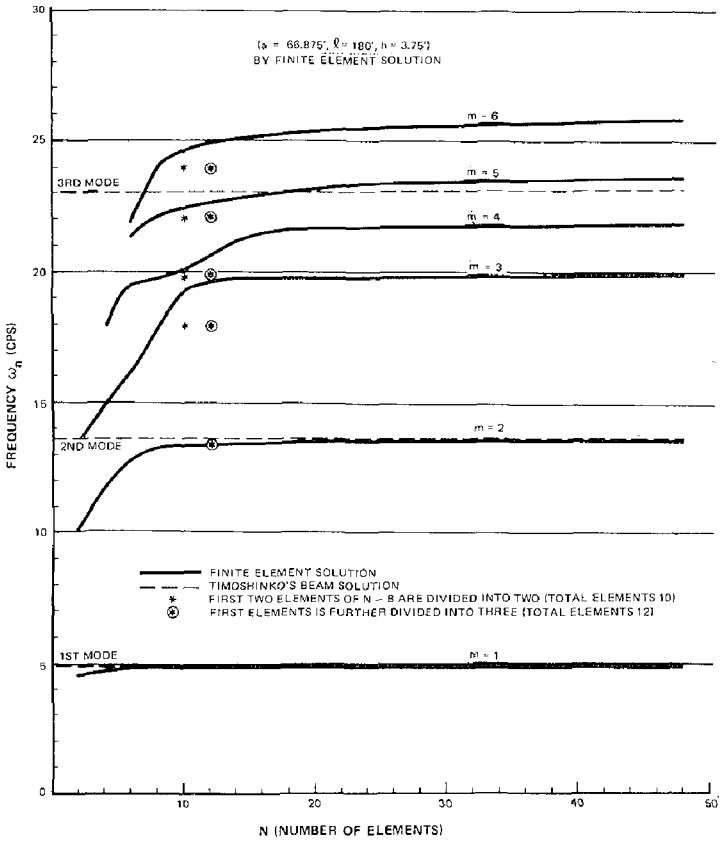

Figure 1

NATURAL FREQUENCIES OF FIXED-FREE CYLINDRICAL SHELL (n = 1)

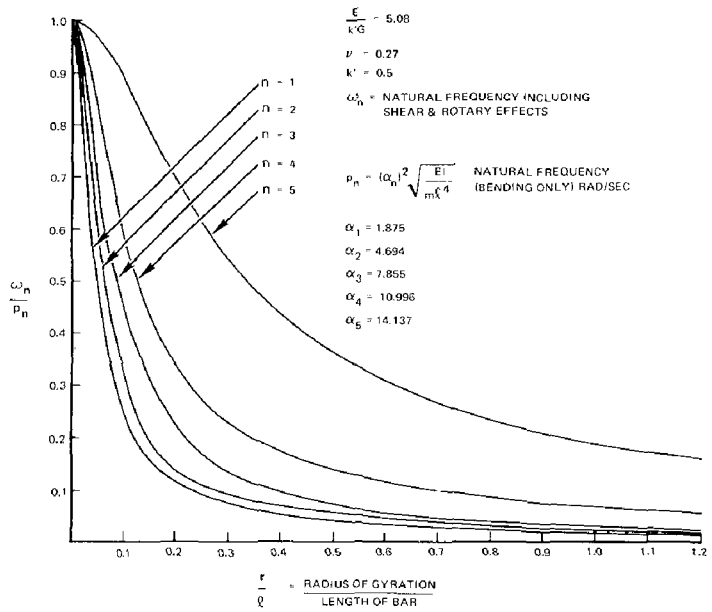

Figure 2.

NATURAL FREQUENCY OF CANTILEVER BEAM

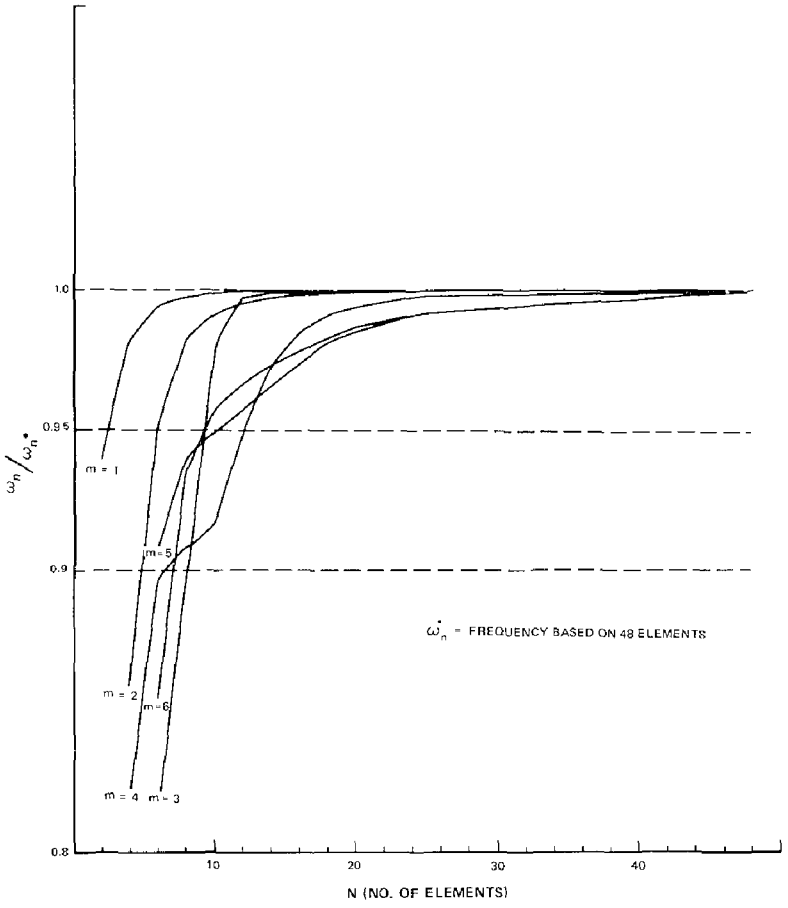

Figure 3.
NORMALIZED NATURAL FREQUENCIES
OF FIXED-FREE CYLINDRICAL SHELL (n = 1)

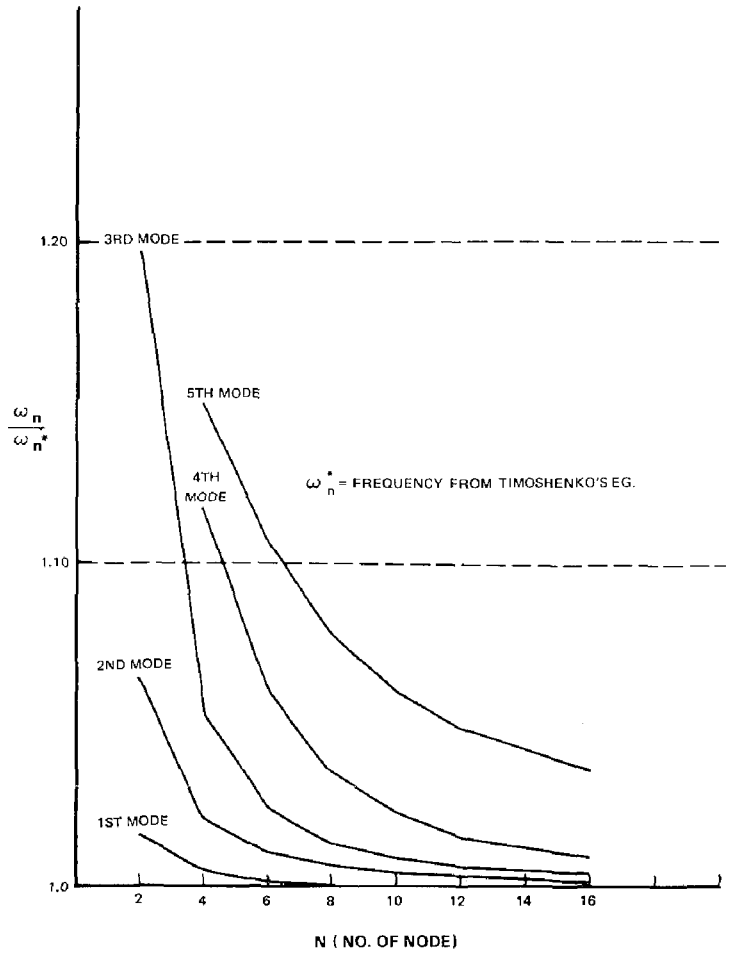

Figure 4
NORMALIZED NATURAL FREQUENCIES
OF CANTILEVER BEAM (LUMPED MASS MODEL)

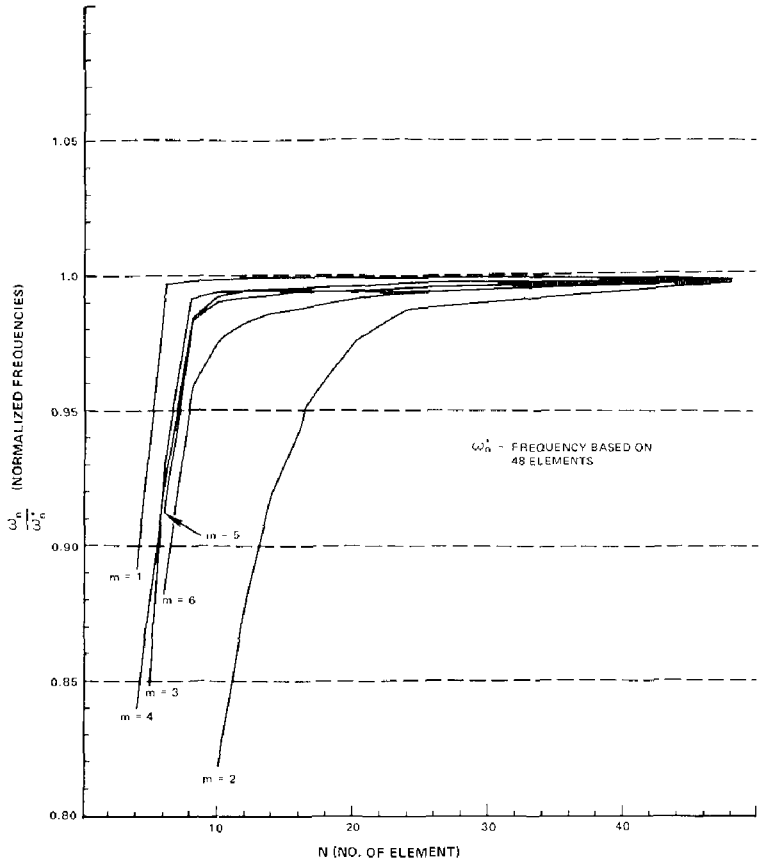

Figure 5

AXISYMMETRIC VIBRATION OF FIXED-FREE CYLINDRICAL SHELL (n = 0)

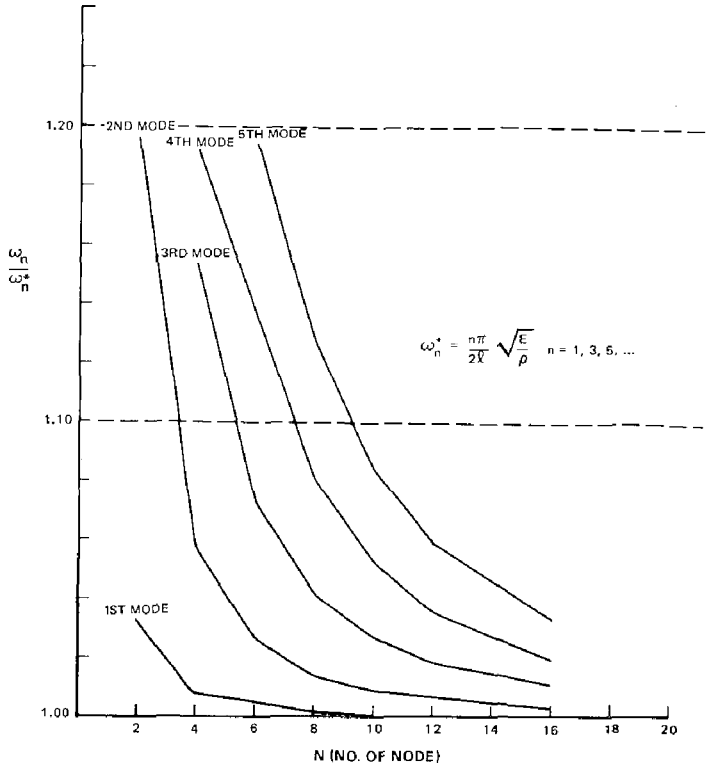

Figure 6

NORMALIZED NATURAL FREQUENCIES
OF LONGITUDINAL VIBRATION OF CANTILEVAR BAR
(LUMPED MASS MODEL)

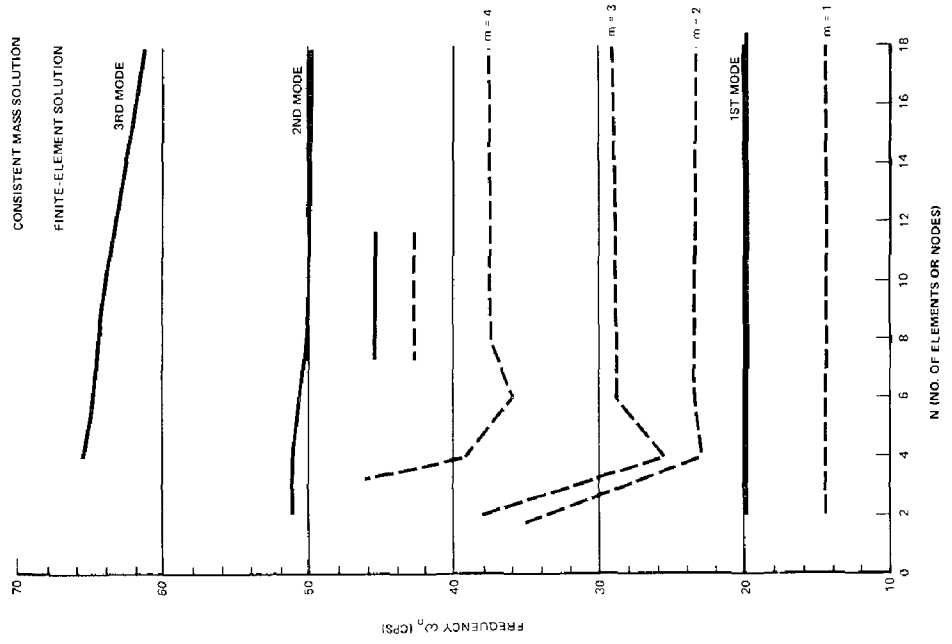

Figure 7
NATURAL FREQUENCIES OF CLAMPED HEMISPHERICAL SHELL (n = 1) (LUMPED-MASS AND FINITE-ELEMENT SOLUTION)

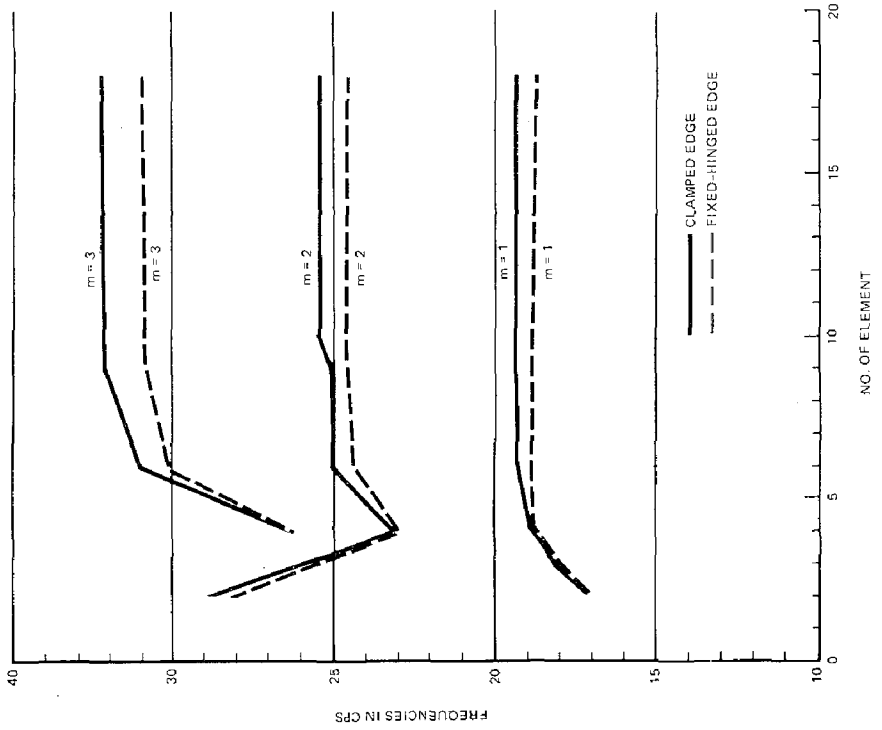

Figure 8
NATURAL FREQUENCIES OF AXISYMMETRIC VIBRATION OF HEMISPHERICAL SHELL (n = 0)

INTERNATIONAL SYMPOSIUM ON
EARTHQUAKE STRUCTURAL ENGINEERING
St. Louis, Missouri, USA, August, 1976

SEISMIC RISK ANALYSIS OF NUCLEAR POWER PLANT SITES INCLUDING POWER SPECTRUM SIMULATION OF FUTURE EARTHQUAKE MOTION

AYBARS GÜRPINAR

Assistant Professor of Engineering Sciences

Middle East Technical University

Ankara, Turkey

SUMMARY

Seismic risk analysis of possible nuclear power plant sites may in some cases be the deciding factor in the site selection process. This article includes the results of a case study for two such sites in Northwestern Turkey, as well as a proposition for a more efficient risk analysis format.

In the case study, site A was found to have higher bedrock peak acceleration risks than site B, but on the other hand, site B had local soil conditions which amplified oncoming wave acceleration by about 2.5 on the average. For site A there was no amplification. Amplification study was carried out using a power spectrum simulation which assumes a band limited white noise spectral density function for the bedrock acceleration. This average amplification of 2.5 was incorporated in seismic risk curves.

Noting the deficiencies of some current methods of seismic risk analysis, a new format is proposed for this purpose. The proposal suggests the use of root mean square value of velocity instead of peak acceleration and includes effects of angle of incidence θ, P wave velocity power spectrum and vertical motion. It is also pointed out that the method enable the risk analyst and structural design engineer to work in closer and more efficient cooperation.

INTRODUCTION

The problem of seismic risk very often turns out to be the most crucial factor in the site selection process of nuclear power plants. On the other hand the data necessary to solve this delicate problem is usually inadequate. Only in the combination of seismically active and technologically developed regions of the world there may be sufficient amount of data to be satisfactorily incorporated in seismic risk calculations. This data should include; (a) historical records of very large earthquakes,

(b) seismograph records of all significant earthquakes (say $M \geq 4.0$) of this century with their corresponding coordinates and focal depths, (c) strong motion records of recent earthquakes. Information from (a) and (b) will enable the engineering seismologist to determine the necessary frequency-magnitude relationship. Strong motion records, on the other hand, will be extremely useful when constructing a realistic attenuation relationship for the region. They will also serve as a valuable starting point for both time history and spectral simulation of future earthquake motion.

Facing a shortage of important data and a critical decision to make, there must be a tendency for extra caution, which on the other hand may yield to over conservatism. For the problem of nuclear power plants, over conservatism may result in either; (a) an order of magnitude of increase in cost, or (b) abandoning of the site. Either of the alternatives (a) or (b) is unattractive yet sometimes unavoidable, when it is impossible to show clearly that probability of "danger" is "acceptable". In other words, every location is dangerous until it is proven otherwise. Then, the task of the engineering seismologist is to be able to prove this provided, of course, that the state of nature in fact is suitable. This is only possible when the data and knowledge at hand are used efficiently.

In the following, a brief summary of a case study will be presented for the purpose of pointing out some difficulties. Then, a proposition will be put forth which can circumvent some of the stated difficulties.

CASE STUDY

Nuclear Energy Division of the Turkish Electricity Authority had selected two sites (A and B) in the seismologically very active region of Northwestern Turkey, for the purposes of locating a nuclear power plant. The selection had been made because of other merits of these two sites and the decision process had been an arduous one. The study was to be a comparative one (between A and B) and it was to include seismic risk considerations as well as any amplification to be expected from local soil conditions. A detailed account of this study has already been published and can be found elsewhere(1).

First of all, quadratic frequency-magnitude relationships for the two sites were determined by using recent catalogues (2,3,4). Earthquakes that occurred after 1900 and with $M \geq 4.3$ were used in the analysis. These relationships are given in Equations 1 and 2 for sites A and B respectively.

$$\log n_m = 1.718 - 0.4068\,(m-4.3) - 0.01521\,(m-4.3)^2 \qquad (1)$$

$$\log n_m = 2.014 - 0.4802\,(m-4.3) - 0.02636\,(m-4.3)^2 \qquad (2)$$

Here n_m denotes the number of earthquakes with magnitudes greater than or equal to m. That the region considered for site B contains more epicenters is due to the fact that a radius of 200 km. was taken for site B whereas a radius of 120 km. was used for site A. This was because increasing of the radius for site A would have included epicenters from a different tectonic formation; hence statistical homogeneity of the data would have been tampered with.

Secondly, a hypothesis was put forth about statistical independence of the magnitudes of successive earthquakes. This hypothesis was tested by using a chi-square control chart and it was found that it cannot be rejected even at very small levels of significance (even for α=0.0001). This may be seen in Table 1. The fact that there is statistical independence between successive earthquakes justifies the use of the Poisson process as a legitimate model in seismic risk analysis. It turns out that this may not always be true. Ferraes (5), for example, showed that the assumption of statistical independence is not justified for Mexico City earthquakes.

Seismic risk curves for the two sites were drawn by using Esteva's (6) attenuation relationship and Mertz and Cornell's (7) method. These curves may be seen in Figures 1 and 2 for sites A and B respectively. Risk values are very high for both sites and site A has a seismic risk of about an order of magnitude greater than that of site B.

It was found, however, that local soil conditions of site B amplified the root mean square (rms) of the bedrock acceleration by about 2.5 times, wheares no amplification occurred for site A. Simulated acceleration spectral density functions are drawn in Figure 3 for these two sites using a method developed elsewhere (8,9). The method, briefly, assumes a shape for the spectral density function of the bedrock motion and using the transfer matrix method and a two dimesional layered model for the soil medium obtains the P and SH wave spectral density function on the ground surface. Figure 4 shows adjusted seismic risk curves for site B in which the factor of 2.5 has been incorporated.

PROPOSED SEISMIC RISK ANALYSES

The basic problem with a seismic risk analysis as outlined above seems to be the use of "maximum acceleration" at a site as the decision criterion. The use of maximum values in establishing attenuation relationships and incorporating these values into seismic risk evaluation gives rise to "rigid" decision making and diminishes the attractiveness of probabilistic assessment. Furthermore, considering all the aspects of the problem of seismic risk and vibrational characteristics of nuclear power plants, only maximum ground acceleration and the probability of axceedance of that acceleration in so many years is insufficient information for

the design engineer. Solving the design problem as uncoupled from the seismic risk problem may be possible but certainly not feasible as it will lead to many repetitions concerning location and activities of possible epicenters, attenuation relationships, etc., necessary for either theoretical or computer (digital or analog) simulation of the probable future earthquake motion.

To be able to combine the problem of the engineering seismologist with that of the design engineer of the nuclear power plant, one should also remember that the frequency content of ground motion is generally as important as the maximum value. This is due to the fact that the power plant contains an assortment of structural elements and mechanical equipment which possess natural frequencies ranging from very low to very high values.

In the light of the above discussion, the following points will be suggested:

1. Statistical independence of magnitude of successive earthquakes must be established before using a Poisson model for seismic risk analysis (see Table 1).

2. Acceleration should not be the only criterion in seismic risk analysis as it usually is not correlated very well with response quantities and potential damage. Kobayashi's work (10) can be cited in support of this and the correlation coefficients relating ground acceleration, velocity and displacement to response quantities can be seen plotted against natural period in Figure 5. If one of these quantities (ground acceleration, ground velocity, ground displacement) had to be chosen, it should be ground velocity because; (a) it is correlated best with response quantities within the widest range of natural periods, (b) it can more easily be converted to either acceleration or displacement.

3. Use of maxima (either acceleration or velocity) should be avoided. rms values can be used in attenuation relationships. These values can be used in the barrier crossing problem, i.e.

$$\nu_a^+ = \nu_o^+ \exp\left(-\frac{a^2}{2\sigma^2}\right) \qquad (3)$$

and the expected frequency of crossing any arbitraty level "a" can be determined instead of one maximum. "a" can be chosen appropriately for the problem at hand. In Equation 3;

ν_a^+: expected frequency of upcrossings of the level "a"
ν_o^+ : expected frequency of upcrossings of zero level
σ^2 : variance ($\sigma^2 = (\text{rms})^2$ if the process has zero mean).

4. Using epicentral location and focal depths of past earthquakes, angles of incidence, θ, should be determined. Even a simple histogram may be useful. The effect of this angle of incidence should be investigated, as it may be an important factor in power spectrum simulation (8,9). Figures 6 and 7 illustrate this dependence for "firm" soil conditions.

5. Influence of P waves should also be investigated as they may contribute to higher frequencies appreciably especially for "firm" soil conditions, (8,9). Figure 8 shows the comparison of P and SH wave power spectra for "firm" type soil. For "soft" soil conditions (alluvial) it was established that P wave is more critical than SH wave in the region $T > d/6.76$ where d is the total depth of layers down to bedrock (8,9).

6. Tracing a typical oncoming wave through the multilayered soil medium, the angle of emergence of the motion may be determined. Then, taking into account the contribution of P and S waves amount of vertical motion may be estimated. This is especially important for mechanical equipment and piping design. It was shown elsewhere that vertical motion coupled with horizontal motion may increase the probability of failure of some structural element by as much as 5000 (11).

REFERENCES

(1) Gürpınar, A. et al., Local Earthquake Study for Nuclear Power Plant Sites, Pro. No. 75-04-09-01, Middle East Technical University, 1975 (in Turkish)

(2) "Balkan Region-Catalogue of Earthquakes", UNESCO, Skopje, 1974

(3) "Earthquake Data File", Edinburgh Center, (computer output), 1975

(4) Alsan, E., Tezuçan, L. and Bath, M. "Earthquake Data File, Kandilli Observatory, İstanbul, (computer output), 1975

(5) Ferraes, S.G., "Earthquake Magnitude Probabilities and Statistical Independence for Mexico City Earthquakes", BSSA, x.63, No. 6, pp. 1913-1919, Dec. 1973

(6) Esteva, L., "Criteria for the Construction of Spectra for Seismic Design", Third Panamerican Symposium on Structures, Venezuela, 1967

(7) Mertz, H.A. and Cornell, C.A., "Seismic Risk Analysis Based on a Quadratic Magnitude-Frequency Law", BSSA, vol.63,pp. 1999-2000, 1973

(8) Özgür,D. and Gürpınar, A. "Theoretical Simulation of Earthquake Acceleration Spectra", Proc. 5WCEE, Roma,1973

(9) Gürpınar, A.,"Power Spectrum Representation of Earthquake Motions", Proc. 5ECEE, İstanbul, 1975

(10) Kobayashi, H. and Nagahashi, S. "Intensity of Earthquake Motion for the Design of Structures", Tokyo Institute of Technology, 1973

(11) Gürpınar, A. and Yao, J.T.P., "Design of Columns for Seismic Loads", Journal of the Structural Division, ASCE, ST9, September 1973

Table 1. Control Chart for Statistical Independence of Magnitudes of Successive Earthquakes

i \ j	4.5	5.0	5.5	6.0	6.5	7.0	7.5	
4.5	16 (16.49)	13 (12.95)	6 (7.46)	2 (1.96)	3 (1.57)	1 (1.18)	1 (0.39)	42
5.0	13 (12.95)	10 (10.17)	7 (5.86)	2 (1.54)	0 (1.23)	1 (0.93)	0 (0.31)	33
5.5	8 (7.46)	7 (5.86)	3 (3.37)	0 (0.89)	0 (0.71)	1 (0.53)	0 (0.18)	19
6.0	2 (1.96)	1 (1.54)	1 (0.89)	1 (0.23)	0 (0.19)	0 (0.14)	0 (0.05)	5
6.5	2 (1.57)	1 (1.23)	1 (0.71)	0 (0.19)	0 (0.15)	0 (0.11)	0 (0.04)	4
7.0	2 (1.18	0 (0.93)	1 (0.53)	0 (0.14)	0 (0.11)	0 (0.08)	0 (0.03)	3
7.5	0 (0.39)	0 (0.31)	0 (0.18)	0 (0.05)	1 (0.04)	0 (0.03)	0 (0.01)	1
	42	33	19	5	4	3	1	

observed

(expected)

$\sum_i \frac{(o_i - e_i)^2}{e_i} = 21.19$

Impossible to reject independence hypothesis up till $\gamma = 0.999$

ACKNOWLEDGEMENT

The author wishes to acknowledge contributions of Professors Polat Gülkan and Çetin Soydemir, principal co-authors of Reference 1, from which this article's case study was outlined.

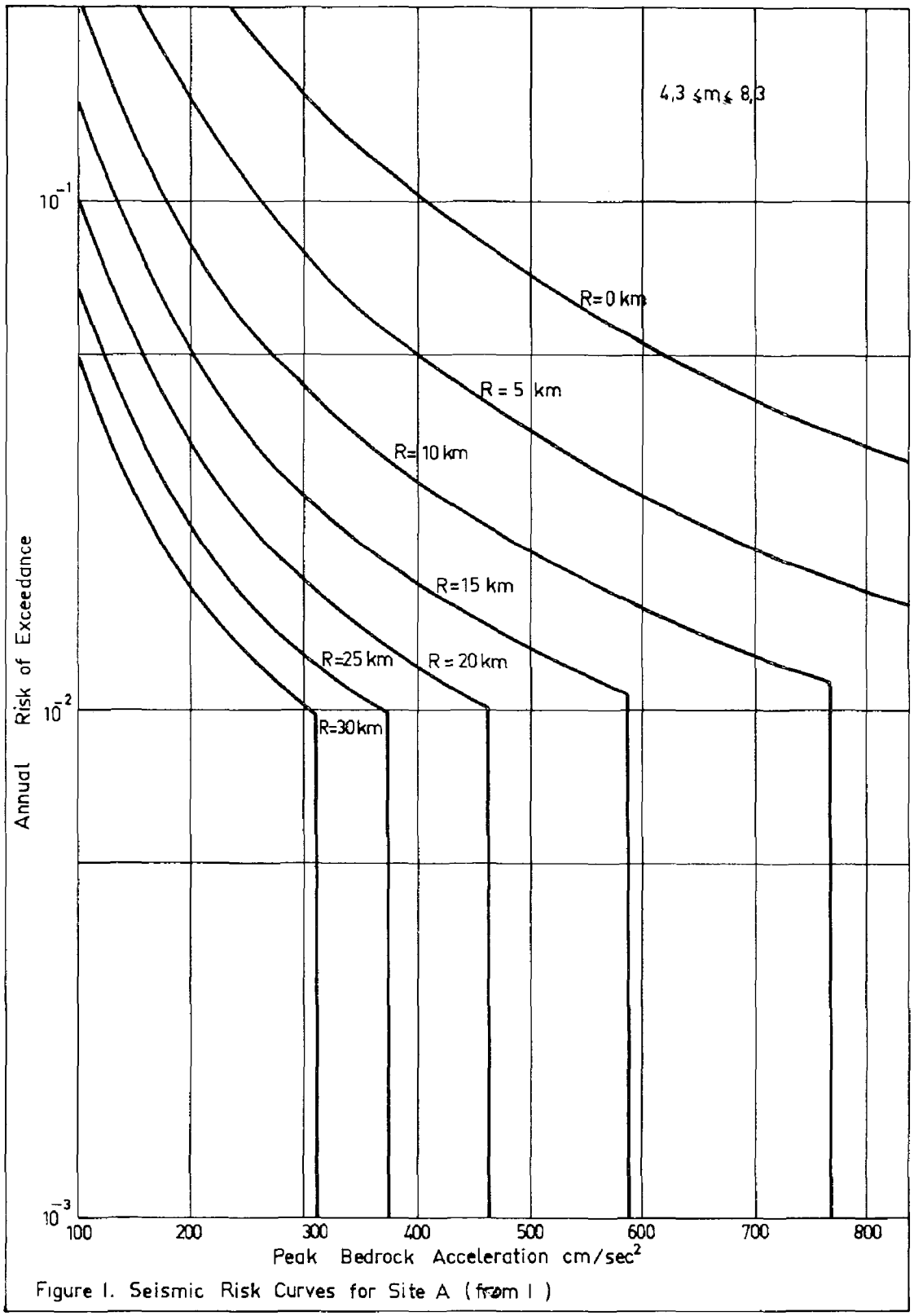

Figure 1. Seismic Risk Curves for Site A (from 1)

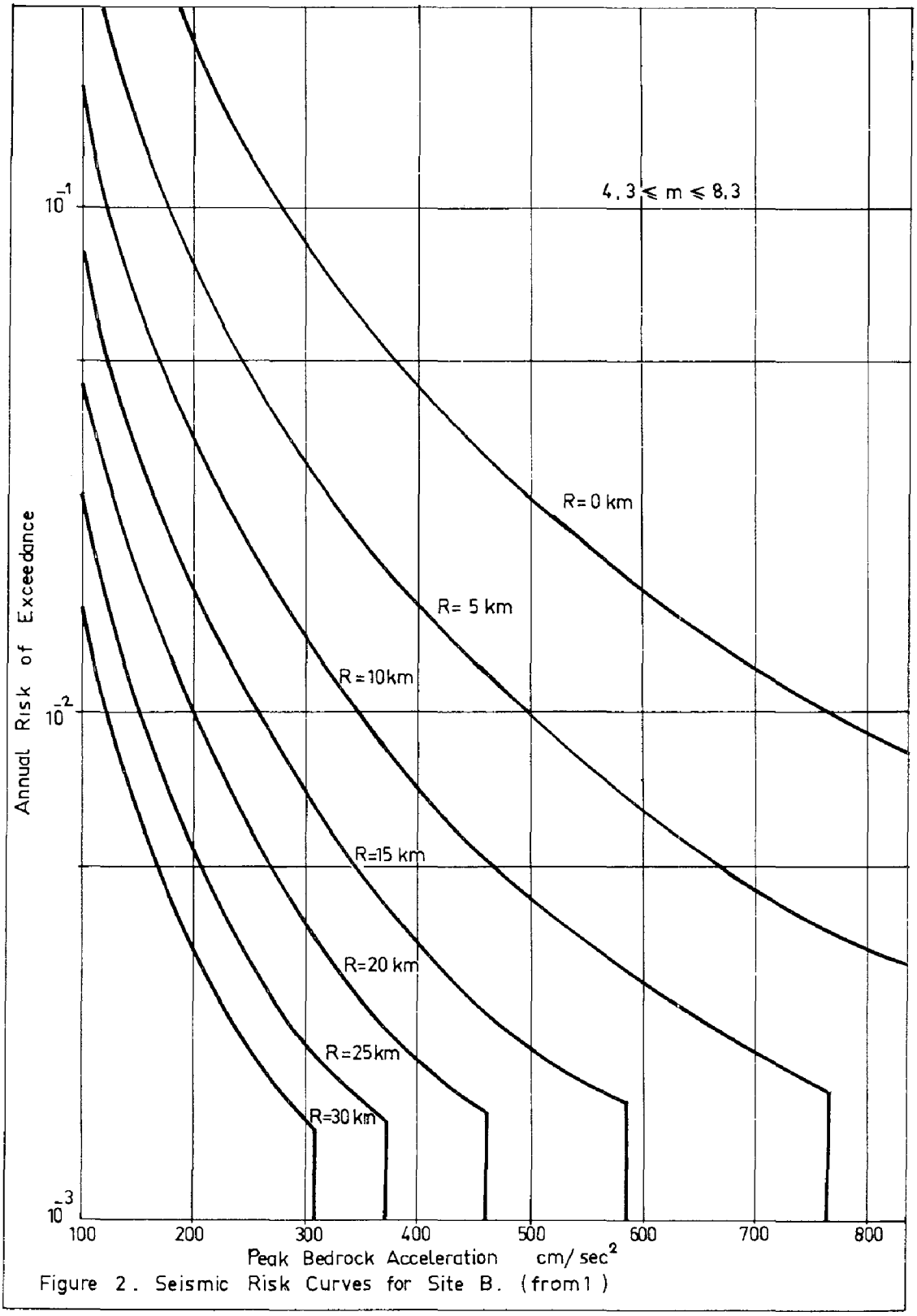

Figure 2. Seismic Risk Curves for Site B. (from 1)

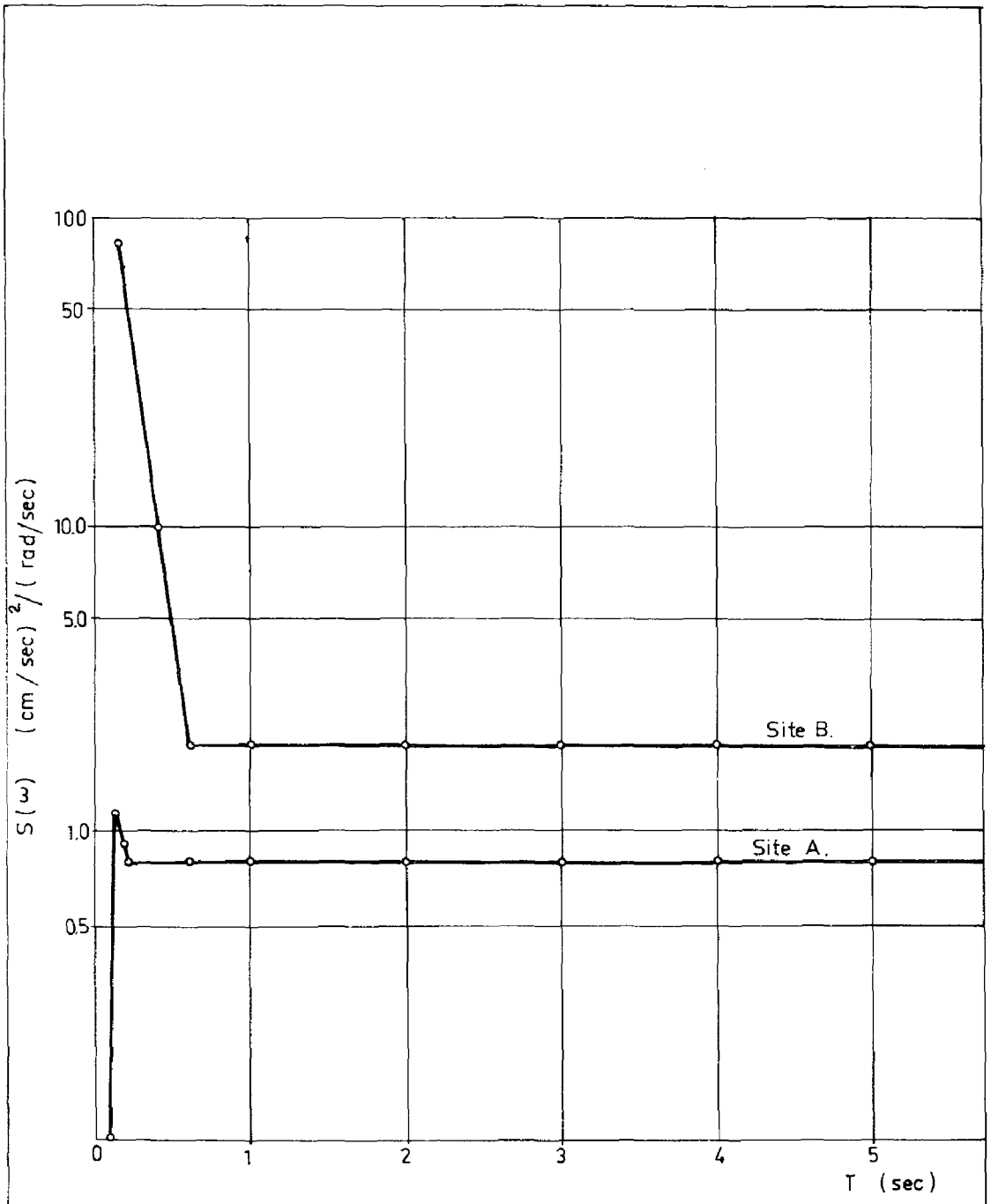

Figure 3. Simulated S Wave Acceleration Spectral Density Functions for Sites A and B (from 1)

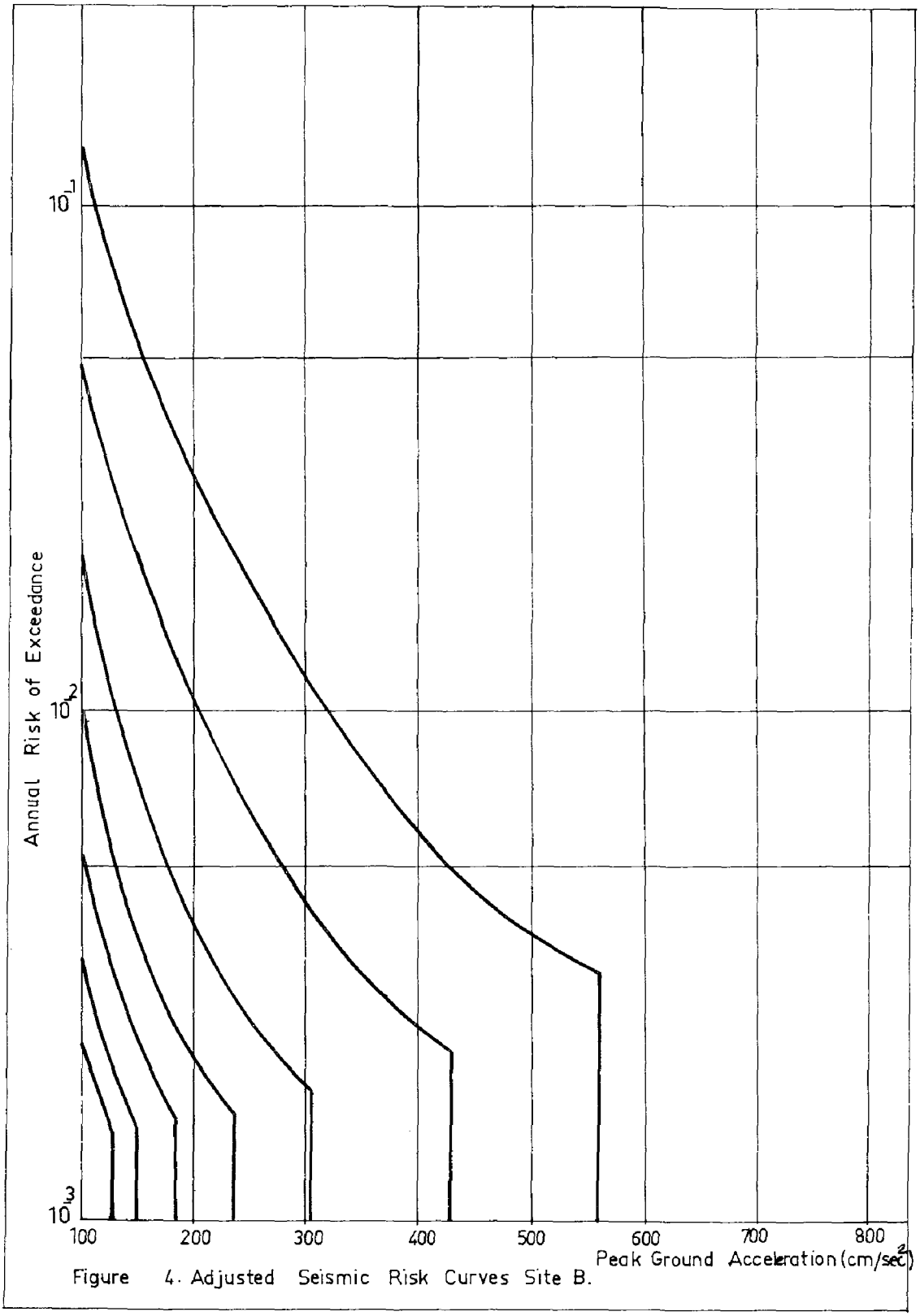

Figure 4. Adjusted Seismic Risk Curves Site B.

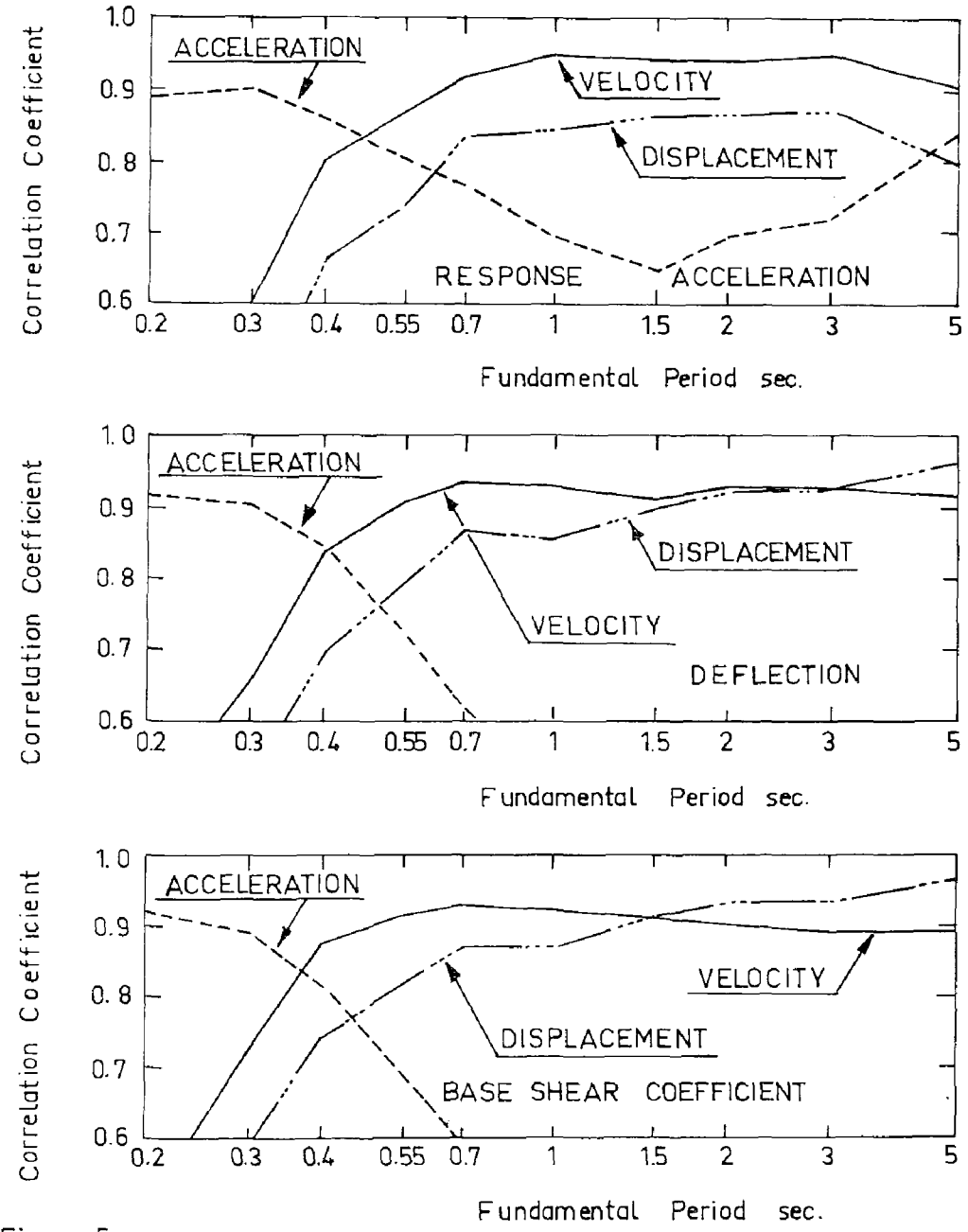

Figure 5.

VARIATION OF CORRELATION COEFFICIENT BETWEEN GROUND MOTION AMPLITUDE AND RESPONSE OF STRUCTURE AGAINST fundamental PERIOD OF STRUCTURE. (From 10)

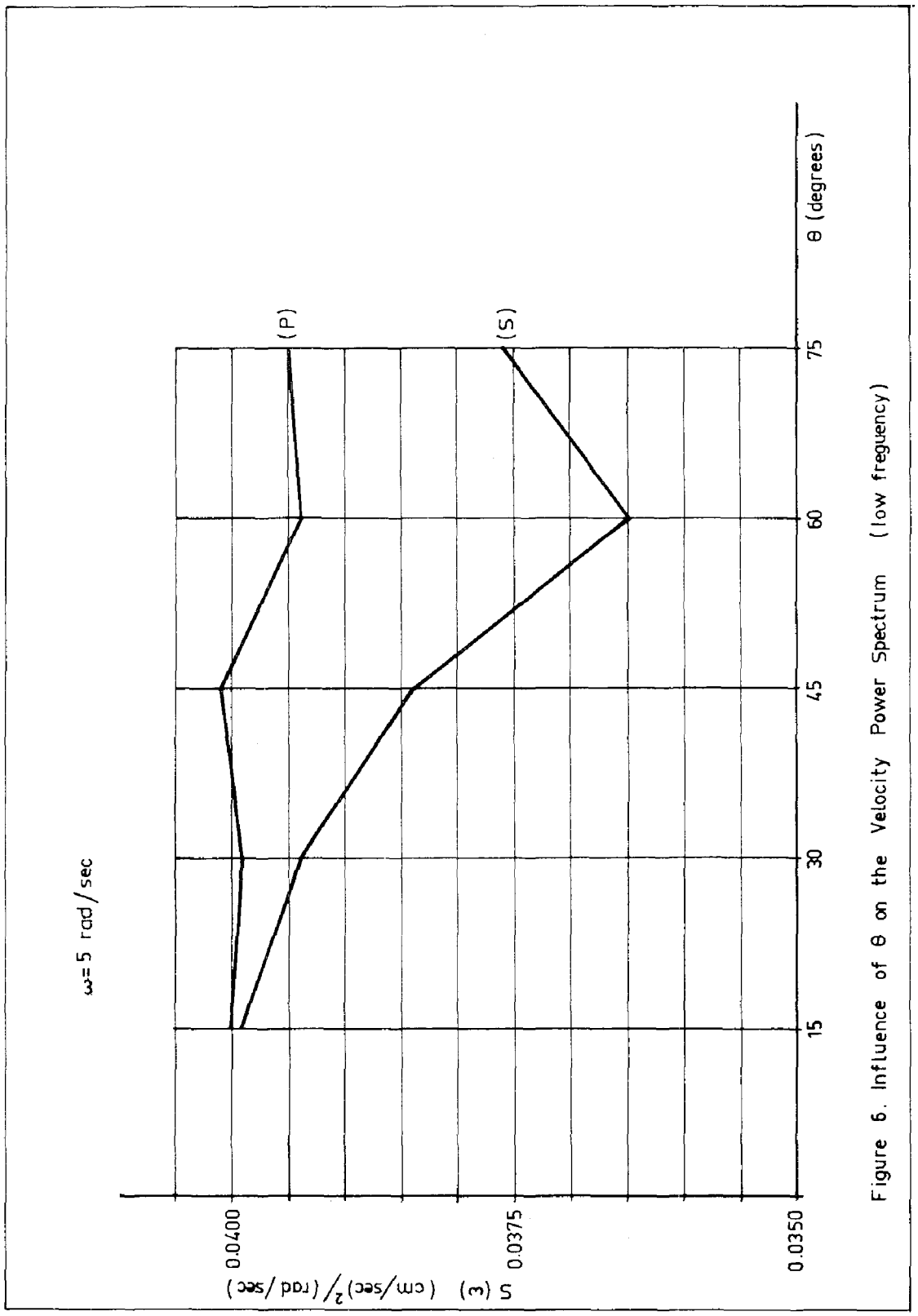

Figure 6. Influence of θ on the Velocity Power Spectrum (low freguency)

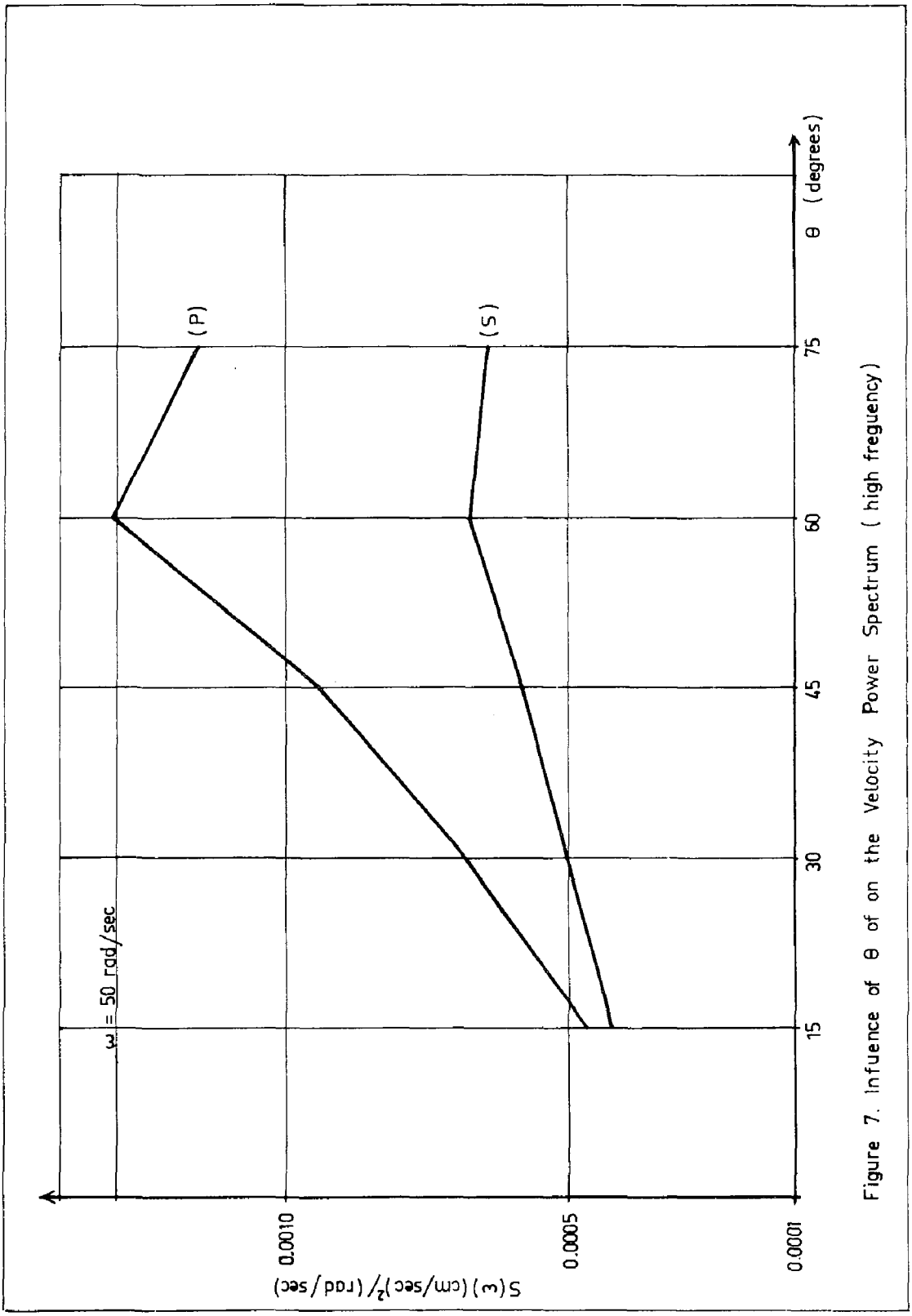

Figure 7. Influence of θ of on the Velocity Power Spectrum (high freguency)

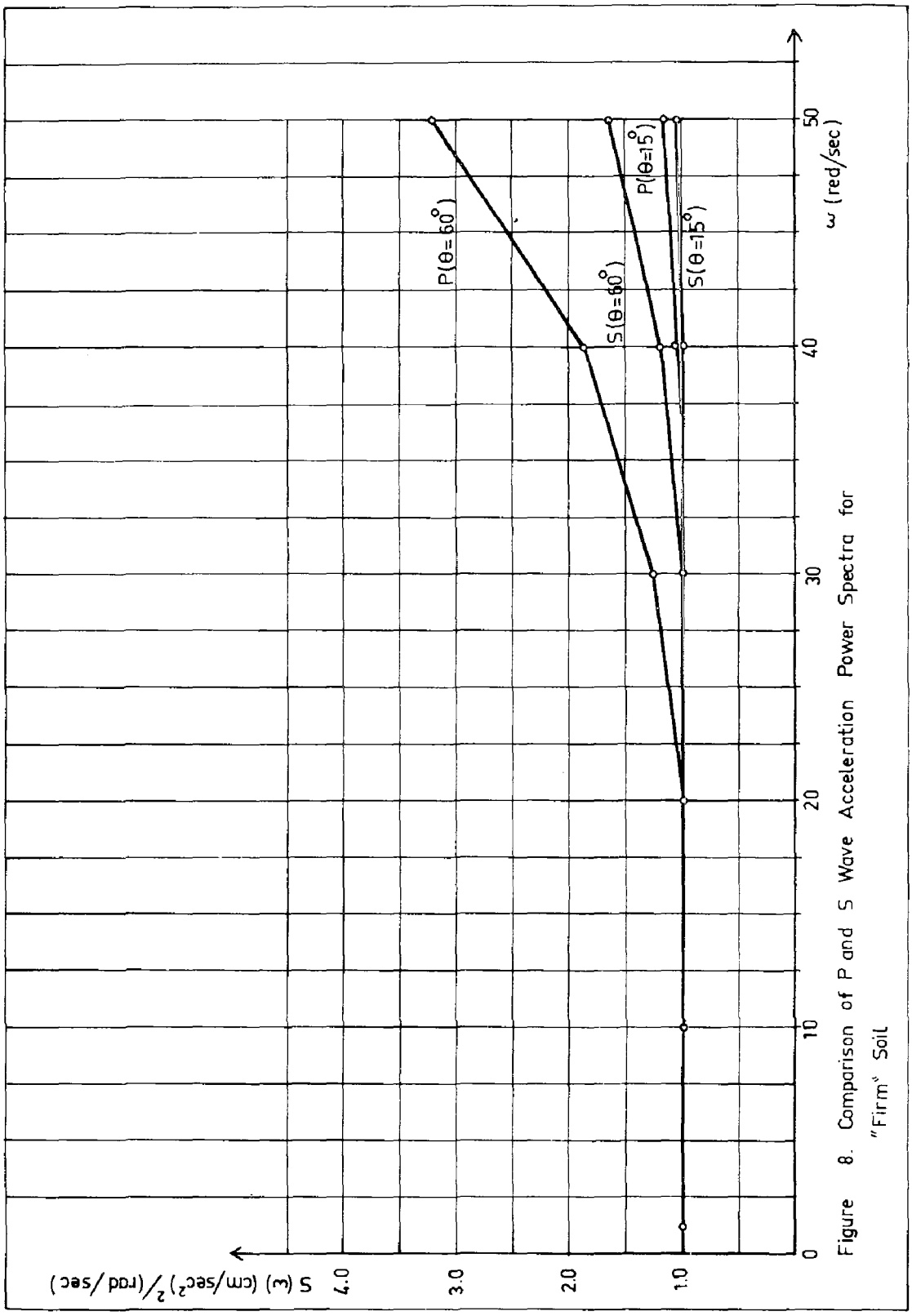

Figure 8. Comparison of P and S Wave Acceleration Power Spectra for "Firm" Soil

INTERNATIONAL SYMPOSIUM ON
EARTHQUAKE STRUCTURAL ENGINEERING
St. Louis, Missouri, USA, August, 1976

SAFETY OF SEISMIC PROTECTIVE SYSTEMS WITH RESERVE ELEMENTS

by I.M.EISENBERG,

Sc.D., Head, Laboratory of Structural Earthquake Resistance Central Research Institute of Building Structures (TsNIISK Kutsherenko) Moscow, USSR.

I. SUMMARY

Some results of the approximate analysis of safety of the earthquake protective systems with reserve disengaging elements are presented. Systems with one and several reserve elements are considered. The overshoot random vibration theory is used for analysis. A wide-band random vibration approximation - a white noise prosses-is assumed as a mathematical model of earthquake ground motion. A numerical example is given. It is shown that the failure probability of reserve elements structures is considerably lower, and the safety is much higher comparing with such characteristics of structures without reserve elements.

II. INTRODUCTION

During the recent earthquakes buildings with a "soft" lower storey displayed a poor behaviour. A variety of examples on collapsing columns of the lower storey during the earthquakes in Ashkhabad (1948), Agadir (1960), Skopje (1963) is given in the book by S.V.Polyakov /17/. The failure of the columns of the lower staircase floor in Olive View Hospital as a result of the San Fernando earthquake (1971) is described by Bertero and Collins /1/. While the upper floors in these buildings had little damage as compared to other buildings, the failure of the lower floor columns was so significant that it threatened with the collapse of the entire building. These facts yielded scepticism on the part of many specialists as to the use of buildings with a "soft" lower storey which in former times were viewed as a method of seismic isolation. Bertero and Collins /1/ even suggest that the use of such structures, unless substantiated by the non-elastic state dynamic design, be prohibited in the code.

It can be supposed that the observed failure of the flexible floor columns was caused by different effects.

We shall mention three of them which seem to be most significant.

Effect A. Sometimes the so called "soft" stories were, in fact, rather "weak", than "soft" not strong enough. For example, according to the design depicted by Bertero and Collins in their report /1/ the fundamental vibration period of the staircase's amounts 0,25 sec. and 0,5 sec. But these periods exactly correspond to the maximum accelerations at the earthquakes in California, in San Fernando (G. Housner and others /12/), in particular.

Effect B. In some regions earthquakes are caused by the activity originating in different sources which are on different distances of the site. The predominant periods of earthquake motion are known to be dependent on the distance from the epicentre and on the magnitude of the earthquake (Shebalin /21/, Triffunac and Udwadia /22/, and others). If the epicentre is situated close to the site, the accelerations predominant in the earthquake spectrum, correspond to higher frequences. In the case of such earthquakes buildings with "soft" lower storey - if it really is flexible - can display a good behaviour. It is but natural that being flexible, the lower storey columns should not be too weak.

But at the same site earthquakes from far away epicentres can occur, and those of great magnitudes. In this case the maximum accelerations can correspond to lower frequences part of spectrum. The quantity of the earthquake response of flexible structures can be quite great, greater than that of rigid structures. This can cause the failure of the lower storey columns.

Effect C. In the usual frame buildings there are different "non-bearing" constructive members (partitions, the filling of the frame, staircase walls). Being not in most cases designed for earthquake loads they, nevertheless, often help the buildings to resist the earthquake. S.V.Polyakov /17/, refers to the cases when the presence of the filling or of the partitions in the parts of the lower storey protected the adjacent columns against damages. When there are the so-called "non-bearing" elements, a kind of two earthquake guard"defence lines" are formed. The importance of the second"defence line", as a means of the earthquake protection has lately been paid much attention on the part of many specialists. This consideration was emphasized, for instance, by Prof. G.Berg (the University of Michigan, USA) in his report at the UNESCO EE Seminar in Bulgaria (Varna, 1975).

The "soft" lower storey is often intentionally designed to be free of partitions, filling in, etc. Consequently it has only one "defence line".

It seems that in each particular case the poor behaviour of the flexible lower floors was caused either by one of the effects (those mentioned above or some other), or by a certain combination of them. The effects B and C can take place not only in buildings with flexible lower floors, but also in other buildings, mentioned below. In the last years a research programme was carried out at the CNIISK, on the basis of which effective adaptive systems with disengaging reserve elements for earthquake protection were proposed /3-8/. The application of these systems either eliminates or essentially smoothes out the unfavourable influence the aforementioned factors of the type of the effects B and C can have on the earthquake resistance of buildings. The reserve elements are designed as additional elements of the structure, e.g. which are supposed to be able to disengage, partly or completely, from the performance of the load carrying system of the construction during earthquake. After the reserve elements are disengaged the construction, possessing now different dynamic characteristics as compared to those original, can accept independently the total permanent vertical load and a certain part of the earthquake load. These reserve elements can be placed, for example, on special panels between the lower storey columns, being attached either to the girders of the frame or to the foundation beams, etc (Fig. 1a). The reserve elements however, should not necessarily be employed in buildings with "soft" lower storey. These elements can be represented, for instance, by crowning rigid beams or shear walls in buildings with vertical shear walls (Fig. 1b) and by other structures /5, 7/. The disengaging reserve elements are quite simple and not expensive. They do not require the use of any devices, special or unusual for building construction. They are easily restored in case of disengagement during an earthquake. Buildings provided with the earhquake protective systems with reserve elements either have already been built in some seismically dangerous regions of the USSR /7/ or are under design - for others. Similar, in essence, structures of systems with special reserve elements or with changing dynamic properties were proposed in the recent years in other countries, too /11, 13, 15/. The earthquake behaviour of buildings with reserve elements bears a relation to the aforementioned effects B and C. The adaptive properties of a trasforming earthquake protective system with reserve elements (RES) under the conditions of possible earthquakes of different types and with different spectra (e.g. in terms of the"effect B") are analyzed, for example, in /4/. The problems were also studied /5,8/ concerning the case when the changing of the dynamic parameters is caused by the accumula-

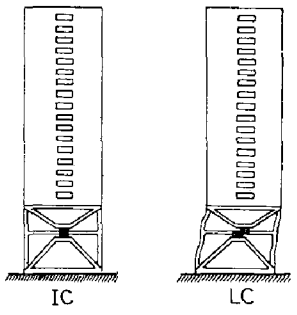

Fig. 1a

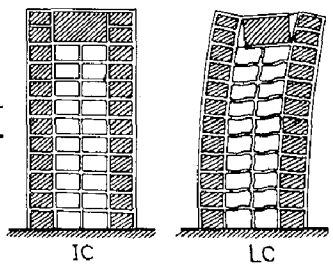

Fig. 1b

tion of cracks and other local damages, but not by the disengagement of special reserve elements. In connection with this various models of systems with degrading stiffness, (ideal elastic plastic, R.Clough and Johnston /2/, exponential /5,8/) were considered.

The positive role of the transformation of the dynamic parameters consists in the elimination or smoothing out of the unfavourable influence of the "effect B". It takes place owing to the system's adaptation (self-adjustment) to one or another possible spectrum of the earthquake action. This positive feature of systems with reserve elements displays it self primarily when the earthquake ground motion is predicted as a class of narrow-band processes.

The other property of RES is related just to reservation, to additional "defence lines" creation, it is related to the mentioned "effect C". In the present paper namely this aspect is analysed.

As it is mentioned in a number of publications /16, 20/ at some sites earthquake motions possessing a relatively wide-band spectrum can happen parallel with narrow-band one's. In the present paper an ultimate case of a wide-band process is employed for an approximated analysis, e.g. the model of the earthquake motion is represented by a random process of a white noise type.

III. SAFETY OF A SYSTEM WITH ONE RESERVE ELEMENT

Let us consider a simple mathematical model of a structure with one reserve element (Fig. 2). It is assumed that after the first exceeding of the level x_r of horizontal displacements the reserve element disengages and the sistem's dynamic structure immediately transforms. The system at the initial state (IC) and at the limit state (LC), e.g. before and after the reserve element is disengaged, is assumed linear and elastic.

For a complete failure of the system the probability of exceeding a certain level x_n of the limit system's horizontal displacements is taken.

The probability of the system's complete failure for the design service period of the construction can be determined according to the total probability formula /6/.

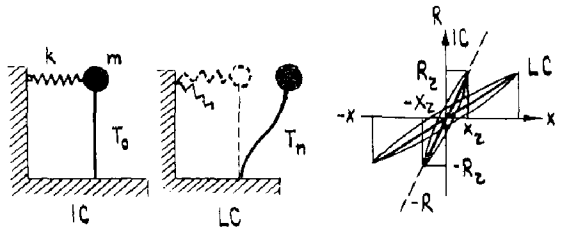

Fig. 2

$$P = \sum_{j}^{m} P(\Phi_j) \cdot P_j \qquad (1)$$

where $P(\Phi_j)$ - probability of the events of the j-variety of the earthquake actions out m possible (predicted) in the time T_p;
$P_j = P\{(x > |x_n|)/\Phi_j\}$ - conventional probability of the complete failure of the structure under the action of Φ_j.

Taking into consideration the fact that the complete failure can occur when the limit level / x_n / is exceeded that is only after the reserve element is disengaged, P_j can be expressed as a product

$$P_j = P_{rj} \cdot P_{nj} \qquad (2)$$

where $P_{rj} = P\{(x > |x_r|)/\Phi_j\}$ - probability of the system's transition from IC to LC;
$P_{nj} = P\{(x > |x_n|)/\Phi_j\}$ - conventional probability of the system's failure at LC (provided the event of the transition from IC to LC has happened).

The quantity $G = 1 - P$ will be the system's safety characteristic (guarantee against failure).

The probability of level - exceeding can be determined on the basis of the random processes overshoot theory.

If high response levels are considered with the probabilities of the level exceeding being small, the response amplitudes may be assumed non-correlated. The probability of exceeding the level of the earthquake response can therefore be considered governed by Poisson's law.

Based on Poisson's distribution and the given expression (2), the formula for the conventional probability of the system's complete failure can be written as the probability of at least one level / x_n / passage

$$P_j = (1 - e^{-n_{x_r,j}}) \cdot (1 - e^{-n_{x_n,j}}) \qquad (3)$$

where $n_{x_r,j}$ and $n_{x_n,j}$ - the average number of level passages for the levels x_r and x_n respectively, under the action of Φ_j. Further on the index j at n_{x_r}, n_{x_n} and λ_k will be omitted for shortening. The autocorrelation function of the earthquake response $x(t)$ can be written as

$$K_x(\tau) = \sigma_x^2 e^{-\alpha|\tau|}(\cos \bar{\omega}\tau + \frac{\alpha}{\bar{\omega}} \sin \bar{\omega}|\tau|) \qquad (4)$$

In this case

$$n_x = t_{ef} \frac{\sqrt{\sigma_x^2 (\alpha^2 + \bar{\omega}^2)}}{\pi \sigma_x} e^{-x^2/2\sigma_x^2} \qquad (5)$$

where t_{ef} - the effective time of the process Φ_j ; σ_x^2 - variance $x(t)$; α and $\bar{\omega}$ are defined respectively by damping and the natural frequency of the system.

For usual structures $\alpha \ll \bar{\omega}$ this simplifying the formula (4)

$$n_x = \frac{2 t_{ef}}{T} e^{-x^2/2\sigma_x^2} \qquad (5)$$

where T - the period of the system's natural vibration. The values for the variance σ_x^2 can be obtained on the basis of solving the problem of the dynamic response at IC (for n_{x_r}) and LC (for n_{x_n}) when under the earthquake motion of $\Phi(t_{ef})$ and $\Phi(t_{ef} - t_r)$ respectively, with due regard for transition processes.

A peculiarity of the system with reserve elements consists in the fact that the probability of failure P depends on the time of transition t_r of IC to LC ($0 \leq t_r \leq t_{ef}$).

The increase of t_r brings about the decrease of the probability of failure at LC, since the effective time $t_{ef} - t_r$ of the performance of LC decreases. The function $P_j(t_r) = P_0(t_r) \cdot P_n(t_{ef} - t_r)$ has its maximum between 0 and t_{ef}. This maximum is taken as the upper estimate of the probability P_j of the failure of the system with reserve elements $\xi_0 = x_r/\sigma_{x_r}$ and $\xi_n = x_n/\sigma_{x_n}$ are taken to be non-dimentional variables which characterise the ratio connecting the level of response which corresponds respectively, to the system's transformation and complete failure - and the standard deviation of IC and LC response. By substituting various values for ξ_0 and ξ_n in (5) and the values obtained for n_{x_r} and n_{x_n} in (3), appropriate conventional probabilities of failures P_{rj} and P_{nj} can be found, and the total probabilities of failure obtained from (1). Assuming ξ_0 and ξ_n to be governing parameters of the system, the problem of optimizing the system's parameters can be considered.

IV. SAFETY OF AN EARTHQUAKE PROTECTION SYSTEM WITH n RESERVE ELEMENTS ("DEATH PROCESS")

Let us suppose that the reserve elements are disengaging one by one in a consecutive order. This assumption is permissible on the condition that $n \leq 1/P_0$, where n - the number of reserve elements, P_0 - the probability of at least one level / x_r / passage.

The initial condition of the system is designated here by H_0 . With the output process crossing the level /x_r/

one out n -reserve elements disengages, the system transforming into the condition H_1 .

In other words the system can enter the finite number of conditions which corresponds to the member of the disengaging reserve elements. $H_1, H_2, \dots, H_n$ are the symbols for these conditions. The condition H_n corresponds to LC, it can be called "absorbing".

Suppose the given sequence of the system's transition to different states can be described as ordinary and free of consequencies, e.g. it represents Poisson's process.

Then the change of the system's states can be depicted as Markov random process with finite set of conditions.

To analyse the safety of the systems a mathematical model should be used known as a simple "death process" /4/. Fig. 3 gives a graph of the system's possible conditions. The probabilities $P_0(t), P_1(t), \dots, P_n(t)$ are used to characterize the system's position at the moment t at the states $H_0, H_1, H_2, \dots, H_n$, respectively.

The intensities of the transition $\lambda_0, \lambda_1, \lambda_2, \dots, \lambda_n$ at wide band effects of a white noise type are constants. In this case the analysis of the system's safety comes to solving differential equations with constant coefficients for the given initial parameters.

According to Fig. 3 the following set of differential equations can be written

$$P_k'(t) = \lambda_{k-1} P_{k-1}(t) - \lambda_k P_k(t) \qquad (6)$$

where $0 \le k \le n$, $\lambda_{-1} = \lambda_n = 0$

The system (6) is solved for the following initial conditions

$$P_0(0) = 1 , \quad P_k(0) = 0 . \qquad 1 \le k \le n$$

With the intermediate calculations omitted the solution can be expressed as

$$P_k(S) = \frac{\lambda_1 \lambda_2 \dots \lambda_{k-1} \lambda_k}{(S+\lambda_0)(S+\lambda_1)\dots(S+\lambda_{k-1})(S+\lambda_k)} \qquad (7)$$

where $P_K(S)$ - representation of the function $P_k(t)$ transform. Applying Laplacian inverse transform theorem to the formula (7) gives the probabilities $P_0(t), P_1(t), P_2(t), \dots, P_{n-1}(t)$. The probability of the transition of the system with reserve elements to LC can be written as

$$P_n(t) = 1 - \sum_{k=0}^{n-1} P_K(t) \qquad (8)$$

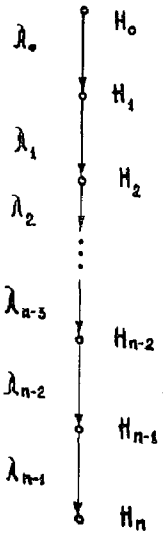

Fig. 3

or

$$P_r(t) = P_n(t) = 1 - \prod_{k=0}^{n-1} \lambda_k \sum_{i=0}^{n-1} \frac{e^{-\lambda_i t_{ef}}}{\lambda_i \prod_{\substack{e=0 \\ e \neq i}} (\lambda_e - \lambda_i)} \qquad (9)$$

The intensities of the transitions $\lambda_0, \lambda_1, \lambda_2, \ldots, \lambda_{n-1}$ can be obtained by the formula

$$\lambda_k = \frac{2}{T_k} e^{-x^2_{r,k}/2\sigma^2_{x_{r,k}}} \qquad (10)$$

If the level x_r is assumed a random variable having a normal distribution, the following expression can be given

$$\lambda_k = \frac{2\sigma_{x_{r,k}}}{T_k \sqrt{\sigma^2_{x_{r,k}} + \sigma^2_{x_r}}} \cdot \exp\left[-\frac{\bar{x}^2_{r,k}}{2(\sigma^2_{x_{r,k}} - \sigma^2_{x_r})}\right] \qquad (11)$$

where $T_k = \frac{2\pi}{\omega_k}$ - the period of the natural vibration of the system at the k-th conditions;

$\sigma^2_{x_{r,k}}$ - the variance of the output process of the at the K-th conditions, transitional processes taking into account;

$\bar{x}_r$ - the mean value of the random variable x_r;

$\sigma^2_{x_r}$ - the variance of the variable x_r.

By using the values P_{rj}, calculated by the formula (9), and P_{nj}, obtained as the probability of at least one crossing of the level / x_n / under the action of $\Phi_j(t_{ef} - t_r)$ the conventional complete failure probability for the system with n reserve elements is determined.

V. NUMERICAL EXAMPLE

Let us study numerically the probability of failure and safety of a given structure. A simplest mathematical model with a single reserve element will be considered.

The earthquake ground motion is represented by a model in the form of a section of stationary Gaussian white noise. The effective duration of the process is taken to be t_{ef} = = 10 sec. The period of the natural vibration of the structure at the limit condition, e.g. after the disengagement of RE, amounts T_n = 2.0 sec. The period of the vibration at the IC T_0 = 0.4 sec. At first the probability of failure P_r of systems with reserve elements (RES) under a given action of the given type will be found. For comparison let us find the probability of failure P_{nr} of a system without reserve elements, possessing the same dynamic parameters as those of RES.

In this example the symbols are used as follows. ξ_0 and ξ_n - the system's relative response to earthquakes at the IC and LC, respectively, e.g., in fact, the steady response of the systems with the periods T_0 and T_n, however, allowing for the time t_r when RE is disengaged;

ξ_{nr} - the relative response of the system without reserve elements allowing for the total time of the earthquake movement, in this particular case t_{ef} = 10 sec;

P_{nr} - the probability of failure of the system without reserve elements for the time t_{ef} = 10 sec.

P_0 and P_n - respectively, the probabilities of the system's transition from IC to LC and the probability of the limit system's failure provided the transformation has happened.

$P_r = P_0 \cdot P_n$ - the probability of failure of RES, P_0, is determined for the time interval t_r, and P_n - for the interval $t_{ef} - t_r$. Assuming t_r can have any value within the interval $0 \leq t_r \leq t_{ef}$ the values P_0, P_n and P_r will be calculated for different values of t_r within the given interval. The probability P_0 naturally increases with the increase of t_r while the probability P_n being dependent on the conventional probability of exceeding $|\alpha_r|$ in the interval $t_{ef} - t_r$, decreases with the increase of t_r. Hence the probability of failure P_r of the entire system has its maximum in the interval t_{ef} = = 10 sec. It is shown in the graphs (Fig. 4). The reserve element can be disengaged at any moment of the time interval $0 \leq t_r \leq$ 10 sec. Strictly speaking, it is possible to obtain the probabilistic distribution of the time moment $t = t_r$ and to utilize the most probable estimates. (It can be asserted a priory that the most probable time will be close to t_{ef}, since we deal with small probabilities P_0). But we shall act differently. To determine the probability of failure we shall take into account the value of t_r to which the maximum of P_r corresponds, that is for comparative estimates it is assumed that $P_r = \max P(t_r)$. Since not all the aspects of the RES's behaviour are studied sufficiently, the aforementioned is the way of allowing for the lack of information by overestimating the corresponding effects comformably to this particular case, by applying the conservative estimates of failure and the underestimates of safety as compared to the systems without reserve elements.

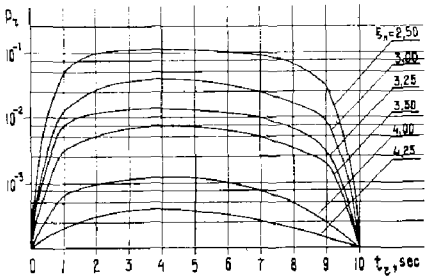

Fig. 4

Thus by comparing RES to the structures without reserve elements we obtain estimates, least favourably characterizing the safety of RES as compared to the non-reserved systems.

The results of the failure probability analysis are given in Table 1a,b,c. The formulae (2) - (5) were used for calculations.

Tables 1a and IIa contain the values of $P_r = \max P(t_r)$ at six different ξ_0 and ξ_n -values.

Table 1a

Maximum values of conventional failure probability for systems with one reserve element: $P_r \cdot 10^3$

ξ_0 / ξ_n	2,50	3,00	3,25	3,50	4,00	4,25
2,50	136,9	37,4	17,3	6,9	1,05	0,39
3,00	47,4	14,0	5,9	2,4	0,36	0,13
3,25	23,2	6,87	2,9	1,18	0,176	0,065
3,50	10,56	3,1	1,32	0,54	0,08	0,024
4,00	1,5	0,39	0,18	0,07	0,011	0,004
4,25	0,49	0,29	0,062	0,025	0,004	0,001

Table 1b

Maximum values of conventional failure probability for systems without reserve elements

ξ_{nr}		2,50	3,00	3,25	3,50	4,00	4,25
$P_{nr} \cdot 10^3$	T_{nr}=0,4sec	889,2	423,1	221,2	104,2	14,9	6,0
	T_{nr}=2,0sec	356,0	104,20	44,88	19,8	3,0	1,1

Table 1c

Correlation between the maximum values for the conventional probabilities of failure of systems without reserve elements and those of systems with one reserve element at $\xi_0 = \xi_n$

ξ		2,50	3,00	3,25	3,50	4,00	4,25
P_{nr}/P_r	T_{nr}=0,4sec	6,5	30,2	76	193	1360	6000
	T_{nr}=2,0sec	2,6	7,4	15,2	36,7	272	1100

Similar characteristics of the probability P_{nr} of the non-reserved system's failures are given in Tables1b and 1c.

Table 1c contains ratios P_{nr}/P_r of the failure probabilities of the systems without reserve elements to the failure probability of the system with one reserve element conformably to the particular case of $\xi_0 = \xi_n$.

The same relation-ship is described by the graphs (Fig. 5). The solid lines refer to the system with $T_0 = 0{,}4$ sec., the dotted lines corresponding to the system with $T_0 = 1{,}0$ sec.

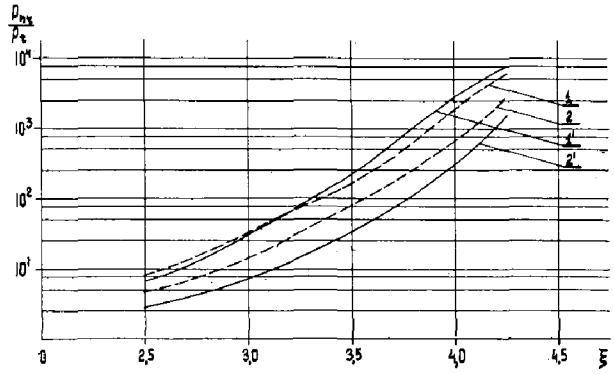

Fig. 5

As it can be seen from Table 1 and the graph (Fig. 5) the failure probability of the systems with reserve elements is considerably higher than that of the non-reserved systems.It needs to be mentioned that the higher is the level of the design relative earthquake response ξ, the higher is the ratio p_{nr}/p_r and, consequently, the effectiveness of using the reserve elements. To put it in other words the use of the reserve elements is most effective in terms of creating highly safe structures.

Now let us calculate the safety $G = 1 - p$ of the structure with a reserve element and assess approximately the design earthquake load relative values conformably to constructions with reserve elements and without them. The value of p can be obtained by the formula (1). In this formula p is represented as the sum that corresponds to the family of actions which are predicted for the design term of service T_p of the construction. If to consider that the successive earthquake intensities (as in seismic scale, for example, MM or MSK) are two times different, it is possible to take into account, for the approximate analysis, only one term of the sum (1), which corresponds to the maximum - in - intensity member φ_j. The analysis testifies as to the error while determining the safety not exceeding 5 - 7 %.

Suppose the design term of service of the structure is 50 years, the mean value of the time between two eartquakes of the design maximum intensity being 1000 years. Then proceeding from the assumption that an earthquake represents Poisson's process, the probability can be obtained

$$P(\varphi_j) = 0{,}05 \text{ and } G = 1 - 0{,}05\, p_j,$$

the values for p_j are taken from Table 1.

Table IIa containsthe calculated values of the safety (guarantee against failure) of the RES. For the systems without reserve elements the values for G at $T_{nr} = 0{,}4$ sec. and $T_{nr} = 2$ sec. are given in Table IIb.

Table IIa

Values for the safety G_r (guarantee against failure) of systems with one reserve element:

ξ_0 \ ξ_n	2,50	3,00	3,25	3,50	4,00	4,25
2,50	0,99315	0,99813	0,99914	0,99966	0,99995	0,99998
3,00	0,99736	0,99930	0,99971	0,99988	0,99998	0,99999
3,25	0,99884	0,99966	0,99986	0,99994	0,99999	0,99999
3,50	0,99947	0,99985	0,99993	0,99997	0,99999	0,99999
4,00	0,99993	0,99998	0,99999	0,99999	0,99999	0,99999
4,25	0,99998	0,99999	0,99999	0,99999	0,99999	0,99999

Table IIb

Values for the safety G_{nr} (guarantee against failure) of systems without reserve elements:

ξ		2,50	3,00	3,25	3,50	4,00	4,25
G_{nr}	T_{nr}=0,4 sec	0,95554	0,97885	0,98894	0,99479	0,99926	0,99969
	T_{nr}=2sec	0,98210	0,99479	0,00776	0,99901	0,99985	0,99995

The comparison of Tables IIa and IIb shows that with the equal values of ξ_r and ξ_{nr} the safety of RES is considerably higher than that of the systems without reservation.

In certain publications /10/ the values for the safety of building, ship and some other constructions are given within the following limits $G = 0,999 - 0,9999$. Let us now compare the values of ξ_r and ξ_{nr} at the equal values of safety.

Table IIc contain the values of ξ_r (at $\xi_0 = \xi_n$) and of ξ_{nr} calculated at two values of G: $G = 0,999$ and $G = 0,9999$; Table IIc gives ξ_r for RES with $T_0 = 0,4$ sec; $T_n = 2,0$ sec.

Now let us estimate approximately the values of the design seismic load for the constructions with one reserve element and without reserve elements.

Table IIc

Values of relative seismic response ξ for systems with one reserve element and without the reserve elements at a given safety ($\xi_r = \xi_0 = \xi_n$)

G		0,999	0,9999
ξ_r		2,95	3,40
ξ_{nr}	= 0,4 sec.	3,98	4,45
	= 2 sec.	3,50	7,20
ξ_r / ξ_{nr}	= 0,4 sec.	0,74	0,76
	= 2 sec.	0,83	0,81

The values of ξ describe the earthquake response design level (in the units of standard response deviation) at the given safety. These values are indirect characteristics of the required load-carrying capacity of the construction. The ratio ξ_r/ξ_{nr} can therefore be viewed as the characteristic of the ratio of the design earthquake loads for RES and for systems without reserve elements. These ratios at the equal values of safety are given in the bottom lines of Table IIc. If, for instance, to compare two systems with a 2 second period of natural vibrations, one of which is with a reserve element while, the other is without it, - it will appear that at the relative values of the earthquake load for the system with a reserve element are 0,83 of the load for the system without reserve elements when $G = 0,999$, being 0,81 of this load when $G = 0,9999$.

Thus, owing to the use of the systems of reserve elements the design earthquake load can be reduced at least by 20 - 30 % with no drop in safety.

In the second line from the bottom of Table IIc the values of the ratios ξ_r/ξ_{nr} are given for the case, when the natural vibration periods of the systems without reservation are $T_{nr} = 0,4$ sec. As we can see, the relative design seismic load for RES is reduced in these cases still more - by 36 %.

At correct designing this reduction of design loads yields considerable reduction of the structure's cost.

In the examples given the case of RES with one reserve element was considered by way of simplification. Based on the "death process", the analysis of the systems with

reserve elements shows their effectiveness to be higher than that of RES with one reserve element.

VI. CONCLUSIONS

1. An approximate analysis of the probability of failure and of safety of simple structures with disengaging elements is carried out. Systems with one and many reserve elements are considered. The problem is solved on the basis of the overshoot theory (of the probability of at least one level-crossing). In the case of systems with n reserve elements the "death process" is employed. A numerical example of calculations is given, in which particular systems with a reserve element and without reserve elements are compared.

2. The analysis results as presented in the given paper and in some other publications mentioned in the references reveal the role of the reserve elements as the effective means of structural earthquake protection. There are at least two positive effects in connection with the behaviour of systems with reserve elements subjected to earthquakes.

One of the effects is relevant to the situation when the structural design has to take into account several types of narrow-band soil movements, different in their dominant periods. The disengagement of the reserve elements in this case favours the adaptation of the structure to high frequency earthquake movements owing to the transformation of dynamic characteristics, e.g. rigidity and natural frequencies.

The structural seismic response in this case can be several times lower than that in the case of the construction with constant dynamic characteristics.

The other effect concerns the reservation proper, that is the formation of so to say, additional "defence lines". This effect works not only in the case of narrow-band processes, but also in the case of wide-band earthquake processes when the frequencies of the system at IC and LC belong to the effective section of the earthquake movement spectrum, as was substantiated by the numerical example, the design seismic load acting on the systems with reserve elements can be by 20 - 30% lower than that in the case of the similar systems, but without the reserve elements.

Therefore the transforming systems with reserve elements are effective at any kind of earthquake motion as well as when taking into account wind loads besides of earthquake action.

Qualitatively the efficiency characteristics of the transforming systems with reserve elements are different depending on the predicted types of actions.

Designing such systems permits to achieve one of the two aims, or a certain combination of the them:

1) structural safety increase at a given cost of earthquake protection;
2) cost reduction of earthquake protection at the safety equal to the safety of usual systems.

3. The numerical analysis has shown a particular efficiency of the use of the reserve elements in terms of creating highly safe systems, the design of which allows for high intensity design actions, e.g. nuclear reactors and other specifically important structures.

4. Based on the research on the optimum design of the transforming earthquake protective systems with reserve elements which is being carried on at the CNIISK, projects have been elaborated in the USSR and a number of structures with disengaging elements built.

The systems of reserve disengaging elements may be different in terms of their constructive embodiment. In the case of buildings with frame "soft" lower storey or several storeys, the reserve elements can be attached to special panels or other rigid supports which can at the same time, restrict the horizontal displacements after the reserve elements are disengaged.

The function of the reserve elements can be performed by reinforced beams, diaphragms and other elements which connect the vertical diaphragms and the vertical reinforced cores in high buildings and constructive elements, such as partitions, crosspieces, etc.

VII. BIBLIOGRAPHY

1. Bertero V.V., Collins R.G. Investigation of the failure of the Olive View stairtowers during the San Fernando earthquake and their implications on seismic design. Report NO EERC 73-26, University of California, Berkley, California, 1973.

2. Clough R.W., Johnston S.B., "Effect of stiffness Degradation on Earthquake Ductility Requirements", Proc. of Japan Earthquake Engineering Symposium, Tokyo, 1966.

3. Eisenberg J.M. "Seismic Effects on Mechanical systems with Changing Parameters" (in Russian), Trudy Instituta Phyziki Zemli, AN SSSR, Moscow, No 10, 1965.

4. Eisenberg J.M. "Adaptive Systems with Disengaging Ties and their Calculation when the Seismological Information is incomplete" (in Russian). Journal "Stroitelnaya mechanica i raschot sooruzhenij", Moscow, 1972.

5. Eisenberg J.M. "Disengaging reserve elements structures

for earthquake regions" (in Russian) "Stroyizdat" Publishers, Moscow, 1976.

6. Eisenberg J.M. Safety of reserve elements structures under seismic loads. (in Russian) CINIS, Gosstroy USSR, Sbornic "Seismostoikoe stroitelstvo", No 1, Moscow, 1976.

7. Eisenberg J.M., Nazin V.V., Polyakov S.V. Multistorey earthquake-proof Building. (in Russian) Patent No 2062984/29-33. 1975.

8. Eisenberg J.M., "Earthquake Response Analysis of Nonlinear Degrading Stiffness Systems" (in Russian). Trudy CNIISC "Seismostojkost zdanij i ingenernyh sooruzhenij", Strojizdat, Moscow, 1969.

9. Eisenberg J.M., Abakarov A.D. Reliability of reserve elements earthquake resistance systems using "death prosses" procedure (in Russian). Sbornic "Seismostoikoye stroitelstvo", CINIS, Gosstroy USSR, Moscow, No 3, 1976.

10. Ekimov V.V. Stochastic methods in structural mechanics of a chip (in Russian) Publishers "Sudostroyenie", Leningrad, 1966.

11. Fintel M., Khan F.R. Shock-absorbing soft storey concept for multistorey earthquake structure. Proc. ASCE, May, 1969.

12. Housner G.W. a.a. Engineering features of the San Fernando Earthquake of February, 9, 1971. Report No EERL 71-02, Pasadena, California, 1971.

13. Ikonomou A.S. The earthquake Guarding System. Technica chronica, 41, No 10, 1972.

14. Kozlov B.A., Ushakov I.A. Text-book on reliability analysis. (in Russian). Publishers "Sovetskoe Radio", Moscow, 1975.

15. Muto K. Earthquake-proof design gives rise to first Japanese skyscrapers. Civil Engineering, No 3, 1971.

16. Newmark N.M., Rosenblueth E. Fundamentals of Earthquake Engineering. Prentice-Hall, Inc. Englewood Cliffs, N.I., 1971.

17. Polyakov S.V. Design of earthquake resistant structures. "Mir" Publishers, Moscow, 1974.

18. Polyakov S.V., Eisenberg I.M., Papelishvili V.V., "Earthquake-proof multi-storey building" (in Russian). Patent No 371335, "Bulleten izobretenij", No 12, 1973.

19. Racicot R.L., Moses F.A. First-Passage Approximation in Random Vibration. Journ. of Appl. Mech., Trans ASME. vol. 38, Series E, No 1, 1971.

20. Rascon O.A., Cornell C.A. Strong motion earthquake Simulation. Cambridge. Massachusetts, MIT, 1968.

21. Shebalin N.V. "Remarks on the predominant Periods Spectra and Strong Earthquake Focus" (in Russian), Sbornik "Seismicheskie issledovania dlya stroitelstva", Izdatelstvo "Nauka", Moscow, 1971.

22. Trifunac M.D., Udwadia F.E., "Variations of Strong Earthquake Ground Shaking in the Los Angeles Area", Bulletin of the Seismological Society of America, vol. 64, No 5, 1429-1454, 1974.

INTERNATIONAL SYMPOSIUM ON
EARTHQUAKE STRUCTURAL ENGINEERING
St. Louis, Missouri, USA, August, 1976

SEISMIC DYNAMIC PARAMETRIC STUDY ON FINITE ELEMENT MODEL OF NUCLEAR POWER PLANT FACILITY

J S TERASZKIEWICZ
Senior Engineer
Ebasco Services, Inc.
New York, USA

Summary

This paper presents the steps taken to establish a finite element model for the seismic dynamic analysis of a nuclear power plant facility embedded 72 ft (25 m.) in a sandstone site. A parametric study was undertaken to establish the extent of the rock to be included in the model, as well as the distribution and number of dynamic degrees of freedom.

The responses of the structures in several models of different widths and depths of rock were compared, and it was found that only small differences were exhibited when the lateral boundaries were taken 940, 1440 and 1940 ft apart (290, 440 and 590 m, equivalent to about 3W, 4W, and 5½W, where W is the width of the base). When the depth was increased from 370 ft to 570 ft (113 to 175 m), small reductions in the peak responses were obtained. As a result of this study a model with lateral boundaries 1440 ft (440 m) apart, and of a 570 ft (175 m) depth was adopted for the analysis.

Rock models without structures were developed to establish the effect of the distribution of dynamic degrees of freedom, and it was found that in order to reproduce the criterion acceleration time history at grade, a uniform distribution of dynamic degrees of freedom had to be maintained throughout the rock, especially for vertical excitation.

The resulting model, adopted for the analysis, retained 486 uniformly spaced dynamic degrees of freedom and 204 Eigenvectors in order to obtain responses up to the frequency range of 20 - 30 Hz. The responses 595 ft (180 m) from the centerline of the plant showed that the rock-structure interaction effects were still present. This parametric study suggests that the boundary does not necessarily have to be placed outside the interaction region, in order to obtain sufficiently accurate responses for the design of this particular plant.

In all of the above analyses, the normal mode method was used, since it was established that for this particular rock site, the damping ratio and the shear modulus was almost constant in the strain range of interest.

Introduction

Finite element models have been used by several investigators for the seismic analysis of nuclear power plants deeply embedded in soil (Reference 1). One of the problems encountered has been the determination of the size of the model to adequatly represent the practically semi-infinite soil. In order to perform the analysis economically, a sufficient amount of soil should be modeled to obtain reasonably accurate responses for the design of the plant. If the boundaries are placed too close to the plant, the responses of the structures are adversly affected by the distortions of the ground motions, and by the lack of material to absorb energy by damping. An acceptable check on the adequacy of the size of the model is to compute whether the soil-structure interaction effects have disappeared near the boundary. Seed et al. (Ref. 1) found that for clay or sandy sites, where the material damping has been relatively high, free-field motions are developed within a distance of 400-500 ft (120 - 150m.) from the plant. However, for a site where the material damping is low, such as the present site, the interaction effects are felt a considerable distance away, suggesting that the model would be too large for current computer programs.

In order to overcome this difficulty a parametric study was undertaken to determine the variation in plant response with increasing size of model.

Since the models inherently contain a large number of dynamic degrees of freedom (1 horizontal and 1 vertical at each grid-point) a condensation has to be performed in order to reduce the problem to a size that can be managed by the current computer programs. In the present investigation rock models without structures were developed in order to determine the effects of condensation.

Description of the Plant

The plant is situated in a region subjected to earthquakes of Intensity VII on the modified Mercali Intensity Scale of 1931. The maximum horizontal ground acceleration is established to be 32 percent of gravity by Seismological investigations. The rock, which exists from grade to a depth of about 5000 ft (1500m.) is a fresh-weathered sandstone with a shear-wave velocity in the range of 3000 to 4300 feet per second, (900 to 1300m/s) and a material damping of 2 to 2.4 percent of critical as determined by laboratory and in-situ testing. The plant studied and reported on herein is embedded 72 feet (25m.) in the rock; a common mat 340 feet (100m.) square in plan and 12 feet (3.7m.) thick supports the internal structure, the containment vessel, the Shield Building, and the Reactor Auxiliary/Fuel Handling Building (Figure 1). The buildings are arranged concentrically about the internal structure, with the Reactor Auxiliary Building on the outside. The ratio of the embedment to the least-base dimension is 21 percent, and to the height of the outer shear walls is 41 percent. This design has been dictated by the unusually large sliding forces and overturning moment produced by the postulated safe Shut-down Earthquake.

Finite Element Models

The models developed for the parametric study are summarized in Table 1. A typical finite element model is shown in Figure 2. The buildings are modeled as beam elements, and the rock as two-dimensional plain-strain elements. Since the models are two-dimensional, three models are used to seismically analyze the structures: Two horizontal, following East/West and North/South directions, and one vertical model. In this particular study, there were two nuclear power plants, side by side, in the East/West direction, therefore, only half of the site was modeled, a center line being established half-way between the models. In a typical model there are about 1,200 grid points, 68 elements, and about 1100 membrane elements representing the sandstone. For accuracy the height of the membrane element is made equal to 1/8 of the wave length of a vertically propagating shear wave, having a frequency of 33 Hz (Ref. 1). In the present project, frequencies up to 20 - 33 Hz were of interest for the design of the structures and equipment. For accuracy, the width of the membrane element is kept equal to not more than five times the height of the element.

Width Study

In the first three models studied, the side boundaries were established 300, 550, and 800 feet (90, 170 and 240m.) away from the external walls. The depth was kept constant at 500 feet (150m) below the mat, and 75 to 99 dynamic degrees of freedom were used (Table 1).

The criterion earthquake time history was an artificial time history developed to match the criterion response as defined by the U S Nuclear Regulatory Commission in Regulatory Guide 1.60 of October 1973. The criterion earthquake time history was applied at the base of the models.

As can be seen from Figure 3 the responses of the narrowest model were only slightly higher than those of the other two models, which were practically indistinguishable. One can postulate that for this particular sandstone site a model with laterel boundaries 1440 ft (440m.) apart would be adequate.

The responses in Figure 3 were practically constant for frequencies greater than 6 Hz although it was expected that there should be a gradual decrease in acceleration with increasing frequency since the input time history exhibited that trend. On examination of the rock modes, it was found that there were no rock modes at frequencies greater than 6 Hz, thereby producing a filtering effect on the input time-history. It was determined therefore to increase the number of dynamic degrees of freedom to obtain rock modes at least up to the frequency range of 20-30 Hz.

Depth Study

For the Depth Variation Study, the width of the model was kept constant at 1440 feet (440m.), and the depth was varied from 370 to 570 feet (113 to 175m.). In these models the number of dynamic degrees of freedom was increased from 87 to 350 in order to increase the range of responses, and a deconvoluted time history was used at the base of the rock. The criterion

time history was assumed to act at the foundation level, and a wave propagation program was used to obtain the motions at the base level (Reference 2). Figure 4 shows that by increasing the D.D.O.F.'s to 350, the range of responses was increased to the required 33 Hz, and that the shallower model exhibited only slightly higher responses at the mat than the deeper model. It was therefore decided that an even deeper model would not produce any further significant differences, and the 570 ft (175m.) depth was chosen for the final analysis.

Both models exhibited the highest mat responses at about 13 Hz. Further examination of the results showed that the internal structure exhibited accelerations as high as 15 g's, and it was felt that these results were unreasonable. Seed et al. (Reference 1) reported that unrealistic response values can occur because of the specification of impossible control motion at a key location, such as the mat elevation. Therefore, in the models used for the final analysis, the criterion motion was assumed at grade. This is now reflected in the U. S. Nuclear Regulatory Commission's criteria, as defined in the Standard Review Plan, June 1975.

Dynamic Degrees of Freedom

In this study the purpose was to determine whether the number and distribution of dynamic degrees of freedom (D.D.O.F.) in the model with a depth of 570 ft (175m) was reasonable. In that model, in an attempt to utilize the maximum D.D.O.F.'s available in the program to the best extent, a non-uniform distribution had been adopted, with a higher concentration under the structures than further away in the free field. Two rock models, without structures, but with the same distribution of D.D.O.F.'s were used in order to see whether the criterion time-history spectra at grade could be reproduced by the models (Table 1).

As can be seen in Figure 5, the horizontal response spectrum at grade corresponds fairly closely to the criterion spectrum and even more closely to the results of the wave propagation program. The spectrum of the artificial time history was omitted for the sake of clarity because it closely matches that of the wave propagation program. However, for the vertical response spectrum (Figure 6) the match is poor, indicating that the non-uniform distribution of D.D.O.F.'s tends to amplify certain frequencies and attenuate others. An examination of the natural frequencies of the rock model shows that the non-uniform distribution tends to introduce modes of greater participation at certain frequencies, producing the peaks, and elimination of modes at other frequencies, producing valleys. The model with a uniform distribution of D.D.O.F.'s shows that the criterion spectrum was reproduced at grade. It was resolved therefore, to keep the distribution uniform for the final analysis, thereby requiring more than 350 D.D.O.F.'s to be retained in the analysis.

For the final analysis, 486 dynamic degrees of freedom were used for the North/South model, and 405 degrees were used for the East/West model, since it was narrower as a result of the center line between the two units. The results for the horizontal and vertical model are shown in Figures 7, 8, and 9. Far from the plant, at grade, there is fairly good correlation with the criteria response except that the interaction effects

were still present probably due to the low material damping. Spectral amplifications of the order of 2 occur at about 3 Hz, which happens to be the natural frequency of the largest building (Reactor Auxiliary Building). The horizontal North/South and East/West responses are slightly different probably partially due to the structure - structure interaction effects in the East/West model.

In all of the analyses, the normal mode method was used, without iteration for changes in rock properties with strain, since it was established by laboratory and site tests that the shear modulus only changed 10 per cent, and that the damping changed from 1 to 3 per cent in the strain range of .0001 to .01.

Conclusions

For sites where the material damping is extremely low, the normal guidelines for establishing the extent of the site to be included in the model produce models that are too large for current computer programs. It is suggested therefore, that parametric studies be undertaken to establish the sensitivity of the plant responses to the size of the model, in order to build a practicable model. In this study it was found that in adequate models the response at grade far from the plant will match the control motion to the extent that it is unaffected by rock - structure interaction.

This study confirms the findings of Seed et al. (Reference 1) that even at considerable distance away from structures, the motions do not approach the free-field values when the damping ratio is low. It also confirms that unrealistic response values can occur if a broad spectrum is assumed for criteria motions at the mat depth in the free field.

References

1. Seed, H. B., Lysmer, J., Hwang, R.

"Soil Structure Interaction analysis for Seismic Response."
Journal of the Geotechnical Engineering Division, ASCE
May 1975, Volume 101, No. GT-5

2. Schnabel, P. B., Lysmer, J., and Seed, H. B., "Shake: A Computer Program for Earthquake Response Analysis of Horizontally Layered Sites."
Report No. EERC, 72-12 Earthquake Engineering Research Center
University of California, Berkely, California - December 1972

Table 1 Models for Parametric Study

Model	Width of rock (ft) (m.)	Depth of rock (ft) (m.)	Purpose	Applied time-history	D.D.O.F. (*)
1	940 (290)	570 (175)	Width variation	Criterion	75
1	1440 (440)	570 (175)		horizontal	87
3	1940 (590)	570 (175)			99
4	1440 (440)	570 (175)	Depth variation	Deconvoluted (1)	350
5	1440 (440)	370 (113)		horizontal	350
6	720 (220)	570 (175)	Distribution of	Deconvoluted (2) Horizontal (3)	174
7	720 (220)	570 (175)	D.D.O.F.*	Vertical (3)	174
8	390 (120)	570 (175)		Vertical (4)	350
9	1440 (440)	570 (175)	Final models for	Deconvoluted (2) Horizontal N-S	486
10	1230 (380)	570 (175)	Seismic analysis	Horizontal E-W	405
11	1230 (380)	570 (175)	of plant	Vertical	405

* D.D.O.F. = dynamic degrees of freedom
(1) Deconvoluted time-history obtained by assuming criterion T-H at mat
(2) Deconvoluted time-history obtained by assuming criterion T-H at grade
(3) Non-uniform distribution of D.D.O.F.'s
(4) Uniform distribution of D.D.O.F.'s

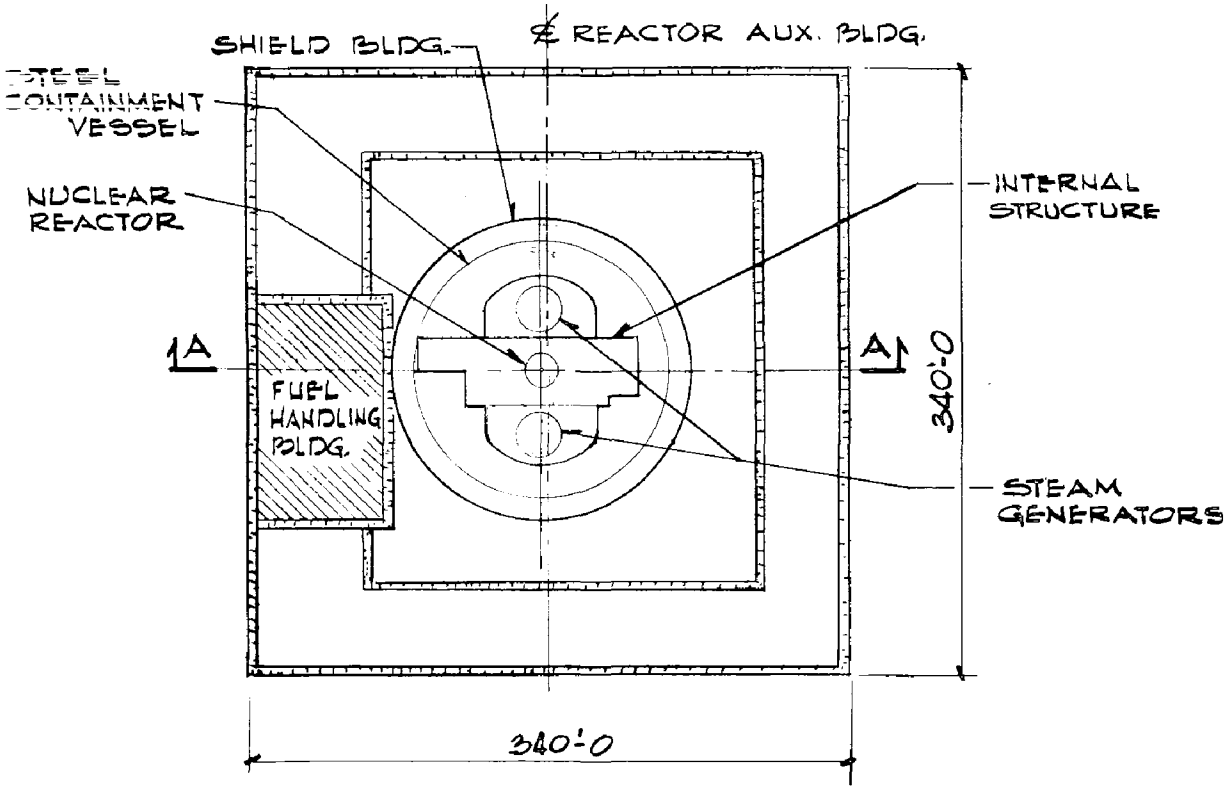

PLAN AT EL 330.00'

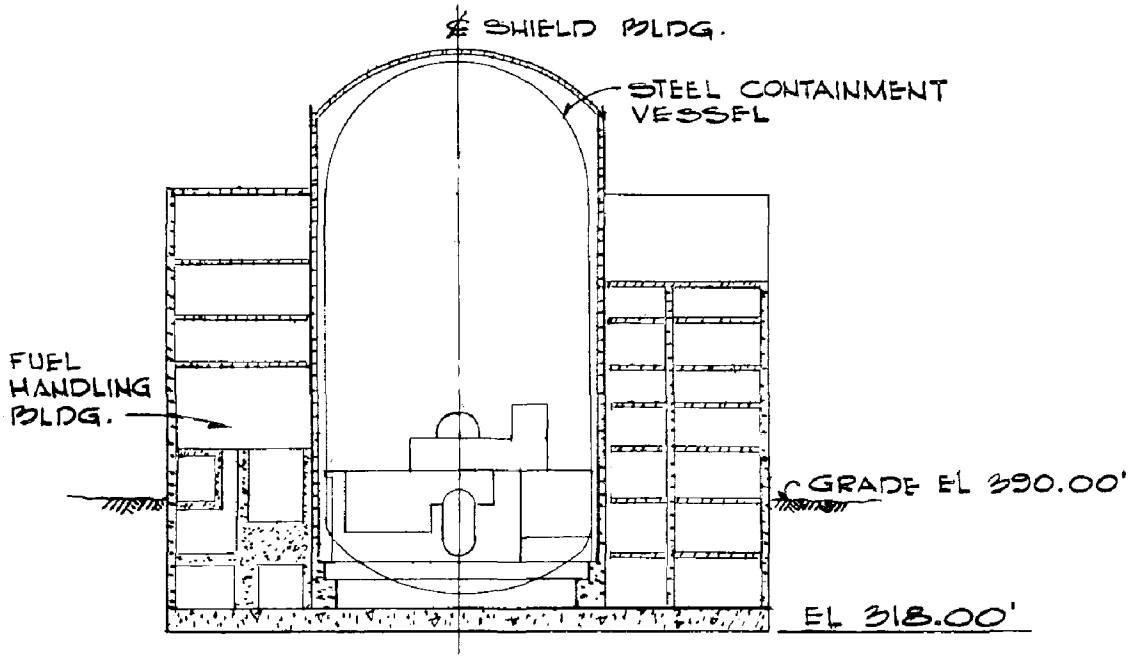

SECT A-A

FIG. 1 - GENERAL ARRANGEMENT OF NUCLEAR POWER PLANT

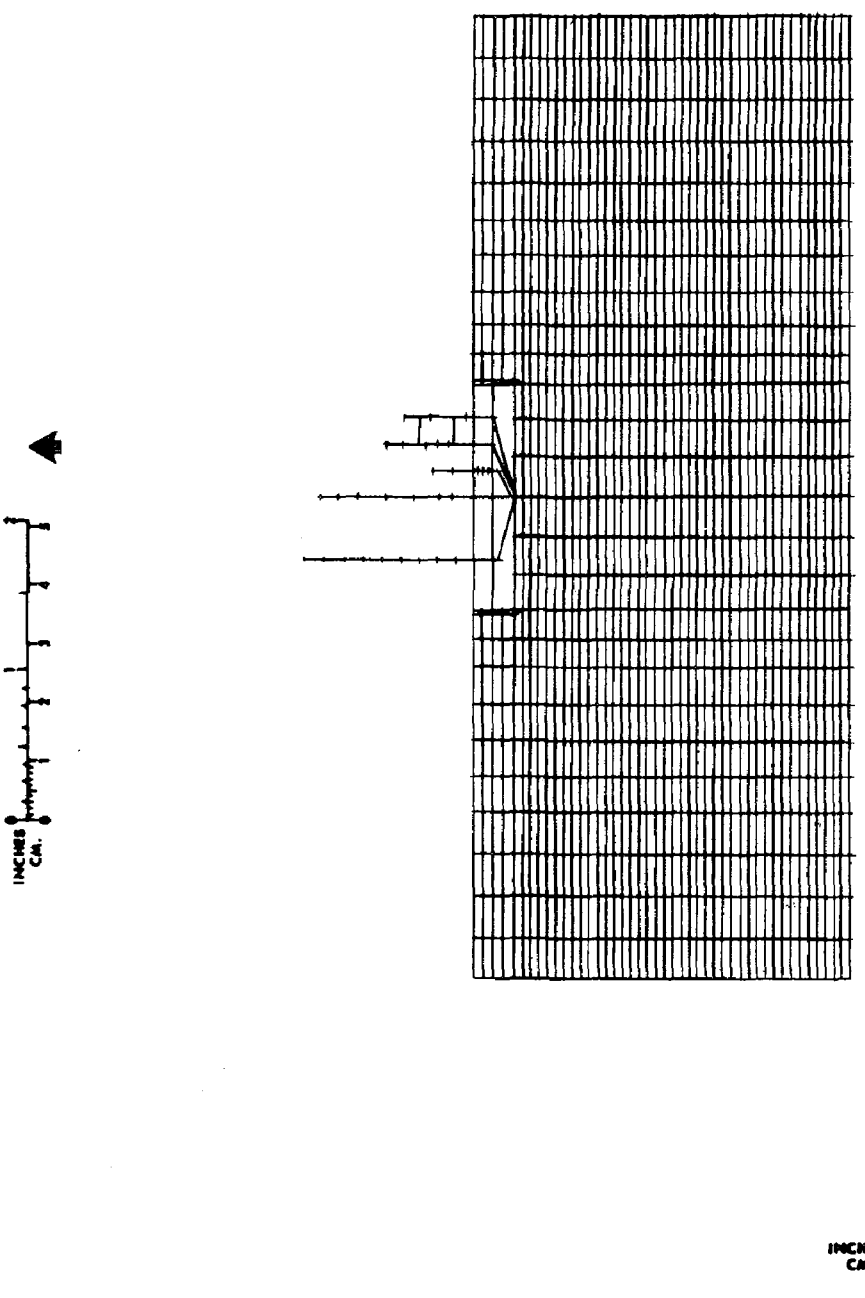

FIG 2 TYPICAL F.E. MODEL

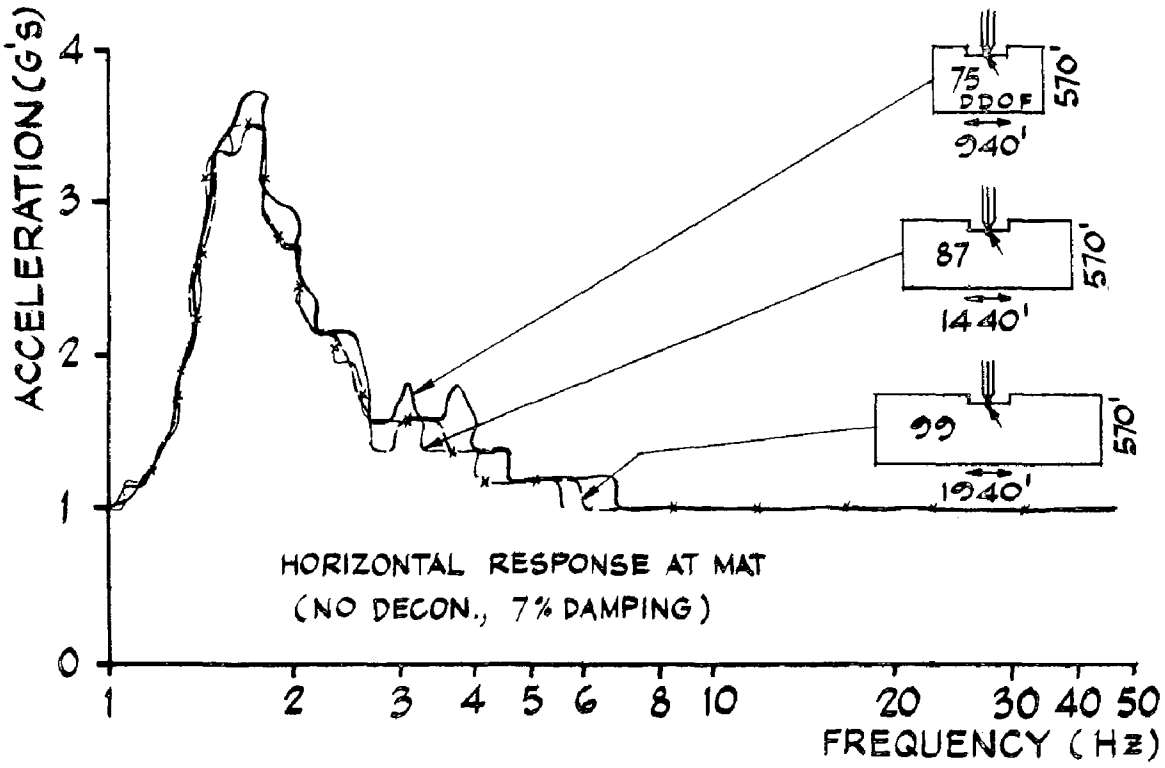

FIG 3 WIDTH VARIATION

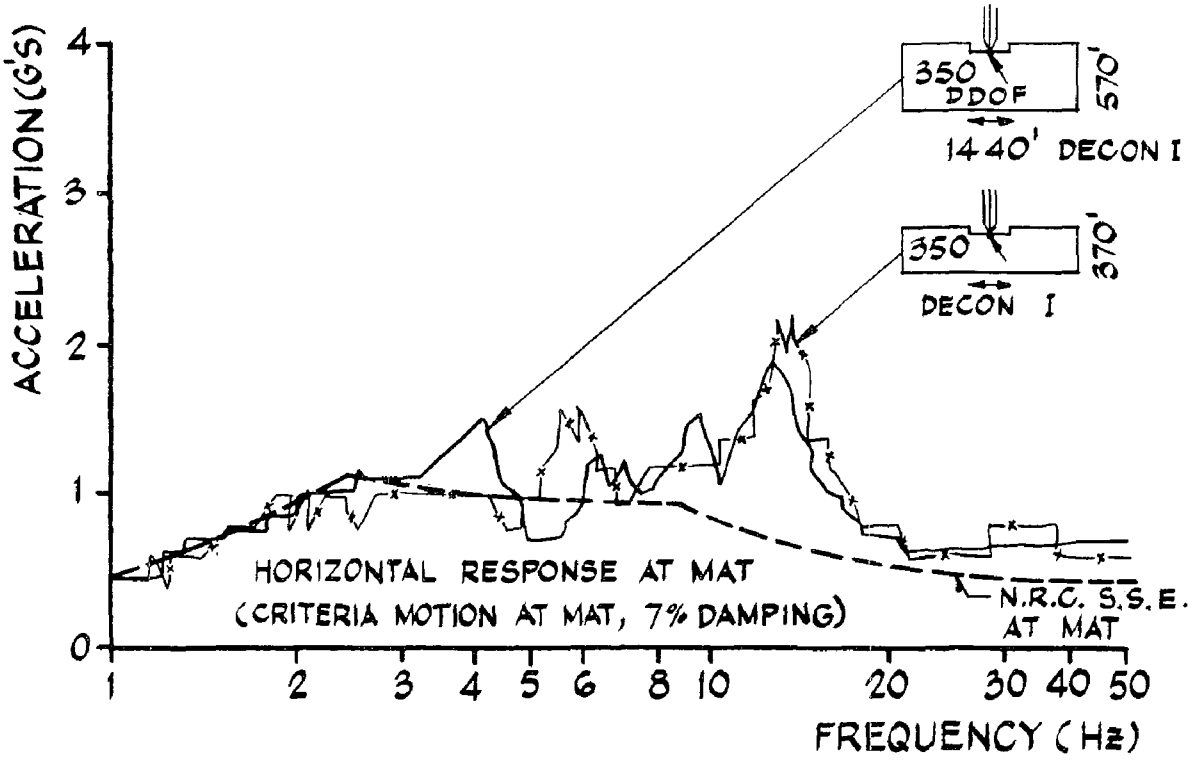

FIG 4 DEPTH VARIATION

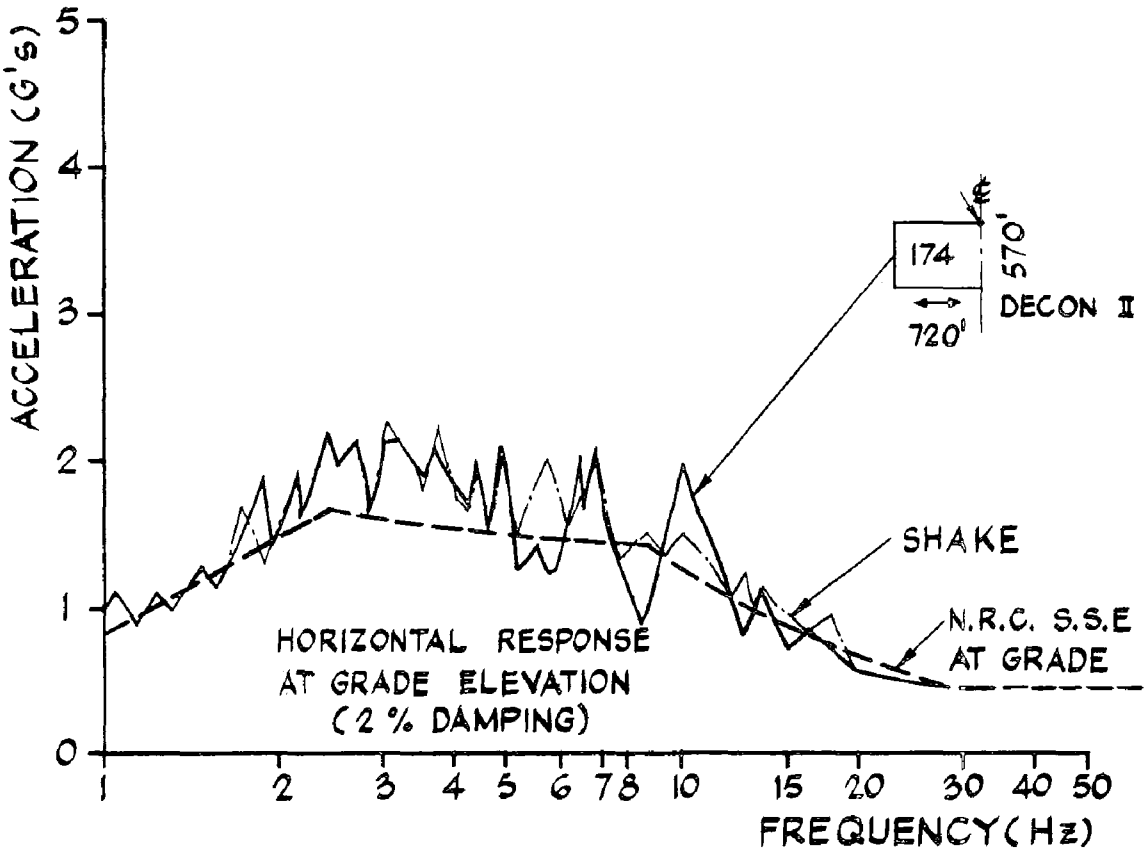

FIG 5 NON-UNIFORM DISTRIBUTION OF DYNAMIC DEGREE OF FREEDOM FOR HORIZONTAL EXCITATION

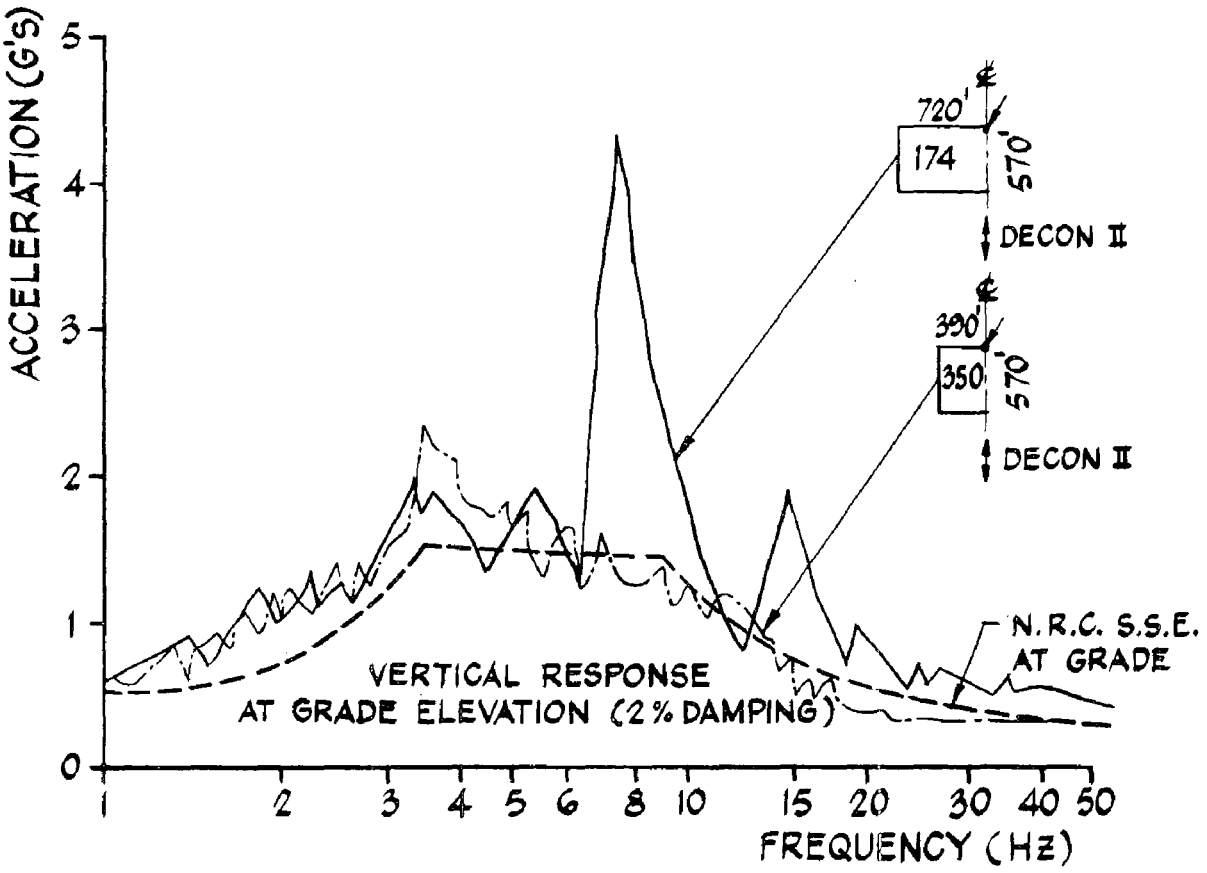

FIG 6 NON-UNIFORM DISTRIBUTION OF D D O F FOR VERTICAL EXCITATION

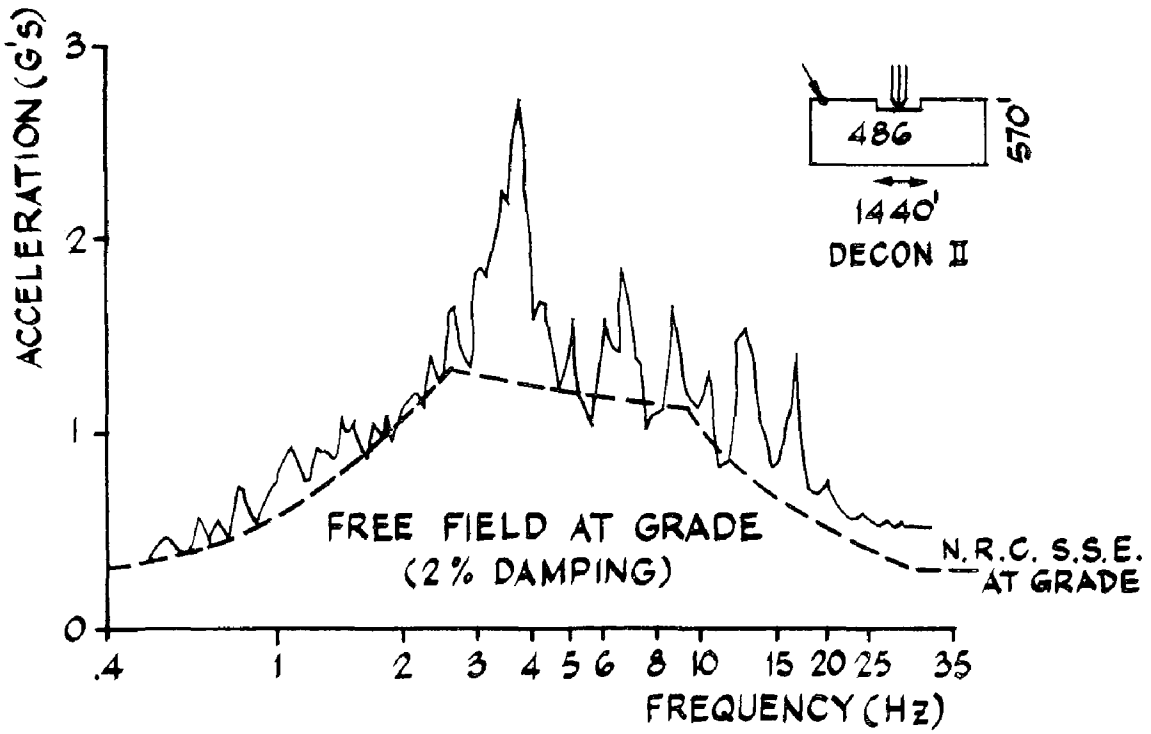

FIG 7 HORIZONTAL N-S RESPONSE FOR UNIFORM DDOF

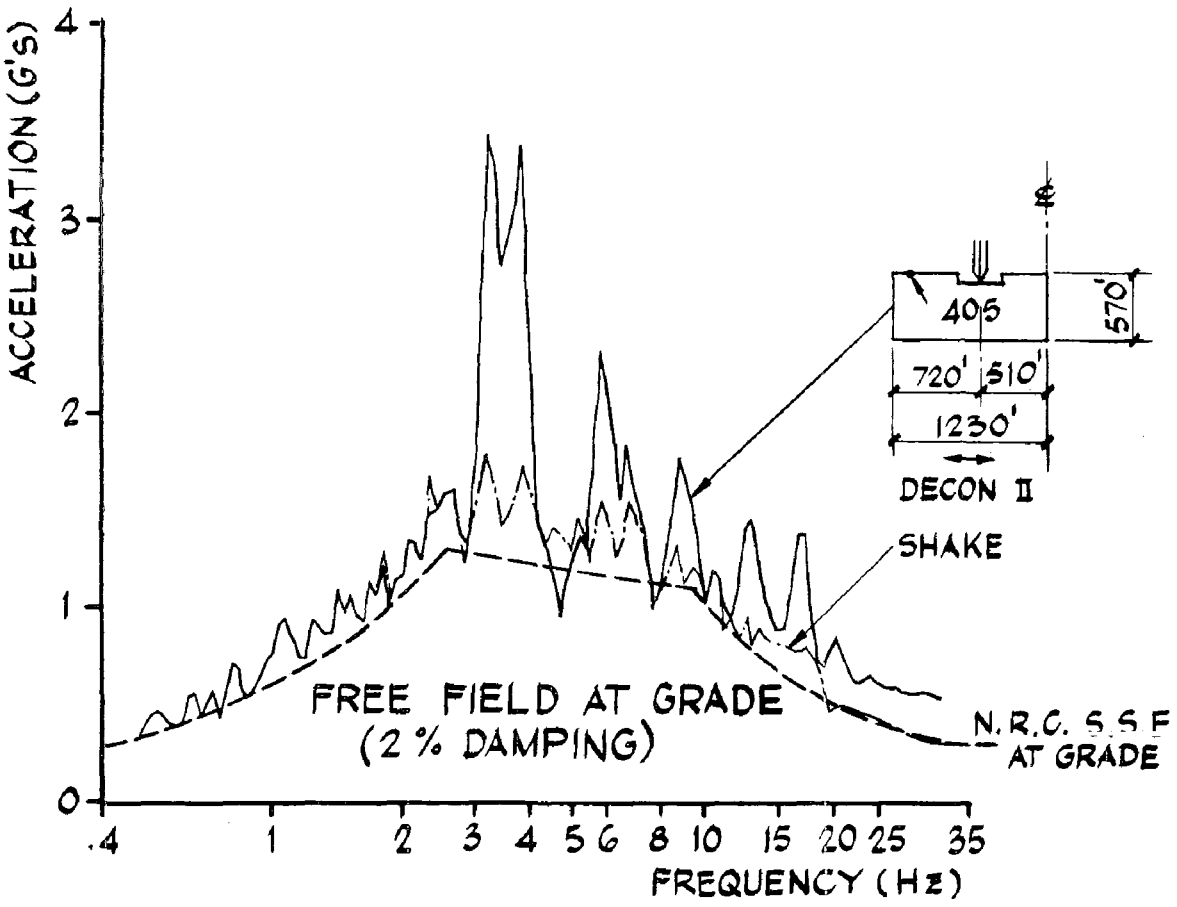

FIG 8 HORIZONTAL E-W RESPONSE FOR UNIFORM D D O F

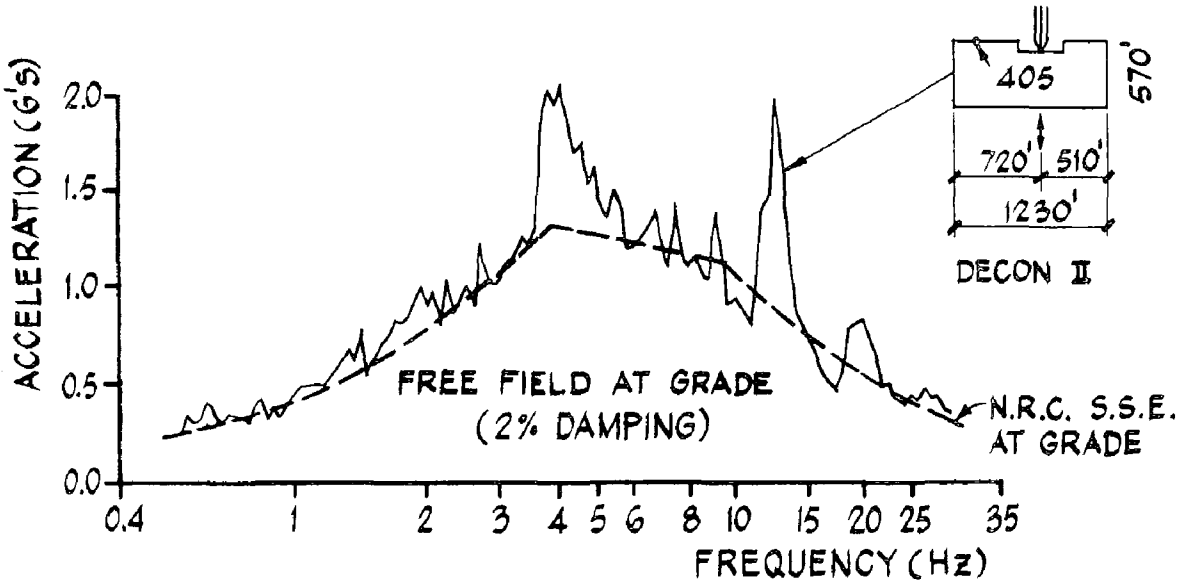

FIG 9 VERTICAL RESPONSE
FOR UNIFORM D D O F

INTERNATIONAL SYMPOSIUM ON
EARTHQUAKE STRUCTURAL ENGINEERING
St. Louis, Missouri, USA, August, 1976

APPROXIMATE RANDOM VIBRATION ANALYSIS OF ELASTOPLASTIC MULTI-DEGREE-OF-FREEDOM STRUCTURES

GEORGE GAZETAS AND ERIK H. VANMARCKE

Department of Civil Engineering

Massachusetts Institute of Technology

Cambridge, Massachusetts, USA

SUMMARY

The paper presents a probabilistic dynamic analysis of the inter-story displacement response to earthquake-like excitation of multistory, elastoplastic, shear structures. The paper consists of two parts. In the first, time-histories of story distortions of a 4-dof structure excited by simulated earthquake motions are presented and the effects of yielding on the apparent mode of vibration of the various stories and on the amount of energy dissipated are shown. In the second part, two (mathematical) models, predicting the expected values of story ductility factors, are presented. The crude, "independent-springs" model gives rough, upper bound solutions, which appear to be too conservative for very stiff structures. The "improved" model combines the elastic random vibration theory of multi-degree-of-freedom structures, the elastoplastic random-vibration theory of simple oscillators, and accounts for the effects that the yielding of a story has on the other stories. The results of the method for these 4-dof structures compare very well with the statistics from 15 simulated motions.

INTRODUCTION

A large number of technical papers dealing with the probabilistic response of inelastic one-degree-of-freedom structures have been published in the last ten years. There does not appear to be any published work attempting to obtain the seismic response of inelastic multi-degree-of-freedom structures by direct random vibration analysis. In several simulation studies reported in the literature (Ruiz and Penzien, 1971, Peyrot, 1972), no attempt is made to develop a mathematical, probabilistic model of the inelastic behavior of the structure. This is not surprising if one considers the large number of factors involved, and hence, the difficulty to modify the already sophisticated mathematical methods used in the study of one-dof structures.

The very large variability in the response stems from the fact that the inelastic activity tends to concentrate in the "weaker" story quite disproportionately; therefore, even if a structure is designed to develop a uniform ductility factor under a certain excitation, it may actually

develop, locally, very large ductility factors when subjected to a different motion.

Several mathematical methods have been extensively used to predict the probability distribution of the response of inelastic simple (1-dof) oscillators, such as perturbation methods (3), equivalent linearization methods (1), equivalent nonlinearization methods (8), "exact" methods such as solving the Fokker-Plank Equation (16) and others. All these methods are quite complicated and it seems extremely difficult to appropriately modify them so that they can predict the response of multi-dof systems as well. Besides, the validity of these methods is limited to the case of small plastic deformations and, therefore, they are not generally applicable.

The scope of this research has been to model the elastoplastic vibration of multi-dof structures by an approximate random-vibration analysis. The research consists of two parts. First, an "empirical" investigation is conducted. Time-histories of story-distortions of a 4-dof shear-type structure, excited by simulated earthquake motions, are studied. The emphasis is on obtaining as much information as possible with regard to the energy dissipated during yielding and the frequency with which each floor vibrates before and after yielding.

Then, an attempt is made to develop a mathematical model accounting, qualitatively and quantitatively, for the above-mentioned observed effects. In fact, two such models are presented in this report. The first is a very crude one, treating each story as being an independent elastoplastic spring, with elastic r.m.s. value, σ, obtained by modal superposition for the m-dof structure. The model is intended to give rough upper bound solutions to the problem. This seems to be the case for the structures examined, although in some cases the predictions were too conservative. An improvement to this model is made by accounting for the effect that the yielding of a story has on the vibration of the others (energy dissipation and change in the mode of vibration). An approximate, intuitive method of combining the yielding activities of the various stories is developed.

TIME-HISTORIES OF STORY DISTORTIONS

Starting from a smooth elastic response spectrum and an assumed total strong motion duration, s, a "compatible" spectral density function (SDF) is computed. Inputing this SDF in the SIMQKE program, fifteen statistically independent acceleration time-histories are computed which are then used as input accelerations to compute the response of the 4-dof structures.

The structural model of all the structures tested was the close coupled or shear model (see Figure 1). Table 1 presents the elastic properties of the three categories of structures used (stiff, flexible, very flexible). The relative drifts (distortions) of each story are studied, considering especially the following quantities: (a) the apparent frequency of vibration, (b) the maximum value of elastoplastic drift, as measured by the ductility factor, μ, and (c) the hysteretic energy dissipated and the change in mode of vibration during yielding.

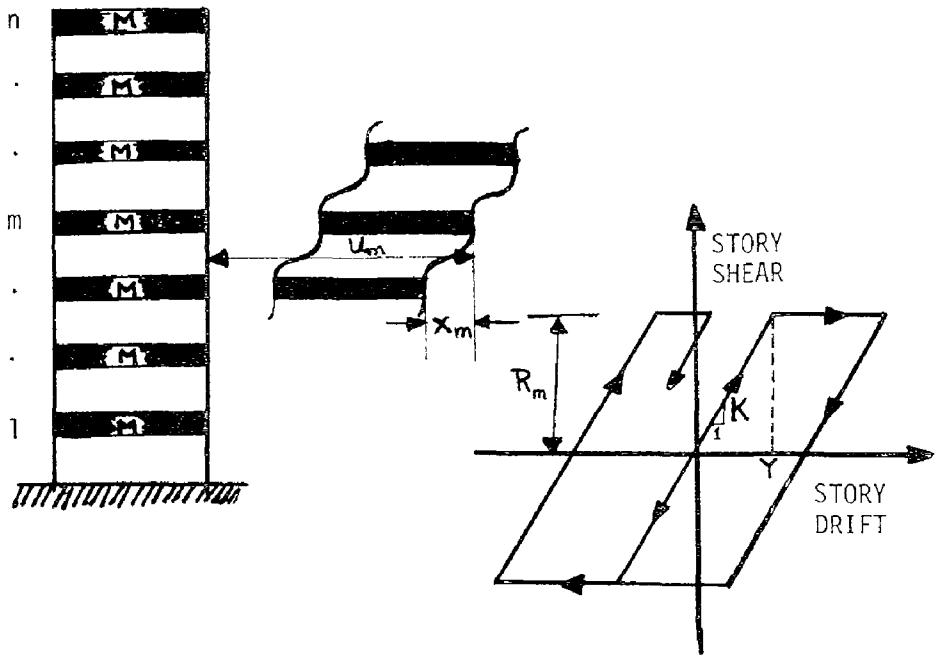

Figure 1 - The Structural Model

STRUCTURE #1 (T_1 = 0.377 sec)		STRUCTURE #2 (T_1 = 1.13 sec)		STRUCTURE #3 (T_1 = 2.26 sec)	
STIFFNESS (ALL STORIES)	MASS (ALL FLOORS)	STIFFNESS (ALL STORIES)	MASS (ALL FLOORS)	STIFFNESS (ALL STORIES)	MASS ALL FLOOR
1152.0	0.5	128.0	0.5	32.0	0.5
MODE	FREQUENCY	MODE	FREQUENCY	MODE	FREQUENCY
1	16.64	1	5.545	1	2.78
2	47.94	2	16.00	2	8.00
3	73.49	3	24.51	3	12.25
4	90.20	4	30.07	4	15.03

Table 1 - Properties of the 3 Structures

(a) Apparent Frequency of Vibration

In the case of linearly elastic stiff structures, when only the fundamental mode is significant, the apparent frequency of vibration corresponds to the mean rate-of-zero-crossings, or the mean rate-of-peaks. When higher modes contribute (for the flexible structures), the mean rate-of-peaks is faster than the mean rate-of-zero-crossings and the apparent frequency for each story is in between the above two rates. This frequency is computed by a weighted superposition of all the modes of vibration of the structure:

$$\Omega_m = \left\{ \sum_{k=1}^{n} p_{km} \, \Omega_k^2 \right\}^{\frac{1}{2}} \qquad \begin{matrix} m = 1,2,\ldots,n \\ \text{(all stories)} \end{matrix} \qquad (1)$$

where the weighting factors p_{km} represent the fraction of total response of the m^{th} story contributed by the k^{th} mode and the apparent modal frequency Ω_k is a superposition of the modal frequency (eigenvalue) and of the frequency content of the input motion.

The comparison of the elastic frequencies computed by (1) with the frequencies measured from the time-histories of the response of the buildings 1 to 3 (Table 2) leads to the conclusion that the elastic formulas compute a frequency which corresponds approximately to an average between the mean rate-of-zero-crossings and the mean rate-of-peak-occurences, and seems to be quite satisfactory for all practical purposes.

Several authors have investigated the effect of yielding on the effective period of vibration (Vanmarcke et al., 1970; Ruiz and Penzien, 1971; Frank, 1975). Combining the information obtained from the time-histories of the story distortions (in this study) with the results reported in previously mentioned papers, a (tentative) curve is constructed, giving the percent reduction in the apparent frequency of vibration as a function of the ductility factor, as is shown in Figure 2. Although the authors feel that more data is required to improve the accuracy of the curve, it seems that the curve is sufficient for practical purposes; it is employed in the analyses reported below.

(b) Distribution of Plastic Response Over the Height of the Structure

At the beginning of the motion, all the stories remain elastic. In order to assess what story will yield first, the ratio of the yield distortion over the r.m.s. value of the associated linear system, $r = Y/\sigma_X$, is a very good index. The smaller the r value of a story, the greater the threat of inelastic action starting first and being larger. This is especially true for cases where the apparent frequencies of vibration are very similar for all stories (stiff structures).

Table 3 portrays and compares the r ratios with the ratios of average elastic response over the r.m.s. value of the associated linear system, m/σ_X, and the average ductility factors, $\bar{\mu}$, for the three structures mentioned previously.

Looking at the elastic response, one can see that while for the stiff structure, the statistical mean of the story drift is proportional to the elastic r.m.s. value, σ_X, the top stories of the two

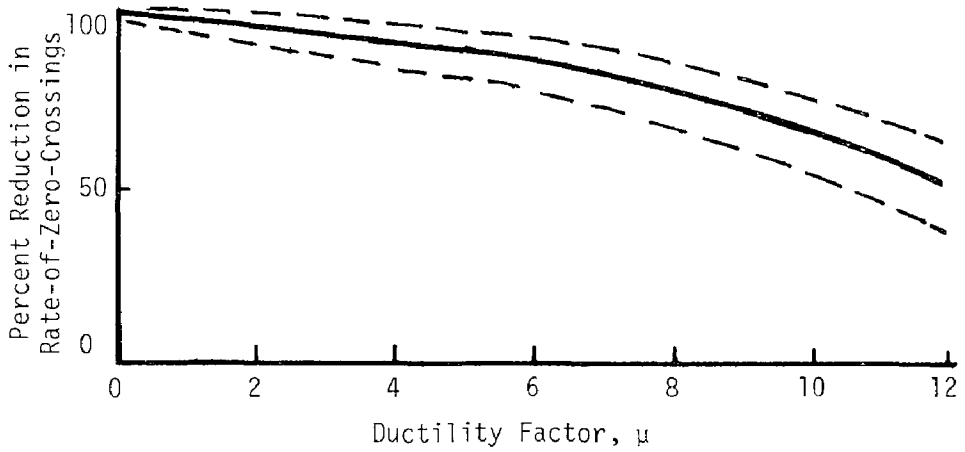

Figure 2 - Reduction in Rate-of-Zero-Crossings due to Yielding

STRUCTURE	FLOOR	COMPUTED	MEASURED (APPROXIMATELY)	
			RATE-OF-ZERO-CROSSING	RATE OF PEAKS
1 (Stiff)	1	16.67	16.7	16.7
	2	16.67	16.7	17.0
	3	17.10	16.8	18.0
	4	18.30	17.0	20.0
2 (Flexible)	1	6.97	6.3	7.2
	2	6.22	6.3	~6.3
	3	7.93	6.8	8.5
	4	11.68	7.6	15.0
3 (Very Flexible)	1	4.58	4.2	4.7
	2	4.47	4.2	4.5
	3	4.88	4.5	5.0
	4	6.27	5.0	7.8

Table 2 - Apparent Frequencies of Vibration - Computed Vs. Measured

TABLE 3

STRUCTURE #1

STORY	$r = Y/\sigma_x$	$1/r$	m/σ_x	$\bar{\mu}$
1	0.7465	1.34	3.00	4.538
2	0.7445	1.343	2.96	2.859
3	0.7421	1.347	2.97	5.142
4	0.7324	1.365	3.01	8.088

STRUCTURE #2

STORY	$r = Y/\sigma_x$	$1/r$	m/σ_x	$\bar{\mu}$
1	0.580	1.724	2.38	4.44
2	0.593	1.686	2.40	3.20
3	0.562	1.780	2.46	5.00
4	0.489	2.05	2.78	13.84

STRUCTURE #3

STORY	$r = Y/\sigma_x$	$1/r$	m/σ_x	$\bar{\mu}$
1	0.456	2.194	2.05	3.672
2	0.463	2.161	2.01	2.690
3	0.443	2.256	2.10	4.266
4	0.390	2.564	2.37	9.095

flexible structures suffer an elastic response which relative to its r.m.s. value is much larger than for lower stories. This is due to the higher frequencies with which the top stories of flexible structures vibrate, compared to the bottom stories.

The average ductility factors of all the stories, with the exception of the first story of the stiff structure, reflect the pattern of $1/r$ ratios, but the differences from one story to another are much larger than the $1/r$ ratios suggested. The fact that ductility factors of the top story are significantly larger than the ductilities of all the other stories, for example, should be attributed to three factors, one of which is the smaller r value. The other is the higher frequency of vibration. Both of these factors make the top story yield more often than the others and thus dissipate energy which is reduced from the energy that the other floors are receiving. Therefore, the amplitudes of vibration of the other floors are smaller than if the top floor were not yielding, and hence the difference in ductility ratios is much larger than in the ones of an equivalent one-dof system, with r values differing so little.

Comparing the responses of the three structures among themselves, one observes that although the r ratios decrease with increasing flexibility of the structure, the average over the height ductility factors show no similar trend. This is believed to be due to the fact that the frequency of vibration of the stiffer structures is higher and hence the rate of plastic excursions faster than that of the more flexible structures. Since the maximum response is the result of randomly occuring positive or negative plastic excursions, the probability of a large number of the same

sign of plastic excursions occuring increases with increasing frequency of vibration. This result can be compared with the behavior of simple elastoplastic oscillators. For very stiff structures, the response is acceleration-controlled and the elastoplastic total displacement is μ times larger than the elastic one, while for flexible structures, the elastoplastic displacement is (almost) equal with the elastic displacement.

(c) Effect of the Yielding of One Story on the Vibration of the Whole Structure: Energy Dissipation and Change in Mode of Vibration.

As a result of the research presented here, it can be concluded that there are basically two ways in which the yielding of a story effects the vibration of other stories. First, due to hysteretic dissipation of energy in the yielding story, in addition to the one dissipated by viscous damping, the other stories receive less energy than if the response were elastic; this causes the amplitudes of response to decrease. And, secondly, when a story is yielding significantly, the apparent mode of vibration of the part of the structure above the yielding story changes; this may have different effects depending on which story yields and on the flexibility of the structure.

Two figures are presented to demonstrate these two effects. In Figure 3, the responses of two relatively stiff structures are compared. The two structures differ only in the shear strength of the top story: the strength in the second structure is only 75% of the strength in the first one. Thus, most of the inelastic action in the second case is concentrated in the top story, which suffers a ductility factor of 6.9 as compared with the 2.9 of the first structure. The effect of this increased yielding activity can be seen in the figure. It is clear that the only change in the response of the first three stories is a small change in the amplitudes of vibration; the apparent frequencies of vibration remain the same and the whole appearance of the time-histories of the two structures clearly indicates that the apparent modes of vibration are the same.

Figure 4 portrays the responses of a structure excited by two ground motions with maximum accelerations 0.1 g and 0.3 g, respectively. In both cases, the first story suffers the greater ductilities. In the second case, however, when very large plastic displacements take place, the first story yields almost 35% of the total response time. This increases the apparent frequencies of vibration of the upper stories, as can be very clearly seen in the figure. It seems reasonable to argue that the top three stories behave as a 3-dof system most of the time and, therefore, have higher frequencies of vibration during this time.

All these observations are used as a guide to model the elastoplastic dynamic behavior of multi-degree-of-freedom structures through approximate random vibration analysis.

ATTEMPTS TO MODEL THE ELASTOPLASTIC DYNAMIC BEHAVIOR OF M-DOF STRUCTURES

a) A Crude Model

The first model to approximately predict the elastoplastic response of multi-story structures during earthquakes is based on the assumption

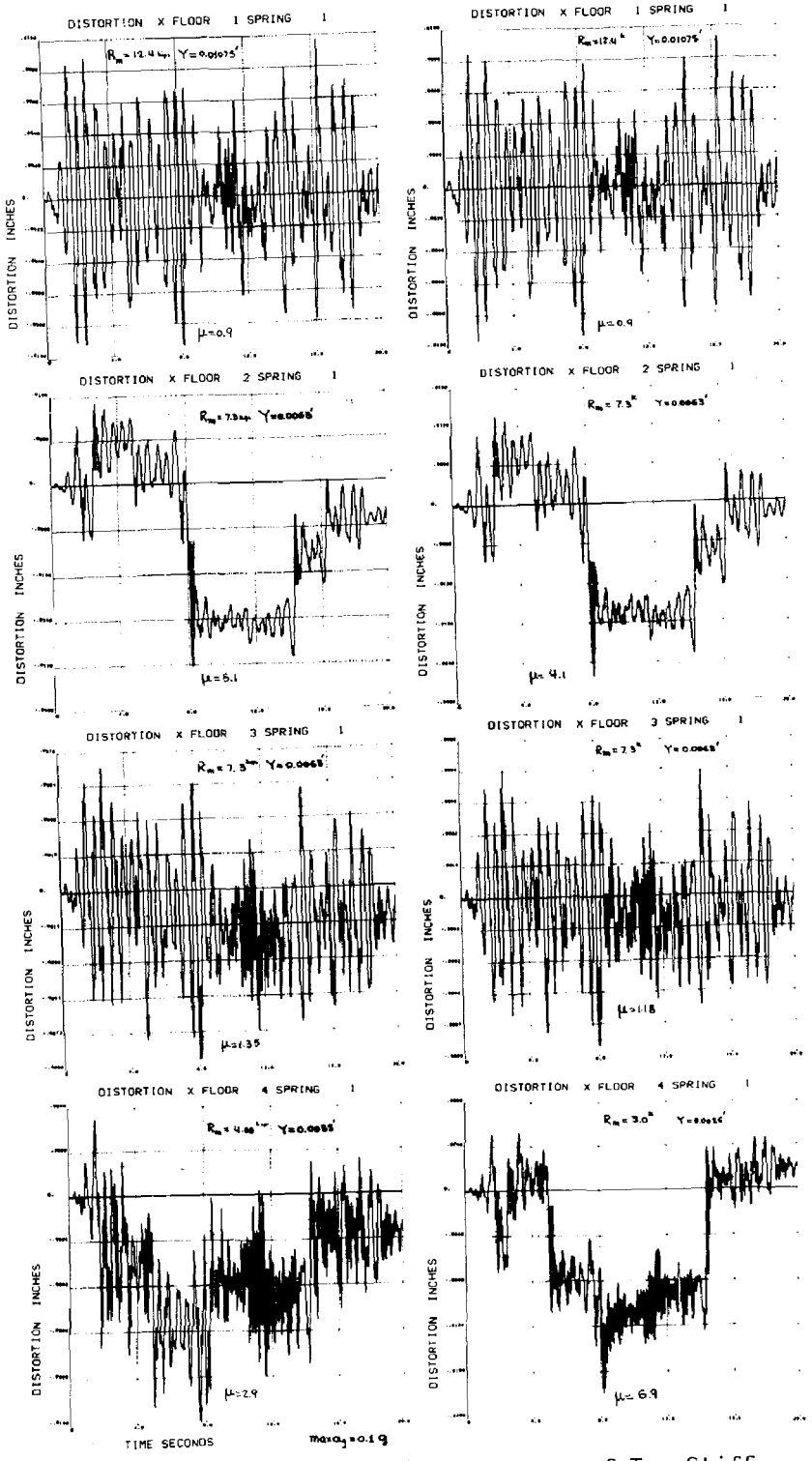

Figure 3 - Comparison of the Responses of Two Stiff Structures (max a_g = 0.1 g)

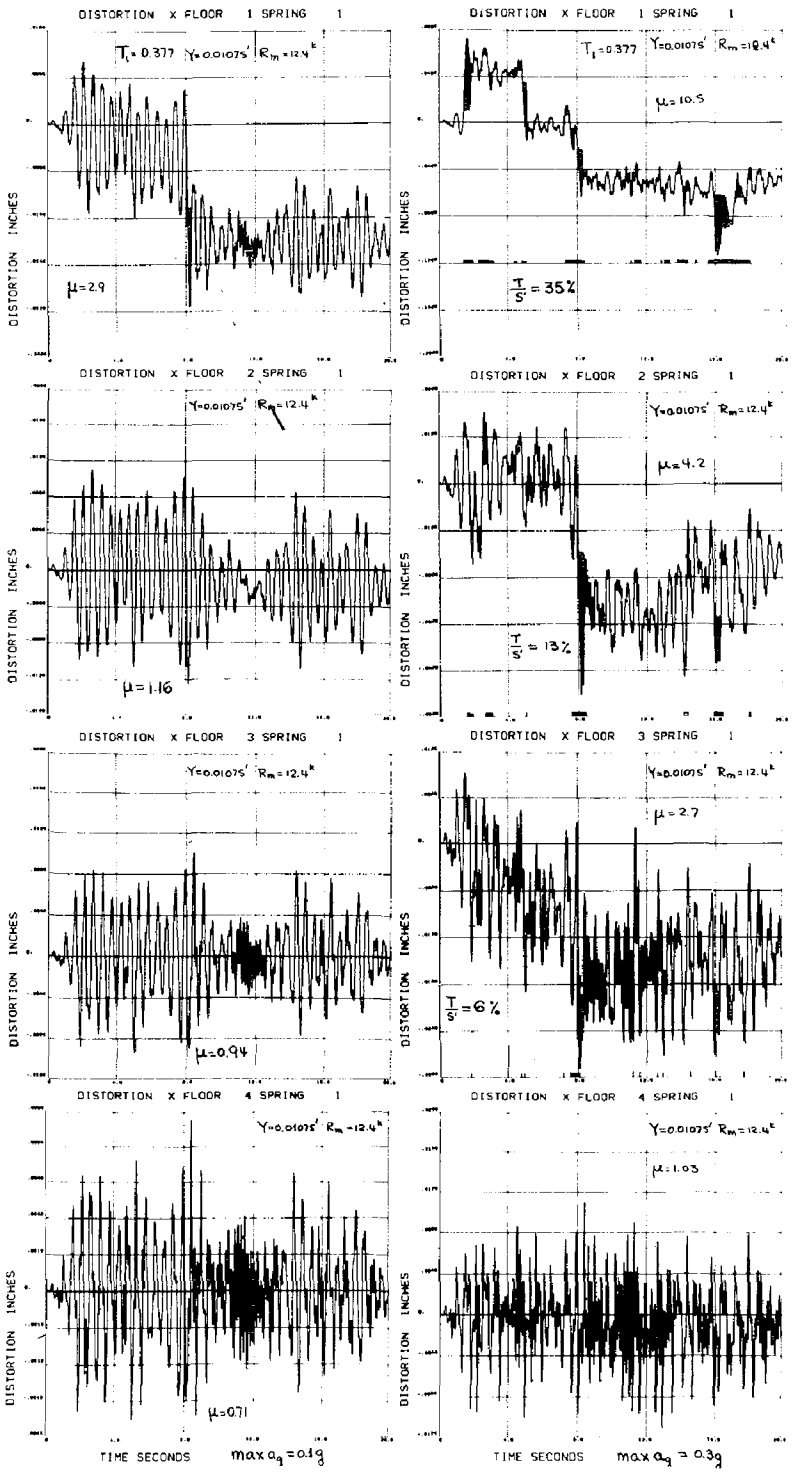

Figure 4 - Comparison of the Responses of a Stiff Structure for 2 Different Ground Motions

that the structure is composed of independently acting springs whose elastic r.m.s. value is computed by modal superposition for the whole structure. The method is intended to give rough upper bound solutions, since it does not account for the reduction in the elastic r.m.s. value of a story while other stories are yielding.

The method suggested by Karnopp and Scharton (7) and extended by Vanmarcke et al.(12-14) is used to compute statistics of the elastoplastic response of simple oscillators. The method treats the vibration process as a two-state Markov process and uses the results of the linear theory of level crossings of stationary random functions. The basic idea is that when no plastic action occurs, i.e., between response excursions into the plastic domain, the elastoplastic system behaves like an elastic oscillator having the same frequency of vibration as the initial natural frequency of the structure. During these elastic intervals, the response is assumed to be stationary with zero mean and r.m.s. value equal to σ, as defined previously. By treating the plastic clumps as "points in time", the time between clump arrivals is exponentially distributed with mean value τ_o given approximately by

$$\tau_o = E[T_o] = \frac{1}{2\nu} e^{r^2/2} \left\{1 - \exp[-r\sqrt{2\beta}]\right\} \qquad (2)$$

where T_o = time between yielding
$\nu = \frac{\Omega}{2\pi}$ is the frequency of vibration
r = ratio Y/σ_x
β = structural damping of the system ($\beta = 0.02$ in this paper)

The amount of deformation due to a plastic excursion is derived (7) by equating the kinetic energy before yielding ($\frac{1}{2}M\dot{x}^2$) with the hysteretic work dissipated during yielding ($R_m|d|$) and is given by

$$\delta \equiv E[d] \simeq \sigma_x^2/2Y = \sigma_x/2r \qquad (3)$$

The cumulative probability distribution of the maximum inelastic deformation, M_s, has the form of a Type I Extreme Value Distribution (13)

$$P[M_s \leq d] = \exp\left\{-\int_0^s \nu_y p_d dt\right\} \cong \exp\left\{-(e^{\nu_y s} - 1)e^{-d/\delta}\right\} \qquad (4)$$

where s = total strong motion duration
$p_d(t)$ = probability that a plastic set contribution at time t results in an upcrossing of the level d, and
$\nu_y \simeq 1/\tau_o$ rate of plastic clump occurences

Combining the results of equation (1) to (4), the expected ductilities of all the stories of these structures are computed. These results are compared in Figure 5 with the average values from the 15 simulated motions (5). In all three cases, the method gives answers which are upper bounds of the response. For the stiff structure, the results are too conservative and do not reflect the pattern of decreased ductilities of the middle stories over the first, but the results for the two flexible structures are satisfactory considering the crudeness of the assumption underlying the method.

(b) Improved Model Accounting for Energy Dissipation and Change in Mode of Vibration During Yielding.

To compute the rate of energy dissipation due to the yielding of a given story, say k, this story is assumed to be unaffected by the possible yielding of other stories. In that case, the yielding story will behave as an independent elastoplastic spring while the other stories vibrate elastically with reduced r.m.s. values and, possibly, increased apparent frequency of vibration. The expected total amount of hysteretic energy dissipation in the k^{th} story is

$$E[H^k] = R_m^k \; E\left[\sum_{i=1}^{N(s)} D_i^{*k}\right] \quad , \; N(s) \text{ is the number of plastic clumps} \qquad (5)$$

where R_m^k is the shear strength of the k^{th} story and D_i^{*k} is the sum of the absolute values of all plastic displacements during a single "plastic clump" of the k^{th} story. Assuming that the consecutive peaks of a plastic clump are independent of the amount of a single plastic excursion and of the position of the peak within the clump, the expected value of D_i^* is computed by the relation

$$E[D_i^*] \simeq E[N_1] \cdot E[d] \simeq 0.5 \Big/ \left\{1 - \exp[-r\sqrt{2\beta}\,]\right\} \cdot \sigma_x / 2r \qquad (6)$$

where the expected number of peaks in a "plastic clump", $E[N_1]$, was derived by combining theoretical arguments with results from time-history analyses.

In a similar semi-empirical way, the quantity $E\left[\sum_{i=1}^{N(s)} D_i^*\right]$ is derived as well as the total expected time which a story spends in yielding, E[T]. The power dissipated can then be evaluated in the following approximate way:

$$E[P^k] \simeq \frac{E[H^k]}{E[T^k]} \simeq 2\nu_k \; K_k \; \sigma_k^2 \qquad (7)$$

The new (elastic) r.m.s. value of the m^{th} story due to the yielding of the k^{th} story, σ_{mk}^*, is related to the "initial" r.m.s. value, σ_m, as follows:

$$\sigma_{mk}^* \simeq \sigma_m \cdot \left\{1 - 2\,r_m^2 (\nu_k \; K_k \; \sigma_k^2) \Big/ \sum_{i=1}^{n} (\nu_i \; K_i \; Y_i^2)\right\}^{\frac{1}{2}} \qquad (8)$$

To assess the change in the mode of vibration with accuracy is almost a formidable task. One can only develop an approximate method based on the theoretical arguments and the empirical evidence discussed previously. The lower stories continue to vibrate with the same frequency as before yielding; the higher stories vibrate as a new m-dof system (having a smaller number of stories than the whole structure and, therefore, a higher frequency of vibration). In this paper, the frequencies of all possible "clusters of upper stories" were roughly estimated by interpolation between the frequency of one story ($\omega_{top} = \{[K/M]_{top}\}^{\frac{1}{2}}$ and the fundamental frequency of the whole structure, ω_1.

The problem left is how to combine the effects of yielding of the various stories. An intuitive approach is followed: The change in the r.m.s. value and the frequency of vibration of all the stories due to the yielding of each story, i, is first computed. Based on these values, the "partial expected ductility factor" of each story m, μ_m^1, is computed

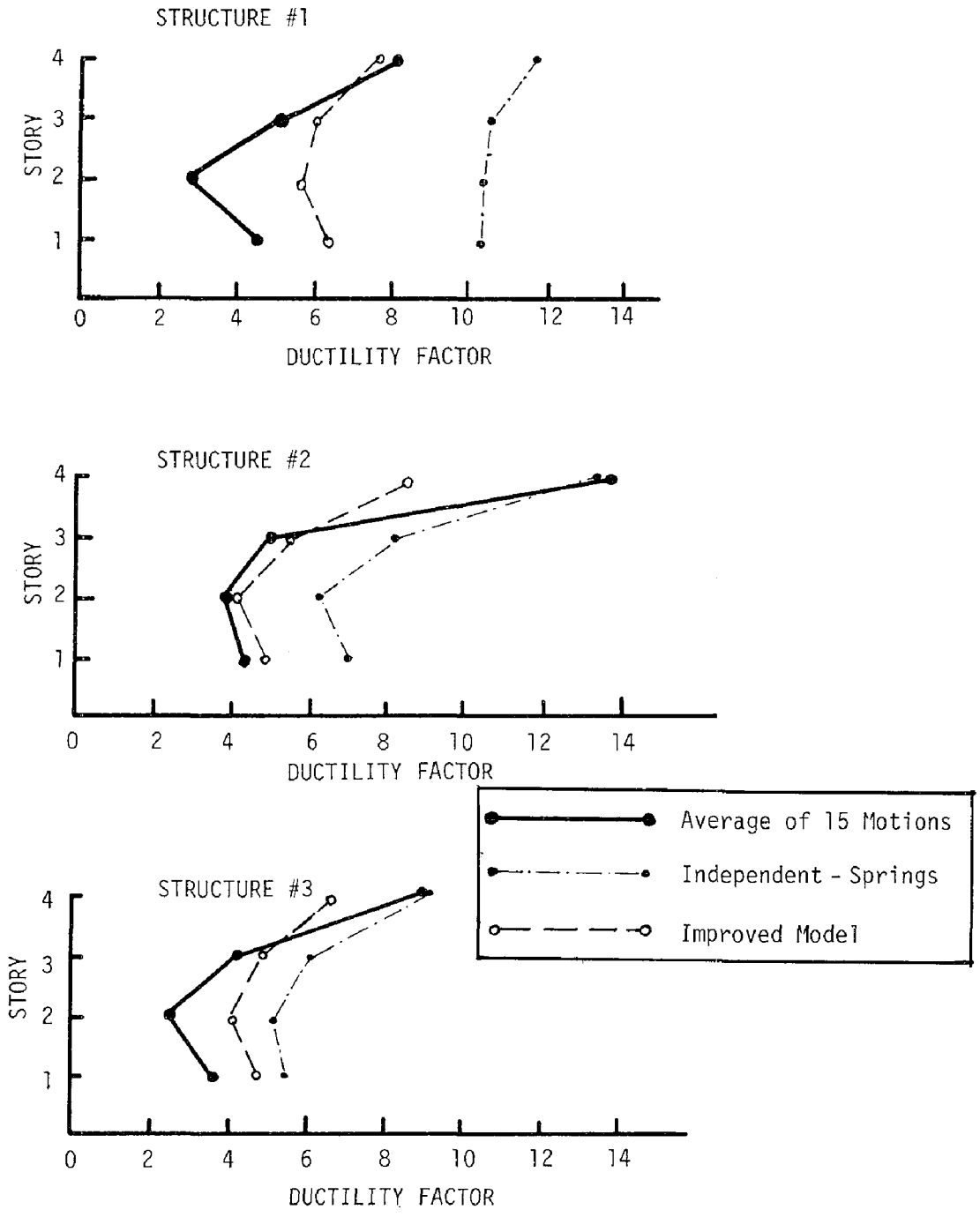

Figure 5 - Comparison of Predicted with the Actual Ductilities

as if each story were independent of the others. The final expected ductility factor, μ_m, is obtained by superimposing all the combinations of yielding actions, conditioned by the probability of occurence of each combination, f_i, i.e.:

$$\mu_m = \sum_{i=1}^{n} (f_i \, \mu_m^i) \qquad (9)$$

In the present "improved model", the probability f_i is taken to be inversely proportional to the square of the expected time between yielding clumps, τ_o.

The results of the method are compared in Figure 5 with the statistics from the 15 simulated motions (5) and the results of the crude model. The overall agreement is quite satisfactory. The greater difference exists in the top story ductilities of the two flexible structures, which are underpredicted by this method. A probable reason for this discrepancy is the crude way the increased frequencies of the upper stories are computed: the fundamental frequency certainly underestimates the frequency of the top stories of flexible structures.

CONCLUSIONS

The conclusion of the empirical research is that the effect of the yielding of a story on the lower stories is to reduce the power they recieve, while the higher stories, besides the reduced power, vibrate with higher frequencies than before yielding. The frequency of the yielding story decreases due to yielding.

The models presented and evaluated in this report lead to the, tentative at least, conclusion that it is possible to model the elastoplastic dynamic behavior of a m-dof structure in a random vibration fashion. This can be done by properly combining the elastic random-vibration results of the m-dof system, the elastoplastic random-vibration results of the one-dof system and the previously mentioned effects of yielding on the behavior of a structure (energy dissipation and change in mode of vibration). Attempts to further improve the presented model have to be made in the near future to either verify or reject the above conclusion.

BIBLIOGRAPHY

1. Caughey, T.K., "Equivalent Linearization Techniques," Journal of the Acoustical Society of America, Vol. 35, 1963, pp. 1706 - 1711.

2. Chopra, A.K., Clough, D.P. and Clough, R.W., "Earthquake Resistance of Buildings with a 'Soft' First Story," Journal of Earthquake Engineering and Structural Dynamics, Vol. 1, 1973, pp. 347 - 355.

3. Crandal, S.H., "Perturbation Techniques for Random Vibration of Nonlinear Systems," Journal of the Acoustical Society of America, Vol. 35, November 1963, pp. 1700 - 1705.

4. Crandal, S.H., "First-Crossing Probabilities of the Linear Oscillator," Journal of Sound and Vibration, Vol. 12, 1970, pp. 285 - 299.

5. Frank, R., "A Statistical Study on the Nonlinear Response of MDOF Systems to Real and Artificial Earthquake Ground Motions," Internal Study Report under "Seismic Safety of Buildings" Research Project, M.I.T., 1975.

6. Frank, R., "A Study of the 'Effective Period' Change for SDOF Systems Responding Inelastically to a Sinusoidal Base Motion," Internal Study Report under "Seismic Safety of Buildings" Research Project, M.I.T., 1975.

7. Karnopp, D. and Scharton, T.D., "Plastic Deformation in Random Vibration," Journal of the Acoustical Society of America, Vol. 39, 1966, pp. 1154 - 1161.

8. Lutes, L.D., "Approximate Technique for Treating Random Vibration of Hysteretic Systems," Journal of the Acoustical Society of America, November 1969.

9. Newmark, N.M. and Rosenblueth, E., "Fundamentals of Earthquake Engineering", Prentice-Hall, Englewood Cliffs, New Jersey, 1971.

10. Peyrot, A.H., "Probabilistic Response of Nonlinear Buildings During Earthquakes," Journal of the Structural Division, ASCE, Vol. 98, No. ST11, November 1972.

11. Ruiz, P. and Penzien, J., "Stochastic Seismic Response of Structures", Journal of the Engineering Mechanics Division, ASCE, Vol. 97, No. EM2, Proc. Paper 8050, April 1971, pp. 441 - 456.

12. Vanmarcke, E.H., Yanev, P.I. and DeEstrada, M.B., "Response of Simple Hysteretic Systems to Random Excitation," M.I.T. Department of Civil Engineering Research Report R70-66, September 1970.

13. Vanmarcke, E.H. and Veneziano, D., "Probabilistic Seismic Response of Simple Inelastic Systems," Proceedings, Fifth World Conference on Earthquake Engineering, Rome, 1973.

14. Veneziano, D. and Vanmarcke, E.H., "Seismic Damage of Inelastic Systems: A Random Vibration Approach," M.I.T. Department of Civil Engineering Research Report R73-5, January 1973.

15. Veletsos, A.S. and Vann, W.P., "Response of Ground-Excited Elastoplastic Systems," Journal of the Structural Division, ASCE, Vol. 97, No. ST4, April 1971.

16. Wen, Y.K., "An Approximate Method for Nonstationary Nonlinear Random Vibration," ASCE Specialty Conference on Probabilistic Methods in Engineering, Stanford University, June 1974.

ACKNOWLEDGEMENT: This research has been supported by the National Science Foundation under Grant No. ATA 74-06935.

INTERNATIONAL SYMPOSIUM ON
EARTHQUAKE STRUCTURAL ENGINEERING
St. Louis, Missouri, USA, August, 1976

PROBABILISTIC APPROACH TO ULTIMATE ASEISMIC SAFETY OF STRUCTURES

M. YAMADA* and H. KAWAMURA**

*Professor, **Res. Assistant
Faculty of Engineering
Kobe University
Kobe, Japan

Summary: In this paper, "Steady-State Forced Vibration" is adopted as a medium to make possible the direct comparison between earthquake loadings, dynamic responses and ultimate states of structures on a common basis. First, ultimate state criteria of structures subjected to regulated cyclic loadings are given by probabilistic descriptions with the following three random variables, resonance capacity relating to hysteretic energy absorption, deformation amplitude (or equivalent natural period) and number of cycles. Second, it is shown that the characteristics of earthquake loadings and structural dynamic responses are able to be expressed by probabilistic distributions of regulated waves and to be illustrated in the space with acceleration amplitude-, period- and number of waves- coordinate axes.

Finally, combining both the probabilistic properties of ultimate state conditions and dynamic responses of structures, their ultimate aseismic safety is able to be evaluated as a probability of survival. It is emphasized here that fracture conditions of structures should be based on experimental results and that the probability of survival shoud be used as an objective function in ultimate aseismic optimum design.

1. INTRODUCTION

In many researches on the aseismic safety or reliability of structures, the following approach is commonly adopted [5] [4] [3]. When earthquake loadings are given as stochastic processes, on the basis of the well known linear differential equation of motion, structural responses to them are also solved as stochastic ones. Using a fracture criterion, e.g. critical deformation or cumulative damage, aseismic reliability of structures is able to be estimated as a threshold-crossing problem or a peak-distribution problem. This approach, however, is available only in the case that structures always show linear or approximately linear properties until fracture, even if such a linear differential equation is applied by means of equivalent linearlization.

On the other hand, the fracture criterion of structures or materials subjected to low cycle loadings which show plastic strains until fracture

is able to be theorized on the basis of the Manson-Coffin's hypothesis [7] [1]. Its application in the case of dynamic structural responses, however, is impossible unless cyclic loadings are deterministically given [2], because of the hysteretic characteristics of structures and materials. If the Manson-Coffin's hypothesis should be able to be dealt with in the same linear ways as the Miner's law, a probabilistic approach might become possible [6]. Anyway, in probabilistic approach to ultimate aseismic structural safety, it seems at present to be an alternative problem which should be selected the linearlization of dynamic responses or of fracture criteria.

The purposes of this paper are to fill the gap between dynamic responses and fracture criteria of structures subjected to earthquake loadings and to establish a method to evaluate the aseismic safety of structures in their ultimate states. Aiming at these purposes, the following new idea is adopted here. By means of probabilistic distribution of "steady-state forced vibration" phenomenon, is it impossible to describe the characteristics of future earthquake loadings, dynamic responses and ultimate states of structures? If possible, all these properties are able to be compared directly, and then the ultimate aseismic safety is able to be estimated as a probability of survival.

2. STEADY-STATE FORCED VIBRATION

A critical coherent phenemenon "steady-state forced vibration" is adopted here as a fundamental medium which ensures the direct comparison between earthquake loadings, dynamic responses and ultimate aseismic properties of structures. When a structure is subjected to earthquake excitations, in reality, such a steady-state response will seldom occur because of the randomness of earthquake loadings. However, if earthquake waves are described as a probabilistic distribution of various sinusoidal waves, the dynamic responses of structures are also able to be described in terms of a probablistic one of steady-state forced vibration.

On the other hand, aseismic characteristics of structures subjected to regulated cyclic loadings are able to be obtained easily and directly by means of proper experimental or analytical operations and to be described of course in terms of probabilistic expressions. Consequently, the dynamic responses and the aseismic characteristics of structures are able to be compared directly, and the aseismic safety of the structures is estimated as a probability of survival.

Anyway, although "steady-state forced vibration" is an imaginary phenomenon in earthquake responses, it is useful and effective enough to describe expected future earthquake waves and to carry out well defined cyclic tests on structures. Rigorously saying, "steady-state forced vibration" adopted in this paper differs from the conventional one in vibrational theory. Presice definition is given in the later chapter.

3. RESONANCE-FATIGUE-CHARACTERISTICS

3-1. Resonance Capacity

When a structure is subjected to constant vertical load W and alternately repeated cyclic horizontal load P and has a deflection amplitude δ_a as shown in Fig. 1, that structure shows such a P - δ hysteresis loop as shown in Fig. 2 at N_cth cycle. Denote the area of the hysteresis loop, A, and "Resonance Capacity" C_R is defined by

$$C_R = \frac{1}{\pi} \frac{A}{\delta_a} \qquad (1).$$

3-2. Fatigue Characteristic

Under the condition of a constant "Resonance Capacity" C_R, which corresponds to the "steady-state forced vibration" defined in this paper, generally, a structure shows a curved line S'X' in δ_a - N_c plane, which starts from point S' and ends at fracture point X' as shown in Fig. 3. Using C_R as parameter, the structure has many lines which are limited by curve Y'Z' corresponding to its fracture. That fracture line Y'Z' is defined as the one on which the deflection amplitude δ_a diverges to infinity.

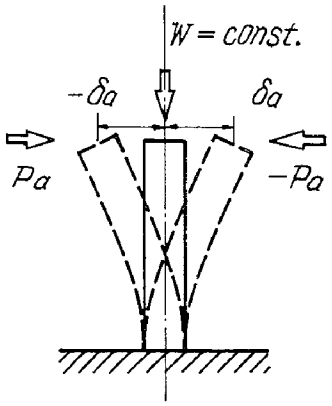

Fig.1 Structure Subjected to Cyclic Loading

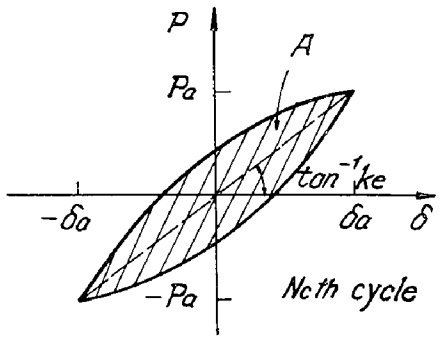

Fig.2 P - δ Hysteresis Loop at N_cth Cycle

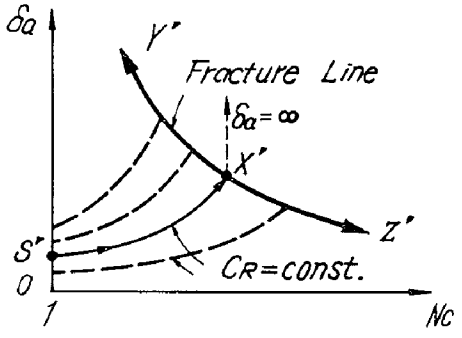

Fig.3 Resonance-Fatigue-Characteristic in δ_a - N_c Plane

3-3. Resonance-Fatigue-Space

Considering C_R - δ_a - N_c space, called resonance-fatigue-space in this paper, the fatigue characteristic shown in Fig. 3 is able to be illustrated by a curved surface with boundary line YZ as shown in Fig. 4. The curved line SX on that surface is parallel to δ_a - N_c plane, and the lines Y'Z', S'X' on δ_a - N_c plane are the projections from YZ, SX to that plane.

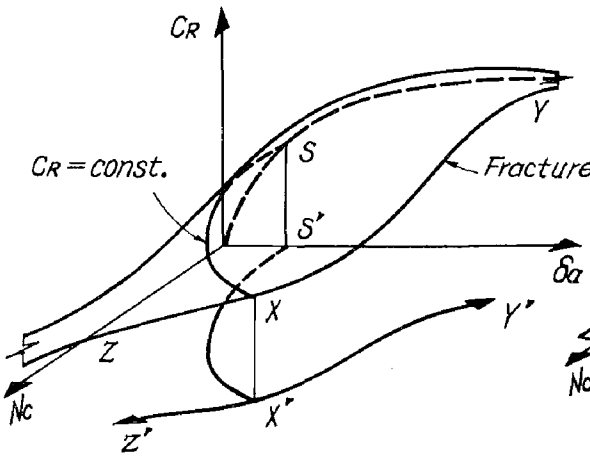

Fig.4 Resonance-Fatigue-Characteristic in C_R - δ_a - N_c Space (Resonance-Fatigue-Space)

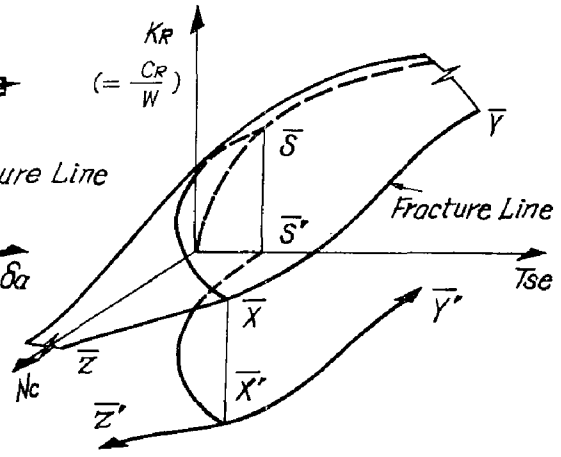

Fig.5 Modified Resonance-Fatigue-Characteristic in K_R - T_{se} - N_c Space (Modified Resonance-Fatigue-Space)

3-4. Modified Resonance-Fatigue-Space

When the structure in Fig. 1 is considered as a one mass oscillator, the equivalent mass m_e and stiffeness k_e are given as follows;

$$m_e = W/g \qquad (2), \qquad k_e = P_a/\delta_a \qquad (3),$$

where P_a is the horizontal load amplitude of the loop in Fig. 2. As for an equivalent one mass oscillator, the coordinate axes C_R, δ_a in C_R - δ_a - N_c space are reasonably replaced by resonance shear coefficient K_R and equivalent natural period T_{se} expressed as follows;

$$K_R = C_R/W \qquad (4), \qquad T_{se} = 2\pi\sqrt{(W/g)(\delta_a/P_a)} \qquad (5).$$

In K_R - T_{se} - N_c space called modified resonanace-fatigue-space in this paper, a curved surface analogous to the one in Fig. 4 may be drawn as shown in Fig. 5. For example, the boundary line YZ corresponding to the fracture one in Fig. 4 is transformed to $\overline{YZ}$ in Fig. 5.

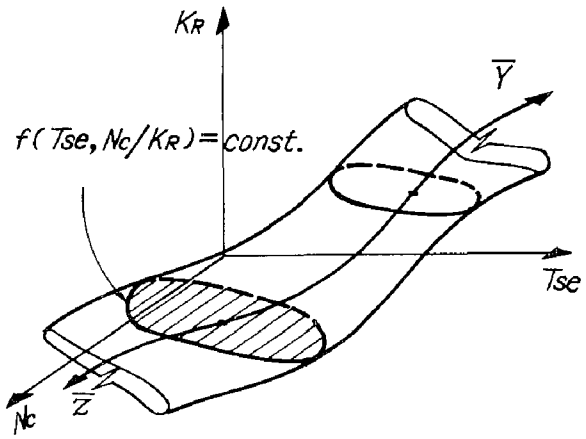

Fig.6 Fracture Condition Expressed by Probabilistic Description

3-5. Probabilistic Description

The fracture line $\overline{YZ}$ of a structure in K_R - T_{se} - N_c space is, generally able to be expressed in terms of a probability distribution or density function, $F(T_{se}, N_c/K_R)$ or $f(T_{se}, N_c/K_R)$, containing the mechanical and material characteristics of that structure. Taking

$f(T_{se}, N_c/K_R)$ as parameters, tubes including $\overline{YZ}$ are made visible in K_R - T_{se} - N_c space as shown in Fig. 6. It must be remembered well that the resonance-fatigue-characteristics shown in Figs. 3,4,5,6 are able to be obtained by means of physical, i.e. experimental operations (8).

4. EARTHQUAKE-WAVE-CHARACTERISTIC

4-1. Acceleration Amplitude, Period and Number of Waves

During a life of a structure, in general, some random ground motions due to earthquakes are expected to attack it. These ground motions are expressed as acceleration waves with various acceleration amplitudes and periods as shown in Fig. 7. Assuming that these waves are composed of many pseudo-sinusoidal waves with acceleration amplitude α_E, period T_E and number of such waves N_E, the sets of α_E, T_E, N_E are cosidered to represent the feature of earthquake waves as an assembly of sinusoidal ones.

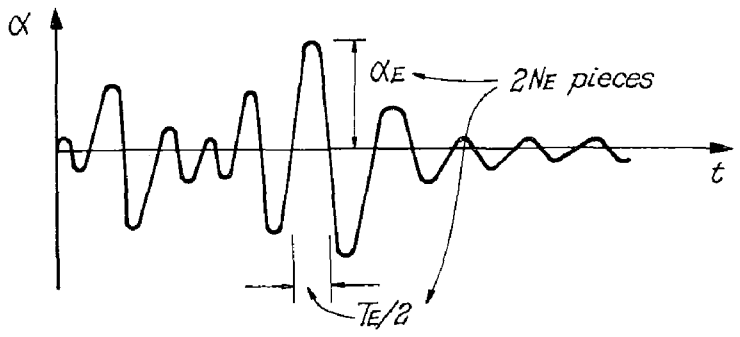

Fig.7 Acceleration Waves of Earthquake Excitations

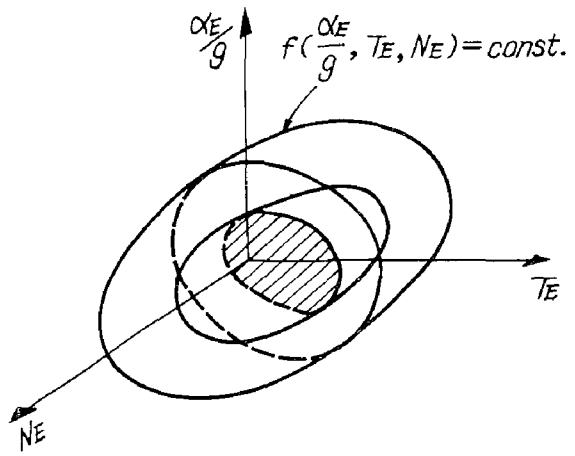

Fig.8 Earthquake-Wave-Characteristic Expressed by Probabilistic Description in α_E/g-T_E-N_E Space

4-2. Earthquake-Wave-Space

In the same way as used to represent the resonance-fatigue-characteristic of a structure in Fig. 5, earthquake-wave-space with α_E/g, T_E, N_E coordinate axes is introduced to express the properties of earthquake waves as shown in Fig. 8. It is of importance that these factors, α_E/g, T_E, N_E have the same meanings as the factors, K_R, T_{se}, N_c defined in Chapter 3.

4-3. Probabilistic Description

No one can foreknow the real features of earthquake waves expected to occur in future, and moreover they are considered to be random very much. Consequently, it is the most reasonable to express them by means of probabilistic description. Using α_E/g, T_E, N_E as random variables, therefore, a probability distribution or density function, $F(\alpha_E/g, T_E, N_E)$ or $f(\alpha_E/g, T_E, N_E)$, is able to be defined in earth-

quake-wave-space as shown in Fig. 8. In other words, the features of expected earthquake waves are able to be represented by a probabilistic distribution of sinusoidal waves with the same α_E, T_E, N_E.

5. RESONANCE-RESPONSE-CHARACTERISTIC

5-1. Steady-State Resonance Acceleration

When a one mass oscillator with mass m and restoring force function f(x) is subjected to ground motions of sinusoidal acceleration waves with amplitude α_E, period T_E and phase difference ϕ as shown in Fig. 9, assume that the oscillator reaches steady-state forced vibration and that the restoring force function shows a hysteresis loop with displacement amplitude x_a and area A as shown in Fig. 10, and the following differential equation of motion is able to be derived;

$$m\ddot{x} + f(x) = -m\,\alpha_E \cos\left(\frac{2\pi}{T_E}t + \phi\right) \qquad (6).$$

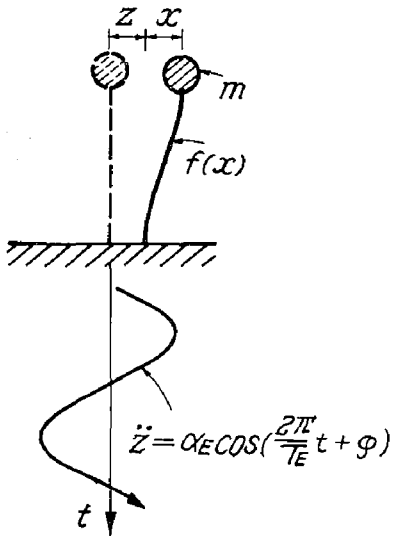

Fig.9 One Mass Oscillator Subjected to sinusoidal Waves

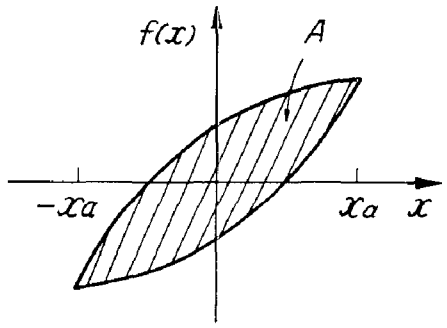

Fig.10 Restoring Force Function at Steady-State Vibration

If the response displacement x is approximately given by

$$x = x_a \cos\frac{2\pi}{T_E}t \qquad (7),$$

integrating both the sides of Eq. 6 with respect to x over one cycle, finally, the following energy equilibrium equation is derived;

$$\frac{A}{\pi x_a} = m\,\alpha_E\,|\sin\phi| \qquad (8).$$

Refer to Eqs. 1,2,4, then Eq. 8 is reduced to

$$K_R = \alpha_R^*/g \qquad (9), \qquad \alpha_R^* = \alpha_E|\sin\phi| \qquad (10),$$

where α_R^* is defined here as steady-state resonance acceleration amplitude

of an oscillator or an equivalent structure.

Consequently, the "steady-state forced vibration" adopted in this paper is able to be defined by the following phenomenon; a structure subjected to regulated input waves with constant acceleration amplitude α_E shows constant steady-state response acceleration amplitude α_R^*, constant resonance shear coefficient K_R and then constant resonance capacity C_R.

5-2. Response Wave Characteristic

When a one mass oscillator is subjected to such earthquake excitations as shown in Fig. 7, response acceleration waves are generally illustrated in Fig. 11. Denote response acceleration amplitude, period and number of waves, α_R, T_R and N_R, and in the same way as earthquake waves the response wave characteristics are described by means of probability distribution of pseudo-sinusoidal waves with α_R, T_R and N_R. Here, applying "steady -state forced vibration", although α_R, T_R, N_R are equal to α_R^*, T_E, N_E, respectively, α_R^* is obviously given as a function of T_S/T_E, where T_S is the natural period of that oscillator. Precisely saying, there exists a probability in the occurrence of steady-state vibration itself. To consider such a probability, it is reasonable to regard phase difference $|\sin\phi|$ in Eq.10 as a function of the relativity between N_R and N_E.

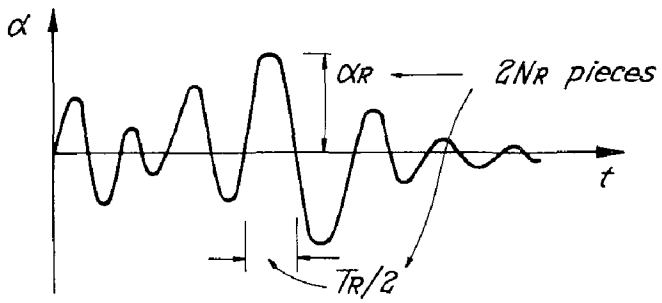

Fig.11 Response Acceleration Waves

In this paper, therefore, resonance-response-space with rectangular coordinate-axes, α_R^*/g, T_S, N_R, is defined so that it represents response wave characteristics of structures which are of course given as a function of α_E/g, T_E, N_E.

5-3. Probability of Steady-State Resonance and Forced Vibration

According to linear vibration theory, the phase difference ϕ in steady-state forced vibration is given by

$$|\sin\phi| = 2h\frac{T_S}{T_E}\Big/\sqrt{\{1-(\frac{T_S}{T_E})^2\}^2 + 4h^2(\frac{T_S}{T_E})^2} \qquad (11),$$

where h is the damping factor of that oscillator. As for an oscillator with hysteretic restoring force function, h is replaced by equivalent viscous damping factor h_e, which is, in case of reinforced concrete members, about 0.3 to 0.4 for flexural yielding type and about 0.1 to 0.2 for shear failure type [8]. From another point of view, Eq. 11 is able to be considered to represent the probability of the occurrence of steady-state resonance.

On the other hand, regarding $|\sin\phi|$ as the probability of the occur-

rence of steady-state forced vibration expressed by a function of N_R, N_E, the tendency of $|\sin\phi|$ is proposed here as follows;

$$|\sin\phi| = 1 - K \exp(-\frac{1}{N_R/N_E}), \quad 0 \leq K \leq 1, \tag{12}$$

where K is constant. $|\sin\phi|$ is given as a decreasing function of N_R/N_E, because the less N_R and the more N_E become, the more the probability of steady-state vibration is naturally considered to become. In the more rigorously way, $|\sin\phi|$ in Eqs. 11,12 should be given by means of probabilistic description, but it is given here by deterministic function for simplification of the later discussions. Supposing that T_s/T_E is independent of N_R/N_E and combining Eq. 11 and Eq. 12, $|\sin\phi|$ is illustrated as shown in Fig. 12.

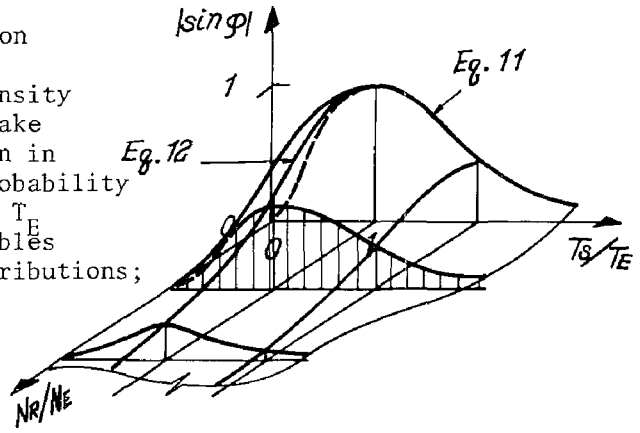

Fig.12 Probability of Steady-State Resonance and Forced Vibration

5-3. Probabilistic Description

From the probability density function of expected earthquake waves, $f(\alpha_E/g, T_E, N_E)$ as shown in Fig. 8, the following two probability density functions with α_E/g, T_E and α_E/g, N_E as random variables are derived as marginal distributions;

$$f(\alpha_E/g, T_E) = \int_0^\infty f(\alpha_E/g, T_E, N_E)\, dN_E \tag{13},$$

$$f(\alpha_E/g, N_E) = \int_0^\infty f(\alpha_E/g, T_E, N_E)\, dT_E \tag{14}.$$

Combining Eqs. 13,10,11, a new probability density function with random variables α_R^*/g, T_E and parameter T_s is given by $f(\alpha_R^*/g, T_E/T_s)$ as shown in Fig. 13. From this, the following probability density function with random variable α_R^*/g and parameter T_s is derived as mrginal distribution;

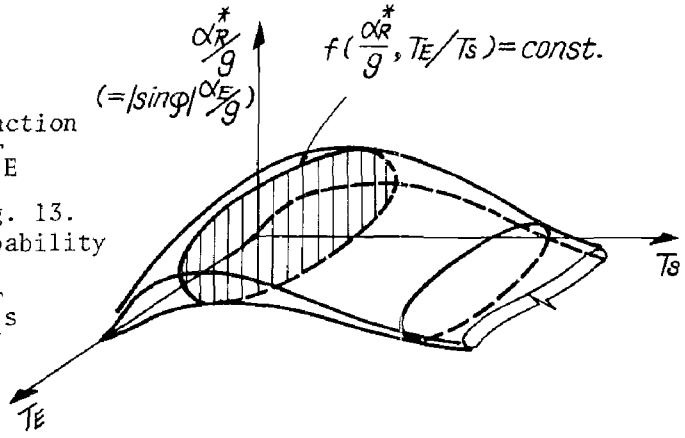

Fig.13 Probabilistic Resonance-Response Surface in α_R^*/g-T_s-T_E Space

$$f(\alpha_R^*/g\ /T_s) = \int_0^\infty f(\alpha_R^*/g, T_E/T_s)\, dT_E \tag{15},$$

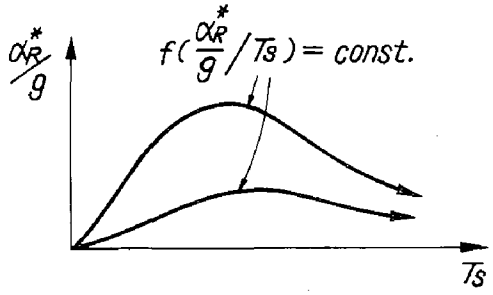

Fig.14 Probabilistic Resonance-Response Curve in α_R^*/g-T_s Plane

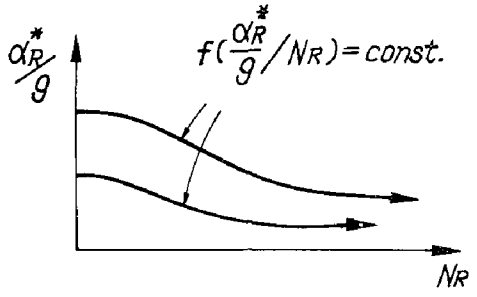

Fig.16 Probabilistic Resonance-Response curve in α_R^*/g-N_R Plane

which is shown in Fig. 14.

In the same way as adopted above, using Eqs. 14,10,12, a new probability density function $f(\alpha_R^*/g, N_E/N_R)$ is derived as shown in Fig. 15. Integrating with respect to N_E, the following probability density function is given as marginal distribution;

$$f(\alpha_R^*/g\ /N_R) = \int_0^\infty f(\alpha_R^*/g, N_E/N_R)\,dN_E \qquad (16),$$

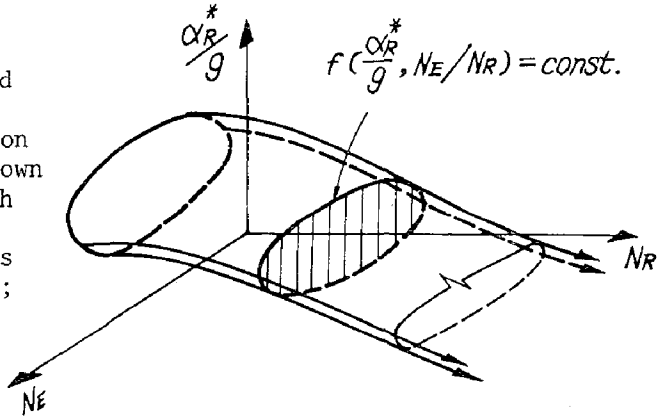

Fig.15 Probabilistic Resonance-Response Surface in α_R^*/g-N_R-N_E Space

which is shown in Fig. 16.

In the same way mentioned above, a probability density function with random variable α_R^*/g and parameters T_s, N_R, $f(\alpha_R^*/g\ /T_s, N_R)$ is easily reduced as shown in resonance-response-space in Fig. 17. This shows a probabilistic description of response characteristics of an oscillator subjected to earthquake excitations shown in Fig. 8.

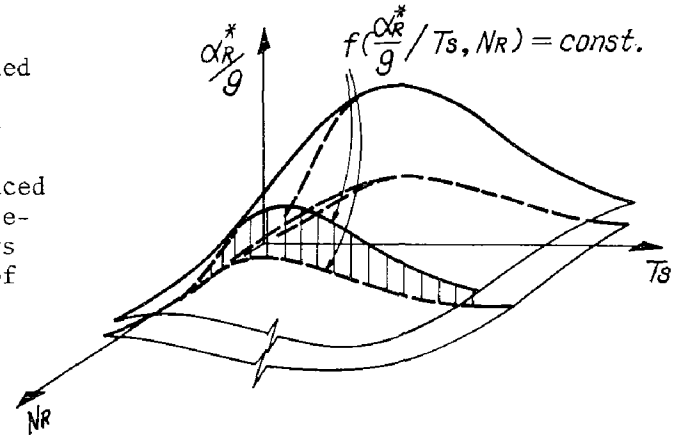

Fig.17 Resonance-Response-Characteristic Expressed by Probabilistic Description in α_R^*/g-T_s-N_R Space (Resonance-Response-Space)

6. ULTIMATE ASEISMIC SAFETY

The modified resonance-fatigue-space with K_R, T_{se}, N_c coordinate axes defined in Figs. 5,6 has the same physical meanings as the resonance-response space with α_R^*/g, T_s, T_R coordinate axes defined in Fig. 17, because Eq. 9 shows that K_R is equal to α_R^*/g, Eq. 5 shows that T_{se} is equivalent to T_s, and Both N_c and N_R mean a number of cycles. Consequently, a probability of survival of a structure p_s is able to be calculated as follows;

$$p_s(K_R,T_s,N_R) = \int_{T_s}^{\infty}\int_{N_R}^{\infty} f(T_{se},N_c/K_R)dT_{se}dN_c \int_{o}^{K_R} f(\alpha_R^*/g\ /T_s,N_R)d\alpha_R^*/g \qquad (17).$$

p_s is given as a function of K_R, T_s, N_R, because these factors have been used as parameters. From the technological point of view, the following three kinds of p_s-value may be available; the minimum, the mean and the maximum, i.e. p_{smin}, p_{smean} and p_{smax}, which are calculated within a region Ω of K_R, T_s, N_R. Let $V(\Omega)$ be the volume of the region Ω, p_{smean} is given by

$$p_{smean} = \int_{\Omega} p_s(K_R,T_s,N_R)dK_R dT_s dN_R/V(\Omega) \qquad (18),$$

which is proposed as a barometer of ultimate aseismic structural safety in this paper, although it is also a function of Ω.

7. CONCLUSIONS

On the basis of steady-state forced vibration, ultimate resonance-fatigue-characteristics of structures as shown in Fig. 6 are defined by means of probabilistic expression so as to represent their ultimate earthquake-resisting capacities. Furthermore, resonance-response-characteristics of structures as shown in Fig. 17 are introduced in terms of probabilistic description so as to express the response level of structures subjected to earthquake loadings which are also described by probabilistic distribution of regulated waves as shown in Fig. 8. Comparing them directly, a probability of survival of structures against expected future earthquakes p_s is able to be given as a function of K_R, T_s, N_R shown by Eq. 17, and the mean value of p_s defined by Eq. 18 is proposed as an index value on the ultimate aseismic safety of structures.

It is true aseismic optimum design of structures to make the value p_s maximum under social and economical confinements.

8. BIBLIOGRAPHY

[1] Ferry Borges,J.; Safety Concepts for Non-Repeated and Repeated loadings, Introd. Rept., IABSE Symp., Lisbon, 1973, pp. 101-124.
[2] Kasiraj,I. and Yao,J.T.P.; Fatigue damage in Seismic Structures, Proceedings, ASCE, ST8, Aug. 1969, pp. 1673-1692.
[3] Lin,Y.K.; Probabilistic Theory of Structural Dynamics, McGraw-Hill, 1967, Chapter 9, pp.293-338.
[4] Newmark,N.M. and Rosenblueth,E.; Fundamentals of Earthquake Engineering, Prentice Hall, 1971, Chapter 9, pp. 267-303.
[5] Shinozuka,M.; Method of Safety and Reliability Analysis, International Conference on Structural Safety & Reliability, Editted by A.M.Freudenthal, Pergamon Press, 1972, pp. 11-45.
[6] Tang,J.P. and Yao,J.T.P.; Expected Fatigue Damage of Seismic Structures, Proceedings, ASCE, EM3, June 1972, pp.695-709.
[7] Yamada,M.; Effect of Cyclic Loading on Buildings, Planning and Design of Tall Buildings, ASCE-IABSE Joint Commitee, Vol.II, 1973, pp.725-739.
[8] Yamada,M. and Kawamura,H.; A Resonance Capacity Criterion for Evaluation of the Aseismic Capacity of Reinforced Concrete Structures, ACI Symp. on Reinforced Concrete Structures in Seismic Zones, 1974, Special Publication, (to be published).

INTERNATIONAL SYMPOSIUM ON
EARTHQUAKE STRUCTURAL ENGINEERING
St. Louis, Missouri, USA, August, 1976

SEISMIC ANALYSIS OF HYPERBOLIC COOLING TOWERS BY THE RESPONSE SPECTRUM METHOD

by

Phillip L. Gould
Professor of Civil Engineering
Washington University
St. Louis, Missouri

Subir K. Sen
Senior Engineer
Bechtel Power Corporation
Ann Arbor, Michigan
formerly Post-Doctoral Fellow
Department of Civil Engineering
Washington University
St. Louis, Missouri

Herman Suryoutomo
Associate
Earthquake Engineering Systems
San Francisco, California
formerly Research Assistant
Department of Civil Engineering
Washington University
St. Louis, Missouri

SUMMARY

A free vibration finite element analysis for rotational shells is developed and applied to the seismic analysis of hyperbolic cooling towers. In the numerical studies, particular attention is drawn to the influence of the system of supporting columns on the dynamic stresses and deformations.

INTRODUCTION

Hyperbolic cooling towers are a visable part of many nuclear power plants and form an important link in the return of cooling water to the source. These structures have been constructed to heights approaching 500 ft. and are basically thin shells of revolution supported atop a system of closely spaced columns which border the air intake space. The ring of columns forms a rather abrupt discontinuity between the shell and the foundation and plays an important role in the response of the structure to seismic excitation. A typical tower is depicted in Figure 1 along with some structural details.

The effect of wind forces on hyperbolic cooling towers is rather severe as compared to a rectangular building structure of similar proportions. This occurs because of the geometric form and the surface characteristics. As a result, cooling towers designed for extreme wind conditions can often meet earthquake design criteria as well. However, in some situations the seismic conditions may control and the problem merits careful attention in any case.

The response spectrum method is generally accepted as a realistic basis for the seismic analysis of cooling towers. From a structural engineering standpoint, the information required to perform such an analysis is obtained chiefly from an undamped, free vibration analysis. For doubly curved shells such as cooling towers, a dynamic analysis is best approached with a variationally based method which produces a consistent mass matrix and a consistent loading vector. The principal reason for requiring this degree of sophistication is that purely physical lumping of the masses and loads is difficult and often inaccurate with curvilinear coordinates. Also the presence of the column system at the base of the shell obviously influences

the natural frequencies and mode shapes, particularly those due to a horizontal seismic excitation where the shell may translate with respect to the base of the columns.

The purpose of this paper is to outline a response spectrum analysis procedure suitable for hyperbolic cooling towers and other shells of revolution. Some aspects of this work have been presented elsewhere[1,2] but are repeated here for clarity and continuity so that all essential steps can be discussed.

FINITE ELEMENT FORMULATION

A high-precision finite element procedure originally developed for the static analysis of arbitrarily loaded, thin elastic shells of revolution[3] has been generalized to include dynamic effects based on Hamilton's variational principle[4]. The element geometry, Fig. 2, is expressed in terms of the curvilinear coordinates φ and θ, and the displacements, rotations, and stress and moment resultants are defined as shown in Fig. 3.

With the shell discretized into n elements and the displacements and rotations taken in harmonic form in the circumferential direction and represented by high-order interpolation polynomials, the equations of motion, in the absence of surface loadings, take the form

$$\sum_{i=1}^{n} [K_i^{(j)}] \begin{Bmatrix} \delta_i^{(j)} \\ q_i^{(j)} \end{Bmatrix} + [C_i^{(j)}] \begin{Bmatrix} \dot{\delta}_i^{(j)} \\ \dot{q}_i^{(j)} \end{Bmatrix} + [M_i^{(j)}] \begin{Bmatrix} \ddot{\delta}_i^{(j)} \\ \ddot{q}_i^{(j)} \end{Bmatrix} = \{0\} \qquad (1)$$

in which

$[K_i^{(j)}]$, $[C_i^{(j)}]$, $[M_i^{(j)}]$ = element stiffness, viscous damping and consistent mass matrices for harmonic j; $\{\delta_i^{(j)}\}$, $\{q_i^{(j)}\}$ = element vectors of nodal displacements and higher order terms for harmonic j; and (˙) indicates differentiation with respect to time. The order of $\{q_i^{(j)}\}$ is equal to the number of coefficients in the displacement interpolation polynomials less the number of defined nodal displacements. In this formulation, since transverse shear and rotatory inertia effects are retained, $\{\delta_i^{(j)}\} = \{u_i^{(j)}\ v_i^{(j)}\ w_i^{(j)}\ \beta_{\varphi i}^{(j)}\ \beta_{\theta i}^{(j)}\}$ where the elements of $\{\delta_i^{(j)}\}$ are the Fourier coefficients for the corresponding displacements shown in Fig. 3.

From Eq. (1) it may be observed that the retention of variables $\{q_i^{(j)}\}$ in the formulation significantly increases the order of the stiffness and mass matrices, especially when higher order comparison functions are used to approximate the displacement field. Since the solution of the dynamic equations of motion for large systems involves significant computational effort, it is desirable to eliminate these variables prior to the actual solution. In the static case, the elimination of $\{q_i^{(j)}\}$ by static condensation resulted in a very efficient formulation[5]. For the dynamic case an analogous technique, kinematic condensation, can be applied. However, in contrast to the static technique, kinematic condensation is not exact. A rigorous development of this method is given by Geradin[6] assuming harmonic motion. The technique is further explored in Ref. 4 where it is shown that provided certain limitations on the order of the interpolation polynomials are observed, the vector $\{q_i^{(j)}\}$ and the corresponding terms of the stiffness and mass matrices may be condensed on the element level without appreciable loss of accuracy.

After assembly of the condensed element mass and stiffness matrices, the undamped free vibration equations follow as

$$\left([\bar{K}^{(j)}] - \omega^{(j)2} [\bar{M}^{(j)}] \right) \{\delta^{(j)}\} = 0 \qquad (2)$$

in which $\omega^{(j)}$ = circular natural frequency; $[\bar{K}^{(j)}]$, $[\bar{M}^{(j)}]$ = reduced global stiffness and mass matrices, and $\{\delta^{(j)}\}$ = global vector of nodal displacements.

The solution to Eq. 2 is accomplished using the EASI method as presented by Gupta[7]. The validity of the basic formulation was verified by comparisons of the free vibration response with several numerical and experimental studies found in the literature. The studies include shells of conical, cylindrical, hemispherical and hyperboloidal geometries with various idealized boundary conditions. In all cases very good results were obtained with comparatively few elements using cubic displacement polynomials[4].

An equivalent discrete elastic support element which is compatible with the rotational shell element is derived in Ref. 8. For this element, the axial and bending stiffness properties of the closely spaced columns are expressed in terms of the shell coordinates and then assumed to be uniformly distributed around the circumference. The elastic support element is then combined with regular shell elements to model the hyperboloidal geometry for the vibration analysis. Upon the completion of the dynamic analysis, the stress free condition between columns is enforced with a self-equilibrated edge loading[9,10]. The ring beam which is generally present as a transition between the columns and the shell proper, as shown in Fig. 1, is modeled using tapered rotational shell elements.

The earthquake excitation is assumed to be represented by uniform ground motion. Only the j = 0 harmonic and the j = 1 harmonic, for vertical and horizontal motion respectively, participate for linear elastic behavior.

It is convenient to separate $\{\delta^{(j)}\}$ into

$$\begin{Bmatrix} \delta_A^{(j)} \\ \delta_B^{(j)} \end{Bmatrix} = \begin{Bmatrix} y_A^{(j)} \\ y_B^{(j)} \end{Bmatrix} + \begin{Bmatrix} x_A^{(j)} \\ x_B^{(j)} \end{Bmatrix} \tag{3}$$

in which

$\{y^{(j)}\}$ = shell displacements due to uniform ground motion

$\{x^{(j)}\}$ = shell displacements relative to ground motion

and the subscripts A and B refer to coordinates above and at the base. The corresponding equations of motion, reduced by kinematic condensation and partitioned in accordance with Eq. 3, are

$$[\bar{K}_{AA}^{(j)}]\{x_A^{(j)}\} + [\bar{C}_{AA}^{(j)}]\{\dot{x}_A^{(j)}\} + [\bar{M}_{AA}^{(j)}]\{\ddot{x}_A^{(j)}\} = \{f^{(j)}(t)\} \tag{4}$$

in which

$$\{f^{(j)}(t)\} = -[\bar{K}_{AA}^{(j)}]\{y_A^{(j)}\} - [\bar{K}_{AB}^{(j)}]\{y_B^{(j)}\} - [\bar{C}_{AA}^{(j)}]\{\dot{y}_A^{(j)}\}$$
$$- [\bar{C}_{AB}^{(j)}]\{\dot{y}_B^{(j)}\} - [\bar{M}_{AA}^{(j)}]\{\ddot{y}_A^{(j)}\} - [\bar{M}_{AB}^{(j)}]\{\ddot{y}_B^{(j)}\} \tag{5}$$

and

$[\bar{C}_{AA}^{(j)}]$ = reduced viscous damping matrix.

In Eq. 5, the first two terms must cancel because they correspond to rigid body motion. Further the damping terms are generally small compared to the inertial terms and therefore will be neglected. The remaining terms may be expressed in terms of the uniform ground acceleration $\ddot{z}_g$ through a transformation between the Cartesian coordinates and the curvilinear coordinates as

$$f^{(j)}(t) = -\left([\bar{M}_{AA}^{(j)}]\{R_A^{(j)}\} - [\bar{M}_{AB}^{(j)}]\{R_B^{(j)}\}\right)\ddot{z}_g^{(j)} \tag{6}$$

For vertical ground motion, j = 0, only displacements u, w and β_φ need be retained and

$$\lfloor R_A^{(0)} \rfloor = \lfloor \sin\varphi_1 \; -\cos\varphi_1 \; 0 \ldots \sin\varphi_i \; -\cos\varphi_i \; 0 \ldots \sin\varphi_n \; -\cos\varphi_n \; 0 \rfloor$$
$$\lfloor R_B^{(0)} \rfloor = \lfloor \sin\varphi_{n+1} \; -\cos\varphi_{n+1} \; 0 \rfloor \tag{7a}$$

For horizontal ground motion, j = 1, all five displacements are present and

$$\lfloor R_A^{(1)} \rfloor = \lfloor -\cos\theta\cdot\cos\varphi_1 \;\; \sin\theta \;\; -\cos\theta\cdot\sin\varphi_1 \;\; 0 \;\; 0 \ldots -\cos\theta\cdot\cos\varphi_i \;\; \sin\theta \;\; -\cos\theta\cdot\sin\varphi_i \;\; 0 \;\; 0 \ldots -\cos\theta\cdot\cos\varphi_n \;\; \sin\theta \;\; -\cos\theta\cdot\sin\varphi_n \;\; 0 \;\; 0 \rfloor$$

$$\lfloor R_B^{(1)} \rfloor = \lfloor -\cos\theta\cdot\cos\varphi_{n+1} \;\; \sin\theta \;\; -\cos\theta\cdot\sin\varphi_{n+1} \;\; 0 \;\; 0 \rfloor \tag{7b}$$

In Eq. 7, φ_i indicates the meridional angle at node point i as shown in Fig. 2.

It is assumed that the damping matrix $[\tilde{C}_{AA}^{(j)}]$ is a linear combination of the stiffness and mass matrices and that

$$\{x_A^{(j)}\} = [\Phi^{(j)}]\,\{\eta^{(j)}(t)\} = [\{\varphi_i^{(j)}\}\ldots\{\varphi_k^{(j)}\}\ldots\{\varphi_n^{(j)}\}]\{\eta^{(j)}(t)\} \tag{8}$$

in which $[\Phi^{(j)}]$ = the mode shape vectors and $\{\eta^{(j)}(t)\}$ = the corresponding generalized coordinates. Then, the equations uncouple into

$$\sum_{k=1}^{n} \ddot{\eta}_k^{(j)} + 2\,\lambda_k^{(j)}\,\omega_k^{(j)}\,\dot{\eta}_k^{(j)} + \omega_k^{(j)2}\,\eta_k^{(j)} = \frac{P_k^{(j)}}{M_k^{(j)}}\;\ddot{z}_g^{(j)}(t) \tag{9}$$

in which

$$\omega_k^{(j)} = \left(\frac{K_k^{(j)}}{M_k^{(j)}}\right)^{1/2} = \text{circular natural frequency for mode k of harmonic j}$$

$$\lambda_k^{(j)} = \frac{C_k^{(j)}}{2\,\omega_k^{(j)}\,M_k^{(j)}} = \text{damping ratio for mode k of harmonic j} \tag{10}$$

and

$K_k^{(j)}$ = k$^{\underline{th}}$ term of generalized stiffness = $\lfloor \Phi_k^{(j)} \rfloor [\tilde{K}_{AA}^{(j)}] \{ \Phi_k^{(j)} \}$

$C_k^{(j)}$ = k$^{\underline{th}}$ term of generalized damping = $\lfloor \Phi_k^{(j)} \rfloor [\tilde{C}_{AA}^{(j)}] \{ \Phi_k^{(j)} \}$

$M_k^{(j)}$ = k$^{\underline{th}}$ term of generalized mass = $\lfloor \Phi_k^{(j)} \rfloor [\tilde{M}_{AA}^{(j)}] \{ \Phi_k^{(j)} \}$

$P_k^{(j)}$ = k$^{\underline{th}}$ term of generalized force = $\lfloor \Phi_k^{(j)} \rfloor \{f^{(j)}(t)\}$

The maximum value of the generalized coordinate $\eta_k^{(j)}(t)$ which corresponds to the j^{th} circumferential mode and k^{th} longitudinal mode is given by[1]

$$\left(\eta_k^{(j)}\right)_{max} = \rho_k^{(j)} \frac{S_{vk}}{\omega_k^{(j)}} \tag{11}$$

in which

$$\rho_k^{(j)} = \frac{P_k^{(j)}}{M_k^{(j)}} = \text{the participation factor for mode k of harmonic j}$$

and

$$S_{vk} = \text{the spectral velocity corresponding to } \omega_k^{(j)} \text{ and } \lambda_k^{(j)}$$

Then, the maximum relative displacements for each mode are

$$\left\{x_{Ak}^{(j)}\right\}_{max} = \left\{\varphi_k^{(j)}\right\} \left(\eta_k^{(j)}\right)_{max} \tag{12}$$

The total maximum displacement for harmonic j may be estimated by the absolute sum or the root-mean-square average of the displacements computed using $\left(\eta_k^{(j)}\right)_{max}$ for each term of vector $\eta^{(j)}(t)$ in Eq. 8.

NUMERICAL STUDIES

Free Vibration Analysis

To assess the effect of base flexibility in the case of a prototype tower, free vibration analyses were performed on a simplified model of the Trojan tower constructed in the western U.S.A.[11]. This cooling tower is about 450 ft. high with a throat diameter of 246 ft. and a base diameter of 365 ft. and is significantly larger than those which collapsed at the Ferrybridge power station in England[12]. The trend in recent tower construction indicates that similar or even larger towers will probably be built in the future.

Three different base conditions were considered in the analysis: (1) fixed base without ring beam; (2) flexible base without ring beam; and, (3) flexible base with ring beam. Some selected results for frequencies and mode shapes corresponding to different base conditions are given in Table 1 and Figure 4. It is seen that the base flexibility can have a significant effect on the results and therefore should be taken into consideration in the analysis. Generally speaking, the flexible base will reduce the natural frequencies and increase the displacements near the base. The ring beam, however, is observed to have comparatively little influence on either the frequencies or the mode shapes. This is further verified from a further analysis, Case 4, in which the thickness of the ring beam and the depth of the columns were increased nearly 1.7 times. The resulting natural frequencies shown in Table 1 and the mode shapes vary little from those of the previous case. Since, in the second analysis, the tangential stiffnesses of the columns were nearly the same as before while the bending stiffnesses in the normal direction were increased by three times, it is evident that the bending stiffness of the

columns has relatively little effect on the frequencies of the tower.

Displacements

A spectrum analysis for a horizontal earthquake (j=1) was performed on the first two cases previously described, fixed base and flexible base without ring beams. The design spectrum used is based on a .12g base acceleration and 4% damping. This spectrum was specified for the actual design of a representative large tower[13].

In Table 2, the generalized coordinates are computed for the first three modes (k=1,2,3) of the j=1 harmonic following Eq. 11. Figures 5-7 show both the absolute and root-mean-square combinations of the three modal responses. Again, the significance of the base flexibility on the dynamic displacements is evident.

Stresses

For the computation of stress resultants and couples, the kinematic relationships and constitutive law are incorporated and applied within the dynamic analysis. The vector of shell displacements for mode k of harmonic j, as given by Equation 12, consists of a discrete set of deflections and rotations at each nodal circle of the shell. For the computation of strains and changes in curvature, it is required to differentiate the displacements with respect to the spatial variables; the absence of internodal values precludes an accurate determination of these derivatives from $\{x_{Ak}^{(j)}\}_{max}$ alone. This is especially acute for the high-precision models under consideration here since the elements are relatively large and the nodes rather sparsely spaced so as to achieve the realized efficiency.

To obtain accurate values for the derivatives of the displacements, the comparison functions originally employed to represent the dependent

variables in the Ritz method solution of the variational problem should be used. The form of these polynomials is given elsewhere[4]; it is sufficient here to note that they contain excess coefficients over the basic number required to enforce the minimum C^o continuity at the nodes. To reduce the degrees-of-freedom in the eigenvalue problem and thereby achieve efficiency, these coefficients were eliminated by kinematic condensation. Therefore, following the eigenvalue solution of the reduced problem, the eliminated coefficients are recovered and back-substituted into the polynomials to provide continuous displacement functions which can subsequently be differentiated accurately[4]. Again, the kinematic and constitutive relationships are applied to the displacements on an individual mode basis and the final results obtained by an appropriate combination.

The column-supported-base boundary condition is modeled in two distinct stages. First, the properties of the column system are taken as uniformly distributed around the circumference in the dynamic analysis. The resulting stress resultants and couples are compared to corresponding values from a fixed base condition. These base conditions are designated continuous-flexible and continuous-fixed, respectively. Secondly, the discontinuous application of the individual column reactions is approximately accounted for by an additional static correction to the results from the continuous base dynamic analyses[8,9,10]. These corrected results are called the discrete-flexible and discrete-fixed conditions.

In Figures 8-11, selected results from both RMS and ABS combinations for the first three modes (k=1,2,3) of the j=1 harmonic are shown. The meridional stress resultant N_φ, shown in Figure 8, is about the same near the base for the continuous-fixed and continuous-flexible conditions with the RMS combination. On the other hand, the difference between the ABS

flexible and fixed base values is greater. Large differences between both the RMS and ABS comparisons of the fixed and flexible base results for N_θ, the circumferential stress resultant, are evident from Figure 9. The influence of the flexible base on the meridional and circumferential stress couples, M_φ and M_θ, respectively, is shown on Figures 10 and 11 and is particularly pronounced in the circumferential direction.

The discontinuous contact between the columns and the shell along the base is accounted for by the previously mentioned statical correction to the stress resultants and couples. It should be noted in this regard that a ring beam or transition section is generally provided to facilitate the distribution of the column reactions into the shell. The significant influence of this detail on the dynamic response of the shell has been discussed earlier. For the subsequent static correction which is being considered at present, the effect of the ring beam on the magnitude and distribution of the stress resultants and couples is not pronounced[8]. The thickened section, however, increases the capacity of the shell to resist the amplified forces and moments produced by the discontinuity and is therefore quite effective.

The comparative results from the discrete as opposed to the continuous base condition are conveniently shown by amplification factors, AF. For example,

$$AF\ (N_\varphi)_{flexible} = \left| \frac{(N_\varphi)_{discrete\text{-}flexible}}{(N_\varphi)_{continuous\text{-}flexible}} \right| \qquad (13)$$

These factors are shown for RMS combinations of k=1 and k=2 results for selected stress resultants and couples on Figures 12 and 13. Generally, the amplification factors for a given resultant or couple are much larger than the difference between the continuous-flexible and fixed base results. Along with the increased magnitude indicated by the rather large amplification factors, the extent of the penetration of the amplification into the

shell is quite important for design. For the example under consideration, the penetration of the amplified stress couples is particularly significant.

CONCLUSION

A dynamic analysis on a representative hyperbolic cooling tower shell using a high-precision curved rotational shell finite element indicates that the inclusion of the flexibility of the supporting columns significantly reduces the natural frequencies and increases the displacements. The effects of accurately representing the ring beam properties and the column bending flexibility appears minor as compared to the inclusion of the axial flexibility of the columns in the model. The incorporation of the flexible, discrete base model into the seismic analysis produces significantly different stress magnitudes and distributions as compared to an idealized fixed, continuous base condition. This emphasizes the desirability of realistically modeling the base region of such shells in a dynamic analysis.

ACKNOWLEDGMENT

This work was supported by National Science Foundation Grant No. GK-19779. The assistance of the Computer Facilities of Washington University, is also acknowledged.

1. Gould, P. L., Sen, S. K., and Suryoutomo, H.
"Dynamic Analysis of Column-Supported Hyperboloidal Shells", J. Earth. Engr. and Struct. Dynamics, Vol. 2, 1974, pp. 269-279.

2. Gould, P. L., Suryoutomo, H., and Sen, S. K.
"Stresses in Column-Supported Hyperboloidal Shells", J. Earth. Engr. and Struct. Dynamics (in press).

3. Brombolich, L. J. and Gould, P. L.
"A High-Precision Curved Shell Finite Element", Proceedings of the 12th Structure, Structural Dynamics and Materials Conference, AIAA, ASME, Anaheim, Calif., April, 1971, (Synoptic, AIAA Journal, Vol. 10, No. 6, June, 1972, pp. 722-728).

4. Sen, S. K. and Gould, P. L.
"Free Vibration of Shells of Revolution Using FEM", Journal of the Engineering Mechanics Division, ASCE, Vol. 100, No. EM 2, April, 1974, pp. 283-303.

5. Brombolich, L. J. and Gould, P. L.
"Finite Element Analysis of Shells of Revolution by Minimization of the Potential Energy Functional", Proceedings of the Symposium on Application of Finite Element Methods in Civil Engineering, Vanderbilt University, Nashville, Tennessee, 1969, pp. 279-307.

6. Geradin, M.
"Error Bounds for Eigenvalues Analysis by Elimination of Variables", Journal of Sound and Vibration, Vol. 19, 1971, pp. 111-132.

7. Gupta, K. K.
"Eigenproblem Solution by a Combined Sturm Sequence and Inverse Iteration Technique", Int. J. of Num. Meth. in Engrg., Vol. 7, 1973, pp. 17-42.

8. Sen, S. K. and Gould, P. L.
"Hyperboloidal Shells on Discrete Supports", Technical Note, Journal of the Structural Division, ASCE, Vol. 99, No. ST 3, March, 1973, pp. 595-603.

9. Gould, P. L. and Lee, S. L.
"Hyperboloids of Revolution Supported on Columns", Journal of the Engineering Mechanics Division, ASCE, Vol. 95, No. EM 5, October 1969, pp. 1083-1100.

10. Gould, P. L. and Lee, S. L.
"Column-Supported Hyperboloids under Wind Loading", Publications, International Association for Bridge and Structural Engineers, Zurich, Switzerland, 1971, pp. 47-64.

11. Billington, D. B.
"Design of Cooling Towers in the USA", Colloquium on Cooling Towers, International Association for Shell Structures, Brussels, Belgium, May 1971.

12. Central Electricity Generating Board (1966), Report of the Committee of Inquiry into Collapse of Cooling Towers at Ferrybridge, November 1, 1965, Her Majesty's Stationary Office, London.

13. Abel, J. F., Cole, P. P. and Billington, D. B. "Maximum Seismic Response of Cooling Towers", Research Report 73-SM-1, Dept. of Civil and Geological Engineering, Princeton University, March, 1973.

TABLE 1 NATURAL FREQUENCIES (Hz) for j = 1

Case	Base Condition	Mode 1	Mode 2
1	Fixed (no ring beam)	2.71	5.75
2	Flexible (no ring beam)	2.30	3.89
3	Flexible (ring beam)	2.33	3.83
4	Flexible (thicker ring beam)	2.35	3.75

TABLE 2 RESULTS OF RESPONSE SPECTRUM ANALYSIS

	Fixed Base				Flexible Base			
Mode	$\omega_k^{(1)}$	$\frac{\rho_k^{(1)}}{\omega_k^{(1)}}$	S_{vk} in/sec	$\eta_k^{(1)}$	$\omega_k^{(1)}$	$\frac{\rho_k^{(1)}}{\omega_k^{(1)}}$	S_{vk} in/sec	$\eta_k^{(1)}$
1	2.7087	0.0909	4.629	0.4207	2.2966	0.1078	5.092	0.5488
2	5.7513	0.0219	2.432	0.0532	3.8892	0.026	3.609	0.0921
3	9.1177	0.0126	1.237	0.0155	7.7279	0.0035	1.528	0.0013

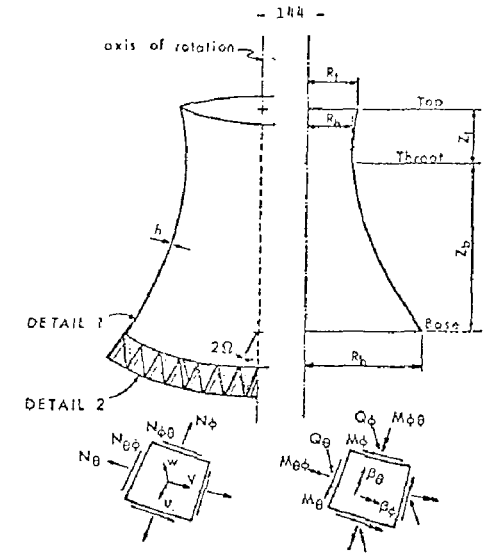

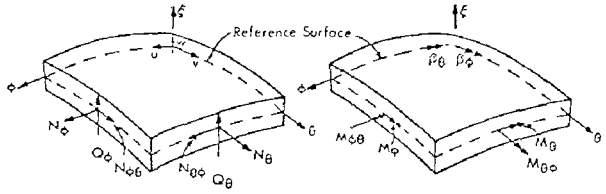

Figure 2. Stress Resultants and Displacements Acting on a Differential Shell Element.

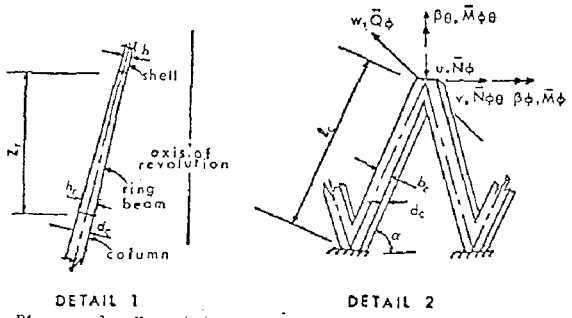

Figure 1. Hyperboloidal Shell on Column Supports.

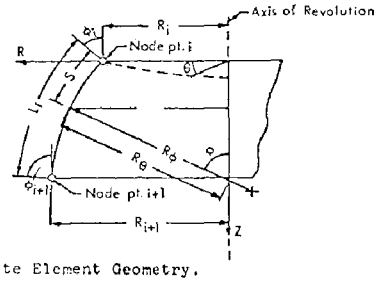

Figure 3. Finite Element Geometry.

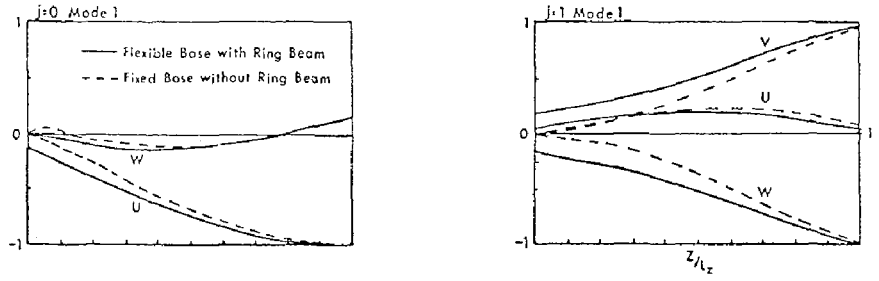

Figure 4. Mode Shapes for a Cooling Tower with Different Base Conditions.

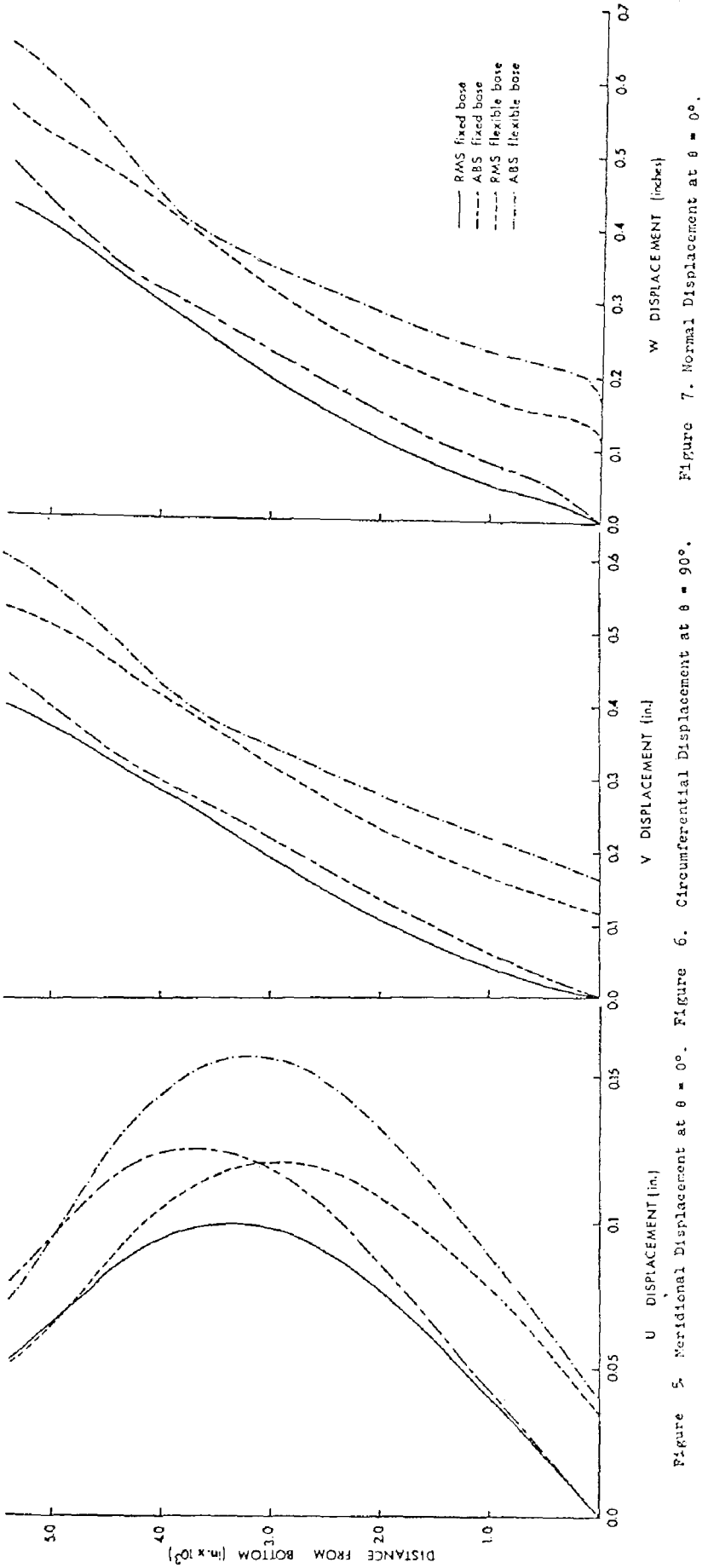

Figure 5. Meridional Displacement at θ = 0°. Figure 6. Circumferential Displacement at θ = 90°. Figure 7. Normal Displacement at θ = 0°.

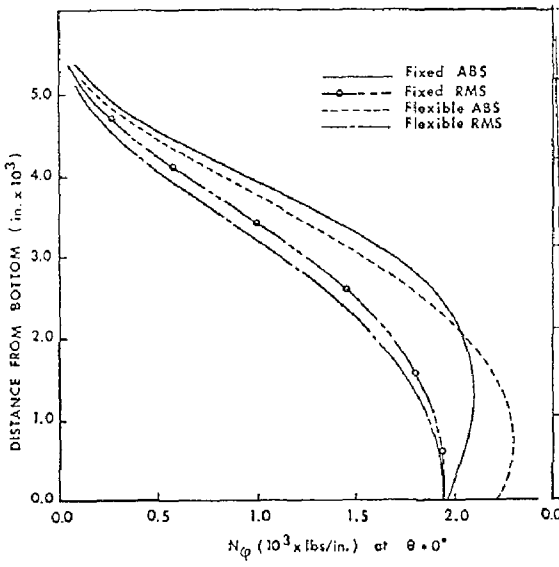

Figure 8

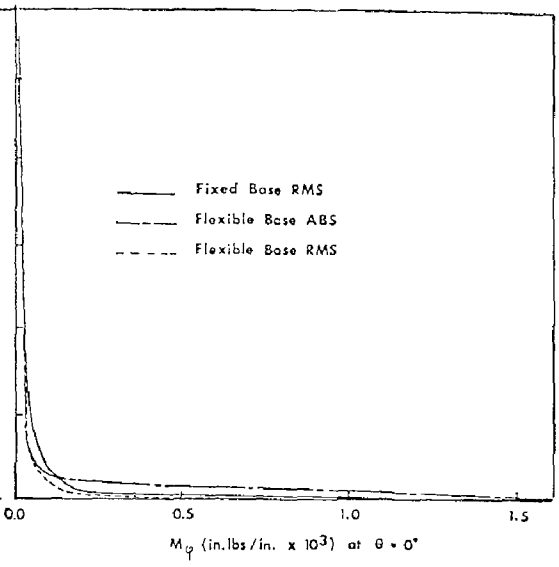

Figure 10

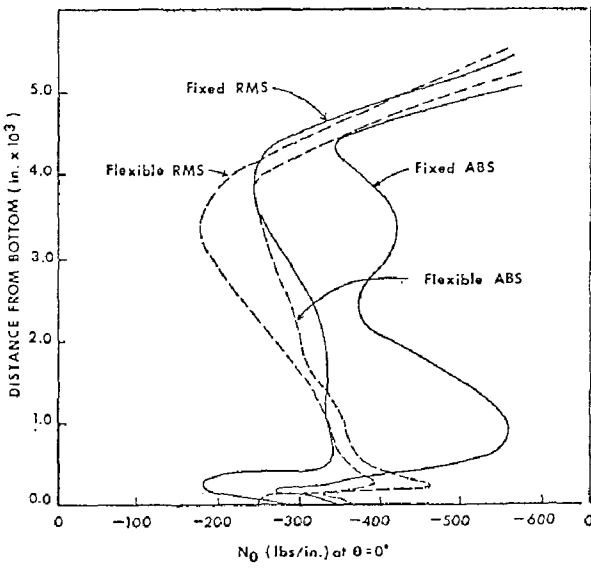

Figure 9

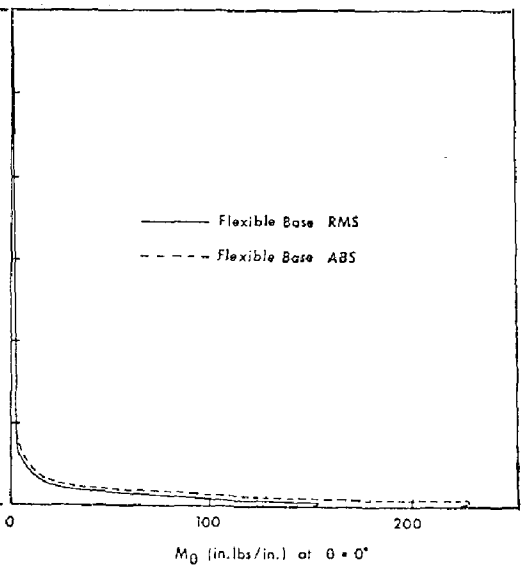

Figure 11

RESPONSE SPECTRUM ANALYSIS FOR DIFFERENT CONTINUOUS END CONDITIONS

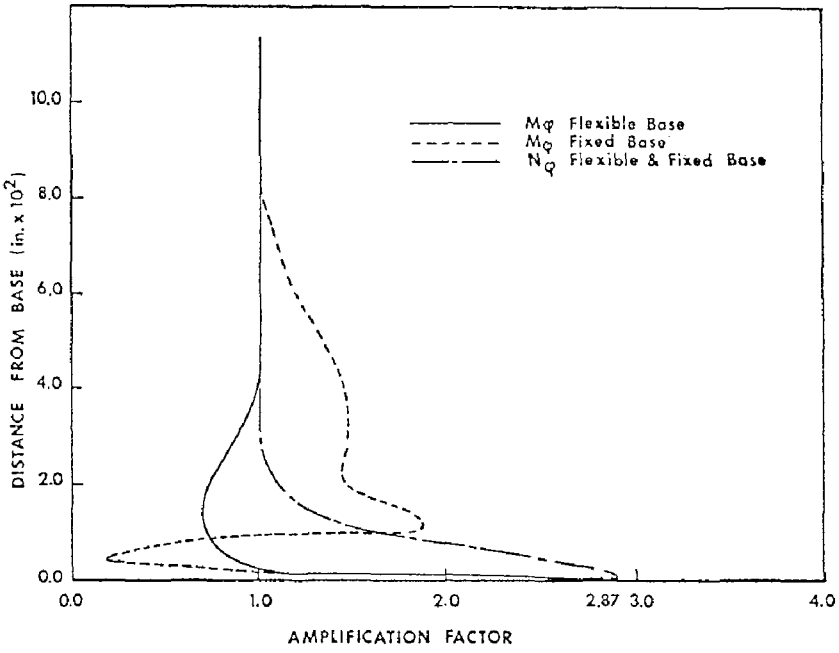

Figure 12 DISCRETE BOUNDARY RESPONSE SPECTRUM ANALYSIS

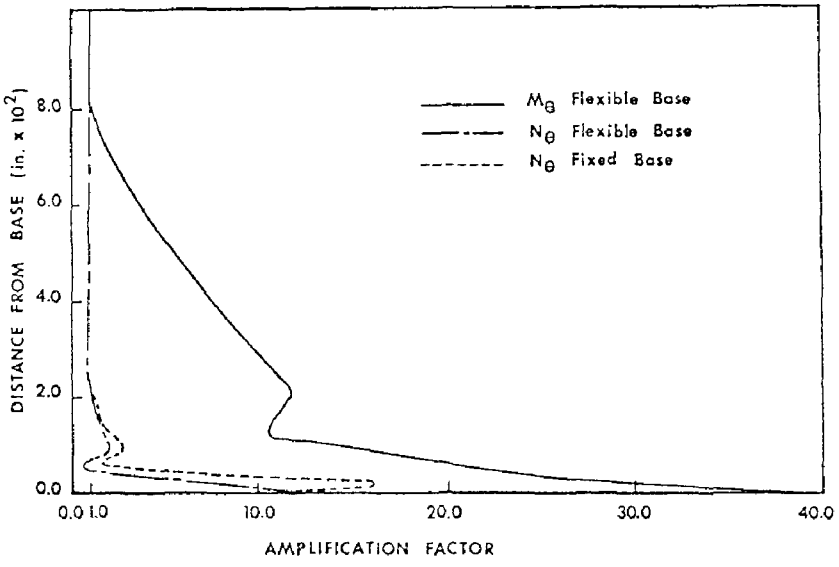

Figure 13 DISCRETE BOUNDARY RESPONSE SPECTRUM ANALYSIS

INTERNATIONAL SYMPOSIUM ON
EARTHQUAKE STRUCTURAL ENGINEERING
St. Louis, Missouri, USA, August, 1976

METHODOLOGY FOR INCORPORATING PARAMETER UNCERTAINTIES INTO SEISMIC HAZARD ANALYSIS FOR LOW RISK DESIGN INTENSITIES

Robin K. McGuire

Structural Engineer

U.S. Geological Survey

Denver, Colorado, U.S.A.

Summary

A methodology is described for incorporating into seismic risk analysis statistical uncertainties in the rate of earthquake occurrences, the maximum epicentral intensity, and the division of the study region into seismotectonic provinces. Using this methodology, a seismic risk analysis is performed for a chain of sites on the east coast of the United States between Florida and Maine. The Modified Mercalli intensity associated with an annual risk of 10^{-4} is found to be between VIII and IX for the sites considered. This result holds for a wide variety of hypothesized seismotectonic provinces. Also, at any given site the calculated intensity is not sensitive to the seismotectonic provinces adopted for the analysis. Further conclusions are that the available earthquake history is adequate to estimate accurately the recurrence rate of events but not the maximum possible epicentral intensity in typical seismotectonic provinces. Thus statistical uncertainty in the recurrence rate has a minor effect on design intensities, but uncertainty in the upper bound intensity of provinces must be accounted for explicitly. At Modified Mercalli intensity levels of interest, annual risks at a site change by approximately a factor of 6 for a change of one unit in intensity level. Thus the Modified Mercalli intensities associated with annual risks of 10^{-6} are between X and XII for the sites considered.

Introduction

The incorporation of parameter uncertainties into seismic risk analysis procedures has been proposed and illustrated by several authors (Esteva, 1969; Veneziano, 1975). Parameter uncertainties are especially important in areas of low seismicity when design intensities associated with high reliability (low probability of being equaled or exceeded) are sought. To date no comprehensive study of seismic risk for many sites along the east coast of the United States has been reported which incorporates uncertainties in seismic source area hypothesis, activity rate, and maximum energy release. Such a study is the purpose of the research reported here.

Throughout this study, Modified Mercalli (M.M.) intensity is used as the measure of ground shaking and of earthquake size. M.M. intensity is taken to be a continuous, rather than a discrete, random variable; results for the discrete variable are easily drawn from those of the continuous variable. Conclusions regarding the effect of parameter uncertainties on design ground motions are not affected by the use of M.M. intensity in the risk analysis.

Data for the study consisted of a catalog of 467 events occurring between 1534 and 1974 in the United States and Canada east of longitude 95°W, for which epicentral M.M. intensities between V and XII had been assigned. This catalog was obtained by removing obvious aftershocks from a larger data set. The data are plotted on a map of the Eastern United States in figure 1; at locations where several epicenters are listed, only the largest M.M. intensity has been plotted.

Parameters for Risk Analysis

Several parameters are required for seismic risk analysis at a site. These are the specification of seismic source areas or seismotectonic provinces within which the earthquake occurrence process may be treated as spatially and temporally homogeneous, the mean rate of occurrence of events in each source area, the relative distribution of earthquakes of different sizes, the largest event possible (largest epicentral intensity) in each area, and the attenuation function describing the transmission of motion from source to site.

In this analysis the distribution of epicentral intensities is taken to be exponential, below some limiting intensity (to be discussed). This distribution has been used by several authors (Chinnery and Rogers, 1973; Cornell and Merz, 1975), and is consistent with a linear log number versus magnitude relation (Richter, 1958) and a linear relation between magnitude and epicentral intensity (Gutenberg and Richter, 1956). The b value describing the slope of the log number versus epicentral intensity relation was estimated using the entire earthquake catalog by plotting the annual rate of earthquakes observed at each intensity level versus intensity, on semi-logarithmic paper. The length of time used for calculating the rate of each intensity level was taken to be the length of time over which reporting of that level was thought to be complete. The value obtained for b was 0.57, identical to that reported by Chinnery and Rogers (1973) for New England data. A smaller value for b reported by Cornell and Merz (1975) for Eastern Massachusetts events is due at least in part to incomplete reporting of the lower intensities. This b value of 0.57 was used for all seismic source areas in this study.

Several alternate hypotheses were examined for specification of source areas within which the earthquake recurrence process can be considered spatially and temporally homogeneous. The first hypothesis is based on the assumption that seismicity within the entire Eastern United States is uniformly distributed, i.e. that areas of high or low rate of occurrence cannot be distinguished, and that events of M.M. intensity up to XII can occur anywhere. The area used to calculate the occurrence rate under this hypothesis is shown in figure 1.

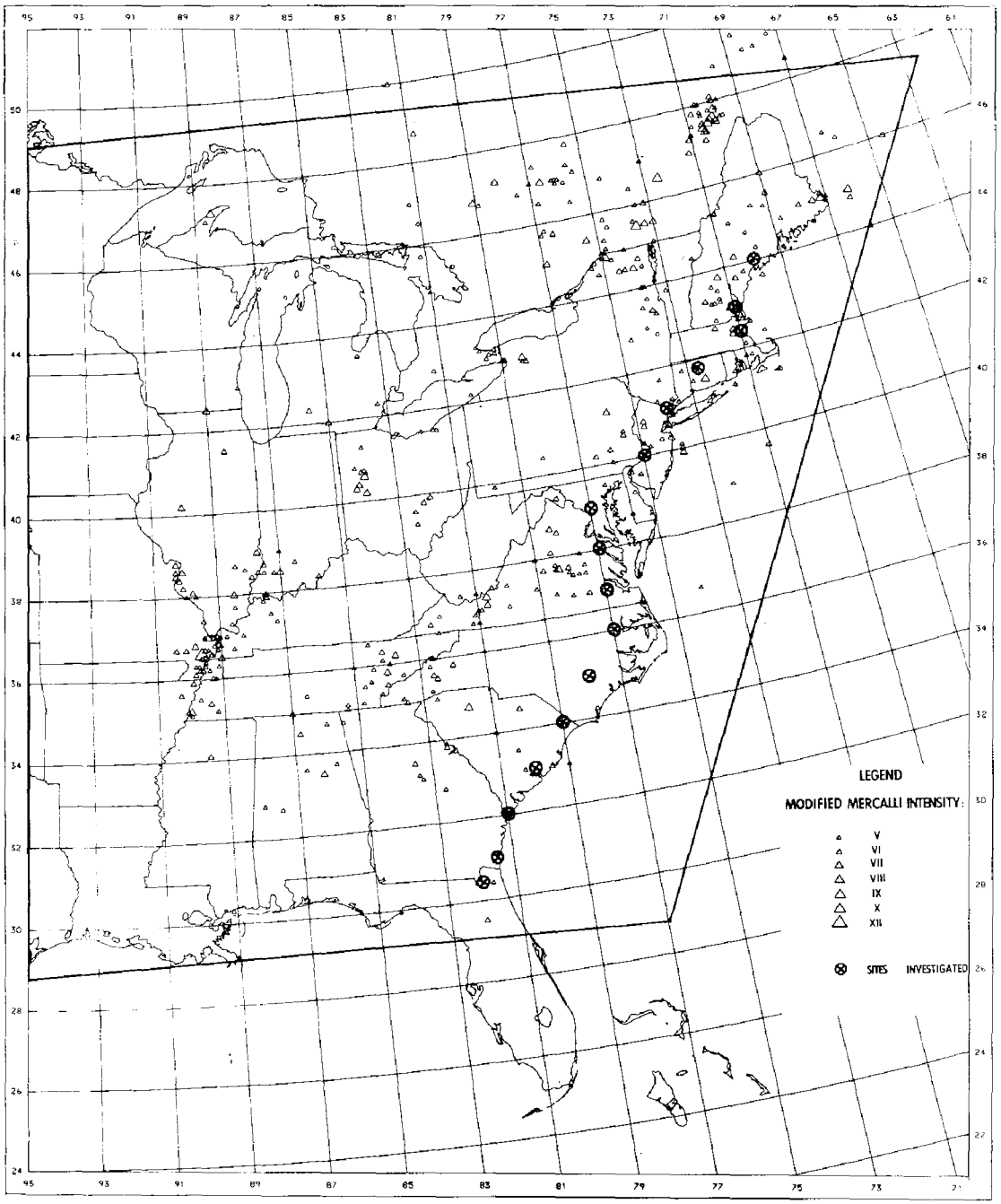

FIGURE 1

Earthquake epicenters, single source area,
and sites examined

A second hypothesis for the specification of source areas examined is that used in a recent seismic risk study of the United States (Algermissen and Perkins, written communication). These source areas were determined using historical seismicity and available geologic and tectonic evidence, and are shown in figure 2.

The third hypothesis used to specify source areas was derived from a seismotectonic map of the Eastern United States (Hadley and Devine, 1974). Again, this seismotectonic map was compiled by interpretation of historic seismicity and tectonic data. The source areas used in this study, derived from the Hadley and Devine map, are shown in figure 3. Some slight modifications of the areas as originally published by Hadley and Devine were required for computer input, such as the use of straight line segments rather than curves to define area boundaries. These changes in no way affect the results or conclusions reached in this study.

Under each of the three hypotheses, the earthquake recurrence process is assumed to be spatially homogeneous for each source area. The rate of occurrence and maximum epicentral M.M. intensity are determined from the historical events which have been observed within the source area.

The occurrence-rate of events with epicentral M.M. intensity greater than or equal to V, and the maximum intensity possible, were treated as random variables. Earthquakes were assumed to occur as Poisson arrivals; this process has been found to describe adequately the occurrence of large events when aftershocks are disregarded (Lomnitz, 1966, 1973; Gardner and Knopoff, 1974). With the further assumption that sizes of successive events are independent, and with the exponential distribution on epicentral M.M. intensity I_e, the joint likelihood function of the mean rate of occurrence ν of intensities i_o or greater and the maximum epicentral M.M. intensity I_m, given observations of intensity $i_1, i_2, \ldots i_n$ in time τ, is (Raiffa and Schlaifer, 1961; Benjamin and Cornell, 1970)

$$L(\nu, I_m | i_1, i_2, \ldots i_n \text{ in } \tau) = P[i_1, i_2, \ldots i_n \text{ in } \tau | \nu, I_m]$$

$$= P[n \text{ in } \tau | \nu] \quad P[i_1, i_2, \ldots i_n | I_m]$$

$$= \frac{e^{-\nu\tau}(\nu\tau)^n}{n!} \frac{\beta^n \exp(n\beta i_0 - \beta \sum_{j=1}^{n} i_j)}{(1-\exp(-\beta(I_m - i_0)))^n} \qquad (1)$$

where $\beta = b \ln 10$, i_0 is the lower bound intensity, here taken (as a continuous variable) equal to 5.0, and $I_m \geq i_1, i_2, \ldots i_n$.

From the form of equation (1), it is apparent that, given the n observations in time τ, ν and I_m are independent. Thus the joint likelihood function for ν and I_m is the product of the individual likelihood functions which may be considered separately.

From the likelihood function for ν it is possible to determine the effect of statistical uncertainty in this parameter on the risk calculated at a site

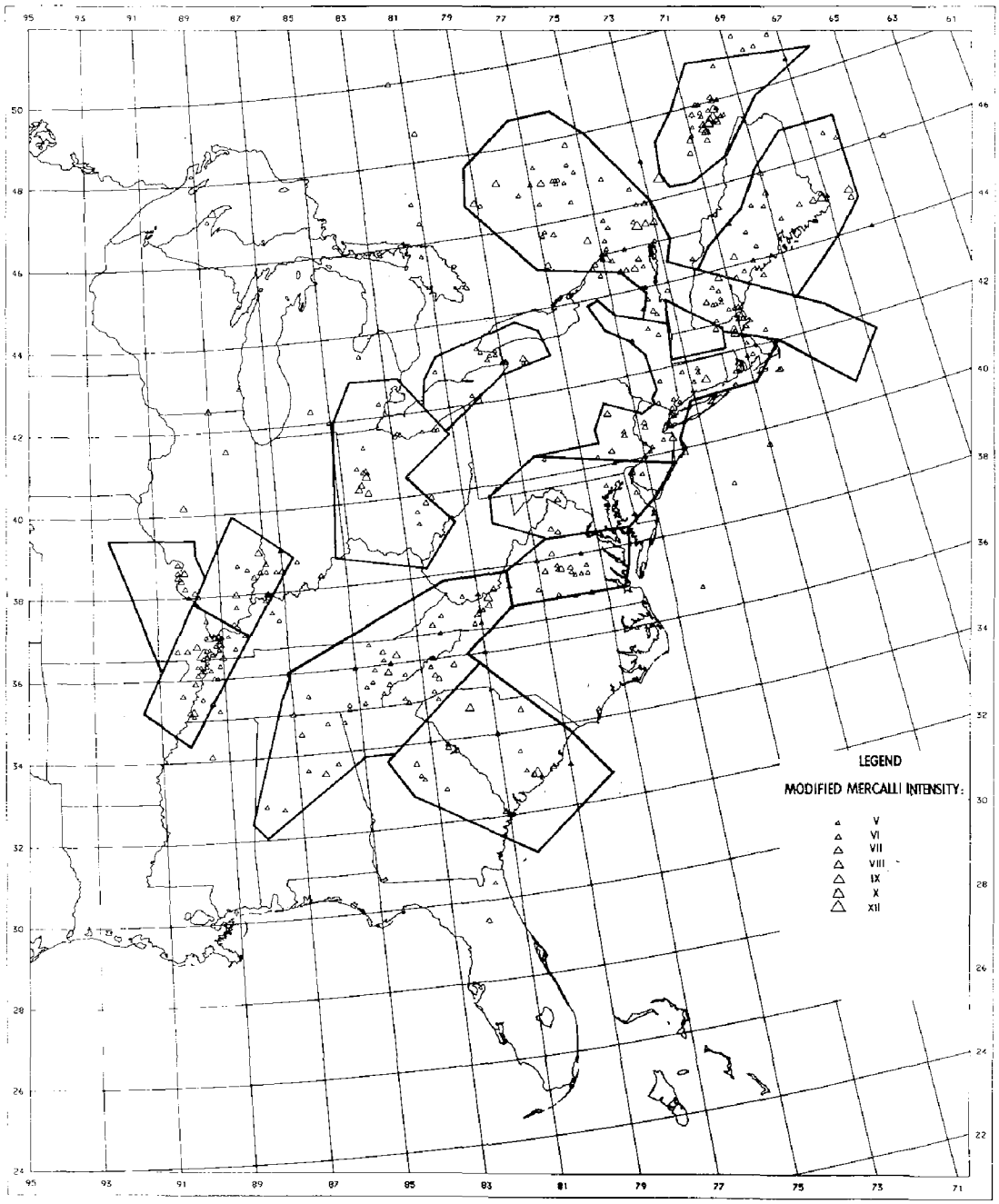

FIGURE 2

Seismic source areas after Algermissen and Perkins

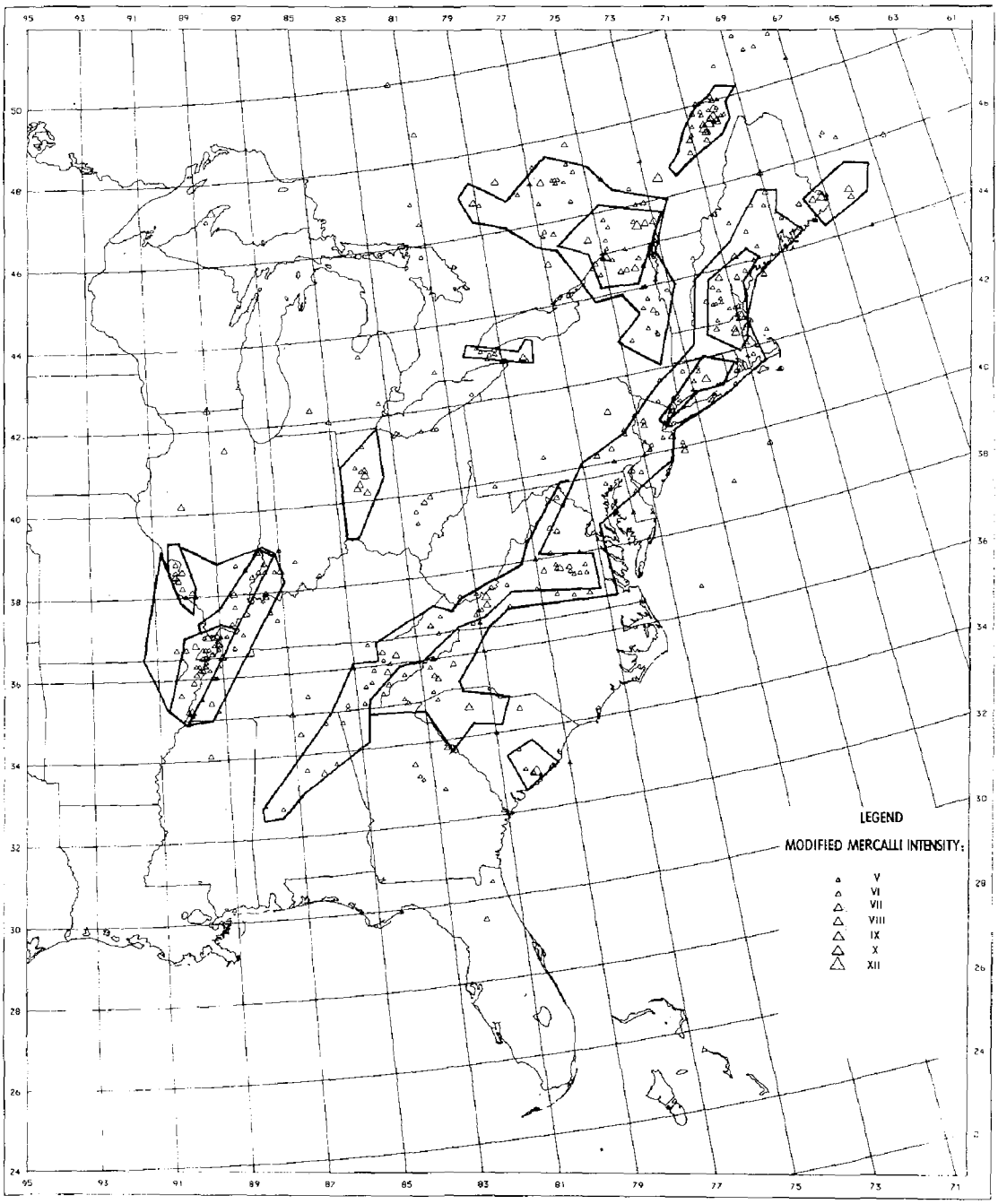

FIGURE 3

Seismic source areas after seismotectonic map
of Hadley and Devine (1974)

for a chosen intensity level. The density function for ν is obtained by normalizing the likelihood function so that the integral over ν from 0 to ∞ unity. This gives

$$f_\nu(\nu)= \frac{\tau}{n!} \quad e^{-\nu\tau}(\nu\tau)^n \tag{2}$$

Let $G_1(i_s)$ be the complementary-cumulative probability for intensity i_s at a site from a single event of random intensity and location in a source area. Under the Poisson process assumption, if ν is known exactly, the complementary-cumulative distribution of the maximum site intensity in time t is (Benjamin and Cornell, 1970)

$$G_{max}(i_s)=1-\exp(-\nu t G_1(i_s)) \tag{3}$$

Uncertainty in the rate ν can be accounted for by multiplying the right side of equation (3) by the density function on ν and integrating over all values, yielding

$$G_{max}(i_s)=1-\left[\frac{\tau}{\tau+t\ G_1(i_s)}\right]^{n+1} \tag{4}$$

For the values of n, τ, t, and G_1 of interest in this study it is easily shown that the ratio of risk given by equation (4) to that given by (3) is approximately 1+1/n. The term 1/n thus indicates the increase in risk due to uncertainty in the rate of occurrence of events. For n as small as 5, there is only a 20% increase in the calculated risk using equation (4) rather than (3). As shall be shown, an increase of 20% in risk results in a very small change in the design intensity associated with that risk. From this point of view there certainly have been enough earthquakes recorded in the Eastern United States to define rates of occurrence in seismotectonic provinces, for the purposes of calculating design intensities through risk analysis.

For the practical case when the catalog is considered complete for varying lengths of time for different intensity levels, a similar analysis is straightforward. Equation (4) may be used to account for statistical variability in ν, replacing n by $n_1+n_2+n_3+\ldots$ and τ by $\tau_1+p_2\tau_2+p_3\tau_3+\ldots$, where n_1 is the number of events in time τ_1 during which the lowest intensity level is considered complete, n_2 is the number of events during the previous time τ_2 during which the next higher intensity is considered complete, and p_2 is the probability of observing an event of the second intensity level or greater given that an event occurs, and so on. The effect of accounting for statistical variation in ν thus is plainly not sensitive to the length of time during which the upper intensity levels are assumed complete.

From the likelihood function for maximum epicentral intensity I_m, the degree to which I_m is accurately determined by historical events may be examined. From equation (1), the likelihood function for I_m is:

$$L(I_m | i_1, i_2, \ldots i_n \text{ in } \tau) = (1-\exp^{(-\beta(I_m - i_0))})^{-n} \qquad (5)$$

where, again, $I_m \geq i_1, i_2, \ldots i_n$. Corresponding results are easily derivable when the various intensities are complete for different time periods. Assuming that the largest event possible is associated with M.M. intensity XII, the value of the likelihood function at this largest intensity is very close to unity. For any given source area and associated historic seismicity, the value of $L(I_m | i_1, \ldots i_n \text{ in } \tau)$ evaluated at I_m equal to the maximum observed intensity indicates the likelihood (relative to intensity XII) that the maximum observed intensity is in fact the maximum intensity possible in that source area.

Values for $L(I_m | i_1, \ldots i_n \text{ in } \tau)$ were calculated at the maximum observed intensity for the source areas studied here (as described above). The majority of values obtained were less than 1.50; in general the values were less than 2.0. (Some values greater than 2.0 were obtained for Hadley-Devine source areas which were drawn specifically to exclude events of M.M. intensity greater than VI.) The conclusion is that, for most source areas, the observed maximum M.M. intensity does not have much greater likelihood than higher intensities, up to and including intensity XII, of being the maximum intensity possible in the region. Although the maximum observed intensity is always most likely to be the maximum possible intensity in a source area, the probability that this hypothesis is correct is on the order of 0.2 for many source areas. Thus, it is not justifiable statistically to take the maximum observed intensity as the maximum possible intensity, for all source areas. This, of course, does not deny the possibility of excluding larger intensities on geologic or tectonic bases.

The likelihood function for I_m, equation (5), could be used to generate a density function with which alternate hypotheses for I_m could be weighted to calculate risk at a site. However, when different lengths of complete records for different intensity levels are accounted for, it is found that the actual value of $L(I_m)$ (and hence of the density function) at the maximum observed intensity level is highly sensitive to the assumed completeness of the historic record for the larger intensities. Thus, to avoid the subjectivity associated with estimating the length of the complete record for the larger intensity levels, it is appropriate to assume a uniform distribution on I_m between the maximum observed intensity and XII. This assumption is always conservative, and in most cases is very accurate because the largest contribution to the total risk comes from (weighted) hypotheses that the maximum intensity is X, XI, or XII; the weights used for these hypotheses are not sensitive to the assumed length of completeness of the record, when the maximum observed intensity is VII, VIII, or IX. The uniform distribution on I_m is adopted in this study.

The attenuation function used here was derived from 783 intensity reports from the 1886 Charleston, South Carolina, earthquake (Bollinger, 1976). The resulting equation for mean site intensity I_s is:

$$\begin{aligned} I_s &= I_e + 3.08 - 1.34 \ln \Delta \qquad \Delta \geq 10 \text{ km} \\ I_s &= I_e \qquad \Delta < 10 \text{ km} \end{aligned} \qquad (6)$$

where Δ is epicentral distance in km and I_e is epicentral intensity. In figure 4, equation (6) is compared to several other attenuation relations

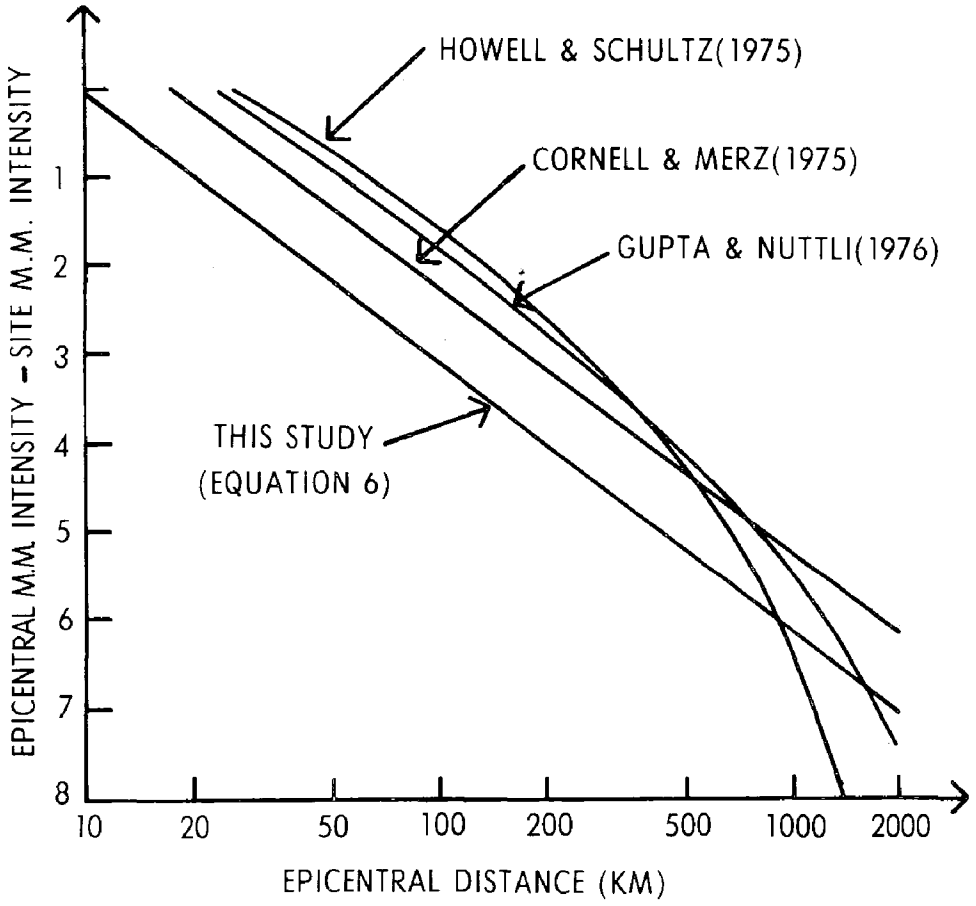

FIGURE 4

Epicentral M.M. intensity minus site M.M. intensity, as a function of epicentral distance; several reported relations for the central and eastern U.S., and the relation used in this study

reported for the Central and Eastern United States. For epicentral distances less than 500 km, the slopes of the various equations are approximately the same; equation (6) lies 1 to 1.5 intensity units below the other relations because these others were derived using distances to isoseismals rather than individual intensity reports. Use of the individual reports is the appropriate method to predict intensities at a site. From examination of residuals about equation (6), it is found that scatter in the attenuation relation can be modeled using the normal distribution with a standard deviation of 1.19 intensity units. There is no apparent upper truncation in the residual distribution, at least up to 3.5 standard deviations above the predicted value; in the risk analysis, the distribution

of residuals is truncated so that site intensities cannot be greater than the epicentral intensity. This implies the assumption (which is not critical) that the epicentral intensity is the maximum intensity observed.

Risk Analysis

Risk analysis was performed at sites on the east coast to determine the annual probability that each of several M.M. intensity levels will be equaled or exceeded, using a computer program to perform the calculations (McGuire, 1976). The method used is described elsewhere in detail (Cornell, 1968, 1971; McGuire, 1974). Briefly, the risk associated with a chosen intensity level at a site is calculated by summing the risk due to all events affecting the site, using the attenuation equation (6) to quantify the decrease with distance of expected intensity level from source to site. The risks corresponding to several intensity levels were examined at each site; the sites investigated are shown in figure 1. A separate analysis was performed for each of the source area hypotheses shown in figure 1, 2, and 3. Under each hypothesis, the seismicity was assigned to each area according to the events in the catalog within that area. For the areas shown in figures 2 and 3, the events which did not lie in any source area were treated as "background seismicity;" the observed maximum intensity and rate per unit area were obtained from these background events and were used to define the seismicity not associated with discrete source areas.

For each source area and for background seismicity, the activity rate and maximum intensity were treated probabilistically, as described above. Thus the occurrence of an event with M.M. intensity XII was considered possible at all locations, for all source area hypotheses. (For the source areas of figures 2 and 3, the probability of occurrence of this event varied greatly from one location to another, due to differences in the occurrence rate and maximum observed intensity.)

Results

Figure 5 shows the annual risks associated with equaling or exceeding several levels of intensity, for several sites and the various source area hypotheses. (The risk associated with a discrete M.M. intensity level of, say, VII, corresponds to the risk shown on the continuous scale of figure 5 at level 7.0.) The risk versus intensity curve for the source area of figure 1 is the same for all sites; this results from the uniform seismicity assumed throughout the region.

The curves in figure 5 have approximately the same slope. This is expected for this analysis, because the slope is proportional to the b value (Veneziano, 1975) and this has been assumed identical for all source areas.

The slope of the curves in figure 5 provides some insight into the sensitivity of design intensities to the associated levels of risk. Changing the risk by a factor of 2 will change the corresponding design intensity by only about 0.4 intensity units. Thus, the effect of statistical variation in the occurrence rate for, say, seismicity defined by only five observations is to increase the risk by 20% over that computed for a rate without accounting for statistical variation; the corresponding

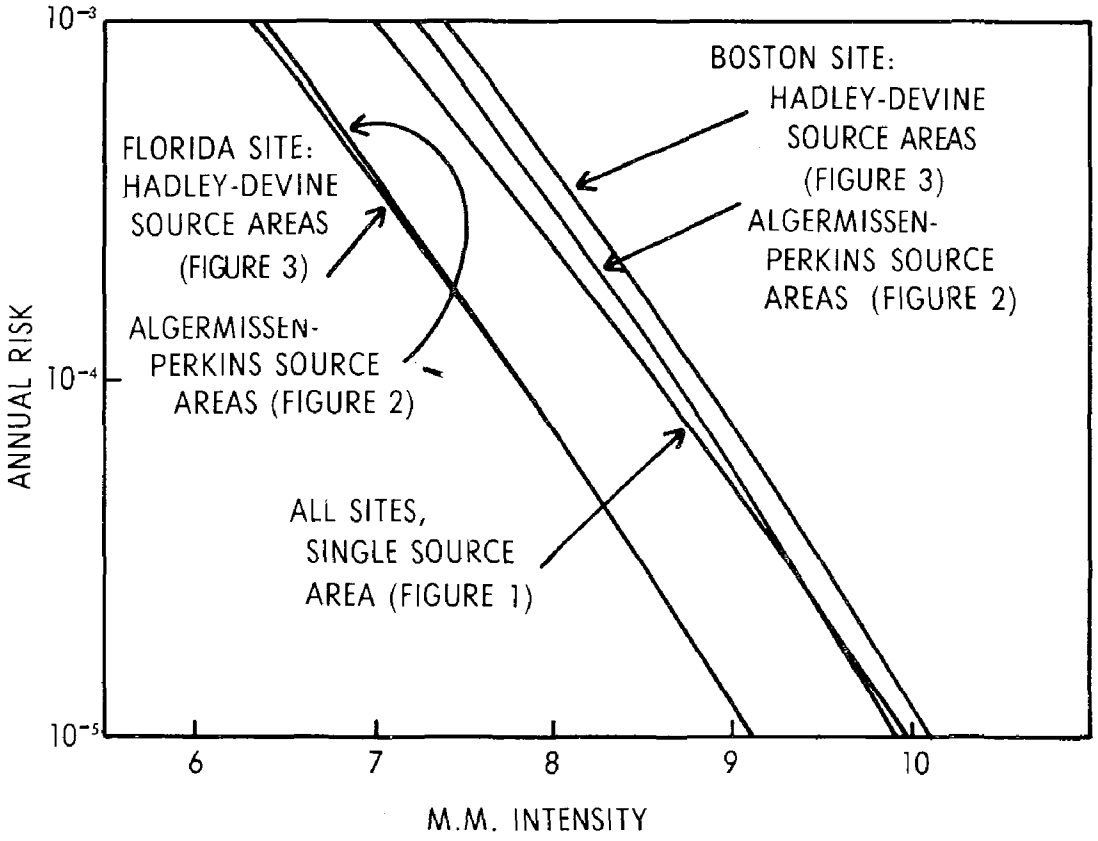

FIGURE 5

Risk versus intensity curves for several sites and source area hypotheses

increase in the design intensity (at whatever risk level is chosen) is about 0.1 intensity units. For the source areas examined in this study, each area encompassed more than five earthquakes in the catalog. Thus statistical uncertainty in the recurrence rate has a very minor effect on the design intensity level. Similarly, any other variation of hypothesis which changes the calculated risk at a site by 20% will change the corresponding design intensity by 0.1 units.

Figure 6 shows the M.M. intensities associated with a risk of 10^{-4} per year for the sites shown in figure 1 and for the three source area hypotheses of figures 1, 2, and 3. The most striking observation about this comparison is the closeness of intensities at most sites for the different hypotheses used. The range in intensities under the three hypotheses is less than 0.35 intensity units for the majority of sites, and in no case is it greater than 0.75 units. It is evident from figure 5 that the range of intensities at a site will not change for risk levels other than 10^{-4} per year; the curves of figure 6 simply shift up or down for smaller or larger risks, respectively.

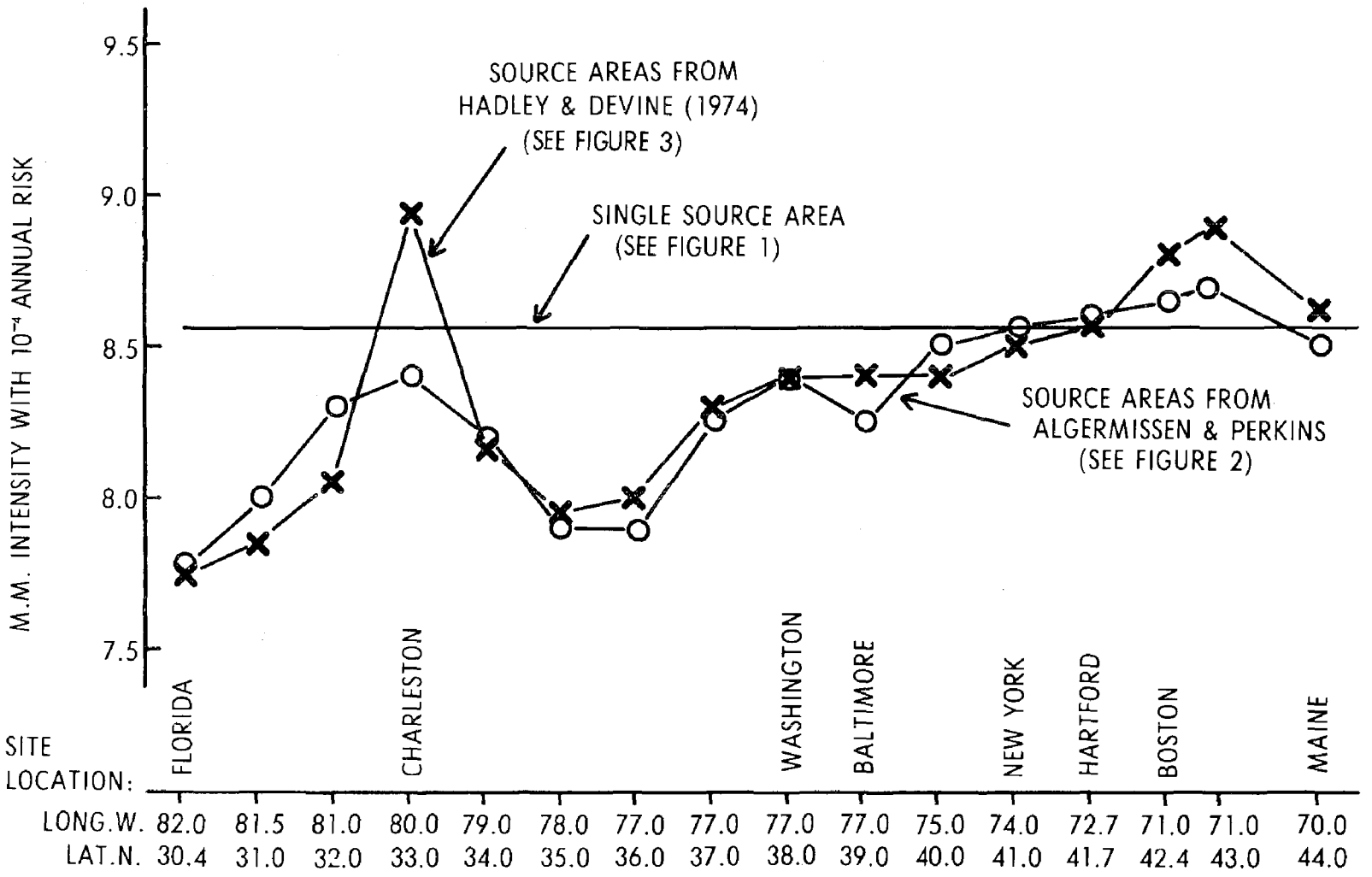

FIGURE 6

M.M. Intensity with annual risk of 10^{-4} for sites on the east coast of the U.S., under various source area hypotheses

The reason for this closeness in intensities at any given risk level is that the various source area hypotheses do not result in large changes in seismicity, as this seismicity affects risk analysis. Again, the insensitivity of intensity levels to changes in risk is important; changing rates of occurrence by a factor of 2 (by using an alternate set of source areas) will change risks at any intensity by a factor of 2, but will change design intensities (at a given risk level) by only 0.4 intensity units. Also, the effect of high occurrence rates (per unit area) in the articulated source areas of figures 2 and 3 (as compared to that of the single source area in figure 1) is partially offset by accounting for the possibility of maximum M.M. intensities less than XII in these articulated source areas.

This insensitivity of design intensity to the source areas used to define seismicity must not be considered a conclusion of universal applicability for all sites in the Eastern United States. Design intensities will usually vary most at a site in a region which is considered highly seismic under one hypothesis and aseismic under another. In such cases, it is always possible to assign subjective probabilities to each hypothesis (e.g. Cornell and Merz, 1975) and to weigh the conditional risks to obtain the total risk at various intensity levels. This procedure will always give a design intensity which lies within the range of the intensities indicated by the individual hypotheses.

The advantage, however, of using risk analysis is that, for many sites, design intensities produced by the method are not sensitive to the exact geometry of the source areas used to define seismicity. The Algermissen-Perkins source areas of figure 2 were derived independently from those of Hadley and Devine (figure 3), and the two sets of areas look quite different. Yet the site design intensities (associated with a chosen risk level) for each interpretation of seismic history and geology are virtually identical (except at Charleston where the difference is one-half intensity unit). Even the comparison between these discrete source areas and the single source area of figure 1 shows little difference in design intensities. Thus, arguments concerning which source area hypothesis best represents the "correct" set of seismotectonic provinces can be avoided for most sites, as the precise choice of source area geometry does not greatly affect design intensities for a given risk level.

A further advantage of the statistical treatment of upper bound intensity is that the intensity associated with a chosen risk level at a site is insensitive to the maximum intensity observed in the hypothesized source areas. For the sites examined here, and for the source areas of figures 2 and 3, altering the maximum observed intensity in each source area by one intensity unit would change the intensity associated with an annual risk of 10^{-4} by approximately 0.1 intensity unit. Thus, arguments about the precise intensity of some historical earthquake which was the largest observed event in a zone would have minor importance, since the design intensity would not be sensitive to this largest value. In contrast, under the deterministic procedure of designing for the largest observed intensity, changing this intensity by one unit will change the design intensity by one unit.

Conclusions

The primary conclusion from this study is that, using a risk analysis procedure which accounts for uncertainty in activity rates and maximum possible intensities of seismic source areas, the M.M. intensity associated with a chosen level of risk at many sites on the east coast of the U.S. is not sensitive to the source areas used to represent seismicity. This allows many alternate methods to be used to combine geology, tectonics, and seismic history to draw source areas, without greatly affecting design intensities at many sites. For other sites in the Eastern United States, the geometry of source areas may be critical; this needs further investigation.

From this study, it is evident that as few as five or ten earthquake observations are adequate to define the occurrence rate in an area, for the purpose of deriving risk-associated design intensities. The seismic history of the Eastern United States is not, however, adequate to define accurately the maximum possible intensity in chosen source areas. In the absence of geologic or tectonic evidence which would limit the size of events in the area, it is logical and conservative to assume a uniform distribution on the maximum possible M.M. intensity, between the maximum observed value and XII.

This analysis places in perspective many of the objections to using probabilistic analysis to determine seismic design levels. In general there is sufficient information, in terms of seismic history and geology, to produce seismic design values at very small levels of risk, given the present understanding of the physical processes governing earthquake occurrences in the Eastern United States. Furthermore the results obtained here provide a means of evaluating the conservativeness and consistency (in terms of risk) of deterministic analyses which assume that the maximum epicentral intensity possible in an area is the maximum intensity which has been observed in recorded history.

References

Benjamin, J. R., and Cornell, C. A., Probability, Statistics, and Decision for Civil Engineers, McGraw-Hill, New York, 1970.

Bollinger, G. A., "Reinterpretation of the Intensity Data for the 1886 Charleston, South Carolina, Earthquake," submitted to Bull. Seis. Soc. Am. for publication, 1976.

Chinnery, M. A., and Rogers, D. A., "Earthquake Statistics in Southern New England," Earthquake Notes, Vol. XLIV, Nos. 3-4, pp 89-103, July-Dec., 1973.

Cornell, C. A., "Engineering Seismic Risk Analysis," Bull. Seis. Soc. Am. Vol. 58, No. 5, pp 1583-1606, October, 1968.

Cornell, C. A., "Probabalistic Analysis of Damage to Structures Under Seismic Load," Chapter 27 in Dynamic Waves in Civil Engineering, ed. by D. A. Howells, I. P. Haigh, and C. Taylor, Wiley Interscience, London, pp 473-488, 1971.

Cornell, C. A., and Merz, H. A., "Seismic Risk Analysis of Boston", Journal of the Structural Division, ASCE, Vol. 101, No. ST10, pp 2027-2043, October, 1975.

Esteva, L., "Seismicity Prediction: A Bayesian Approach," Proceedings, 4th W.C.E.E., Vol. 1, Santiago, Chile, 1969.

Gardner, J. K., and Knopoff, L., "Is the Sequence of Earthquakes in Southern California, with Aftershocks Removed, Poissonian," Bull. Seis. Soc. Am., Vol. 64, No. 5, pp 1363-1368, October, 1974.

Gupta, I. N., and Nuttli, O. W., "Spatial Attenuation of Intensities for Central U.S. Earthquakes," Bull. Seis. Soc. Am., Vol. 65, No. 3, in press, July, 1976.

Gutenburg, B., and Richter, C. F., "Earthquake Magnitude, Intensity, Energy, and Acceleration (Second Paper)," Bull. Seis. Soc. Am., Vol. 46, No. 2, pp 105-145, April 1956.

Hadley, J. F., and Devine, J. F., "Seismotectonic Map of the Eastern United States," U.S. Geological Survey, Miscellaneous Field Study MF-620, 1974.

Howell, B. F., Jr., and Schultz, T. R., "Attenuation of Modified Mercalli Intensity with Distance from the Epicenter," Bull. Seis. Soc. Am., Vol. 65, No. 2, pp 651-665, June, 1975.

Lomnitz, C., "Statistical Prediction of Earthquakes," Reviews of Geophysics, Vol. 4, No. 3, August, 1966.

Lomnitz, C., "Poisson Processes in Earthquake Studies," Bull. Seis. Soc. Am., Vol. 63, No. 2, pp 735, April, 1973.

McGuire, R. K., "Seismic Structural Response Risk Analysis, Incorporating Peak Response Regressions on Earthquake Magnitude and Distance," M.I.T. Dept. of Civil Engineering, Report R74-51, August, 1974.

McGuire, R. K., "Fortran Computer Program for Seismic Risk Analysis," U.S. Geological Survey, Open-File Report 76-67, January, 1976.

Raiffa, H., and Schlaifer, R., Applied Statistical Decision Theory, M.I.T. Press, Cambridge, 1961.

Richter, C. F., Elementary Seismology, W. H. Freeman and Co., San Francisco, 1958.

Veneziano, D., "Probabalistic and Statistical Models for Seismic Risk Analysis," M.I.T. Dept. of Civil Engineering, Report No. 21, June, 1975.

INTERNATIONAL SYMPOSIUM ON
EARTHQUAKE STRUCTURAL ENGINEERING
St. Louis, Missouri, USA, August, 1976

EPOXY REPAIR OF STRUCTURES*

JOSEPH M. PLECNIK
Assistant Professor in Civil Engineering
California State University, Long Beach
Long Beach, Calif., USA

JAMES E. AMRHEIN
Director of Engineering
Masonry Institute of America
Los Angeles, Calif., USA

WILLIAM H. JAY
Graduate Research Assistant
California State University, Long Beach
Long Beach, Calif., USA

JAMES WARNER
Warner Engineering Services
Los Angeles, Calif., USA

SUMMARY

This paper presents a brief review of a portion of the experimental results obtained in the Structures Laboratory at California State University, Long Beach. The results deal with the behavior of epoxy repaired structural masonry elements subjected to static and dynamic (seismic) load conditions. The conclusions show that damaged concrete masonry structural elements properly repaired with various epoxy adhesive materials are essentially restored to the strength levels which existed prior to sustained damage. Furthermore, several aspects concerning epoxy repair procedures are discussed in relation to their effects on the strength of the repaired structural elements. Lastly, presented in the following text are experimental results demonstrating the behavior and strength properties of epoxy repaired structural masonry elements.

* Research sponsored in part by the National Science Foundation under Contract ENG 75-11292.

INTRODUCTION

The use of epoxy materials for repair of structures was introduced before 1960 (1). However, extensive structural repair in California utilizing epoxy materials did not occur until after the 1971 San Fernando Earthquake. This earthquake damaged a considerable number of concrete and concrete masonry structures in the Los Angeles area. Many of these damaged structures have been or are presently being repaired with epoxy compounds (2). The current research project briefly described herein has concentrated on two specific types of epoxy materials widely used for structural repair in California.

Epoxy materials represent a wide range of chemical polymers that may be mixed with various organic or inorganic additives, the resulting materials providing extremely diverse physical properties (1,3,4,5,6). A particular group of epoxy adhesive systems with compressive strengths of approximately 3 to 8 times that of concrete have been developed for structural repair purposes (4). Aside from ultimate strength, the viscosity of the epoxy adhesive is of particular importance in the repair process. Therefore, two commonly used high and low viscosity epoxy adhesives are discussed in this report.*

The low viscosity epoxy material designated as Delta Plastics' LV 17-9044 general purpose epoxy adhesive possesses compressive and tensile strengths of 1,200 kg/cm^2 and 700 kg/cm^2 respectively at 20° C. The viscosity of this adhesive is approximately 450 cps at 20° C (4). As for most epoxies, these and other physical properties are significantly affected by the ambient temperature conditions. The high viscosity epoxy material designated as Delta Plastics' TM 15-7018 epoxy adhesive system for structural bonding applications has approximately the same compressive and tensile strengths as the LV material but with approximate viscosity of 15,000 cps at 20° C.

The unique advantages of structural epoxy repair techniques include (a) minimum total repair costs on some projects, (b) minimum loss of utilization time of the damaged structure, (c) minimum or no change in architectural and aesthetic features of structures, and (d) restoration to the original design strength of a properly epoxy repaired structure. The primary disadvantages of epoxy repair techniques include (a) sensitivity of epoxy adhesives to temperature and (b) lack of knowledge concerning the behavior of epoxy repaired structures subject to seismic loading and adverse environmental conditions.

INJECTION OF EPOXY ADHESIVES

Epoxy injection techniques for structural repair may be divided into two categories based on mixing procedure. The first technique involves pre-mixing the epoxy resin and hardener in a container followed by injec-

---

* All epoxy adhesives described in this report were provided by Delta Plastics Company, Visalia, California.

tion using a common caulking gun or a specially fitted pressure pot similar to those used in spray painting. The second technique includes a pumping system required to generate sufficient injection pressure for full penetration and a continuous mixing unit where the epoxy resin and hardener are combined, mixed and immediately injected. Ref. 8 provides an excellent discussion on this latter injection technique.

Both of the above injection techniques are employed in this research project. The epoxy resin and hardener must be mixed according to predetermined volume or weight ratio in order to assure complete curing. Such designed mixing ratios can be achieved readily in the pre-mixing injection technique; however, considerable care and experienced work crews appear to be essential in the continuous mixing injection technique. Pre-mixing techniques are more time-consuming than continuous mixing techniques. References 1 and 2 provide additional discussion on practical aspects concerning injection of epoxy adhesives into structures.

Verification of full penetration of epoxy adhesives into cracks is presently accomplished by standard core sampling methods. Core samples are, at best, a statistical verification rather than an assurance of full penetration and complete curing. All specimens repaired with LV epoxy in this research project are checked for void formations and curing utilizing high intensity light source since the LV epoxy is nearly transluscent. This method is highly efficient and practical for laboratory purposes but not useful for crack formations normally found in structures. Therefore, x-ray techniques are presently being investigated. X-ray techniques have been attempted on the repair of the 26-story Los Angeles City Hall structure with good technical results; however, the economics of this method are often discouraging (4). Moreover, x-ray techniques may fail to detect uncured epoxy regions.

SPECIMEN DESIGN AND BOND, SHEAR AND TENSILE STRENGTH RESULTS

To investigate the static and dynamic strength properties of epoxy repaired concrete masonry structures, a series of experimental tests have been devised. The tests involve small scale specimens consisting of individual components within the masonry wall matrix including block, mortar and grout. Figures 1,2, and 3 provide schematic diagrams of the three masonry wall components experimentally investigated in this research program.

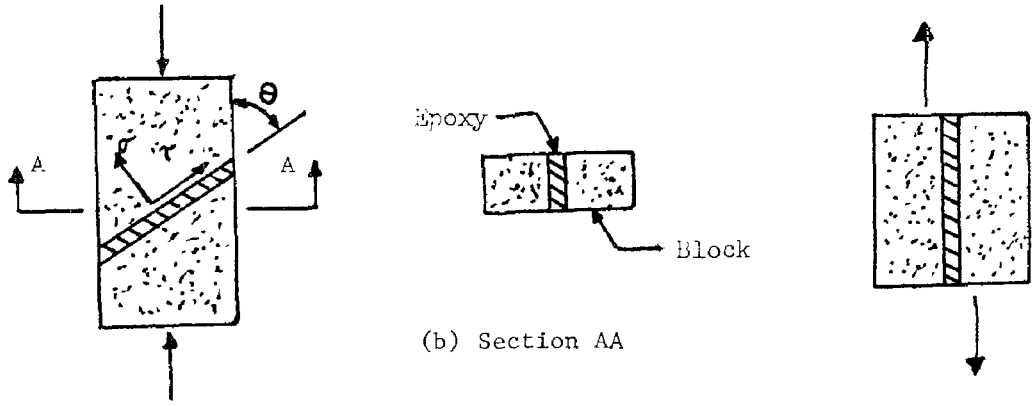

(a) Compression Loading (b) Section AA (c) Direct Shear Loading

Fig. 1 Epoxy Repaired Block Specimens

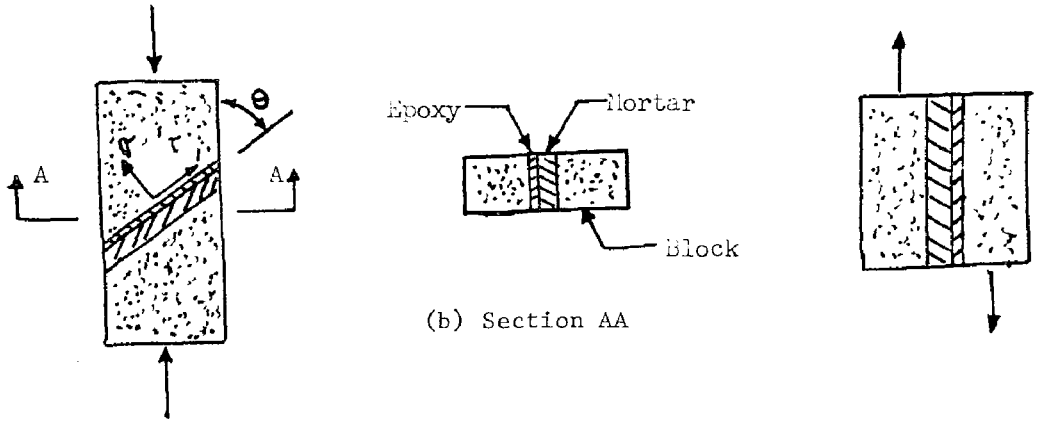

(a) Compression Loading (b) Section AA (c) Direct Shear Loading

Fig. 2 Epoxy Repaired Block Joint Specimens

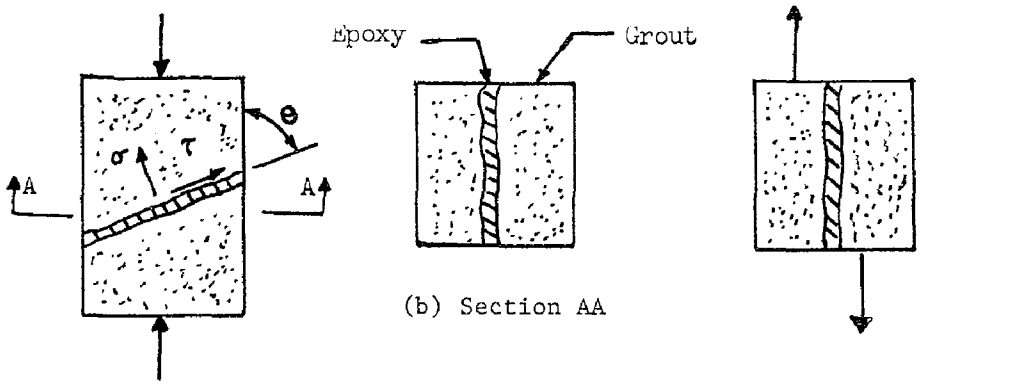

Fig. 3 Epoxy Repaired Grout Specimens

The epoxy injected cracks were created in most specimens by a rotary carbide saw. The sawed surfaces were thoroughly washed in water and subjected to high air pressures in order to dislodge all loose material. This procedure produced crack surfaces very similar to the irregular crack surfaces encountered in damaged structures. With sound irregular crack surfaces, epoxy bond strength was sufficient for nearly all specimens including direct shear tests. The tensile strength of the epoxy materials described earlier was much greater than the tensile strength of such structural materials as block, mortar, grout, and concrete. Therefore, the tensile strength of properly epoxy repaired specimens was determined by the tensile strength of the structural material for both static and dynamic load conditions.

Direct shear loading tests illustrated in Figures 1,2, and 3 likewise demonstrate that the direct shear strength of properly epoxy repaired concrete masonry structures is determined by the shear strength of the structural material. Ref. 9 provides a complete summary of all test procedures and experimental results. The compressive strength results will be discussed later in this paper.

CURING OF EPOXY ADHESIVES

All specimens were constructed, stored, and tested under normal laboratory conditions. Mortar and grout specimens were tested approximately 90 days after casting. All experimental tests on the epoxy repaired specimens were performed at least seven days after epoxy injection. Care during epoxy injection and specimen construction was exercised in order to simulate as closely as possible the actual field conditions.

As noted earlier, proper and complete curing of epoxy resin and hardener is achieved only if the volume or weight ratio of these two components is maintained according to specified limits. Therefore, several possible conditions causing deviation in specified limits are here discussed. First, mixing according to specified ratios is of extreme importance. For the pre-mixing injection technique only carelessness can result in erroneous ratios. However, the continuous injection technique requires diligent and experienced crews in order to insure proper ratios. Second, the low viscosity epoxy adhesive may experience minor segregation of either the epoxy resin or hardener. For example, the density of the low viscosity epoxy hardener is approximately 12% less than that of the epoxy resin. After mixing the amber colored hardener with the colorless epoxy resin, slight segregation is observed. These two factors may explain why nearly 7% of all low viscosity epoxy repaired specimens contained uncured areas ranging from negligible percentage to approximately 8% of the total crack area. Such uncured regions reduce effective stress area and create stress concentrations resulting in reduced strength capacities of up to 15%.

Additional stress concentrations and reduced effective stress areas may also be created by absorption of epoxy adhesive into the structural material resulting in appreciable void formations. Such void formations were never observed for high viscosity epoxy adhesives but were observed in approximately 6% of all specimens injected with low viscosity material. The highly viscous material was not readily absorbed into the cracked surfaces; hence, void formations were not likely to occur after injection was completed. For low viscosity epoxy adhesive, absorption to depths of up to 5 mm were observed. Since the absorption process continued after injection was completed, void formations most likely occurred. Additional void formations resulted from trapped or disolved air bubbles, although the structural significance of such minute air bubbles appeared to be negligible.

The above paragraphs indicate the importance of choosing appropriate epoxy adhesives for specific applications. Possible occurrance of reduced effective stress areas and stress concentrations should be considered when selecting epoxy adhesives. The optimum viscosity for structural repair is a function of many variables including crack size, relative difference in temperature between epoxy and structural materials, speed of injection, and injection pressures (8,9). Other physical properties such as wetting capabilities, surface tension, pot life and reactivity to damp surfaces must also be considered when selecting epoxy adhesives for specific applications. These latter properties are usually supplied by the epoxy manufacturer (4,5).

SIMULATED SEISMIC LOAD PATTERNS

Due to the vast difference in physical properties of epoxy repaired concrete masonry or concrete structures, considerable care must be exercised in selecting experimental load patterns for simulation of the seismic response of epoxy repaired structures. Sinusoidal function with frequencies ranging from 2 to 5 hertz are rather common in laboratory experiments (10). However, the simulation of the almost random variation of the amplitudes in the response spectra is a subject of considerable

debate, especially where epoxy materials are also present.

Based on the fracture and impact properties of plastics and epoxy adhesives, a linearly increasing sinusoidal amplitude for applied experimental loads was chosen as shown in Fig. 4. Initial stress, σ_o = 105.5 kg/cm^2 was applied to all compression tests described in Figures 1, 2, and 3. This value was selected for the purpose of producing compression failure in all experimental tests between the sixth and twelfth stress cycles.

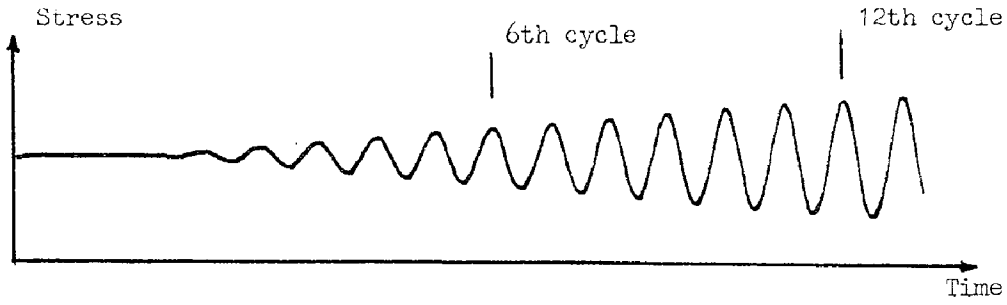

Fig. 4 Dynamic Load Pattern (3 hertz)

FRACTURE AND IMPACT PROPERTIES

Impact properties (Izod test) of epoxy materials at 20° C vary from below 0.020 kg-m/cm for rigid epoxy adhesives to above 1.10 kg-m/cm for flexible epoxy sealing materials (3,4,11). Fracture studies on structural epoxies apparently are not available; however, extensive fracture studies have been performed on many common polymers such as polymethylmethacrylate (PMMA) and polystyrene (11,12,13,14). These studies show that for most strain rates little or no correlation is possible between impact and fracture properties of polymers. Since epoxy adhesives are considered as polymers, it is logical to assume that fracture properties such as crack behavior cannot be derived from impact test results. Additional research is essential before such conclusions can be experimentally substantiated.

For the low viscosity epoxy materials described earlier, the listed Izod impact test value is 0.022 kg-m/cm (4). Observations of epoxy fractured surfaces also show characteristics of brittle behavior. Ultimate fracture stress for no pre-crazed dumb-bell crystal polystyrene test specimens at 25° C is approximately 640 kg/cm^2 (15). Such fracture stress values are not available for epoxy materials described herein. However, in comparing physical properties of crystal polystyrene (Izod impact strength of about 0.027 kg-m/cm at 20° C) with the epoxy materials, the probable ultimate fracture strength of epoxy materials described herein is greater than the ultimate tensile strength of concrete ($6\sqrt{f'c}$ to $7\sqrt{f'c}$) or concrete masonry. This conclusion is substantiated by experimental results since fracture was never initiated in the epoxy material where bonding problems were not encountered (9). Once initiated, fracture usually propagates across the epoxy repaired crack.

COMPRESSION TEST RESULTS

Tables 1, 2, and 3 provide a summary of partial compression test results conducted on epoxy repaired masonry components. Approximately 120 compression tests described in Figs. 1, 2, and 3 were conducted under static and dynamic test conditions. Slight debonding occurred in only two specimens. Uncured epoxy material and void formations due to absorption were important factors in reduction of ultimate strength capacities. Extensive care was excercised to assure full penetration of the epoxy material.

TABLE I

Compression Block Rib Test Results

Specimen Number	Crack Angle (Degrees)	Epoxy Type	Crack Width(cm)	Test Condition	Max. Applied Stress(kg/cm^2)
B1*	90	TM	.25	Static	184.63
B2	90	TM	.25	Static	167.13
B3	90	LV	.25	Static	182.31
B4	90	LV	.25	Static	153.06
B5	90	TM	.05	Dynamic	236.24
B6	90	TM	.05	Dynamic	238.35
B8	90	LV	.05	Dynamic	237.79
B9	90	TM	.25	Dynamic	234.84
B10	90	TM	.25	Dynamic	198.27
B11	90	LV	.25	Dynamic	273.65
B12	90	LV	.25	Dynamic	249.39
B13	75	TM	.25	Static	216.55
B14	75	TM	.25	Static	212.34
B15	75	LV	.25	Static	229.28
B16	75	LV	.25	Static	186.88
B17	75	TM	.05	Dynamic	188.43
B18	75	TM	.05	Dynamic	242.43
B19	75	LV	.05	Dynamic	247.28
B20	75	LV	.05	Dynamic	251.43
B21	75	TM	.25	Dynamic	247.28
B22	75	TM	.25	Dynamic	251.43
B23	75	LV	.25	Static	205.66
B24	75	LV	.25	Dynamic	260.50
B25	60	TM	.25	Static	180.70
B26	60	TM	.25	Static	196.87
B27	60	LV	.25	Static	171.06
B28	60	LV	.25	Static	167.97
B30	60	TM	.05	Dynamic	185.62
B31	60	LV	.05	Dynamic	260.15
B32	60	LV	.05	Dynamic	279.76
B33	60	TM	.25	Dynamic	281.80
B34	60	TM	.25	Dynamic	252.83
B35	60	LV	.25	Dynamic	251.08
B36	60	LV	.25	Dynamic	250.23
B37	90	TM	.25	Dynamic	256.77

* The letter B denotes block rib specimens.

TABLE 2

Compression Grout Test Results

Specimen Number	Crack Angle (Degrees)	Epoxy Type	Crack Width(cm)	Test Condition	Max. Applied Stress(kg/cm^2)
G1*	90	TM	.25	Static	150.25
G2	90	TM	.25	Static	147.65
G3	90	LV	.25	Dynamic	162.06
G4	90	LV	.25	Static	128.67
G5	90	TM	.05	Dynamic	162.13
G6	90	TM	.05	Dynamic	222.18
G7	90	LV	.05	Dynamic	222.18
G9	90	TM	.25	Dynamic	174.37
G10	90	TM	.25	Dynamic	222.74
G11	90	LV	.25	Dynamic	223.59
G12	90	LV	.25	Dynamic	234.13
G13	75	TM	.25	Static	163.82
G14	75	TM	.25	Static	163.82
G15	75	LV	.25	Static	162.77
G16	75	LV	.25	Static	246.09
G17	75	TM	.05	Dynamic	223.23
G18	75	TM	.05	Dynamic	174.72
G19	75	LV	.05	Dynamic	162.56
G20	75	LV	.05	Dynamic	223.30
G21	75	TM	.25	Dynamic	161.71
G22	75	TM	.25	Static	246.09
G23	75	LV	.25	Dynamic	221.69
G24	75	LV	.25	Dynamic	198.98
G25	60	TM	.25	Static	256.56
G26	60	TM	.25	Static	227.80
G29	60	TM	.05	Dynamic	186.18
G30	60	TM	.05	Dynamic	221.48
G31	60	LV	.05	Dynamic	232.02
G32	60	LV	.05	Dynamic	233.99
G33	60	TM	.25	Dynamic	186.32
G34	60	TM	.25	Dynamic	196.45
G35	60	LV	.25	Static	201.37
G36	60	LV	.25	Dynamic	198.98

* The letter G denotes grout specimens.

TABLE 3

Compression Block Joint Test Results

Specimen Number	Crack Angle (Degrees)	Epoxy Type	Crack Width(cm)	Test Condition	Max. Applied Stress(kg/cm^2)
J1*	90	TM	.25	Static	131.48
J2	90	TM	.25	Static	103.36
J3	90	LV	.25	Static	145.61
J4	90	LV	.25	Static	165.23
J7	90	TM	.25	Static	157.99
J10	90	TM	.05	Dynamic	174.58
J11	90	TM	.05	Dynamic	208.75
J12	90	LV	.05	Dynamic	226.40
J14	90	TM	.25	Dynamic	194.34
J15	90	TM	.25	Dynamic	190.33
J16	90	LV	.25	Dynamic	231.32
J17	90	LV	.25	Dynamic	241.80
J18	75	TM	.25	Static	185.62
J19	75	TM	.25	Static	162.42
J20	75	LV	.25	Static	132.67
J21	75	LV	.25	Static	163.26
J24	75	TM	.25	Dynamic	206.01
J27	75	TM	.05	Dynamic	216.55
J28	75	TM	.05	Dynamic	228.72
J29	75	LV	.05	Dynamic	247.98
J31	75	TM	.25	Dynamic	193.35
J32	75	TM	.25	Dynamic	209.52
J33	75	LV	.25	Dynamic	223.37
J34	75	LV	.25	Dynamic	196.31
J35	60	LV	.25	Static	152.99
J36	60	TM	.25	Static	151.17
J37	60	LV	.25	Static	143.50
J38	60	TM	.25	Static	146.96
J48	60	TM	.25	Dynamic	169.45
J50	60	LV	.25	Dynamic	212.69
J51	60	LV	.25	Dynamic	192.58
J63	90	LV	.05	Dynamic	216.41

* The letter J denotes block joint specimens.

Crack widths of 0.5 mm and 2.5 mm have also been investigated. Experimental results summarized in Table 1 indicate that if void formations and curing problems do not exist, the thickness of the epoxy injected crack does not affect strength results within the stated thickness range. Furthermore, strength results in Tables 1, 2, and 3 indicate that the strength of the epoxy repaired specimens is approximately the same for both the high and low viscosity epoxy adhesives.

The results in Tables 1, 2, and 3 will now be summarized in graphical form. Fig. 5 presents the compression test results for block ribs under

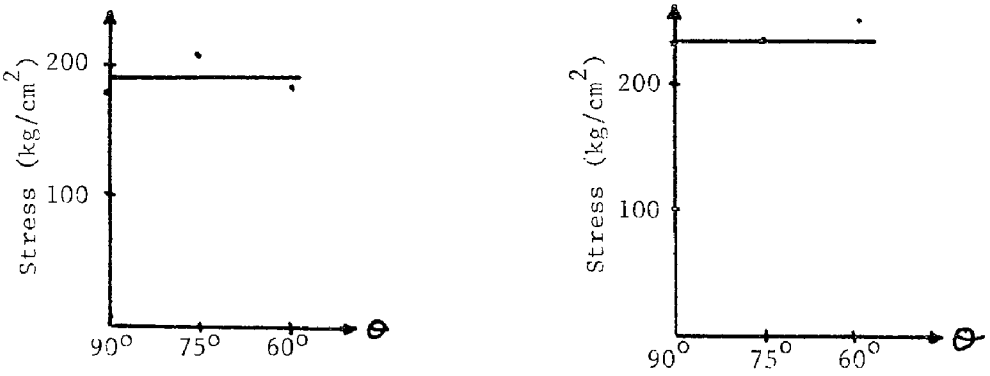

(a) Static loads (b) Dynamic loads

Fig. 5 Compression Test Results for Block Ribs

static and dynamic load conditions. These results show that crack angle, θ , does not influence the ultimate strength of block rib specimens. Dynamic strengths are approximately 24% greater than the corresponding static conditions. These strength results indicate the extensive influence of applied strain rate on ultimate strength (16).

Fig. 6 provides a summary of static and dynamic compression test results for masonry joints. The compressive strength is independent of the

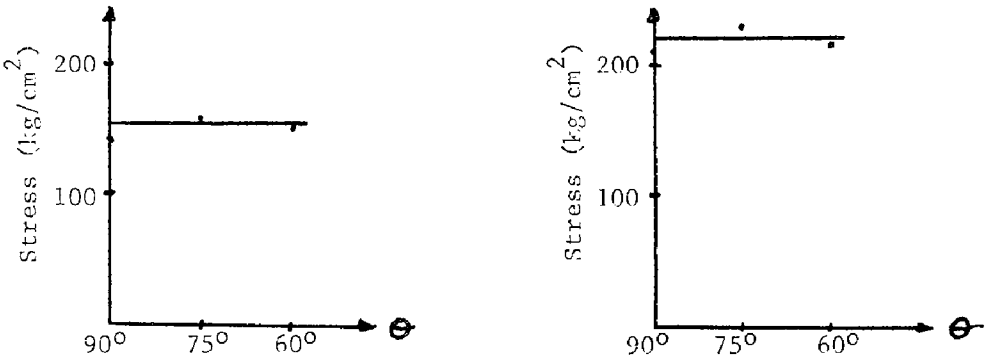

(a) Static loads (b) Dynamic loads

Fig. 6 Compression Test Results for Block Joints

crack angle, θ . The compressive dynamic strength is approximately 44% greater than the static compressive strength. Since extensive absorption of the epoxy into the mortar has the same effect as reduced mortar thickness, the compressive strength of epoxy repaired masonry joints is probably greater than the corresponding undamaged and unrepaired masonry joints.

Fig. 7 provides a summary of compressive strength results for grout specimens. The 28-day compressive strength of standard grout cylinders

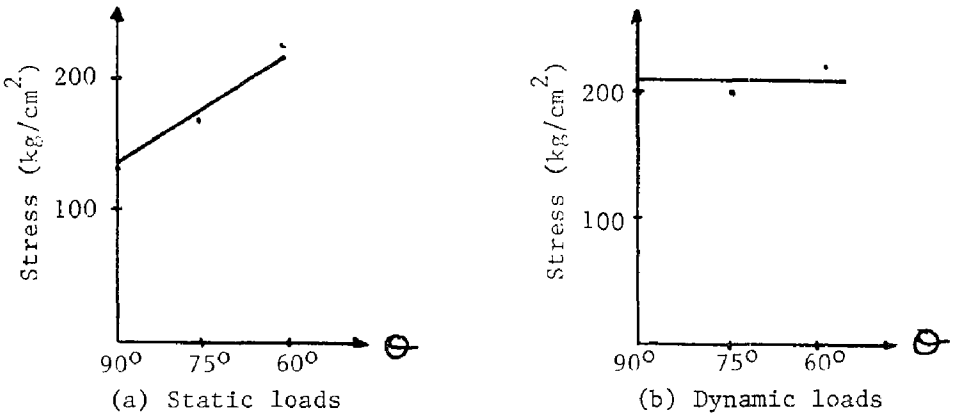

Fig. 7 Compression Test Results for Grout Specimens

is 183 kg/cm^2. The dynamic test results show that the crack angle, θ, has minor effect on the compressive strength. However, the static test results seem to show considerable interaction between compressive strength and crack angle. Finite element analysis of the grout specimens indicate that the three dimensional Poisson effect and the complex stress patterns created at the epoxy-grout interface may partially explain such extensive dependence of compressive strength on crack angle. Future tests will be performed to further substantiate or refute these static experimental results on grout specimens.

CONCLUSIONS

Experimental test results described in this paper show that properly epoxy repaired structural masonry components usually possess compressive and shear strengths equal to or greater than the original (undamaged) design strengths (large scale tests currently in progress confirm this conclusion). However, if full penetration is not attained or voids and uncured epoxy regions are formed, the strength of the epoxy repaired specimens may be extensively diminished due to stress concentrations and reduced effective stress area. Therefore, properly selected and correctly injected epoxy adhesives provide sufficient strength properties when utilized in the repair of concrete masonry structures subjected to static or dynamic load conditions. Additional research on fire-proofing and creep behavior of epoxy repaired structures is being prepared in order to obtain a more complete understanding of the behavior of those structures subjected to seismic loads and adverse environmental conditions.

ACKNOWLEDGEMENTS

The authors gratefully acknowledge the monetary and technical contributions from Russell A. Skiff of Delta Plastics Company of Visalia, California. The low viscosity epoxy material was injected by the continuous injection system provided by James Warner of Warner Engineering Services of Los Angeles, California. Several other epoxy manufacturers also contributed their materials and ideas to this research program. Lastly, the authors are appreciative of the monetary support from the National Science Foundation and extensive contributions from A. M. Plecnik, J. D. Cunningham and W. E. Whitman.

BIBLIOGRAPHY

1. Epoxies with Concrete, ACI Publication SP-21, 1968.

2. Hohman, R., Survey Report on the Repair of Structures Damaged by the 1971 San Fernando Earthquake, Building and Permits Dept. of Van Nuys, California.

3. Lee, H. and K. Neville, Handbook of Epoxy Resins, McGraw-Hill Book Co., New York, 1967.

4. Skiff, R., Delta Plastics Handbook, Delta Plastics Co., Visalia, California, 1975.

5. Con/Chem., "Technical Bulletin on Epoxy," Con/Chem Company, Los Angeles, California, 1975.

6. Rathbun, S., Hunt Process Co., Inc., Report on Epoxy Properties, Hunt Process Co., Inc., Santa Fe Springs, California, 1974.

7. Sika Data Book, Sika Chemical Corp., Lyndhurst, New Jersey, 1975.

8. Warner, James, "Ventura City Hall Restoration," ASCE preprint #2366, Oct. 1974.

9. Plecnik, Joseph, "Report on Epoxy Repaired Structures," NTIS Report in preparation.

10. Hegemier, G. A., Earthquake Response and Damage Prediction of Reinforced Masonry Multistory Buildings--A Research Proposal Submitted to NSF, University of California, San Diego, Ca., 1974.

11. Van Krevelen, D. W., Properties of Polymers, Elsevier Publishing Co., New York, N. Y., 1972.

12. Williams, J. G., "Visco-Elastic and Thermal Effects on Crack Growth in PMMA," Int. J. of Fracture Mechanics, Vol. 8, No.4, pp. 393-401, Dec. 1972.

13. Marshall, L. E., L. E., Culver, and J. G. Williams, "Fracture Phenomena in Polystyrene," Int. J. of Fract. Mechanics, Vol. 9, No. 3, pp.295-306, Sept. 1973.

14. Andrews, E. H., Fracture in Polymers, Elsevier Publishing Co., Inc., New York, N. Y., 1968.

15. Pratt, P. L., Fracture 1968, Chapman and Hall Ltd., London, Eng., 1969.

16. Davis, H. E., G. E. Troxell, and C. T. Wiskocil, The Testing and Inspection of Engineering Materials, McGraw-Hill Book Co., New York, N. Y., 1964.

INTERNATIONAL SYMPOSIUM ON
EARTHQUAKE STRUCTURAL ENGINEERING
St. Louis, Missouri, USA, August, 1976

A CALIFORNIA STRUCTURAL ENGINEER SHARES THREE YEARS OF ON-SITE EXPERIENCES IN THE DESIGN OF REPARATIONS FOR BUILDINGS IN MANAGUA

PATRICK J. CREEGAN

Structural Engineer

Chairman of the Board CREEGAN & D'ANGELO, INC., Cal.
President - CREEGAN Y D'ANGELO, S. A.
Managua, Nicaragua

SUMMARY

In the introduction, the author summarized the events of 12/23/72 at Managua, and indicates how a rating on the Richter Scale can be misleading to the engineer. Then discussed are the "politico-engineering" decisions related to recovering from the effects of the earthquake; fire; Building Code; the insurance surveys; surveys for the owners; the economics of reparation; inflation; special comments on torsion, excessive frame deflections, soft story, yielding in the plastic range, elevators, secondary damage, progressive failures, epoxy for concrete cracks, specifications and inspection.

INTRODUCTION

On Dec. 23, 1972, at 12:29 AM, Central Standard Time, the climactic shocks of about 24 hours of diastrophic activity struck Managua, Nicaragua. The event was scarcely felt in Leon - a city 60 miles to the west. The estimated magnitude of the principal terremoto was only between 5.5 and 6.5 Richter Scale. And yet there resulted in Managua - a modern capital city, whose buildings were all less than 40 years old - the total destruction of 5 square miles of city, and the partial destruction of an additional 5.4 square miles. This destruction left

5,000 - 6,000 dead.

20,000 injured to the point of requiring medical treatment.

220,000 - 250,000 homeless.

530,000 housing units lost or seriously damaged.

20,000 housing units sustaining "25% damage".

4,000,000 square feet of commercial buildings and warehouses lost.

3,400,000 square feet of public and private office space lost (40% of the national total).

4 hospitals (1,650 beds and 40% of the national total) lost or seriously damaged.

740 school rooms, lost or seriously damaged.

51,700 persons thrown out of work.

for about $845,000,000 in total damages - which approximated 85% of the GNP of Nicaragua.

By that earthquake, Managua - nestled on the axis of Nicaragua's volcanos - has proven one of nature's great laboratories. Those seismic events of Dec. 23, 1972 and their results have been well studied and have been the subject of much in our technical literature. This was the theme of the Conference at San Francisco in November, 1973 - sponsored by the Earthquake Engineering Research Institute - wherein 41 papers were presented and published - covering virtually all aspects of the earthquake. This report is brought to you well after the fact and cites impressions and reactions of a Structural Engineer who arrived at the scene on Apr. 2, 1973 and has been practicing his profession in that City since that date.

THE RICHTER SCALE

Much has been inferred that the Managua earthquake really wasn't that big a shake. The position has been taken - and the author has joined in it - that had the buildings of the City been properly designed and constructed there would have been little loss of life, and far less structural damage of the irreparable type. Those conclusions are probably true. But as regards the magnitude of the shake - make no mistakes about it, there was an unbelievable impact on the City.

Photographs of the results of this earthquake are numerous in the literature - and to a certain extent lose their effectiveness if viewed in mass. So to illustrate the degree of impact that can be experienced in a "mere" 5.6 Richter event only three photos have been selected. These are from the Cathedral at Managua. Figure #1 shows the Cathedral - a relatively squat building with a structural steel frame encased in rather massive concrete. Figure #2 is a view from inside the right hand (southerly) bell tower - looking at the N-W column of that tower. Figure #3 shows the fracture of flange and web of the N-W column of the southern bell tower. Figure #4 shows the structure of the column in cross-section.

The study of these photos could be the subject of a graduate thesis. The point of failure of this column was about 65 feet of the ground, with about 40 feet of tower above it. Failure was apparently during the first mode of response. Ignoring all of the energy that was absorbed by the concrete (Figure #2), it would take 5.25 pounds of 80% "Hi-Velocity" Gelatin to shear that steel column in that manner. I don't think "5.6 on the

FIG. #1

FIG. #2

FIG. #3

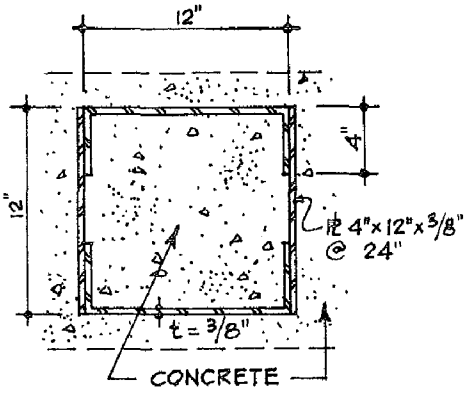

COLUMN SECTION

FIG. #4

Richter Scale" adequately describes to the engineer what he is to expect.

The Richter Scale is a means of classifying earthquakes according to an estimate of the "total amount of energy released" as measured at seismographs 60 Km. from the epicenter. But at Managua the epicenter was shallow - and right under the city. Perhaps some other concept such as "total energy released per square mile" would lead to a better yard stick to guide the engineers in determining how much energy their individual buildings should be capable of safely absorbing.

THE POLITICO-ENGINEERING DECISIONS

Immediately following a catastrophic earthquake there are a multitude of actions necessary for the protection of life and property. Naturally it is impossible to anticipate just what conditions will be, but it certainly helps if a contingency plan exists - say, as part of the general civil defense plan of each major city - to be followed, rather than developed, when disaster strikes. In retrospect it appears that these activities were handled in Managua in three phases:

Emergency

Post Emergency

Recovery

The decisions to be set forth in each phase include:

Emergency

What type of law - civil or marshall?

Chain of command.

Police protection.

Appraisal of conditions.

Medical stations and hospital facilities.

Evacuation and registration of refugees.

Feeding, housing and clothing of refugees.

Rescue operations.

Burial and registration of the dead.

Treatment of the injured.

Uniting of families.

Restoration of vital services - water, power, sanitary services, communication, fire protection, fuel supply, etc.

Post Emergency

General damage survey.

Condemnation to occupancy of those buildings rated dangerous.

Cordoning areas unsafe for occupancy.

Dynamite demolition of those buildings in imminent danger of collapse.

Control against looting.

Specific damage survey classifying each condemmed building as subject to obligatory demolition; or reparation at the owner's option.

Clean up.

Recovery Period

Does the extent of the damage warrant:

a revision in the City Plan?

a revision in the City Zoning?

Fault mapping and seismic risk survey for the city.

Adoption of a Building Code - where the law has been silent in this respect.

Establishment of governmental controls over new construction and reparation:

a) Planning department.

b) Building department.

Plan and design review.

Construction inspection.

Materials testing.

A Master Plan of the economic limits to be imposed on the reconstruction program, recognizing:

a) Money sources - Insurance; private capital; local public capital; international grant and loan.

b) Problems of artificial inflation under too accelerated a construction program.

c) Limitations of the local labor market - as regards numbers and expertise.

A Master Plan for the permanent establishment of all public (including governmental) services interrupted by the earthquake.

Raising the money to finance the recovery.

Implementing the recovery.

FIRE

As in San Francisco 1906, the Managua 1972 quake again pointed up the importance of concern for fire protection in the wake of this type of catastrophe. In Managua the power was knocked out - which may have been a blessing. Water supply was also interrupted - and the fire department was completely incapacitated, with all trucks buried in the rubble of the single fire house. In spite of this the report was "no fires" as of 24

hours after the event. But then either the vandals or the underinsured set the torch which probably accounted for as much physical damage as the terremoto.

The point is, fire can be expected after a major earthquake. Be prepared - and don't have "all those eggs in one basket". The fire fighting equipment should be decentralized. It will be needed for rescue even if there is no fire. There should be ample isolation valves in the water distribution system to be able to quickly reestablish service in fire mains even after several major breaks have been experienced.

BUILDING CODE

There are lots of you at this Conference that will be shocked to hear that there are many places in the world where there is no legally adopted Building Code. Managua was such a place, and to this time (Jan. 1976) is operating under an emergency code, formulated during two weeks of February 1973 and adopted in April 1973. Fortunately that Code embraces the ACI and AISC codes, which accounts for a lot of the construction. But it is completely silent in the areas of timber construction; reinforced masonry (traditional systems); fire resistive standards; stairs; exits and occupant loads; wall openings, etc.

At present there is a Nicaraguan Code in preparation. But it will be a special Code, for Nicaragua. In the writer's opinion this is a procedural error.

It can quite safely be assumed that a country that has no formally adopted Building Code is underdeveloped. Small, underdeveloped countries, by their nature, have an engineering profession so small as to be unable to competently maintain a "living" Building Code. It is the author's continuing opinion that, in this circumstance, the Code adopted, should be an existing and "living" code - that is, a Code kept continuously current by the work of Code committees of the various professional societies. Without intending to be provincial, an example of such a code would be the Uniform Building Code, which has served so well in the Western United States these many years. Such a Code can always be supplemented by local law to accommodate any peculiar local construction practices. There are many such Codes in existence throughout the world.

INSURANCE SURVEYS

Just as soon as possible after the event, the Insurance adjustors like to move in, make their investigations and settle all legitimate claims. At this stage of negotiations there is quite a demand for professional engineering opinion - both on the part of the insurance companies - and the owners. The early pay-out is desirable on both sides. The insurance company escapes as much of the effect of inflation as possible (inflation will be inevitable in a small country, badly hit). The owners need the money (this is about the first money available to the reconstruction program).

The typical engineering services called for at this time in respect to a given building are:

a) A careful inventory of damage.

and b) An evaluation of the damage.

Where there has been a catastrophe, the insurance decisions are often based on a "broad brush" analysis. A convenient formula for this is to estimate:

Percentage of loss in structure.

Percentage of loss in the electrical system.

Percentage of loss in the mechanical system.

Percentage of loss in architectural finish.

This approach permits quite a valid ultimate opinion.

SURVEYS FOR THE OWNER

If there is no insurance claim - or once the insurance claim is settled, the owner then has to make the decision of whether to demolish and reconstruct - or to repair. This often requires engineering consultation.

The Engineer's first responsibility is to formally inquire of the governmental agency in jurisdiction if the structure - if completely repaired - would still conform to the zoning, land use and City plan (if these have changed since the earthquake). If the official response at this point indicates that the option to repair is actually available, then the Engineer's function is to:

a) Make a detailed damage survey and report.

b) Analyze the original building to determine if part or all of the damage was due to a deficiency in the original design.

c) Make a preliminary design of compensatory construction that will satisfy any deficiencies of (b).

d) Prepare an estimate of the cost of the total reparation and structural remodelling - and compare this to the costs of demolition and reconstruction.

e) Present technical conclusions and observations in such a manner as to either make a definite recommendation - or give the owner the facts necessary for him to make the decision wisely.

As implied in (e) it is not always possible or appropriate to give the owner a definite recommendation, because of certain intangibles. For instance:

Is the building architecturally obsolete?

Can architectural obsolescence be overcome by remodelling during reconstruction?

Will the "post terremoto" location of the property be as desirable as before?

What other economic and aesthetic consideration besides "direct cost" will pertain to a wise decision?

Above all don't be misled by what you see. In Managua the vandals had an absolute field day. The cordoning of the disaster area had the effect of keeping the owners out and the looters in, with the result that in a short time many buildings not protected by armed guard were literally stripped not only of movable chattel but fixed improvements such as roofs, tile floors, elevators, doors, plumbing fixtures, windows, banister rails, etc. A standing building which at first sight appears not too badly damaged may on closer examination be found to be but a structural shell, which might have a value (if not obsolete) of only 15 or 20 percent of the total.

THE ECONOMICS OF REPARATION

As a rule, the Engineer's responsibility at this decision level stops with the presentation of the estimate of direct costs of reparation vs. new construction. But he should be aware of the other economic factors involved - because very often the owner will rely on the private opinions of his engineer.

A lot depends on the use of the building (residential, commercial, industrial, public facility, etc) and the type of client (private or public). Remember, virtually any building that is standing in a reasonably plumb position after an earthquake can be saved and repaired. The point is, is it worth it. For instance a 400 year old cathedral which is a cultural treasure might unhesitatingly be repaired - whereas a 40 year old cathedral with similar damage might be unhesitatingly scheduled for demolition.

How have the land values changed? Is the building still appropirate in that particular location of the reconstructed City? Would an elegant home end up in an undesirable neighborhood? Under revised land use would a one story warehouse site now be more appropriately the site at a high rise office building? Was a low rent area now a high rent area - or vice versa?

Again there is the subject of architecural obsolescence. Commercial landlords compete on the basis of desirability of location and attractiveness of accommodations. Many times it is just not practical to give the architectural face lifting necessary to really bring the building up to competitive standards.

How does the time factor enter the decision? The addage that "time is money" is particularly true in this type of situation - and especially where inflation will be a factor. Will there be a shortage of construction labor and materials, such that new construction, at costs comparable to those of reparation, would take much longer? Can a dollar factor be assigned to this time differential, recognizing the effects of escallating costs, early revenue, early termination of emergency rentals, etc. (one usually can - regardless of the type of building).

INFLATION

Already there have been several references to inflation. Normal escalation in construction costs is always one thing to consider - but artificial inflation can be really bad. If San Jose, California were to be levelled by an earthquake you wouldn't expect to experience artificial inflation during the recovery period. This is not true in many small countries of the world, however. Managua, for example, is about the same size as San Jose, but a much higher percentage of the national work force is required for the recovery process than would be the case in San Jose. Also, Nicaragua is an economic island among nations. It's national product is basically raw material and although it produces cement, stone, masonry units and timber, it imports all steel (even nails, nuts and bolts) mechanical and electrical products - and most items of architectural finish. The merchants and manufacturers of the country have long lived together and learned to let live. Consequently there is not a great deal of competition between vendors. There are many hardware dealers, for example - but they don't all sell the same items, and the overlapping of items sold is not that much.

So it is that the shortage of labor can cause an inflation in labor costs. The shortage of material and the low degree of competition invite an artificial inflation in material costs.

COMMENTARY ON THE TECHNICAL ASPECTS OF REPARATION ENGINEERING

Once it has been decided to save a given building, the engineer moves into a very specialized field of structural engineering. He becomes a doctor of buildings - making well ones out of sick ones. This calls for the scientific expertise of the engineer of new construction, plus a special application of the art of engineering, and a lot of sound judgment.

First, when moving into a new locale, make a careful study of local building practices, available construction materials and the construction techniques in current favor. This doesn't mean to imply that you should conform to these - for they may have contributed to the failures involved. But they should be evaluated and the decision made as to which to follow - and which to modify.

With respect to the repair of a specific building, the first thing is to be satisfied that all necessary temporary shoring is in place. Then make a careful damage survey. Study the failures to determine why they happened in the way they did. This will invariably provide the clue or clues as to what was wrong with the building in the original design (make no mistake about it - our best designs have flaws).

At this point there is a judgment to make:

1) Does the building fall into Class "A" - where the damage was tolerable, and acceptable again if repeated in a future earthquake of design magnitude.

or 2) Does the building fall into Class "B" where a repetition of the damage is not desirable and the overall performance characteristics of the building should be improved.

Remember, a building is not a "One Hoss Shay" - it will invariably have weak points. Sometimes these are just as acceptable as the shear keys in a machine that are designed to fail under overload before more expensive parts are damaged. An outstanding example of the Class "A" structure was the famous Banco de America building of Managua. It was the tallest building in the city and it's principal damage was the systematic failure of some spandrel beams at each floor of the elevator shaft. It was decided that this "weakness" could be tolerated in the future and the beams were merely repaired to their original condition.

This matter of making repairs to restore a building to it's original condition is necessary for all buildings being repaired. To those whose performance characteristics are to be improved (Class "B") there will also be some "compensatory" construction (additional shear walls, reduction of torsion, tying certain elements together, closing certain wall openings, providing some sliding connections, etc.) - designed to prevent the repetition of the type of failure experienced. Most reparation falls into this latter category.

SPECIAL TOPICS

Code. Usually the building being repaired will not have been designed to the letter of the currently existing Building Code. And so, early in the design the engineer must decide whether to bring the building into full conformance with the existing Code - or to make repairs to some reduced standards. The Nicaragua emergency code permits this type relaxation of requirements, providing the building official concurs with the Engineer's judgment in the matter.

Classical examples are with the roof or the seismic factor.

Often, the specifications for the reparation permit the continued existence of a roof system that cannot carry the full live loads per Code, without excessive deflections. But so what? If everything else is in order, the roof's only function in service may be to keep out the rain.

The design seismic factors in Managua are quite high now (for instance, 0.33 for a concrete block wall, box system). The Engineer may propose a reduced factor, on the proviso that all connections are in order.

In exercizing this particular type of judgment be careful not "to throw the baby out the window with the bath water" - but to still end up with a safe building.

Torsion. Torsion is no myth. A very popular type construction in Managua for intermediate floors and some roof slabs was 2" reinforced concrete slab with 2" wide tee stems at 12" on center with 6", 8" or 10" deep hollow clay or concrete tile between the stems. These made excellent rigid horizontal diafragms, and generally speaking sustained very little damage in the

earthquake. But as they rotated under lateral load due to the eccentricity between the c.g. of the load and the c.g. of the resisting elements, they wrought incredible wall damage.

Perhaps one of the two great lessons emphasized in Managua relates to this subject of torsion.

Lesson #1. "The most important phase of a seismic design is during the basic architectural layout at the very conception of the project. Structural symmetry is good. Large structural eccentricities are bad."

Excessive Frame Deflections. Because all steel must be imported to Nicaragua the concrete frame was a popular method of construction during the 50's and 60's. These frames were designed for vertical load - and whether by design or simply by virtue of their joinery - had a certain capacity to resist lateral loads...albeit with excessive deflection. As a matter of fact the frames in many of these frame structures behaved well - of themselves - and were perfectly feasible of being repaired. But because of the deflections the "non-structural" partitions and masonry infill walls were ruined.

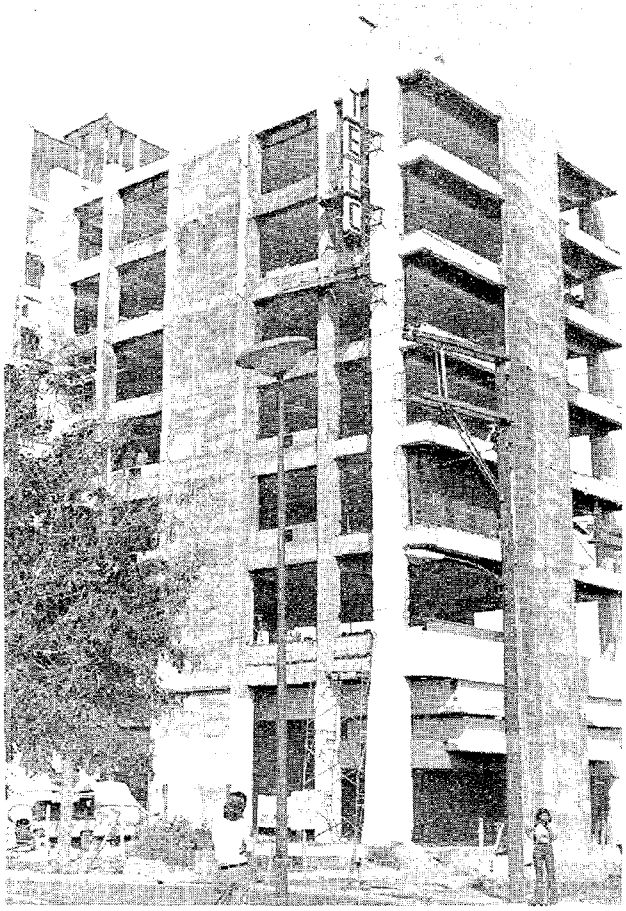

FIG. #5

The ACI has recognized this lesson and now will be requiring that moment resisting frames of and above certain minimum dimensions be supplemental and stiffened by shear walls. And actually this is an excellent concept of design. If there is a frame alone and the frame fails, the building is gone. Similarly with the "box" system, once the shear walls fail, the building is gone. But to use the two in combination is ideal... because due to the great differences in flexibility the two systems do not work together. This means that the shear walls can "take it all" and sustain a tremendous amount of damage. Then the frame is left to save the building until repairs can be made.

Figure #5 gives an illustration of these points. This is the 7 story "TELCOR" building. It was a concrete frame with clay tile infill walls. These walls were brittle and almost "exploded" in their shattering. But the photo is as of December 1975, showing the building is being saved. Note the new and symmetrically positioned shear walls being added.

This discussion has related to concrete frames. Steel frames would have been found just as lacking under the same design philosophy. This points up the second great lesson emphasized in the behaviour of buildings in Managua.

Lesson #2. "A building element - structural or "non-structural" - not free to deflect as much as all else around it tends to - will catch the load. It had better be able to take it - or fail".

Soft Story. This is merely an editorial observation directed at the concept of the "soft story". The idea of the soft story is that the first floor framing be quite flexible under lateral load, as compared to the upper stories. If it works right this story will damp out the effects of earthquake ground motion such that the response in the upper stories would be practically nil. All damage would be concentrated in the first story and would be readily subject to repair.

There were many "soft story" buildings in Managua. They were not designed with that in mind - but they turned out that way. They were 5 and 6 story buildings that abruptly became 4 and 5 story buildings - respectively - with little damage in the surviving floors. So the soft story, per se, may not be such a good idea.

But an idea that is "almost" on target shouldn't necessarily be abandoned. This concept of buffering the shock before it gets into the main building elements is fundamentally sound. But the place to do it is probably in the foundations.

Shock absorbers in the foundations may not always be possible - and certainly will always be costly. But so has this concept of "fighting the forces" (that our profession has followed to date) been costly. It is a fair prediction that much thought will be devoted to this field of shock absorbing - either before the shock enters the structure or in the joints once it's there. Figure #3 is a reminder of the dynamic nature of the seismic load. It would seem that static structures and dynamic loads may not be the answer.

Yielding in the Plastic Range. This is another editorial comment, but this time directed at a concept that is generally accepted in the profession. The desirability of ductility and toughness - as opposed to brittleness are certainly at the very heart of aseismic design. But a lot of steel has been sold on the merits of it's ability to absorb earthquake energy by deforming in the plastic range. That's fine for saving lives and selling steel - and surely some plastic yielding in some joints can do a lot of good and not much harm - but there were a lot of buildings in Managua that "leaned and stayed leaning" because of this phenomenon. By definition the hysteresis loop does not close back to zero in this type of yielding.

But again, the idea is on the right track. Energy has to be absorbed and dissipated as heat. The profession should keep working and progressing along that line of thought.

Elevators. At Managua elevators consistently jambed, and a common failure with cable systems was that the cables jumped the grooves of sheaves and fairleads and bound between the sheave and the cheekblock. This was one more warning like San Fernando. But it is encouraging to see that California, as of last October, has inaugurated new seismic safety standards for elevators. Incidentally, these new controls are administered by the State Division of Industrial Safety - and no doubt correctly so. Let us hope that other agencies follow suit. The point is that if ships at sea can survive typhoons with all elevators in working order, then building elevators can be made to survive an earthquake and operate as long as the shaft stays intact.

Secondary Damage. In 45 years this profession has made pretty good progress in the field of aseismic design. Joinery has improved. A lookout is kept for that short stiff element that wants to catch all the load. There is a better understanding of the nature of the loads and how to handle them. Protection of life has been the aim. But in Managua probably more than half the total damage was secondary damage of the type herebefore described under"Excessive Deflections". The building stood, but all the walls, architectural finish, mechanical and electrical works were gone. It is very difficult to explain this to an owner. His principal consolation is that the same thing happened to his neighbor. It is just like a Doctor reporting that "the operation was a success - but the patient died".

This point is made to indicate to the Engineer that his work is not done when he designs the structural skeleton. He must look to the building as a whole to work as a whole - and hopefully perfect his design to the point where at least for a "5.6 Richter" most of this secondary damage will be avoided.

Progressive Failures. Beware of the series type connection where the extreme connector can be overloaded while the interior ones are under stressed. "Ten were needed and ten there were. One failed, and then there were nine, etc." This "bewareness" should become ingrained. It is particularly important to have when conceiving the overall building performance. Fail Safe!

Repair of Concrete Cracks by Epoxy. Not enough can be said in praise of the system developed for injecting epoxy into the cracks of concrete building elements. Principal beams and columns that have hinged can be restored to conditions better than new. Remember though, that this merely brings the structure back to what it was. Chances are that with some reasonably unsophisticated "compensatory construction" the original design can be substantially improved upon.

Specifications. The cost-plus contract is ideal for reparation work because the true scope of work is a bit nebulous. But it is not absolutely necessary. Restoration contracts can be let on the basis of a fixed price, competitively bid, for all work clearly specified to be done. But there should always be ample provision - either by means of a prespecified contingency fund within the bid price - or through broad latitude of discretion given the Engineer to make field changes and additions to the work. It is usually impossible to discover all of the structural deficiencies of a building during the design period. This is because the building is not totally exposed to inspection until the contractor actually starts working. It is for this time that the Engineer should reserve authority to himself to modify or amplify the reparation work and authorize extra payment to the contractor on-the-spot.

Inspection. There , no doubt, will be situations in the future similar to what Managua 1972 was. In Managua, the construction labor force jumped 800% after the earthquake, so that inspection not only became a goal of guarding against unscrupulous practices, but overcoming an honest but genuine ignorance factor. With the best of contractors inspection is necessary to see that the intent of the design is followed.

This is especially important with respect to those details of joinery fundamental to aseismic design.

INTERNATIONAL SYMPOSIUM ON
EARTHQUAKE STRUCTURAL ENGINEERING
St. Louis, Missouri, USA, August, 1976

TROIKA FOR EARTHQUAKE-RESISTANT BUILDING DESIGN
ENGINEER - BUILDING CODE - CONTRACTOR

JOHN R. TISSELL, P. E.

Research Engineer
AMERICAN PLYWOOD ASSOCIATION

Member
STRUCTURAL ENGINEERS ASSOCIATION OF WASHINGTON
Tacoma, Washington, U.S.A.

SUMMARY

A team of structural engineers from the American Plywood Association investigated the behavior of plywood systems in the San Fernando earthquake of February 9, 1971. They found that the good performance of schools showed that current design and careful building techniques could produce plywood and wood buildings that performed well, even in a high intensity quake. Poor performance of some industrial buildings showed that less careful design and construction was soon reflected in performance. Performance of hospitals demonstrated that an "importance factor" should be applied to such buildings. And a comparison of earthquake durations, together with the exemplary performance of well-built buildings, showed that the duration-of-load adjustment, for wood under seismic load, should be raised from 1.33 to 1.75.

INTRODUCTION

Definitions

Webster's Seventh New Collegiate Dictionary defines "troika" as: "(1) Russian vehicle drawn by three horses abreast; also, a team for such a vehicle. (2) A group of three closely related persons or things."

"Engineer" includes both engineers and architects who are qualified to do, and are engaged in the practice of, the structural design and detailing of buildings.

"Building code" is defined as including both the written code and the officials in a position to enforce it.

"Contractor" includes the management as well as the workmen who are engaged in the actual construction of the building.

The definition of the 3-member troika appears to omit the very essential 4th member, the owner, of any building program. Actually the owner

should be considered as the driver and vehicle being drawn by the troika. This definition indicates that the progress of the owner is dependent upon sufficient cooperation between the members of the troika so that they are all moving uniformly in the same direction. Also implied is the fact that the owner, as driver, can give instructions to the troika which they will accept, if they are in accord with their training.

Tests of Seismic Designs

Engineering design methods, and other theories developed in the scientific community should be, and normally are, verified by testing. While building components and materials can be tested, however completed buildings are too large to be tested. Development of the shaking table has made it possible to simulate 3-directional earthquake motion, but here again, the largest table in the United States is 20 ft x 20ft (6m x 6m) which restricts its use to testing of models or components. Structures cannot be scaled down to models of manageable size and still preserve dynamic similitude, and even if the costs of full-size tests were not prohibitive, no means exists for generating the earthquake forces at full scale.

It is imperative, therefore, that evidence bearing on the theories or design processes be gleaned from actual earthquakes whenever they occur. The earthquake can be looked upon as an experiment conducted by nature. The experiment is completely uncontrolled, but the troika must use it to gather whatever information they can.

Since an actual earthquake is the only means of testing a completed structure, each earthquake, of sufficient intensity to cause damage, must be thoroughly investigated. The investigators commonly represent such areas as the academic community, professional engineering organizations, building-code officials, and trade associations of construction material manufacturers

Investigation, following an earthquake, must be prompt so that evidence indicating the nature and cause of any failures is not destroyed by repairs or cleanup. While pictures and accounts of dramatic failures are a very obvious purpose of the investigation, it is equally important that buildings that survive with little or no damage also be investigated to determine the reason for their good performance.

An ideal situation for the investigative team is when two relatively similar buildings with a wide disparity in the amount of damage are located in the same vicinity and were probably subjected to the same earthquake forces. This situation occurred in the 1971 San Fernando earthquake (10)* and in the 1973 Managua, Nicaragua earthquake (4, 24, 25)*. While the exact significance of these comparisons may be argued by advocates of various building materials or design methods, the widely differing performance must not be ignored by members of the troika, particularly the engineer and building code.

A point to be considered in evaluating building performance is the importance of that performance. A warehouse or industrial building might

* Numbers in parentheses refer to Bibliographical References, at end of paper.

have been built on a tight budget with full realization that it would be damaged in an earthquake. A hospital or fire station, however should not have been so designed or built.

American Plywood Association Investigation

After the San Fernando earthquake of February 9, 1971, a team of structural engineers from the American Plywood Association investigated the behavior of plywood systems in the quake. The purpose of the investigation was to determine if design methods for plywood diaphragms were realistic. Did the failures indicate a fundamental design weakness, inadequate engineering, or poor construction? Were they the result of an easily corrected "weak link" in the design or construction?

The function of diaphragms and shear walls should be understood to appreciate fully the significance of the actual building successes and failures. A diaphragm is a horizontal structural element, like a roof or a floor. It is designed to resist lateral loads, such as those caused by high winds or earthquakes. The diaphragm functions as an oversize beam, with the sheathing forming the web and the boundary members, the flanges. The boundary members, or chords, carry flexure, acting in direct tension or compression. The intermediate framing members stiffen the diaphragm against buckling and splice the sheathing and the roof or floor surface to carry shear.

Walls and partitions can be designed to function as vertical diaphragms, commonly referred to as shear walls, which serve as cantilever beams to transfer loads from their upper edges to the foundation.

Earthquake or wind forces generated in building walls, perpendicular to the direction of the forces, are transferred to the foundation and to the roof acting as a diaphragm. The roof, in turn, transfers the load from the walls, as well as any wind or earthquake forces on the roof, to the shear walls that are parallel to the force.

The buildings in this region ranged from masonry or wood framed single residences to high-rise buildings framed in steel or concrete. The investigation reported in this paper is limited to discussion of buildings using lumber framing overlaid with plywood to develop the shear resistance required to withstand earthquake forces. This type of construction was commonly used for both walls and roofs, in schools, homes, and apartments. Another major use was for roofs only in light industrial or warehouse buildings using masonry or concrete tilt-up walls. The design methods for this type of construction have been developed through a long series of laboratory tests at the American Plywood Association laboratories, the U.S. Forest Products Laboratory, and Oregon State University. Since the San Fernando earthquake produced the strongest accelerations ever recorded, San Fernando provided an opportunity to study the behavior of plywood structures at "probably close to the maximum values (of ground motion) to be expected for an earthquake of even the largest size." (7)

OBSERVATIONS FROM THE SAN FERNANDO EARTHQUAKE

High Intensity

Intensity of the San Fernando earthquake was the highest ever recorded, as measured by the acceleration, which caused the actual building damage.(1) Seismologists have referred to the San Fernando earthquake as a minor quake since its magnitude was only 6.5 on the Richter scale. Intensity, however, not magnitude, determines the strength of the damaging forces.

The high lateral forces in San Fernando caused building stresses that were far above the design load. In places, these forces were equal to or greater than the building code design force multiplied by normal "load factors". In other words, they were forces at which well-designed structures would be expected to fail.

Successes

In general, well-designed and well-constructed diaphragms performed well, as illustrated by the performance of a number of schools visited. Schools commonly used large amounts of plywood and used it in a way that provided adequate strength to match the earthquake.

At Olive Vista Junior High School, there were several temporary classrooms, which were completely sheathed with plywood on walls, roofs, and floor. They survived without damage, even though the quake was sufficient to destroy the foundations beneath them. These classrooms fell to the ground when the post-type foundation tipped under the lateral force of the earthquake. At the time of the inspection, about two weeks after the quake, they had already been lifted, the foundations had been restored, and the rooms were in use.

Also observed at Olive Vista was a large, two-story building with a plywood diaphragm and plywood shear walls. It had survived the earthquake with both diaphragm and shear walls doing their job. The only failure was at the bottom of one end shear wall, where lateral forces had been so great that the anchor bolts actually caused splitting of the bottom plate. Here again, repairs were well underway with the replacement of the bottom plate.

The damage to this building, even though minor and easily repairable, becomes significant when judged against the performance of the adjacent building. The two buildings were identical and parallel, but with reversed floor plan. The two buildings were basically symmetrical about a line midway between them. The only known difference in the construction of the two buildings was the omission of the hold-down anchors at either end of the damaged shearwall. (10)

Failures

Most of the buildings inspected, with structural failure, were industrial structures. Typically, these structures had plywood diaphragm roofs and concrete tilt-up walls. The majority of these buildings had failed through outward movement of an end wall, and collapse of a portion of the roof adjacent to that wall.

The usual industrial building was rectangular in shape, with the main roof framing glulam beams parallel to the shorter end walls. Purlins were placed parallel to the longer side walls, and spanned between the glulams. Plywood roof panels were preframed with 2x4 sub-purlins, and spanned between the purlins. The failures generally occurred in the end bays, along the shorter, end walls. There was no tension connection at the ends of the purlins, other than that formed by the plywood sheathing.

The lack of tension ties between the roof purlins and the end walls was prominent in all failures. This lack caused the diaphragm perimeter nailing to be loaded in three ways. First, it was serving its primary function of transferring shear from the roof diaphragm into the wall ledger (chord). Second, it was filling the role of a tension tie between the roof diaphragm and the wall. Third, it was transferring uplift forces from the roof to the wall.

Since the end bays are also the areas of highest shear, the question naturally arises as to whether the failure was primarily due to high shear or to the lack of tension ties. The partial failures in three buildings offer strong proof that the primary cause of the failure was lack of tension ties rather than excessive shear.

The first of these buildings was a warehouse that was approximately 100 ft (30 m) square. Since the building was square, for equal forces the shears would be equal in either direction. In this building, the failures occurred in the bays where the purlins were perpendicular to the end walls (where there were no tension ties). There were no failures in the side walls, where the glulam seats provided tension ties.

The framing in the second building is even more significant, since it was a typical long rectangular building. In this building, however, the purlins were perpendicular to the long side walls instead of to the short end walls. With such framing, plywood panels are oriented so that the continuous plywood panel joints are parallel to the high shear forces. The close nail spacing observed indicated that the engineer recognized this fact and adjusted the nail spacing accordingly. In this building, the failures occurred along the side walls, where the purlins lacked tension connections to the wall, but where the shear forces were actually lower than at the ends.

The third building was a large manufacturing facility; it had the typical failures in the end bays. Four large sawdust collectors, on the roof, were supported by the roof framing in an end bay. This particular bay failed except for the area supporting the sawdust collectors. Further investigation indicated that the purlins supporting the sawdust collectors had been increased in size, due to the increased vertical load. More important, they were securely anchored at each end in a way to resist vertical forces as well as any outward tensile force from the wall. (20)

While several investigators (2, 18) report no wall to roof separations in buildings with good ties between walls and roof framing, one report (2) does contain reference to such a building where there were major failures in the interior portion of the diaphragm. Obviously, when one weakness is corrected, the next weakest link will become critical. In the case of roof

diaphragms, when the inadequate tension connection between framing and walls are strengthened, quite possibly the next weakest link would be where the roof purlins are supported on either side of the major roof beams without provision for transmitting tensile forces across the beams. While it is not intended to minimize necessity for checking all connections for forces in all possible directions, reference to Figure 1, showing the building mentioned in the report, indicates that differential ground movement was so great at this location that not even a well designed and well built building could have survived undamaged.

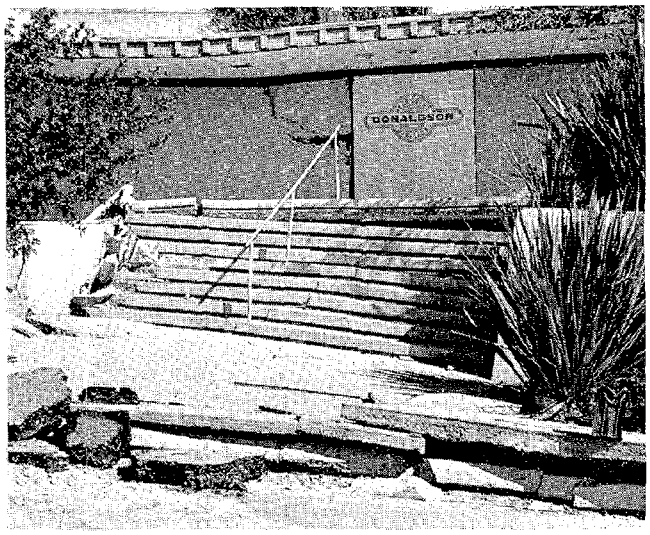

FIGURE 1

Extensive differential ground movement at 12366 Montero Avenue

It was paradoxical that, of the 58 fatalities recorded in the San Fernando earthquake, 50 occurred in hospitals. Admittedly 47 of these lives were taken by collapse of non-earthquake-resistant buildings at the Veterans Administration Hospital, which were built before earthquake requirements were added to the code. Several hospitals, however, were damaged to the extent that they were non-functional at a time when they were needed most, even though they had been designed and constructed recently under modern building codes.

Duration of Load

Assuming that the addition of the tension tie between the roof framing and the wall would correct the only appreciable weakness of this type of construction, the performance of the buildings would then have been far above expectations. This assumption is not unreasonable since the buildings in the area, with ties, escaped serious damage. Then the extremely high actual earthquake accelerations, compared to the design load specified by the building code, would indicate that load factors of 4 and 5 and, in cases, even 6 were common. These load factors are considerably higher than the factor of 2 1/2 to 3 that is accepted for wood construction, and they indicate that wood has a considerable reserve strength available for short term loading.

A question arises on the assigned load increase allowable for seismic design - partially from field observation, and partially from study of the records of the San Fernando and other previous earthquakes.

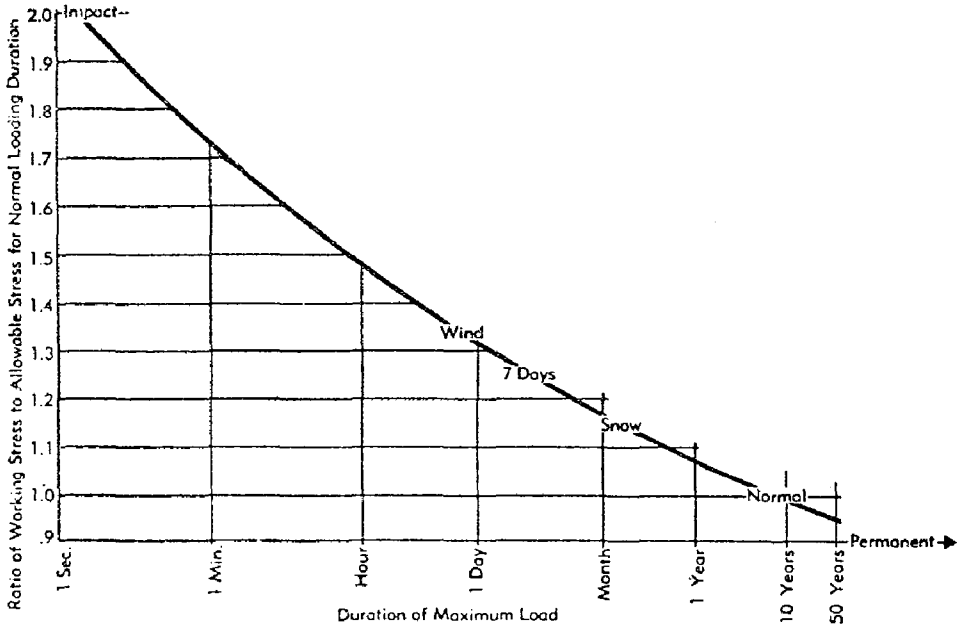

FIGURE 2

ADJUSTMENT OF WORKING STRESSES FOR VARIOUS DURATIONS OF LOAD
(Derived from Forest Products Laboratory Report No. R 1916)

The ability of wood to take short-time loads has been commonly recognized, with a relationship between working stress and duration, as shown in Figure 2, established by the U. S. Forest Products Laboratory. This figure shows a one-third increase in allowable design stresses for a cumulative total duration of load of one day in the life of the structure. It also shows a 75% increase applicable to a load duration of one minute. Presently a one-day duration of load is understood to include both wind and earthquake.

It does not seem reasonable to place wind load and earthquake load in the same classification. It is easy to believe that the actual cumulative duration of maximum wind load over the life of a building will total one day. In contrast it is hard to justify over one minute of cumulative earthquake loading, at maximum stress, even for buildings with an expected life of 100 years. The high-intensity duration of the San Fernando earthquake, for instance, was 12 seconds, and the entire earthquake lasted about 60 seconds. (3, 12, 26)

William Cloud arbitrarily established the damaging intensity of earthquakes at 2% gravity and above. His figures, shown in Table 1, indicate that such strong past earthquakes as El Centro or Kern County (Taft) have had a duration of only approximately 2/3 of a minute above the level of 2% g. While there is no record of the Alaska-Prince William Sound earthquake, reliable witnesses (19) estimate its duration as being considerably longer.

TABLE 1

DURATION OF EARTHQUAKES HAVING STRONG-MOTION RECORDS

Date	Magnitude (Richter Scale)	Station	Distance to Epicenter (Miles)	Timbe above 2% gravity (seconds)
May, 1940	7.1	El Centro, CA	7	30
Apr., 1949	7.1	Olympia, WA	10	50
Apri., 1949	7.1	Seattle, WA	38	49
July, 1952	7.6	Taft, CA	27	43
July, 1952	7.6	Pasadena, CA	75	26
July, 1952	7.6	Hollywood, CA	76	31
Aug., 1959	7.1	Bozeman, MT	56	27
May, 1962	7 to 7.25	Mexico City Mexico	160	27

On the other hand, to consider 2% gravity as the threshold of damaging intensity is probably overly conservative for a building designed for earthquake accelerations of 10% g. Setting the damaging intensity, for properly designed buildings, at a more realistic level, well above 2%, would greatly decrease the damaging duration of past quakes below the intervals shown in Table 1. Jennings and Housner feel that accelerations of 15% mark the threshold of serious damage for most poorer, pre-1933 buildings. (8)

The cumulative duration of earthquake loading of one minute or less indicates that normal design stresses for wood should be increased 75% for earthquake loading, using the relationship of working stress to duration of load shown in Figure 2.

DISCUSSION OF OBSERVATIONS

The importance of thorough design and construction inspection were shown by the striking difference between the excellent performance of school buildings and the relatively poor showing of industrial buildings in San Fernando.

One observer, referring to the industrial buildings, stated, "the construction of these buildings is a highly competitive undertaking with a strong pressure to keep the cost low, and hence, the tendency is to just satisfy the requirements of the building code." (5)

The results of inadequate inspection, design or detailing were obvious in the damage to buildings at San Fernando. Figure 3 shows a portion of a reinforced masonry shear wall that has a conspicuous absence of grout in the voids containing the vertical reinforcing steel. (22) Inspection of the diaphragm chord and its attachment to the wall indicates the thoroughness of the engineers design.

FIGURE 3

Collapsed shear wall, 15151 Bledsoe Street. Note ungrouted void containing vertical reinforcing steel.

FIGURE 4

Ledger anchor bolt embedded approximately 1 1/2", 12460 Gladstone Avenue.

Analysis of the construction drawings of another building that suffered severe, but repairable, damage shows that the structure generally was designed in accordance with requirements of the Los Angeles City Building Code. However, examination of the damaged portions of the building indicated that the horizontal wall reinforcing steel was not spliced at the columns as detailed on the construction drawings. Another cause of failure in this building was the shallow embedment of anchor bolts. A typical bolt is shown in Figure 4 and other bolts were found embedded even less. The construction drawings show the bolts being embedded to within 1 inch of the far surface of the wall. (23)

School design and construction, on the other hand, are described by the following:

> "However, the primary difference between school construction and other work is in the scrutiny given to details and connections, and in the added job-site surveillance by the architect, engineer, inspector, and a field engineer of the Schoolhouse Section of the Office of Architecture and Construction." (13)

and again:

> "Possibly the most significant provision of the (Field) Act is the requirement for strict construction supervision." (14)

These accents on details, connections, and inspection could well be the "other reasons" referred to by Jennings and Housner in the following quote:

> "The lateral force requirements for the school buildings are essentially those of the building code and the successful performance of the one- and two-story school buildings reflects the fact that these structures actually possess, for other reasons, lateral resistance substantially in excess of the minimum code requirements." (9)

Importance of a conscientious and competent contractor is required even with inspection. A full-time inspector cannot watch every workman continuously or verify every minute detail. Thorough as inspection requirements are for schools, under the Field Act, connection details were observed to have been omitted in at least two schools. First was the omission of the holddown anchors mentioned earlier at Olive Vista Junior School. At a second school a weld was omitted between reinforcing steel and a steel beam. Also a reinforcing bar was not hooked around the anchor bolts as specified. These details appeared several places in a total of three buildings. (7, 11)

LESSONS FROM SAN FERNANDO

These are lessons to be learned from the San Fernando earthquake, for all three members of the troika.

For the engineer, one of the very first lessons which should have been learned from study of San Fernando is the need for incorporation of the structural lessons in the engineer's initial and continuing education. This need for education seems obvious while the memory of the various damaged buildings is still fresh. It can be soon forgotten, however, as illustrated by the fact that R. Hanson and H. Degenkolb's eleven lessons "learned" (6) published after the July 29, 1967 Caracas, Venezuela earthquake, had to be "relearned" from San Fernando.

The engineer's next lesson is the need to complete thoroughly each building design, including close attention to all details and connections.

The building code has learned one of its lessons well. The need to incorporate new provisions in the Uniform Building Code has been realized, and many changes have been implimented.

The collapse of numerous school buildings during the 1933 Long Beach earthquake, and the realization of the immensity of the catastrophe that would have been involved had the schools been in session, shocked the California Legislature into effective action. The Field Act was passed, governing school construction, eleven weeks after the earthquake. Similarly, extensive damage to several hospitals in the February 1971 San Fernando earthquake caused the California Legislature to pass a bill in 1972 to insure that hospitals be constructed with the same attention to earthquake resistance as required in school construction under the 1933 Field Act.

The code and the engineer also need to learn to emphasize the importance of inspection. The construction inspection should be by both the engineer, to be certain that his design drawings are correctly interpreted, and by the building code to be doubly certain that the design and construction are in accord with the code.

The third member of the troika, the contractor, is equally important to the success or failure of a building. He must learn to accept the responsibility associated with this importance. Buildings properly designed, meeting the requirements of the latest building code and using the latest building technology can still fail if items such as reinforcing rods are omitted or improperly spliced, or fewer or shorter nails are used than those specified. A competent, knowledgeable contractor, combined with inspection during construction, is insurance that the building is constructed as the designer intended, as well as providing an opportunity for a final check for errors or omissions on the part of the designer.

An important lesson for all three members of the troika and for the owner, is the need for an understanding of the degree of earthquake resistance designed and built into the building. It is necessary in certain cases to design above the minimum requirements specified by the code, by adding what has often been called an "importance factor" to the code requirements. Ideally, the amount of the increase can be determined in a free and open discussion between the members of the troika and the owner, based on the number of people exposed to danger should the building be damaged in an earthquake, and on the time that a building would be nonfunctional, for repairs, following an earthquake.

Interviews with owners, after the San Fernando earthquake, showed that they did not understand the need to define importance. They had been under the impression that a building, even marginally in compliance with the code, was expected to sustain little or no structural damage in an earthquake. The building code, on the other hand, like most building codes, had been written to provide minimum standards for the protection of public health and safety - not property.

Failures, of hospitals and other emergency facilities, at San Fernando indicated that higher importance factors should be considered for such structures as: hospitals, fire stations, communication centers, and electrical switching and distribution centers.

COST OF APPLICATION

Obviously it will cost money for the increased engineering time required for more completely detailed design, the addition of full-time inspection in the construction phase, and increased material and construction time required to build a more earthquake-resistant building.

Traditionally it has been considered that the owners resisted expenditures of this type since they were apparently willing to gamble that an earthquake would not occur. Undoubtedly owners of buildings damaged in San Fernando, while hoping that another earthquake of this magnitude will not strike for another 50 years, see the justification

for spending a small amount of money in building construction to prevent the potentially large amount of damage later on.

Perhaps additional incentive could be given owners to build more highly earthquake resistant buildings if the premium rate for earthquake insurance could be related to the designed ability of the building to resist the maximum expected potential earthquake.

Several studies have been made to determine the increase in building costs that can be attributed to earthquake-resistive construction. The first of these studies was in 1961; it concluded that the increase in cost for earthquake resistant construction as required by Title 21, California Administrative Code (the Field Act), generally amounts to no more than 1% of the total cost of a building designed to meet the usual vertical and wind load requirements. (17)

Another study (15, 21) was based on the redesign of several buildings damaged in the San Fernando earthquake. Included among these buildings were a school and a typical industrial building with tilt-up reinforced concrete walls and a plywood roof diaphragm. This study resulted in 9.7% construction cost increase for the industrial building and a 30% increase in the necessary engineering. The increased cost for the school was 1% in construction and 15% in engineering.

The 1% estimate increase in construction cost for the school indicates the large reserve strength built into the school under the Field Act. The original school design was for a typical lateral force of 13% of gravity and normal design stresses were used for the building materials. The redesign assumed a maximum potential earthquake lateral force of 44% gravity (almost 3-1/2 times the original design). In the redesign, unit stresses were used that averaged approximately twice those specified in the Uniform Building Code. The load factor (safety factor) was cut in half since the absolute maximum expected earthquake force was used rather than the nominal force specified by the code. (16)

CONCLUSIONS

Investigation after the San Fernando earthquake led to the following conclusions.

1. A combination of complete and detailed design, proper code requirements, and careful construction can result in a building with a high level of performance, even when subjected to the extreme loads of San Fernando. The exceptional performance of schools constructed under the Field Act proved that fact.

2. Additional design detail and inspection during construction can result in buildings with good earthquake resistance, at a very nominal increase in cost over those with inadequate resistance. Examination of buildings with structural failures showed how little extra would have been required.

3. An "importance factor" should be developed for each design. The destruction of hospitals and electrical distribution centers in

San Fernando underlined need for this factor.

4. The duration-of-load adjustment for wood under seismic load should be raised to 1.75 from the present 1.33. This increase is justified by the outstanding performance of well designed and properly constructed wood-framed buildings, even subject to what can be considered an "ultimate earthquake".

REFERENCES

1. Bolt, Bruce A., Los Angeles Times, February 19, 1971.

2. Briasco, Ezio, "Behavior of Joist Anchors Versus Wood Ledgers". San Fernando California Earthquake of February 9, 1971, Vol. 1, 1973, U.S. Department of Commerce, p.121 - 125.

3. Degenkolb, Henry J., "Preliminary Structural Lessons from the Earthquake, The San Fernando, California Earthquake of February 9, 1971," U.S. Department of the Interior, U.S. Department of Commerce 1971,p.133.

4. Fintel, Mark, "Quake Lesson from Managua: Revise Concrete Building Design", Civil Engineering Vol. 43,No. 8, August 1973, p. 60-63.

5. Frazier, G. A., Wood, J. H.,Housner, G. W. (1971), "Earthquake Damage to Buildings", Chapter 3 in "Engineering Features of the San Fernando Earthquake EERL 71-02," California Institute of Technology, Pasadena, p. 233.

6. Hanson, R. D., and Degenkolb, H. J., "The Venezuela Earthquake, July 29, 1967", American Iron and Steel Institute, 1969, p. 125 - 130.

7. Hudson, D. E. and Jepcott, D. K., "The San Fernando Earthquake and Public School Safety", Bulletin of the Seismological Society of America, Vol. 64, No. 6, December 1974, p. 1669.

8. Jenning, P. C., Housner, G. W. (1971) "Conclusions and Recommendations." Chapter 8 in "Engineering Features of the San Fernando Earthquake, EERL 71-92", California Institute of Technology, Pasadena, p. 478.

9. Ibid., p. 484.

10. Jephcott, D. K. and Hudson, D. E., "The Performance of Public School Plants During the San Fernando Earthquake", California Institute of Technology, September 1974, p. 186.

11. Ibid. p. 102

12. Kachadoorian, Reuben, "An Estimate of the Damage, The San Fernando, California Earthquake of February 9, 1971," U. S. Department of the Interior, U. S. Department of Commerce 1971, p. 5.

13. Lew, H. S., Leyendecker, E. V., Dikkers, R. D. (1971) "Engineering Aspects of the 1971 San Fernando Earthquake," U.S. Department of Commerce 1971, p. 269.

14. Ibid., p. 406.

15. Martin, J. A. & Associates, "Redesign Report Building No. 11", An Evaluation of a Response Spectrum Approach to Seismic Design of Buildings; September 1974, Applied Technology Council, p. 56.

16. Ibid p B-166.

17. Meehan, J. F., "The Response of Several Public School Buildings in Anchorage, Alaska, to the March 27, 1964 Earthquake", The Prince William Sound,Alaska Earthquake of 1964 and Aftershocks 1967, U.S. Department of Commerce, p. 221.

18. Nosse, John, "Plywood Diaphragms", verbal presentation to 1st Western Roundup of Structural Engineers Associations, Sun River, Oregon, June 1975.

19. Steinbrugge, Karl V., Manning, John H., Degenkolb, Henry J.,"Building Damage in Anchorage", The Prince William Sound, Alaska Earthquake of 1964 and Aftershocks, Volume 11, U. S. Department of Commerce (1967), p. 14.

20. Walters, Kenn. Personal communication to author December 1975.

21. Wichman, R. H. & Associates, "Redesign Report Building No. 9". An Evaluation of A Response Spectrum Approach to Seismic Design of Buildings, September 1974, Applied Technology Council, p. 54.

22. Wheeler and Gray, "Stone's Liquor Store", San Fernando California Earthquake of February 9, 1971, Vol. 1, 1973, U. S. Department of Commerce, p. 45 - 50.

23. Ibid. "Vector Electronics", p. 75 - 81.

24. _____, "Managua Dozes Wreckage, Sorts Out What's Salvageable" Engineering News Record Vol. 190, No. 2, January 11, 1973, p. 10 - 11.

25. _____, "Earthquake - Resistant Construction" Concrete Construction Vol. 18, No. 6, June 1973, p. 266 - 267.

26. _____, "The California Earthquake: February 9, 1971, "Earthquake Information Bulletin, U. S. Department of Commerce, March-April 1971, p. 8.

INTERNATIONAL SYMPOSIUM ON
EARTHQUAKE STRUCTURAL ENGINEERING
St. Louis, Missouri, USA, August, 1976

SAFETY OF CITIES DURING SEVERE EARTHQUAKES

O. CLARKE MANN, P.E.

O. Clarke Mann, P.E.; Consulting Engineers

Memphis, Tenn. U.S.A.

SUMMARY

The safety of modern cities during a severe earthquake is explored using simulation methods. The loss parameters were derived from recent earthquakes. The population and construction were modeled in accord with recent demographic projections for the area. The simulation indicates that 1.5% of the population may die or be seriously injured in a severe earthquake unless earthquake resistant structures are built. Before a higher level of safety is attained, the public must accept its responsibility to pay more for safer structures.

INTRODUCTION

The question to be explored in this paper is "How safe are modern cities during a strong earthquake?".

Serious questions have recently been raised about the safety of modern cities because most cities do not require earthquake loading in the design of buildings, and dramatic damage occurred to numerous aseismic buildings during recent earthquakes at Anchorage, San Fernando, Caracas, and Managua. These recent damages have deeply disturbed many people who are responsible for public safety because of the collapse or severe damage to structures that were built to modern building codes with seismic requirements.

In this paper the author will explore the safety of modern cities using simulations. Simulation methods were chosen for this analysis because they are capable of accounting for seismic history, variations in populations, and building technology, while predicting life losses. The exploration will indicate life losses and injuries which occur in different types of structures when exposed to severe earthquakes.

The exploration will be illustrated with results of a risk assessment for the metropolitan Memphis area.[5] This illustration will be of interest to the reader since Memphis' risks are similar to risk in other cities. There, structures range from old to new and from large to small for each class of construction. Soil conditions vary from medium to poor, and the population approaches a million. The area has a seismic history since the 1811-12 earthquake at New Madrid, Mo. was felt very heavily there.

SEISMIC DESIGN HISTORY

In order to appreciate the probable response of existing buildings to severe earthquakes, it is informative to look backward at the design criteria that have been in effect over the past 70 years.

Prior to 1950 seismology was in its formative stages, and there was no organized body of engineering information that defined seismic risk in the United States.

Except in the western United States, the law has been silent on earthquake requirements. Not until after the Long Beach earthquake of 1933 did California pass the Field Act directed to providing safe school buildings.

In 1949 the U.S. Coast & Geodetic Survey[9] published its first "Earthquake Risk Map", Fig. 1. During the following years seismological activities increased at an extraordinary rate. In 1969 the U. S. Coast & Geodetic Survey published a second "Earthquake Risk Map", Fig. 1, compiled by Algermissen[1]. This second map indicated an increased risk in many geographic areas, and also indicated an awakening to the reality of earthquake risks throughout this country.

The public does not in general understand seismic language, but everyone does understand the catastrophic message of falling buildings and many deaths. The translation from technical to lay language is best done through simulation analysis. Simulations start with data on magnitude, intensity, time, construction and population, and end with life losses and injuries. Since the simulation process is relatively new, a short description will be given.

RECURRENCE MODEL

The first element used in a simulation is a "Recurrence Model" in which current and past seismic acitivities of a geologic area are summarized. A recurrence model expresses the seismicity of a geological area by defining the range of credible earthquakes, and the average frequency with which they have occurred in recorded history.

Figure 2 presents recurrence models for earthquakes in the New Madrid and Memphis area. These were constructed by Howe[5] using the earthquake catalog of McClain and Myers[7]. The models indicate that an earthquake of intensity comparable to the great earthquake of Charleston, S.C. has a recurrence rate of once in 150 years.

CONSTRUCTION MODEL

The seismic safety of a given city depends upon its construction. Thus, the second element required for a simulation is a construction model which identifies the amount, location, and quality of each type of construction throughout the city.

Early seismologist ranked earthquake intensity in terms of visible manifestations and the damage to buildings was the major observation used. In the simulation process the sequence is reversed in that building damages and deaths are derived from Modified Mercalli (MM) intensity values.

Loss of life is used to measure safety, but since deaths usually result from building damage, it is appropriate that a few brief comments be made on building damage. To facilitate the simulation process construction is divided into four classes: structural steel frames are Class A, concrete frames are Class B, buildings with masonry bearing walls and piers are Class C, and wood framed residences with or without masonry veneers are Class D. The damage and danger associated with different classes of construction varies widely. Dutton[2] and Freeman[3] have pointed out the extreme damages to ordinary masonry construction during medium earthquakes. This makes Class C structures extremely dangerous. Steinbrugge[8], Hanson and Degenkolb[4], and Freeman[3] have described a wide range of damages to concrete structures in medium and severe earthquakes. When used as high-rise construction, one collapsing structure can bring many deaths as in Caracas. Wood frames, Class D residences, of good construction offer little danger to life even during severe earthquakes.

Construction throughout the United States is essentially homogeneous and this condition is helpful to the risk analyst. From the records of earthquakes throughout the country, it is possible to draw an adequate picture of the degree of damage to different classes of construction for each intensity of earthquake. Uniformity of construction makes it possible to apply throughout the United States the mathematical parameters that define property damages and life losses, even when these parameters are derived from widely separated events.

POPULATION

Because the question of seismic safety is to be answered in terms of people, population distributions are the third element used in this set of simulations. The distribution establishes a unique relation between people and type of structures at a chosen time.

An earthquake may occur at any time point, and substantial losses may occur at many different time points. Simulation points are chosen to reflect significant population patterns and are defined in terms of the number of people occupying each type construction. Winter weekdays reflect the school and work population pattern, and winter nights reflect the residential pattern. For this paper a winter weekday pattern was chosen as the time point for illustration.

Population distributions for Memphis in the years 1970 and 2020 are shown in Fig. 3. Each population is distributed first for day and night, and then subdistributed for each class of construction. For the full fifty year period it can be seen that Class D construction houses the greatest part of the population but the percentage is declining. The author[5] recently surveyed a group of planners, demographers, and bankers and found that Americans are moving from the single family house toward multi-family structures. This group expects a three-fold to five-fold increase in apartment dwellings built of types A and B construction by the year 2020. The "three fold" change is shown in Fig. 3. Notice that in Class B the nighttime population increases from 3% to 9%, and the daytime population increases from 9% in 1970 to 22% in 2020.

LIFE LOSS

The next type of information that is needed in making a simulation is information related to life losses.

Earthquakes of damaging intensities have occurred in many parts of the United States within the last 100 years. Engineers, insurance investigators, and seismologists have surveyed the striken areas. Their records indicate the form and degree of damage and life losses related to each type of construction.

When making a risk study the analyst draws heavily from these records. Earthquakes of the chosen intensity, occurring where construction and soils are comparable to the subject area, are used as references. As an example, an earthquake of intensity 8.0 to 9.0 (MM) struck Long Beach, Calif. in the late afternoon of March 10, 1933. Much of the construction has been described by Martel[6] as of poor quality Class C. In the area of poor conditions there were 48 deaths in a population of 142,000. Thus, for poor quality, Class C

construction, the specific mortality ratio occurring in the Long Beach earthquake was 34 deaths per 100,000 population. It can be estimated from this record that should an earthquake of intensity 8.0 (MM) strike another area where 200,000 people lived in poor quality masonry structures, 68 people would lose their lives.

SIMULATIONS

A simulation is a mathematical process by which a specified set of initial conditions are hypothetically interacted in order to study the results. In preceding sections the elements or conditions for earthquake simulations have been described. They were earthquake recurrence, construction and population models, and life loss information or mortality ratios. Using these elements, simulations are made on the premise that a given type of construction, exposed to a given intensity earthquake, will perform substantially the same regardless of its time or place.

The simulation for a given intensity is made by summing the life loss determination for each class of construction and population distribution as indicated by Equation 1.

$$ {}_tLL_i = \sum_{n=A}^{n=D} \left[MR_n \times \Delta P_n \right] \qquad \text{EQ-1} $$

- i Earthquake intensity
- n Class of construction
- t Time point
- LL_i Life loss for intensity 'i'
- MR_n Mortality ratio for construction 'n' during intensity 'i'
- ΔP_n Population within construction

To illustrate a simulation the writer chose a weekday morning in the year 2000 and the city of metropolitan Memphis, Tenn. The "Recurrence Model", Fig. 2, indicates that the maximum intensity expected is 9.0 MM, which occurred during the 1811-12 earthquake; a recurrence of that event was assumed. A number of population projections have been recently made for Memphis and the consensus of the projections indicates a population of about 1,300,000 in the year 2000. From the population distribution data shown in Fig. 3, the population in each class of construction was interpolated. This calculation indicates that 24% of the people will be in Class A construction, 18% in Class B, 13% in Class C, and 45% in Class D. Mortality ratios were derived from the San Fernando, Caracas and Anchorage earthquakes. These simulation conditions are shown in Fig. 4.

The present Memphis building code, like many other cities, has no earthquake design requirements. The first simulation was made on the assumption that no code changes will be made. A second simulation was made assuming that construction of Classes A, B, and C buildings built after 1975 will be designed to Uniform Building Code 1968-Zone 3 requirements. These two simulations are henceforth referred to as Option 1 and 2.

Option 1 simulation indicates that under a severe earthquake a total of 3620 people will die, and 16,000 will be so seriously injured as to require extended hospitalization. The distribution of deaths between different types of construction is shown in Fig 4; ie, Class A-too few to estimate; Class B - 2350; Class C - 1200; and Class D - 70. Thus, for 20,000 people the city of Memphis, during a severe earthquake, will not be safe if Memphians continue to build buildings that are not designed to resist earthquakes.

On the other hand, if Option 2 is chosen the city will be a great deal safer. If the building code is changed and all buildings, except Class D residences, built after 1975 are designed and built for Uniform Building Code-Zone 3 earthquake loading, the number of deaths can be cut in half. The death total can be reduced from 3620 to 1710. The number of deaths in Class B construction can be reduced from 2350 to 1400, and in Class C from 1200 to 240.

If the number of deaths is used to index safety, the city designed and built to resist a severe earthquake is twice as safe as one that is not. Simulations show that if present building practices are continued, 1.5%of the population in a typical American city is in serious danger during a severe earthquake. The number of persons in serious danger can be reduced in half if new buildings are built to resist earthquakes in a manner set forth in the Uniform Building Code of 1968.

It is understandable that many people have asked why all buildings are not made earthquake resistant. The answer is that earthquake resistance adds substantially to building costs.

EARTHQUAKE PROTECTION COSTS

An in-depth treatment of earthquake protection costs is beyond the scope of this paper, but the omission of a few brief remarks about costs would be a disservice to the reader and to the general public.

To provide Option 2 protection for the Memphis area would increase building costs over the next 24 years by about $280 million.[5] Since Memphis can reasonably be assumed to be a representative city, it is estimated that society must pay

about $150,000 for each life saved. The writer has found that most people are not willing to pay such a high price for protection against an earthquake, and are often strongly opposed to revising building codes to require earthquake resistant structures.

The opposition to higher building costs arises from the fact that the frequency of severe earthquakes is too small to impress people. Also, there are other more pressing, even though less dramatically dangerous, needs competing for the same dollars. In addition, people inherently take risks rather than spend their money, especially when the probability of the loss is small.

RESPONSIBILITY FOR PROTECTION

Since the question to which this paper is addressed is "How safe are modern cities?", it is reasonable that a meaningful answer should point to who is responsible for that safety. Responsibility is shared by the seismologists, geologist, the engineer, and the public. This interaction is illustrated by the Venn diagram in Fig. 5.

The technical limits of safety are defined by the engineer, seismologists, and geologists and contributions of each are indicated by sets "S" and "E". The limits of safety are thus defined by the union of these sets which form subset "G". But, society enjoys only a part of this potential asset because society opposes higher building costs and funding is currently inadequate. Public willingness to provide additional funds for earthquake protection is generally nil. This condition is schematically defined by set "MO" which corresponds to Option 1. Half of the unrealized potential can be enjoyed if society is willing to expand the funding set to "M 3" which reflects Option 2.

Thus the final decision on seismic safety must be made by society in its own behalf.

CONCLUSIONS

This paper addresses the question of "How safe is a typical modern city during a severe earthquake?" and answers it with three conclusions:

1. There is a substantial risk of death or serious injury to people living in a typical city in the United States. Simulation analysis indicates that as many as 1.5%of a city's population may be seriously injured or killed during a severe earthquake.

2. The engineering profession has the technical ability to design buildings that are many times safer than most of those being built. But, society in general has not shown a willingness to pay for safer buildings.

3. In our social system it is society who must make the final decision regarding its own safety. But it is appropriate that engineers and scientists speak out to the end that society can make an informed decision on so vital an issue as seismic safety.

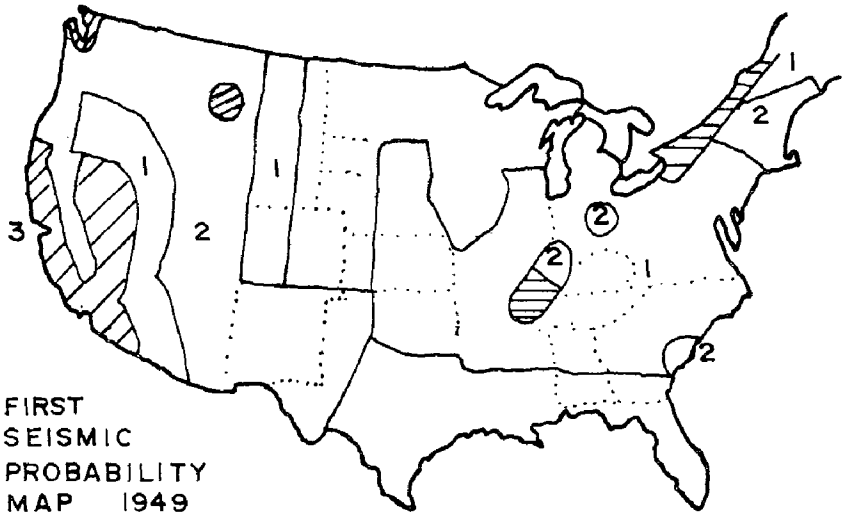

FIRST
SEISMIC
PROBABILITY
MAP 1949

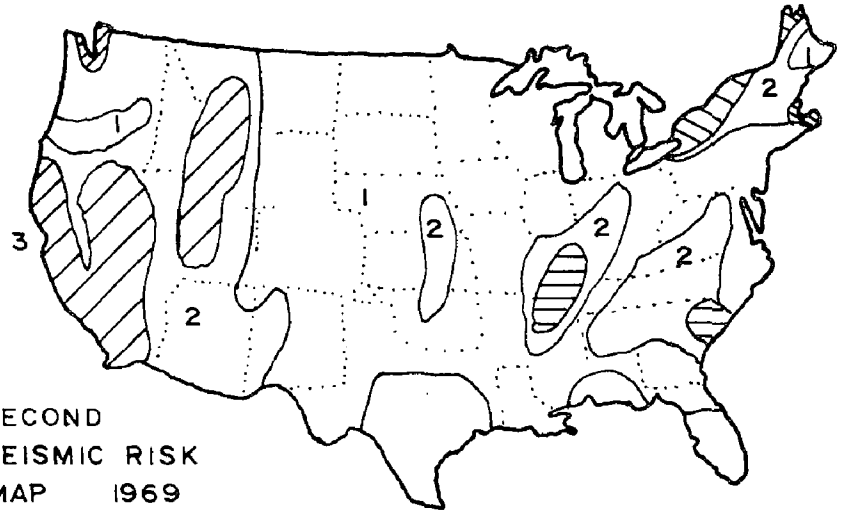

SECOND
SEISMIC RISK
MAP 1969

(by Algermissen)

SEISMIC RISK MAPS BY U.S. COAST & GEODETIC SURVEY

FIGURE 1

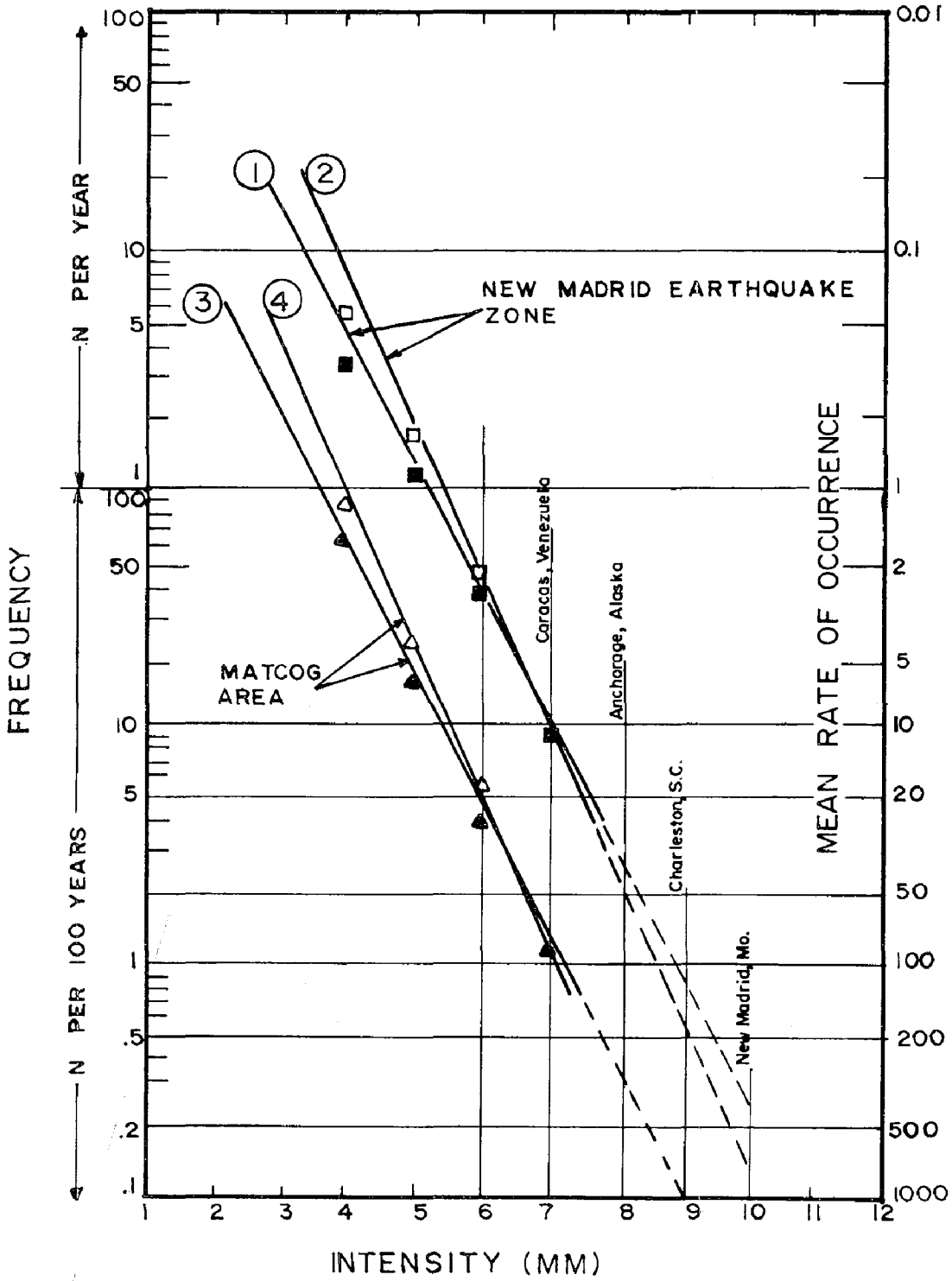

RECURRENCE MODEL

After HOWE

FIGURE 2

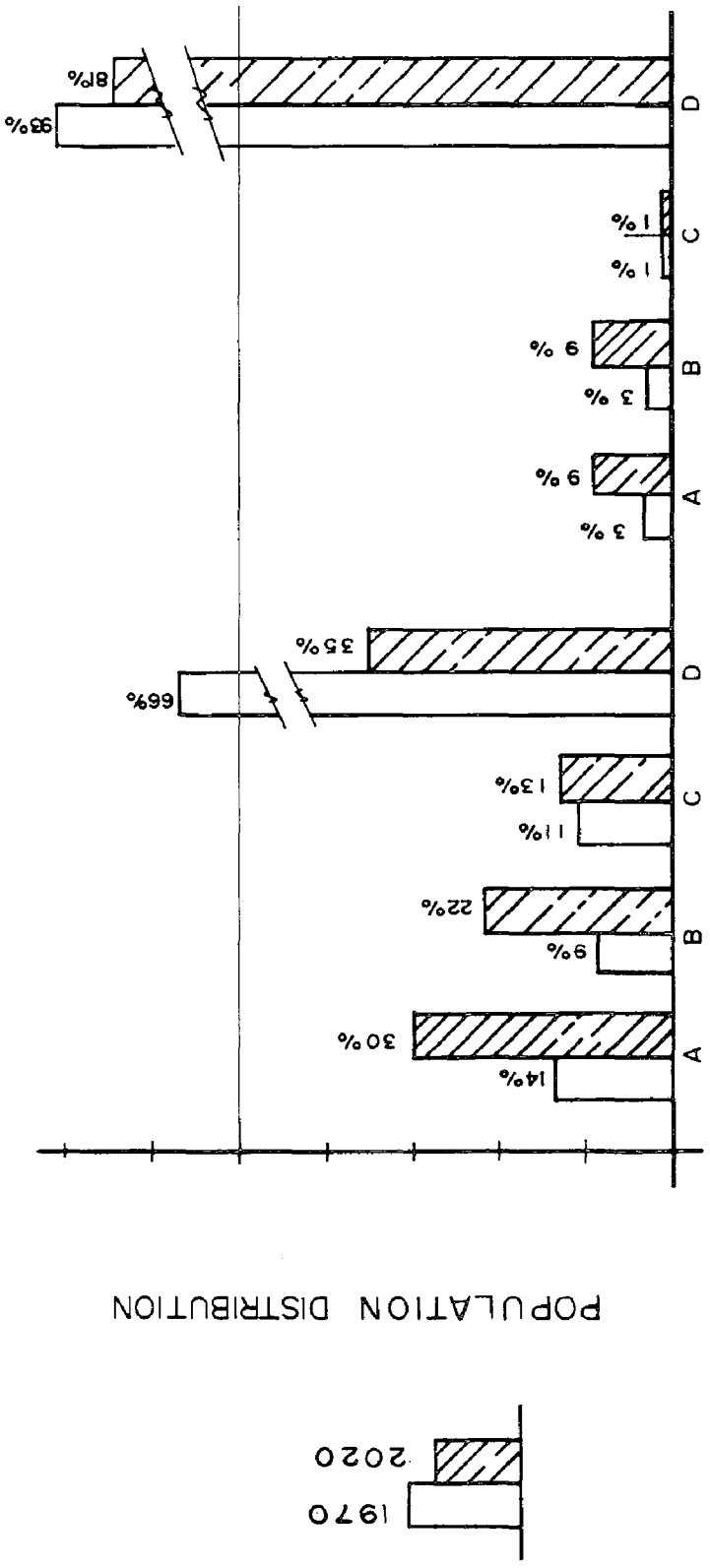

POPULATION DISTRIBUTION BY CONSTRUCTION TYPE
MEMPHIS, TN. 1970 & 2020
Mann

FIGURE 3

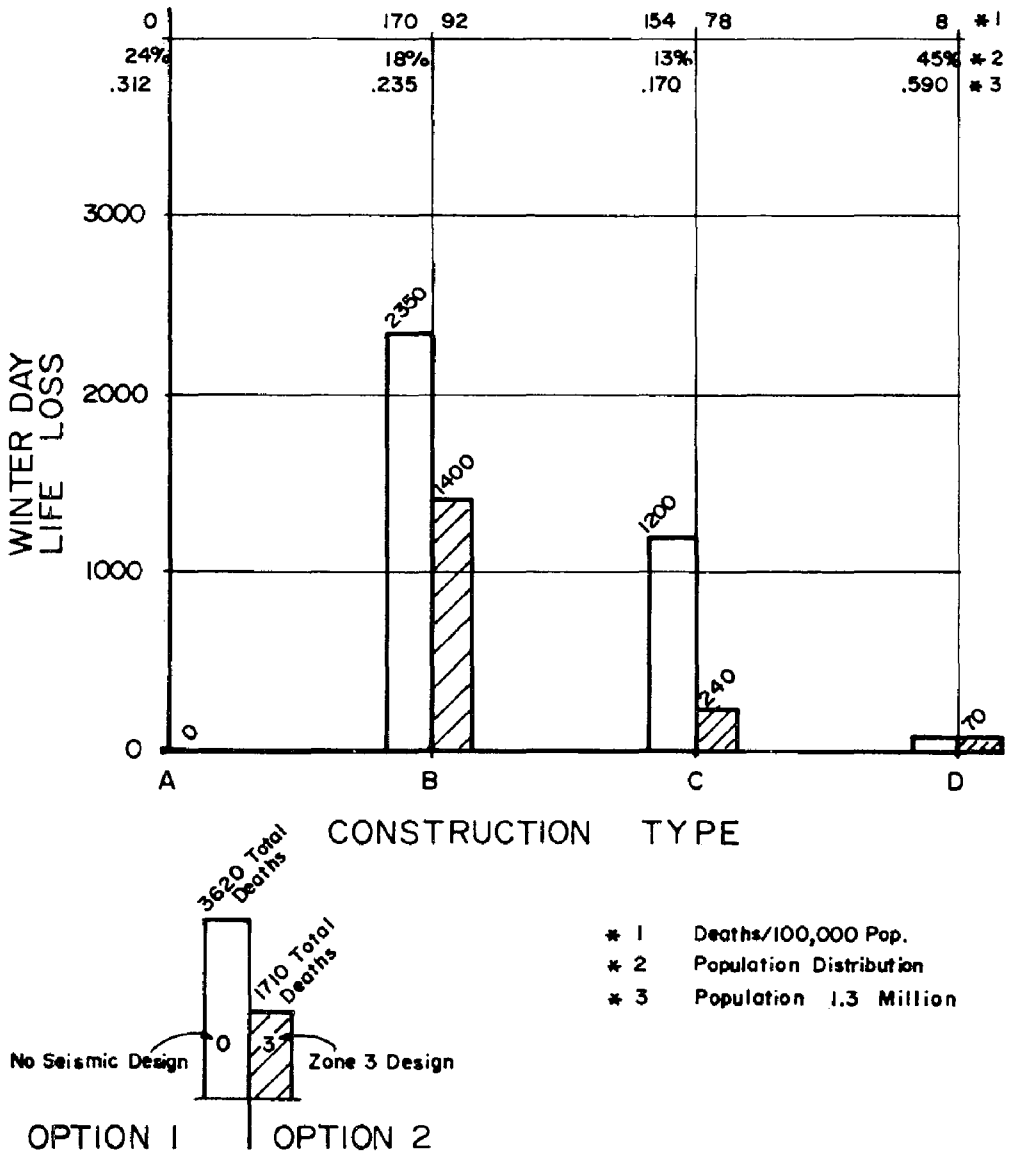

LIFE LOSS IN MEMPHIS YEAR 2000 - INTENSITY 9(MM)

MANN

FIG. 4

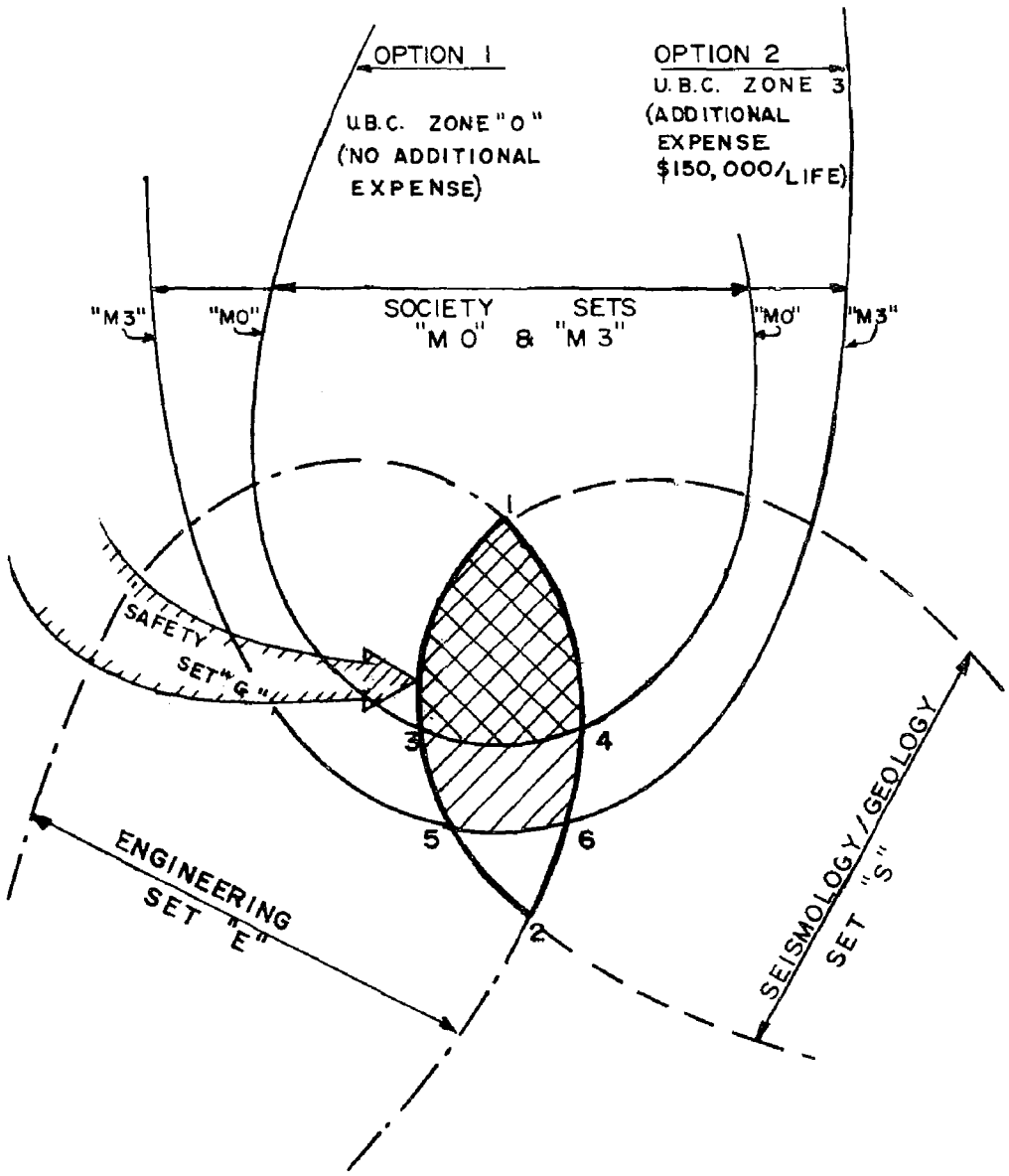

EARTHQUAKE PROTECTION RESPONSIBILITIES

Mann

FIGURE 5

BIBLIOGRAPHY

1. Algermissen, S.T., "Seismic Risk Studies in the United States", 4th World Conference on Earthquake Engineering, Santiago, Chile, 1969, ESSA/Coast & Geodetic Survey.

2. Dutton, C.E., "The Charleston Earthquake of August 31, 1886", U.S. Geological Survey, Ninth Annual Report 1887-1888.

3. Freeman, J.R., "Earthquake Damage & Earthquake Insurance" McGraw Hill Book Co., 1932.

4. Hanson, R.D., Degenkolb, H.H., "The Venezuela Earthquake of July 29, 1967", American Iron and Steel Institute, New York, 1969.

5. M & H Engineering (Mann, O.C. & Howe, W.) & Memphis State University (Kellogg, F.H.), "Regional Earthquake Risk Study", Mississippi-Arkansas-Tennessee Council of Governments/Memphis Delta Development District, funded by Department of Housing & Urban Development, 9/30/74.

6. Martel, R.R., "Earthquake Damage to Type III Buildings in Long Beach, 1933", in Earthquake Investigations in the Western United States 1931-1944, Carder, D.C.Editor, Publication 41-2, U.S. Department of Commerce, U.S. Coast & Geodetic Survey.

7. McClain, W.C., Myers, O.H., "Seismic History and Seismicity of the Southeast Region of the United States", Oak Ridge National Laboratory,(ORNL-4582), June 1970.

8. Steinbrugge, K.V., Schrader, E.E., Bigglestone, H.C., Weers, C.A., "San Fernando Earthquake, February 9, 1971" Pacific Fire Rating Bureau, San Francisco.

9. U.S. Coast & Geodetic Survey, "Seismic Probability Map", 1949.

INTERNATIONAL SYMPOSIUM ON
EARTHQUAKE STRUCTURAL ENGINEERING
St. Louis, Missouri, USA, August, 1976

EVALUATION OF GREEK STRONG MOTION RECORDS

P. G. CARYDIS J. G. SBOKOS

Assistants at the National
Technical University of Athens
Greece

Summary

In this paper the two horizontal components for every one of four rather strong Greek earthquakes are presented. For every one recorded motion, the absolute acceleration, relative velocity and relative displacement response spectra are evaluated. Further, their ground acceleration, velocity and displacement as well as the energy flux are plotted as a function of time. In a separate table some information concerning these earthquakes are given, like the name, location and date of occurance, epicentral distance, magnitude, intensity, kind of soil, maximal values of the ground motions and their duration.

Introduction

The installation of the Strong Motion Network in Greece started at 1971, after the participation of the country in the project "Survey of the Seismicity of the Balkan Region" under the program of UNESCO & UNDP offices. The total number of Strong Motion Accelerographs that will be installed before the end of this year will be more than 20 units. All of them are of the same type SMA-1, except the one installed at Cephalonia which is SMAC-B type.

From this network of Strong Motion Accelerographs, was possible to register eight in total earthquake motions. For the first two earthquakes ever registered in Greece, namely these of Sept.17 and of Oct.30, 1972 at Cephalonia, the two horizontal components of the ground acceleration was not possible to be used accurately, due to some malfunction of the vertical component of the instrument. For the other six earthquakes all three components of the ground acceleration was possible to be recorded and to be used with confidence for further analysis.

For every one of the registered eight earthquakes some valuable information is presented in Table I. As it is shown in this Table, every earthquake receives his name from the region where the epicenter was located*, and

* Better, from the region where the most damages occured.

this name is characterized by the two last digits of the year when the earthquake occured, and further by his serial number of occurance within that year. Every component receives an identification after the above mentioned characteristic numbers, namely the letters "L", "T" and "V" for the component which is parallel to the longitudinal, tranversal and vertical axis of the instrument respectively.

In Table I are given the location of the epicenter as is officially casted by the National Observatory of Athens, as well as the local time of occurence of the earthquake. Further, the epicentral distance of the site of the accelerograph, the magnitude calculated from the surface waves and the epicentral Intensity according to the Mercalli scale as these are given by the NOA are also presented in Table I. It is well known that the soil filters the seismic waves according to its elastic and non elastic characteristics. For this reason in the Table I the kind of soil for every recording site is given. For the sake of comparison the duration of every component of the recorded ground motions for accelerations higher than 10% of their maximum acceleration is given in the last column of the same Table.

The Background Theory

It is well known that a seismic analysis of any kind of structure can be very well performed by the so called modal superposition method,when the behavior of the structure is expected to be at the most linear. As an inevitable result of the application of this method of analysis is the use of the response spectra as this has been elsewhere theoretically proved [4]*.

Since the aseismic regulations deal with the linear behavior of structures,or are basically refered to that,the response spectra are established as the basic reference for the study of an earthquake from the structural engineering point of view and for the rational development of the various aseismic codes as well.

The behavior of a multidegree of freedom elastic system,subjected to earthquake ground motion is given [4] by the solution of the differential equations:

$$[m]\{\ddot{v}\}+[C]\{\dot{v}\}+[K]\{v\} = -\ddot{y}\{m\} \qquad (1)$$

where: $[m]$ and $\{m\}$ are the diagonal and column vector mass matrices of the system respectively
$[C]$ the damping matrix
$[K]$ the stiffness matrix
$\{v\},\{\dot{v}\},\{\ddot{v}\}$ the column vector of the displacements,velocities and accelerations of the various levels of the system and
$\ddot{y}$ is the ground seismic acceleration as input motion to the elastic system.

Introducing the well known transformation for every level i:

$$v_i(t) = \sum_{r=1}^{n} \Delta_{ir}\phi_r\gamma_r(t) \qquad (2)$$

where: Δ_{ir} are the normalized half amplitudes of the r mode
ϕ_r the participation factor of the r mode and
$\gamma_r(t)$ the dynamic translation of a single degree of freedom oscillator of cyclic frequency ω_r and damping ratio ζ_r.

* Numbers in brackets corresponds to the bibliography,given at the end of this paper.

Expanding eq.(2) one receives the time histories of the translations $v_i(t)$, but this is a time consuming process,while the engineering applications only maximum probable values are of main importance. Thus the following relation is proposed in [5] and elsewhere.

$$\max v_i(t) = \sqrt{\sum_{r=1}^{n} \left(\Delta_{ir}\psi_r \max\gamma_r(t)\right)^2} \qquad (3)$$

The $\max\gamma_r(t)$ is given [4] after the solution of the equation:

$$\ddot{\gamma}_r(t)+2\zeta\omega_r\dot{\gamma}_r(t)+\omega_r^2\gamma_r(t) = -\ddot{y}(t) \qquad (4)$$

From eq.(4) one concludes that $\gamma_r(t)$ depends,besides the $\ddot{y}(t)$,on the values of ζ and ω_r. For five different values of the damping ratio,for a wide range of probable frequencies that can appear in an engineering structure and for every ground motion $\ddot{y}(t)$ the $\max\gamma_r(t)$ have been plotted against the periods of oscillation $T_r = 2\pi/\omega_r$. These curves, i.c.the response spectra, for the Greek shocks $\ddot{y}(t)$ are presented in this paper, and briefly explained in the following.

Evaluation of the Response Spectra

In order to calculate the maximum spectral values, standard techniques and computer programs [6] have been used. The digitization was done using a Hewlett Packard manual digitizer, with unequal time intervals.

A fundamental preliminary task was the baseline correction,due to some errors that could interfere during the recording,the development and digitization. This correction has been performed after A.G.Brady [1] and [6] with the use of a parabolic baseline.

The time duration of the ground motions for the computation of response spectra was taken longer than that shown in Table I, but eventhough this is relatively short. The digitized points for almost every record were more than 1000, corresponding to more than 120 points per second. After the abovementioned baseline correction, the corrected ground acceleration,velocity and displacement were computed. The maximum values of these quantities are shown at the respective columns of Table I.

Only four of the earthquakes that have been registered until now in Greece, has been possible to be evaluated at present. These earthquakes are: the main shock of the Cephalonia event of Sept.17,1972,and the two shocks, separate from each other with 20m time difference, those of the Leukas events of Nov.4,1973, and fourth , the Patras event of Jan. 29, 1974.

In Fig.1 the absolute acceleration response spectra are shown for the two horizontal components of every one of the abovementioned first three events, and for 0% and 5% damping ratios respectively (upper and lower part of the figure). In Fig.2 the relative velocity response spectra are given corresponding to the abovementioned events and for the same damping ratios, while the same yields for Fig.3 where the relative displacement response spectra are presented. Finally, for the two horizontal components of the Patras event of Jan.29,1974,the absolute acceleration response spectra are presented in Fig.4. As far as the ground shaking concerns its corrected acceleration, and after one integration its velocity and further its displacement

time histories are given in Figs 5,6 and 7 for every one horizontal component of the three earthquakes respectively.

In Fig.8 the energy flux or action of every one of these components have been plotted, since the authors believe that this quantity is a special feature of every earthquake shock,because figures out the way that the earthquake energy is released,being very important for seismic structures,as this has been first presented in [5], 1968.

Finally in Fig.9 the ground acceleration,velocity,displacement and energy flux is shown for both horizontal components of the Patras event.

Conclusions

Although the Leukas (73-1) earthquake,being one of the five strongest ever recorded [2] ground accelerations,shows peak acceleration equal to 0.54g which is more than three times higher than that of the Cephalonia (72-1) earthquake,its maximum undamped spectral acceleration has been found to be just 1.6 times higher than the latter one. This relation changes completely,when it is refered to damped spectral curves. This could be nicely explained by the following two reasons: One is the mechanism of the earthquake energy release and the other is the frequency content of every shock.

a) The cuves of the energy fluxes according to [3] give the picture of the way that the earthquake energy is released. The Cephalonia (72-1) event shows more constant energy release per unit of time,which according to [3] means a more sinusoidal character,evidently resulting to higher undamped spectral values. The energy release during the Leukas (73-1) event is done at one or two separate shocks,which has not relation [3] with any sinusoidal character,resulting thus to relatively smaller undamped spectral values.

b) The frequency content fo the abovementioned ground motions has a relation to item a) and to the soil quality,since the epicentral distance is almost the same. The soil where the seismograph at Cephalonia has been installed is rather hard,while that of Leukas is rather soft.To this fact could rely the reason of the quick dampening of the Cephalonia spectral values.

It must be noted here that not any substantial damage has been reported for the Leukas earthquake of peak acceleration equal to 0.54g.

The explanation given at the above item b) yields also for the difference at the frequency content between the Leukas (73-2) and Patras (74-1) earthquakes. The soil at Patras is rather hard. To this fact may rely the great difference between their curves of the total earthquake energy release, having a ratio 8:1,though these two earthquakes show almost the same peak accerations.

A great similarity can be drawn for the Leukas (73-1) and the Parkfield [7] earthquake. These two events show almost the same shape of the curve of the energy flux,as well as the same maximum value,with almost the same time duration,maximum ground acceleration and velocity.

From the analysis given above,one could conclude that neither the sole accelerogram nor the spectral diagrams are adequate data for the complete configuration of the character of an earthquake. The curve that shows the way of the earthquake energy release could be a very helpful feature after a comprehensive engineering judgment [3].

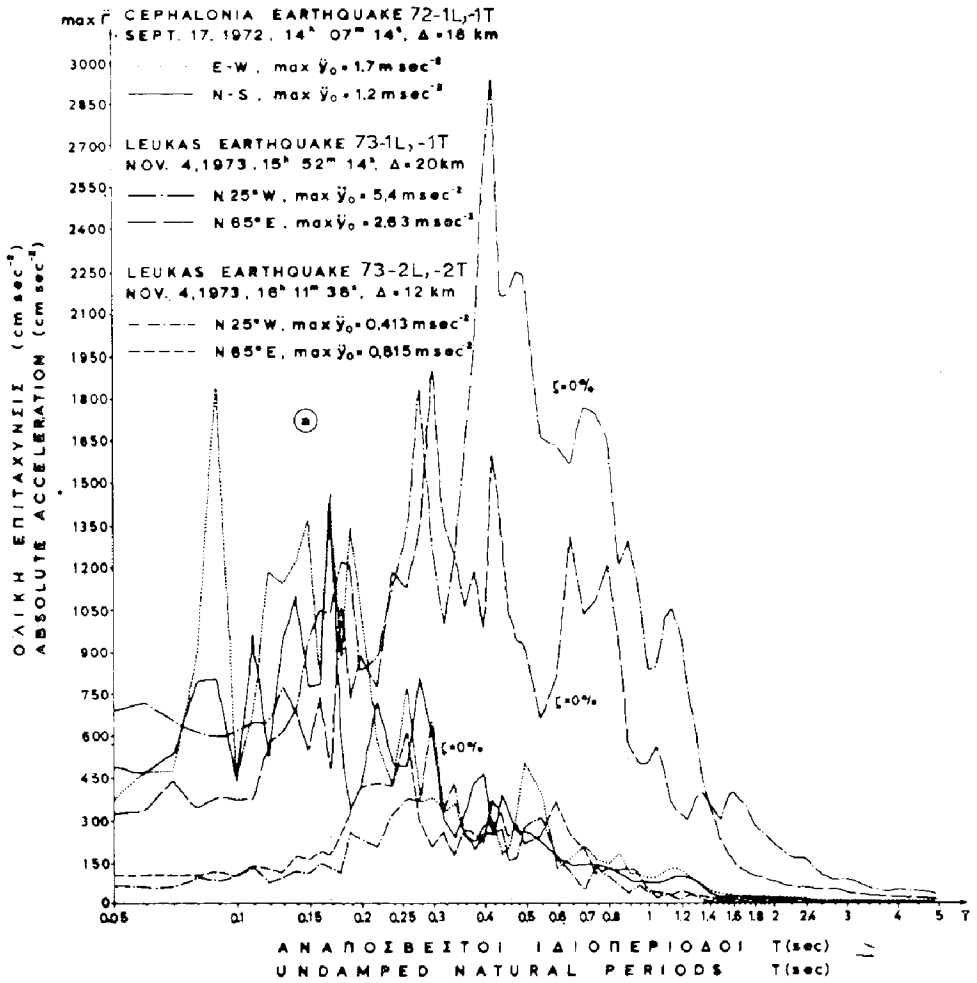

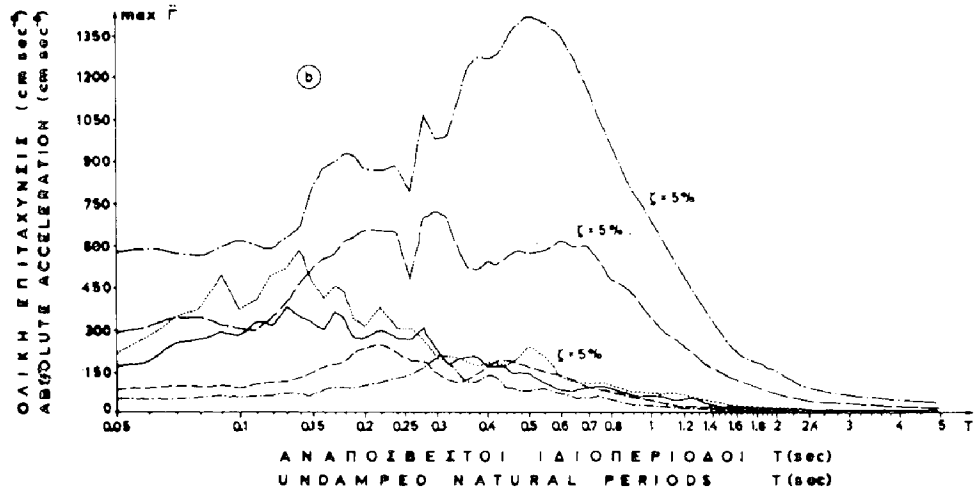

Fig.1 ACCELERATION RESPONSE SPECTRA OF THE 72-1(L&T),73-1(L&T) AND 73-2(L&T) EARTHQUAKES,FOR 0% AND 5% DAMPING RATIOS.

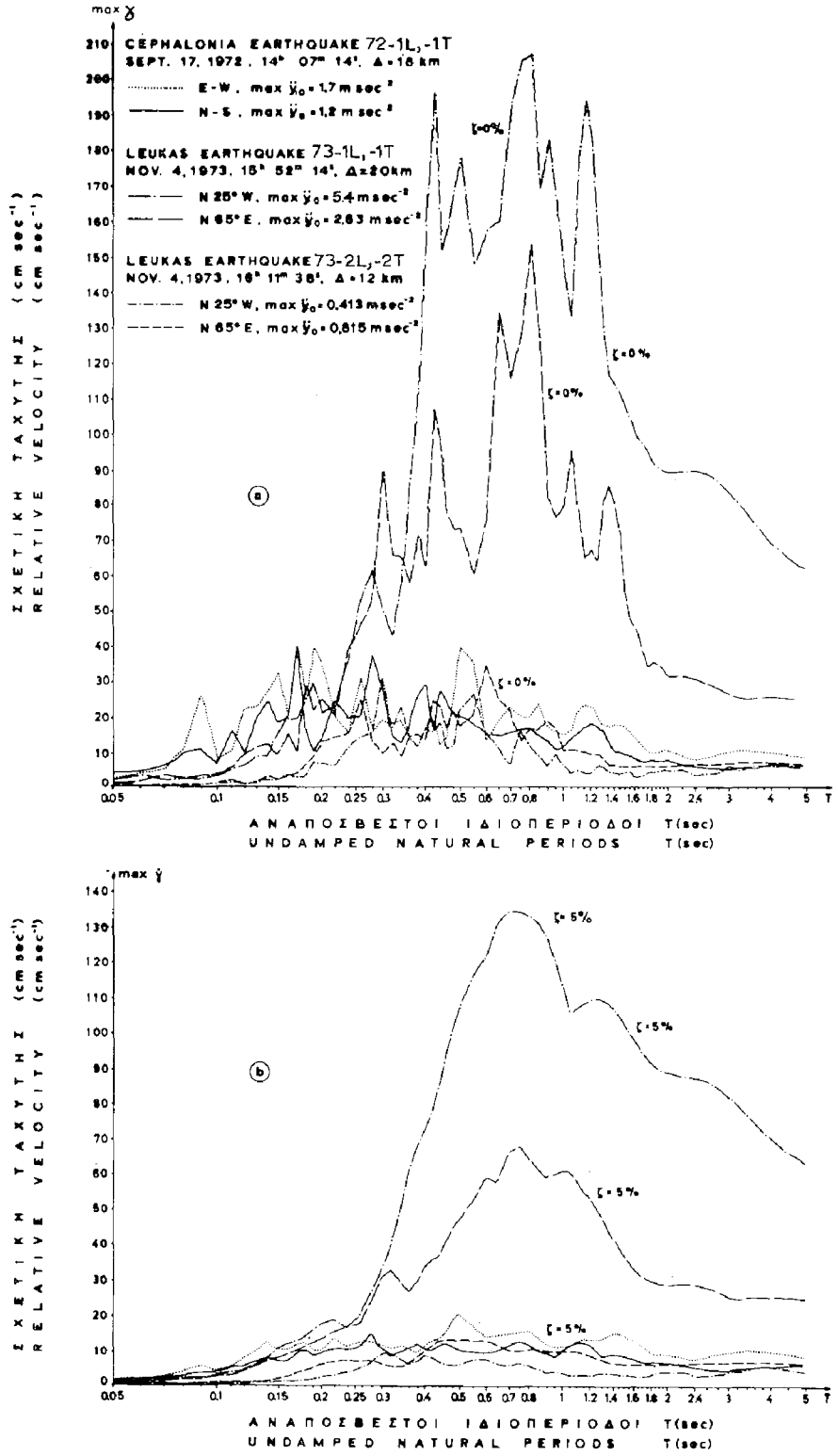

Fig.2 RELATIVE VELOCITY RESPONSE SPECTRA OF THE 72-1(L&T), 73-1(L&T) AND 73-2(L&T) EARTHQUAKES, FOR 0% AND 5% DAMPING RATIOS.

Bibliography

1) Brady A.G.,"Studies of Response to Earthquake Ground Motion", EERL, Calif.Inst. of Techn., Pasadena, 1966.

2) Galanopoulos A.G.,J.C.Drakopoulos, "A T Phase recorded on an Accelerogram", BSSA, Vol.64, No 3, June 1974, pp.717-719.

3) Carydis P.G., "Simplification of the Solution of the General Dynamic Aseismic Problem by Converting the Random Seismic Movement to equivalent Harmoni Vibrations", Doctoral thesis at NTU of Athens, 1968.

4) Kokinopoulos F.E.,P.G.Carydis, "Multidegree Plane Elastic Structures under the Action of Horizontal Seismic and other Dynamic Excitations". Scientific Publ.of NTU, No 23, Athens 1972.

5) Kokinopoulos F.E.,P.G.Carydis, "Proposal for a Dynamic Aseismic Design of Multidegree Structures", Athens 1973.

6) Nigam N.C.,P.C.Jennings, "Digital Calculation of Response Spectra from Strong-Motion Earthquake Records", EERL, Calif.Inst.of Techn.,Pasadena, June 1968.

7) Sarma S.K.,"Energy Flux of Strong Earthquakes", Tectonophysics, Vol.11,1971, pp.159-173.

TABLE I

NAME-LOCATION-DATE	Δ km	Ms	Ie	SOIL	COMPON/ IDENT.	max $\ddot{y}_o$ cm sec^{-2}	max $\dot{y}_o$ cm sec^{-1}	max y_o cm	Duration 10%max $\ddot{y}_o$ sec
72-1 CEPHALONIA SEPT. 17. 1972 $14^h\ 07^m\ 14^s$ 38.2° N, 20.4° E	18	6.2	VII	Lime-stone	E-W/72-1L	170	8	1.8	6
					N-S/72-1T	120	5	1.7	8
					Z/72-1V				
72-2 CEPHALONIA OCT. 30. 1972 $14^h\ 32^m\ 10^s$ 38.3° N, 20.4° E	22	5.5	V	Lime-stone	E-W/72-2L	165			6
					N-S/72-2T	70			8
					Z/72-2V				
73-1 LEUKAS NOV. 4. 1973 $15^h\ 52^m\ 14^s$ 38° 46′ 48″ N, 20° 33′ 00″ E	20	6.0	VII*	Saturated Alluvium	N 25° W/ 73-1L	530	65	26.8	9
					N 65° E/ 73-1T	263	30	12	12.5
					Z/73-1V	123	7.3	6.4	13
73-2 LEUKAS NOV. 4. 1973 $16^h\ 11^m\ 38^s$ 38° 45′ 36″ N, 20° 39′ 00″ E	12	5.0		Saturated Alluvium	N 25° W/ 73-2L	40	2.5	3.5	16
					N 65° E/ 73-2T	82	5.1	3.2	13
					Z/73-2V	27	2.3	2.3	15
74-1 PATRAS JAN. 29. 1974 $15^h\ 12^m\ 43^s$ 38.3° N, 22.0° E	17	4.4	V*	Alluvium	N 56° E/ 74-1L	41	1.5	0.6	7
					N 34° W/ 74-1T	40	2.1	1.1	7
					Z/74-1V	22	0.9	0.15	9
75-1 PATRAS APR. 4. 1975 $05^h\ 16^m\ 18^s$ 38.1° N, 22.1° E	32	5.5	VI	Alluvium	N 56° E/ 75-1L	21			14
					N 34° W/ 75-1T	46			14
					Z/75-1V	20			14
75-2 XYLOKASTRON MAY. 13. 1975 $00^h\ 22^m\ 50^s$ 38.2° N, 22.7° E	15	4.3	V*	Alluvium	E/75-2L	74			6.5
					N/75-2T	60			6.5
					Z/75-2V	26			6.5
75-3 CORINTHOS OCT. 12. 1975 $08^h\ 23^m\ 10^s$ 37.9° N, 23.1° E	16	5.0	VI	Alluvium	N 35° E/ 75-3L	27			14
					N 55° W/ 75-3T	30			14
					Z/75-3V	19			14

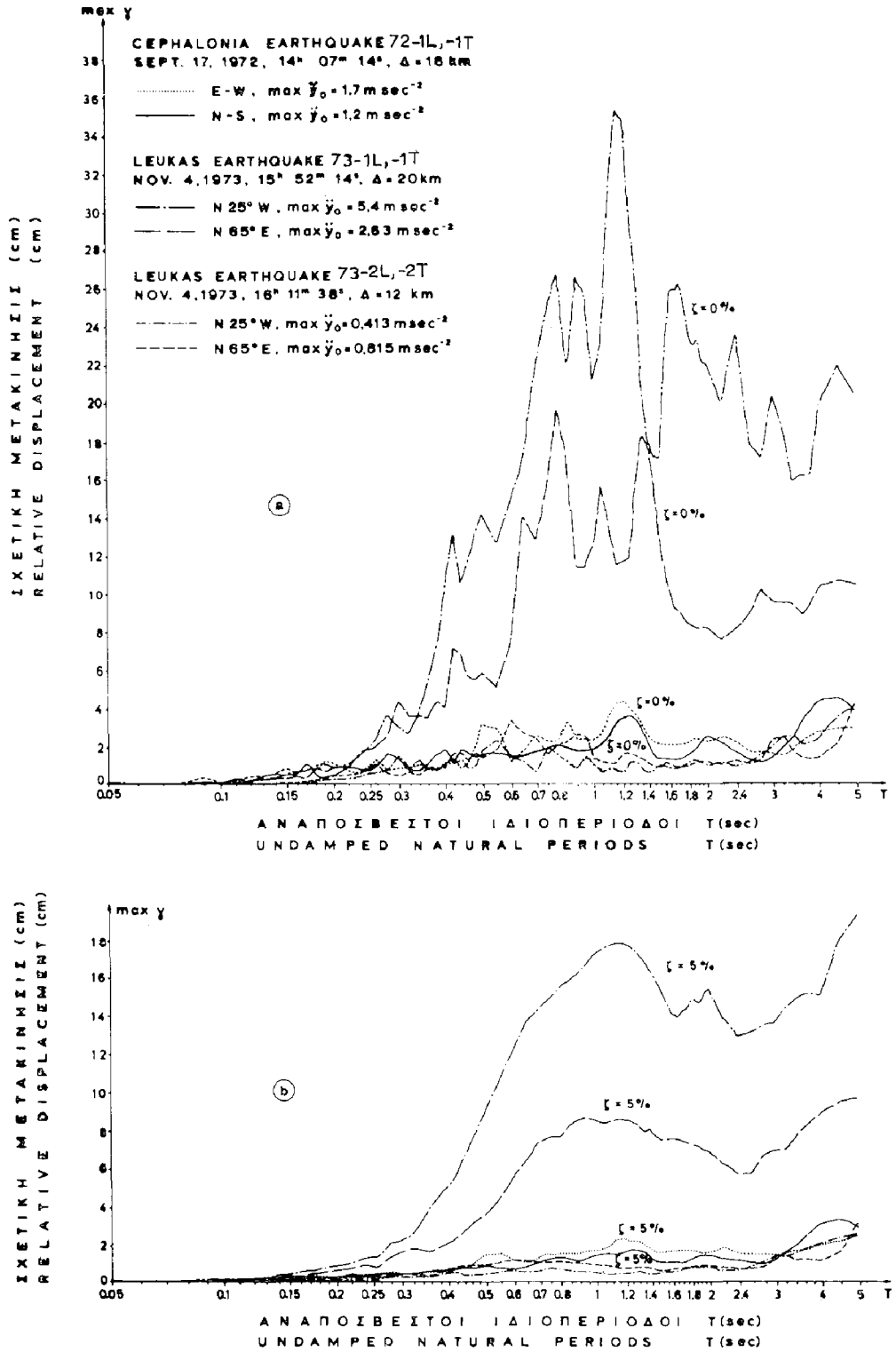

Fig.3 RELATIVE DISPLACEMENT RESPONSE SPECTRA OF THE 72-1 (L&T), 73-1 (L&T) AND 73-2 (L&T) EARTHQUAKES, FOR 0% AND 5% DAMPING RATIOS.

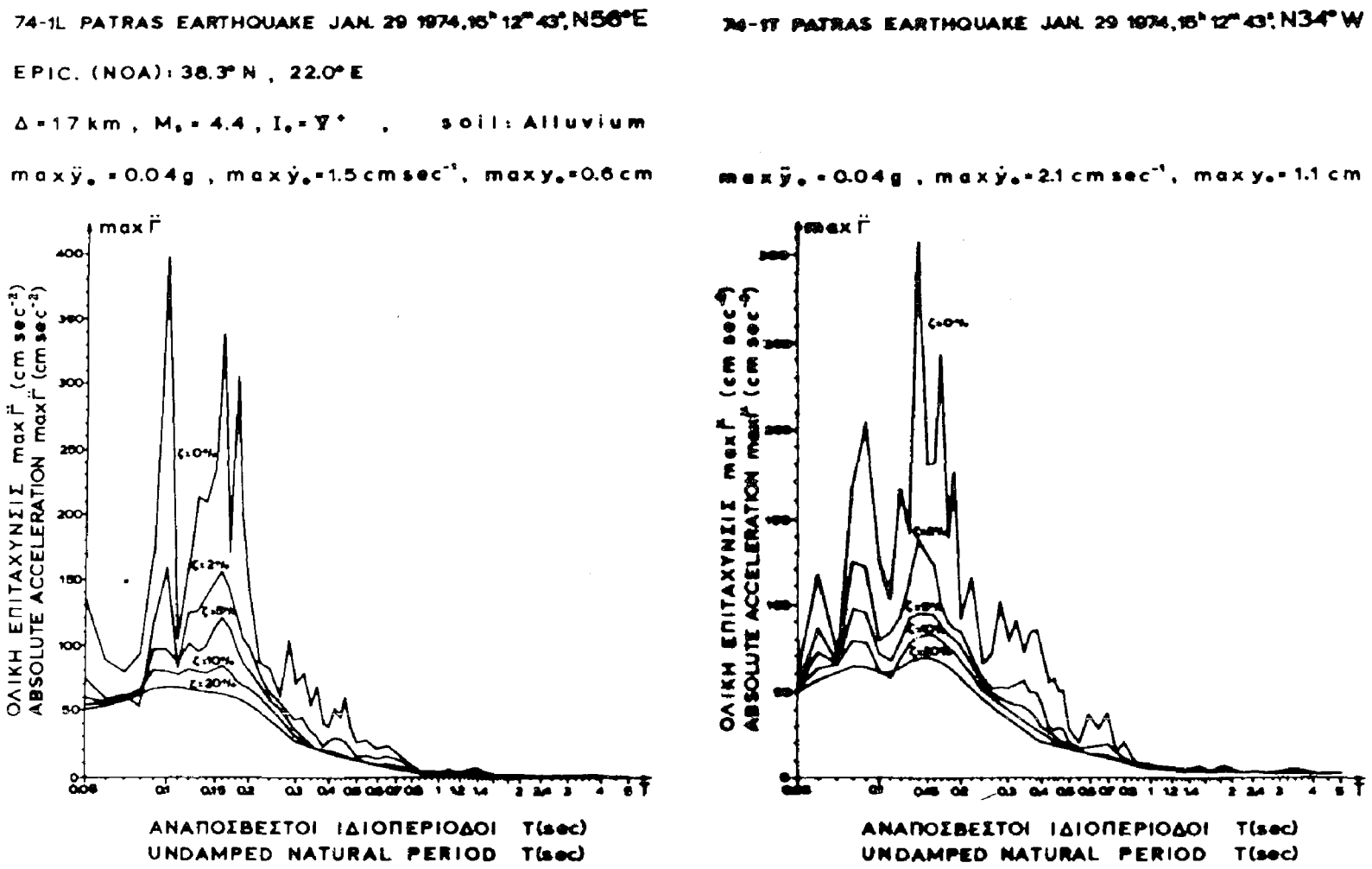

Fig.4 ACCELERATION RESPONSE SPECTRA OF THE 74-1 EARTHQUAKE (Longit.& Transv.) FOR 0%,2%,5%,10%,20% DAMPING RATIOS.

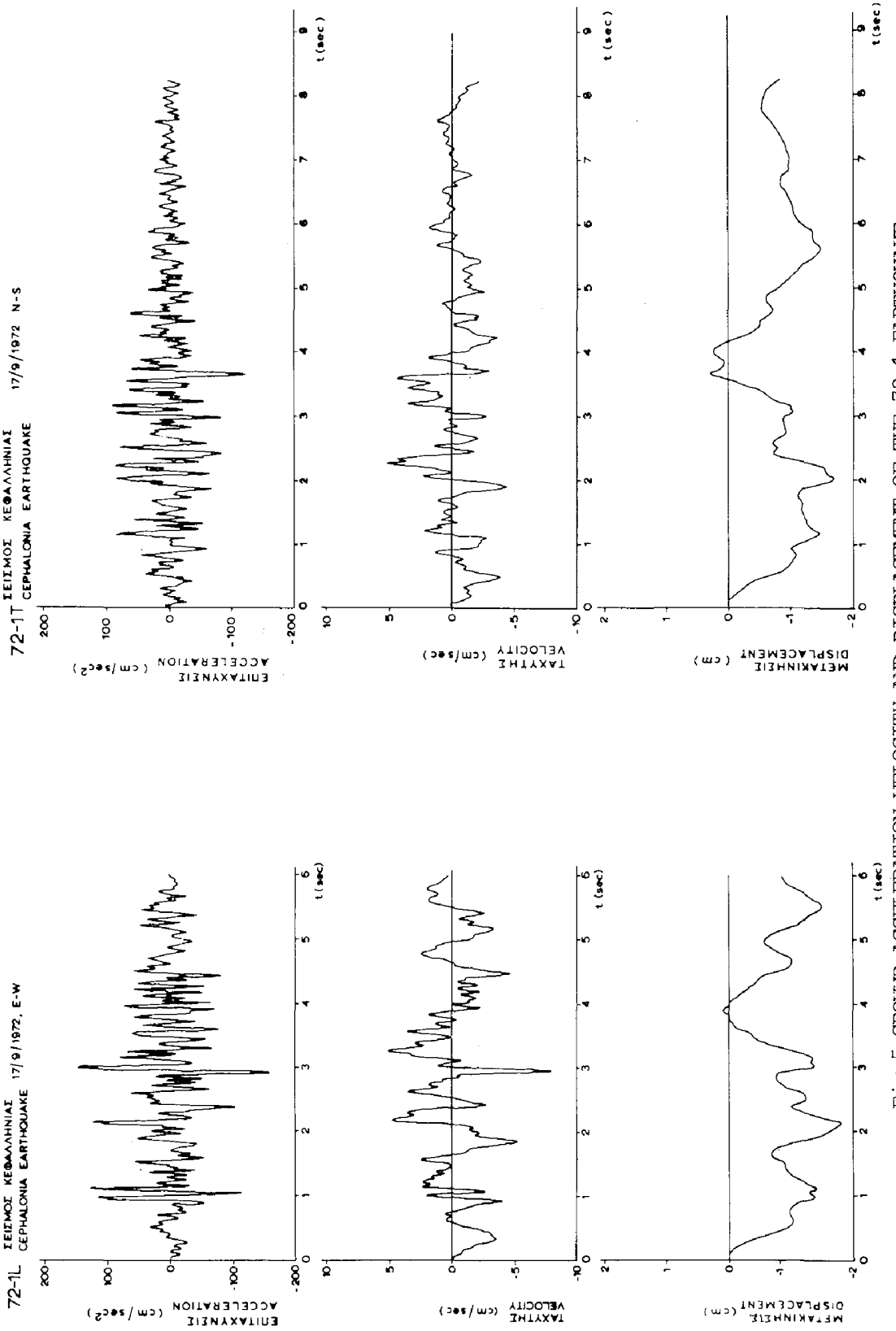

Fig.5 GROUND ACCELERATION, VELOCITY AND DISPLACEMENT OF THE 72-1 EARTHQUAKE

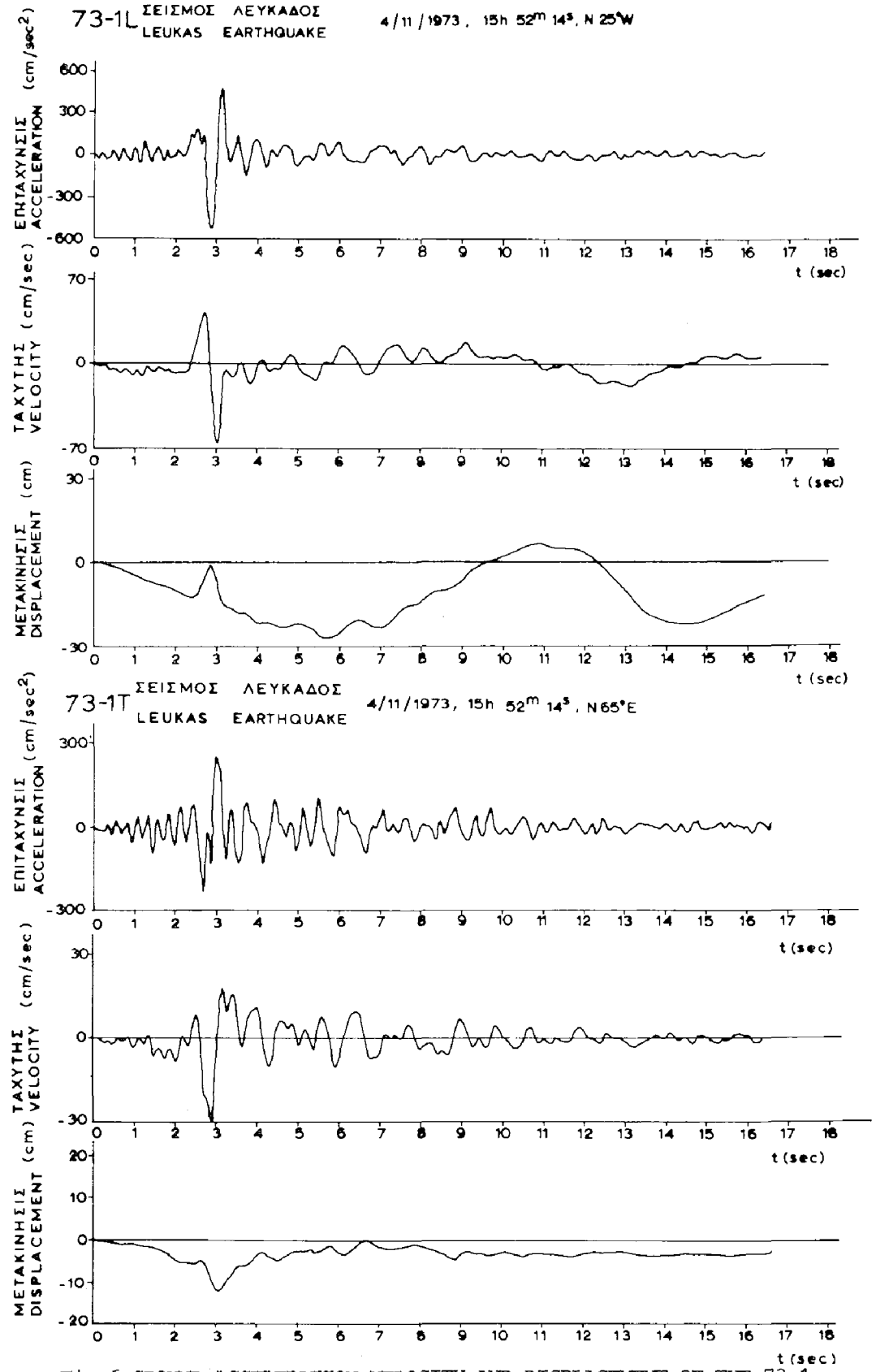

Fig.6 GROUND ACCELERATION, VELOCITY AND DISPLACEMENT OF THE 73-1 EARTHQUAKE (Longit.& Transv.COMPONENTS)

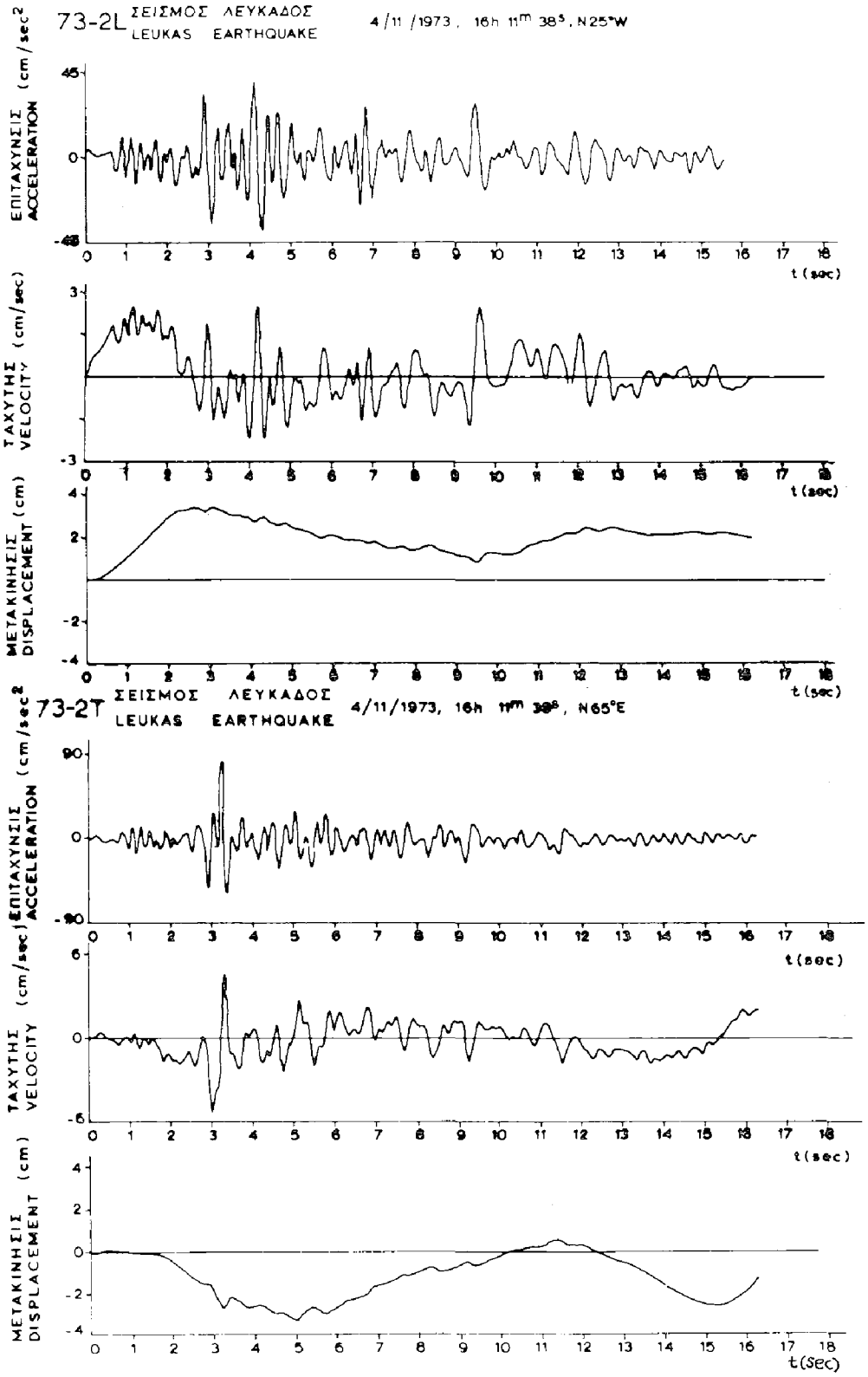

Fig.7 GROUND ACCELERATION,VELOCITY AND DISPLACEMENT OF THE 73-2 EARTHQUAKE(Longit.& Transv.COMPONENTS)

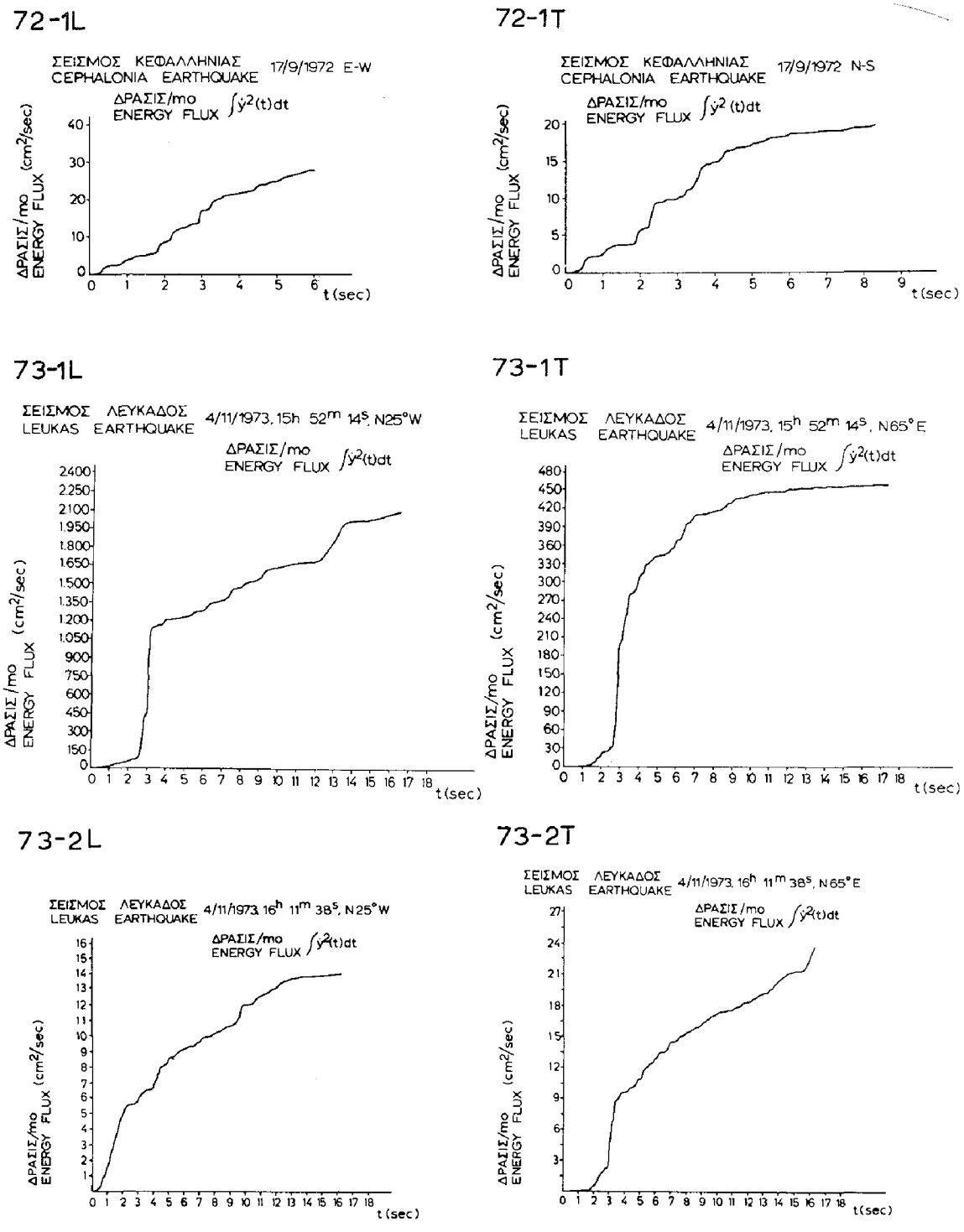

Fig.8 ENERGY FLUX OF THE 72-1(L&T),73-1(L&T) AND 73-2(L&T) EARTHQUAKES.

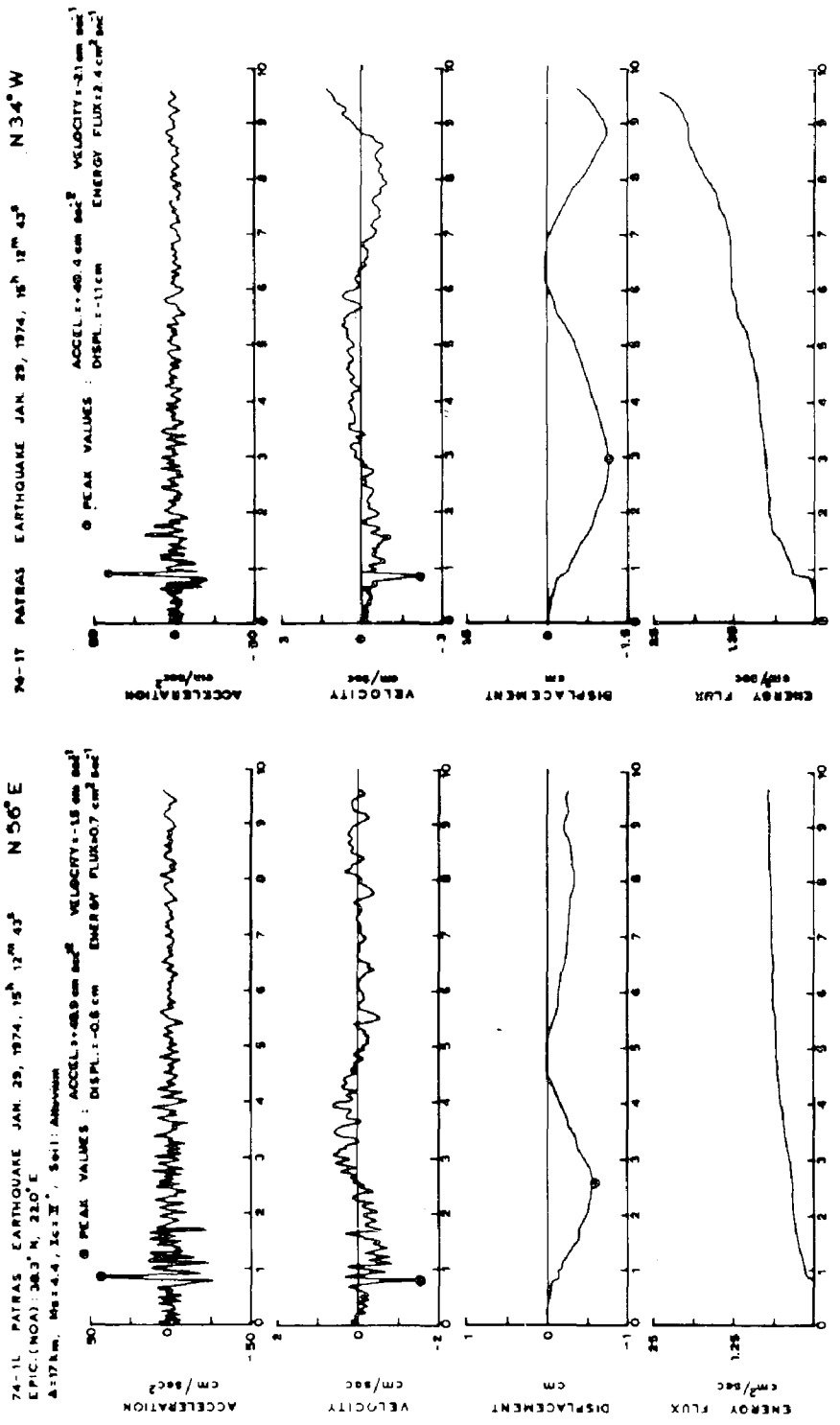

Fig. 9 GROUND ACCELERATION, VELOCITY, DISPLACEMENT AND ENERGY FLUX OF THE 74-1 EARTHQUAKE (Longit.&Transv.COMPONENTS).

INTERNATIONAL SYMPOSIUM ON
EARTHQUAKE STRUCTURAL ENGINEERING
St. Louis, Missouri, USA, August, 1976

BEHAVIOR OF REINFORCED CONCRETE STRUCTURES DURING THE MANAGUA EARTHQUAKE

by

Gabriel Estrada-Uribe, Ph.D., P.E.

Consulting Engineer, Bogota, Colombia.

Buildings in Managua may be considered typical of the present practice in many other seismic areas around the world. The strong earthquake that destroyed Managua for the second time on December 23, 1972 provides a means of evaluating such practice as well as some code provisions. The 1972 Managua earthquake has established by itself a new standard for building structures in seismic countries.

The author flew to Managua few hours after the occurrence of the earthquake and stayed there for several weeks inspecting a number of buildings. He turned in reports to the Nicaraguan government, concerning sixteen of the most important buildings. He was one of the seven international experts nominated by the government of Nicaragua to write the Antiseismic Building Code for Managua. He brought back with him a number of samples of construction materials currently us ed in Managua and subjected them to a series of physical as well as chemical tests.

The experience that the author gathered on the site, and the results of the laboratory tests are presented. The characteristics of the earthquake and the ground acceleration in the city are discussed. Typical failures of reinforced-concrete structures are illustrated to show the advantages and disadvantages of design and construction practices currently used in several seismic areas around the world, and the need for revising such procedures.

* * *

Although Nicaragua did not have its own building code before the earthquake -there is one now (1)-, construction in Managua and in the rest of the nation followed some of the regulations (2,3) currently used in other countries. Therefore, analysis, design and construction procedures used in Managua are, in some respect, typical of the present practice in many other seismic areas. The strong earthquake that destroyed Managua for the second time on December 23, 1972 provides a means of evaluating such standard practices.

An investigation (4) of the damage suffered by some reinforced concrete structures in Managua indicates the need for re-examining the state

of the art as far as methods of analysis, design procedures, construction techniques, and regulations are concerned. The 1972 Managua earthquake has established by itself a ne standard for building structures in seismic countries.

Following a summary of the characteristics of the earthquake motion, a few cases are discussed and illustrated by photographs which show typical actual ways of failure in reinforced concrete structures subjected to high seismic loads and particularly to strong vertical accelerations.

THE EARTHQUAKE. In spite of the fact that Managua is located in an active volcanic area, the earthquake that destroyed the city last Christmas Eve was of tectonic rather than volcanic nature and had its origin in the various geological faults that surround and cross the city. The epicenter was located near downtown Managua, and the focal depth ranged between 12 and 15 kilometers. From the accelerograms recorded at La Refinería, 6 km. west of the center of the city, it was possible to measure maximum ground acceleration peaks of 0.35 g on the horizontal component and 0.28 g on the vertical component. Such values correspond to a Righter magnitude of 6.8 degrees, and to a calculated intensity (4) of 9.1 degrees in the Modified Mercalli Intensity Scale. The corresponding released energy was figured out as 10^{22} ergs.

Originally, the ground acceleration near the epicenter was believed to be around 0.5 g, but some calculations (4) performed on seven simple oscillatory systems located at various places showed that the maximum value of 0.35 g held for most of the city. The very large vertical and horizontal accelerations, the shallow focus, and the location of the epicenter so close to the city, besides poor construction and materials, caused the collapse of almost 80 percent of Managua.

THE BUILDINGS. Other than few steel structures and the very popular adobe construction, most buildings and homes had a reinforced concrete structure of some sort. Frames and shear-wall cores were very common in medium and tall buildings, whereas reinforced masonry was used in the majority of one- and two-story homes. The behavior of several of such reinforced concrete structures under this particular earthquake loads is discussed hereinafter.

Columns and shear walls. Very often, structures are designed for vertical accelerations of half or less the corresponding horizontal values, and some times those axial dynamic effects are completely neglected. However, the Managua experience showed how important vertical accelerations are when they can reach values of 80 percent of the horizontal maxima. Of course, the largest effect of vertical accelerations is to increase axial loads and bending moments in columns. A vertical acceleration of 0.28 g produces considerable additional axial forces that can reach figures beyond the reserve strength provided by the static safety factor (5). Indeed, such vertical accelerations were, to some extent, responsible for the fact that many structures in Managua collapsed due to failures in the columns. A few first and top stories disappeared completely because of disintegration of the columns.

Tied columns of various cross sections were the most commonly used.

Fig. 1 shows a campanile composed of five triangular-section tied columns at Santo Domingo church, downtown Managua. The columns were connected to each other at different heights by beams that also served as supports for the bells. At the top of the longest columns there was a 6 meter tall reinforced concrete cross which failed in bending at the bottom section due to large inertia forces developed there, and leaned westward approximately 40°. The longitudinal reinforcement at that section was 18 bars 9.5 mm. in diameter. For 2815 kg/cm^2 steel and 210 kg/ cm^2 concrete as indicated by a Schmidt test hammer, the ultimate moment capacity calculated using fast-loading stress-strain curves (6) is 178 tons-cm. To make the section fail a force of 0.245 tons had to be applied at the center of gravity of the cross. Therefore, the acceleration at the base of the cross was 0.511 g.

The average stiffness of each column was calculated as 0.74 tons/cm. Consequently, the corresponding natural frequency of the continuous system is 1.44 Hz. Using the pseudo-velocity spectrum for El Centro, 1940 earthquake that had approximately the same acceleration peak as the Managua, 1972 earthquake, and assuming a 5 % damping, an amplification factor of 1.6 is obtained. Therefore, the acceleration at the base of the columns, i.e. the ground acceleration at that place was 0.32 g which agrees closely with the values recorded at La Refinería seismological station.

These tied columns behaved within the elastic limit and did not show any cracks. On the other hand, all of the short beams connecting them failed at the joints. Reinforced concrete columns in earthquake resistant structures must have adequate transverse reinforcement either as ties or as a continuous spiral to provide both a good confinement of the core and enough ductility in the member. In general, when this requirements are satisfied so is the shear strength of the column.

Fig. 2 shows a typical column at the Pureza de María School. These ties were scarce and equally spaced along the column. They were obviously ineffective to provide adequate confinement of the core. Such a failure may be hopefully avoided in the future with the new and more rigorous regulations (1,2).

The column shown in Fig. 3 had ties so widely spaced that did not have even the necessary shear strength. This column was located in the third floor of the four-story building under construction at the Universidad Centroamericana campus on the outskirts of the city. The first two floors already had reinforced masonry partitions that made the frame stiffer there than in the last two stories. The lack of such walls and, of course, the lack of adequate transverse reinforcement caused the shearing off of all the columns in the third floor in the same way shown in Fig. 3.

Unfortunately, very few structures had spiral columns. Fig. 4 shows a typical spiral reinforced concrete column in the first floor of the Automotriz building. The large bending moments concentrated at the bottom end of the column cased the shell to spall off but the core resisted it without damage because of the confinement provided by the closely spaced spiral reinforcement. The building located downtown on Roosevelt Ave. had minor damage. Spiral columns proved very effective in earthquake resistant structures.

On the other hand, the circular hollow columns at the entrance of the Distrito Nacional building did not have a core to confine, so when the shell spalled off the entire column collapsed as shown in Fig. 5. Evidently, this type of columns are not appropriate for earthquake zones.

Most tall buildings in Managua had composite frame-shear wall structural systems. The majority of failures occured in the columns as discussed earlier, but it was not rare to find serious cracks in the shear wall cores, though. Typical shear-wall failures are shown in Figs. 6 and 7. The former shows a compression failure in the shear wall core in the first floor of the 6-story Enaluf building near the Tiscapa flooded crater. The shear-wall core was a 3 x 6 meter reinforced concrete shaft that housed the elevators. It behaved as a cantilever beam under lateral load, and, thus, opposite core faces in the E-W direction acted as compression and tension fibers. Consequently, the east face of the wall in the first floor had a tension failure whereas the west face (Fig. 6) failed in compression. Altough later load reversals widened the cracks, the buckling of the bars is still noticeable in the photograph. Typical bending shear cracks were found in the north and south faces of the core in the first three floors.

Fig. 7 corresponds to an upper left corner of the south face of the shear-wall core at the 6-story Palacio de Justicia. The crack occured in the first floor and was the only one observed after inspecting the shear wall core up to the top floor. It was evidently a local failure most probably caused by poor concrete vibration during construction.

Reinforced concrete beams. It is obviously preferred to have the formation of plastic hinges and the occurrence of cracks and failures in the beams rather than in the columns. A few cases of beam failures were observed in Managua. One of such failures occurred at the Bank of America building, the tallest in the city -19 stories-. The structure consists of 4 shear-wall cores connected by stiff beams and arranged in a tube fashion. In the outside, there are columns forming an exterior tube. The beams connecting the cores had an openning for airconditioning ducts at midspan and failed as shown in Fig. 8 due to the high vertical shear stresses developed there. Notice a few broken stirrups in the photograph.

Fig. 9 shows another typical failure that happened in the first story beams of the 8-story Telcor building. The beams span 13 meters between the two exterior columns. The high stresses in the beams were caused by the horizontal torsion due to the asymmetrical stiffness distribution. The formation of those cracks was governed by local shear stresses rather than by bending moments and thus cannot be considered as plastic hinges.

Next door to the Telcor building there was a two-story reinforced concrete frame that housed the machinery of La Prensa daily. The hollow clay-block filler walls broke down completely letting the frame go for large deformations. Since most of the energy was released through plastic deformations the frame remained in a "frozen" deformed shape as shown in Fig. 10. This shows how pure bending plastic hinges formed in the beams at approximately the quarter points, indicating the need for adequate reinforcement at those places where the bars are usually bent up or cut off.

The columns did not suffer any damage. The frame shown has only two spans and what seems to be slender columns at midspan are just broken remainings of the reinforced masonry walls. Such "columns" did not restrict the bending of the beams since they were at the points of contraflexure. As far as the location of the plastic hinges is concerned, the behavior of the structure was proper: plastic hinges should never occur in the columns.

Beam-column connections. Many structures had the weakest link in the beam-column connections. That was the case of Los Sagrados Corazones building under construction downtown Managua. The two-story reinforced concrete frame shown in Fig. 11 collapsed for the joints were unable to resist the bending moments produced by the high lateral inertia forces. The importance of a good connection detailing cannot be over emphasized. Those structures that had drop panels at the joints showed none or very little damage. However, some of them had construction joints in the columns right underneath the drop panel making it completely usless.

Anchorage. Because of the lack of anchorage in the reinforcement, many reinforced concrete and reinforced masonry structures collapsed. That was the cause, for instance, of the auditorium of the Central Bank building on Roosevelt Ave. Fig. 12 shows the auditorium and part of the 14-story building. There was a deep ring beam supporting the roof. Due to the high vertical accelerations the bars in the columns supporting the beams pulled out. Then, the free beam moved away from the columns making the whole roof collapse. Fig. 13 shows a detail of the beam-colum connection.

In the same fashion, reinforced masonry walls anchored to columns felt down because of the pulling out of the bars. Typical of such common failures is the one shown in Fig. 14 that occurred at the Don Bosco center. In many other buildings that had no structural damage, such "minor" collapse of partition walls and ceilings caused a large number of deadths. The same happened with appendages that were not properly anchored to the main structure.

Stairways. There were serious failures in some stairways endangering the lives of many people that crowded there to evacuate the buildings. The majority of such failures were due to the same mistake in detailing the reinforcement. A typical stairway failure at the Social Security building is shown in Fig. 15. The bottom bars had been bent following the bottom face of the stairway. Then, as a result of the bending moments induced by the lateral forces the bars made the cover spall off, turned loose and caused the failure of the concrete cross section due to the corresponding increase in depth to the neutral axis. After the earthquake, the stairway was pending from the steel bars and could barely support any vertical loads. Altough there was not any damage in the rest of the building there was no security at all to evacuate it in such an event, particularly under the panic developed.

Shell roofs. Very few of the reinforced concrete shell structures collapsed in Managua. They proved that the strength derived from their shape was adequate even when subjected to large horizontal as well as vertical loads. The onesthat collapsed did so because of failures in the supports. The cylindrical shell roof shown in Fig. 1, for instance, resisted the earthquake without any damage except for the cantilever sec-

tion that failed due to the large vertical inertia forces acting on it. That cantilever was supported only by the "edge" beams and had not the additional strength provided by the shape action of the shell.

Precast members. Once again, the danger of insuficient connections between precast members and their supporting structures was disclosed. A large number of new homes at the Ciudad Jardín development in Managua had precast concrete roof slabs anchored to the masonry walls. The high inertia forces acting on the heavy slabs made them breake the anchors, slide 10 to 20 cm. in both horizontal directions and fall down in the living room as shown in Fig. 16. Had the homes been ocupied already many people would had been killed there.

CONCLUSIONS. The earthquake that occurred in Managua on December 23, 1972 has established a new standard for building structures in seismic zones and showed the need for reexaminimg current analysis, design and construction trends as well as present regulations. The following general conclusions and recommendations for earthquake resistant reinforced concrete structures may be drawn from the previous discussion and photographs:

1. Vertical accelerations equal to 80 percent of the horizontal maxima should always be taken into account in the design process.

2. Adequate transverse reinforcement should be provided in columns either as closely spaced ties or spiral to assure a good confinement of the core and enough ductility in the member. Whereas spiral columns proved very effective for earthquake loads, hollow columns are not recommended for seismic zones even if spiraly reinforced.

3. Shear walls should be designed and checked for proper beam action during severe earthquakes.

4. Plastic hinges should occur in the beams rather than in the columns; adequate reinforcement should be provided at the points where those hinges are expected to occur.

5. The importance of a good beam-column connection design and detailing cannot be over emphasized. Drop panels help achieve good earthquake resistant connections.

6. The safety of the structure depends largely upon the adequate anchorage of reinforcement, partition walls and appendages. Stairways are very important in the event of a strong earthquake and should be designed and detailed accordingly.

7. Reinforced concrete shells are excellent for earthquake zones provided the supporting structures do not fail or suffer large deformations. Precast members need very good connections to supporting structures.

REFERENCES:

1. Decree 90 of January 15, 1973 based on the Bill Proposal "Normas de Emergencia para Diseño Antisísmico de la Ciudad de Managua" ("Emergency Regulations for Antiseismic Design of Managua") prepared by the International Consulting Committee nominated by the Government of Nicaragua as follows: Dr. Luis Esteva, Ing. Enrique del Valle (Mexico); Dr. Abdel Karim Conrado, Ing. Federico Fiedler (Nicaragua); Ing. José Adolfo Peña, Ing. José Luis Alonso (Venezuela), and Dr. Gabriel Estrada-Uribe (Colombia).

2. ACI Committee 318, "Building Code Requirements for Reinforced Concrete Structures", American Concrete Institute, 1971.

3. "Recommended Lateral Force Requirements and Commentary", Structural Engineers Association of California, 1968.

4. Gabriel Estrada-Uribe, Managua Antisísmica, 1st. edition, Colciencias, Bogotá, 1973, 230 pp.

5. R.C. Reese, "Safety Requirements in Structural Design and ACI 318-71", ACI Journal, Proceedings V. 70, No. 3, March 1973, pp. 190-198.

6. G. Winter, L.C. Urquhart, et al., Design of Reinforced Concrete Structures, 7th ed., McGraw-Hill, N.Y., 1964.

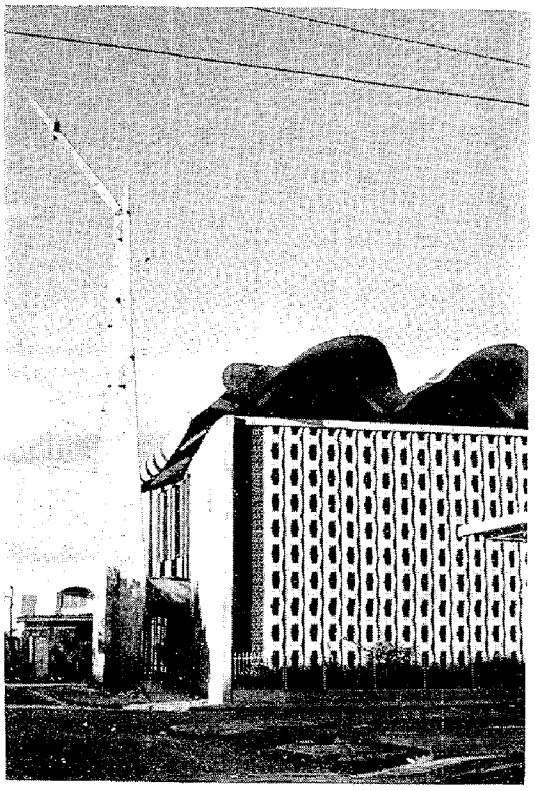

Fig. 1 Collapsed shell roof and cross

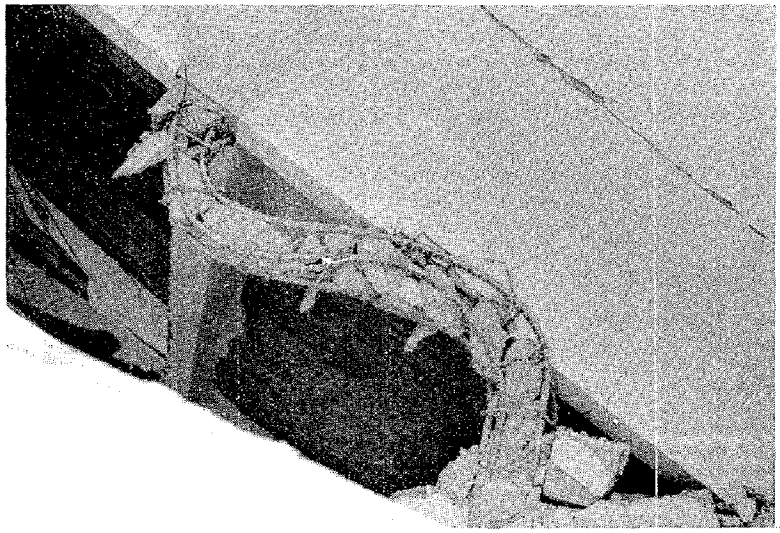

Fig. 2 Failure of tied column

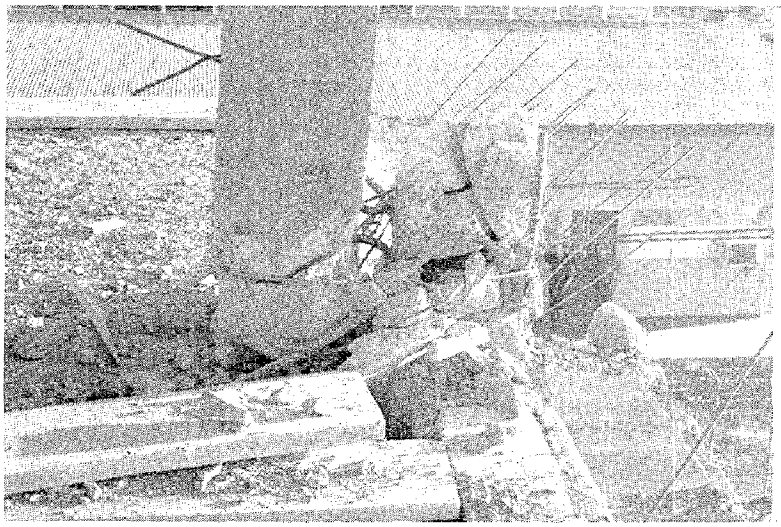

Fig. 3 Sheared off column

Fig. 4 Spiral reinforced column

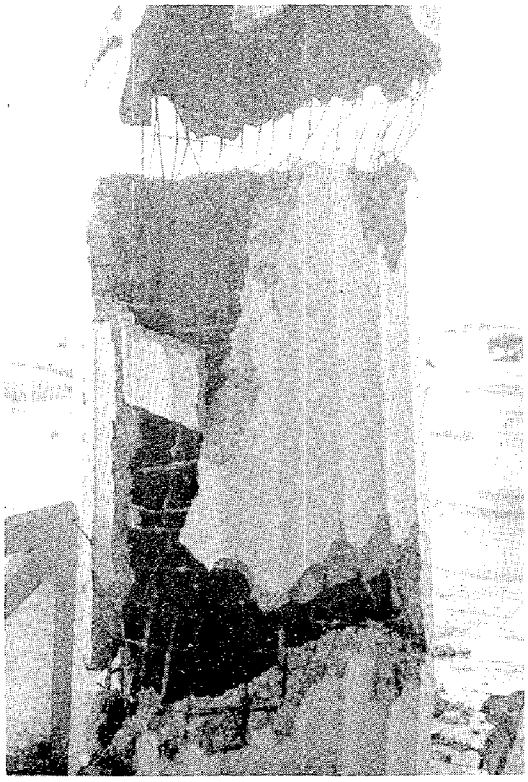

Fig. 5 Hollow column

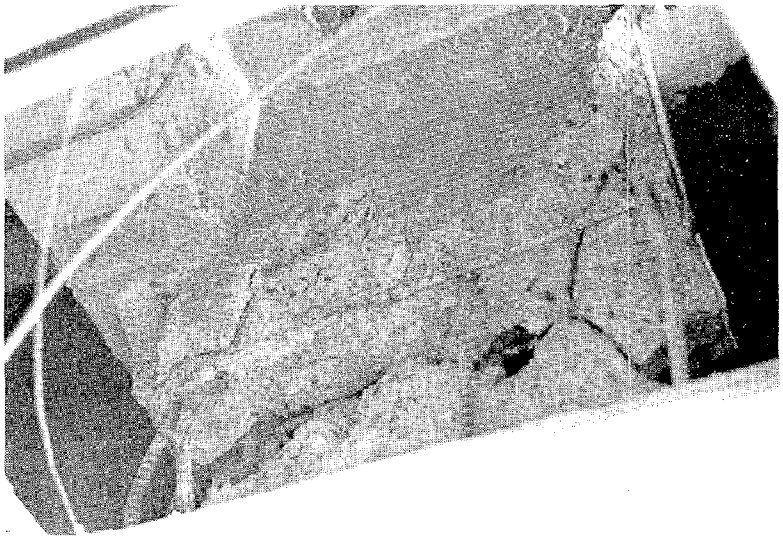

Fig. 6 Compression failure in shear wall core

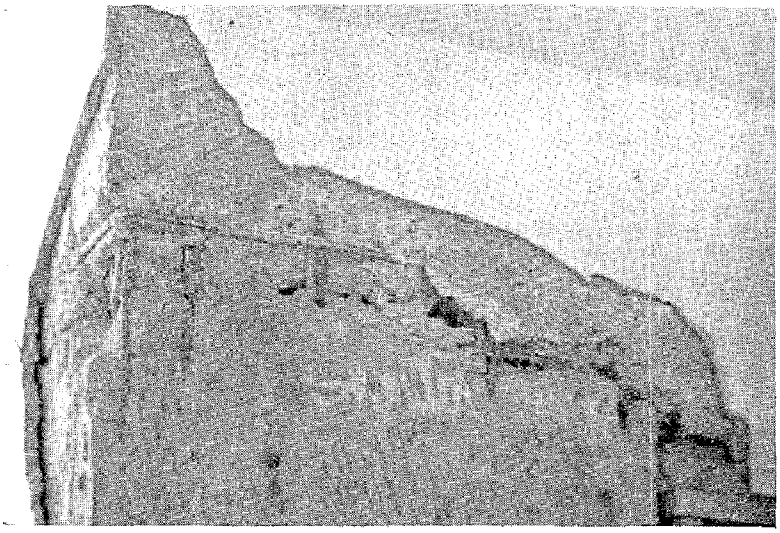

Fig. 7 Poorly vibrated concrete

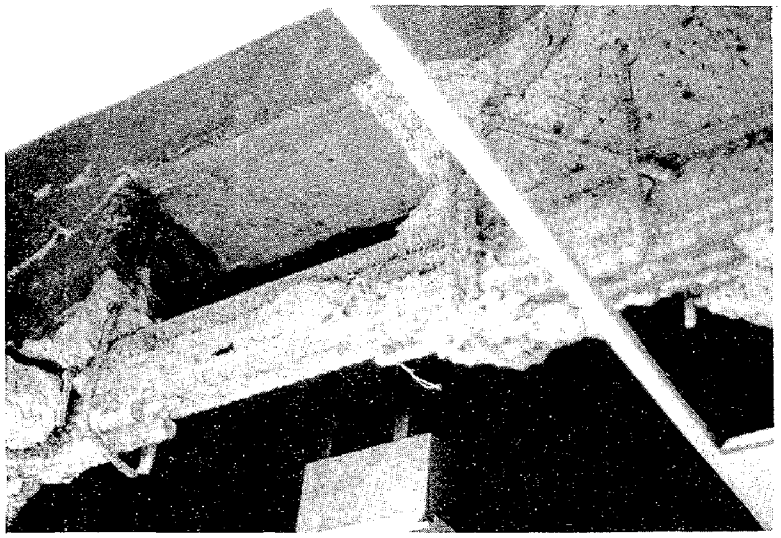

Fig. 8 Failure of beams connecting shear wall cores

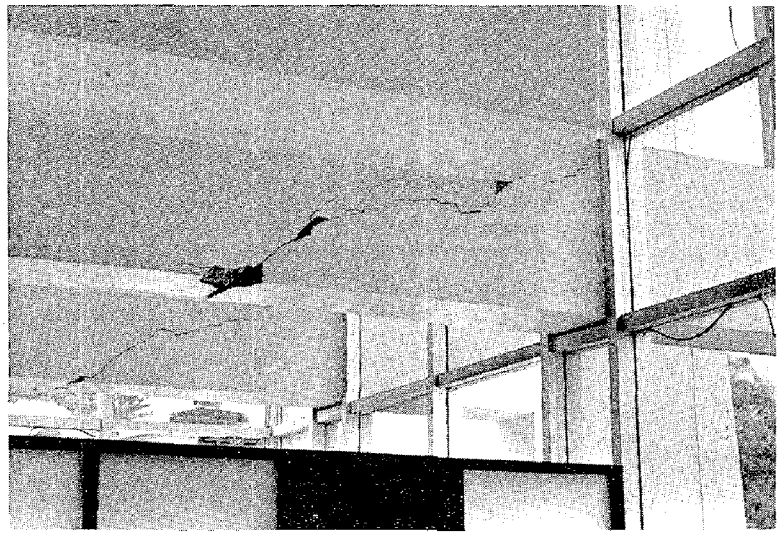

Fig. 9 Shear flexural cracks

Fig. 10 "Frozen" deformed shape of frame

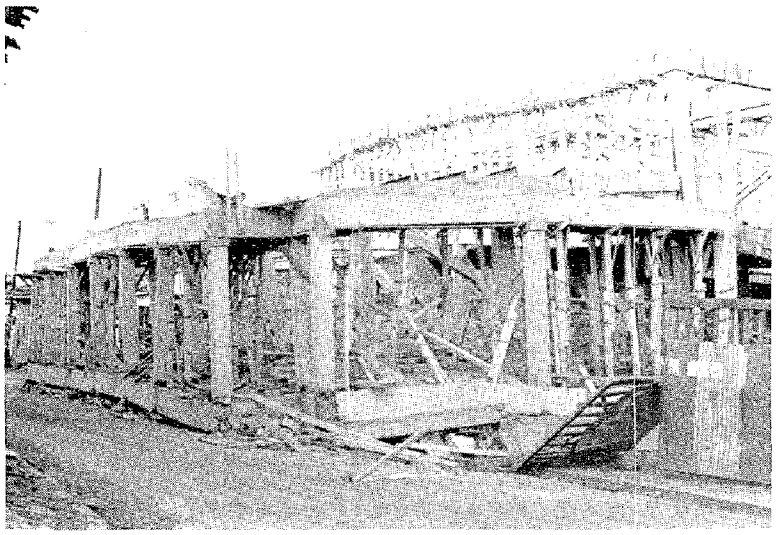

Fig. 11 Collapsed frame under construction

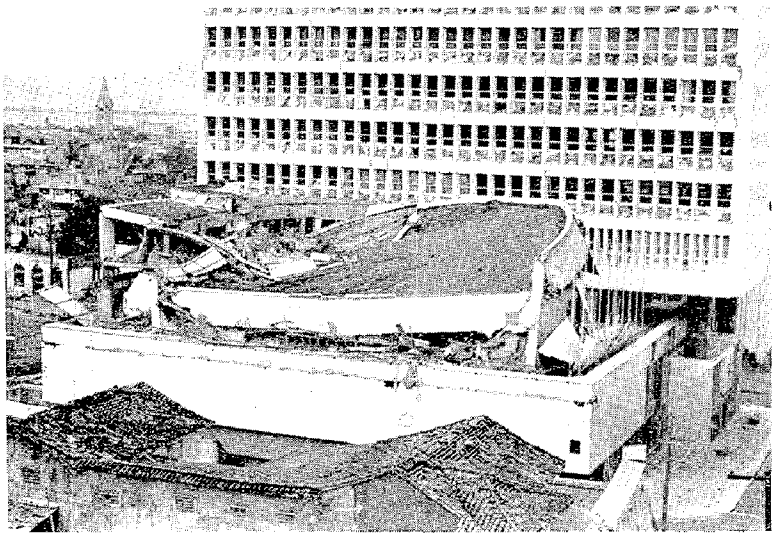

Fig. 12 Collapsed auditorium roof

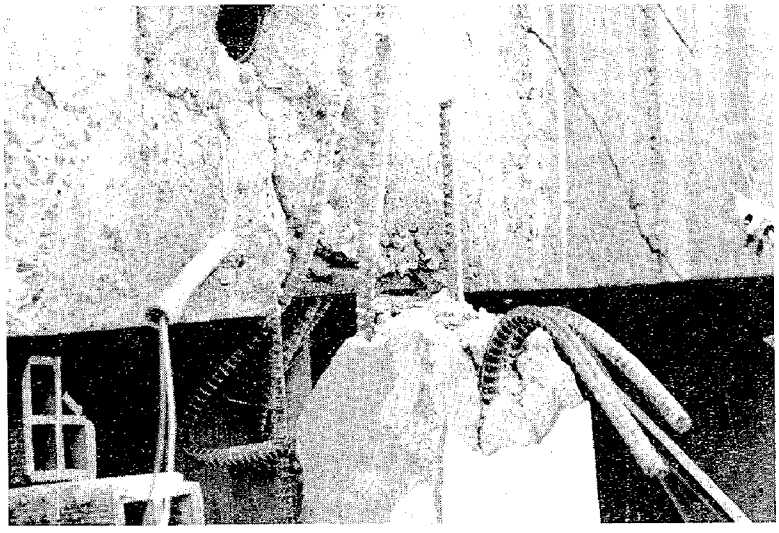

Fig. 13 Anchorage failure

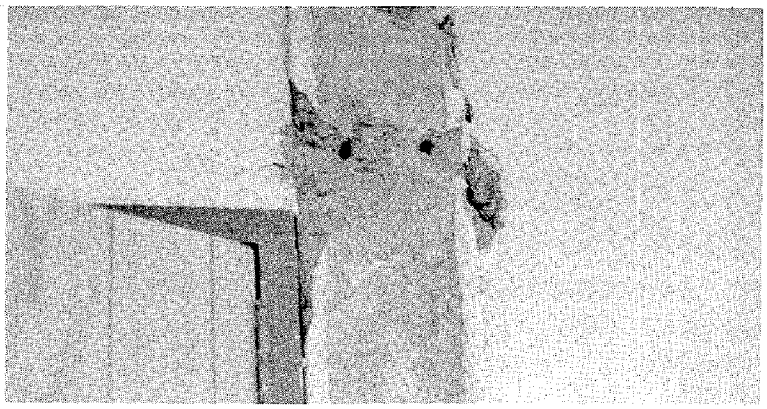

Fig. 14 Pull out failure

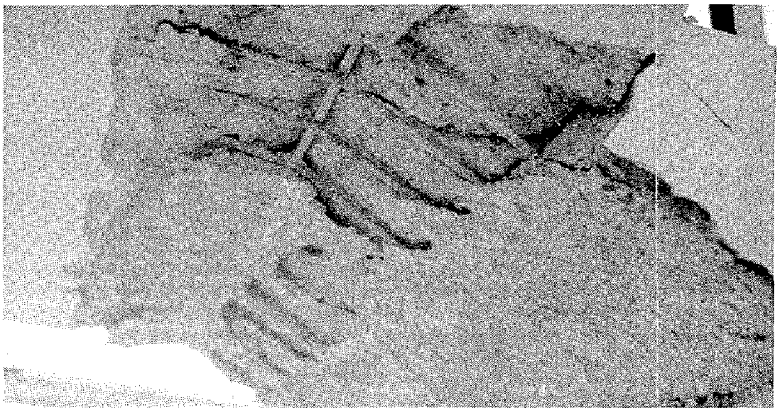

Fig. 15 Collapsed stairway

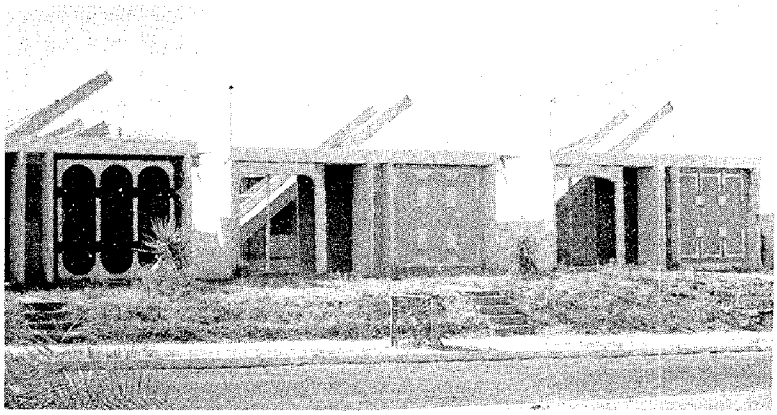

Fig. 16 Failure of precast roof slabs

INTERNATIONAL SYMPOSIUM ON
EARTHQUAKE STRUCTURAL ENGINEERING
St. Louis, Missouri, USA, August, 1976

SITE RESPONSE ANALYSIS FOR EARTHQUAKE LOADING

Y.S. LOU, S.J. DIXON and C.R. MacFADYEN

Respectively, Senior Engineer,
Executive Vice President
and Vice President

Converse Davis Dixon Associates

Pasadena, California

SUMMARY

Several methods for evaluating the site response during earthquakes are presently available. Most of these methods are based on the assumption that the site response is induced by the upward propogation of shear waves from the underlying bedrock. However, the question of how accurate these methods can predict the site response has not yet been substantiated by using actual recorded bedrock and surface motions for comparison.

Following the San Fernando Earthquake of 1971, the Metropolitan Water District of Southern California initiated a study to evaluate the earthquake damage at Joseph Jensen Filtration Plant, near Sylmar, California(7). Part of that study was to monitor aftershocks. A number of rock and ground motion time histories were obtained and the soil profiles of these recording stations were evaluated by field exploration.

A site response study was performed using these actually recorded bedrock and surface motions, and the popular shear wave propogation technique developed by Schnabel, Lysmer and Seed(2) was used in site response calculation. The result of this study indicates that this technique does predict different site response than those actually recorded. However, it should be realized that the technique developed by (2) is still a valuable tool in site response analysis to date. It is also concluded that engineering experience and profound judgment are still important factors in evaluating site response under earthquake loadings.

INTRODUCTION

The response of a soil deposit near the ground surface during an earthquake plays an important role in seismic design of

structures to be situated on that soil deposit. Several methods for evaluating the site response during earthquakes are presently available (e.g., Tsai(1) and Schnabel, Lysmer and Seed(2)). Most of these methods are based on the assumption that the site responses to an upward propogation of shear waves from the underlying bedrock. The purpose of this paper is to compare the accuracy of one of these methods using recorded bedrock and ground surface motions.

Following the San Fernando Earthquake of 1971, the Metropolitan Water District of Southern California initiated a study to evaluate the earthquake damage at Joseph Jensen Filtration Plant, near Sylmar, California(7). As the part of that study, two strong motion accelerometers were installed at the site. Instrument No. 1 was located on a cut section of sedimentary rock (Saugus formation) and Instrument No. 2 was installed on the soil deposit. The horizontal distance between these two instruments is 1200 feet. Figure 1a shows the geotechnical profile on which the No. 2 earthquake instrument was located. The subsurface material properties shown in this figure were derived from field exploration and laboratory tests.

The proximity of the instruments enable obtaining both the outcropping rock and surface soil earthquake motions, and thereby provided a unique situation for evaluating the site response using the existing techniques mentioned above. Eleven aftershocks were recorded at the site between March 6 to April 15, 1971. The strongest aftershock recorded during this period was selected for the purpose of this study and its characteristics were tabulated in Table 1 shown as follows:

TABLE 1

EARTHQUAKE CHARACTERISTICS

Date of Event	Richter Magnitude	Epicenter Distance (Miles)	Maximum Acceleration (in g's)					
			Instrument No. 1 (Sedimentation Rock)			Instrument No. 2 (Fill)		
			E-W	V	W-S	E-W	V	N-S
3/31/71	4.9	4.5	0.095	0.075	0.075	0.111	0.087	0.1

The recorded time history motions are presented in Figure 2 and the horizontal components are used in this study. The study involved the following two stages:

1. Using a measured rock motion at Instrument No. 1 as input to the bottom of the geotechnical profile at Instrument No. 2, ground surface motions were calculated, assuming the motion propogates upwards. The calculated ground motions were then compared with those recorded at the surface; and

2. Using the measured ground motions at Instrument No. 2 as input to the top of the geotechnical profile and apply the deconvolution technique, the bedrock motions were calculated, assuming the motion propogates downward to the bottom of the geotechnical profile (bedrock). The calculated bedrock motions were then compared with those actually recorded rock motions.

The computer program SHAKE developed by Schnabel, Lysmer and Seed(2) is used to carry out the computation mentioned above.

SITE RESPONSE ANALYSIS

The procedure of site response analysis used in this study can be illustrated by the flow chart shown in Figure 3.

The site response of geotechnical profile shown in Figure 1a was carried out using the recorded rock motions (E-W and N-S) as input to the base of this profile, and the ground surface responses were calculated using computer program SHAKE. The calculated and recorded acceleration and velocity spectra were compared and results were presented in Figures 4 and 5. The comparison indicated that the calculated response was substantially different from the one recorded.

Realizing that the site response is sensitive to its soil properties assigned, and in order to consider the possible variation in soil properties evaluated, three more cases (Cases 2, 3 and 4) are also investigated. Case 2 represented the site response of geotechnical profile and its soil properties in Figure 1a with a 20 percent reduction in shear wave velocity (V_s). Using the recorded bedrock motion as input to the base of that profile, the ground surface response was calculated and the result of calculated and recorded acceleration response spectra were compared as shown in Figure 6. Cases 3 and 4 represent the same situation as Case 2 except that Case 3 (Figure 7) represented the site response as a result of 20 percent increase in shear wave velocity and Case 4 (Figure 8) represented the site response as a result in changing the relative density (D_γ). Both cases indicated that the calculated site response was substantially different from the recorded response.

The procedure shown in Figure 3 also indicates that when ground surface motion is defined, the bedrock motion can also be calculated by so-called deconvolution process(2). In this study, the ground surface motions (E-W, N-S) recorded at Instrument No. 2 were used as input to the top of geotechnical profile shown in Figure 1a and the base rock responses were calculated using computer program SHAKE. The calculated and recorded bedrock acceleration response spectra were compared and results were presented in Figures 10 (E-W) and 11 (N-S). The comparison also indicated that the calculated bedrock response does not agree with those recorded.

It should be noted that the soil conditions at which Instrument No. 2 was located were also investigated by other consulting firms(3) and the result was presented in Figure 1b. The response of this profile was also analyzed using the E-W component of the recorded earthquake following the same procedure as described in Case 1. The calculated ground acceleration response spectra were then compared with those recorded (see Figure 9) and the result also indicated that the calculated responses do not reasonably match those recorded.

In order to examine the dynamic characteristics of recorded and calculated earthquakes, the so-called PAD (Period-Amplitude-Duration) diagrams (4, 5) were constructed and results were shown in Figures 12 and 13. Since the dynamic characteristics (frequency content, load cycle and the amplitude, etc.) of calculated and recorded earthquakes are indeed substantially different, it illustrated the reason why the calculated responses were different from those recorded.

SUMMARY AND CONCLUSION

In examining these cases studied in this paper, the results can be summarized as follows:

1. The results of the calculated site response (acceleration and velocity) are higher than those actually recorded. The difference in maximum response ranging from 50 to 100 percent or more (see Table 3).

2. The dominant periods (the period at which the maximum response acceleration occurred) predicted by calculated earthquakes are, in general, higher than those actually recorded (e.g., see Figures 4, 7 and Table 3). However, in some cases, they are reasonably close enough to be acceptable (e.g., Figures 5, 9 and Table 3).

3. Based on the spectrum intensity (SI) concept defined as the area under the velocity response spectrum by Housner(6), which can be related to the intensity of shaking as regarding effects on structures, the results of this study indicated that the spectrum intensities of calculated earthquakes are about 40 percent higher than those actually recorded (see Table 2). This implies that the earthquakes derived by SHAKE could over-estimate the intensity of shaking on soils as well as on structures.

4. The "strongness" of those calculated earthquakes relative to those actually recorded ones had been demonstrated by PAD diagrams (see Figures 12 and 13). For example, when appropriate amplitude scales are used, one can realize that the calculated motions are clearly stronger than those recorded ones, therefore substantiate the reason why the calculated responses were greater than those recorded.

In conclusion, the authors realized that more study is needed before any definite conclusion can be reached. The authors intend to continue this type of study using other available earthquake information and also to examine other available techniques in site response analysis.

However, it is reasonable to conclude that, based on the study performed in this paper, the technique developed in Reference 2 does predict somewhat different site response than those actually recorded. It is hoped that the results of this study will provide some kind of guideline in future site response analysis. It is also concluded that engineering experience and profound judgment are still important factors in evaluating site response under earthquake loadings. However, it should be realized that the technique developed in Reference 2 is still a valuable tool in site response analysis to date.

REFERENCES

1. TSAI, N.C., Influence of Local Geology on Earthquake Ground Motion, Ph.D., Thesis, California Institute of Technology, Pasadena.

2. SCHNABEL, P.E., LYSMER, J., and SEED, H.B.; SHAKE, A Computer Program for Earthquake Response Analysis of Horizontally Layered Sites, Report No. EERC 72-12, University of California, Berkeley.

3. WOODWARD-LUNDGREN AND ASSOCIATES, Evaluation of the Effects of the February 9, 1971 San Fernando Earthquake on the Balboa Water Treatment Plant, December 3, 1971.

4. LOU, Y.S. and SHYN, Y.S., Seismic Analysis Criteria of Nuclear Plant Components, ASCE National Structural Engineering Meeting, Print 2232, April 22-26, 1974, Cincinnati, Ohio.

5. LOU, Y.S., Stochastic Simulation of Earthquakes, Ph.D Thesis, University of Pennsylvania, Philadelphia.

6. HOUSNER, G.W., Spectrum Intensities of Strong-Motion Earthquakes, Proc. Symp. Earthquake and Blast Effects on Structures, Earthquake Engineering Research Institute.

7. DIXON, S.J. and BURKE, J.W., A Liquefaction Case History, ASCE National Structural Engineering Meeting, April 9-13, 1973, Preprint No. 1977, San Francisco, California.

TABLE 2

COMPARISON OF SPECTRUM INTENSITY

SPECTRUM INTENSITY			
Case	Calculated (SI) (1)	Measured (SI) (2)	(1)/(2)
1a	0.84 (E-W)	0.60	1.40
1b	0.80 (N-S)	0.79	1.00
2	0.90	0.64	1.41
3	0.85	0.60	1.42
4	0.94	0.72	1.31
5	1.21	0.84	1.43
6	1.34	1.44	0.93
7	1.60	1.23	1.31

TABLE 3

COMPARISON OF MAXIMUM RESPONSE ACCELERATION

	Recorded(1)				Calculated(2)				(2)/(1)	
	Damping		At Period		Damping		At Period		Damping	
Figure	0%	10%	0%	10%	0%	10%	0%	10%	0%	10%
4	1.06	0.32	0.30	0.30	1.88	0.59	0.45	0.45	1.77	1.84
5	1.00	0.34	0.18	0.19	1.57	0.48	0.20	0.20	1.57	1.41
6	1.10	0.29	0.23	0.22	1.77	0.58	0.20	0.20	1.61	2.00
7	1.06	0.31	0.25	0.75	1.85	0.58	0.47	0.47	1.75	1.87
8	1.05	0.30	0.75	0.25	1.57	0.52	0.47	0.25	1.50	1.73
9	1.07	0.31	0.15	0.25	1.54	0.49	0.25	0.25	1.44	1.58
10+	0.68	0.22	0.20	0.10	0.58	0.12	0.28	0.28	0.85	0.55
11+	0.48	0.15	0.28	0.10	0.43	0.12	0.28	0.28	0.89	0.80

+ Bedrock Responses

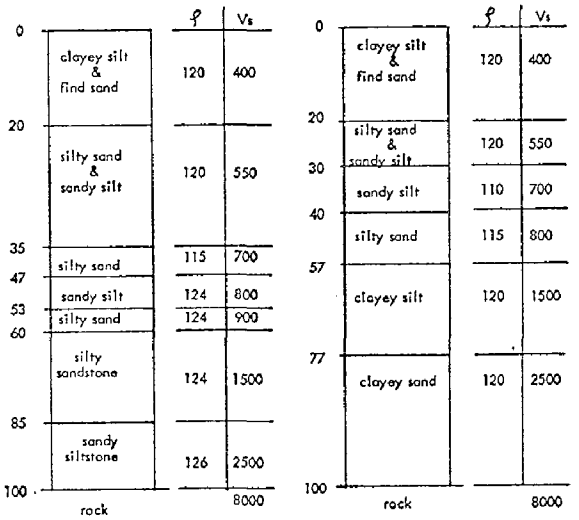

Figure 1a Geotechnical Profile by CDOA

Figure 1b Geotechnical Profile by Other

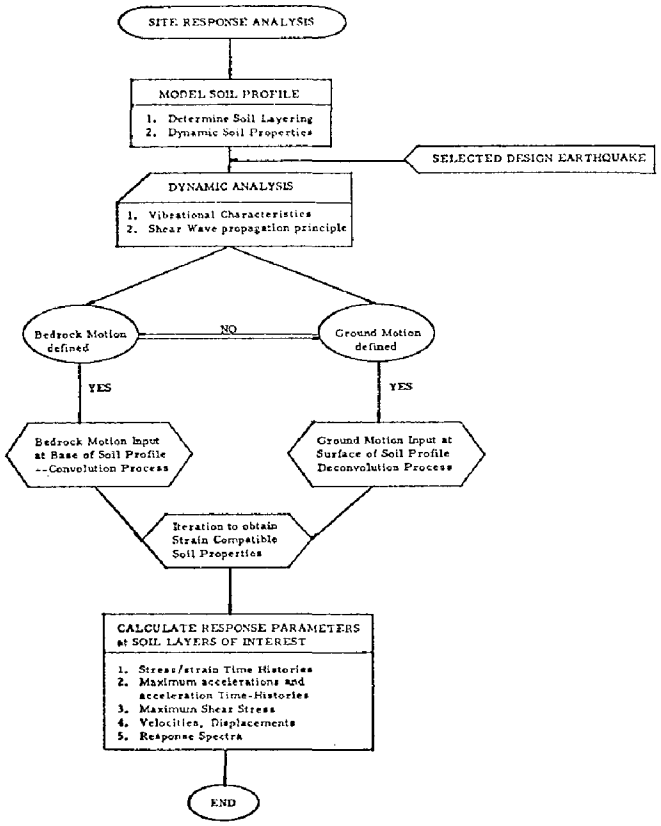

Figure 3 Site Response Analysis Procedure

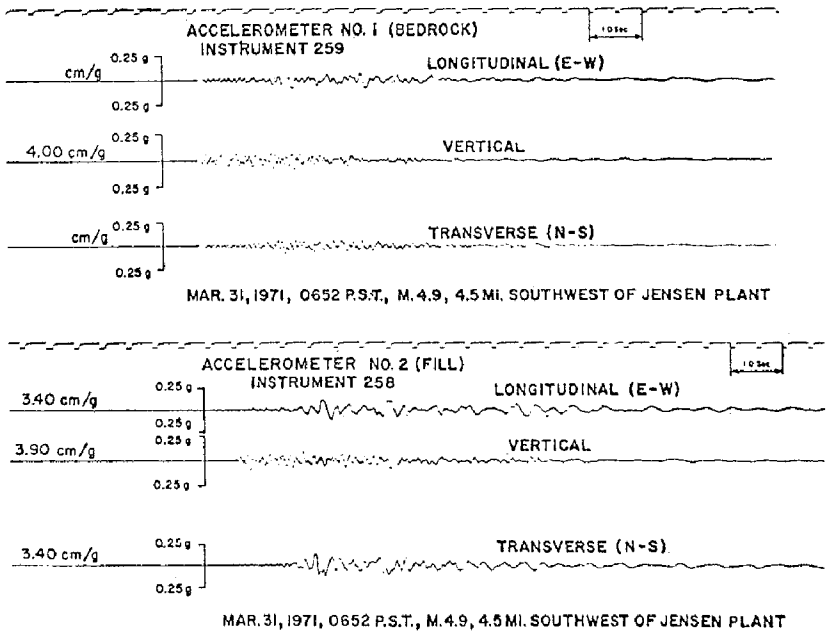

Figure 2 Recorded Aftershock

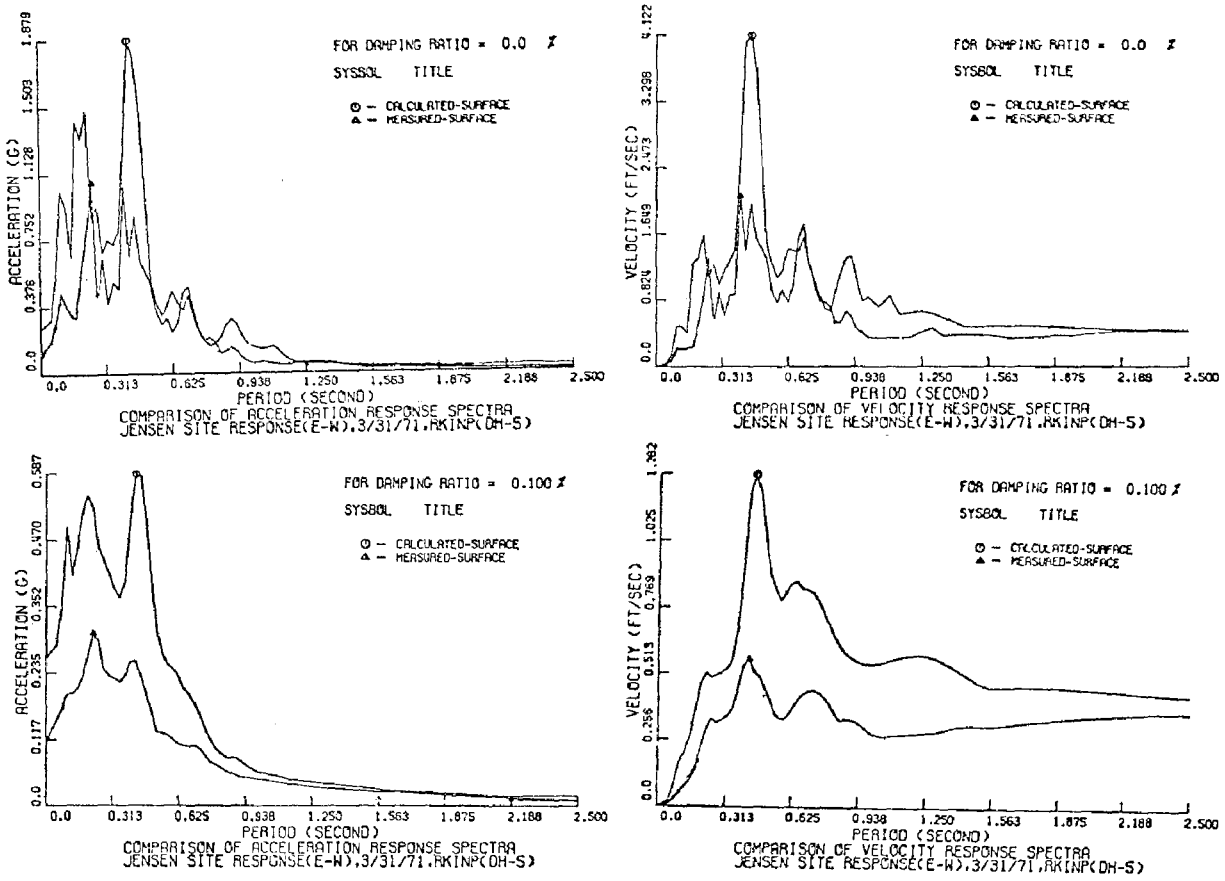

Figure 4 Comparison of Spectra, Case 1a.

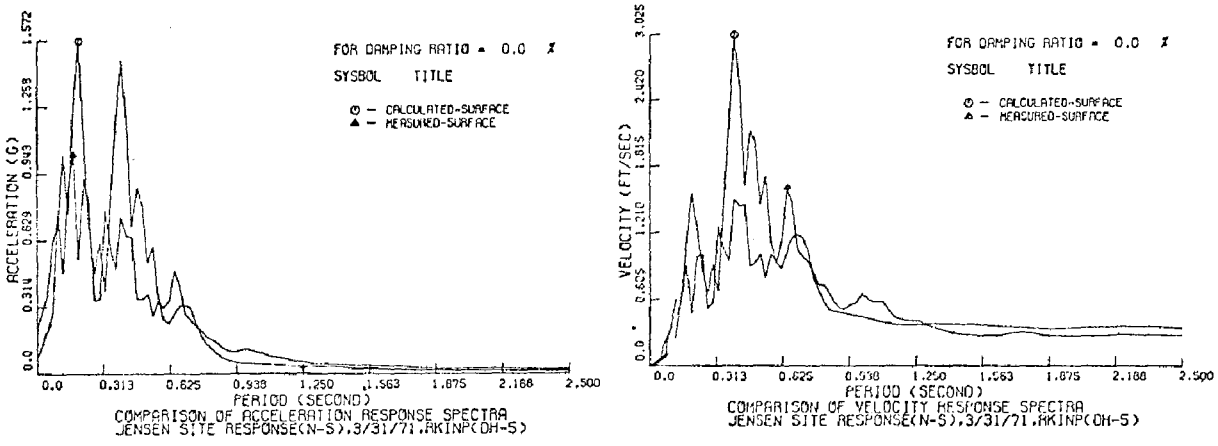

Figure 5 Comparison of Spectra, Case 1b.

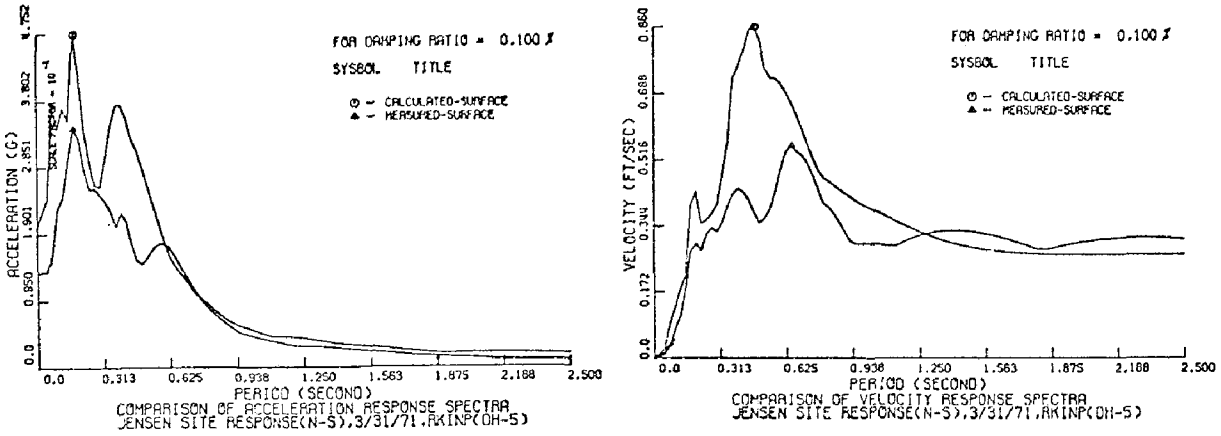

Figure 5 Comparison of Spectra, Case 1b (Cont'ed).

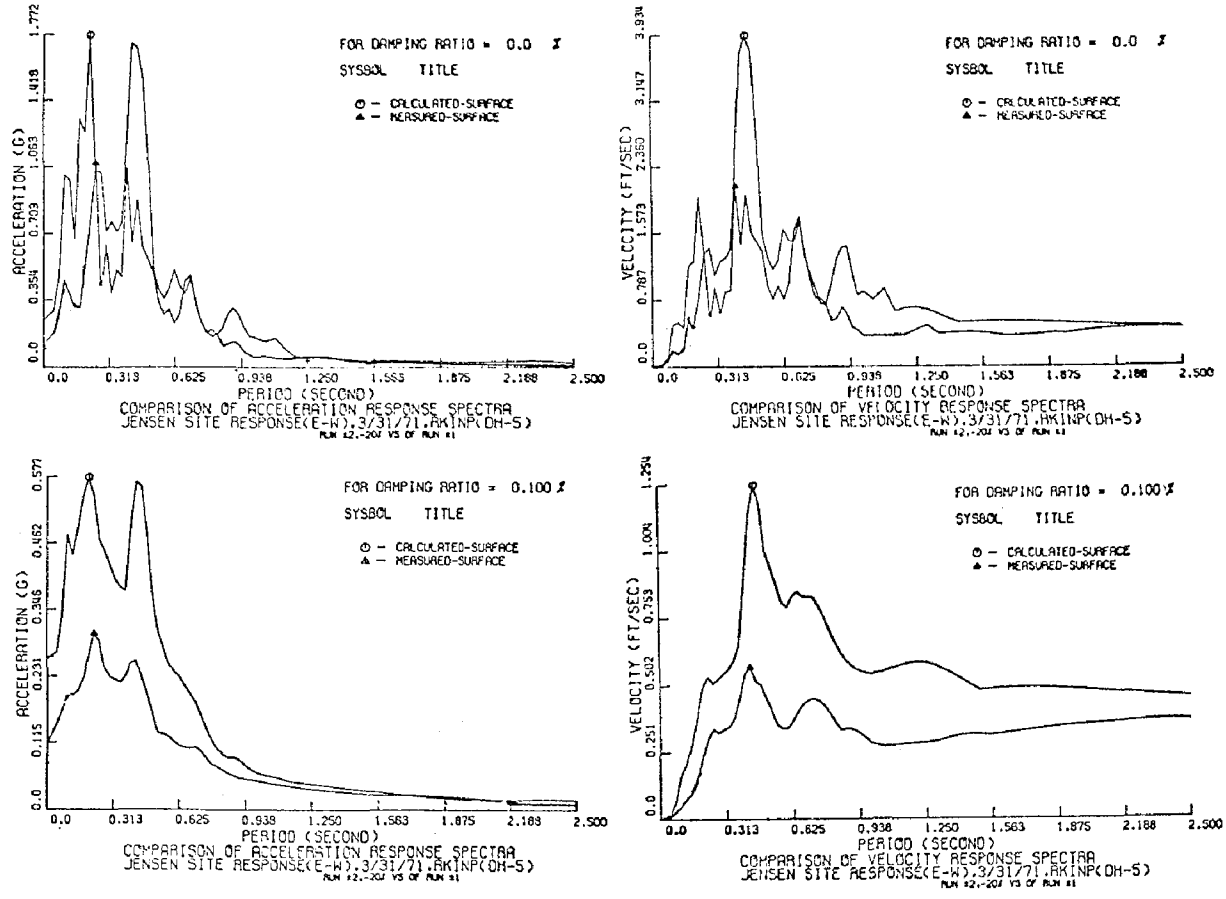

Figure 6 Comparison of Spectra, Case 2.

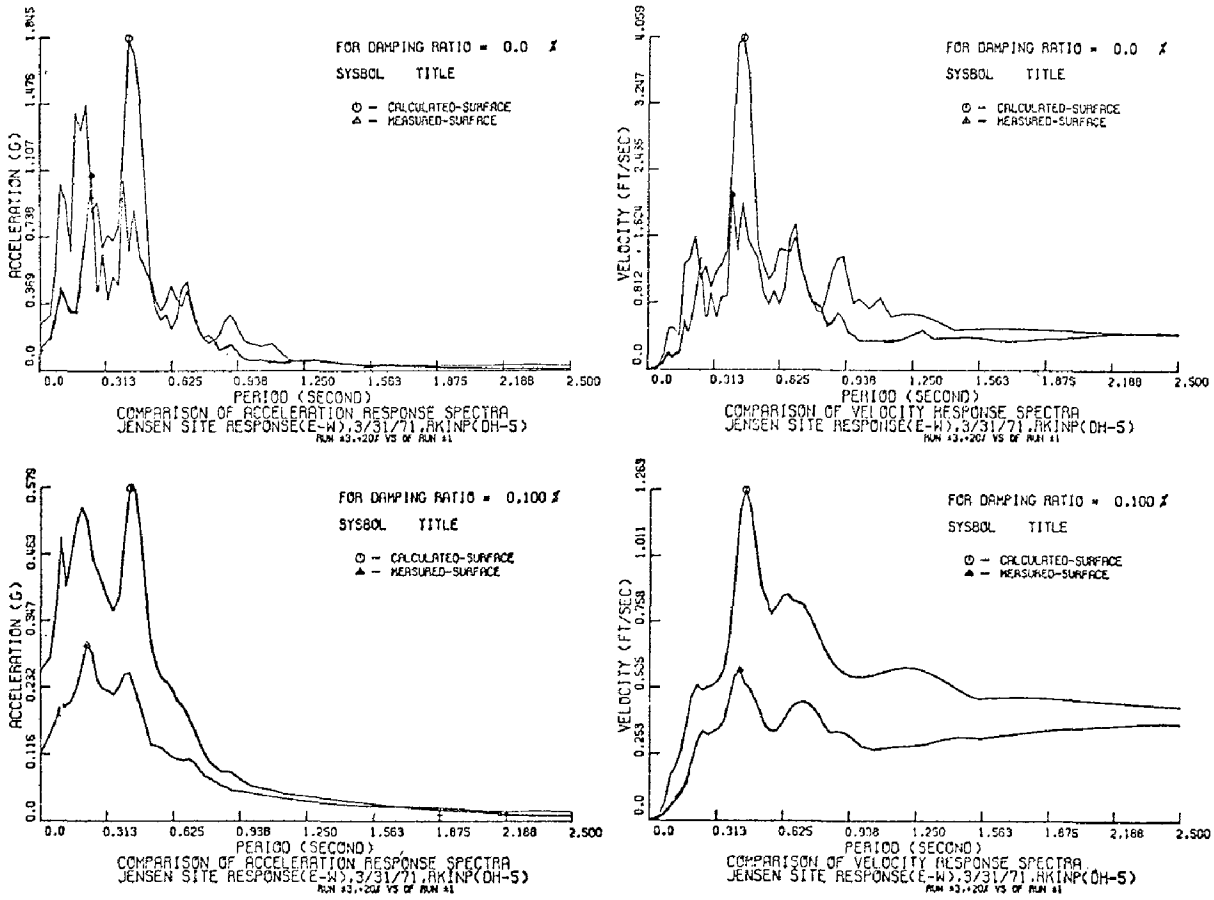

Figure 7 Comparison of Spectra, Case 3.

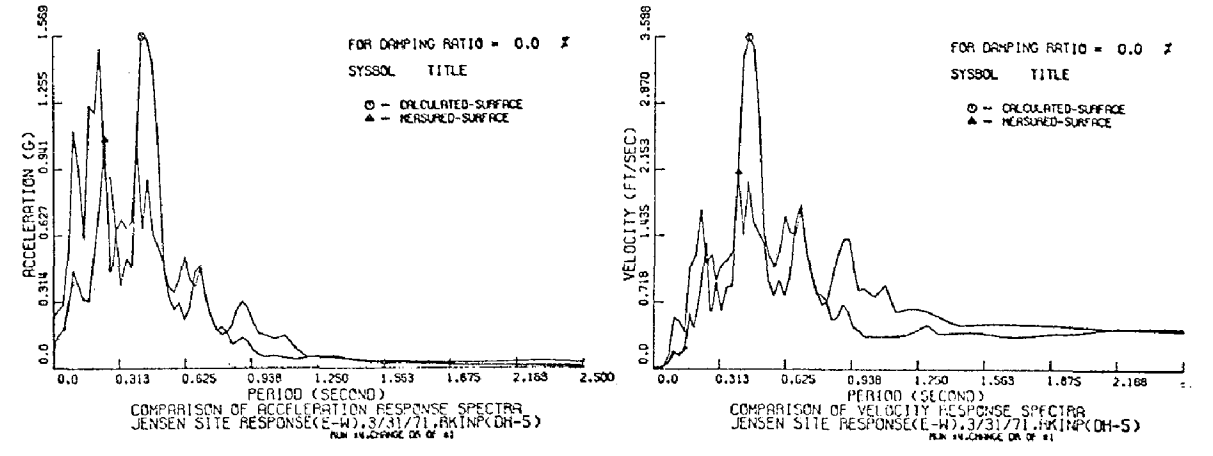

Figure 8 Comparison of Spectra, Case 4.

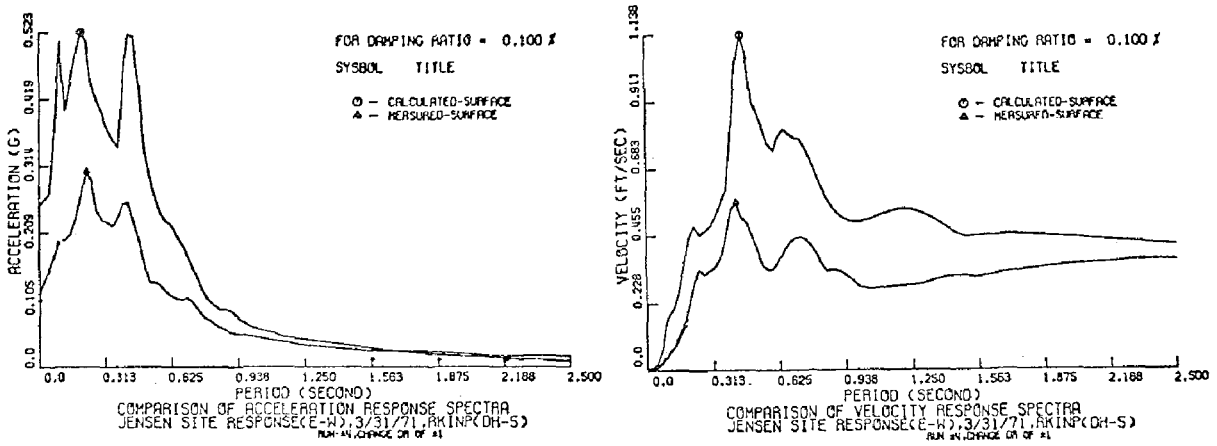

Figure 8 Comparison of Spectra, Case 4 (cont'ed).

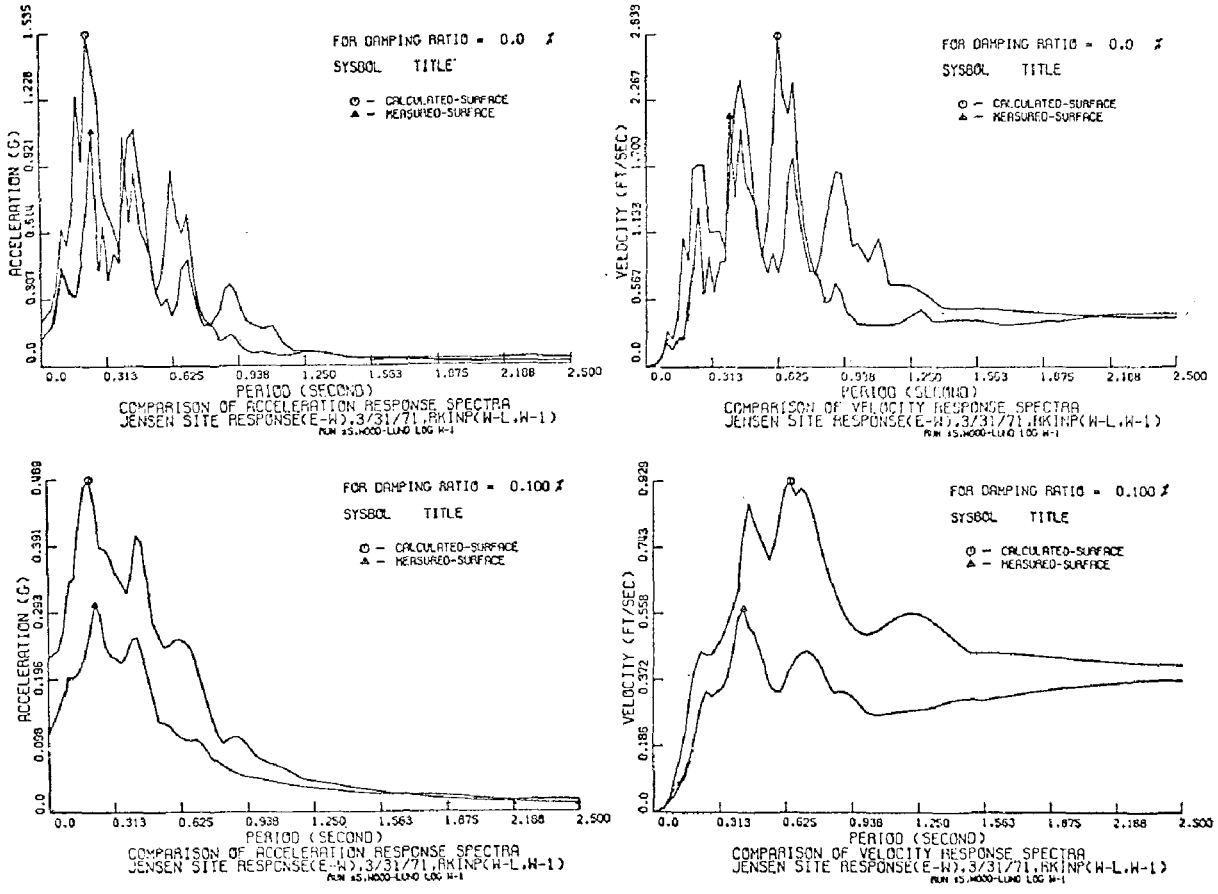

Figure 9 Comparison of Spectra, Case 5.

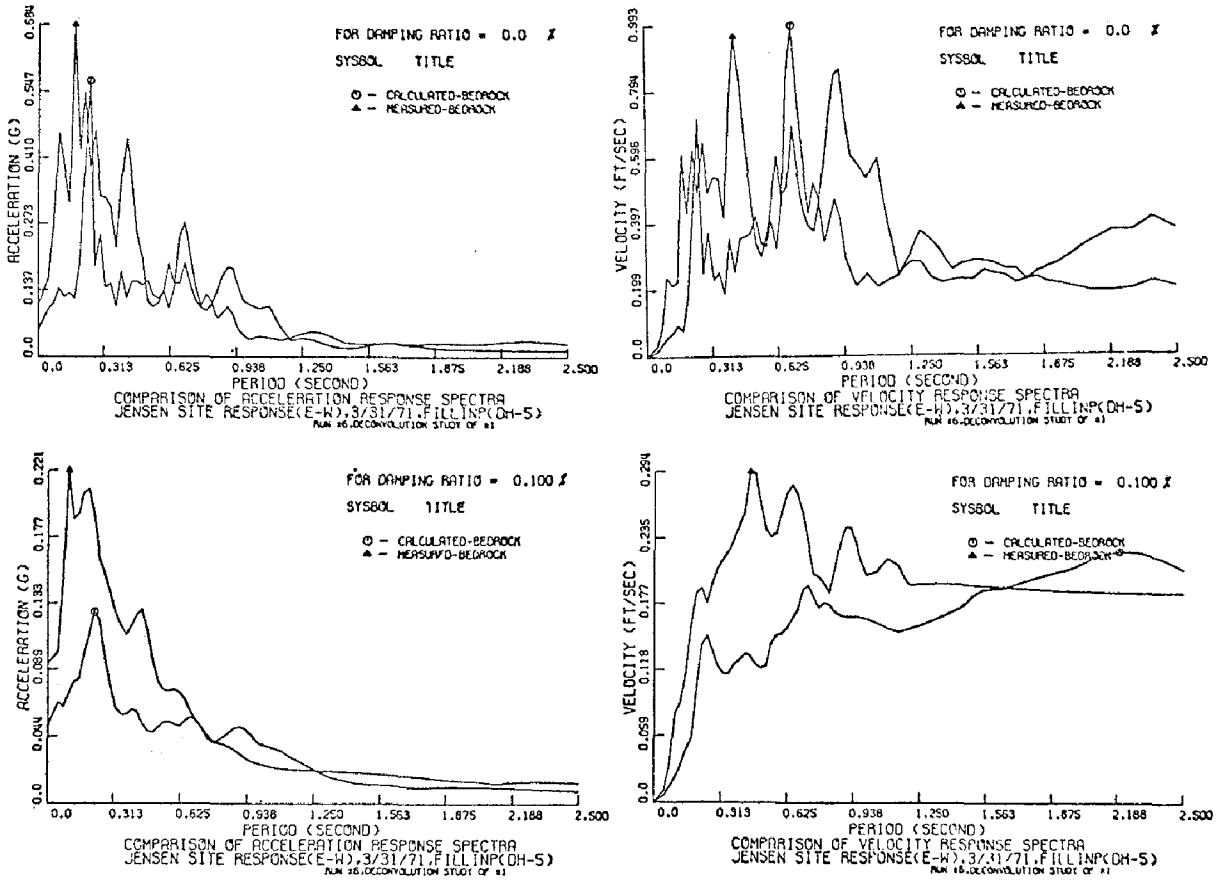

Figure 10 Comparison of Spectra, Case 6.

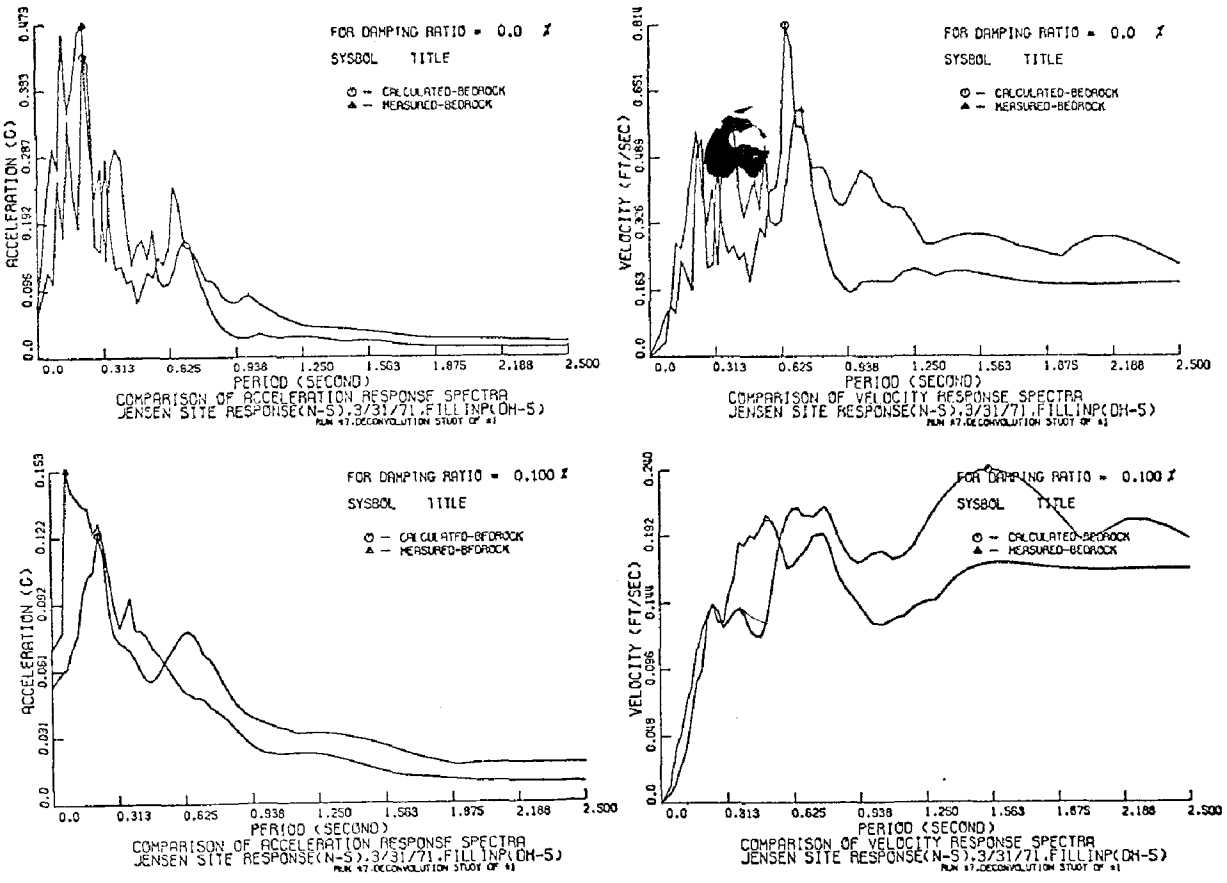

Figure 11 Comparison of Spectra, Case 7.

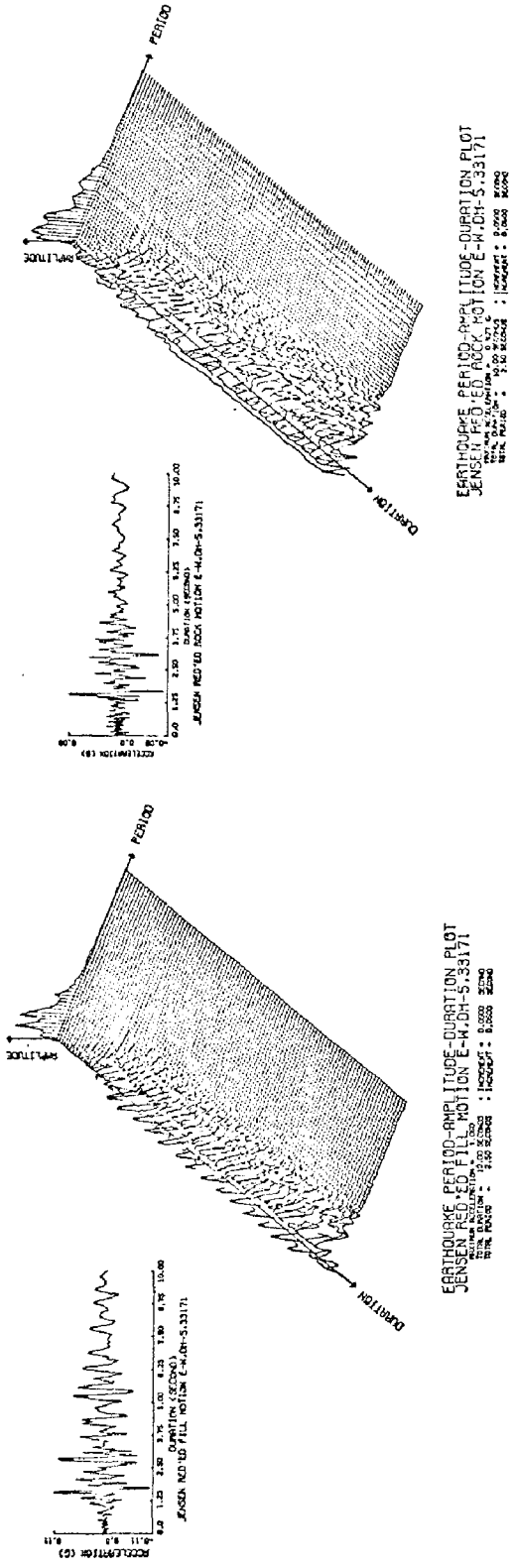

Figure 12 PAD Diagrams for Fill Motions

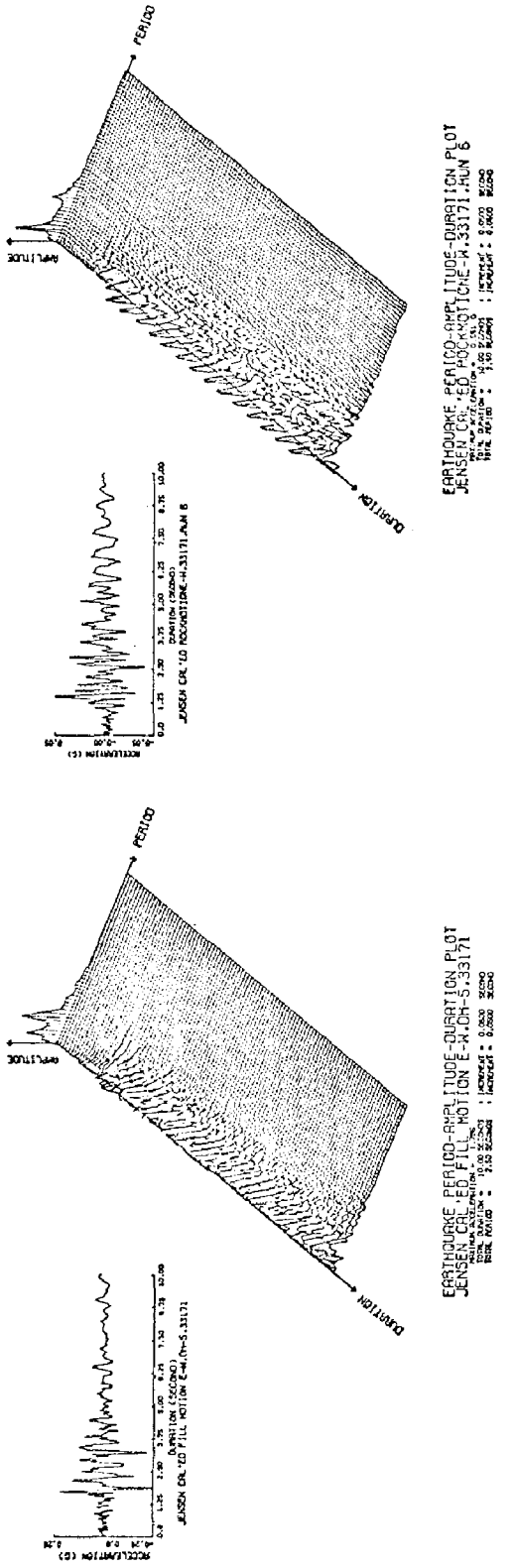

Figure 13 PAD Diagrams for Rock Motions

INTERNATIONAL SYMPOSIUM ON
EARTHQUAKE STRUCTURAL ENGINEERING
St. Louis, Missouri, USA, August, 1976

OBSERVATIONAL STUDIES ON THE EARTHQUAKE RESPONSE OF BUILDINGS IN JAPAN

by

Y. OSAWA[1], M. MURAKAMI[2], T. MINAMI[3] and K. ISHIDA[4]

SUMMARY

The present state of earthquake observation projects in Japan is introduced with special emphasis on soil-structure interaction effects. The analyses are made on the records obtained for moderate earthquake motions at three building sites and one spherical tank site as illustrative examples. The results indicate that the interaction effects can be observed in a form of spectral ratio between Fourier spectra of records at the base of structures and the surface of the ground and that the shear wave velocity in a soil layer plays an important role in determining the suitable model of soil-structure interacting system.

INTRODUCTION

It is widely recognized that research based on the earthquake observation of buildings and other structures is of great importance in the field of earthquake engineering. The earthquake observation may be divided into two categories: (1) observation of the behavior for strong earthquake motions that rarely occur, in which the structure is sometimes stressed beyond the elastic limit; and (2) observation of the behavior for moderate or weak earthquake motions that occur relatively often, in which the structure is in most cases stressed only in the elastic range.

---

1) Professor and Director, Earthquake Research Institute, Univ. of Tokyo. 2) Associate Professor, Faculty of Eng., Chiba Univ. 3) Research Associate Earthquake Research Institute. Univ. of Tokyo. 4) Research Fellow, Earthquake Research Institute, Univ. of Tokyo.

In Japan the first category observation program started early in the 1950's by installing strong motion accelerographs in several buildings, and at present about one thousand strong motion accelerographs, about 600 of which are installed in buildings, are in operation. The second category observation started in the 1960's by installing several sensitive seismographs in a reinforced concrete building and in its surrounding subsoil layers. Such an observation study has been carried out in Japan at many buildings and other structures.

The main purpose of the second category observation is to clarify the characteristics of an earthquake input into structures and to obtain the necessary information for constructing the model of soil-structure system used for dynamic analysis to earthquake motions. Although the results obtained by these observational studies should be complemented by other investigations such as elasto-plastic characteristics of soils and structural elements with large deformations or strains, rich data can be expected for many observation points within a short period as the moderate or weak earthquake motions occur rather frequently.

It is inteded in this paper first to introduce the outline of the second category observation system that has been carried out in Japan mostly for building structures, and second to give a rather detailed description (dimension of structures, subsoil properties, instrumentations, analyses of records obtained, etc.) for four different types of observation systems.

OUTLINE OF EARTHQUAKE OBSERVATION SYSTEMS

Most buildings in Japan are built on relatively soft ground and their earthquake responses are often subjected to an interaction effect between the building and its surrounding soil. Thus the observational study of second category for building structures is focussed to clarify the soil-structure interaction effect and to establish a suitable method of modeling the soil-structure interaction system used for dynamic analyses.

Table 1 shows an outline of the second category observation systems that have been carried out at various buildings and building-like structures in Japan. These systems are chosen from those reported in the publications of the Architectural Institute of Japan, and therefore, those for civil engineering structures such as dams and bridges are excluded.

As is seen in Table 1, the earthquake observation has been made for various types of buildings such as university, school, apartment, office, hotel and model buildings, and

for various types of structures such as reinforced concrete (RC), steel(S) and steel framed reinforced concrete(SRC) with or without piles. It should be noted that in most cases the observation has been made on the rigid structure on soft ground where the soil-structure interaction is expected to predominate.

Among those observation systems listed in Table 1 Nos.1, 4, 13 and 37 are chosen to describe the details of the system and the results obtained from observations.

BUILDING A - REINFORCED CONCRETE UNIVERSITY BUILDING

Outline of the Building and Subsoil

The building is a six story reinforced concrete structure with one basement story. It is 15.8m x 84m in plan as shown in Fig. 1. The west part of the building was first constructed during 1962 - 1963 and extensions were made three times up to 1970. Each construction stage is indicated in Fig. 2.

The main lateral resisting elements of this building are the walled type reinforced concrete frames, which have a walled girder (Spandrel) and a walled column, in the longitudinal direction, and the reinforced concrete shear walls in the transverse direction. In both directions there are slightly reinforced concrete and concrete block partition walls that are considered to be non-structural members. The building is supported by individual footings without piles at 5 meters below the ground level.

The antiseismic design of the building was made in accordance with Japanese Building Standard Law and AIJ (Architectural Institute of Japan) Structural Standards.

The fundamental natural period of the building determined by forced vibration tests is 0.29 sec in the longitudinal direction and 0.32 sec in the transverse direction. The rocking vibration is predominant in the transverse direction.

The subsoil below the building is Kanto loam layer, alternative layers of fine and sandy loam, alternative layers of fine sand and silty or clayey sand, and a gravel layer, on that order from the surface. The water-level is 8.8m below the ground surface. The soil profile and penetration test results (N-values) are shown in Fig. 3.

Measurement System

The electromagnetic seismometers were used to measure the earthqake motion under, around and inside the building. The location of the seismometers is shown in Fig. 4.

Seismometers A, B, C, D and E are placed along the vertical line from the top of the building to the soil layer 42m below the surface. Seismometers F, G and H are arranged also along the vertical line and are 60m distant south from the above group in a horizontal direction, intending to clarify the subsoil-superstructure interaction by comparing the records of two groups, the former group being affected by the superstructure while the latter being expected to be free from the interaction effect. Seismometer K is arranged at the depth of 82m below the ground level. This is expected to supply relatively pure earthquake, not much affected by the free surface. Each seismometer under the ground was installed at the bottom of a bore-hole, which was refilled after the installation so that seismic waves would not be afftected by the bore-hole.

Observed Earthquakes

Since the measurement was begun in 1964, seismograms of 24 earthquakes have been recorded. Intensity levels at the site are I, II and III according to JMA Intensity Scale. All the earthquake data are listed in Table 2.

Distribution of Maximum Amplitudes

Maximum amplitudes observed at the vertical building line (A, B, C, D, E) are normalized by those at the top of the building and plotted in Fig. 5 together with the mean values at each observation point.

Power Spectral Ratios

Mean values for the spectral ratios RF/BF, BF/GL and GL/-42m are illustrated in Fig. 6 together with the 95% confidence interval of mean values under Normal distribution assumption. The fluctuation in the spectral ratios decreases in order from GL/-42m (40%), BF/GL to RF/BF (10%), indicating a large amount of uncertainties inherent in soils rather than in the superstructures.

To compare the observed spectral ratios with computed ones, a building-soil interacting model as shown in Fig. 7 was adopted in this study. The dynamic ground compliance of a rectangular footing on an elastic half space is employed to evaluate the ground stiffness. The results plotted in Fig. 8 show a relatively good agreement with the observed spectral ratios where the peaks at 0.38 - 0.40sec in RF/GL indicates the fundamental natural period of the soil-building system, while the peak and valley at 0.30sec in RF/BF and BF/GL corresponds to the natural period of the superstructure. It is noted here that much attention should be taken in determining the shear wave velocity of the ground, which appears to be the most sensitive factor to the dynamic response of soil-building systems.

BUILDING B - PRECAST CONCRETE APARTMENT

Outline of the Building and Subsoil

The building where earthquake-motion measurement has been carried out is a seven story apartment house made of precast lightweight concrete as is shown in Fig. 9. It is supported on P.C. piles which are driven into a dense sandy layer 12m below the surface. The main structural components are walled frames in the longitudinal direction and shear walls in the transverse direction. The dimensions are 55.8m in Y direction, 13.2m in X direction and 19.1m in Z direction excluding the penthouse.

The natural periods of the building obtained from the forced vibration tests are 0.19sec in X and 0.24sec in Y direction. Translational and rotational displacements at the top are quite large and account for about half of the top displacement.

The surrounding soil consists mainly of sand and partly of silt or clay. (Fig. 10) The superficial layer (4 - 5m) has been recently reclaimed.

Measurement System

The seismometers are installed on two vertical lines, i.e., building line and soil line. (Fig. 10) Building line consists of 5 points, RF and 1F in the building, GL-4m, -12m and -24m just below the building. Soil line is parallel to the building line 15m from the building and consists of 4 points at the same levels.

The recorder is optical type and triggered when acceleration over 1 gal acts at GL-12m below the building.

Observed Earthquakes

Since the measurement was begun in Dec. 1971 more than 80 earthquakes have been observed. Intensity levels at the site are 1V or less in JMA scale. The epicentral distances, focal depths and magnitudes are less than 80km, around 50km and below 6.0 for more than half of the observed earthquakes, respectively.

Distribution of Maximum Amplitudes

The average amplitude ratios of maximum accelerations for 20 earthquakes regulating 1F to unity are shown in Fig. 11 where the thick continuous line and broken line denote the building line and soil line respectively both with standard deviations shown by lateral bars.

Amplification is great above GL-4m where existed the

ancient sea bed. Maximum amplitude of GL is about 1.5 times that of 1F, and no significant difference is seen between the building line and the soil line at lower levels. Amplification factors from GL-24m to 1F and from 1F to RF are 2.45 and 2.52 in the X direction, and 2.34 and 2.83 in the Y direction, respectively.

Power Spectral Ratios

The average power spectral ratios, RF/1F, 1F/GL and GL/-24m are plotted in Fig. 12 together with the 95% confidence interval of mean values under Normal distribution assumption. The fluctuation increases, in general, as the amplification factor becomes large and the maximum difference between the upper confidence limit and the sample mean is about 50% in this case. The variation in the natural periods of the building, soil and soil-building interacting system are about 10%.

The transfer characterestics, RF/1F, 1F/GL and GL/-24m, are calculated using the model shown in Fig. 7 and plotted in Fig. 13. The apparent shear wave velocity of the ground is increased 45% in order to take account of pile effects. A relatively good agreement is obtained between the observed and calculated spectral ratios.

Comparison Between Building Line and Soil Line

Fourier spectral ratios between the building line and the soil line at corresponding levels are calculated for a typical earthquake (No. 58) and shown in Fig. 14. For the ratio 1F/GL, a peak at 0.34sec and a valley at 0.24sec, corresponding to the natural periods of the soil-building system and of the superstructure, respectively, are clearly recognized. Such a tendency due to the soil-building interaction effects is greatly weakened as the depth from the ground surface increases.

Earthquake Response Analysis

Using the lumped mass model shown in Fig. 15, earthquake response analysis has been made for the observed wave forms. A typical example shown in Fig. 16 indicates a reasonable agreement between the observed and calculated time history of the response. Damping factors adopted in the analysis for the first several natural modes are so determined that the observed and calculated spectral ratios may become close as possible.

BUILDING C - STEEL FRAMED APARTMENT HOUSE

Outline of the Building and Subsoil

The building is an eleven story steel structure with

fire-proof covering of concrets. It is 8.5m x 92.7m in plan and 30.4m high above the ground level as shown in Fig. 17. It is supported by steel piles reaching the sand layer about 12m below the ground level with penetration resistance of $N > 50$.

The lateral resisting elements of this building consists of steel frames at lines A and C in the longitudinal direction and steel braced frames in the transverse direction. The beams at lines A and C and the bracings are encased in reinforced concrete and prefabricated together with reinforced concrete panels including the beams at line B. The columns and slabs are concreted at the site after the precast beams and panels are erected.

The subsoil below the sample building consists of several layers. The subsoil profile and the penetration test results are shown in Fig. 18 together with the location of the instruments.

Measurement System

16 sets of the electro-magnetic seismometers are installed to measure the earthquake accelerations under, around and inside the building as shown in Fig. 18.

The observation system was designed so as to know the dynamic behavior of the building and its surrounding soil during earthquakes and to establish an appropriate dynamical model for the soil-building systems. The following items are taken into consideration.

1) Participation factors of the natural vibrations associated with the horizontal slab deformation, which are distinguishable up to the 4th modes in forced vibration tests.
2) The rocking and swaying displacements measured at the top of the building.
3) Support excitation measurements along the longitudinal direction.
4) Soil-building interaction effects by comparing the observed earthquake records on the building and soil lines at different levels.

Observed Earthquakes

During the period 1970 - 1975, 41 sets of earthquake records were obtained, among which 15 earthquake data have been analized in this study. (Table 3) Root mean square values of the maximum ground accelerations in two horizontal components exceed 5 gals for 12 earthquakes denoted by * in Table 3.

Fourier Spectra

A pair of horizontal accelerograms is rotated from 0° to 90° by 22.5°, resulting in 8 different wave forms. Average Fourier amplitude spectra at the locations G0 and G30 are shown in Fig. 19. It is seen in this figure that the curves are random and scattered for both locations.

Distribution of Maximum Amplitudes

The average maximum amplitude ratio of 12 earthquake records denoted by * in Table 3, normalized to unity at GL-30m is plotted in Fig. 20, 21 together with the standard deviations. The amplitude ratios in the transverse and longitudinal directions along the vertical lines are shown in Fig. 20 a,b respectively, while the horizontal distr-butions of the maximum accelerations at the 1st and 11th floors are given in Fig. 21. Large fluctuations of the maximum amplitude ratios due to the different earthquakes can be seen in each figure.

Fourier Spectral Ratios

Fourier amplitude spectral ratios between two observation points characterize the transfer function between them. NC11/NB30 and EC11/EB30 shown in Fig. 22 represent the transfer characteristics between the top of the building and 30m below the ground level in the transverse and longitudinal directions. NC11/NC1, EC11/EC1, NC11/NG0 and EC11/EG0 in Fig. 23,24 reflect amplification characteristics of the building for the ground motion and base excitations, respectively. NC1/NG0 and EC1/EG0 in Fig. 25 indicate considerable effects of soil-building interaction. It is noted that the variation of the spectral ratios is smaller than that of the maximum amplitude ratios (Fig. 20) and Fourier spectra of the ground motions (Fig. 19).

Earthquake Response Analyses

A mathematical model of the soil-building system which includes in-plane slab deformations is employed in this study to represent the dynamic characteristics of the building in the transverse direction. The natural periods of the building obtained from earthquake observations, forced vibration tests and dynamic analyses are shown in Table 4. Theoretical transfer functions calculated by another model based on the dynamic ground compliance theory are also plotted by broken lines in Figs. 24 and 25.

The response analysis was carried out for the transverse direction in such a way that the observed accelerograms at different points along the base of the building are applied to the model with 2% of critical damping. The response accelerations at the top of the building are compared with the

Fig. 31 (a) for all 16 earthquakes. The 90% confidence interval of the mean values and 95% confidence interval of the standard deviation under the assumption of Normal distribution for the spectral values are drawn on both sides of the sample mean in (b) of the same figure.

In Fig. 32 (a), (b), (c), observed spectral ratios between the observation points 5/4, 3/1 and 4/3 are illustrated in the same manner of Fig. 31 (b), respectively. A large fluctuation in the spectral ratio between the top and base of the tank is due to the fact that the natural period of the tank changes according to the amount of the contained butane liquid.

It is also noted that the spectral ratio 4/3 has a wide valley at 0.22sec which seems to be the natural period of the tank with a small peak at a shorter period but no peaks in the longer period range. This fact, a seeming contradiction to the common concepts of dynamic ground compliance theory of semi-infinite medium, may be due to the interaction effects of the tank and layered soils especially when the predominant period of the ground coincides very closely with the natural period of the tank.

Apparent Effective Mass of the Contained Liquid

As mentioned previouly, the natural period of the tank changes according to the amount of contained liquid, and coversely, the apparent effective mass of the liquid may be determined from the observed natural period of the tank (including the base rotation). Fluctuation of the natural period versus total amount of the liquid is plotted in Fig. 33 together with the ratio of the apparent effective mass of the contained liquid.

CONCLUDING REMARKS

The analyses have been made on the records obtained for moderate earthquake motions at three buildings and sites and one spherical tank site which are chosen as illustrative examples of many earthquake observation projects that have been carried out in Japan for the purpose of clarifying soil-structure interaction effects. The results of the analysis may be summarized as follows:

(1) Distribution of maximum accelerations. The maximum acceleration at the top of the structure is alomst always larger than that at the base and at the soil layer due to amplification effect. The amplification factor is rather scattered but varies between 2 to 4 in most cases. Significant reduction of the maximum acceleration at the base of the structure as compared with that at the ground surface is observed. This implies the effect of soil-structure interaction.

observed ones in Fig. 26 which shows a reasonably good agreement.

SPHERICAL TANK

Outline of the Tank and Subsoil

The tank where the earthquake measurement has been carried out is a spherical shell supported by 12 steel pipes (700x9) with a pair of steel-bar bracings (2x80ϕ) between them. The heights to the crown and the circumference, and the diameter of the shell are 20.4m, 11.5m and 17.9m, respectively.

The soil layer formation at the observation site and the S-wave travel-time curve measured at the boring hole for installation of the underground seismometers are shown in Figs. 27 and 28 respectively.

Measurement System

The Tuss type accelerometers (f=5 c/s, h=0.6) are installed at 5 observation points along 2 vertical lines, as shown in Fig. 29. Output voltage of seismometers is amplified with automatic control of sensitivity (1:1/3:1/9) and recorded on a magnetic tape by the trigger of thresholed current from the seismometer at the deepest observation point. All the records are digitized simultaneousely, with the time interval of 0.02 sec, by the automatic A-D converter and stored directly in computer files.

Observed Earthquakes

Among all the earthquakes which have been observed since the measurement was begun in 1973, 16 significant earthquakes, which are analized herein, are listed in Table 5. Maximum amplitudes of the ground motion are 2 - 40 gal, earthquake magnitudes being 4.3 - 7.6, epicentral distances and focal depths being 20 - 500 km and 10 - 420 km, respectively.

Distribution of Maximum Amplitudes

The maximum amplitudes of all the 16 sets of records are plotted in Fig. 30, where the solid lines and the broken lines indicate the data on ground and tank lines, respectively. Significant reduction of the maximum amplitudes at the base of tank of 40% as compared to those at the ground surface, presumablly due to the soil-tank interaction effects, is observed.

Power Spectra and Spectral Ratios

Power spectra of the ground acceleration are averaged between two horizontal components (EW,NS) and plotted in

(2) Transfer functions. Considerable amount of variation is seen in the observed spectral ratios, although it is much smaller than those in the ground motion spectra. The fluctuations increase in the spectral ratios between the top and bottom of the buildings, between the base of the building and the ground surface, between the surface and the deeper soil layers, indicating considerable uncertainties inherent in the subsoils rather than in the superstructures. The spectral ratios between the base of structures and the free surface, however, show general tendencies that a peak corresponding to the fundamental natural period of soil-structure systems exists in a longer period range than a valley which represents the natural period of the superstructures. This fact, having been indicated by the theories e.g., the dynamic ground compliance for a long time, gives rigid framework for the futher development of the theoretical studies.

(3) Simulation models. Because of the large fluctuations observed in the transfer characteristics of soil-structure systems, it seems to be difficult to establish rigorous models for simulation analyses. Nevertheless, some models which represent the principal statistical features of the observed nature of the systems may be provided without much difficulty if the system parameters are suitablly adopted. It is mentioned here that the shear wave velocity of the ground is one of the most sensitive parameters for the overall characteristics of the soil-structure systems.

At an early stage of the earthquake observation projects, all the records themselves provided a valuable clue to study the earthquake response of soil-building systems. As the number of such projects increased, however, more systematic, more orderly planned and better equipped measurement systems are required. Possible technical improvements extend over wide categories; intentional choice of the site and structure; proper arrangement of instruments; stability and accuracy of instruments including periodic calibrations of underground seismometers; wide range measurement in amplitudes and frequencies; automatization of data processing and so on. Since the earthquake measurement projects cost high in general, cooperation and coordination between the projects are indispensable in order to provide systematic data not only for research on soil-structure interaction effects but for comparative studies of incident seismic waves.

ACKNOWLEDGMENT

The authors would like to acknowledge the continuing guidance and encouragement of Professor H. Umemura of the University of Tokyo. In preparing the present paper the authors' colleagues, Dr. Y. Kitagawa of the Building Research

Institute and Dr. S. Kawamura of the Taisei Construction Co. contributed a great deal. The authors also would like to take pleasure in acknowledging the important part played by them.

REFERENCES

(1) Strong-Motion Earthquake Observation Council, Tokyo, "The Project for Observation of Strong-Motion Earthquake and Its Results in Japan." Some Recent Earthquake Engineering Research and Practice in Japan, May 1973.

(2) Osawa, Y., Kitagawa, Y. and Ishida, K., "Recent Analyses of Earthquake Motions Observed In and Around a Reinforced Concrete Building Including Building-Subsoil System.", Proc. 5th W.C.E.E., 1973, Rome.

(3) Kawamura, S., Osawa, Y. and Umemura, H., "Earthquake Motion Measurement and Analysis of Pile-Supported Building and Its Surrounding Soil.", Proc. Review Meeting, U. S. - Japan Cooperative Research Program in Earthquake Engineering, Aug. 18 - 20, 1975, Honolulu, Hawaii.

(4) Murakami, M., et all, "Earthquake Resistance of a Steel Frame Apartment House with Precast Concrete Panel", 5th W. C. E. E., 1973, Rome.

(5) Minami. T., Osada, K. and Osawa, Y., "Earthquake Observations On a Spherical L. P. G. Tank and The Surrounding Ground.", Proc. 4th Japan Earthquake Engineering Symposium, 1975.

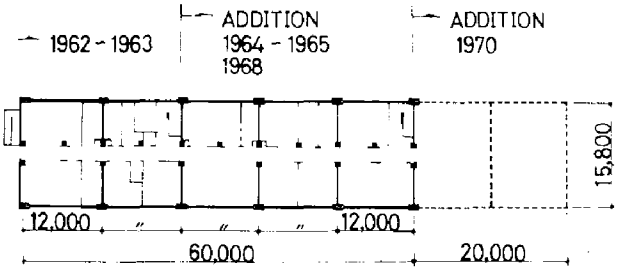

Fig.1 Plan of Building A

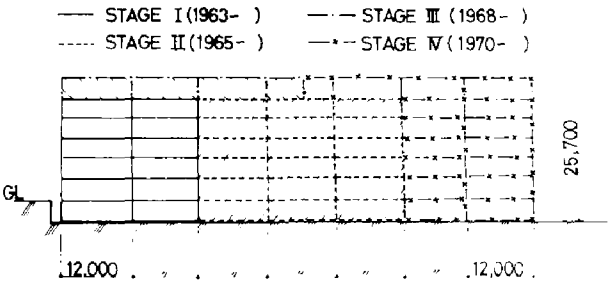

Fig.2 Construction Stage (Bldg. A)

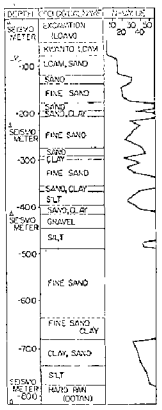

Fig.3 Soil Profile (Bldg. A)

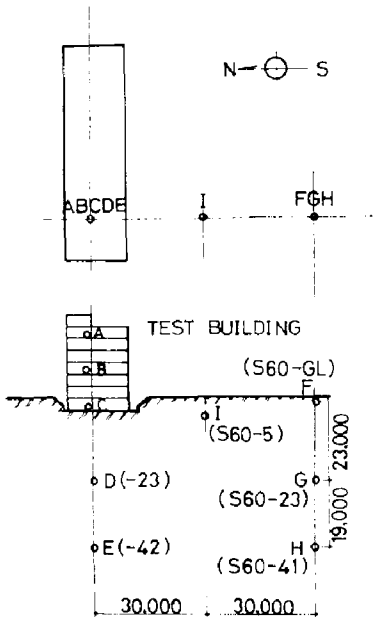

Fig.4 Location of Seismometers (Bldg. A)

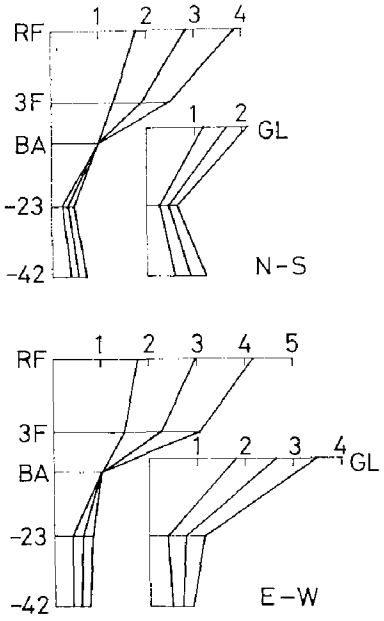

Fig.5 Maximum Amplitude Ratios (Bldg. A)

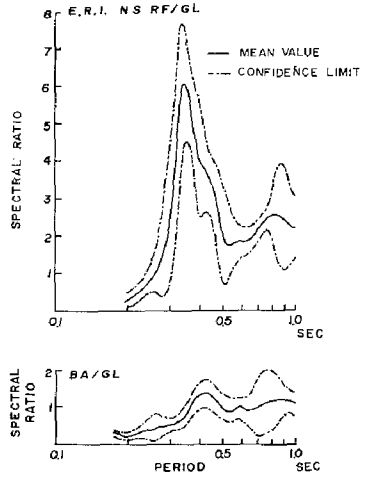

(a) RF/GL and BA/GL (EW)

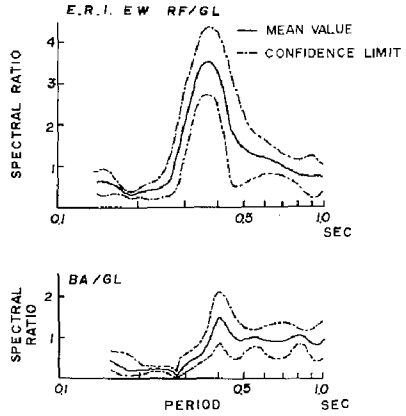

(b) RF/GL and BA/GL (NS)

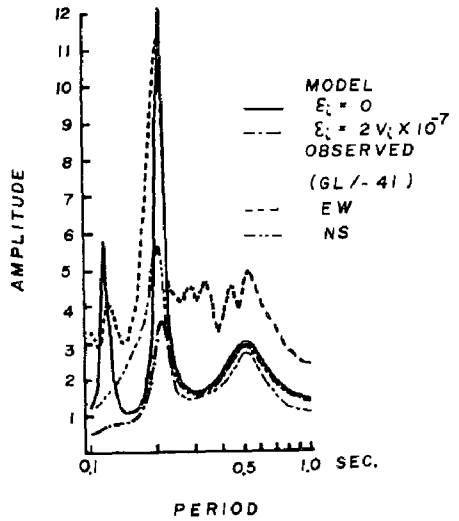

(c) Comparison of Observed and Calculated Spectral Ratios

Fig.6 Spectral Ratios (Bldg.A)

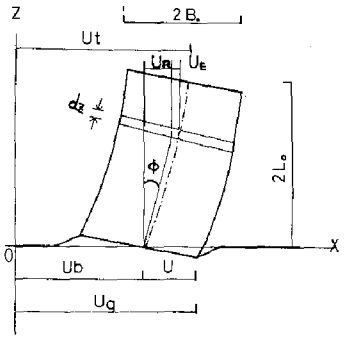

Fig.7 Analytical Model

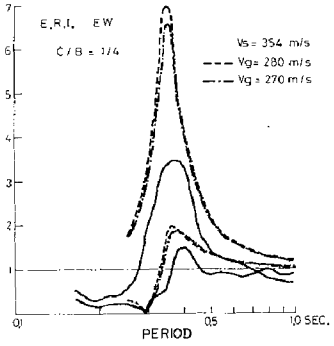

Fig.8 Computed Spectral Ratios RF/GL, BA/GL

V = 130	ρ = 1.4	H = 5.5
V = 170	ρ = 1.8	H = 2.5
V = 250	ρ = 2.0	H = 4.0
V = 400	ρ = 2.0	H = 17.0
V = 230	ρ = 1.9	H = 8.0
V = 800	ρ = 2.0	——

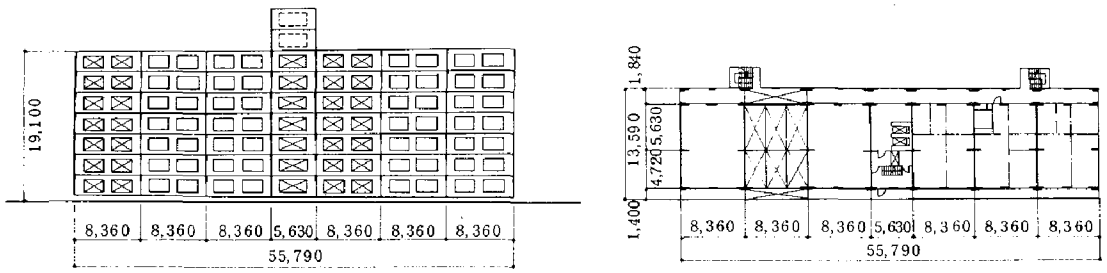

Fig.9 Plan and Section of Building B

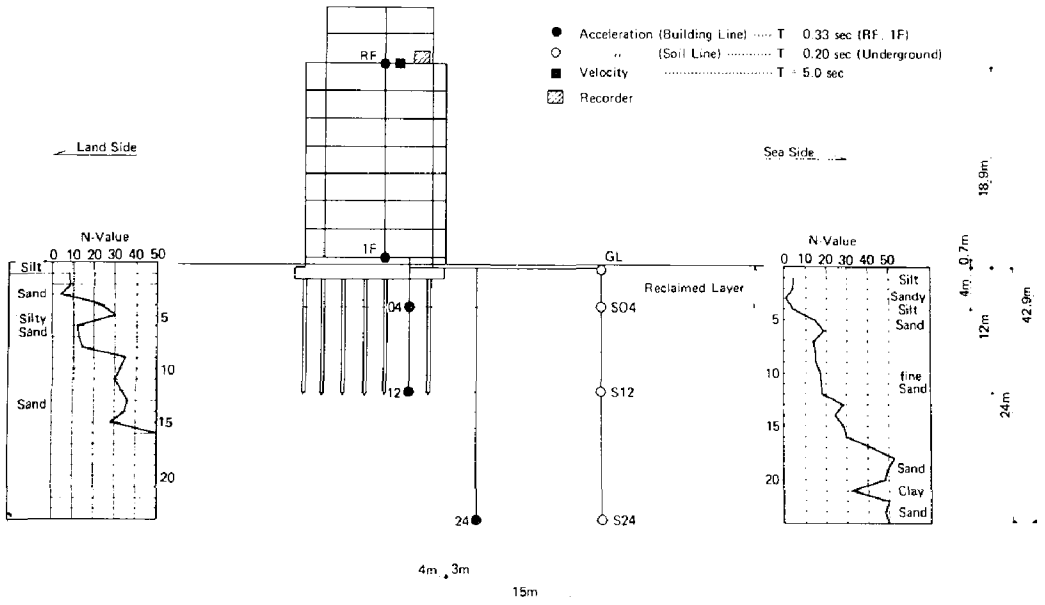

Fig.10 Location of Instruments and Soil Profile (Bldg. B)

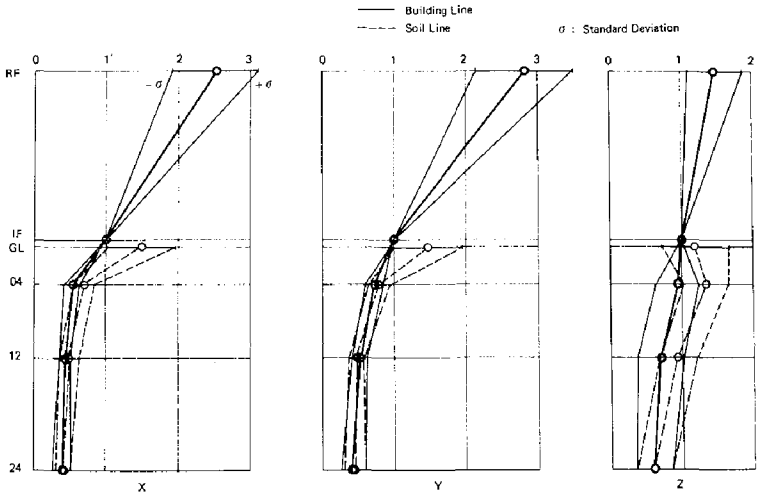

Fig.11 Average Maximum Acceleration Pattern (Bldg. B)

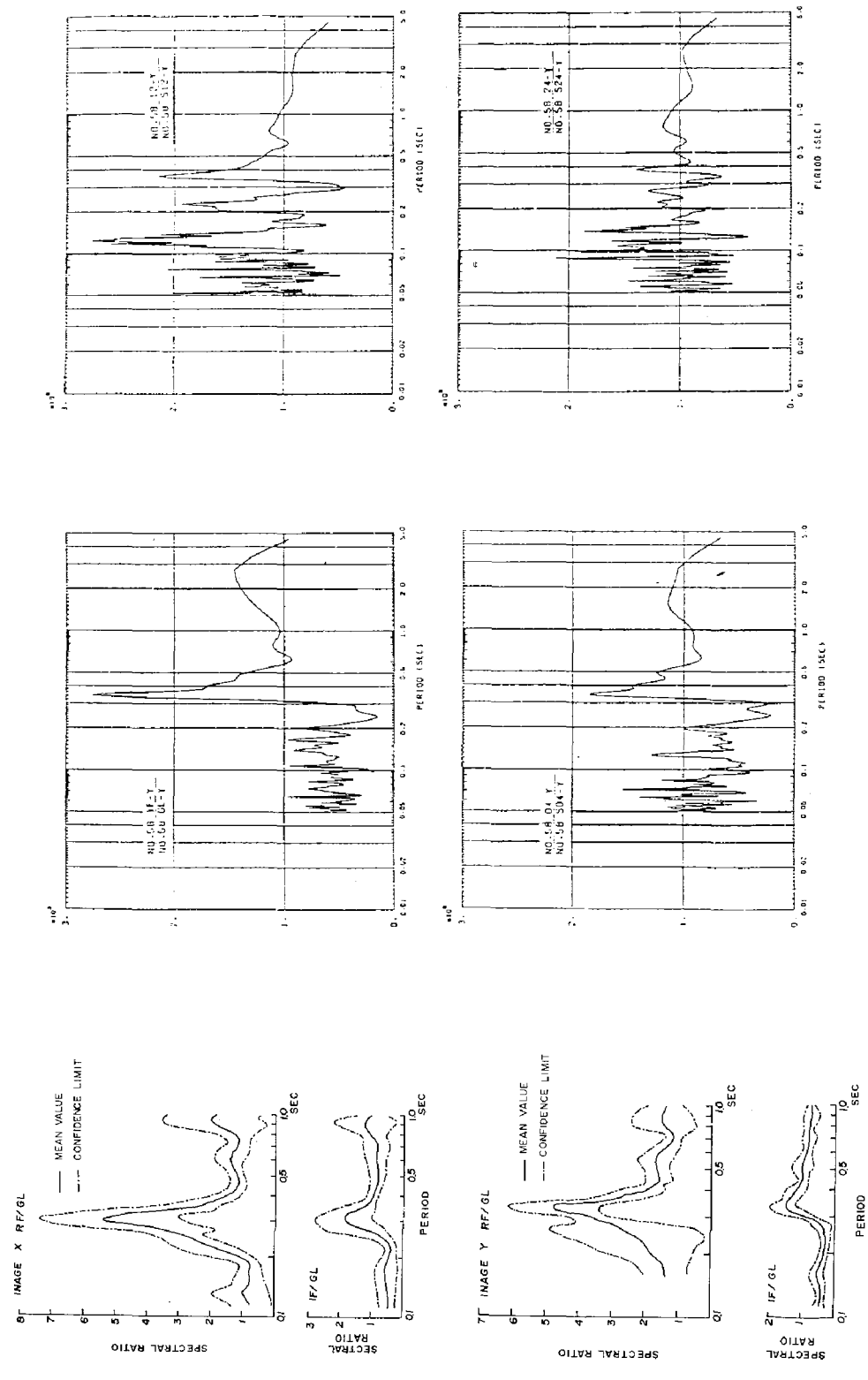

Fig.12 Spectral Ratios RF/G1 and 1F/GL

Fig.13 Fourier Spectral Ratios Between Building Line and Soil Line (Bldg. B)

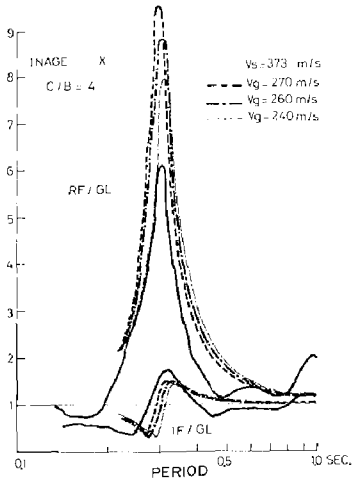

(a) X Direction

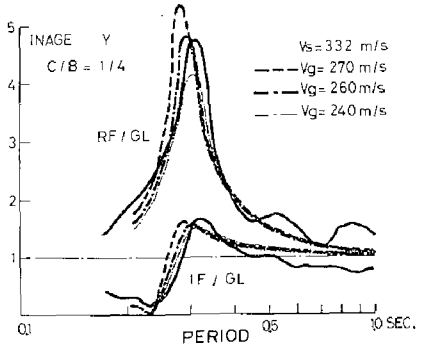

(b) Y Direction

Fig.14 Computed Spectral Ratios (Bldg. B)

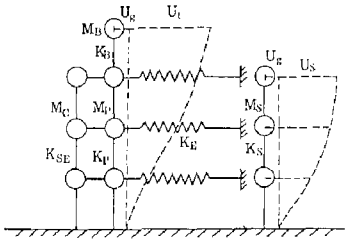

M_B: Mass of Building, M : Mass of pile
M_C: Additive Mass, M : Mass of Soil Column
K_B: Stiffness of Building
K_P: Stiffness of Pile
K_S: Stiffness of Soil Column
K_E: Interaction Spring
K_{SE}: Shear Spring between Additive Masses
U_g: Ground Motion
U_t: Displacement of Structure
U_s: Displacement of Soil Column

Fig.15 Analytical Model for Soil-Pile-Building System (Bldg. B)

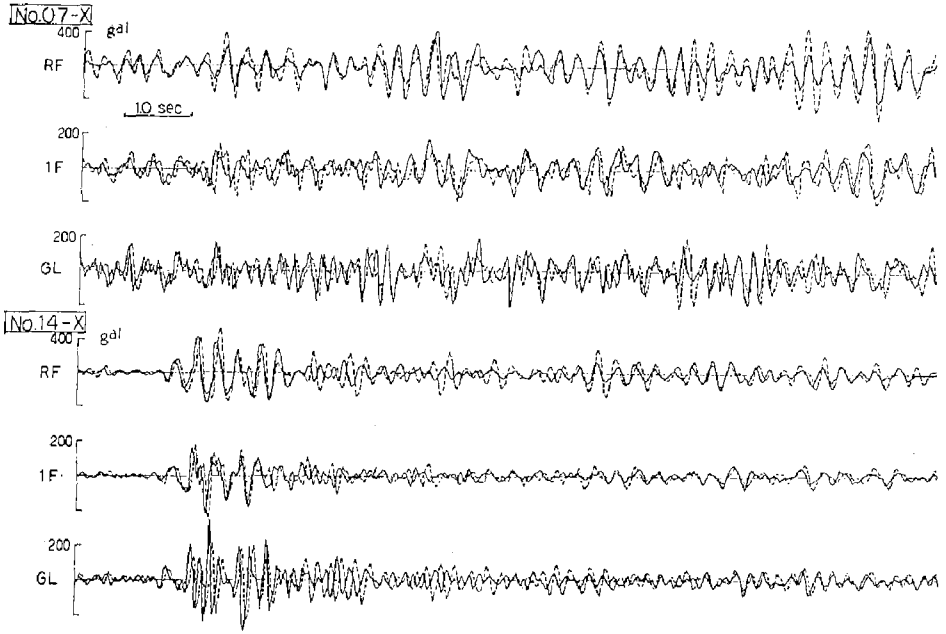

Fig.16 Comparison Between Observed and Calculated Waves (Bldg. B)

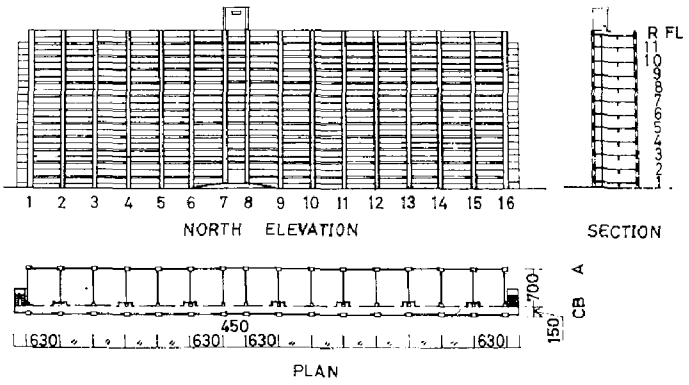

Fig.17 Outline of Building C

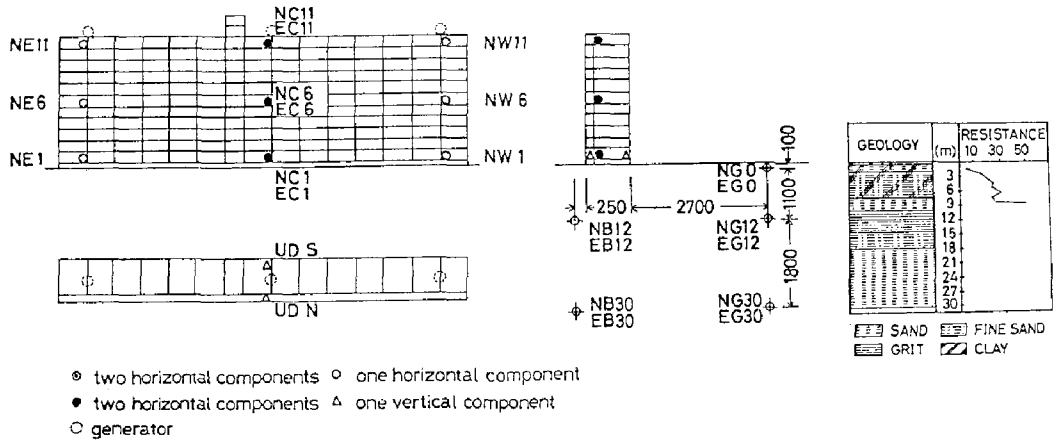

Fig.18 Location of Instruments and Soil Profile (Bldg. C)

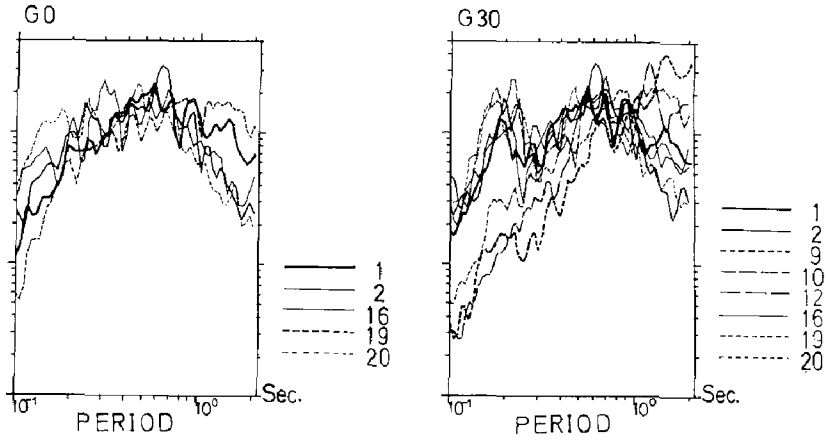

(a) Base of Building (b) Free Surface

Fig.19 Mean Values of Fourier Amplitude Spectra (Bldg. C)

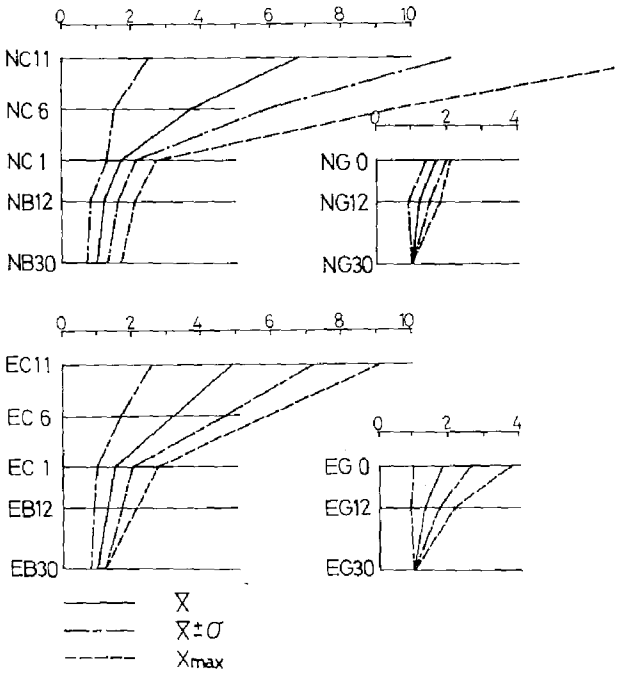

Fig.20 Maximum Amplitude Ratios (Bldg. C)

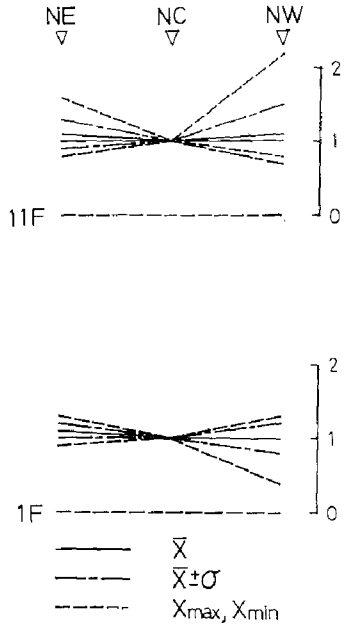

Fig.21 Horizontal Distribution of Maximum Amplitudes (Bldg. C)

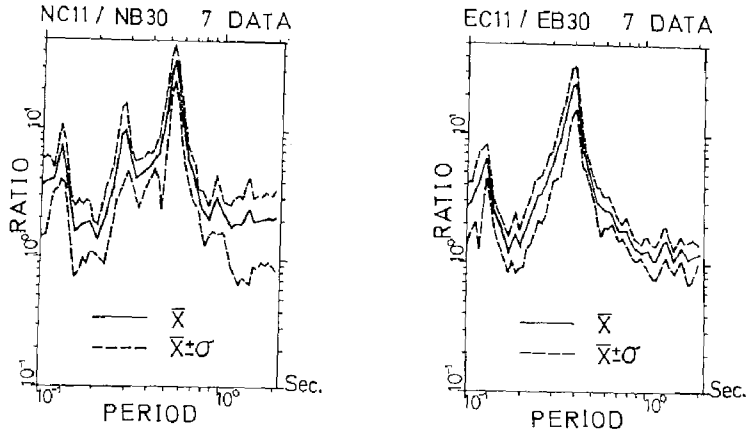

Fig.22 Fourier Spectral Ratios NC11/NB30 and EC11/EB30

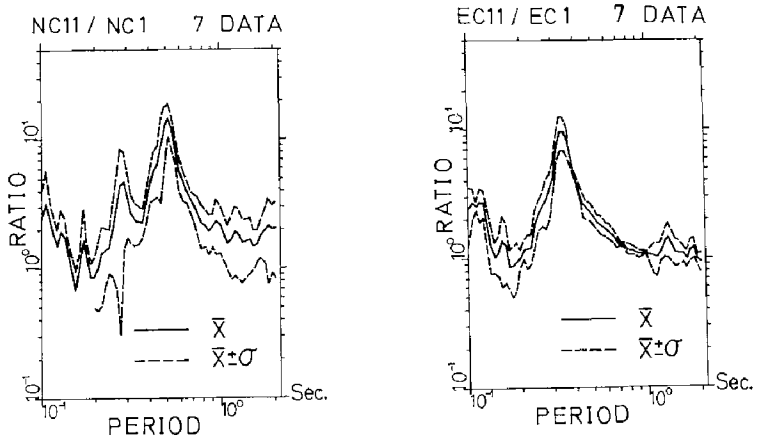

Fig.23 Fourier Spectral Ratios NC11/NC1 and EC11/EC1

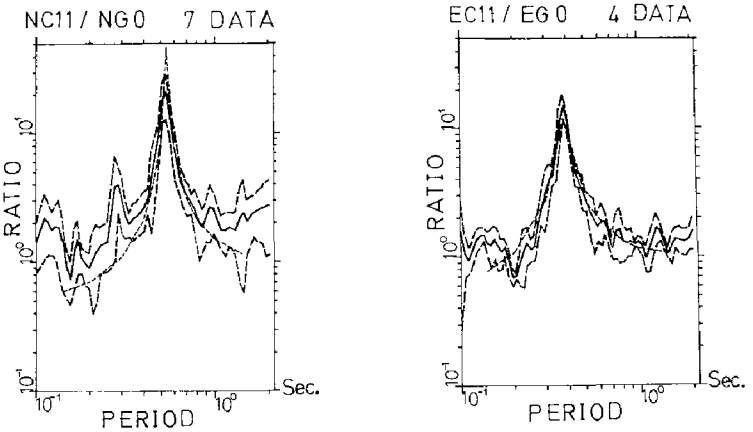

Fig.24 Fourier Spectral Ratios NC11/NGO and EC11/EGO

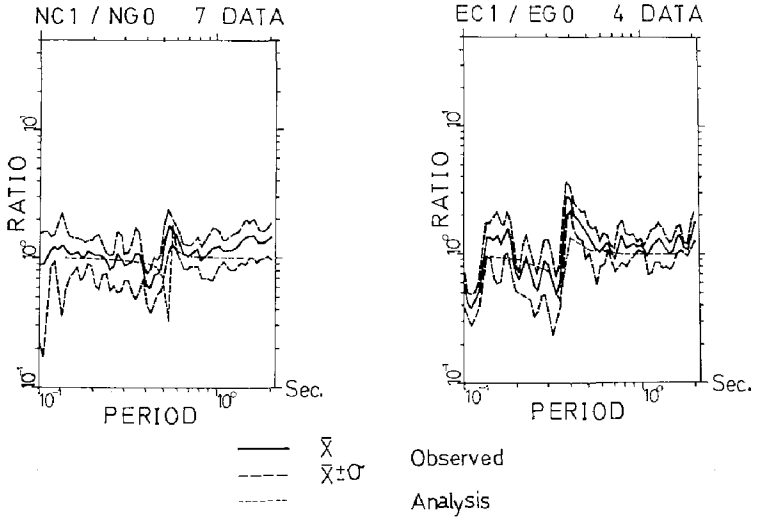

Fig.25 Fourier Spectral Ratios NC1/NGO and EC1/EGO

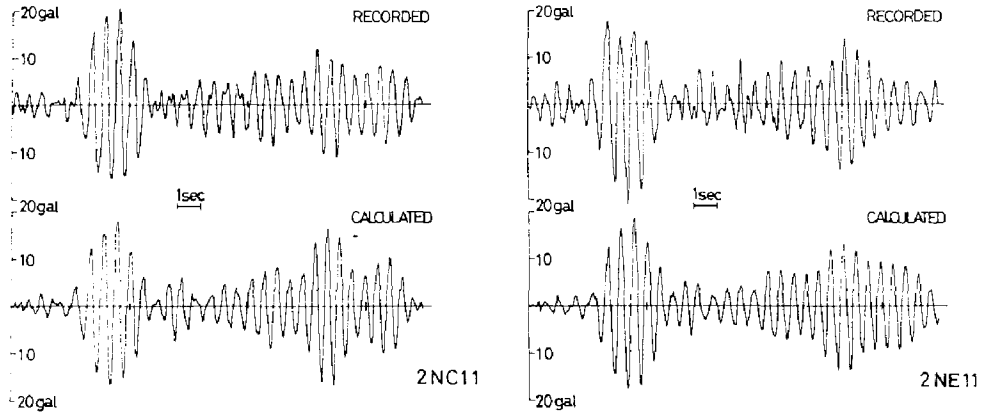

Fig.26 Comparative Time History of Recorded and Calculated Accelerations (Bldg. C)

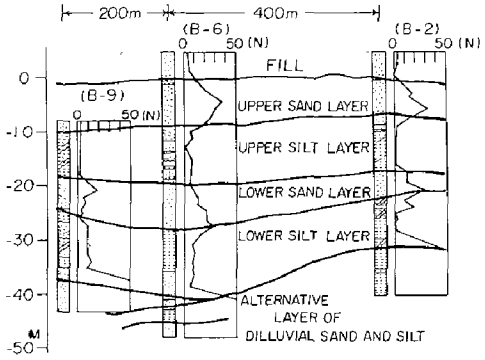

Fig.27 Soil Layer Formation (Tank)

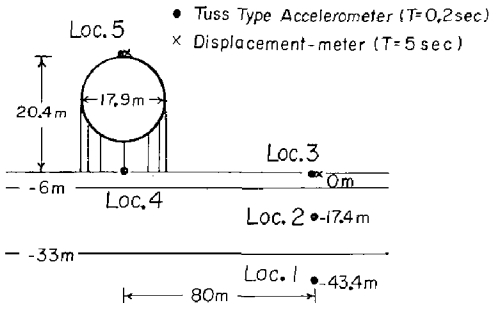

Fig.29 Location of Instruments (Tank)

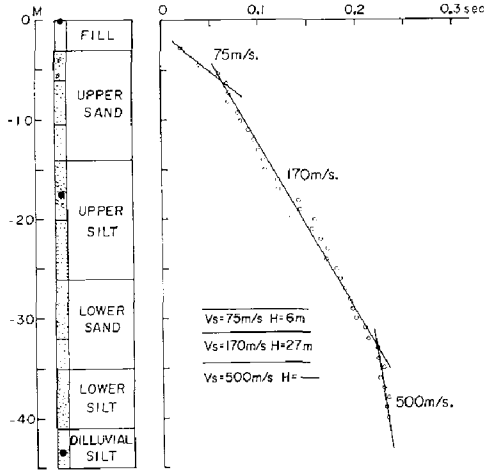

Fig.28 S-Wave Travel Curve (Tank)

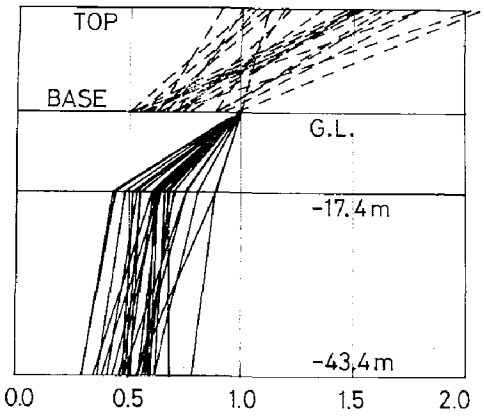

Fig.30 Maximum Amplitude Ratios (Tank)

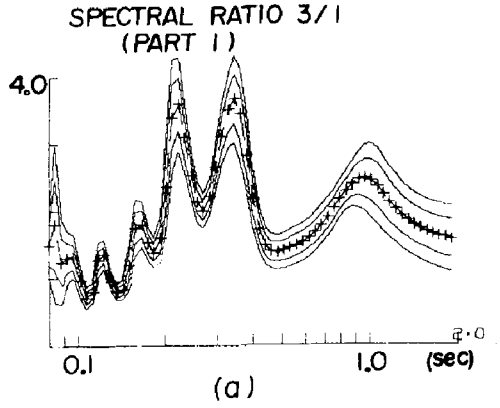

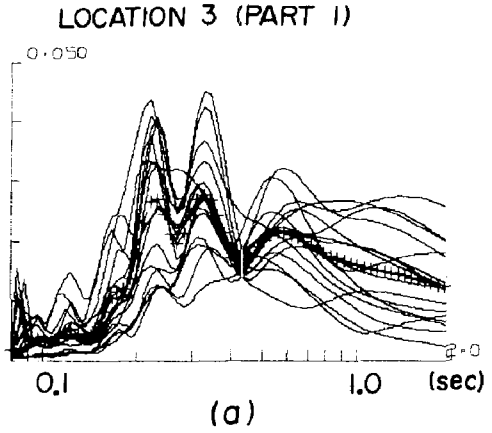

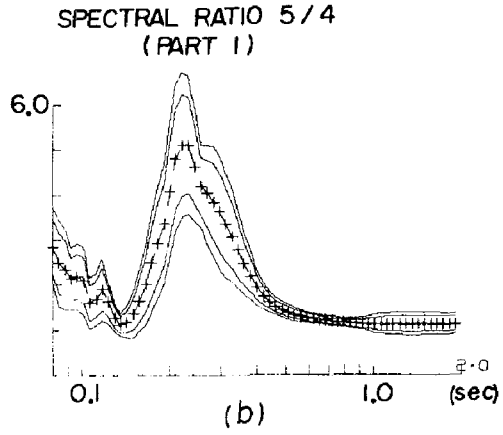

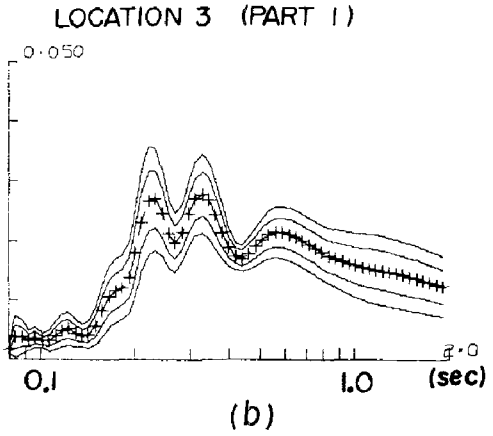

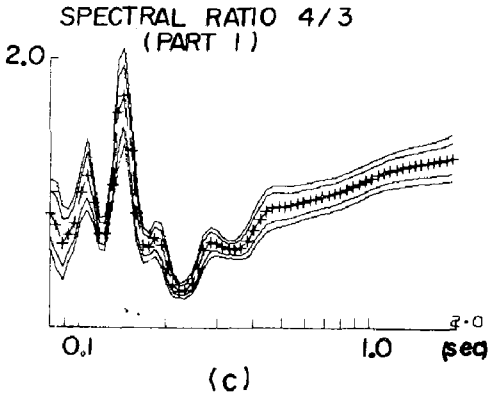

Fig.32 Spectral Ratios (Tank)

Fig.31 Power Spectra of Ground Motion (Tank)

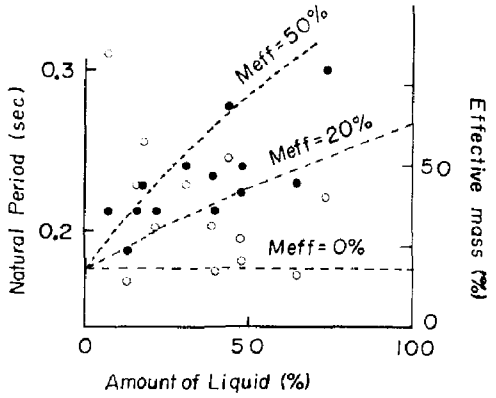

Fig.33 Effective Mass of Contained Liquid (Tank)

Table 1 Earthquake Observation Projects in Japan

No	Type of Building	Type of structure Number of stories Type of foundation	Organization	Date	Observation Points
1	University building	RC 6F individual	Univ. of Tokyo	1964	RF,4F,1F,GL-23m,GL-42m Ⓢ GL,GL-23m, GL-41m
2	High school building	RC 2F (ℓ=13m)	Kyoto Univ.	1965	RF.2F.1F Ⓢ GL,GL-1m, GL-10m,GL-20m
3	University building	RC 4F individual	Shinshu Univ.	1967	3F,1F Ⓢ GL
4	Apartment building	RC 7F PC pile(ℓ=12m)	Univ. of Tokyo	1971	RF,1F,GL-4m,G1-12m,G1-24m Ⓢ GL,GL-4m,GL-12m,GL-24m
5	Apartment building	RC 5F continuous	Ministry of Const.	1971	RC,3F,GL,GL-2m,GL-10m,GL-50m Ⓢ GL-2m
6	High school building	RC - RC pile(ℓ=32m)	Architectural Inst. of Japan	1972	RF,1F, GL-32m
7	Experiment building	RC 5F+B2F mat	Shimizu Const.	1972	RF,1F, B2F, GL-20m
8	Steam power station	RC 5F steel pipe pile (ℓ= 20m)	Chugoku Electric power Ohbayashi-gumi	1973	FL-38m,FL-55m, FL-23.75m Ⓢ GL-73m, GL-70m
9	Apartment building	RC 18F pier(ℓ=20m)	Kajima Co.	1974	RF,9F,B1F,GL-24m Ⓢ GL-1m, G1-27m
10	University building	RC 5F+B1F -	Nihon Univ.	-	B1F Ⓢ GL-3m, -15m, -30m
11	University building	RC 5F+B1F pile(=19m)	Tokyo Inst. of Tech.	-	B1F
12	Office building	S 36F+B3F mat	Kajima Co.	1968	RF,23F,13F,B2F(SMAC) B2F,GL-80m
13	Apartment building	S 11F H steel Pile (ℓ=12m)	Chiba Univ.	1970	11F,6F,1F,GL-12m,GL-30m Ⓢ GL-1m,GL-12m,GL-30m
14	Model building	S 5F individual	Kyoto Univ.	1971	RF,4F,1F,GL-50m,GL-12m, GL-50m
15	Office building	S 3F individual	Nippon Telegraph & Telephone Public Co.	1972	RF,3F,1F(SMAC),GL-5m GL-15m
16	Apartment building	S 11F earth drill pile (ℓ=11m)	Shimizu Const.	1972	11F,1F,GL-10m
17	Office building	S 30F mat	Ohbayashi-Gumi	1973	R1F,24F,15F,1F,B2F
18	Apartment building	SRC 15F steel pile	Waseda Univ.	1968	RF(SMAC),GL-4m,GL-44m

(to be continued)

19	University building	SRC 9F (ℓ=12m)	Tohoku Univ.	1970	RF,7F,3F,1F.
20	Apartment building	SRC 14F PC pile	Ministry of Const.	1972	14F,8F,B,P. Ⓢ GL-9m,GL-16m,GL-26m,GL-60m.
21	Office building	SRC 12F mat	Kumagaya-Gumi	1974	RF,6F,B2F
22	Apartment building	SRC 11F Benoto pile	Technology Center for National Land Developement Kajima Co.	1974	RF,1F,GL-13m,GL-26m Ⓢ GL-2m,GL-55m,GL-9m,GL-13m, GL-35m,GL-100m
23	Apartment building	SRC 9F -	Kajima Co.		RF,BF,GL-10m,GL-20m s GL-2m,GL-20m
24	Laboratory building	SRC 7F+B3F continuous	Central Res. Inst. of Electric Power - Industry	1975	RF,7F,6F,4F,3F,1F,B1F,B3F
25	Reactor	RC,S - -	Architectural Inst.of Japan	1963	
26	Rigid structure model No.1	RC 1F mat	Architectural Inst. of Japan	1965	RF,1F,B1F, Ⓢ GL-2m,GL-4m,GL-14m,GL-20m
27	Rigid structure model No.2	RC 2F mat	Architectural Inst. of Japan	1967	RF,2F, 1F Ⓢ GL,GL-20m

28	Rigid structure model No.3	RC 2F mat		1967	RF,1F,B1F, Ⓢ GL-3m,GL-14m,GL-20m
29	Reactor	RC 5F+B1F mat	Tokyo Electric Power Kajima Co.	1970	RF,5F,footing GL-14,GL-24,GL-50 Ⓢ GL-14
30	Reactor	RC 5F+B1F mat	Chygoku Electric Power Kajima Co.	1973	RF,5F, footing,GL-35m Ⓢ GL
31	Model with PC pannel	RC 1F H steel pile (ℓ=10m)	Nippon Steel Univ. of Tokyo	1968	RF,1F,Gl-5m Ⓢ GL-5m
32	Model building	RC 3F -	Japan Electric Association	1968	RF,3F,2F,1F Ⓢ GL
33	Model footing	S 1F mat	Ministry of Const.	1975	RF, footing Ⓢ GL-0.5mx2,-15m,-41m
34	Tower	S 81m	Ministry of Const.	1967	GL+81,GL Ⓢ GL
35	Office building with tower	building SRC 15F+B5F tower S mat 140m	Kajima Co.	1973	GL+200m,GL+107m,15F(SMAC) B5(SMAC)
36	Tank	25m steel pipe pile (ℓ=38m)	Shimizu Const.	1973	top, footing,GL-2m,GL-18m, GL-39m Ⓢ GL-2m,GL-18m,GL-38m,GL-71m
37	Tank	20m steel pipe pile (ℓ=31m)	Univ. of Tokyo	1974	top,footing Ⓢ GL,GL-17.4m,GL-43.4m

(to be continued)

38	Chimney	S 230m steel pipe pile (ℓ=40m)	Tokyo Electric Power Mitsubishi Heavy Instustries	1974	GL+222m,GL+112m,GL+0.5m GL-10m, GL-31m,GL-38m
39	Plant tower	S 50m, 30m steel pipe pile (ℓ=45m)	Mitsui Petro-Chemical Taisei Co.	1974	T49,T30,P1,F2,GL-10m,GL-45m, GL-85m Ⓢ GL

RC ; Reinforced concrete structure
S ; Steel structure
SRC; Steel framed reinforced concrete structure
Ⓢ ; Observing point distant from building

Table 2 Observed Earthquakes (Bldg.A)

No	Date	Epicentre	Depth	Magnitude	Intensity (JMA)
A-01	05h, 03m 29d, VIII,'66	35.5°N,139.9°E	80km		III: Ôshima I : Tokyo
A-02	22h, 20m 28d, X,'66	35.7°N,140.3°E	60	5.0	III: Ôshima II : Tokyo
A-03	14h, 25m 26d, XI,'66	35.9°N,140.2°E	100		II : Tokyo
A-04	20h, 04m 14d, XII,'66	36.2°N,138.9°E	60	4.9	III: Utsunomiya II : Tokyo
A-05	20h, 59m 17d, 1, '67	38.3°N,142.2°E	30	6.3	IV : Sendai II : Tokyo
A-06	20h, 21m 13d, II, '67	36.1°N,140.0°E	54.9	4.9	III: Utsunomiya II : Tokyo
A-07	17h, 17m 02d, III, '67	35.5°N,140.1°E	80		III: Yokohama II : Tokyo
A-08	02h, 50m 19d, III, '67	36.3°N,140.1°E	80		III: Tokyo
A-09	06h, 54m 21d, III, '67	36.2°N,140.0°E	50	5.1	III: Utsunomiya II : Tokyo
A-10	11h, 42m 22d, V, '67	36.1°N,139.8°E	70		III: Tokyo
A-11	21h, 13m 03d, VIII,'67	36.1°N,139.9°E	50	4.5	II : Utsunomiya I : Tokyo
A-12	05h, 07m 14d, VIII,'67	35.5°N,135.8°E	360		III: Onahama II : Tokyo
A-13	22h, 38m 19d, VIII,'67	36.1°N,140.9°E	100		II : Utsunomiya
A-14	11h, 06m 30d, VII,'67	35.0°N,140.0°E	70		III: Chiba II : Tokyo
A-15	17h, 09m 30d, VIII,'67	36.1°N,140.3°E	80		III: Utsunomiya II : Tokyo
A-16	09h, 28m 15d, IX, '67	35.5°N,141.1°E	40	5.6	III: Yokohama II : Tokyo
A-17	19h, 56m 19d, IX, '67	430 °N,145.1°E	90		IV : Kushiro I : Tokyo
A-18	09h, 32m 20d, XI, '67	36.1°N,140.2°E	80		III: Tokyo

(to be continued)

A-19	21h, 07m 19d, XI, '67	36.3°N, 141.1°E	40		III: Onahama II : Tokyo
A-20	21h, 08m 28d, II, '68	32.9°N, 137.9°E	340		III: Tokyo II : Chiba
A-21	09h, 12m 06d, III, '68	36.05°N, 139.9°E	50	5.2	III: Tokyo II : Maebashi
A-22	09h, 49m 16d, V, '68	40.7°N, 143.6°E		7.9	VI : Tomakomai II : Tokyo
A-23	19h, 39m 16d, V, '68	41.4°N, 142.9°E	40	7.5	V : Uraga II : Tokyo
A-24	22h, 42m 12d, VI, '68	39.4°N, 143.1°E		7.2	IV : Sendai II : Tokyo

Table 3 Observed Earthquakes (Bldg. C)

MODE			EXPERIMENT			ANALYSIS	OBSERVATION
	FRAME	SLAB	PERIOD sec	DAMPING %	SHAKING TYPE	PERIOD sec	
NS	1st MODE		0.48	2~3		0.48	0.51
			0.43	2~3		0.43	0.42
			0.25	2~3		0.25	0.29
			0.13	—		0.13	—
	2nd MODE		—	—	—	0.09	—
			—	—	—	0.09	—
EW	1st MODE		0.31	3~4		—	0.32
	2nd MODE		0.10	—		—	—

* Due To Eccentric Mass & Shaking Type

Table 4 Natural Periods and Mode Shapes (Bldg. C)

NO.	DATE	TIME	EPICENTER	(N)	(E)	DEPTH (Km)	EPICENTER DISTANCE (Km)	MAGNI-TUDE	INTENSITY (J.M.A.) (CHIBA)	(MAX.)		
1	'70. 5.17	23:52	SE OFF BOSOH PEN	34°36'	141°06'	60	140	-	I	II	:TATEYAMA	#
2	'70.12. 8	6:36	OFF TORISIMA	29°32'	140°36'	180	690	-	II	-	:	#
3	'72. 2.29	18:23	E OFF HACHIJOJIMA	33°11'	141°16'	70	310	7.0	IV	V	:HACHIJOJIMA	* #
9	'72. 9. 8	18:23	CENTRAL CHIBA PREF	35°32'	140°23'	70	50	-	II	II	:CHIBA	*
10	'72.10. 6	20:31	SW OFF IZU PEN	34°24'	138°31'	30	160	5.5	II :TATEYAMA	IV	:OMAEZAKI	#
12	'72.10.18	10:48	NORTHERN CHIBA PREF	35°44'	140°07'	80	50	-	III	III	:CHIBA	* #
16	'73.12.22	10:20	SOUTHERN CHIBA PREF	35°13'	140°17'	70	40	-	II	III	:TATEYAMA	*
19	'74. 2.22	9:37	OFF KII PEN	33°08'	137°07'	400	370	6.9	II	III	:TATEYAMA	* #
20	'74. 3. 3	13:50	E OFF CHIBA PREF	35°34'	140°53'	60	90	6.1	III	IV	:CHOSHI	* #
21	'74. 4. 3	10:52	S COAST OF CHIBA PREF	35°01'	140°11'	50	40	4.3	I :TATEYAMA	II	:TOKYO	* #
22	'74. 5. 9	8:33	S COAST OF IZU PEN	34°34'	138°48'	10	130	6.9	III	V	:IROUZAKI	*
25	'74.11.16	8:32	OFF CHOSHI	35°45'	141°15'	40	130	6.1	II	IV	:CHOSHI	*
27	'74.11.30	7:06	NEAR TORISIMA	30°36'	138°46'	420	540	7.6	II	IV	:TATEYAMA	*
31	'75. 4. 2	17:44	NEAR HACHIJOJIMA	33°42'	140°47'	40	200	5.8	I	IV	:HACHIJOJIMA	*
41	'75. 8.12	23:22	S OFF CHUBU	31°57'	138°12'	400	410	6.9	II	III	:TOKYO	*

* AGO≧5 # DIGITALIZED

Table 5 Observed Earthquakes (Tank)

Earthq. No.	Date, Time (y,m,d,h,m)	Origin	Depth (km)	M	Max. Accel. EW	Max. Accel. NS
1	'73.4.21 19.44				2.9	3.4
5	'73.5.5 12.52	N37.07 E141.30	50	5.3	2.6	3.2
14	'73.6.9 17.37	N 35.53 E140.03	80		2.2	2.0
17	'74.3.19 21.01	N 35.15 E141.00	50	4.8	2.5	2.9
19	'74.4.3 10.52	N 35.01 E140.11	50	4.3	3.9	4.8
21	'74.4.5 04.33	N35.58 E140.09	70	4.3	2.9	4.2
28	'74.5.5 23.19	N 37.45 E141.51	40	5.5	1.5	1.9
29	'74.5.9 08.33	N 34.34 E138.48	10	6.9	9.9	14.2
31	'74.6.27 10.49	N 33.45 E139.12	10	6.1	4.0	1.8
32	'74.8.4 03.16	N 36.01 E139.55	50	5.8	22.2	39.8
33	'74.9.27 12.10	N 33.43 E141.31	60	6.4	17.1	10.4
34	'74.10.9 04.42	N 36.03 E139.55	60	4.8	18.1	15.7
35	'74.11.16 08.32	N 35.45 E141.15	40	6.1	13.7	9.6
36	'74.11.30 07.06	N 30.36 E138.46	420	7.6	14.7	7.8
37	'75.1.21 02.31	N 34.59 E141.21	30	5.9	4.1	2.4
38	'75.2.8 01.41	N 35.48 E140.06	50		20.7	26.5

INTERNATIONAL SYMPOSIUM ON
EARTHQUAKE STRUCTURAL ENGINEERING
St. Louis, Missouri, USA, August, 1976

DISCRETE MODELING OF SYMMETRIC BOX-TYPE STRUCTURES

A. H. HADJIAN AND T. S. ATALIK

Engineering Specialist and Engineer

Bechtel Power Corporation, Los Angeles Division

Norwalk, California, U.S.A.

SUMMARY

The dynamic modeling of box-type structures with simple lumped mass models is evaluated. Shear deformations, rotatory inertia and shear lag effects have important contributions to the overall response depending on the characteristics of the structure. To routinely incorporate these effect, a simplified procedure is described. The effects of shear deformation and rotatory inertia effects on the mass properties of the structure are accounted for by heuristically reducing the consistant mass matrix of a beam element into a diagonal form. These effects are then isolated and checked against the analytical solutions with acceptable results. The incorporation of shear lag effects is approached from a statics point of view. Based on a bending theory developed by Reisner, the stiffness of the beam is modified such that the use of the elementary bending theory would correctly predict deflections of beams with significant shear lag effects. The effect of shear lag on the inertial properties is investigated only by a few test cases. The procedure developed is tested by a comparison of the results with those from a finite element model of a structure whose properties were intentionally selected such as to accentuate the considerations under investigation.

INTRODUCTION

It is common engineering practice to use simplified lumped mass models in predicting the dynamic characteristics and earthquake response of structures. For complicated structures, such as those encountered in nuclear power plants, a finite element model could, in principle, provide a more appropriate representation. However, due to the associated high computer costs, lengthy modeling labor, the non-availability of large problem solving capabilities and the uncertainties in the other aspect of the problem, it is usually deemed adequate that a simplified lumped mass model would represent the dynamic characteristics of these relatively complicated structures. However, it is important that a) the modeling techniques used be first qualified using simpler structures, b) these simpler structures be studied to identify the important parameters of the modeling process, and c) based on the above two steps, modeling techniques for the more complicated structures be formulated. The first two steps are the subject of this paper. A subsequent paper will deal with the third phase.

The following areas are considered to be particularly important for the modeling of box-type concrete structures: a) The proper location of the shear center. b) The determination of the effective shear area. c) Shear lag effects in the computation of moment of inertias. d) The lumping of mass and of rotatory inertia at selected nodes and the effects of shear deformation on the mass matrix. e) The possible effects of shear lag and effective shear area on the inertial masses.

SHEAR CENTER OF RESISTING ELEMENTS

The shear center is the point through which a transverse loading will not cause any twisting of the cross-section. Although equations for the calculation of the shear center for open sections are available in texts on advanced strength of materials (6), those for closed sections are more difficult to obtain (7). More importantly the application of these concepts to complicated floor plans encountered in nuclear power plant structures is not a trivial task. It is common practice though to calculate instead the center of rigidity in each of the "principal" structure axes by considering only the walls parallel to the direction under consideration. Obviously for an open channel section such as shown in Fig. 1a, this assumption is not justified. Fig. 1b shows an unsymmetrical box where the assumption of the center of rigidity as defined above, is seen to be a very good approximation to the true shear center. A more detailed study of this approximation is in order for more complicated structures; however, such a study is beyond the scope of the present paper. It is obvious that for sections having two axes of symmetry, the shear center and the centroid of the section coincide.

EFFECTIVE SHEAR AREA

In the derivation of the Timoshenko beam equation the effective shear area is introduced to account for the fact that shear stress and shear strain are not uniformly distributed over the cross-section. Although there are many interpretations to the actual meaning of the shear coefficient, K, (1, 2, or 3), the important point to note is that except for Timoshenko's (8), the differences in the actual values are of no significant importance in practical applications in earthquake engineering. Although

the equations for K as reported by Cowper (1) are dependent on Poisson's ratio, ν, the differences between the range of ν commonly used for concrete is not significant at all. Thus a value of $\nu = .17$ is used in this paper. In the present paper both Cowper's equations (1) and that given by Ebner and Billington (2) will be used; however, a direct dimensionless comparison of these shear coefficients will not be attempted in this paper. The intent of such a comparison would be to establish the generality of the Ebner and Billington equation, since it could most suitably be extended to apply to more complicated sections.

A further simplification would be to relate the shear area of the cross-section to the area of the "webs" only. Results of such an attempt, based on Cowper's equation for a box section, are shown in Fig. 2, together with the Cowper results. The variables are explained in the figure. These results indicate that the generality of the Cowper equation for the box section breaks down for certain values of M and N (dashed lines). This conclusion is based on the observation that the shear area of the complete box could not be less than that of the shear area of the webs treated as independent rectangular sections. For $\nu = 0.17$, the Cowper equation gives the shear area coefficient for rectangles as 0.844. The Cowper equation when used will be limited as discussed above.

SHEAR LAG EFFECTS IN BENDING STIFFNESS

Considering bending stiffness only, the elementary beam theory assumes that the normal stress along the flanges (the walls normal to the direction of bending) does not vary. However, because of the shear deformation of the flanges this assumption often leads to errors for wide beams. The problem is illustrated schematically in Fig. 3. For the section shown, bending about the Y-axis would rotate the web of the section assuming plane sections remain plane. However, the flanges would deform as shown; thus in effect reducing the moment of inertia of the section as would have otherwise been calculated according to the elementary beam theory. In the following, a method of obtaining an effective moment of inertia of box sections including shear lag effects is presented.

Using the principle of minimum potential energy Reissner (5) developed the following governing equations for the deflection of a box beam (Fig. 4) when the shear lag effects are present:

$$Z'' + \frac{2}{3}\,\frac{I_f}{I}\,U' + \frac{M}{EI} = 0 \tag{1}$$

$$U'' - \frac{5}{2}\,\frac{G}{E}\,\frac{U}{w^2} + \frac{5}{4}\,Z''' = 0 \tag{2}$$

with the boundary conditions

$$\begin{aligned} &U = 0, \text{ at a section where the flange is fixed} \\ &U' + \frac{5}{4}\,Z'' = 0, \text{ at a section where the flange is free} \end{aligned} \tag{3}$$

In the above equations Z is the transverse deflection, $I_f = 4wth^2$ is the moment of inertia of the flanges, $I_w = 4bh^3/3$ is the moment of inertia of the webs, $I = I_w + I_f$ is the total moment of inertia of the cross-section, M is the moment at the section, E and G are Young's modulus and shear modulus respectively, U = U(x) is a function denoting the magnitude of the shear lag effects and it is assumed that the spanwise flange deformation u(x,y) may be approximated by

$$u(x,y) = \pm h \left[Z' + \left(1 - \frac{y^2}{w^2} \right) U(x) \right] \tag{4}$$

Herein, prime denotes differentiation with respect to the spatial variable x. The variables w, t, h and b describe the dimensions of the cross-section as depicted in Fig. 4.

Differentiating Eqn. 1 once and back substituting into Eqn. 2 one gets a differential equation for the shear lag function U as

$$U'' - k^2 U = \frac{5}{4} n \frac{M'}{EI} \tag{5}$$

with the boundary conditions

$$U = 0, \text{ at the fixed end} \tag{6}$$

$$U' = \frac{5}{4} n \frac{M}{EI}, \text{ at the free end} \tag{7}$$

where $k = \frac{1}{w} \sqrt{\frac{5nG}{2E}}$ and $n = \frac{1}{1 - 5I_f/6I}$ (8)

Once the shear lag function U is found for a specific case from Eqn. 5, the static deflection of the box beam can be solved by a double integration of Eqn. 1 with the appropriate boundary conditions,

$$Z'' = - \frac{M}{EI} - \frac{2}{3} \frac{I_f}{I} U' \tag{9}$$

Since the aim is to obtain a reduction factor for the flange stiffnesses a further simplification of Eqn. 9 is necessary. This can be achieved as follows: For a given moment variation, M = M(x), solve for U = U(x) from Eqns. 5, 6 and 7. Find the constant 'a' such that

$$U'(x) \cong a \cdot M(x) \tag{10}$$

Herein the constant 'a' is found by minimizing the average over the length, of the square of the difference between U'(x) and a · M(x); that is

$$H = \int_0^{\ell} [U'(x) - aM(x)]^2 \, dx \qquad \text{minimum} \tag{11}$$

or
$$\frac{\partial H}{\partial a} = 0 \Rightarrow a = \frac{\int_0^{\ell} U'(x).M(x)dx}{\int_0^{\ell} M^2(x)dx} \tag{12}$$

Back substituting the approximation to U' into Eqn. 9 gives

$$Z'' = -\frac{M}{EI} - \frac{2}{3}\frac{I_f}{I}(aM) \tag{13}$$

or
$$Z'' = -\frac{M}{EI}\left(1 + \frac{2}{3} EI_f\, a\right) \tag{14}$$

The expression within the parenthesis in Eqn. 14 is the factor by which the simple beam deflection field is to be modified to include the effects of shear lag.

To find the reduction factor of the flange stiffness due to shear lag, let

$$\alpha = 1 + \frac{2}{3} EI_f\, a \tag{15}$$

then find β such that

$$\frac{\alpha}{I} = \frac{1}{I_w + \beta I_f} \tag{16}$$

Solving for β one obtains

$$\beta = I/\alpha I_f - I/I_f + 1 \tag{17}$$

The variable β defined in Eqn. 17 may be interpreted as the flange stiffness reduction factor due to shear lag effects.

The changes in β as a function of the ratio of beam length to half flange width for three different loading conditions, namely, an end point load, a uniformly distributed load and a triangular load are given in Figures 5 through 7. Table 1 shows the maximum error in the displacements of typical box-beams, for each of the three loading conditions, when the shear lag effects are introduced approximately using the present approach (column 5). It is observed that the method yields satisfactory results. In addition, Table 1 contains the corresponding errors in the simple beam theory solutions (column 4).

The important conclusions to be drawn from Figures 5 through 7 is that the problem of shear lag is insensitive to the ratio of flange moment of inertia to total moment of inertia; the type of loading has some minor effect and for earthquake type loadings Figure 7 would be the more appropriate curve to use; and finally, that the length of beam to width ratio determines the importance of shear lag in box beams.

ROTARY INERTIA AND SHEAR DEFORMATION EFFECTS ON BEAM MASS

For beams with large radius of gyration to length ratios, r/L, the error in the Bernoulli-Euler theory is considerable even for the lower modes. These discrepancies can be overcome by using the Timoshenko beam theory, whereby the effects of rotatory inertia and shear deformations are introduced. Also in developing lumped mass models it is common practice to assign masses only to translational degrees of freedom. Herein, an attempt is made to define a diagonal mass matrix, which would include shear and rotatory terms in it.

In the literature one may find consistent element mass matrices which contain the effects of shear deformations and rotatory inertia (4). Such a mass matrix is given in Appendix I, where $r^2 = I/A$, $\phi = 12EI/GA_s\ell^2$, ρ = mass density of the beam, A = cross-sectional area, A_s = shear area of the beam, ℓ = length of the beam segment, I = moment of inertia, E and G are respectively Young's and shear moduli of the beam material. To obtain an equivalent diagonal element mass matrix, a simple procedure is attempted: It is assumed that to each degree-of-freedom direction only the deflections which are compatible with that direction contribute (e.g., in U_1 direction U_1 and U_3 contribute); then their contributions are added to obtain a diagonal term (Eqn. Ib, Appendix I). This process results in $\rho A\ell/2$ for the term associated with the translational degrees of freedom. The same results are obtained by the usual concept of rigidly lumping of mass by tributary lengths. Since in the consistant mass matrix shear deformation effects impact on both the translational and rotatory inertia terms, it would be useful to consider rotatory inertia effects alone. Thus setting $G = \infty$ or $\phi = 0$, the "lumped" rotatory inertia term on the "diagonalized" element mass matrix becomes

$$J_{consistent} = \rho A\ell\left(\frac{\ell^2}{420} + \frac{r^2}{10}\right) \tag{19}$$

A comparison of Eqn. 19 with the one obtained by the rigid lumping concept would be useful. The corresponding term in the mass matrix for the latter approach for a segment of a rectangular section is given by

$$J_{rigid} = \frac{1}{2}\rho A\ell\left(\frac{\ell^2 + b^2}{12}\right) = \frac{1}{2}\rho A\ell\left(\frac{\ell^2}{12} + r^2\right) \tag{20}$$

Eqn. 20 would give significantly larger values than Eqn. 19. To illustrate the impact of this difference on the frequencies of a beam, the Timoshenko beam equation is modified to include rotatory inertia and bending effects only. The resulting frequencies are then compared with a lumped mass model using both Eqns. 19 and 20 to calculate rotatory inertia terms. The results for Beam I (refer to Table 2 for beam properties) are shown in Fig. 8. It is obvious that the concept of rigid lumping is more appropriate, suggesting a revision of the m_{22} and m_{44} terms of Eqn. Ib of Appendix I as follows

$$m_{22} = m_{44} = \frac{\left(\frac{\ell^2}{24} + \frac{r^2}{2}\right) + \frac{\phi^2 r^2}{2}}{(1 + \phi)^2} \tag{21}$$

and resulting in the mass matrix of Eqn. Ic, Appendix I. For other than rectangular sections, the terms in parenthesis in the numerator should be interpreted as the polar mass moment of inertia about the nodal points.

To check the adequacy of the derived lumped mass matrix (Eqn. Ic, Appendix I), two uniform beams of constant properties throughout are selected with large r/L ratios to emphasize both the shear and rotatory effects. The properties of these beams are listed in Table 2. The beams are modeled as lumped mass models with equidistant nodes and the resulting frequencies for several number of lumped masses are compared to the theoretical results using the Timoshenko beam solution. The results are shown graphically in Figures 9 and 10. Both figures indicate that the lumped mass model frequencies will be within 10% of the theoretical frequencies if the number of masses are equal to N + 1, where N is the number of the desired N^{th} frequency.

It is instructive to compare Eqns. 20 and 21. Since ϕ is usually a large number for the type of structures considered, the effect of shear deformations on the mass matrix is small, which is as it should be. A study of the Timoshenko beam equation reveals that the translational and rotatory masses are dominant in the inertia effects and that shear deformations are dominant in the stiffness effects.

EVALUATION OF THE MODELING CONCEPT

To evaluate the adequacy of the modeling concepts developed in the paper, the response of a lumped mass model will be compared to that of a finite element model of the same structure. A symmetric box-type two story structure without openings is chosen with dimensions and properties such that the considerations discussed in this paper are accentuated. The structure with both finite element and lumped mass models is shown in Fig. 11. A modulus of elasticity of 51,800 Kips/ft^2 (2.5 x 10^6 N/m^2), a unit weight of 0.145 Kips/ft^3 (197 N/m^3) and Poisson's ratio of 0.17 is used. To make the comparison between the two models compatible, centerline dimensions are used in calculating the properties of the lumped mass model since the finite element model allows only such an analysis. The shell element used in the finite element model is a thin plate element having both membrane and bending isotropic properties (Kirchhoff hypothesis).

The lumped mass model was developed as follows:

a. The shear center and the centroid of the section coincide since the structure has double symmetry.

b. Effective shear area: The area associated with the finite-element model dimensions is given by A = 2 (20 x 1 + 40 x 1) = 120 ft^2 (11.2m^2). Using the Cowper (1) equation K = 0.234 and therefore A_s = 0.234 x 120 = 28.1 ft^2 (2.6 m^2). As shown in Fig. 2 and discussed earlier in the paper the Cowper equation needs to be re-evaluated for certain values of M and N. Thus the shear area is limited to 0.844 (2x20) = 33.8 ft^2 (3.1 m^2). However, using the Ebner and Billington equation (2), A_s = 37.3 ft^2 (3.5 m^2). Two models will be developed using shear areas of 33.8 ft^2 (3.1 m^2) and 37.3 ft^2 (3.5 m^2) respectively.

c. Shear lag effects: Using Fig. 7, for L/w = 1.5, I_f = 8000 ft^4 (69.2 m^4) and I = 9333 ft^4 (80.7 m^4), the flange stiffness reduction factor is given as β = 0.53. Thus the effective moment of inertia of the section is equal to 0.53 x 8000 + 1333 = 5573 ft^4 (48.2 m^2).

d. Mass matrix: From Eqn. Ic (Appendix I) the translational masses are simply obtained by lumping half of each element mass to the adjoining nodes. The floor masses will be assumed concentrated at the floor nodes. Thus the mass matrix elements associated with coordinates 1 through 6 are given by 2.7, 2.7, 6.3, 2.7, 2.7, and 4.95. The terms for rotatory inertia and shear effects can be simplified when it is recognized that for this example ϕ is a large number compared to unity. Thus a very good approximation to these terms can be obtained by $r^2/2$. This simplication serves to eliminate indirectly an issue raised in the calculation of shear areas. A second issue that should be resolved is the question of the shear lag effects on the calculation of the rotatory inertia terms. Among many possibilities two will be employed: a) the full cross-section properties and b) the partial cross-section properties. For the former the square of the radius of gyration is equal to r^2 = 9333/120 = 77.8 ft^2 (7.24 m^2) and for the latter r^2 = 5573/82.4 = 67.6 ft^2 (6.29 m^2). The cross-sectional area used in the latter is related to the reduced flange moment of inertia in an average sense. Thus, the effective area is obtained as 2 x 20 + 2 x 0.53 x 40 = 82.4 ft^2 (7.66 m^2). Similarly the mass per unit length (ρA) should reflect the same considerations. Thus for the first case $\rho A\ell$ = 0.145 x 120 x 5 ÷ 32.2 = 2.7 and for the second case $\rho A\ell$ = 0.145 x 82.4 x 5 ÷ 32.2 = 1.86. A similar consideration should be given the slabs. Although the slabs can be assumed to be rigid for translatory motion, they may not be so assumed for rotatory motion. Using Eqn. 20, for the first case J = 3.6 $(1^2 + 20^2)/12$ = 120. Considering the effects of shear lag, it is reasonable to assume that the portion of the slab that, on the average, is affected by shear lag be excluded. This is simply effected by 0.53 x 120 = 63.6. From the above results the mass matrix elements associated with coordinates 7 through 12 for the first case are calculated as 210, 210, 330, 210, 210, and 225, and for the second case as 126, 126, 189, 126, 126, and 127.

The differences between the shear areas as given by Cowper and Ebner and Billington and between the two concepts of calculating the mass matrix result in four possible lumped mass models. The frequencies of these models are compared in Table 3. It is seen that the effect of using either shear area is negligible. And, except for the third mode, the effect of considering shear lag effects on the rotatory inertia terms is also negligible. (The participation factor of this third mode is extremely small.) Thus the model using the Cowper shear coefficients and neglecting the possible effects of shear lag on rotatory inertia terms would be considered as representative and compared to the finite element model. Since the finite-element model would result in many frequencies that, by the very nature of discrete modeling, are absent from the lumped mass models, an appropriate comparison between the finite-element model and the lumped mass models would be the response spectra of some representative point on the structure. The mid-point of the roof slab is selected for the purposes of this comparison.

These results are shown in Fig. 12. The 1% damping response spectra was selected to emphasize the differences between the two basic models. It is observed that the differences between the finite-element and lumped mass model results are minor and acceptable in an engineering sense. It must be remembered that the degree of refinement in the two models differ by about two orders of magnitude. The finite element model has about 200 nodes and 1000 dynamic degrees of freedom as against 12 degrees of freedom for the lumped mass model.

CONCLUSIONS

From the several results shown in the paper it is concluded that simple dynamic models can be used in the prediction to seismic excitations of box-type structures. The stiffness properties of such structures should include effects of shear lag and the proper shear areas. For the shear lag effects graphical solutions are provided and it is observed that the important parameters affecting shear lag is the height to width ratio of the structure. The question of shear area needs further exploration although existing formulations give adequate results. Rotatory inertia terms should be included in the mass matrix and the assumption that the segment considered is rigid gives acceptable results. Shear deformation effects on the mass matrix are minor and could be neglected. In the absence of conclusive results of the effect of shear lag on the inertial masses it is recommended that the problem be evaluated on a case by case basis.

ACKNOWLEDGEMENTS

The authors thank their colleagues Y. J. Lin for his helpful suggestions and critical review of the paper, H. D. Tabakman for the computation of the shear center for closed sections, R. C. Lee for the results of the sample problem and R. S. Platoni for the results of Fig. 8.

REFERENCES

1. Cowper, G.R. "The Shear Coefficient in Timoshenko's Beam Theory" J. App. Mech., June 1966, pp. 335-340.
2. Ebner, A.M. and Billington, D.P. "Steady State Vibration of Damped Timoshenko's Beams." Journal of the Structural Division, ASCE, Vol. 94, No. ST3, March 1968, pp. 737-759.
3. Mindlin and Deresiewing "Timoshenko's Shear Vibrations of Beams" Tech. Report No. 10, ONR Project NR-064-388, Columbia Univ. 1953.
4. Przemieniechi, J.S., Theory of Matrix Structural Analysis, McGraw-Hill Book Co., New York, 1968.
5. Reissner, E. "Analysis of Shear Lag in Box Beams by the Principle of Minimum Potential Energy," Appl. Math., Vol. IV, No. 3, 1946, pp 268-278.
6. Seely, F.B. and Smith, J.O. Advanced Mechanics of Materials, Section Edition, John Wiley & Sons, New York, 1955, pp 97-111.
7. Tabakman, H.D., "Locating the Shear Center in Thin Closed Sections": Product Engineering, June 1954, pp. 137-141.
8. Timoshenko, S.P. Strength of Materials - Part I. Second Edition, D. Van Hostrand Co., New York, 1940, pp. 170-171.

Table 1. DISPLACEMENT ERROR ANALYSIS OF PRESENT APPROACH

LOADING TYPE (1)	FLANGE MOM. INERTIA / TOTAL MOM. INERTIA (2)	BEAM LENGTH / 1/2 FLANGE WIDTH (3)	MAX. % ERROR IN SIMPLE BEAM (4)	MAX. % ERROR IN MODIFIED SIMPLE BEAM (PRESENT APPROACH) (5)
POINT LOAD	0.85	5.0	13.0	6.53
	0.6	1.41	30.00	3.8
	0.667	1.41	34.47	4.75
	0.75	1.41	39.08	6.08
	0.85	0.92	55.64	5.47
UNIFORMLY DIST LOAD	0.5	5.0	10.80	4.18
	0.6	1.41	34.89	5.85
	0.667	1.41	39.08	7.07
	0.77	1.41	45.79	9.4
	0.86	0.92	59.97	8.30
TRIANGULAR DIST LOAD	0.5	5.0	9.58	4.18
	0.6	1.41	33.83	5.55
	0.667	1.0	44.00	4.7
	0.82	0.9	56.5	6.77

Table 2. BEAM PROPERTIES

	r/L	L (ft)	I (ft^4)	A (ft^2)	K	E (k/ft^2)	G (k/ft^2)	γ (k/ft^3)	ν
BEAM I	0.6	100	8,305,259	2,336	0.5	4.32×10^5	1.85×10^5	0.15	0.17
BEAM II	1.0	100	5.0×10^7	5.0×10^3	0.833	4.32×10^5	1.85×10^5	0.15	0.17

Table 3. FREQUENCY COMPARISON OF FOUR LUMPED MASS MODELS

MODES	NO SHEAR LAG EFFECTS ON MASS MATRIX		WITH SHEAR LAG EFFECTS ON MASS MATRIX	
	$A_S = 37.3$	$A_S = 33.8$	$A_S = 37.3$	$A_S = 33.8$
1	6.17	5.99	6.22	6.03
2	17.15	16.64	18.06	17.45
3	30.37	29.34	37.16	36.04
4	40.03	38.34	40.51	38.72
5	49.40	47.16	49.95	47.64
6	59.43	58.83	68.15	64.95

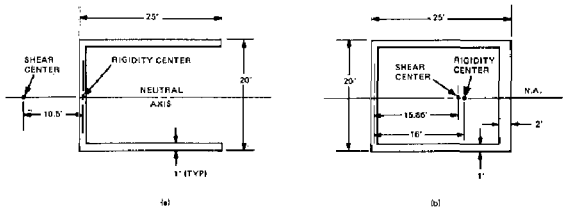

Figure 1. RIGIDITY AND SHEAR CENTER COMPARISON

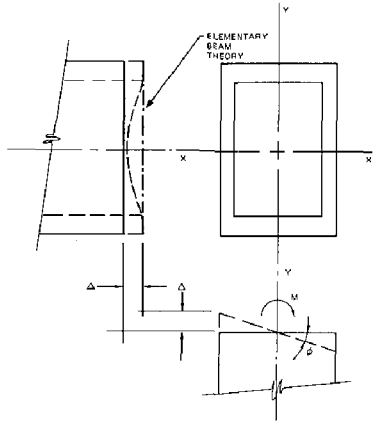

Figure 3. SHEAR LAG EFFECTS SCHEMATICALLY SHOWN

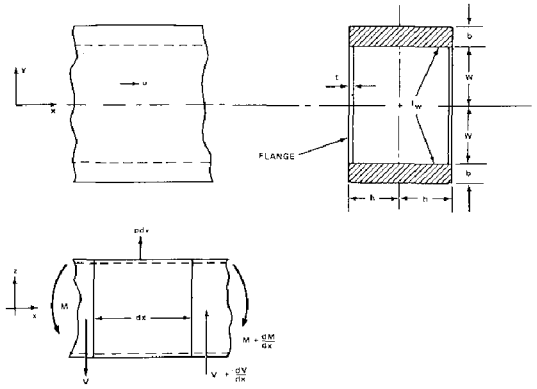

Figure 4. SKETCH OF ELEMENT OF BOX BEAM (USING REISSNER NOTATION)

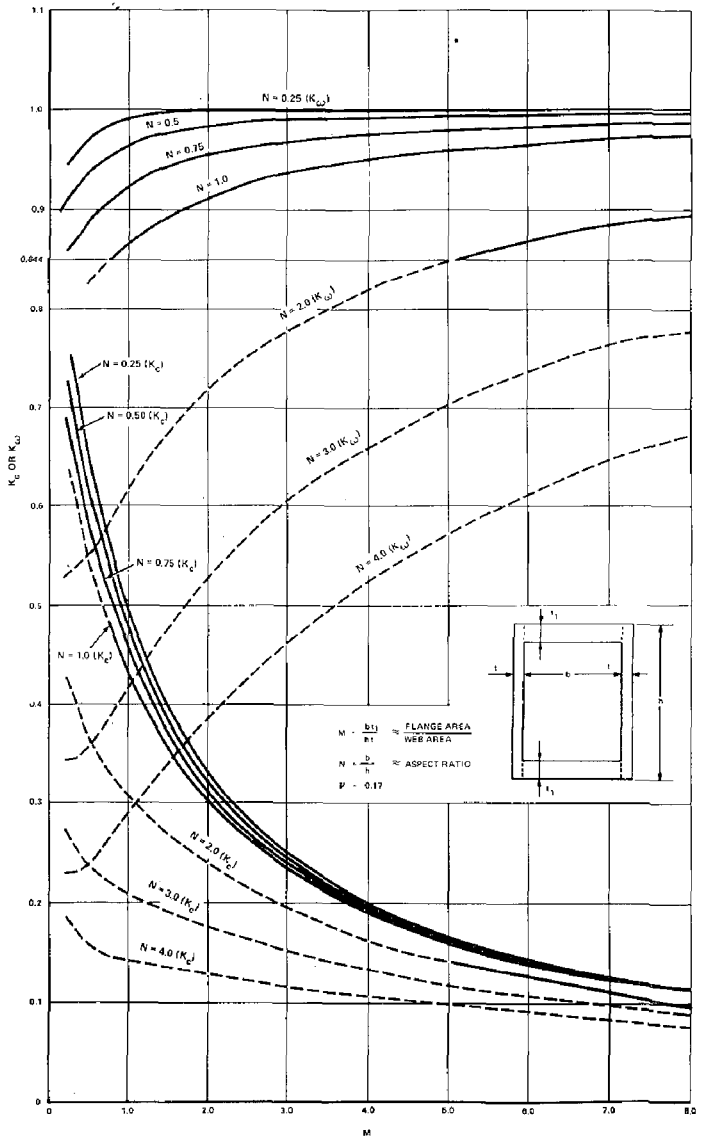

Table 2. SHEAR AREA COEFFICIENTS FOR BOX SECTIONS (AFTER COWPER (1))

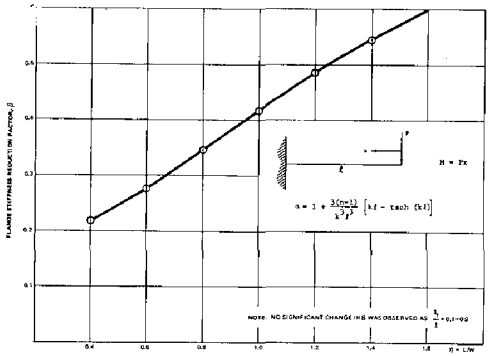

Figure 5. β VERSUS η, CANTILEVER – POINT LOAD

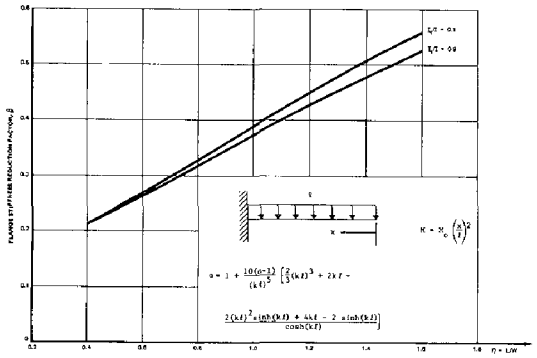

Figure 6. β VERSUS η, CANTILEVER – UNIFORMLY DISTRIBUTED LOAD

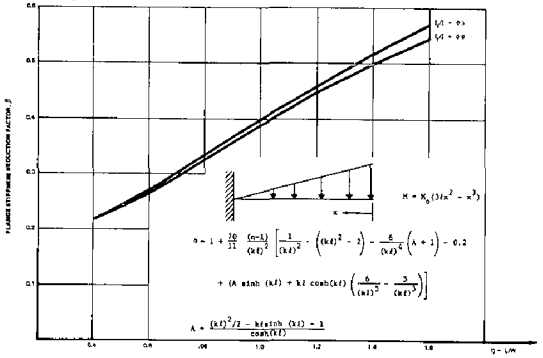

Figure 7. β VERSUS η, CANTILEVER – TRIANGULAR LOAD

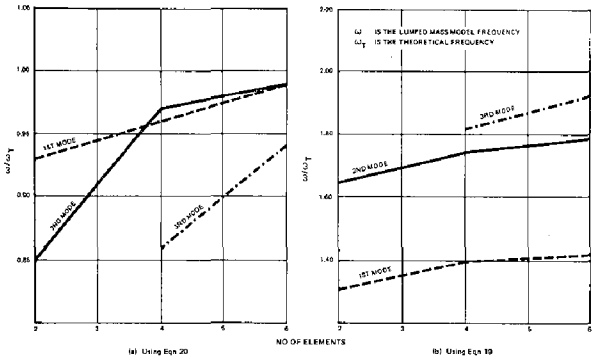

Figure 8. BEAM I CONVERGENCE STUDY – ROTATORY EFFECTS ONLY

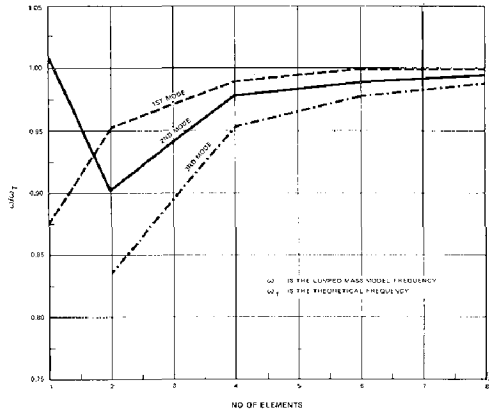

Figure 9. BEAM I CONVERGENCE STUDY – SHEAR AND ROTATORY EFFECTS

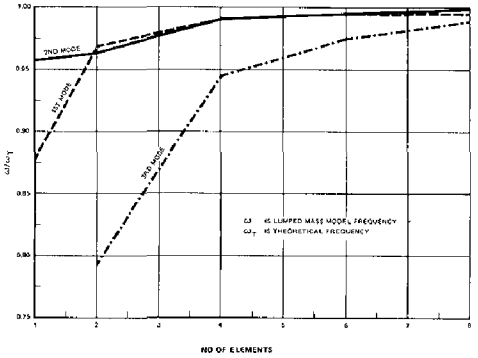

Figure 10. BEAM II CONVERGENCE STUDY – SHEAR AND ROTATORY EFFECTS

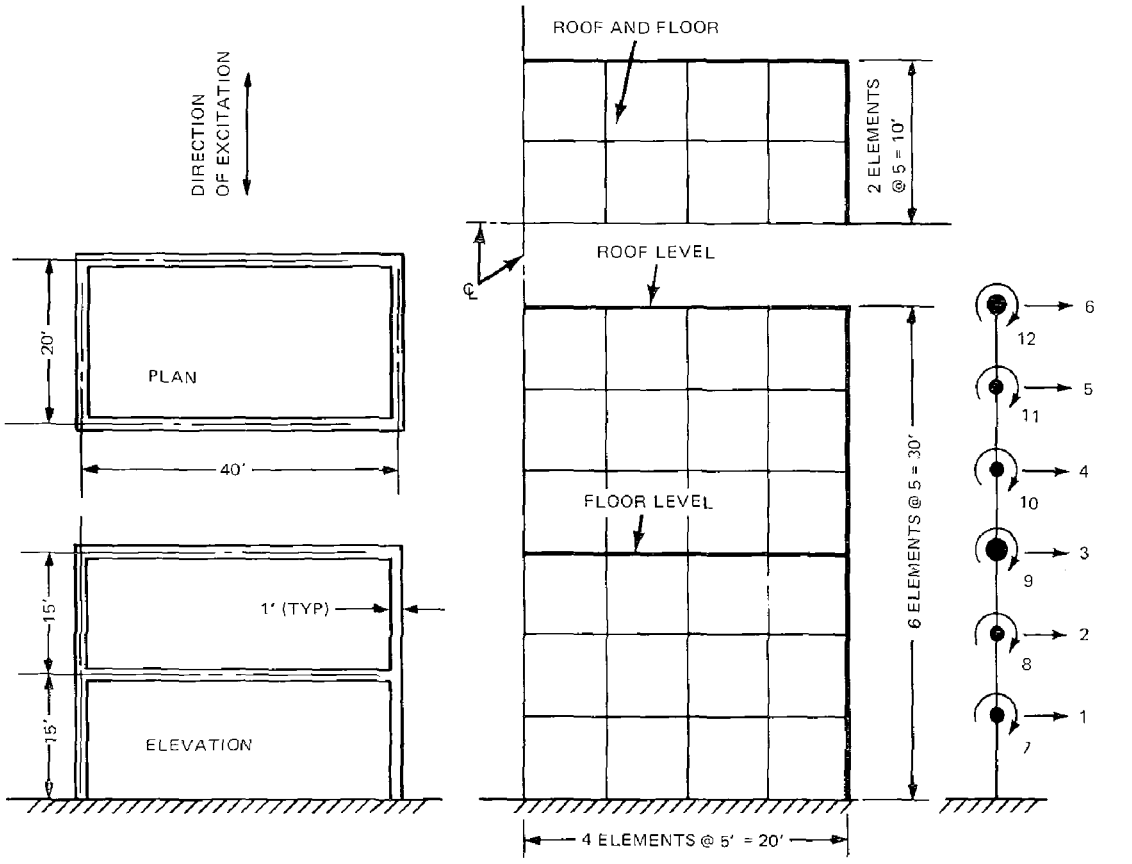

Figure 11 SCHEMATIC REPRESENTATION OF SAMPLE PROBLEM

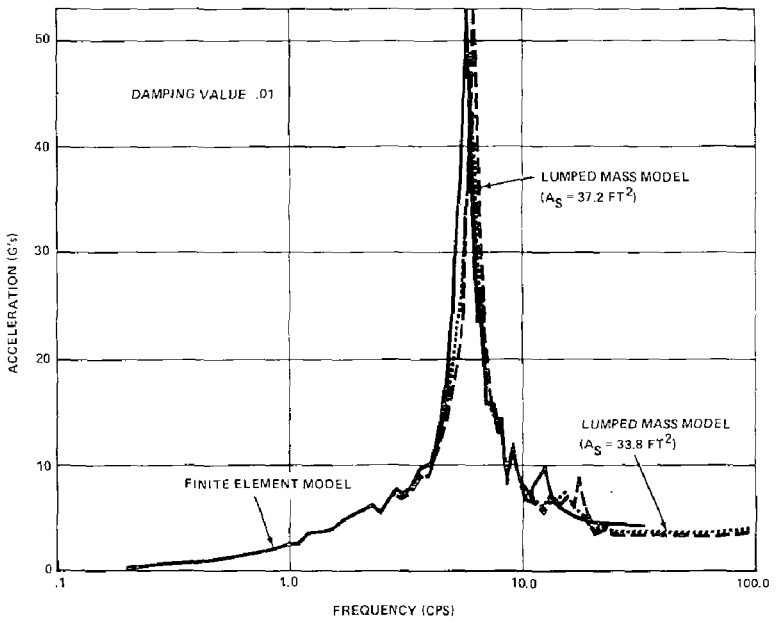

Figure 12 RESPONSE SPECTRA COMPARISON OF FINITE ELEMENT AND LUMPED MASS MODEL, CENTER OF ROOF

APPENDIX I

Ia. CONSISTANT ELEMENT MASS MATRIX (4)

$$m = \frac{\rho A l}{(1+\Phi_s)^2}\begin{bmatrix} \cdot & & & \\ (\frac{1}{21}{}_0 + \frac{1}{12}{}_0\Phi_s + \frac{1}{24}\Phi_s^2)l & (\frac{1}{105} + \frac{1}{60}\Phi_s + \frac{1}{120}\Phi_s^2)l^2 & \text{Symmetric} & \\ \frac{9}{70} + \frac{3}{10}\Phi_s + \frac{1}{8}\Phi_s^2 & (\frac{13}{420} + \frac{3}{40}\Phi_s + \frac{1}{24}\Phi_s^2)l & (\frac{13}{35} + \frac{7}{10}\Phi_s + \frac{1}{3}\Phi_s^2 & \\ -(\frac{13}{420} + \frac{3}{40}\Phi_s + \frac{1}{24}\Phi_s^2)l & -(\frac{1}{140} + \frac{1}{60}\Phi_s + \frac{1}{120}\Phi_s^2)l^2 & -(\frac{11}{210} + \frac{11}{120}\Phi_s + \frac{1}{24}\Phi_s^2)l & (\frac{1}{105} + \frac{1}{60}\Phi_s + \frac{1}{120}\Phi_s^2)l^2 \end{bmatrix}$$

$$+ \frac{\rho A l}{(1+\Phi_s)^2}\left(\frac{r}{l}\right)^2\begin{bmatrix} \frac{6}{5} & & & \\ (\frac{1}{10} - \frac{1}{2}\Phi_s)l & (\frac{2}{15} + \frac{1}{6}\Phi_s + \frac{1}{3}\Phi_s^2)l^2 & \text{Symmetric} & \\ -\frac{6}{5} & (-\frac{1}{10} + \frac{1}{2}\Phi_s)l & \frac{6}{5} & \\ (\frac{1}{10} - \frac{1}{2}\Phi_s)l & (-\frac{1}{30} - \frac{1}{6}\Phi_s + \frac{1}{6}\Phi_s^2)l^2 & (-\frac{1}{10} + \frac{1}{2}\Phi_s)l & (\frac{2}{15} + \frac{1}{6}\Phi_s + \frac{1}{3}\Phi_s^2)l^2 \end{bmatrix}$$

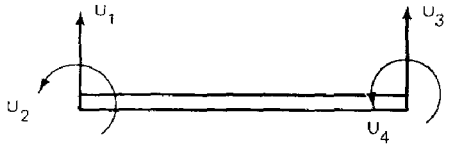

$$\phi_s = 12EI/GA_s\ell^2$$

Ib. "LUMPED" ELEMENT MASS MATRIX FROM Ia ABOVE.

$$m = \rho A \ell \begin{bmatrix} \frac{1}{2}\,\dfrac{\frac{\ell^2}{420} + \frac{r^2}{10} + \frac{\phi^2 r^2}{2}}{(1+\phi)^2} & \frac{1}{2}\,\dfrac{\frac{\ell^2}{420} + \frac{r^2}{10} + \frac{\phi^2 r^2}{2}}{(1+\phi)^2} \end{bmatrix}$$

Ic. MODIFIED "LUMPED" ELEMENT MASS MATRIX

$$m = \rho A \ell \begin{bmatrix} \frac{1}{2}\,\dfrac{\left(\frac{\ell^2}{24} + \frac{r^2}{2}\right) + \frac{\phi^2 r^2}{2}}{(1+\phi)^2} & \frac{1}{2}\,\dfrac{\left(\frac{\ell^2}{24} + \frac{r^2}{2}\right) + \frac{\phi^2 r^2}{2}}{(1+\phi)^2} \end{bmatrix}$$

INTERNATIONAL SYMPOSIUM ON
EARTHQUAKE STRUCTURAL ENGINEERING
St. Louis, Missouri, USA, August, 1976

INELASTIC SEISMIC RESPONSE OF ISOLATED STRUCTURAL WALLS

by

GEORGE N. FRESKAKIS
Senior Structural Engineer

ARNALDO T. DERECHO
Principal Structural Engineer

MARK FINTEL
Director

Engineering Services Department
Portland Cement Association
Skokie, Illinois, 60076, U. S. A.

SUMMARY

This paper presents the results of an analytical investigation to determine the effect of important structural characteristics on the seismic response of isolated structural walls. The properties considered include the fundamental period of vibration as affected by the stiffness, the strength or yield level, the stiffness in the post yield range, strength taper, and viscous damping.

The basic structure considered in the study is a 20 story building. The corresponding analytical model consists of a cantilever with masses concentrated at floor levels. Inelasticity is allowed by point "plastic hinges" which form at the ends of elements when the yield moment is exceeded. The moment-rotation characteristics for these hinges account for the decrease in stiffness resulting from cyclic loading. The input motion used is the first 10 seconds of the E-W component of the 1940 El Centro record, with the acceleration amplitude adjusted to obtain a 5% damped spectrum intensity equal to 1.5 times that of the N-S component of the El Centro record.

The effect of the various structural parameters on the seismic response is evaluated essentially qualitatively with particular attention given to the ductility requirements of the hinging region and the interstory displacements along the height of the building. It is found that increasing the stiffness of a structure, and thus decreasing its fundamental period, results in a reduction in the interstory displacements but an increase in the ductility requirements. An increase in the yield level generally tends to decrease both the ductility requirements and the magnitude of the interstory displacements.

INTRODUCTION

In recent years, observations of the performance of buildings during earthquakes have indicated the effectiveness of structural walls in controlling damage within the structures and in ensuring their general safety.

The establishment of rational seismic design procedures for buildings stiffened with structural walls requires a study of the response of such structures to earthquakes and the determination of the associated deformations and forces. Since the seismic behavior of buildings is affected by their structural properties and the characteristics of the ground motion, this study was undertaken to evaluate qualitatively and quantitatively the effect of the most important structural and earthquake parameters.

This paper presents the results of the study of the effects of structural properties on the seismic response of buildings stiffened with isolated structural walls. The study of isolated walls was motivated not only by the need to obtain information for this type of construction but also to establish a reference with which results for more complex wall systems can be compared in the later stages of the investigation.

PARAMETRIC STUDIES

The influence of the structural properties on seismic response was evaluated within the framework of a parametric study. The properties considered as parameters were those expected to have a significant effect on the response of the structure, particularly in relation to the deformation characteristics of individual members as well as the entire structure. These are the following:

1. fundamental period of vibration, as affected by stiffness,
2. strength or yield level,
3. stiffness in post-yield range,
4. viscous damping,
5. variations in stiffness*, and strength along the height, as well as variations in the height* (number of stories),
6. degree of fixity* at the base of the structure.

To evaluate the effect of the above variables the following general procedure was used.

1. A 20 story building designed on the basis of the Uniform Building Code Zone 3 requirements was established as the reference structure. A number of other designs were considered to determine the practical range of variation of the structural properties.

---

* Results for this parameter are not included in this paper.

2. The reference structure was subjected to a number of strong motion accelerograms. Based on the results of these dynamic analyses[2,3] a ground motion was selected for input in the parametric studies.

3. Dynamic analyses were carried out on walls obtained by varying in the reference structure the particular parameter under consideration while holding the other properties constant.

Basic Building Properties

The basic structure considered in the parametric studies is a 20-story building consisting mainly of a series of parallel structural walls, as shown in Fig. 1. The building is 60 ft. x 144 ft. in plan and rises some 178 feet above the ground. All story heights are 8'-9" except the first story, which is 12'-0" high.

For the purpose of the dynamic analysis, the mass of the structure was calculated to include the dead weight and 40 percent of the live load specified for apartment buildings by the Uniform Building Code[8]. This percentage of live load was deemed reasonable and is consistent with the current specifications for the design of columns in the lower stories of buildings.

The stiffness of the structural wall in the basic building was assumed uniform along the height since this provides a better reference for the evaluation of the effect of stiffness taper. A constant wall cross-section was also assumed throughout the height of the basic structure. However, a reduction in the yield level of sections above the base was included to reflect the effect of axial loads on the moment capacity. The structural elements were assumed to possess unlimited deformation capacity (ductility) since the major objective of the study is the determination of the deformation requirements corresponding to particular parameter values. The building was assumed to be fully fixed at the base except for the cases where the base fixity condition was the parameter investigated. The basic building properties are listed in Table 1.

TABLE 1. Basic Building Properties

Number of stories	20
Height	178.25 ft.
Weight (for mass computation)	4370 k/wall
Stiffness EI for T_1 = 0.80 sec	6.34×10^{11} k-in^2/wall
1.40	2.052×10^{11}
2.00	0.990×10^{11}
2.40	0.684×10^{11}

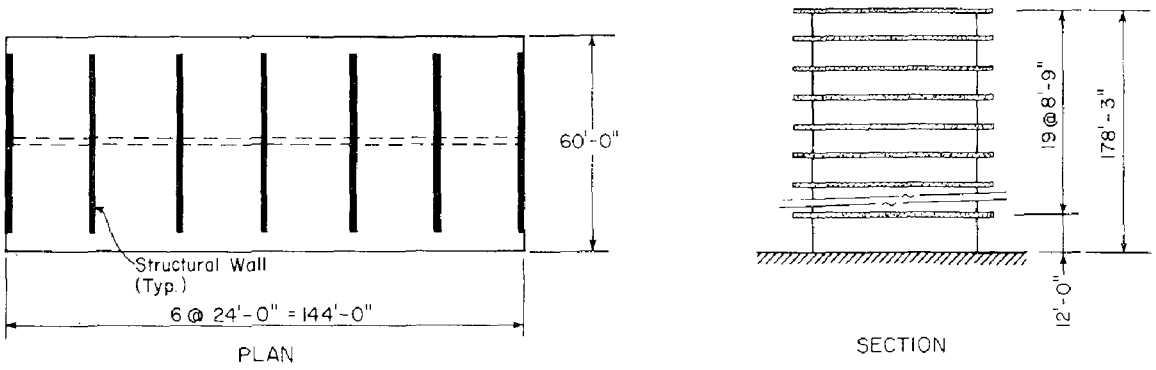

Fig. 1 Twenty story building with isolated structural walls

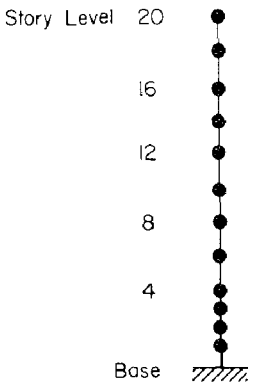

Fig. 2 Dynamic analysis model (12 masses)

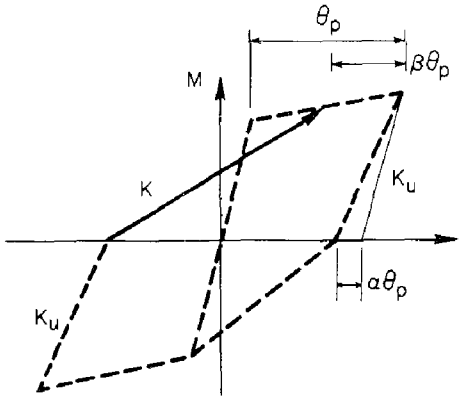

Fig. 3 Decreasing stiffness moment-rotation relationship

Computer Program and Modelling

The dynamic analysis studies were carried out using the computer program DRAIN-2D,[4,5] a general purpose program for the inelastic analysis of plane structures subjected to earthquake excitations. The program uses the direct stiffness method of analysis with the nodal displacements as unknowns. The dynamic response is determined by a step-by-step procedure based on the assumption of a constant acceleration within any step.

For the purpose of the dynamic analysis and based on some preliminary investigations the reference building was represented by the simple analytical 12-mass model shown in Fig. 2. This simplified model has the mass lumped at alternate story levels except in the lower portion where the mass is lumped at nodal points established by requirements of the hinging region of the wall.

The proper modelling of the region of potential hinging at the base of the wall is important if a reliable assessment of the deformation requirements in this critical region is expected. The model of the plastic region should not only be realistic but should allow convenient interpretation of the dynamic analysis results and correlation with experimental data. The program DRAIN-2D accounts for inelastic effects by allowing the formation of concentrated "point hinges" at the ends of elements when the moments at these points equal the specified yield moment. The moment-rotation characteristics of these point hinges are defined in terms of a basic bilinear relationship which develops into either a stable hysteretic loop or one which is an extended version of the Takeda model[7] exhibiting a decrease in reloading stiffness (Fig. 3) with loading cycles subsequent to yield. Since the latter model represents more closely the behavior of reinforced concrete members under reversed inelastic loading, it was used throughout this study. The values of α and β used in this investigation ($\alpha = 0.1$, $\beta = 0$) are within the practical range found in experimental results for members under cyclic loading. It should be noted that dynamic analysis results indicated that the response is not particularly sensitive to variations in these coefficients.

In using elements with potential point hinges at the ends the main difficulty arises in assigning the proper moment rotation characteristics to the hinges. If the elements are made very short the curvature may be assumed uniform along the member or the variation may be closely approximated and the moment rotation curve for the hinges is easily obtained from the moment-curvature relationship of the section. Since in this study it was desirable to divide the wall into the minimum number of elements consistent with the accurate determination of the response quantities, some preliminary analyses were made using different element sizes. Based on the results of these studies the elements were conveniently made one story long in the lower portion of the wall where most of the hinging occurs. In the upper portion the elements were made two stories high.

The integration time step used in the dynamic analyses was determined by trial runs. In general $\Delta t = 0.02$ sec. was used except in the cases of the stiffer structures for which intervals of 0.005 to 0.01 seconds were needed to obtain sufficient accuracy.

The viscous damping assumed for the structures considered in this study consists of a linear combination of stiffness-proportional and mass-proportional damping. The damping distribution among the initial component modes is defined in terms of the percentage of the critical damping for the first mode and the second mode, which are assumed to be equal. Except when damping was the parameter under consideration a damping coefficient of 0.05 was assumed.

Ground Motion Characteristics

The ground motion used in the dynamic analyses has the same frequency characteristics as the E-W component of the El Centro 1940 record. The duration of the motion was set at 10 seconds since preliminary studies indicated that maximum effects were produced during this interval. The intensity was normalized to 1.5 times the spectrum intensity corresponding to the first 10 seconds of the N-S component of the 1940 El Centro record. Studies to determine the effect of different frequency characteristics, duration and intensity on the response are reported in References (2) and (3).

RESULTS

In selecting the response quantities to be studied primary importance was given to the ductility requirements, the displacements, the interstory displacements which provide a measure of the potential damage to structural and non-structural components of a building, and the forces developed during the motion. Particular attention was given to the behavior of the hinging region since it represents the most critical part from the point of view of expected deformations as well as its importance to the behavior of the wall and other structures that may be attached to the wall. Some typical plots of deformations and forces for the reference structure are shown in Figures 4 and 5. The basic plots presented to show the effect of different paramenters are envelopes of maximum values of the response quantities.

The deformation requirements for the elements of the wall are presented in terms of the rotational ductility which is defined as

$$\theta_r = \frac{\theta_{max}}{\theta_y}$$

where θ_{max} is the maximum effective member rotation and θ_y is the effective rotation corresponding to yield. In terms of moments, this definition becomes

$$\theta_r = 1 + \frac{(M_{max} - M_y)}{r_y M_y}.$$

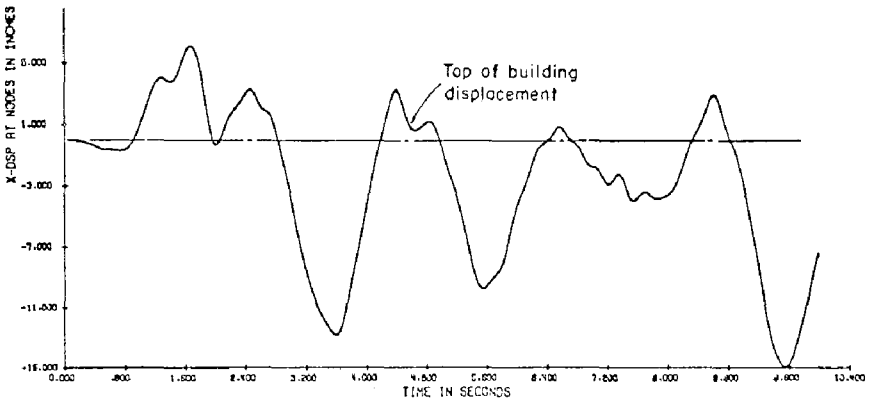

(a) Time history of top of building displacement

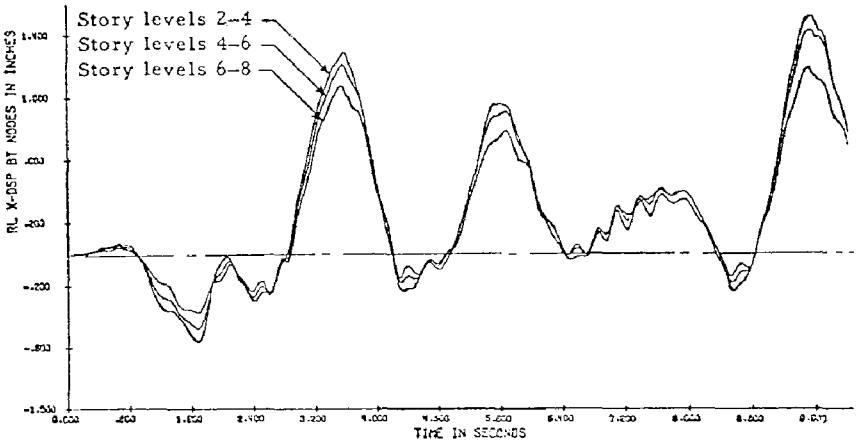

(b) Time history of relative story displacements

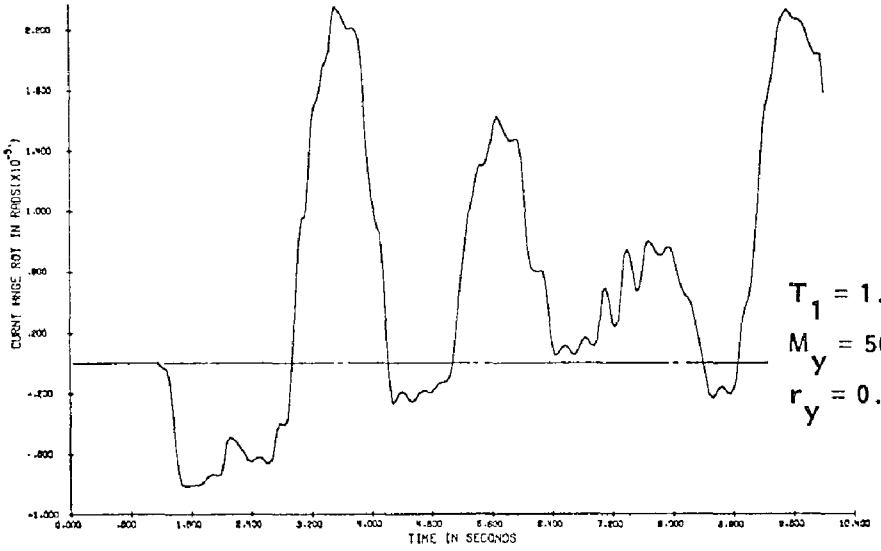

T_1 = 1.40 sec.
M_y = 500,000 in-k
r_y = 0.05

(c) Time history of plastic hinge rotation at base

Fig. 4 Typical dynamic analysis results for reference building

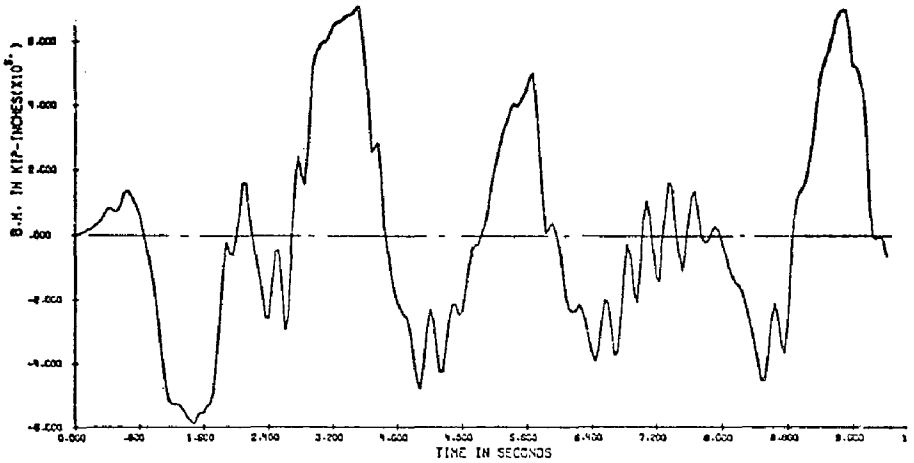

(d) Time history of bending moment at base

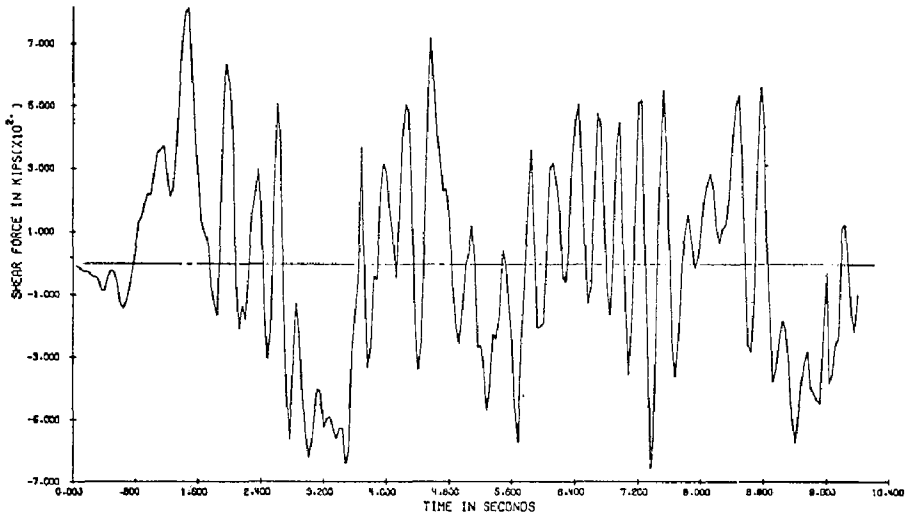

(e) Time history of shear at base

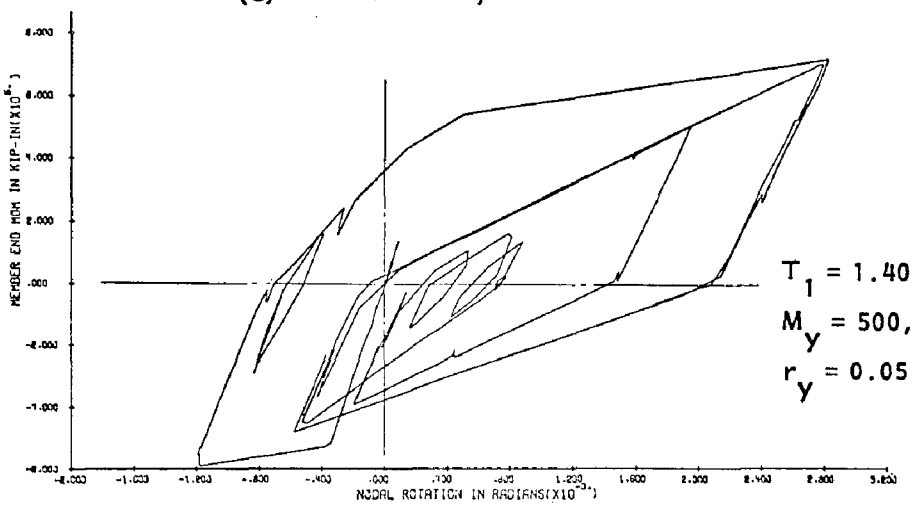

(f) Moment - rotation relationship

Fig. 5 Typical dynamic analysis results for reference building

where r_y is the ratio of the slope of the second, post-yield, branch to the slope of the initial or elastic branch of the primary bilinear moment-rotation curve of the member, i.e., the yield stiffness ratio.

The effect of the various parameters on the response is discussed in the following paragraphs.

Effect of Fundamental Period

The effect of the initial fundamental period was investigated using values of 0.80, 1.40, 2.00, 2.40 seconds to cover the practical range for 20 story buildings. Each of the periods was investigated under varying values of the yield level in order to examine the relationship between these two major variables and the response quantities. Envelopes of maximum values of deformations and forces over the entire height of the building are presented in Fig. 6 for the yield level M_y = 500,000 in-k. and a yield stiffness ratio r_y = 0.05. Results over the entire range of yield levels considered are shown in Fig. 8 for critical sections.

In general, the results indicate a consistent increase in displacements and interstory displacements with increasing period or decreasing stiffness of the structure. The shears corresponding to the same yield level do not vary significantly over the period range considered. It is interesting to note, however, that for the lower yield levels (Fig. 8) the shears are minimum in the period range of 1.40 seconds. The ductility requirements become greater with decreasing fundamental period, a trend also observed by Ruiz and Penzien [6] As indicated in Figures 6 and 8, however, beyond a certain value of the fundamental period, the ductility requirements do not decrease significantly with an increase in period. Thus, the ductility requirements for the structures with periods of 2.0 and 2.4 sec. are about the same.

Effect of Yield Level, M_y

The values considered in studying the effect of the yield level on the seismic response, range from 500,000 to 1,500,000 in-k. Envelopes of maximum response quantities corresponding to T_1 = 1.40 sec. are shown in Fig. 7. The effect of the yield level for other values of the fundamental period is indicated in Fig. 8.

The following general comments apply to all cases shown in these figures: For the same fundamental period, the horizontal and interstory displacements decrease sharply as the yield level increases from 500,000 in-kips to a value associated with nominal yielding at the base. Above this value, the trend is reversed and an increase in yield level is accompanied by an increase in horizontal and interstory displacements. The maximum shears increase sharply with the yield level, for periods equal to 0.80 and 1.40 sec. In the case of the higher periods (2.00 and 2.40 sec.) the effect of the yield level on shears is rather negligible. The rotational ductility requirements increase significantly as

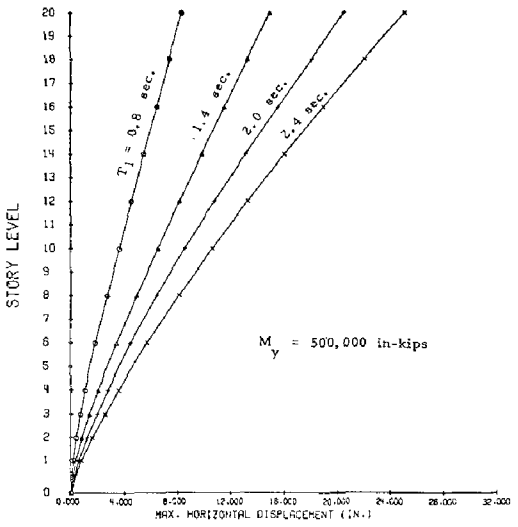

(a) Variation of max. horiz. displacement

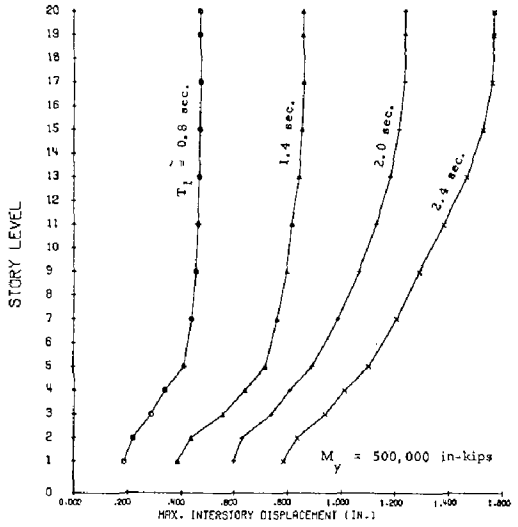

(b) Variation of max. interstory displacement

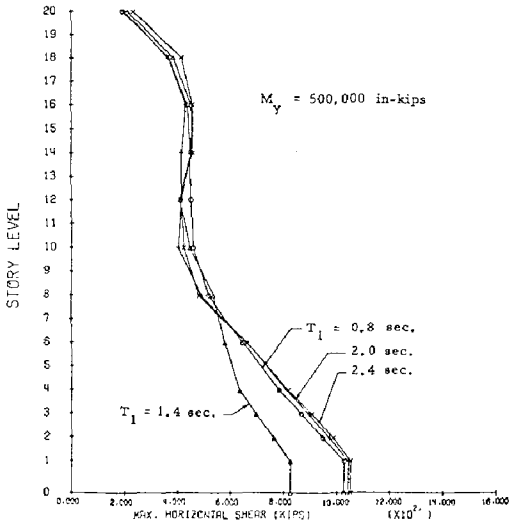

(c) Variation of max. horiz. shear

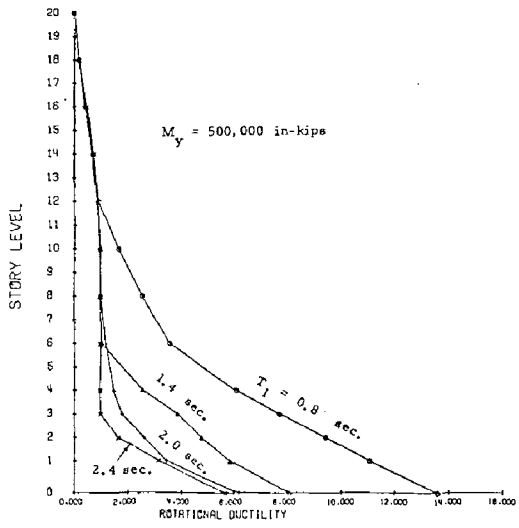

(d) Variation of max. rotational ductility

Fig. 6 Effect of fundamental period of vibration, T_1

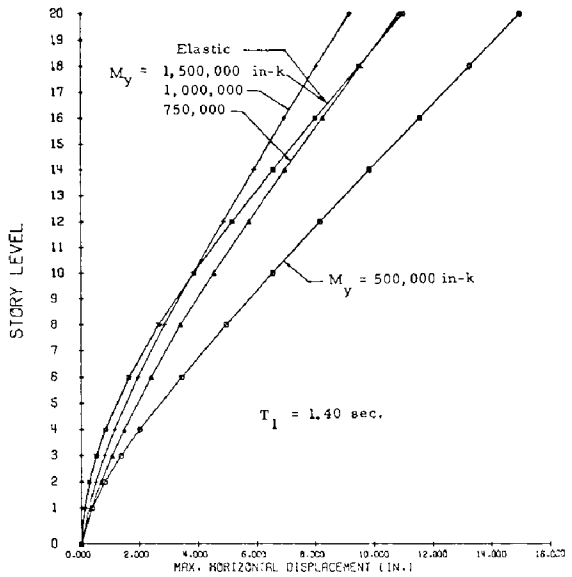

(a) Variation of max. horiz. displacement

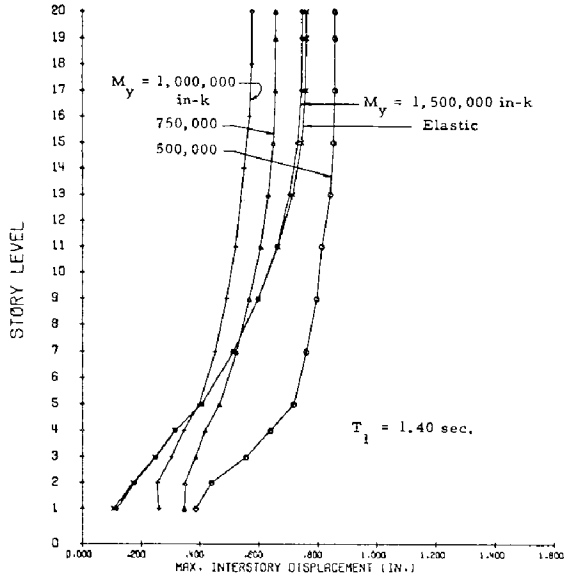

(b) Variation of max. interstory displacement

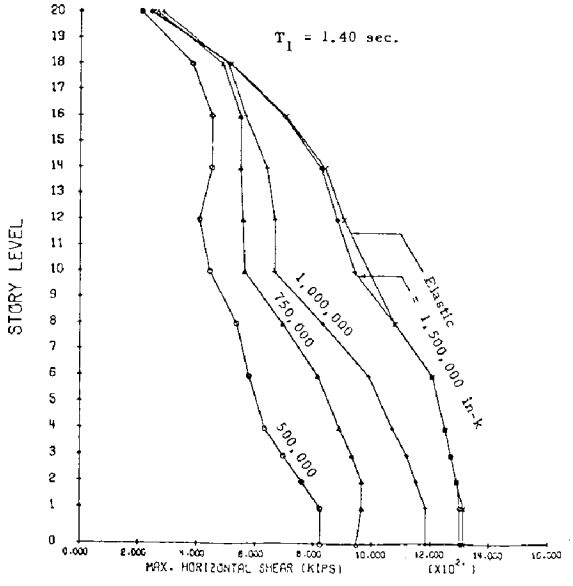

(c) Variation of max. horiz. shear

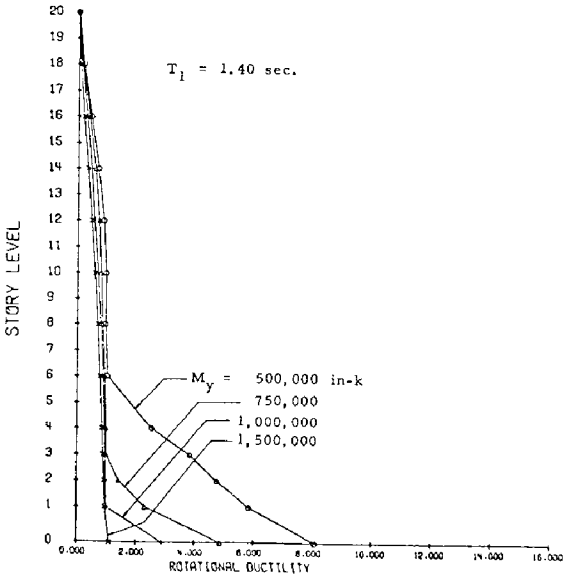

(d) Variation of max. rotational ductility

Fig. 7 Effect of yield level, M_y

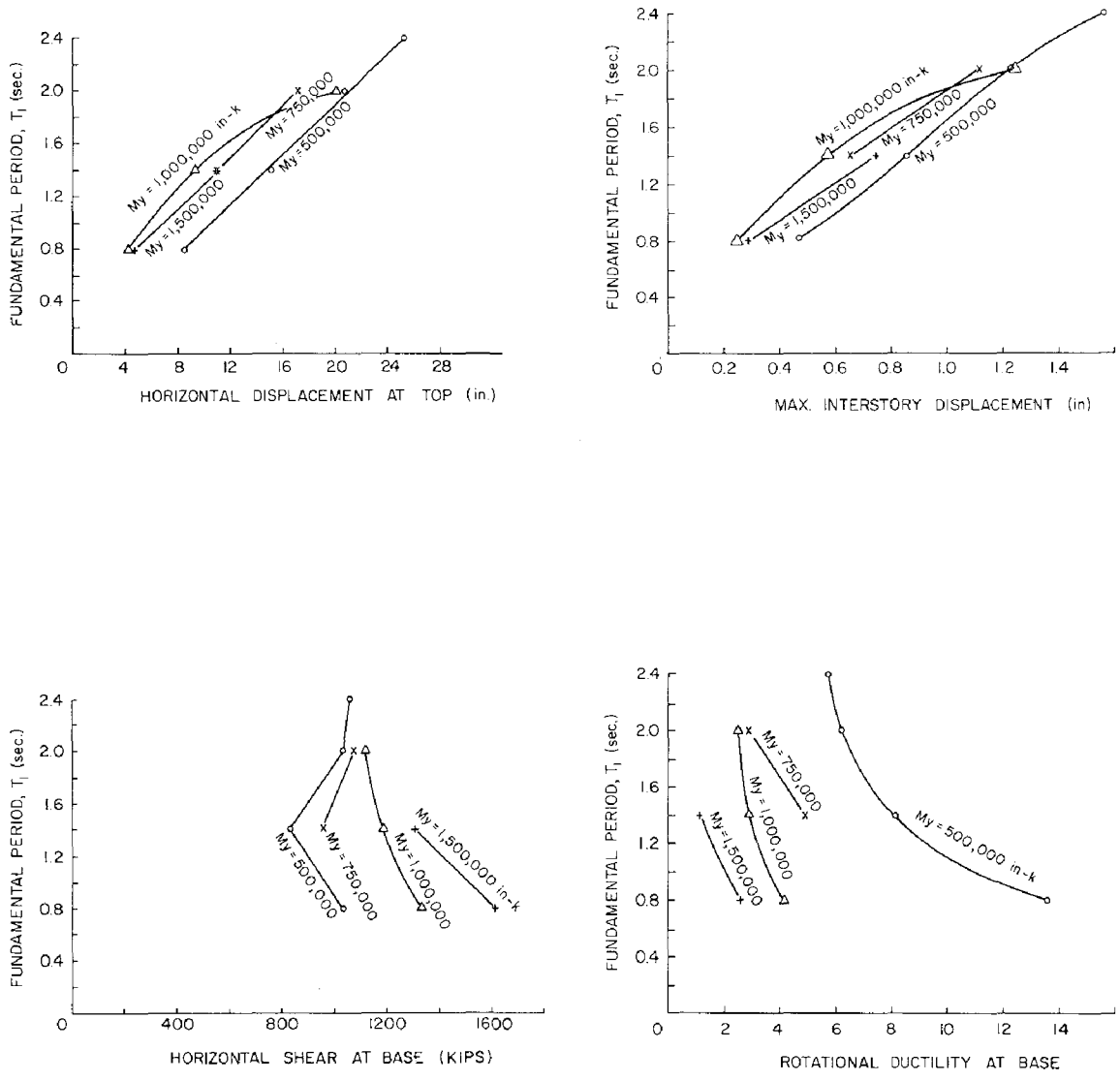

Fig. 8 Effect of fundamental period, T_1, and yield level, M_y

the yield level decreases. This qualitative trend has also been observed in connection with the response of single-degree-of-freedom systems.[1]

Effect of Yield Stiffness Ratio, r_y

The effect of the slope of the second, post-yield branch of the primary bilinear moment-rotation curve of the members which make up the structural wall was investigated by considering values of the yield stiffness ratio of 5% and 15%. The results (Fig. 9) show that an increase in the slope of the post-yield branch of the M-θ curve tends to reduce horizontal and interstory displacements as well as the ductility requirements at the base. The shears at the base increased only slightly with the increase in the value of r_y. In general the effect of r_y is relatively small. This is because for the Takeda model, the response after yielding may be governed not so much by the primary M-θ curve as by the rules governing the slope of the reloading stiffness associated with the model.

Effect of Damping

To study the effect of damping, values of the damping coefficient of 0.05 and 0.10 were considered. As has been observed in other studies, the general effect of increasing the damping in a structure is to reduce the magnitude of the response quantities. For the particular case considered here, increasing the damping coefficient from 0.05 to 0.10 produced only a relatively small (about 10%) reduction in the response quantities.

Effect of Strength Taper

The strength tapers considered in this study are uniform variations in strength along the height with the magnitude of the taper defined as the ratio of the yield moment at the base to that at the top of the building. The results using ratios of 1.0 (uniform strength) to approximately 4.0 show some increase in ductility requirement in the intermediate stories due to a taper in strength but the effect on other quantities was negligible.

SUMMARY AND CONCLUSIONS

The effect of important structural parameters on the seismic response of isolated structural walls has been presented in the form of a parametric study. The significant observations made in connection with this study are summarized below.

The magnitude of the deformation (i.e., ductility requirement) generally increases with decreasing fundamental period (or increasing stiffness) of a structure. The effect is more pronounced in the case of lower yield levels. In hinging regions the magnitude of deformation (ductility) decreases with increasing values of the yield level. An increase in the value of the slope of the post-yield branch of the M-θ relationship, r_y, results in lower ductility requirement.

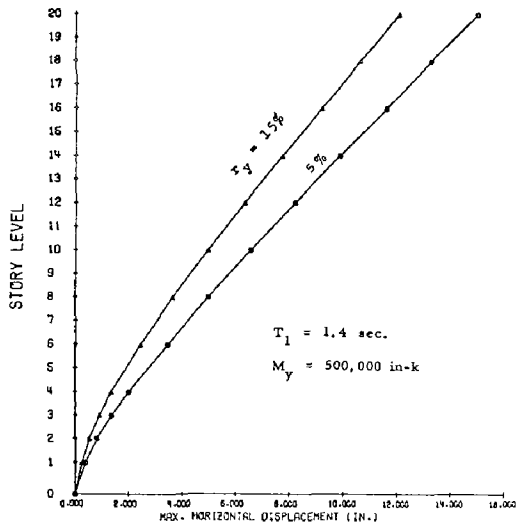

(a) Variation of max. horiz. displacement

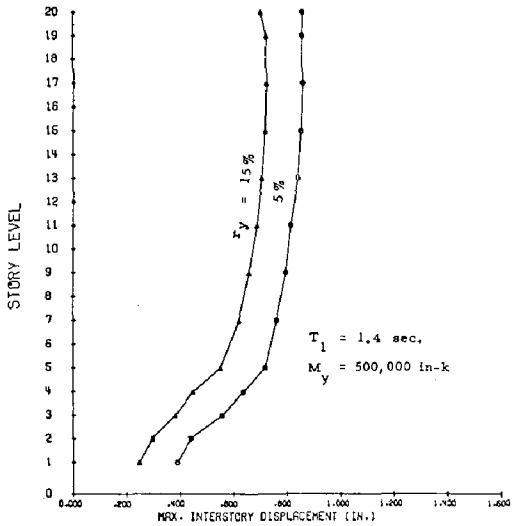

(b) Variation of max. interstory displacement

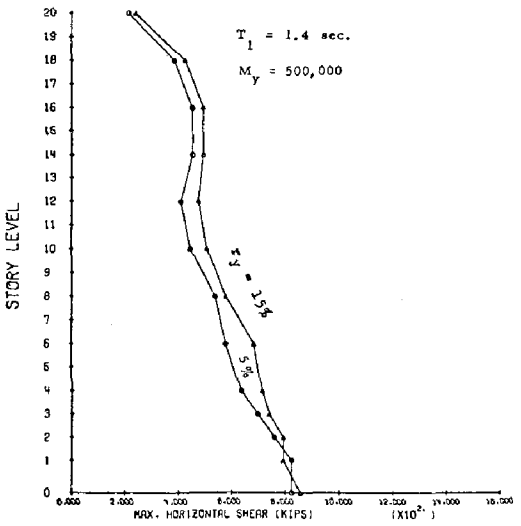

(c) Variation of max. horiz. shear

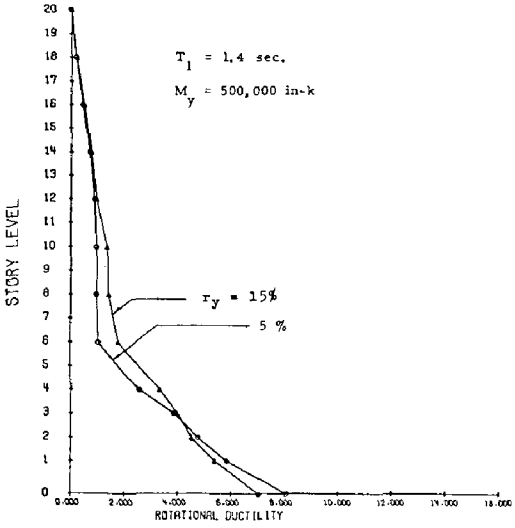

(d) Variation of max. rotational ductility

Fig. 9 Effect of yield stiffness ratio, r_y

A direct result of increasing the stiffness of a structure and decreasing its fundamental period (assuming essentially the same mass) is the reduction of the interstory displacements along the height of the structure. The magnitude of the interstory displacements also tends to diminish with increasing yield levels as long as significant yielding occurs. Within a narrow range, where only nominal yielding occurs, the interstory displacements, particularly in the upper stories of a structure, tend to increase with increasing values of the yield level, until a value is reached when no yielding (purely elastic response) occurs.

The shear forces developed during the motion are generally not affected very significantly by the fundamental period of the structure. Increasing the yield level results in sharp increases in the shear forces for structures with low periods but this effect diminishes for higher periods.

The preceding discussion of the effects of various structural parameters was meant to establish the relative importance of these parameters with respect to the significant response quantities. The response values presented here correspond to a building of a certain height and mass, subjected to a particular ground motion and are not intended for design purposes.

ACKNOWLEDGEMENT

The study reported here is part of a broader investigation directed towards the development of design procedures for earthquake-resistant structural walls sponsored by the National Science Foundation (RANN) under Grant No. GI-43880. This report is based on material presented in Reference 3.

The help extended by S. K. Ghosh in incorporating the necessary plotting routines into Program DRAIN-2D is much appreciated.

REFERENCES

1. Blume, J.A., Newmark, N.M., and Corning, L.H.,"Design of Multistory Reinforced Concrete Buildings for Earthquake Motions", Portland Cement Association, Skokie, Illinois, 1961.

2. Derecho, A.T., Freskakis, G.N., and Fintel, M., "A Study of the Effect of Frequency Characteristics of Ground Motions on Nonlinear Structural Response", Proceedings, International Symposium on Earthquake Structural Engineering, St. Louis, Missouri, August 1976.

3. Fintel, M., Derecho, A.T., Freskakis, G.N., Fugelso, L.E., and Ghosh, S.K., "Structural Walls in Earthquake Resistant Structures - Analytical Investigation - Progress Report", Report to National Science Foundation (RANN), Portland Cement Association, August 1975.

4. Ghosh, S. K., and Derecho, A.T., "Supplementary Output Package for DRAIN-2D, General Purpose Computer Program for Dynamic Analysis of Plane Inelastic Structures", Supplement No. 1 to a Progress Report on the PCA Investigation: Structural Walls in Earthquake Resistant Structures, NSF Grant No. GI-43880, Portland Cement Association, Skokie, Illinois, 60076, August 1975.

5. Kanaan, A.E., and Powell, G.H., "General Purpose Computer Program for Inelastic Dynamic Response of Plane Structures", (DRAIN-2D), Report No. EERC 73-6, Earthquake Engineering Research Center, University of California, Berkeley, April 1973.

6. Ruiz, P., and Penzien, J., "Probabilistic Study of the Behavior of Structures During Earthquakes", Earthquake Engineering Research Center Report No. EERC. 69-3, University of California, Berkeley, March 1969.

7. Takeda, T., Sozen, M.A., and Nielsen, N.N., "Reinforced Concrete Response to Simulated Earthquakes", Journal of the Structural Division, ASCE, Proceedings Vol. 96, No. ST12, December 1970.

8. Uniform Building Code, 1973 Edition, International Conference of Building Officials, 5360 South Workman Mill Road, Whittier, California, 90601.

INTERNATIONAL SYMPOSIUM ON
EARTHQUAKE STRUCTURAL ENGINEERING
St. Louis, Missouri, USA, August, 1976

EFFECTS OF SECTIONAL SHAPE ON THE STRENGTH AND DUCTILITY OF SLENDER STRUCTURAL WALLS IN EARTHQUAKE-RESISTANT MULTISTORY BUILDINGS

S. K. GHOSH
Senior Structural Engineer

MARK FINTEL
Director

Engineering Services Department
Portland Cement Association
Skokie, Ill.,60076, U.S.A.

SUMMARY

An in-depth study on the effects of sectional shape on the behavior of structural walls (shear walls) is reported in this paper. The approach used is a computer simulation of the response of a large number of structural wall sections with varying shapes. Sectional shape is varied by changing three variables: flange width, flange thickness, and web thickness, while keeping a fourth variable, total depth, unchanged. The result for each section analyzed is obtained in the form of its moment-curvature diagram. Each of these diagrams is idealized into a bilinear curve which can be completely defined in terms of four parameters: initial elastic stiffness, yield level, post-yield stiffness, and ductility ratio. Conclusions are drawn concerning the effects on these four parameters of the above three variables.

INTRODUCTION

While the open frame structure represents a highly efficient gravity load-carrying system, deep flexural members such as structural walls are more efficient in terms of lateral stiffness per unit volume of material. The use of structural walls to stiffen multistory buildings against wind loads has, by now, had a long history of satisfactory results. In buildings required to resist earthquake excitations, not only efficient lateral load resistance, but also superior damage control can be attained with the use of properly proportioned and detailed structural walls which have sufficient ductility or energy absorption capacity built into them.

While the analysis for lateral loads of buildings containing structural walls can now be handled with relative ease and sophistication, the current state-of-the-art of structural wall design requires further development. As a step towards the evolution of rational and practical design procedures for slender structural walls governed by flexure, a parametric study directed to a thorough understanding of variables affecting the strength, stiffness and ductility of such walls has recently been undertaken at Portland Cement Association. Some of the results of this ongoing investigation are presented in this paper.

Sectional shape is one of the most fundamental variables affecting the response of a slender structural wall to external loading. This paper presents an in-depth study of this one important variable. The cross-sectional shape of most commonly encountered structural walls may be defined in terms of four variables: total depth, flange thickness, flange width and web thickness. By keeping total depth unchanged and varying the other three parameters, a wide range of sections varying in shape from rectangular to wide-flanged I was studied. Great care was exercised to isolate the variable of interest, or, in other words, to prevent a simultaneous variation in other parameters such as the percentage and location of reinforcement, concrete strength, steel strength, etc.

The approach used in this analytical investigation is a computer simulation of the behavior of the sections studied. A computer program was especially developed for the purpose.[1] The program uses realistic representations of the properties of concrete and steel, and is based on an assumption of linear strain distribution and on the conditions of force and moment equilibrium. The program produces complete moment-curvature diagrams of the sections analyzed. The interpretation of results is facilitated through a superimposition of these curves in various combinations and through suitable idealizations whenever necessary. Such interpretation leads to certain useful conclusions concerning the effects of sectional shape on the response of slender structural walls to external loading.

Monotonic loading only is simulated in this study, since no satisfactory model of the possible effects of cyclic loading on concrete behavior has been developed as yet. Also, a crucial assumption underlying this study is that the behavior of slender structural wall sections is governed by flexure rather than by shear. In other words, it is assumed that the shear capacity of the critical structural wall section is sufficient to permit eventual flexural failure under combined bending and axial load. There are indications that repeated reversed loading of reinforced concrete sections in the inelastic range may lead to a reduction in their shear resistance. Finding ways of adequately reinforcing concrete sections against premature shear failure, even under severe load reversals, is the subject of a current experimental investigation at Portland Cement Association. This investigation, hopefully, will result in reinforcement arrangements, and the corresponding maximum allowable stress levels, sufficient to prevent premature shear failure and to cause no significant reduction of flexural strength under repeated reversals of loading in the inelastic range.

EXTENT OF INVESTIGATION

The one variable of this investigation, as mentioned earlier, was sectional shape. It was varied by varying flange width, flange thickness and web thickness, while keeping total sectional depth unchanged. Ten values of flange width (B), five values of flange thickness (t_F) and three values of web thickness (t_W) were considered, as listed in Table 1 and as indicated in Fig. 1.

Table 1: Geometric Properties of Sections Analyzed

Flange Width Designation		in.	(mm)	Flange Thickness Designation		in.	(mm)	Web Thickness Designation		in.	(mm)
B1	=	12	(304.8)	t_{F1}	=	12	(304.8)	t_{W1}	=	12	(304.8)
B2	=	18	(457.2)	t_{F2}	=	18	(457.2)	t_{W2}	=	18	(457.2)
B3	=	24	(609.6)	t_{F3}	=	24	(609.6)	t_{W3}	=	24	(609.6)
B4	=	36	(914.4)	t_{F4}	=	36	(914.4)				
B5	=	48	(1219.2)	t_{F5}	=	48	(1219.2)				
B6	=	60	(1524.0)								
B7	=	90	(2286.0)								
B8	=	120	(3048.0)								
B10	=	240	(6096.0)								

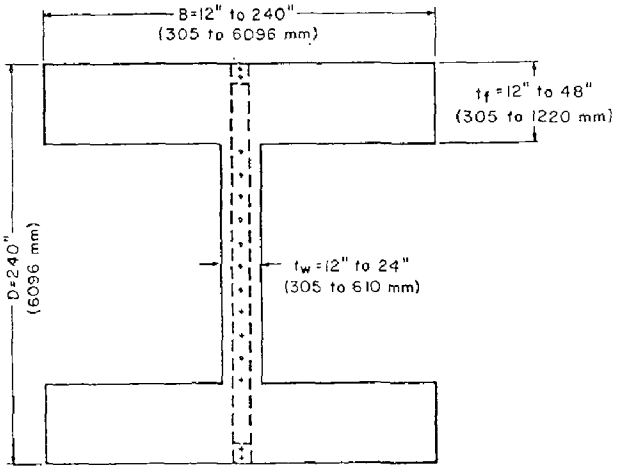

Fig. 1: Sections Analyzed

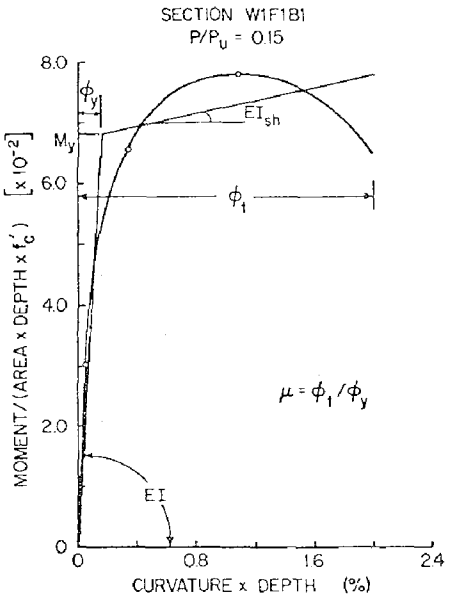

Fig. 2: Idealization of Moment-Curvature Diagrams

Total sectional depth was kept constant at 240 in. (6096 mm). Each analyzed section had a designation indicating a particular combination of the above three parameters. For instance, Section W2F3B4 had a flange width B4 = 36 in. (314.4 mm) a flange thickness t_{F3} = 24 in. (609.6 mm), and a web thickness t_{W2} = 18 in. (457.2 Fifty-four sections in all were analyzed.

The location of the reinforcement, which was kept the same for all sections analyzed, is indicated in Fig. 1. The amount of reinforcement in each flange was 0.5% of the flange area, divided in two layers. The amount of reinforcement in each web was 0.25% of the web area, distributed over eleven layers. Steel and concrete strengths were kept constant at 60 ksi (414 N/mm^2) and 4 ksi (27.6 N/mm^2), respectively. The concrete in each section was considered to be unconfined. Each section was analyzed under an axial load equal to 15% of the axial load capacity of the section. This was considered representative of the axial loads normally carried by structural walls in most common types of construction.

It should be noted that the parameters kept unchanged in this particular investigation are the prime variables in other segments of an extensive parametric study on the behavior of structural wall sections now in progress at Portland Cement Association. The present investigation forms a part of this general parametric study.

RESULTS OF ANALYSIS

The computer output for each section analyzed was obtained in the form of a set of k (non-dimensional neutral axis depth), σ_s (steel stress at the extreme tension layer), φ (curvature), and M (bending moment) values, corresponding to the given magnitude of axial load applied on the section, and to various values of ε_c (concrete strain at the extreme compression fiber) imposed on the section. Three critical stages of sectional behavior were clearly identified in the output for each section. These stages are: (1) cracking, defined by the initiation of tensile concrete strains at the extreme tension fiber, (2) first yielding of the extreme tension reinforcement layer, and (3) the attainment of the moment capacity of the section. The curve in Fig. 2 is a plot of the calculated moments against curvatures for section W1F1B1. The three critical stages mentioned above are clearly identified on the plot.

The program[1] used for sectional analysis in the present investigation does not permit a decrease in reinforcement strains, as the extreme compression fiber concrete strains are increased from one stage to the next. This is because no unloading stress-strain curve with a decrease in strains is defined for steel. At advanced strain stages, where an increase in the extreme compression fiber concrete strain may mean a net decrease in the total compression force because of concrete unloading, a corresponding decrease in the tensile steel stresses and strains may be absolutely necessary for the satisfaction of equilibrium. This is the reason why the satisfaction of equilibrium under the given axial load turned out to be an impossibility for each section, beyond a particular

value of the extreme compression fiber concrete strain which depended upon the properties of the section. As a result, the termination of each moment-curvature diagram obtained in the course of this investigation was at the stage beyond which force equilibrium under the given axial load could not be satisfied.

It is intended in subsequent phases of the present investigation to try to extend the moment-curvature diagrams up to where the moment decreases along the descending branch to 80% of the maximum moment capacity. This is in view of the fact that, particularly in seismic analysis and design, it may be reasonable and practical to define ductility (curvature at the limit of useful deformations divided by curvature at yielding of the section) in terms of such a termination stage. Extension of the moment-curvature diagrams would require a switch from extreme compression fiber concrete strain as the independent variable to curvature as the independent variable in the computer program for sectional analysis.

IDEALIZATION OF MOMENT-CURVATURE DIAGRAMS

To facilitate interpretation of the analytical results, each computed moment-curvature diagram was idealized as indicated in Fig. 2. The principal features of a bilinear idealized curve such as the one in Fig. 2 can be defined in terms of four parameters: the slope of the initial elastic branch, the yield level (moment corresponding to the point where the two branches of the bilinear curve meet), the slope of the post-yield branch, and ductility (defined as curvature at termination of the $M-\varphi$ curve divided by curvature corresponding to the yield level). The slope of the first branch, which is a measure of the stiffness of the section, is a prime factor in determining the initial period(s) of vibration of a structure. The degree to which the behavior of a structure is influenced by the initial period(s) of vibration depends on the yield level of the critical section(s); that is, on how early during its response the structure becomes inelastic. After yielding, the behavior of the structure becomes a function of the characteristics of the hysteretic force-deformation curve, which include the slope of the post-yield branch. Ductility of the critical section(s) governs the deformability as well as the energy absorption capacity of a structure.

A computed moment-curvature diagram is idealized into a bilinear curve by following the steps outlined below:

(1) Compute the slope of the initial elastic branch as follows:

$$EI = \frac{1}{2}\left(\frac{M_c}{\varphi_c} + \frac{M'_y}{\varphi'_y}\right) \qquad (1)$$

where M_c, φ_c, are the moment and curvature, respectively, corresponding to the stage of cracking; and M'_y, φ'_y, are the moment and curvature, respectively, corresponding to first yielding of the extreme tension reinforcement layer.

(2) Locate the yield point of the section such that the area under the computed moment-curvature diagram up to its peak would be equal to the area under an idealized bilinear curve, if the post-yield branch of such a curve were to extend from the yield point to the peak of the computed diagram. This criterion results in the following coordinates of the yield point of the section:

$$\varphi_y = \frac{2A_u - M_u\varphi_u}{EI \cdot \varphi_u - M_u} \tag{2}$$

$$M_y = EI \cdot \varphi_y \tag{3}$$

where A_u is the area under the computed moment-curvature diagram up to its peak point and M_u, φ_u are the moment and curvature, respectively, corresponding to the peak point.

(3) Calculate the moment at termination of the idealized moment-curvature diagram (the idealized and the computed diagrams terminate at the same curvature), such that areas under the idealized and the actual moment-curvature diagrams up to their respective termination points are equal:

$$M_t = \frac{2(A_t - A_y)}{\varphi_t - \varphi_y} - M_y \tag{4}$$

where A_t is the area under the actual $M - \varphi$ diagram up to its termination point,

A_y is the area under the idealized $M-\varphi$ diagram up to the calculated yield point $(= M_y \varphi_y/2)$,

and φ_t is the termination curvature.

(4) Make the following adjustment if M_t, as given by Eq. (4), exceeds M_u:

$$M_t = M_u \tag{5}$$

(5) If the above adjustment is made, relocate the yield point of the section such that the total areas under the idealized and actual $M - \varphi$ diagrams would be equal:

$$M_y = \frac{2A_t - M_u\varphi_t}{EI \quad \varphi_t - M_u} \tag{6}$$

(6) Compute the slope of the post-yield branch and the ductility ratio as follows:

$$EI_{sh} = \frac{M_t - M_y}{\varphi_t - \varphi_y} \tag{7}$$

$$\mu = \varphi_t/\varphi_y \tag{8}$$

The remainder of this paper is devoted to a detailed discussion of the effects of sectional shape on the four parameters--EI, M_y, EI_{sh}, and μ -- of the idealized M - φ diagrams.

EFFECTS OF FLANGE WIDTH ON STRUCTURAL WALL BEHAVIOR

The four idealized M-φ curve parameters--initial elastic stiffness (EI), yield level (M_y), post-yield stiffness (EI_{sh}) and ductility ($\mu = \varphi_t / \varphi_y$)--are plotted as functions of flange width in Fig. 3. The trends evident from this figure are discussed below.

Initial Elastic Stiffness (Fig. 3a): EI increases linearly with an increase in flange width. The rate of increase is dependent on flange thickness and web thickness, with steep increases corresponding to thick flanges and webs.

Yield Level (Fig. 3b): M_y also increases almost linearly with increasing flange widths, the rate of increase being high for sections with thick flanges and webs.

Post-Yield Stiffness (Fig. 3c): EI_{sh} appears to increase with flange width, flange thickness and web thickness, as the flange width is increased beyond a certain value. Until this value is reached, however, the trend as to the effects of these three geometric variables on EI_{sh} is rather confused. Fig. 4, which illustrates the moment-curvature diagrams of a set of sections with the same flange thickness and web thickness, but with varying flange widths, may serve to explain this phenomenon. It is apparent that the M-φ diagrams of sections with narrow flanges terminate at moments along their descending branches which are well below the respective maximum moments. The M-φ diagrams of sections with wider flanges, on the other hand, terminate at or shortly past the maximum moment. This in itself would account for much of the apparent reversal of slope exhibited by the EI_{sh} versus flange width curves in Fig. 3c. A more orderly trend should emerge when the sectional analysis program is extended, and all M-φ diagrams terminate at moments along their descending branches equal to 80% of the respective maximum moments. The kinks in the initial portions of some of the curves in Fig. 3c are apparently attributable to the adjustment effected by Steps 4 and 5 in the idealization of computed moment-curvature diagrams (preceding section). If these kinks persist after all M-φ diagrams are extended to 80% of maximum strength along their descending branches, the process of idealization itself has to be reviewed and modified as necessary.

Ductility Ratio (Fig. 3d): Increasing flange widths cause a highly significant improvement in the ductility of a section. The rate of improvement appears to diminish with increasing flange thickness and web thickness.

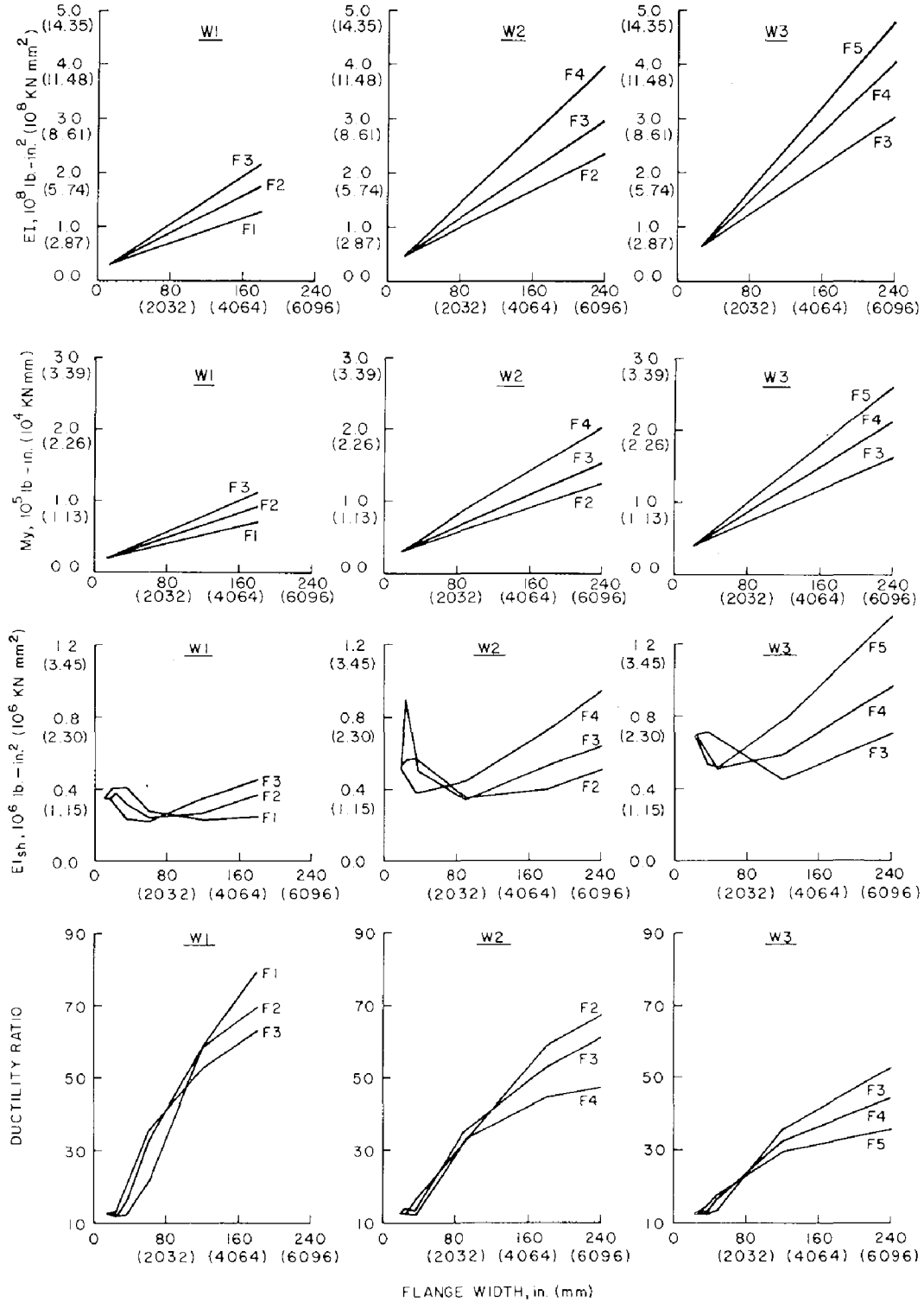

Fig. 3: Effects of flange width on structural wall response.

The magnitudes of the ductility ratio in Fig. 3d may require some comments, these being significantly higher than the comparable ductilities reported in Ref. 2. This is caused by two major changes in the definition of the ductility ratio $\mu = \varphi_t/\varphi_y$. φ_t in Ref. 2 corresponds to the peak of the M-φ diagram, whereas in the present study it is the curvature at termination of the M- φ diagram. φ_y in Ref. 2 corresponds to first yielding of the extreme tension reinforcement, whereas in this study it is the curvature at yielding of the section, as defined by the intersection of the two branches of the idealized M-φ curve. Both these changes cause increases in the value of μ, with the change in the definition of φ_y having a more significant effect. It is believed that such change is unlikely to alter the basic trends exhibited by Fig. 3d, except that the trends are likely to become more orderly, particularly at low values of the flange width.

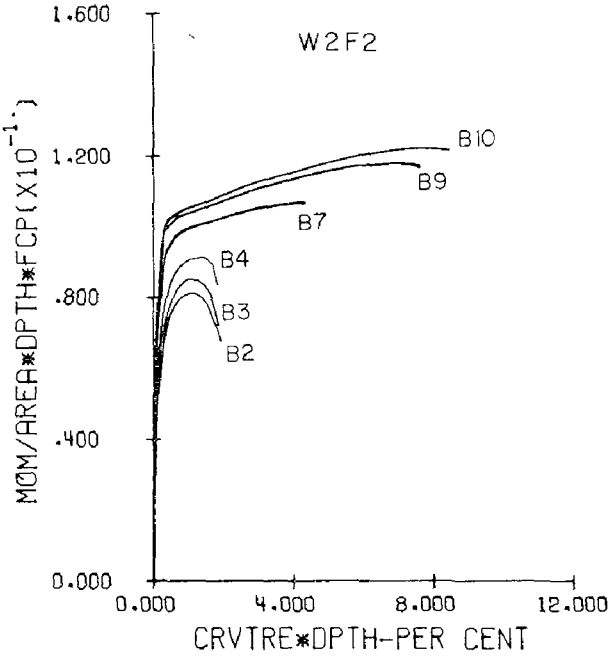

Fig. 4: Moment-Curvature Diagrams of Sections with Varying Flange Width

EFFECTS OF FLANGE THICKNESS ON STRUCTURAL WALL BEHAVIOR

Idealized M-φ curve parameters are plotted as functions of flange thickness in Fig. 5 which presents a clear picture of the influence of this variable on structural wall response. A discussion of this figure follows.

Initial Elastic Stiffness (Fig. 5a): Increasing flange thickness causes an increase in EI values. The rate of increase is higher for sections with wide flanges and thick webs.

Yield Level (Fig. 5b): M_y is affected in the same manner as EI by an increase in flange thickness.

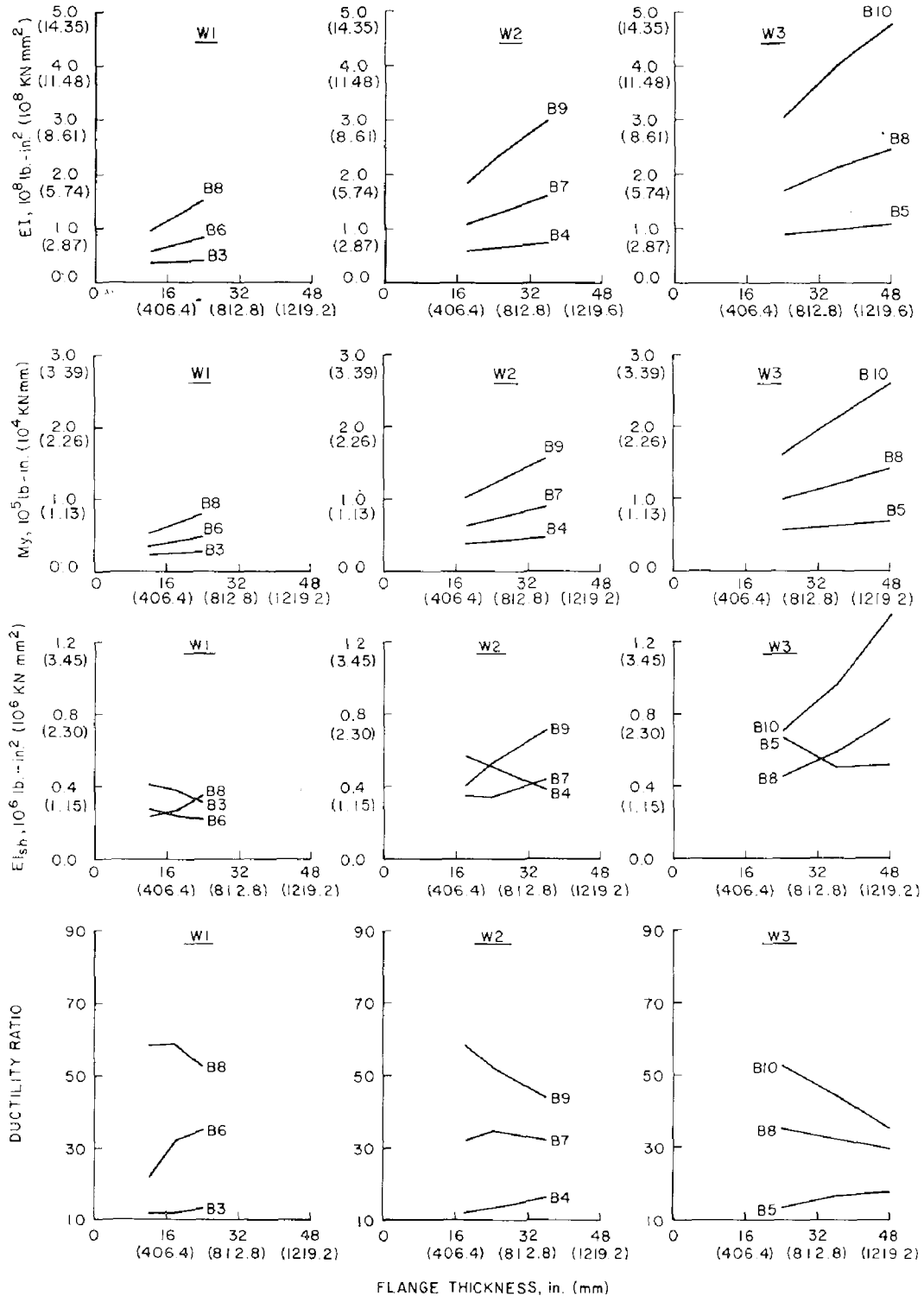

Fig. 5: Effects of flange thickness on structural wall response.

Post-Yield Stiffness (Fig. 5c): The trends exhibited by Fig. 5c are rather confused, because of reasons mentioned in the preceding section. However, if one considers only the wide-flanged sections with their M-φ diagrams terminating at or shortly beyond maximum moment, which makes the EI_{sh} values of these sections suitable for proper comparison, there are clear indications that EI_{sh} increases with increasing flange thickness.

Ductility Ratio (Fig. 5d): Different trends are apparent for wide-flanged sections with their M-φ curves terminating at or just beyond maximum moment, and for sections having narrower flanges with their M-φ curves extending further. However, it is clear that in cases where an improvement in the ductility of a section is desired, increasing the flange thickness is not an effective way of achieving it.

EFFECTS OF WEB THICKNESS ON STRUCTURAL WALL BEHAVIOR

Idealized M-φ curve parameters are plotted as functions of web thickness in Fig. 6, a discussion of which follows.

Initial Elastic Stiffness (Fig. 6a): There is a slight, almost insignificant, increase in EI with increasing web thickness.

Yield Level (Fig. 6b): M_y and EI are influenced in exactly the same way by an increase in web thickness.

Post-Yield Stiffness (Fig. 6c): The effect of an increase in web thickness on EI_{sh} appears to be favorable. However, this trend ought to be confirmed following the extension of the M-φ curves beyond their peak points to 80% of maximum strength.

Ductility Ratio (Fig. 6d): An increase in web thickness appears to have a decidedly unfavorable effect on the flexural ductility of a section.

FURTHER PROCESSING OF RESULTS

An increase in any of the geometric variables considered in this study causes a corresponding increase in the concrete area and the reinforcing steel area of a section. The effectiveness of any of these variables in improving the parameters under consideration (EI, M_y, EI_{sh}, μ) can only be assessed if the changes in these parameters caused by increases in the variables are examined in light of the corresponding changes in concrete and steel areas. Each of the three parameters other than the ductility ratio, which is nondimensional, was divided by concrete area, steel area, and the product of steel and concrete areas, and these ratios were plotted as functions of the variables of interest. Space restrictions will not permit the inclusion of these plots here. Consideration of these plots, however, entered into the drawing of conclusions which follow.

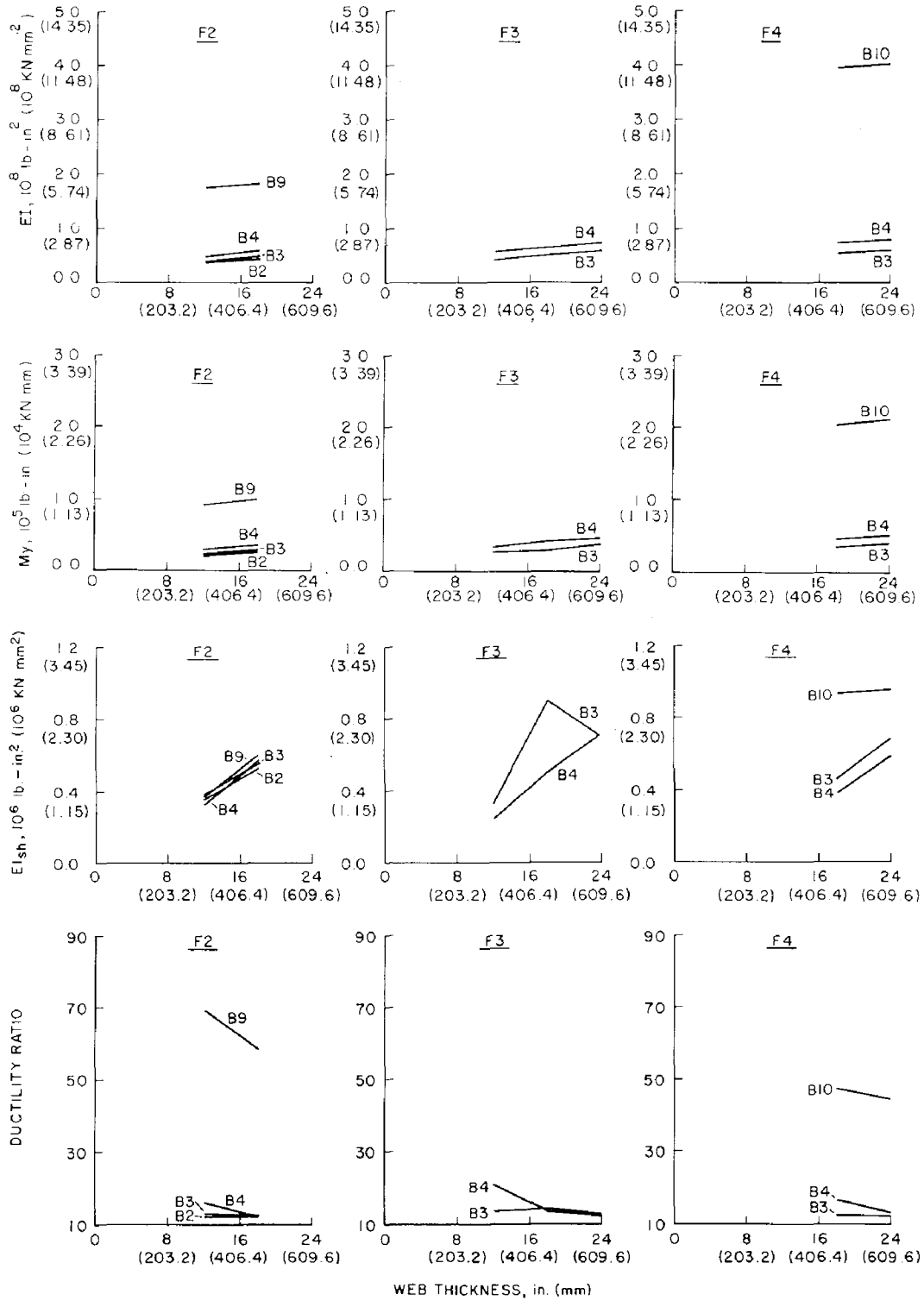

Fig. 6: Effects of web thickness on structural wall response.

CONCLUSIONS

1. Increasing the flange width appears to be the most effective way of improving the initial elastic stiffness, the yield level as well as the ductility of a reinforced concrete structural wall section. Although the post-yield stiffness, in all likelihood, also increases with increasing flange width, this requires further confirmation.

2. An increase in flange thickness also improves the initial elastic stiffness as well as the yield level of a section; however, it is not as effective as a comparable increase in flange width. Moreover, sectional ductility does not appear to be favorably affected by increasing flange thickness. The indicated positive effect of increasing flange thickness on post-yield stiffness awaits further confirmation.

3. An improvement in the initial elastic stiffness or the yield level of a section cannot be achieved efficiently or economically by increasing its web thickness which, moreover, appears to have an adverse effect on the sectional ductility. EI_{sh} appears to be favorably affected by an increase in web thickness. However, this also remains to be confirmed.

Confirmation of some of the trends observed in this study will be forthcoming when the sectional analysis program[1] is enlarged to permit the extension of all moment-curvature diagrams beyond their peak points to 80% of maximum strength. Further investigation must be carried out to examine the validity of the conclusions drawn in this paper in the presence of high shear stresses, and/or under repeated reversed loading into the inelastic range.

ACKNOWLEDGEMENT

This research was supported in part by National Science Foundation Grant No. GI-43880.

REFERENCES

1. Ghosh, S. K., "A Computer Program for the Analysis of Slender Structural Wall Sections under Monotonic Loading", Supplement No. 2 to an Interim Report on the PCA Investigation: Structural Walls in Earthquake Resistant Structures (NSF Grant No. GI-43880), Portland Cement Association, Skokie, Ill., August 1975.

2. Ghosh, S. K., Derecho, A.T., and Fintel, M., "Preliminary Design Aids for Sections of Slender Structural Walls," Supplement No. 4 to an Interim Report on the PCA Investigation: Structural Walls in Earthquake Resistant Structures (NSF Grant No. GI-43880), Portland Cement Association, Skokie, Ill. August 1975.

INTERNATIONAL SYMPOSIUM ON
EARTHQUAKE STRUCTURAL ENGINEERING
St. Louis, Missouri, USA, August, 1976

ON THE SHEAR PINCHED HYSTERESIS LOOPS

MEHMET ÇELEBİ
Associate Professor
Department of Civil Engineering
Middle East Technical University
Ankara, Turkey

SUMMARY

The dependence of shear pinching on high nominal shear stresses acting on critical regions of reinforced concrete beams is discussed. Samples of shear pinched hysteresis loops are presented.

Shear pinching phenomenon is discussed in terms of energy absorption and instantaneous stiffness. The representation of shear pinched hysteresis loops with mathematical models is reviewed. The existing model is compared with a new model based on Ramberg-Osgood curve.

INTRODUCTION

Recent experimental investigations of reinforced concrete beams under various levels of reversed nominal shear stresses resulted in a variety of hysteresis loops as well as important conclusions (1-6, 8, 9, 13, 15-17). Although different types of test specimens and testing techniques have been used by different investigators in order to reach their respective aims, a compilation of the results can be summarized as follows :

a. all specimens reversely loaded by moment and shear exhibit various degrees of deterioration of stiffness (1-6, 8, 9, 13, 15-17).

b. when the nominal shear stresses (v_u) are increased, energy absorption and therefore damping as described by the area of hysteresis loops exhibit distinctively decreasing trends as ductility is increased (4, 8, 13, 16).

c. the shapes of the hysteresis loops of the specimens under pure flexural stresses can be satisfactorily represented by Ramberg-Osgood curve. However, the shapes of the hysteresis loops under high nominal shear stresses ($v_u > 3\sqrt{f'_c}$, when f'_c in psi or approximately $v_u > 0.8\sqrt{f'_c}$ when f'_c in kg/cm^2) divert considerably from Ramberg-Osgood curve (4, 8, 13, 16). The decrease of the area is termed as shear pinching.

d. the shear resistance in the critical regions is an integrated function of the resistance provided by web reinforcement, interlocking, dowelling and grinding actions of the cracked surfaces (8, 13, 14).

e. no significant influence of dynamic loading versus static or quasi-static loading on the stiffness degrading and energy absorption properties of the specimens tested is observed (8).

As a result of experimental work compiled above attempts have been made to model the hysteretic behavior of reinforced concrete members. Besides the model represented by Ramberg-Osgood curve, an elasto-plastic and degrading stiffness model due to Clough (6) exists. These existing models have been successfully used in non-linear analysis; however, they in no way represent realistically those hysteresis loops which are pinched due to existence of shear deformations caused by presence of high nominal shear stresses at critical regions. Recently, a model based on degrading stiffness concept has been qualitatively formulated by Popov, Bertero and Krawinkler (13). An alternative model to represent shear pinched hysteresis loops is presented herein and discussed.

HYSTERESIS LOOPS OF VARIOUS TESTS

In Fig. 1, the hysteresis loops of a beam tested by triangularly shaped loading pattern applied quasi-staticly is seen. The objective of the series from which the sample is taken was to see the influence of varying degrees of nominal shear stresses (v_u) dependent upon the shear span to depth ratio

(a/d) as well as the longitudinal reinforcement percentage (p). The web reinforcement spacing (s) was varied (8).

In Figs.2 and 3, two sample hysteresis loops from two of the specimens recently tested at Middle East Technical University are shown. The objective of this series was to study the influence of varying a/d ratio only (and therefore the nominal shear stresses), keeping p and s constant. The testing specimen as well as the testing set-up of this series was different than that of Fig.1. In this series, strong column-weak girder concept was applied and the detailing of the column, girder and that of the joint was made in accordance with the seismic provisions of ACI 318-71.

Sample of some of the hysteresis loops of specimens tested in Japan are given Fig.4 (1). Most recently, Bertero and Popov (17) obtained the hysteresis loops in Fig.5, the specimen of which was subjected to nominal shear stresses in the range of $5.3\sqrt{f'_c}$ (f'_c in psi. or $1.4\sqrt{f'_c}$ when f'_c is given in kg/cm^2).

Although the aims of each of the laboratory conducted series mentioned above were different, the common result of all tests is in the presence of varying degrees of shear pinching. As one of the rare actual structural tests, Hochinohe Technical College Building tested after the 1968 Tokachi-oki Earthquake in Japan resulted in hysteresis loops that were spindle shaped or pinched (3).

IMPACT AND IMPORTANCE OF SHEAR PINCHING

Theoretical models are available for predicting the moment rotation hysteresis loops of sections of test specimens with low nominal shear stresses when no pinching takes place (12). Therefore, for designs of sections based on web reinforcement detailing provisions of the present codes, these models result in incorrect hysteresis loops because they ignore the influence of shear deformations.

Diversions of hysteresis loops of sections with high nominal shear stresses from those of pure flexure or those of low nominal shear stresses is interprated by mainly two concepts :

a. decrease in the area of the hysteresis loops

b. change of the instantaneous stiffness of the shear pinched hysteresis loop.

Impact of the decrease of the area of the hysteresis loop is that the decreased area is related to energy absorption and therefore to the equivalent viscous damping fraction which is an important parameter in dynamic response prediction. As proposed by Jacobsen (11) and Hudson (10), the equivalent viscous damping fraction (ξ) is given by the equation :

$$\xi = \frac{1}{4\pi} \frac{\Delta W}{W}$$

where ΔW is the actual area of the hysteresis loop and W is the energy defined by the area under triangle formed by the yielding slope at the particular value of displacement for which ΔW is considered. For those specimens in Figs. 1-3, the change of the equivalent viscous damping fraction with ductility is given in Fig.6. The characteristics of the specimens included

in Fig.6 are given in summary in Table I. Clearly, in Fig.6, it is seen that the equivalent viscous damping fraction decreases as the ductility is increased.

TABLE I. RELEVANT CHARACTERISTICS OF SPECIMENS

Specimen	p(%)	a/d	s(cm)	$v_u/\sqrt{f'_c}$	$v_c/\sqrt{f'_c}$
A	1.03	2.31	8.26	0.99	1.99
B1	1.10	3.70	7.00	0.81	1.59
B2	1.10	2.78	7.00	1.06	1.59

$v_u = M_u/abd$, $v_c = 0.53\sqrt{f'_c} + p_w f_y$

The response prediction in dynamic analysis is also dependent on the instantaneous stiffness of the structure and/or the specimen in question since the stiffness term is related to the spring force. It is observed in Figs. 1-5 that the stiffness at unloading can be represented by some fraction of initial or yielding stiffness. However, once the loading starts, then the stiffness of the critical region reflected to the load-displacement hysteresis loop of the test specimen is indeed very low. This can be explained by the mechanism of resistance of the diagonally cracked region. At zero load, there is a permanent set deflection and no interlocking. All cracks are opened. When loading starts, at first the resistance is provided by dowel action only and therefore large deformations (mainly shear deformation) take place until interlocking of the cracked portions takes place; hence, the resistance and therefore the stiffness increases. This mechanism is responsible for the softer stiffness at first loading and then increasing stiffness of the critical region. Therefore, a straight line representation of the loading portion of shear pinched hysteresis loops of the critical regions is not realistic.

TWO MODELS FOR SHEAR PINCHED HYSTERESIS LOOPS

The model proposed by Popov, Bertero and Krawinkler (13), is a simulation based on degraded stiffness model originated by Clough (6). Accordingly, the yielding slope is followed by a strain-hardening slope which becomes the asymptote for the hysteresis curves. The unloading slope is represented by degraded stiffness and given by Popov, Bertero and Krawinkler as

$$K_{unloading} = K_{elastic}\ (1/\mu)^{\alpha}$$

where μ is the ductility and α is a parameter to be determined empirically. At reloading, the stiffness defined by the zero load and the load defined by any previous maximum displacement is taken and then the asymptotic strain-hardening line is followed up to the new displacement (13). This is shown in Fig.7.

Also shown qualitatively in Fig.7 is an alternative model which has been previously proposed by the author (7). This model entails defining a Ramberg-Osgood hysteresis loop given the yielding load, yielding displacement and the maximum displacement and the maximum load (which can be defined by the strain-hardening asymptotic line) of the hysteresis loop under consideration. Then, from this larger Ramberg-Osgood hysteresis loop, two smaller Ramberg-Osgood hysteresis loops are to be subtracted. The smaller loops will be defined by the displacement at zero load and the maximum displacements. The Ramberg-Osgood parameters are to be determined empirically as a function of v_u, v_c and μ. The softer stiffness at the beginning of the reloading is represented quite satisfactorily by the Ramberg-Osgood curves given in Fig.7. Mathematically the smaller Ramberg-Osgood curves can be easily represented by shifting the axes to zero loading.

CONCLUSIONS

Laboratory conducted experiments on reinforced concrete specimens lead to distinctive trends of shear pinching dependent on the degree of nominal shear stresses. Shear pinched hysteresis loops mean less energy absorption and therefore less damping.

Besides decrease in energy absorption, the stiffness of the shear pinched hysteresis loops change during reloading. At first the stiffness is softer and later after interlocking of the cracked portions of the critical region, the stiffness increases.

Realistic estimation of the shape of the hysteresis loop is therefore important in terms of damping and stiffness. A model based on subtracting two small Ramberg-Osgood hysteresis loops from a larger Ramberg-Osgood loop represents the shear-pinched hysteresis loop satisfactorily.

More important, of course, is to change the detailing of shear reinforcement (of specimens with large nominal shear stresses) such that shear deformations will decrease. This will result in greater energy absorption capacity and aid in regaining the stiffness which otherwise deteriorates rapidly.

REFERENCES

1. _____, "Experimental Studies on Load-Deflection Characteristics of R.C. Columns Subjected to Alternate Loading," Yokohoma National University, March, 1968.

2. Bertero, V.V., Bresler, B. and Liao, H., "Stiffness Degradation of R.C. Members Subjected to Cyclic Flexural Moments," EERC Report 69-12, Univ. of Calif., Berkeley, 1969.

3. Bertero, V.V., "Experimental Studies Concerning Reinforced, Prestressed and Partially Prestressed Concrete Structures and Their Elements," IABSE Symposium, Lisbon, Sept. 1973, p.74.

4. Bertero, V.V. and Popov,E., "Hysteretic Behavior of Ductile Moment-Resisting Reinforced Concrete Frame Components," EERC Report 75-16, Univ. of Calif., Berkeley, April 1975.

5. Brown, R.H. and Jirsa, J.O., "Reinforced Concrete Beams Under Load Reversals", Journal of ACI, May 1971.

6. Clough, R.W., "Effect of Stiffness Degradation on Earthquake Ductility Requirements", Report No. 66-16, Univ. of Calif., Berkeley, Oct. 1966.

7. Çelebi, M., "A Model for Shear Pinched Hysteresis Loops," CENTO Sym. on Earthquake Engineering, Middle East Tech. Univ., Ankara, Nov. 1974.

8. Çelebi, M. and Penzien, J., "Experimental Investigation into the Seismic Behavior of Critical Regions of R.C. Components as Influenced by Moment and Shear," EERC Report 73-4, Univ. of Calif., Berkeley, Jan. 1973.

9. Hanson, N.W. and Conner, H.W., "Reinforced Concrete Beam-Column Connections for Earthquakes," Prelim. Report, PCA, Nov. 1965.

10. Hudson, D.E., "Equivalent Viscous Friction for Hysteretic Systems with Earthquake-like Excitations," PROC. III. WCEE, New Zealand, 1965.

11. Jacobsen, L.S., "Damping in Composite Structures," PROC. II. WCEE, Tokyo, Japan, 1960, pp.1029-1040.

12. Kent, D.C., "Inelastic Behavior of R.C. Members with Cyclic Loading," PhD. Thesis, Univ. of Canterbury, New Zealand, 1969.

13. Popov, E., Bertero, V.V. and Krawinkler, H., "Cyclic Behavior of R.C. Flexural Members with High Shear," EERC Report 72-5, Univ. of Calif., Berkeley, Oct. 1972.

14. Singh, H.N., Gerstle, K.H., and Tulin, H.G., "Shear Strength of Concrete Beams Under Cyclic Loading," Int'l Symp. on Shear, Bond and Torsion in R.C., Coimbatore, India, Jan. 1969.

15. Umemura, H., Aoyama, H. and Ito, M., "Experimental Studies on R.C. Members and Composite Steel and R.C. Members," Univ. of Tokyo, Dec. 1970.

16. Uzumeri, S.M., and Seçkin, M., "Behavior of R.C. Beam-Column Joints Subjected to Slow Load Reversals," Publication No. 74-05, Univ. of Toronto, March 1974.

17. White, R.N. and Chowdhury, A.H., "Behavior of Multi-Story R.C. Frames Subjected to Severe Reversing Loads," IABSE Symp., Lisbon 1973, p.205.

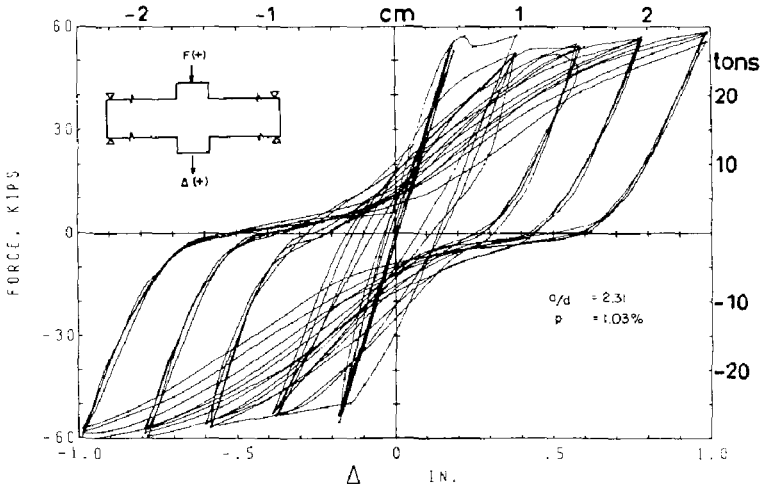

Fig. 1. Shear Pinched Loops (Ref.8)

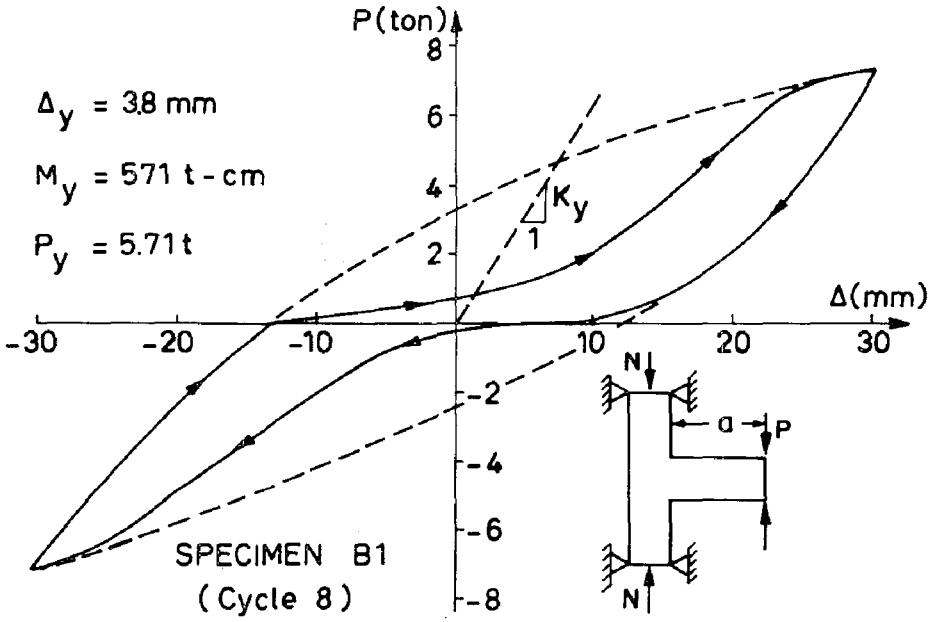

FIG. 2 SHEAR PINCHED LOOP (METU TEST)

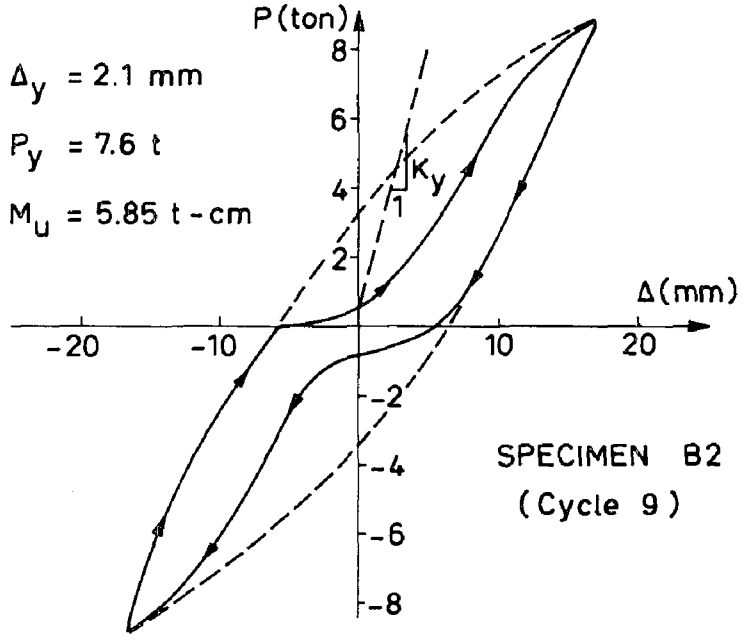

FIG. 3 SHEAR PINCHED LOOP (METU TEST)

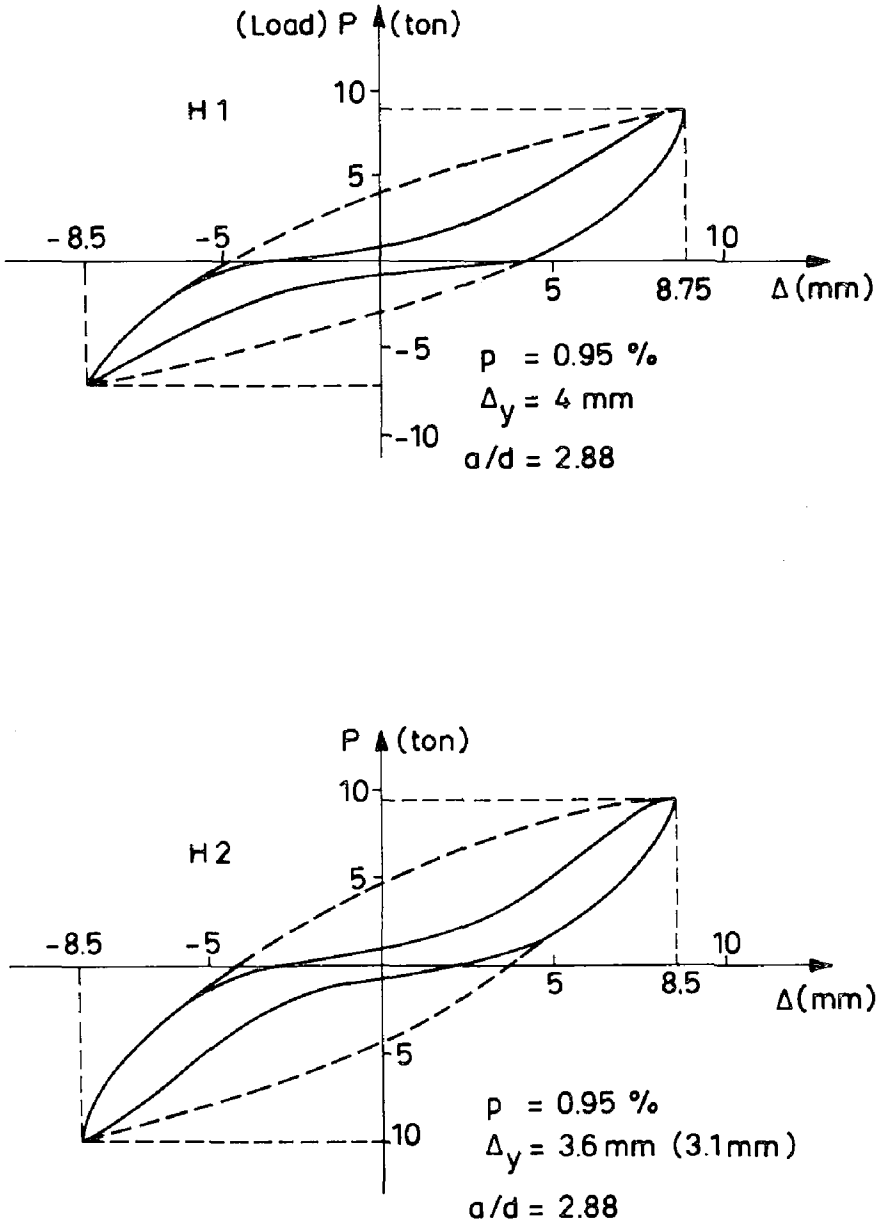

FIG. 4 SHEAR PINCHED LOOPS (JAPAN - REF. 1)

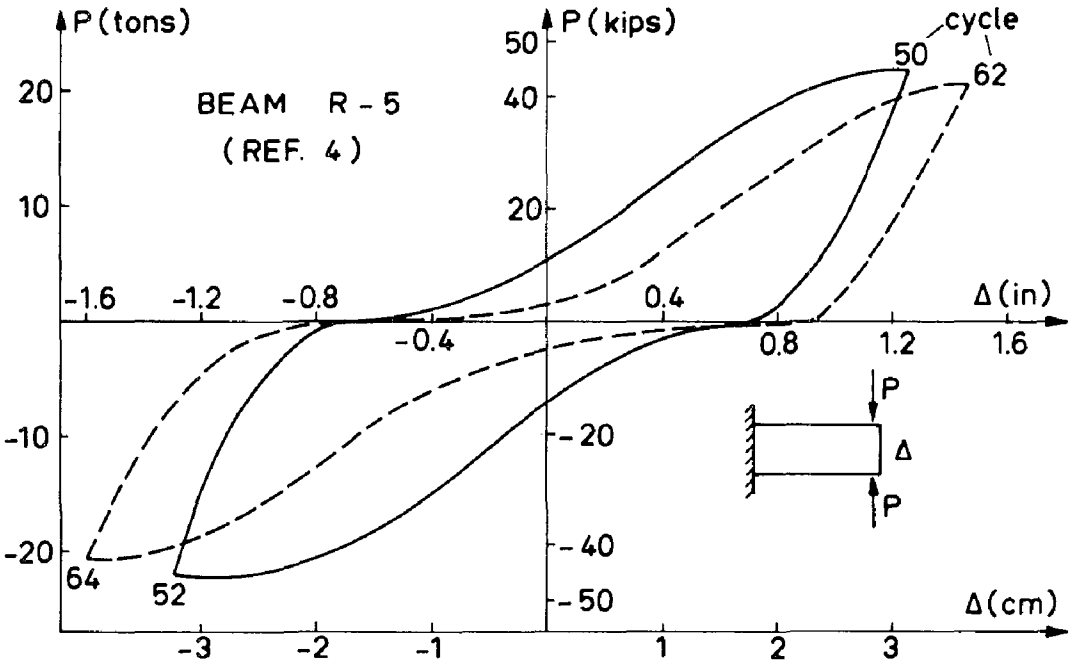

FIG. 5 SHEAR PINCHED LOOPS (REF. 4)

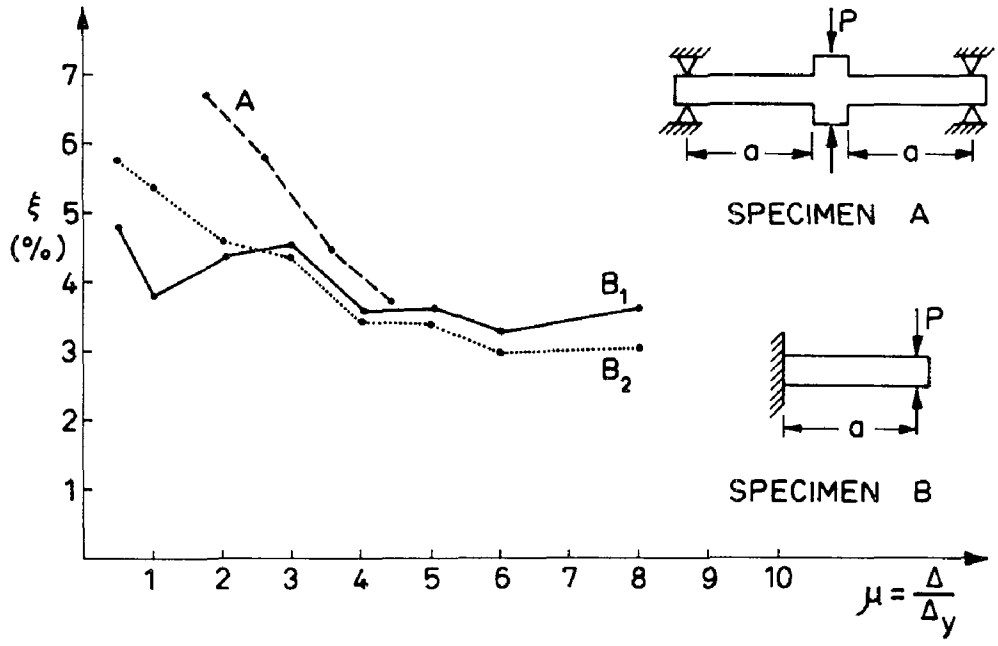

FIG. 6 CHANGE OF DAMPING WITH DUCTILITY

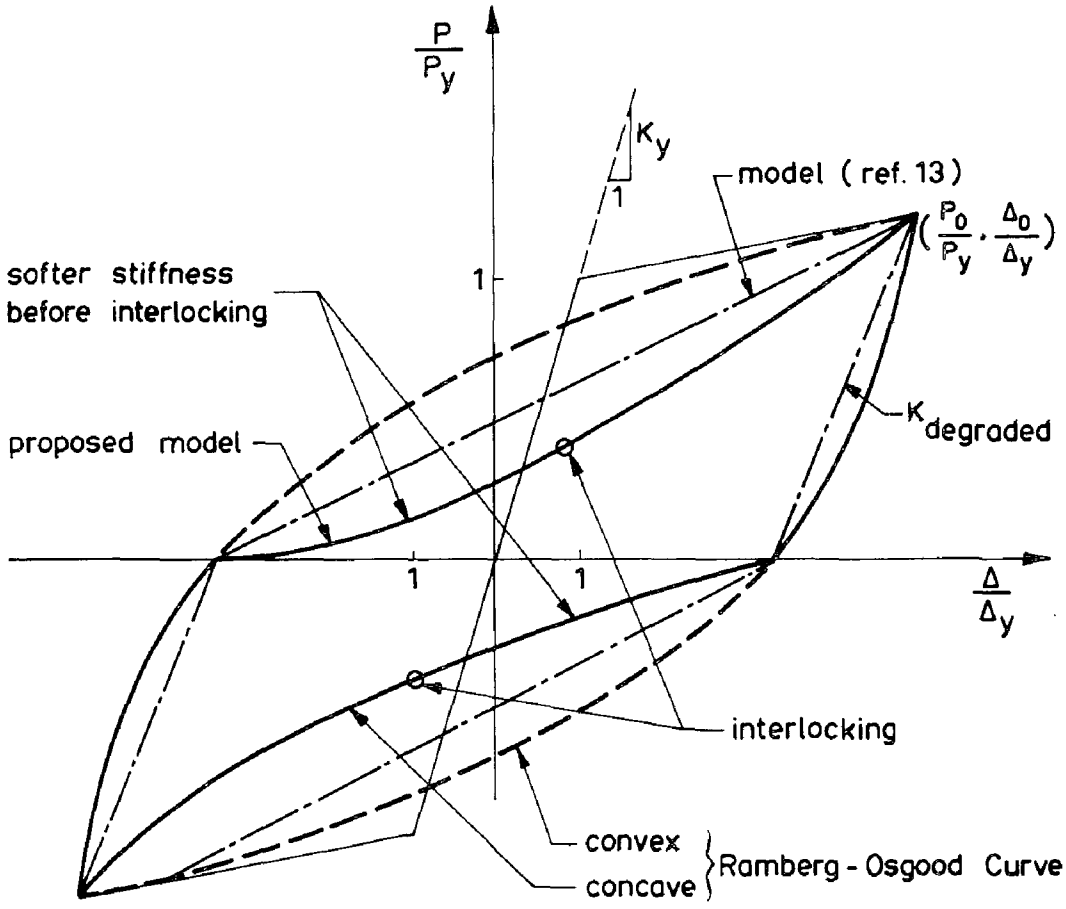

FIG. 7 COMPARISON OF TWO MODELS

INTERNATIONAL SYMPOSIUM ON
EARTHQUAKE STRUCTURAL ENGINEERING
St. Louis, Missouri, USA, August, 1976

CONFINED CONCRETE IN COMPRESSION ZONES OF STRUCTURAL WALLS DESIGNED TO RESIST LATERAL LOADS DUE TO EARTHQUAKES

P. H. KAAR, A. E. FIORATO, J. E. CARPENTER and W. G. CORLEY

Senior Structural Engineer, Senior Structural Engineer
Former Principal Structural Engineer, and Director

Engineering Development Department

Portland Cement Association

Skokie, Ill., U.S.A.

SUMMARY

The Portland Cement Association is carrying out a combined analytical and experimental program to develop design criteria for reinforced concrete structural walls used as lateral bracing in earthquake resistant buildings. The work is sponsored in part by the National Science Foundation under Grant No. GI-43880. As part of this program, tests have been performed on specimens representing full size compression zones of structural walls. The results are being used to evaluate the effects of rectangular hoops as confinement reinforcement and to determine the effective stress versus strain relationship of confined concrete.

The test specimen has been adapted from one developed earlier for the determination of the stress versus strain relationship for plain concrete. Controlled variables included hoop size, hoop spacing, amount of longitudinal reinforcement, concrete strength, and size of specimen.

Analysis of the test results showed that all arrangements of rectangular hoops were effective in significantly increasing the limiting concrete strain. For those specimens with hoop reinforcement meeting the requirements of Appendix A of the ACI Building Code, limiting concrete strains exceeded 0.015.

The spacing and amount of transverse reinforcement were the primary variables affecting the stress versus strain relationship of the concrete. The amount of longitudinal reinforcement had little effect.

INTRODUCTION

An extensive analytical and experimental investigation is under way at the Portland Cement Association to develop design criteria for reinforced concrete structural walls used as lateral bracing in earthquake resistant structures. The experimental program is primarily concerned with the development of details to ensure ductility, energy dissipation, and strength of structural walls subjected to forces simulating an earthquake.

As part of this program, tests are being performed to develop information on the effectiveness of closed rectangular hoops used as confinement reinforcement to increase useful strain capacity of concrete. Several investigators have demonstrated the increase in strain capacity obtained by confining the concrete with spiral or tie reinforcement. [1,3,4,8,9,10] This series of tests considers variables in members representing the compression zones of structural walls. The effective stress versus compressive strain relationship for the confined concrete determined from the experimental data is reported.

TEST PROGRAM

Test Specimens

Tests to determine strain capacity of confined concrete are being performed on C-shaped specimens as shown in Fig. 1. The specimen was adapted from the design first used by Hognestad, Hanson and McHenry[6] to determine the stress versus strain relationship of plain concrete.

Variables in the test program include spacing of confinement reinforcement, size of confinement reinforcement, strength of concrete, amount of longitudinal reinforcement, and size of test specimen. Values chosen for the variables are listed in Table 1. Results described in this report cover the tests in Groups 1, 2, and 3.

The two sizes of test specimen cross section were 10x16 in. (254x406 mm), shown in Fig. 2, and 5x8 in. (127x203 mm). For the larger size specimens, the central value for the hoop size and spacing was No. 4 bars at 4 in. (102 mm). This met the requirements of ACI 318-71[2] for lateral confinement as specified in Appendix A, Section A.6.4.3. The volumetric ratio, ρ_s, required by this Code Section for the dimensions of the hoop used in 0.0067. The area required for one leg of the hoop bar is 0.19 sq. is. (123 sq. mm) which is satisfied by a No. 4 bar having an area of 0.20 sq.in. (129 sq.mm)

Values of the volumetric ratio, ρ_s, provided for each specimen are shown in Table 1. The hoop size and spacing were increased and decreased from the central value to determine the influence on the effective stress versus strain relationship of the concrete. The specimens were constructed using concrete having a design compressive strength of 3000 psi (211 kgf/cm^2).

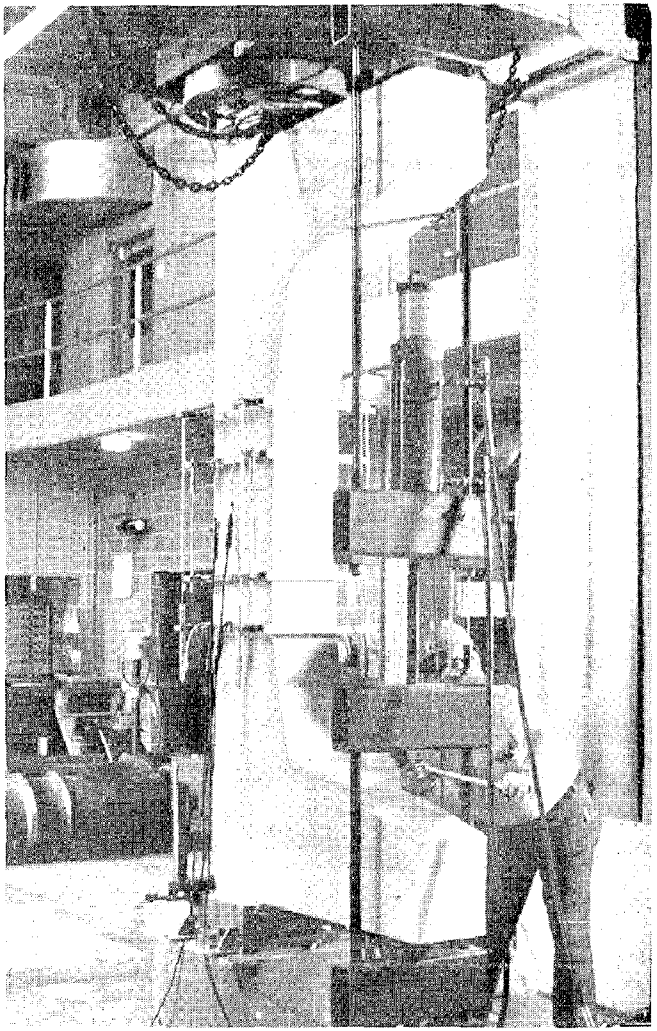

Fig. 1 Specimen Ready for Testing

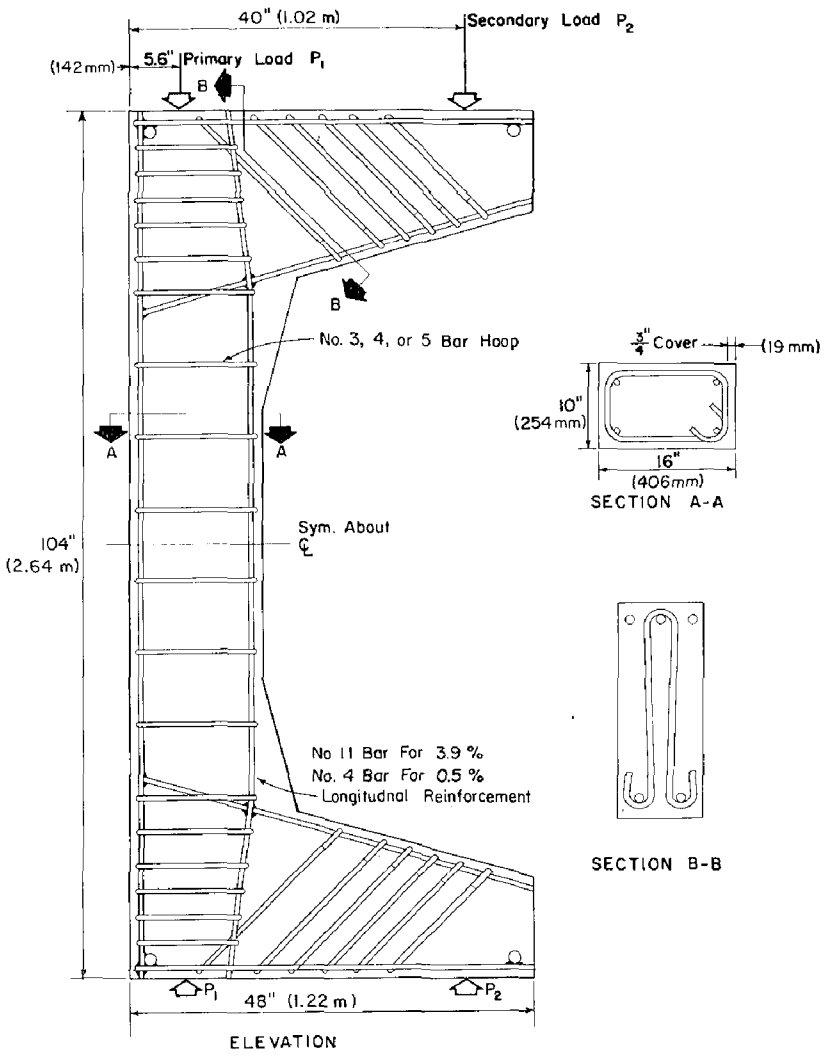

Fig. 2 Details of Large Specimen

TABLE 1 DETAILS OF TEST SPECIMENS

Group	Dimensions of Crossection in.	Concrete Comp. Str. ksi	Long. Reinf. Ratio ρ'	Hoop Size Bar No.	Hoop Reinf. Ratio ρ_s	Specimen No. and Hoop Spacing				Comments
						2-in.	4-in.	8-in.	∞	
Specimens Reported										
1	10x16	3	0		0				1P*	Plain Concrete
				3	0.010		7			
				4	0.037	2				Meets ACI Hoop Req.
2	10x16	3	0.005	4	0.019		3P*			Meets ACI Hoop Req.
				4	0.009			4		
				5	0.029		6P			Meets ACI Hoop Req.
				3	0.010		13P			
				4	0.037	8				Meets ACI Hoop Req.
3	10x16	3	0.039	4	0.019		9*			Meets ACI Hoop Req.
				4	0.009			10		
				5	0.029		12			Meets ACI Hoop Req.
Specimens for Future Tests										
4	5x8	3	0		0				20	Plain Concrete
5	5x8	3	0.005	2	0.019	16				
6	5x8	3	0.044	2	0.019	19				
7	5x8	6	0		0				17	Plain Concrete
8	5x8	6	0.005	2	0.019	18				
9	5x8	6	0.044	2	0.019	15				

Notes: Groups 4, 5 and 6 are repetitions, in half scale, of the specimens marked with asterisk* in Groups 1, 2 and 3, respectively. Groups 7, 8 and 9 are repetitions in 6 ksi concrete, of Groups 4, 5 and 6, respectively.

1 in. = 25.4 mm 1 ksi = 70.3 kg/cm^2

Longitudinal reinforcement was provided by four bars, one in each corner of the cross section. Two sizes of bars were used, No. 4 and No. 11. This gave vertical reinforcement percentages of 0.5 and 3.9, respectively. These values were chosen to approximate the range that might be used in practice. The larger specimen with 10x16-in. (254x406 mm) cross section is shown in Fig. 1. Other dimensions of the specimen are given in Fig. 2.

In addition, future tests will be carried out on specimens having dimensions one-half those of the large specimens. Hoop reinforcement made from 6 mm deformed bars at 2-in. (51 mm) spacing will be used with 0.5% and 4.4% longitudinal reinforcement. Specimens in the smaller size will be tested using 3000 (211 kgf/cm^2) and 6000 psi (422 kgf/cm^2) concrete compressive strength.

Hoops were held in place at the desired spacing by tying them to the longitudinal reinforcement. The four longitudinal bars were placed at the rectangular hoop corners so that concrete cover over the hoops was 3/4 in. (19 mm). Flexural and shear reinforcement was added to the arms of the "C" shaped specimen to prevent distress in this region during the test. A photograph of a reinforcing cage in the plywood form is shown in Fig. 3. All specimens were cast in a horizontal position.

The concrete contained a blend of Type I portland cements and 3/4-in. (19 mm) maximum size Elgin sand and gravel aggregate. Mix proportions per cubic yard were 346 lb. cement, 2093 lb. aggregate, 1228 lb. sand, and 248 lb. water. Each specimen was moist cured under a plastic sheet at 70F for three days after casting. Subsequently the concrete was cured at 70F and 55% relative humidity.

Concrete strengths given in Table 2 are the average determined by three 6x12-in. (152x305 mm) cylinders taken from the concrete region on which strain measurements were made during the test. Also shown in this table are the modulus of elasticity determined from cylinder tests and from test specimens. The arms of the specimen were cast at the same time as the main portion, but a higher strength concrete was used.

All reinforcement met the requirements of ASTM Designation A615[5] Grade 60.

Test Procedure

The major load P_1, shown in Fig. 2, was applied by a testing machine having a 1,000,000 lb. (453,600 kgf) capacity. Force was applied through a system of bearing plates and rollers that accommodated rotation of the specimen during the test.

The minor load P_2, shown in Fig. 2, was applied by a hydraulic ram through a system of rods, cross-heads, and rollers. This apparatus is also visible in the foreground of Fig. 1.

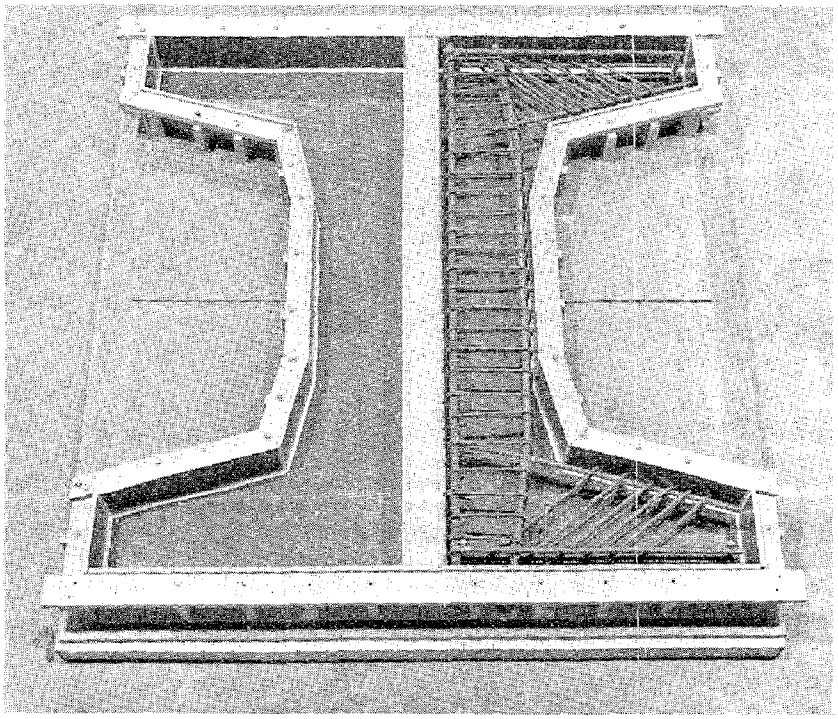

Fig. 3 Reinforcing Cage in Form

During the test, the major load P_1 was increased at a constant rate. By manually controlling the minor load P_2, strain at the extreme fibers at the back of the cross section, the left side in Fig. 2, was kept near zero. Thus, the back face represented the neutral axis boundary of the compression zone of the cross section. On the opposite side of the cross section, the right side in Fig. 2, the fibers are subjected to a monotonically increasing compressive strain representing conditions in the compressive zone.

Instrumentation

Direct current differential transformers (DCDT) measured the distances between reference frames mounted transversely on the specimen. These deformations were used to determine strain both in the plane of the compression face and in the plane of the neutral face. Two pairs of frames were used over gage lengths initially at 16 in. (406 mm) and at 30 in. (762 mm). An additional horizontal DCDT was used to monitor the bending distortion from loading. This information was used to determine changes in the load lever arms necessary for the analysis.

TABLE 2 TEST RESULTS

Specimen	6x12-in.(152x305mm)Cylinders		Test Specimens		
	Compressive Strength psi	Modulus of Elasticity psi	Compressive Strength psi	Modulus of Elasticity psi	Maximum Compressive Strain ε_u
1P	3300	2,670,000	3490	3,190,000	0.003
7	3430	3,060,000	4030	3,850,000	0.009
2	3130	3,400,000	3160	3,370,000	0.042
3P	3040	2,620,000	3550	3,610,000	0.015
4	3250	3,400,000	2990	3,530,000	0.011
6P	3260	2,810,000	3480	3,530,000	0.026
8	3200	2,970,000	2950	3,750,000	0.059
9	3300	3,000,000	3550	3,650,000	0.016
10	3470	2,990,000	3220	3,150,000	0.010
12	3010	3,030,000	3410	3,570,000	0.027
13P	2780	3,030,000	3190	2,850,000	0.015

1000 psi = 70.3 kgf/cm^2

Signals from the DCDT's were recorded at regular intervals during the continuous loading of the specimen. The primary load was applied by a 1,000,000 lb. (453,600 kgf) capacity testing machine. The secondary load was monitored by load cell transducers described elsewhere.[7] Electrical resistance strain gages mounted on the concrete of most specimens provided confirming information on strain distributions prior to spalling of the concrete cover.

Data Analysis

Stresses in the longitudinal reinforcement were calculated from strain data. Resultant reinforcement loads and moments were then subtracted from the total values so that loads and moments on the concrete could be determined. The analysis was similar to that used by Hognestad, Hanson, and McHenry.[6] Closely spaced readings of data during the test enabled the differentials in the following equations to be approximated by finite differences $\Delta f_o/\Delta \varepsilon_c$ and $\Delta m_o/\Delta \varepsilon_c$

$$f_c = \varepsilon_c \frac{df_o}{d\varepsilon_c} + f_o \qquad (1)$$

$$f_c = \varepsilon_c \frac{dm_o}{d\varepsilon_c} + 2\, m_o \qquad (2)$$

where

f_c = compressive stress in concrete

ε_c = strain in concrete

f_o = average compressive stress in concrete

$m_o = \dfrac{\text{applied moment}}{bc^2}$

b = width of rectangular member

c = distance from neutral axis to compressive edge of member

Concrete stresses are calculated on the basis of small differences between large numbers. The differentials $\frac{df_o}{d\varepsilon_c}$ and $\frac{dm_o}{d\varepsilon_c}$ are determined from data differences for the load stage either side of the one considered for stress determination. This process naturally produces some scatter in the data. By using two independent methods to calculate the relationship between stress f_c and strain ε_c, the accuracy of the test data is checked.

Final data were condensed by eliminating readings for which the two values of f_c did not substantially agree. The selected points were then plotted and a smooth curve drawn.

A second analysis was also performed to avoid eliminating readings for which f_c did not agree. A "best fit" polynominal was determined by regression analysis of the data representing the f_o versus ε_c and m_o versus ε_c

relationships. The polynominals were then differentiated so the slope at each load state was known. Stresses were determined as before but avoiding the disadvantage of approximating the slope.

TEST RESULTS

Test results shown in Fig. 4 illustrate the effect on stress versus strain relationship of hoop spacing and size of hoops for specimens reinforced with 0.5% and 3.9% longitudinal reinforcement. The stress versus strain relationship of a plain concrete specimen is shown for reference. The ordinate to each plot is in terms of the ratio of concrete stress to concrete cylinder strength.

The values shown are not strains in the generally accepted sense of the word. Rather, they are shortening per unit gage length measured at the compression face over a length equal to the gage length. The actual maximum strain may be several times higher. These values have a real meaning in terms of calculations of deformation when used in conjunction with the strain of the opposite edge of the specimen at the same location.

Regardless of spacing, the presence of hoops had a beneficial effect upon the stress versus strain relationship. Even specimens containing hoops with 8-in. (203 mm) spacing showed continuing concrete strains of 0.010, a value well above the 0.003 strain often assumed for plain concrete.

All tests of confined concrete specimens ended gradually while tests of unreinforced concrete specimens ended suddenly. The test of the confined specimens ended when the longitudinal reinforcement buckled and load carrying capacity was greatly reduced. Figure 5 shows the buckled bars in the confined concrete specimens after testing and Fig. 6 shows the plain concrete specimen after test.

CONCLUSIONS

Lateral hoop reinforcement meeting or exceeding the ACI Building Code requirement (ACI 318-71) for lateral confinement as specified in Appendix A, Section A.6.4.3, extended the limiting concrete strain beyond 0.015. This is five times the value of 0.003 assumed for ultimate strain of plain concrete. Confinement reinforcement in the range utilized for this report showed no significant influence on concrete strength.

All of the specimens tested with hoop reinforcement had significantly greater concrete strains than could be obtained with plain concrete. The amount of longitudinal reinforcement had little effect on the stress versus strain relationship for concrete. Spacing and amount of transverse hoop reinforcement was of primary importance.

ACKNOWLEDGMENTS

This investigation was carried out in the Structural Development Section of the Portland Cement Association under the direction of Dr.H.G.Russell,

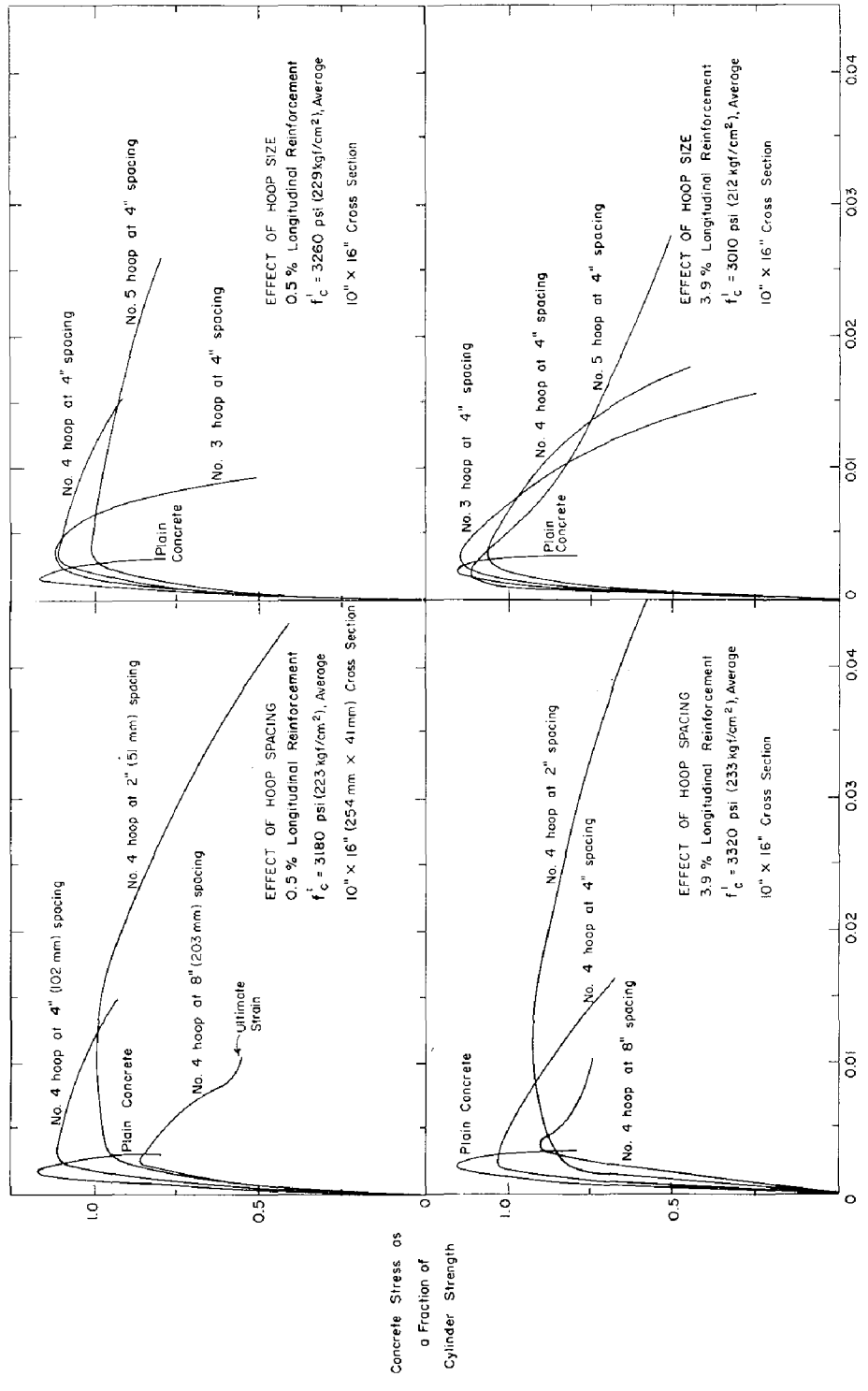

Fig. 4 Stress versus Strain Relationship of Confined Concrete

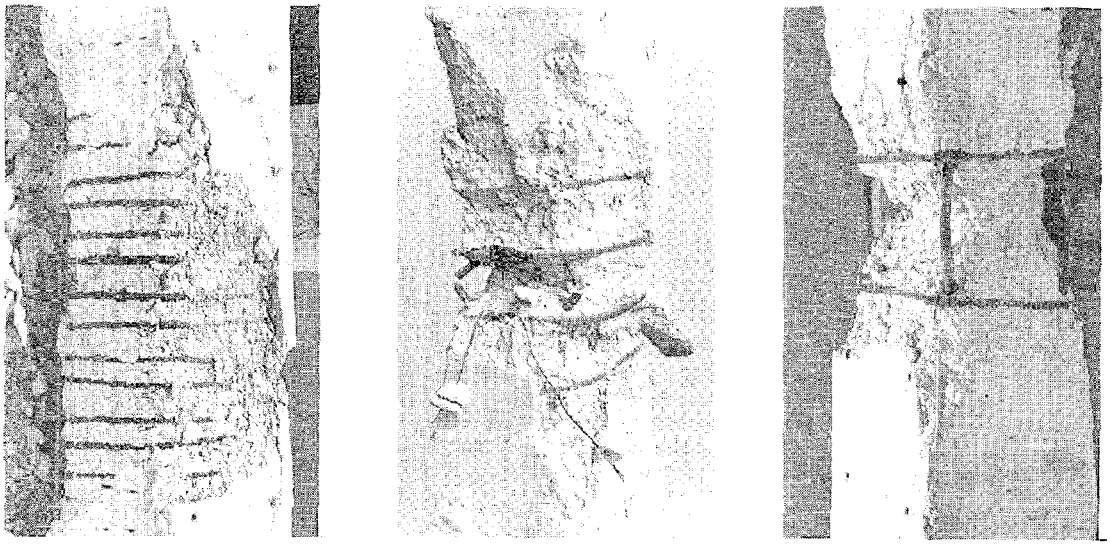

2-in. (51 mm) 4-in. (102 mm) 8-in. (204 mm)

Fig. 5 Buckled Bar Region of Specimens for 2-in., 4-in., and 8-in. Hoop Spacing

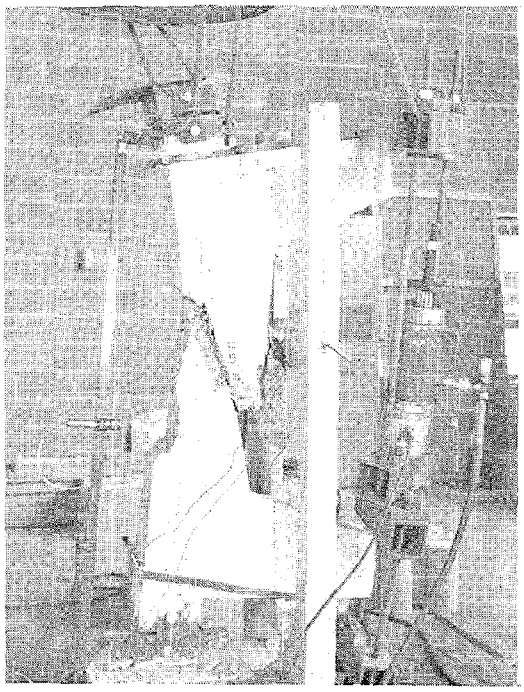

Fig. 6 Plain Concrete Specimen after Test

Manager. Fabrication and testing of the specimens were performed by the Technical Staff of the Section with the assistance of the Staff of the Transportation Development Section.

The work was part of a combined analytical and experimental investigation under the direction of M. Fintel and was sponsored in part by the National Science Foundation through Grant No. GI-43880.

REFERENCES

1. Base, G. D., and Read, J. B., "Effectiveness of Helical Binding in the Compression Zone of Concrete Beams,, Journal of the American Concrete Institute, Detroit, Mich., Vol. 62, July, 1965, pp. 763-781.

2. "Building Code Requirements for Reinforced Concrete (ACI 318-71)." American Concrete Institute, Detroit, Mich., 78 pp.

3. Burns, N. Y., Siess, C. P., "Load-Deformation Characteristics of Beam-Column Connections in Reinforced Concrete," Structural Research Series No. 234, Civ. Engrg. Studies, Univ. of Illinois, Urbana

4. Corley, W. Gene, "Rotational Capacity of Reinforced Concrete Beams," Journal of the Structural Division Proceedings of the American Society of Civil Engineers, Proc. Paper 4939, Vol. 92, ST5, pp. 121-146, Oct. 1966. Also PCA Development Bulletin D108.

5. "Deformed and Plain Billett-Steel Bars for Concrete Reinforcement," (A615-74a) American Society for Testing and Materials, Philadelphia, Pa. 11 pp.

6. Hognestad, E., Hanson, N. W., and McHenry, D., "Concrete Stress Distribution in Ultimate Strength Design,"Journal of the American Concrete Institute, Dec. 1955, Proceedings, Vol. 52, pp. 455-479. Also PCA Development Bulletin D6.

7. Hognestad, E., Hanson, N. W., Kriz, L. B. and Kurvits, O. A., "Facilities and Test Methods of PCA Structural Laboratory," papers under various titles in Journal of the PCA Research and Development Laboratories, Vol. 1, No. 1, Jan. 1959, pp. 12-20, and 40-44; Vol. 1, No. 2, May 1959, pp. 30-37; and Vol. 1, No. 3, Sept. 1959, pp. 35-41; reprinted jointly as PCA Development Department Bulletin D33.

8. Richart, F. E., Brantzaeg, A., Brown, R. L., "The Failure of Plain and Spirally Reinforced Columns in Compression," Bulletin No. 190, University of Illinois Engineering Experimental Station, Urbana, Ill., 1929, 74 pp.

9. Roy, H.E.H., and Sozen, M. A., "Ductility of Concrete," Flexural Mechanics of Reinforced Concrete, Proceedings of the November 10-12, 1964, ASCE-ACI Internatl. Symposium held in Miami, Fla., ASCE, 1965, pp. 213-224.

10. Soliman, M.T.M., and Yu, C. W., "The Flexural Stress Strain Relationship of Concrete Confined by Rectangular Transverse Reinforcement," Magazine of Concrete Research, Vol. 19, No. 61, Dec. 1967, pp. 223-238.

INTERNATIONAL SYMPOSIUM ON
EARTHQUAKE STRUCTURAL ENGINEERING
St. Louis, Missouri, USA, August, 1976

RESPONSE OF AN EMPTY CYLINDRICAL GROUND SUPPORTED LIQUID STORAGE TANK TO BASE EXCITATION

SAMIA HAFIZ SHAABAN*

WILLIAM A. NASH**

*University Fellow
**Professor of Civil Engineering
University of Massachusetts
Amherst, Massachusetts 01002 USA

SUMMARY

The structure under consideration is an elastic cylindrical liquid storage tank attached to a rigid base slab. A finite element analysis is presented for the free vibrations of the empty tank permitting determination of natural frequencies and associated mode shapes. The response of the empty tank to (a) simple deterministic base excitation as well as (b) artificial earthquake excitation is also determined by finite elements.

INTRODUCTION

The problem of free and forced vibration of thin elastic shells has been of practical concern for many years and a 1973 monograph by A.W. Leissa [4] summarizes the significant contributions to that area. In particular, shells subject to dynamic loading have been investigated by P.M. Ogibalov [5], H. Kraus [3], G.B. Warburton [10], P. Seide [8] and others. Usually these investigations are restricted to determination of responses to harmonic excitations applied normal to the shell surface or suddenly applied normal loads that remain constant with respect to time. However, the techniques discussed in these works are not considered practical for application to the case of an applied edge loading that varies rapidly and in essentially a random fashion with time. From an analytical standpoint the case of time-dependent edge loads gives rise to significant complications due to the fact that the boundary conditions are inhomogenous. When a shell is subjected to time-dependent edge displacements rather than time-dependent edge forces the solution of the response problem becomes even more difficult.

The objective of the present investigation is to develop a computerized approach for determination of small amplitude elastic responses of an empty slab-supported cylindrical liquid storage tank subject to arbitrary base excitation. It is assumed that the base slab supporting the tank is rigid and that the tank does not separate from the slab during excitation.

This study will form the basis for a subsequent investigation concerned with response determination of the same storage tank when filled to an arbitrary depth with liquid.

BODY

The slab supported liquid storage tank is excited by seismic forces transmitted from the foundation through the rigid slab to the elastic tank. Thus, excitation to the tank is applied at points of support, i.e. around the tank base. In use of the finite element technique, imposition of support displacements is possible since one can partition the displacement vector U into certain components U_b associated with known support displacements with all other components being associated with the remaining (nonsupported) nodes. Thus, the general equation of motion

$$M \ddot{x} + C \dot{x} + K x = F(t) \tag{1}$$

may be written in the partitioned form [1]

$$\left[\begin{array}{c|c} M_{bb} & M_b^T \\ \hline M_b & M \end{array}\right] \left\{\begin{array}{c} \ddot{U}_{bt} \\ \hline \ddot{U}_t \end{array}\right\} + \left[\begin{array}{c|c} K_{bb} & K_b^T \\ \hline K_b & K \end{array}\right] \left\{\begin{array}{c} U_{bt} \\ \hline U_t \end{array}\right\} = \left\{\begin{array}{c} F_b \\ \hline 0 \end{array}\right\} \tag{2}$$

where damping in (1) has been neglected and U_{bt} and $\ddot{U}_{bt}$ in (2) are known support displacements and accelerations, respectively. All elements in the top line of Equation (2) pertain to base node parameters. Thus, K_{bb} and M_{bb} denote forces at base nodes due to unit displacements and unit acceleration respectively at the base nodes and the superscript T denotes matrix transpose. K_b and M_b in the bottom row are coupling effects between the base nodes and the other (non-base) nodes. All other elements in the bottom row of Equation (2) pertain to non-base nodel parameters. Thus K and M represent stiffness and mass matrices of all non-base nodes.

At any time, the displacement vectors of the non-base nodes can be considered as a summation of two factors. The first vector U_s is a function of the instantaneous ground displacement, thus it can be called static. The second vector U_d is a function of the ground acceleration history, thus it is termed dynamic.

This approach furnishes a suitable method to reduce the equations of motion to the familiar form of forced vibrations:

$$[M] \{U_d\} + [K] \{U_d\} = \{F\} \tag{3}$$

where {F} is a defined driving force vector to be derived later. Thus:

$$\{U_t\} = \{U_s\} + \{U_d\} \tag{4}$$

The equations of motion are

$$\left[\begin{array}{c|c} M_{bb} & M_b^T \\ \hline M_b & M \end{array}\right] \left\{\begin{array}{c} \ddot{U}_{bt} \\ \hline \ddot{U}_s + \ddot{U}_d \end{array}\right\} + \left[\begin{array}{c|c} K_{bb} & K_b^T \\ \hline K_b & K \end{array}\right] \left\{\begin{array}{c} U_{bt} \\ \hline U_s + U_d \end{array}\right\} = \left\{\begin{array}{c} F_b \\ \hline 0 \end{array}\right\} \tag{5}$$

The equations of the off-base elements are

$$[M_b]\{\ddot{U}_{bt}\} + [M]\{\ddot{U}_s\} + [M]\{\ddot{U}_d\} + [K_b]\{U_{bt}\} + [K]\{U_s\} + [K]\{U_d\} = 0 \tag{6}$$

Now it is attractive to define U_s as a displacement vector so that when it is associated with the ground displacement vector U_{bt} the resulting motion of the structure corresponds to no internal strain energy. This condition implies that

$$[K_b]\{U_{bt}\} + [K]\{U_s\} = 0 \tag{7}$$

In other words the vector $\{U_s\}$ is developed through rigid body displacements consistent with $\{U_{bt}\}$. Thus from (7)

$$U_s = -[K]^{-1}[K_b]U_{bt}$$

This phenomena has also been demonstrated numerically and the resulting static displacement U_s is nothing but a series of U_{bt} or

$$\{U_s\} = \begin{Bmatrix} U_{s1} \\ \hline U_{s2} \\ \hline U_{s3} \\ \hline \vdots \\ \hline U_{sN} \end{Bmatrix} \simeq \begin{Bmatrix} U_{bt} \\ \hline U_{bt} \\ \hline U_{bt} \\ \hline \\ \hline U_{bt} \end{Bmatrix} \tag{8}$$

where N is the total number of elements and $\{U_{si}\}$ is the displacement vector of node i = $\{U_{bt}\}$ for all values of i and $\{U_{bt}\}$is a (4x1) vector representing the axial, tangential, and radial displacements as well as the rotation of the generator at the base.

Thus, the off-base node equations yield

$$\begin{aligned} [M]\{\ddot{U}_d\} + [K]\{U_d\} &= -[M_b]\{\ddot{U}_{bt}\} - [M]\{\ddot{U}_s\} \\ [M]\{\ddot{U}_d\} + [K]\{U_d\} &= -[[M_b] - [M][K]^{-1}[K_b]]\{\ddot{U}_{bt}\} \\ &= [\text{effective mass matrix}]\{\ddot{U}_{bt}\} \\ &= [M_{eff}]\{\ddot{U}_{bt}\} \end{aligned} \tag{9}$$

It should be pointed out that for most practical tank dimensions the driving forces developed due to the mass $[M][K][K_b]$ are much larger than those developed by $[M_b]$. This has been demonstrated numerically for a variety of practical tank geometries.

The ground acceleration vector $\ddot{U}_{bt}$ will be

$$\ddot{U}_g(t) \begin{Bmatrix} 0 \\ -1 \\ 1 \\ 0 \end{Bmatrix}$$

where $\ddot{U}_g(t)$ is the ground acceleration amplitude at time t as will be shown later in (12).

Since the base of the tank is excited by a ground displacement and acceleration acting in its plane and in the constant direction $\theta = 0$, no axial acceleration component develops and the ground acceleration will be completely defined by its amplitude value $\ddot{U}_g(t)$:

$$\ddot{U}_g(t) = \text{Peak} \cdot f(t) \tag{10}$$

The peak is an acceleration value independent of time and f(t) is a non-dimensional function of time.

The present study is based upon the shell theory due to J.L. Sanders, Jr. [7]. That theory considers a right, circular cylindrical shell of radius a and thickness h. Let the quantities r, θ, and z denote radial, circumferential, and axial coordinates respectively of a point on the shell middle surface. The corresponding displacement components are denoted by w, v, and u respectively. The shell equilibrium equations in terms of displacements are:

$$\begin{aligned}
&\alpha^2 \frac{\partial^2 u}{\partial z^2} + \left(\frac{1-\nu}{2}\right)\left(1 + \frac{\alpha^2}{4}\right)\frac{\partial^2 u}{\partial \theta^2} + \frac{a}{2}\left[1 + \nu - \frac{3}{4}(1-\alpha)\alpha^2\right]\frac{\partial^2 v}{\partial \theta \partial z} \\
&\quad + a\alpha \frac{\partial w}{\partial z} + \frac{a\alpha^2}{2}(1-\nu)\frac{\partial^2 w}{\partial \theta^2 \partial z} = -\frac{a^2}{k} q_z + \frac{a^2}{k} \rho_s h \ddot{u} \\
&\frac{a}{2}\left[1 + \nu - \frac{3}{4}(1-\nu)\alpha^2\right]\frac{\partial^2 u}{\partial \theta \partial z} + \frac{a^2(1-\nu)}{2}\left(1 + \frac{q}{4}\alpha^2\right)\frac{\partial^2 v}{\partial z^2} \\
&\quad + (1+\alpha^2)\frac{\partial^2 v}{\partial \theta^2} + \frac{\partial w}{\partial \theta} - \alpha^2\left[\frac{\partial^3 w}{\partial \theta^3} + a^2\left(\frac{3}{2} - \frac{\nu}{2}\right)\right]\frac{\partial^3 w}{\partial z^2 \partial \theta} \\
&\quad = -\frac{a^2}{k} q_\theta + \frac{a^2}{k} \rho_s h \ddot{v} \\
&-a\nu \frac{\partial u}{\partial z} + \frac{a}{2}(1-\nu)\alpha^2 \frac{\partial^3 u}{\partial z \partial \theta^2} + \frac{\partial v}{\partial \theta} - \alpha^2\left[\frac{\partial^3 v}{\partial \theta^3} + a^2\left(\frac{3}{2} - \frac{\nu}{2}\right)\right]\frac{\partial^3 v}{\partial \theta \partial z^2} \\
&\quad + w + \nabla_w^4 = \frac{a^2}{k} q_r - \frac{a^2}{k} \rho_s h \ddot{w}
\end{aligned} \tag{11}$$

where

$$\alpha^2 = \frac{1}{12}\left(\frac{h}{a}\right)^2$$

$$\nabla^4 w = a^4 \frac{\partial^4 w}{\partial z^4} + 2a^2 \frac{\partial^4 w}{\partial z^2 \partial \theta^2} + \frac{\partial^4 w}{\partial \theta^4}$$

$$k = \frac{Eh}{(1-\nu^2)}$$

Equations (11) permit representation of the applied loads in the form

$$q_z = \sum_m q_z^m \ (z,t) \ \cos m\theta$$

$$q_\theta = \sum_m q_\theta^m \ (z,t) \ \sin m\theta$$

$$q_r = \sum_m q_r^m \ (z,t) \ \cos m\theta$$

while simultaneously the displacements are expressed as

$$u = \sum_m u_m \ (z,t) \ \cos m\theta$$

$$v = \sum_m v_m \ (z,t) \ \sin m\theta$$

$$w = \sum_m w_m \ (z,t) \ \cos m\theta$$

The associated base-node displacement vector U_{bt} is

$$\begin{aligned} u(o,\theta,t) &= 0 \\ v(o,\theta,t) &= -\ddot{U}_g(t) \cdot \sin\theta = -\text{Peak} \cdot f(t) \cdot \sin\theta \\ w(o,\theta,t) &= +\ddot{U}_g(t) \cdot \cos\theta = +\text{Peak} \cdot f(t) \cdot \cos\theta \\ \frac{\partial w}{\partial z}(o,\theta,t) &= 0 \end{aligned} \qquad (12)$$

Since the excitation function is described in the form (12) to be associated with m = 1, obviously only the first circumferential harmonic will be excited, and thus the vibration of the tank can be prescribed by superposition of certain contributions of different axial modes corresponding to m = 1 only:

$$\ddot{U}_b(t) = \text{Peak} \cdot f(t) \cdot \begin{Bmatrix} 0 \\ -1 \\ 1 \\ 0 \end{Bmatrix} \qquad (13)$$

Let

$$\{P_{eff}\} = \text{Peak} \cdot [M_{eff}] \cdot \begin{Bmatrix} 0 \\ -1 \\ 1 \\ 0 \end{Bmatrix}$$

$\therefore$. The equations of motion reduce to

$$[M]\{\ddot{U}_d\} + [K]\{U_d\} = \{P_{eff}\} \cdot f(t)$$

which is the desired form of forced vibration to which the modal analysis technique will be applied.

Modal Analysis Solutions

$$[M]\{\ddot{U}_d\} + [K]\{U_d\} = \{P_{eff}\} \cdot f(t)$$

Let

$$\{\ddot{U}_d\} = [X]\{\ddot{A}\}$$

$$\{U_d\} = [X]\{A\}$$

$\therefore$. [X] is the rectangular mode matrix formed as a set of mode vectors (n x k) where

n = number of degrees of freedom of the non-base elements

k = number of modes considered in the analysis

{A} = mode participation factor vector = k x 1

$\therefore$. $[M][X]\{\ddot{A}\} + [K][X]\{A\} = \{P_{eff}\} \cdot f(t)$

$\{A\} \equiv \{A(t)\}$; $\{\ddot{A}\} = \{\ddot{A}(t)\}$

$$f(t) = \frac{\ddot{U}_g(t)}{\text{Peak}}$$

Premultiply by $[X]^T$; (k x n)

$\therefore$. $[X]^T[M][X]\{\ddot{A}\} + [X]^T[K][X]\{A\} = [X]^T\{P_{eff}\} \cdot f(t)$

$= \{GP\} \cdot f(t)$

Now, use the orthogonality condition:

$$\{X_n\}^T[M]\{X_k\} = 0 \qquad k \neq n$$

Obviously the resulting matrix $[X]^T[M][X] = [GM]$ is a diagonal matrix since the (generalized k x k mass matrix) nonvanishing terms are only $[X_n]^T[M][X_n] = GM(n,n)$.

The same concept holds for $[X]^T[K][X] = [GS] \equiv$ diagonal matrix where

Ω^2 is the squared eigenvalue diagonal matrix = $[\Omega^2][GM]$:

$$[\Omega^2] = \begin{bmatrix} \omega_1^2 & & & & \\ & \omega_2^2 & & & \\ & & \omega_3^2 & & \\ & & & \ddots & \\ & & & & \omega_n^2 \end{bmatrix}_{k \times k}$$

Thus GM, as well as GS can be considered as vectors,

$$\begin{bmatrix} GM(1,1) \\ GM(2,2) \\ GM(3,3) \\ GM(k,k) \end{bmatrix} \quad \text{and} \quad \begin{bmatrix} GM(1,1) \cdot \omega_1^2 \\ GM(2,2) \cdot \omega_2^2 \\ \vdots \\ GM(k,k) \cdot \omega_k^2 \end{bmatrix} \quad \text{respectively.}$$

Thus k independent equations result:

$$GM(I,I) \cdot \ddot{A}(I) + \omega(I) \cdot \omega(I) \cdot A(I) \cdot GM(I,I) = GP(I) \cdot f(t)$$

where I refers to the mode number.

Thus;

$$\ddot{A}(I) + \omega^2(I) \cdot A(I) = \frac{GP(I)}{GM(I,I)} \cdot f(t)$$

which are the equations of k independent lumped masses each representing the participation of the corresponding i-th mode.

Now, A(I) can be found using Duhamel Integration to account for the initial conditions (just before the instant t), i.e. to consider the whole acceleration record imposed on the structure, viz:

$$A(I) = \frac{GP(I)}{GM(I,I) \cdot \omega(I)} \cdot \int_0^t f(\tau) \cdot \sin \omega(t-\tau) d\tau$$

$$= \frac{PIN(I)}{GM(I,I) \cdot \omega(I)}$$

$$\text{where } PIN(I) = \left(\int_0^t f(\tau) \sin \omega(t-\tau) d\tau\right) \cdot GP(I)$$

$$\therefore A(I) = \frac{GP(I)}{GM(I,I)} f(t) - (\omega(I))^2 \cdot A(I)$$

Now from the original equations of motion the displacement and acceleration nodal vectors are determined:

$$\{U_d\} = [X]\{A\}$$

$$\{\ddot{U}_d\} = [X]\{\ddot{A}\}$$

The accuracy of the method can be examined through the satisfaction of the original external equilibrium equation:

$$[M]\{\ddot{U}_d\} + [K]\{U_d\} = \{P_{eff}\} \cdot f(t)$$

For the structures considered it was found that the superposition of four modes offered only a crude approximation since the external equilibrium equation failed to be satisfied by as much as thirty percent. Use of eight modes reduced the maximum discrepancy to about ten percent. It was worth the effort to cross-check the program by use of a coarse idealization of the tank involving a limited number of degrees of freedom, i.e. a limited total number of natural modes. In that case the external equilibrium equation was satisfied perfectly.

The expressions for displacements and forces arising because of base excitation are well-suited to computer implementation. This is achieved through use of two main programs. The first program, termed the free vibration program, develops the element mass matrix for a typical ring-shaped finite element. It also develops the stiffness matrix, does the assembly, permits application of various boundary conditions, and extracts eigenvalues and natural modes through use of the Cholesky reduction method, then performing the power method. The various displacements and internal forces are also displayed in terms of relative values. The second main program partitions the original mass and stiffness matrices as required in (2), develops the effective mass matrix, and applies modal analysis to obtain the participation factor of each mode employed. It also obtains the nodal displacements through superposition of the modes and their participation factors, as well as the external reaction developed at the base slab, and designated internal stresses. Finally, it carries out an external equilibrium check.

As an example, the slab supported tank discussed in [2] was considered. This structure is 40 feet (12.19 meters) high and 60 feet (18.29 meters) in radius with a steel wall having a thickness of one inch (2.54 cm). Use of the first program for the case of the tank clamped at the base slab and free at the top, with the values found by Edwards [2] being given for comparison yields.

Mode	Frequency (Hz) Ref. [2]	Present work
1	34.04	34.08
2	43.87	43.91
3	44.58	44.64

Mode	Frequency (Hz) Ref. [2]	Present work
4	45.10	45.19
5	45.80	45.92
6	47.97	47.13
7	--	49.03
8	--	51.86
9	--	55.79
10	--	61.91

The case of this same slab-supported tank subject to a single rectangular acceleration pluse was also considered. The acceleration is applied in the direction $\theta = 0°$ and the tank response was determined through use of the second main computer program. The excitation pulse, together with the response of radial displacement w at the tank top for $\theta = 0°$ is illustrated in Figure 1. Also shown in that figure is the behavior of radial displacement w at node 6 (top of the central of the nine ring-shaped finite elements employed) as well as axial displacement at the same node for $\theta = 0°$. Relative values of significant forces and moments per unit length of the shell middle surface (during free vibration) were also displayed by the computer program but are omitted here in the interest of brevity.

The same empty tank was also considered to be subjected to the artificial earthquake accelerogram available through the National Information Service-Earthquake Engineering, at Berkeley, California [6]. This excitation was considered to be the exciting mechanism acting on the rigid base slab in the horizontal direction along the line $\theta = 0°$. The assigned maximum ground acceleration was taken to be g/2 although the record itself is normalized in terms of a unit value of g. This record was imposed upon the base slab for five seconds and the tank response determined at 0.1 second intervals during the time period t = 0 to t = 5 seconds using time increments of 0.001 seconds. The time history of radial displacement at the tank top at $\theta = 0°$ during the time interval t = 4.0 to 4.5 seconds appears as indicated in Figure 2. Significant forces and moments were also determined but are omitted here for brevity. More complete results are offered in [9]. Use of smaller time increments would have led to a more irregular response than indicated in Figure 2. It is anticipated that both computer programs developed in this investigation will be available through the National Information Service-Earthquake Engineering, University of California, Berkeley, California.

CONCLUSIONS

Finite element programs have been developed for determination of natural frequencies and mode shapes of an empty elastic cylindrical storage tank. Programs have also been developed for determination of response of such a tank to arbitrary base excitation.

ACKNOWLEDGMENT

The authors would like to thank the Earthquake Engineering Program of the Division of Advanced Environmental Research and Technology, Research

Applied to National Needs (RANN) of the National Science Foundation for their sponsorship of this work under Grant GI39644. Also, the authors would like to thank Dr. C.I. Wu and Dr. J.M. Colonell for valuable discussions and comments during the course of this work.

BIBLIOGRAPHY

1. Clough, R.W., "Analysis of Structural Vibrations and Dynamic Response," in Recent Advances in Matrix Methods of Structural Analysis and Design, ed. by R.H. Gallagher, Y. Tamada, and J.T. Oden, University of Alabama Press, 1971.

2. Edwards, N.W., "A Procedure for the Dynamic Analysis of Thin Walled Cylindrical Storage Tanks Subjected to Lateral Ground Motion," Ph.D. Dissertation, University of Michigan, Ann Arbor, Michigan, 1969.

3. Kraus, H., Thin Elastic Shells, John Wiley & Sons, New York, 1967.

4. Leissa, A.W., Vibration of Shells, NASA-SP-288, Washington, D.C., 1973.

5. Ogibalov, P.M., Dynamics and Strength of Shells, translated from Russian as NASA TT-F-284, 1966.

6. Ruiz, P., and Penzien, J., "Artificial Generation of Earthquake Accelerograms," Program available as PSEQGN from the National Information Service, Earthquake Engineering, Computer Program Applications, University of California, Berkeley, California 94720.

7. Sanders, J.L., Jr., "An Improved First Approximation for Thin Shells," NASA TR-R24, 1959.

8. Seide, P., Small Elastic Deformation of Thin Shells, Noordhoff International Publishing, Leyden, The Netherlands, 1975.

9. Shaaban, S.H., and Nash, W.A., "Response of an Empty Cylindrical Ground Supported Liquid Storage Tank to Base Excitation," University of Massachusetts, Amherst, Mass. report to the National Science Foundation, August 1975.

10. Warburton, G.B., Dynamics of Shells, Department of Mechanical Engineering, University of Toronto, TP 7307, 1973.

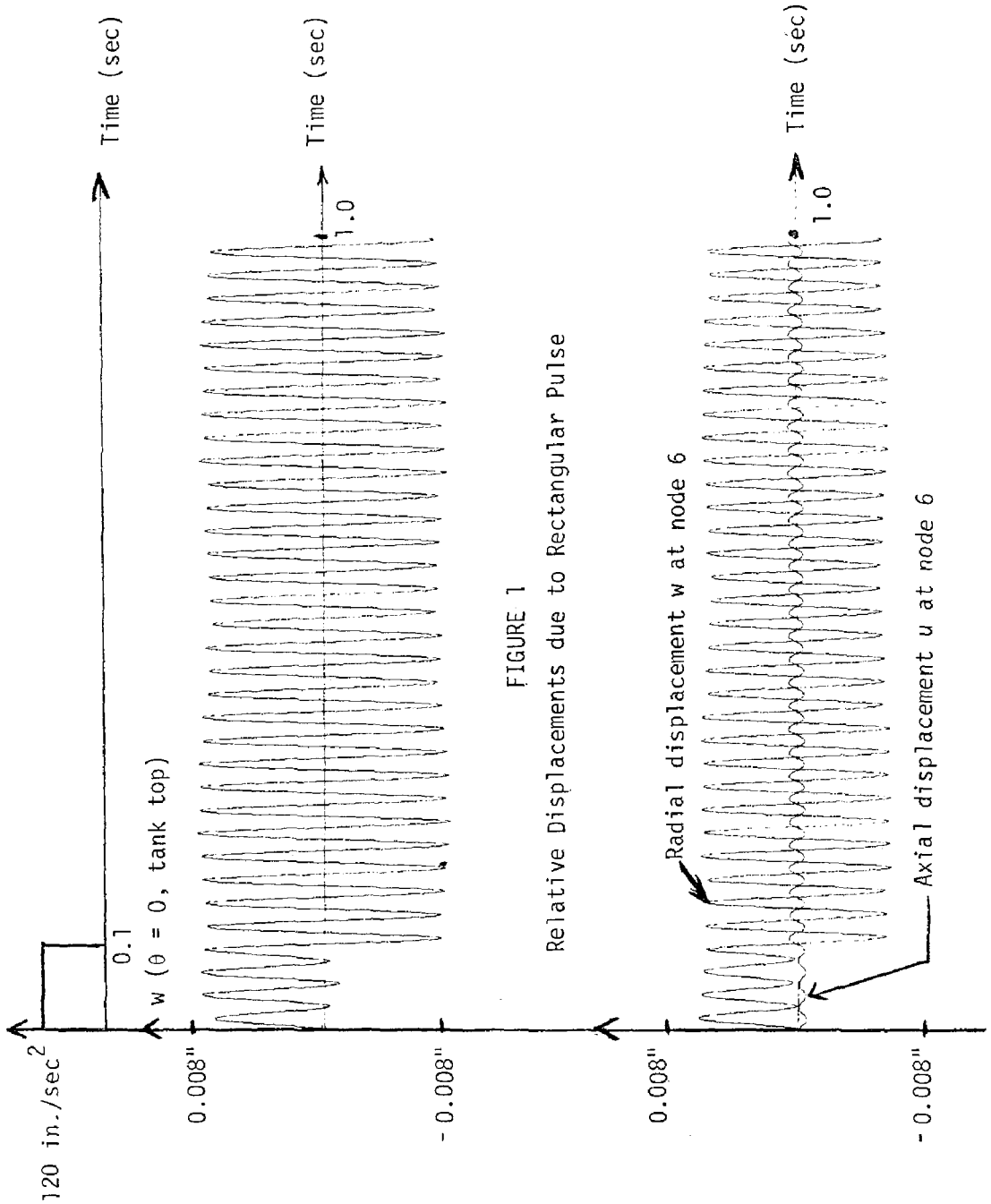

FIGURE 1

Relative Displacements due to Rectangular Pulse

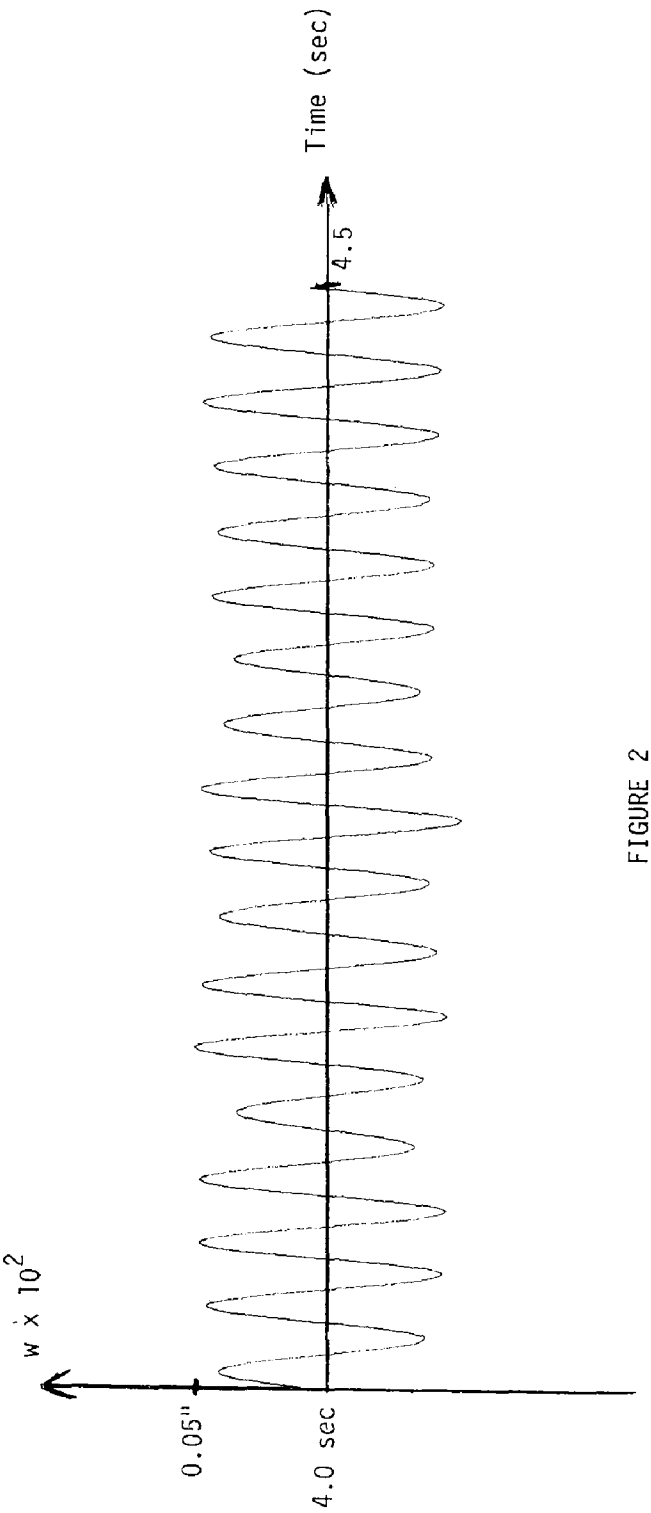

FIGURE 2

Relative Radial Displacement of Tank Top ($\theta = 0$) with Respect to Rigid Slab. Artificial Earthquake Excitation.

INTERNATIONAL SYMPOSIUM ON
EARTHQUAKE STRUCTURAL ENGINEERING
St. Louis, Missouri, USA, August, 1976

SEISMIC DESIGN OF LIQUID STORAGE TANKS TO EARTHQUAKES

P. C. CHEN and R. B. BARBER

Engineering Specialists

Scientific Development, Bechtel Corporation

San Francisco, California, 94119, U.S.A.

SUMMARY

A rigorous and experimentally verified technique (Bauer) which finds the solution to the Laplace equation and satisfies the boundary conditions for hydrodynamic problems was compared with the current tank seismic design procedures (Housner). The current tank design procedures were developed using an approximate approach which did not consider the usual procedures of determining velocity potentials for hydrodynamic problems. Also, it only considered the first mode frequency of fluid oscillation.

Factors included in the comparison were fluid oscillation frequencies, fluid dynamic pressures, equivalent mechanical models, and tank base moments. The NRC seismic design spectra were used in the comparison as the design earthquakes. The results show that for cylindrical tanks, the current design approach generally gives smaller tank base moments than the rigorous approach. For rectangular tanks, the differences in tank base moments between those two approaches are small.

Based upon above results, improved techniques were developed for tank seismic design. These simplified techniques use the rigorous approach for tank analysis and consider higher mode frequencies of fluid oscillation. Parameter charts were also developed which greatly facilitate the seismic analysis and design of liquid storage tanks.

INTRODUCTION

The serious damage suffered by storage tanks in recent earthquakes (4, 8, 10) demonstrates the need for reinvestigating currently used approaches in designing tanks to resist fluid dynamic forces induced by earthquakes. The need is further intensified when one realizes that the spent fuel pool, radioactive storage tanks, and suppression chambers of nuclear power plants are designed using these same approaches. The approaches are based on the assumptions that the tank is rigid and only the first sloshing mode is present in the dynamic analysis (7, 13). The analysis itself is carried out by an approximate method which avoids the usual procedures of finding a solution to the Laplace equation that satisfies the boundary conditions for hydrodynamic problems.

Since the publication of currently used oil storage tank design procedures in 1957 (7), very little research work has been done concerning sloshing forces in civil-type structures. In the meantime, the state of the art has been advanced in the space industry through efforts to minimize the effect of propellant sloshing on the stability of space vehicles (1, 3, 6). The analysis of propellant sloshing is rigorous, and the results for cylindrical tanks have been experimentally verified (2).

The nature of space vehicle propellant sloshing and fixed storage tank liquid sloshing is the same except for the cause of liquid disturbance. For the former, the disturbances are gust loads and the motion of space vehicles; for the latter, the disturbances are caused by earthquakes. Therefore, it is desirable to compare the techniques for space vehicle fuel tank design with the current design approaches for liquid storage tanks in order to determine the adequacy of the latter. Because the formulations of and solutions to the problem of liquid sloshing inside a flexible tank are extremely complex and its analysis is still in the developmental stage (5, 11, 14), the comparison is restricted to the motions of a contained fluid inside rigid tanks.

This paper compares the results of design procedures for both rectangular and cylindrical space vehicle fuel tanks and oil storage tanks. Based on this comparison, improved techniques are suggested for the seismic design of oil storage tanks. Parameter charts which facilitate the seismic analysis and design of such tanks are also developed.

BACKGROUND

The formulation of and solution to the general problem of fluid oscillations in a laterally moving tank are extremely difficult. The assumptions generally employed in such a theoretical analysis are that the tank is rigid, the fluid is homogeneous, incompressible and nonviscous, the flow is irrotational, and the displacements, velocities and and slopes of the fluid surface are small.

The assumption of irrotational flow insures the existence of a single-value velocity potential in a simply connected region, from which the velocity can be derived. Using the equations of motion for a particle in a nonviscous fluid and considering the mass conservation and incompressibility, the velocity potential is the solution to the Laplace equation.

With the boundary conditions that the normal velocity at the interface of the fluid surface and tank wall equals the normal velocity of the fluid particle at that point, the surface pressure is zero, and the fluid particles must stay on the surface, the velocity potential is then determined. The velocity components, pressure distributions, and the fluid surface displacement are then obtained from the known velocity potential. The forces and moments acting on the tank are determined by appropriate integrations of pressure (12).

Using the above basic theory, Graham and Rodriquez (6) derived equations which determine the frequencies, surface displacements, pressures, and forces associated with fluid sloshing in rectangular tanks. Bauer (3) derived the equivalent equations for cylindrical tanks. The tank geometry and coordinate system for the rectangular and cylindrical tanks are shown in Figures 1 and 2 respectively.

The complexity of the solution to the sloshing problem in laterally moving tanks resulted in Housner's (7) approximate approaches. These approaches are based upon the simplification that the pressures acting on the tank during lateral sloshing can be separated into impulsive and convective components (Figure 3). With the separation of pressures into two parts, each part is developed separately so that the usual procedures of determining velocity potentials for hydrodynamic problems are not used. Also, only the first vibration mode of the fluid is considered in the analysis.

The formulas for frequencies, pressures and surface displacements for both the rectangular and cylindrical tanks using the different approaches are summarized respectively in Tables 1 and 2.

The oscillatory motion of fluid in a tank may be near resonance with the motion of the supporting structure and thus may lead to dynamic instabilities or structural failure. In order to minimize possible structural failure and realistically determine the coupled structural response through dynamic analysis, it is sometimes desirable to replace the fluid with a dynamically equivalent mechanical system and combine it with the structural model. This dynamic equivalence is taken in the sense of equal frequencies, masses, resultant forces, and moments acting on the tank walls and bottom. The dynamically equivalent mechanical model for fluid sloshing normally consists of a series of springs and masses attached at specified heights from the tank base, in the plane of symmetry and in the direction of base excitation.

The equivalent mechanical models for lateral sloshing in the rectangular tanks are summarized in Table 3. Their detailed derivations, are given in References 6 and 13. The diagrams of the equivalent mechanical models are shown in Figure 4 for both the Graham and Rodriquez approach and the Housner approach. Similarly, the equivalent mechanical models for lateral sloshing in cylindrical tanks are summarized in Table 4, and their derivations are given in References 3 and 13. The diagrams of the equivalent mechanical models for both the Bauer and the Housner approaches for cylindrical tanks are similar to those for the rectangular tank and are shown in Figure 5.

COMPARISON OF TANK DESIGN TECHNIQUES

Tank design techniques for both the rectangular and the cylindrical space vehicle propellant tanks and oil storage tanks were compared using the Graham and Rodriquez (G&R), Bauer, and Housner approaches. The comparison included frequencies, pressures and tank base moments. Since the resulting moments about the tank base are obtained by the integration of pressures, the results of pressure comparisons are seen from the comparison of resulting moments. The equivalent mechanical models were used to compute the base moments.

(a) Rectangular Tanks

The first mode frequency comparison for two families of rectangular tanks for both the G&R and Housner approaches is given in Table 5. The predicted frequencies are almost identical for the two methods. No higher mode frequencies were compared since Housner's approach gives only the first mode frequency.

Figure 7 compares the resulting tank base moments for the two families of tanks studied. One set of lines in Figure 7 (identified by a=16') is for the family of tanks with a fixed tank width of 16 feet. Moments from the G&R approach and both the IBP (which includes bottom pressures) and EBP (which excludes bottom pressures) cases of the Housner approach are labeled in the figure. The NRC design spectram (9), Figure 6, were used for computing the moments due to sloshing masses for both the G&R and Housner approaches. A fluid damping value of 0.5% and a maximum ground acceleration of 1.0g were assumed. It is interesting to note that for the family of tanks studied, the results of the G&R approach lie between those of the IBP and EBP cases of the Housner approach. The other set of lines in Figure 7 (identified by h=20') is for the family of tanks with a fixed tank height of 20 feet. The results show that moments from the G&R approach have a near constant value, while the Housner approach tends toward a constant moment--close to that moment given by the G&R method--as the tank aspect ratio increases. For tank aspect ratios smaller than 0.5, the Housner approach gives excessively large IBP moments.

(b) Cylindrical Tanks

The first mode frequency comparison of two families of cylindrical tanks for both the Bauer and Housner approaches is shown in Table 6. The comparison shows almost identical results. The higher mode frequencies could not be compared since Housner's approach only gives the first mode frequency.

A comparison of resulting tank base moments for two families of cylindrical tanks is shown in Figure 8. The curves in Figure 8 (identified by D=16') are for tanks with a fixed tank diameter of 16 feet. The results obtained using the Bauer approach and the IBP and EBP cases of the Housner approach are so labeled. The NRC design spectrum with a 0.5% damping value and a maximum ground acceleration of 1.0 g was used for determining the moments due to the sloshing masses. The results show that, except for tank aspect ratios smaller than 1.0, the Bauer approach gives larger moments than the Housner approach.

The curves in Figure 8 (identified by h=20') are for the family of tanks with a fixed tank height of 20 feet. The moments predicted by the Bauer approach at first increase as the tank aspect ratio increases and then approach a constant value. For tank aspect ratios smaller than 0.5, the Housner approach gives unreasonably large IBP moments. For tank aspect ratios larger than 1.0, both the IBP and EBP moments tend to be constant.

The comparison of tank design techniques indicates that for cylindrical tanks, the current design technique (Housner's approach) generally gives smaller base moments than the experimentally verified Bauer approach. A difference of 15% in base moments has been observed (Figure 8). For rectangular tanks, the G&R and Housner approaches generally give only small differences in base moments as shown in Figure 7. This is not surprising, since the Housner approach was developed after the G&R approach was published and used the G&R results for verification (7). For tank aspect ratios smaller than 0.5, the Housner approach gives excessively large IBP moments for both the rectangular and cylindrical tanks. In view of these observations, the more rigorous G&R and Bauer approaches should be used to achieve more reliable tank designs.

DESIGN CHARTS

In order to facilitate tank design using the G&R and Bauer approaches, several design charts were developed. Figure 9, 10, and 11 give the frequencies, masses, and mass locations in the tank for the equivalent mechanical model of lateral sloshing in rectangular tanks. The approximate base moments for rectangular tanks with aspect ratios between 0.25 and 6.0 are shown in Figure 12. The frequencies, masses and mass location in the tank for the equivalent mechanical model of lateral sloshing in cylindrical tanks are given in Figures 13, 14 and 15. The approximate base moments for cylindrical tanks with aspect ratios between 0.25 and 6.0 are shown in Figure 16. The base moments from these charts are at most 10% smaller than the base moments obtained for a rigorous dynamic analysis using the NRC design spectra with a 1.0 g maximum horizontal ground acceleration. If the ground acceleration is smaller than 1.0 g, the tank base moments for these charts should be scaled down proportionally.

CONCLUSION

The comparison of tank design techniques indicates that for cylindrical tanks, the current design technique (Housner approach) generally provides smaller tank base moments than the experimentally-verified Bauer approach. A difference of 15% in base moments has been observed. In rectangular tanks, there is a small difference in tank base moments calculated using the Graham and Rodriguez (G&R) approach as compared to those obtained by the Housner approach. The difference in base moments also reflects the difference in dynamic pressures. Very little difference in the first mode oscillating fluid frequency was observed.

Because of these observations, the more rigorous G&R and Bauer approaches are suggested to be used to achieve more reliable tank design. Design charts are developed to facilitate the use of these approaches for the design of tanks subjected to earthquakes.

REFERENCES

1. Abramson, H.N. ed., "The Dynamic Behavior of Liquids in Moving Containers," NASA SP-106, 1966.
2. Abramson, H.N. et al., "Wall Pressure Distributions During Sloshing in Rigid Tanks," ARS J. Vol. 31, No. 4, April 1961.
3. Bauer, H.F., "Fluid Oscillations in the Containers of a Space Vehicle and Their Influence Upon Stability," NASA TR R-187, 1964.
4. Bug, G. V. and Stratta, J.L., "Anchorage and the Alaska Earthquake of 1964," American Iron and Steel Institute, July, 1974.
5. Cooperative Research Program on the Response of Liquid-filled Storage Tanks to Earthquake Excitation. Current research activity at the University of California, Berkeley, California.
6. Graham, E.W. and Rodriguez, A.M., "The Characteristics of Fuel Motion Which Affect Airplane Dynamics," J. Appl. Mech., Vol. 19, No. 3, September 1952.
7. Housner, G.W., "Dynamic Pressure on Accelerated Fluid Containers," BSSA, Vol. 47, No. 1, January 1957.
8. Husid, R. et al., "Damage Effects and Strong Motions Due to the Lima, Peru, Earthquake of October 3, 1974," the 71st Annual Meeting of the Seismological Society of America, March 1975.
9. Regulatory Guide 1.60, "Design Response Spectra for Seismic Design of Nuclear Power Plants," Directorate of Regulatory Standards, U.S. NRC, October, 1973.
10. Rinne, J.E., "Oil Storage Tanks," The Prince William Sound Earthquake 1964 and Aftershocks, Vol. II, part A, U.S. Department of Commerce, 1967.
11. Shabaan, S.H. and Nash, W.A., Response of an Empty Cylindrical Ground Supported Liquid Storage Tank to Base Excitation, Engineering Research Institute, University of Massachusetts, Amherst, Massachusetts, August, 1975.
12. Stoker, J.J., Water Waves, Interscience Publishers Inc., New York, 1957.
13. TID 7024, Nuclear Reactors and Earthquakes, US AEC, 1963.
14. Wu, C.I., et al., "Response of Ground Supported Liquid Storage Tanks to Seismic Excitation," Proceedings of the U.S. National Conference on Earthquake Engineering, Ann Arbor, Michigan, 1975.

Table 1. Frequency, Dynamic Pressure, and Free Surface Displacement - Rectangular Tank

	Graham and Rodriguez	Housner
Natural Frequency	$\omega_n^2 = g(2n+1)\frac{\pi}{a}\tanh\left[(2n+1)\pi\frac{h}{a}\right]$	$\omega^2 = \sqrt{\frac{5}{2}}\frac{g}{l}\cdot\tanh\left(\sqrt{\frac{5}{2}}\frac{h}{l}\right)$
Excitation	$X_0 \sin\omega t$	Acceleration $\ddot{x}_0$
Pressure on the Wall	$\rho X_0\omega^2\sin\omega t\left\{\frac{a}{2}+\sum_{n=0}^{\infty}(-1)^n\frac{4a}{\pi^2(2n+1)^2}\cdot\left(\frac{\omega^2}{\omega_n^2-\omega^2}\right)\cdot\frac{\sin\left[(2n+1)\frac{\pi}{2}\right]\cosh\left[(2n+1)\frac{\pi}{a}(z+\frac{h}{2})\right]}{\cosh\left[(2n+1)\pi\frac{h}{a}\right]}\right\}$	$\rho\ddot{x}_0 h\left[\frac{y}{h}-\frac{1}{2}\left(\frac{y}{h}\right)^2\right]\sqrt{3}\cdot\tanh\left(\sqrt{3}\frac{l}{h}\right)$ (IMPULSIVE) $\rho\frac{l}{3}\left(\frac{5}{2}\right)\cdot A\omega^2\sin\omega t\cdot\frac{\cosh\left(\sqrt{\frac{5}{2}}\frac{y}{l}\right)}{\cosh\left(\sqrt{\frac{5}{2}}\frac{h}{l}\right)}$ (CONVECTIVE)
Pressure on the Bottom	$\rho X_0\omega^2\sin\omega t\left\{\frac{x}{2}+\sum_{n=0}^{\infty}(-1)^n\frac{4a}{\pi^2(2n+1)^2}\cdot\left(\frac{\omega^2}{\omega_n^2-\omega^2}\right)\cdot\frac{\sin\left[(2n+1)\frac{\pi}{a}x\right]}{\cosh\left[(2n+1)\frac{\pi}{a}h\right]}\right\}$	$\rho\ddot{x}_0 h\left(\sqrt{\frac{3}{2}}\right)\frac{\sinh\left(\sqrt{3}\frac{y}{h}\right)}{\cosh\left(\sqrt{3}\frac{l}{h}\right)}$ (IMPULSIVE) $\rho\frac{l}{2}\left(\frac{5}{2}\right)A\omega^2\sin\omega t\left[\frac{y}{l}-\frac{1}{3}\left(\frac{y}{l}\right)^3\right]\frac{1}{\cosh\left(\sqrt{\frac{5}{2}}\frac{h}{l}\right)}$ (CONVECTIVE)
Free Surface Displacement	$X_0\frac{\omega^2}{g}\sin\omega t\left\{x+\sum_{n=0}^{\infty}(-1)^n\frac{4a}{\pi^2(2n+1)^2}\cdot\left(\frac{\omega^2}{\omega_n^2-\omega^2}\right)\cdot\sin\left[(2n+1)\frac{\pi}{a}x\right]\right\}$	$d_{max} = \frac{0.527 l}{\left(\frac{g}{\omega^2\theta_1 R}-1\right)\tanh(1.58\frac{h}{l})}$ $\theta_1^2 = 1.58\frac{A}{l}\cdot\tanh(1.58\frac{h}{l})$
	X_0 = MAXIMUM AMPLITUDE OF EXCITATION	A = MAXIMUM FLUID OSCILLATION AMPLITUDE

Table 2. Frequency, Dynamic Pressure, and Free Surface Displacement - Cylindrical Tank

	Bauer	Housner
Natural Frequency	$\omega_n^2 = \frac{g}{a}\epsilon_n\cdot\tanh(\epsilon_n\frac{h}{a})$	$\omega_0^2 = \frac{1.84}{R}\cdot g\cdot\tanh(1.84\frac{h}{R})$
Excitation	$X_0 e^{i\Omega t}$	Acceleration $\ddot{x}_0$
Pressure on the Wall	$\rho\Omega^2 X_0 e^{i\Omega t}\cdot a\left\{\frac{r}{a}+\sum_{n=0}^{\infty}\frac{2\cdot J_1(\rho_n)\eta_n^2\cdot\cosh(K_n\frac{z}{a})}{(\epsilon_n^2-1)\cdot J_1(\epsilon_n)\cdot(1-\eta_n^2)\cosh(K_n)}\right\}$	$\rho\ddot{x}_0 h\left[\frac{y}{h}-\frac{1}{2}\left(\frac{y}{h}\right)^2\right]\sqrt{3}\tanh\left(\sqrt{3}\frac{l}{h}\right)$ (IMPULSIVE) $\rho R(0.63)A\omega^2\sin\omega t\cdot\frac{\cosh(1.84\frac{y}{R})}{\cosh(1.84\frac{h}{R})}$ (CONVECTIVE)
Pressure on the Bottom	$\rho\Omega^2 X_0 e^{i\Omega t}\cdot a\left\{\frac{r}{a}+\sum_{n=0}^{\infty}\frac{2\cdot J_1(\rho_n)\cdot\eta_n^2}{(\epsilon_n^2-1)\cdot J_1(\epsilon_n)\cdot(1-\eta_n^2)\cosh(K_n)}\right\}$	$\rho\ddot{x}_0 h\left(\sqrt{\frac{3}{2}}\right)\frac{\sinh\left(\sqrt{3}\frac{y}{h}\right)}{\cosh\left(\sqrt{3}\frac{h}{h}\right)}$ (IMPULSIVE) $\rho R(0.94)A\omega^2\sin\omega t\left[\frac{y}{R}-\frac{1}{2}\left(\frac{y}{R}\right)^3\right]\frac{1}{\cosh(1.84\frac{l}{R})}$ (CONVECTIVE)
Free Surface Displacement	$\Omega^2\frac{a}{g}X_0 e^{i\Omega t}\left\{\frac{r}{a}+\sum_{n=0}^{\infty}\frac{2\cdot J_1(\rho_n)\eta_n^2}{(\epsilon_n^2-1)\cdot J_1(\epsilon_n)(1-\eta_n^2)}\right\}$	$d_{max} = \frac{0.408 R}{\left(\frac{g}{\omega^2\theta_1 R}-1\right)\tanh(1.84\frac{h}{R})}$ $\theta_1^2 = 1.534\frac{A}{R}\cdot\tanh(1.84\frac{h}{R})$
	X_0 = MAXIMUM AMPLITUDE OF EXCITATION	A = MAXIMUM FLUID OSCILLATION AMPLITUDE

Table 3. Equivalent Mechanical Model for Lateral Sloshing - Rectangular Tank

	Graham and Rodriguez	Housner
Natural Frequency	$\omega_m^2 = g_l (2m+1)\frac{\pi}{a} \cdot \tanh[(2m+1)\pi r_1]$	$\omega_1^2 = \frac{1.58}{l} \cdot g \cdot \tanh(1.58 \frac{h}{l})$
Spring Constant	$K_m = m_m \omega_m^2$	$K_1 = m_1 \omega_1^2$
Rates of Slosh Mass to Fluid Mass	$\frac{m_m}{m_F} = \frac{8 \tanh[(2m+1)\pi r_1]}{\pi^3 (2m+1)^3 r_1}$	$\frac{m_1}{m_F} = 0.527 (\frac{l}{h}) \tanh(1.58 \frac{h}{l})$
Rates of Fixed Mass to Fluid Mass	$\frac{M_0}{m_F} = 1 - \sum_{m=0}^{\infty} \frac{m_m}{m_F}$	$\frac{M_0}{m_F} = \frac{\tanh(\sqrt{3}\frac{l}{h})}{\sqrt{3}\frac{l}{h}}$
Rates of Slosh Mass Height to Fluid Depth	$\frac{h_m}{h} = 1 - \frac{\tanh[(2m+1)\frac{\pi}{2} r_1]}{(2m+1)\frac{\pi}{2} r_1}$	$\frac{h_1}{h} = 1 - \frac{\cosh(1.58\frac{h}{l}) - 1}{1.58(\frac{h}{l}) \cdot \sinh(1.58\frac{h}{l})}$ (EBP) $\frac{h_1}{h} = 1 - \frac{\cosh(1.58\frac{h}{l}) - 2}{1.58(\frac{h}{l}) \cdot \sinh(1.58\frac{h}{l})}$ (IBP)
Ratio of Fixed Mass Height to Fluid Depth	$\frac{h_0}{h} = \frac{1}{2} - \frac{1}{(\frac{M}{m_F})} \sum_{m=0}^{\infty} \frac{m_m}{m_F} \cdot \frac{h_m}{h}$	$\frac{h_0}{h} = \frac{3}{8}$ (EBP) $\frac{h_0}{h} = \frac{1}{8}\left\{ \frac{4\sqrt{3}\frac{l}{h}}{\tanh(\sqrt{3}\frac{l}{h})} - 1 \right\}$ (IBP)
	$r_1 = \frac{h}{a}$ m_F = TOTAL FLUID MASS	EBP-EXCLUDING BOTTOM PRESSURE; IBP-INCLUDING BOTTOM PRESSURE

Table 4. Equivalent Mechanical Model for Lateral Sloshing - Cylindrical Tank

	Bauer	Housner
Natural Frequency	$\omega_m^2 = \frac{g}{a} \cdot \epsilon_m \cdot \tanh(\epsilon_m \frac{h}{a})$	$\omega_1^2 = \frac{1.84}{R} \cdot g \cdot \tanh(1.84 \frac{h}{R})$
Spring Constant	$K_m = m_m \omega_m^2$	$K_1 = m_1 \omega_1^2$
Ratio of Slosh Mass to Fluid Mass	$\frac{m_m}{m_F} = \frac{2 \cdot \tanh(\epsilon_m \frac{h}{a})}{\epsilon_m \cdot \frac{h}{a} \cdot (\epsilon_m^2 - 1)}$	$\frac{m_1}{m_F} = 0.318 \cdot \frac{R}{h} \cdot \tanh(1.84 \frac{h}{R})$
Ratio of Fixed Mass to Fluid Mass	$\frac{M_0}{m_F} = 1 - \sum_{m=0}^{\infty} \frac{m_m}{m_F}$	$\frac{M_0}{m_F} = \frac{\tanh(\sqrt{3}\frac{R}{h})}{\sqrt{3}\frac{R}{h}}$
Ratio of Slosh Mass Height to Fluid Depth	$\frac{h_m}{h} = 1 - \frac{2}{\epsilon_m \frac{h}{a}} \cdot \tanh(\epsilon_m \frac{h}{2a})$	$\frac{h_1}{h} = 1 - \frac{\cosh(1.84\frac{h}{R}) - 1}{1.84(\frac{h}{R}) \cdot \sinh(1.84\frac{h}{R})}$ (EBP) $\frac{h_1}{h} = 1 - \frac{\cosh(1.84\frac{h}{R}) - 2}{1.84(\frac{h}{R}) \cdot \sinh(1.84\frac{h}{R})}$ (IBP)
Ratio of Fixed Mass Height to Fluid Depth	$\frac{h_0}{h} = \frac{1}{2} + \frac{1}{\frac{M_0}{m_F}} \sum_{m=0}^{\infty} (\frac{m_m}{m_F})(\frac{h_m}{h})$	$\frac{h_0}{h} = \frac{3}{8}$ (EBP) $\frac{h_0}{h} = \frac{1}{8}\left\{ \frac{4\sqrt{3}\frac{R}{h}}{\tanh(\sqrt{3}\frac{R}{h})} - 1 \right\}$ (IBP)
	ϵ_m = ROOTS OF $J_1'(\epsilon) = 0$	EBP-EXCLUDING BOTTOM PRESSURE; IBP-INCLUDING BOTTOM PRESSURE

Table 5. Comparison of Frequencies, Constant Tank Height, h = 20' Rectangular Tank

HEIGHT / WIDTH	HOUSNER	GRAHAM & RODRIGUEZ
.167	.1018	.1013
.200	.1201	.1195
.250	.1456	.1449
.333	.1834	.1826
.500	.2433	.2424
.667	.2888	.2878
1.00	.3583	.3572
1.33	.4144	.4132
2.00	.5077	.5062
4.00	.7180	.7158

Table 6. Comparison of Frequencies, Constant Tank Height, h = 30' Cylindrical Tank

HEIGHT / DIAMETER	HOUSNER	BAUER
.250	.1347	.1347
.500	.2180	.2180
.750	.2727	.2728
1.00	.3159	.3160
2.00	.4471	.4472
3.00	.5475	.5477
4.00	.6322	.6324
5.00	.7069	.7071
6.00	.7743	.7746

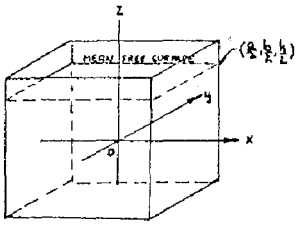

Figure 1. Geometry and Coordinate System, Rectangular Tank, Graham and Rodriguez Approach

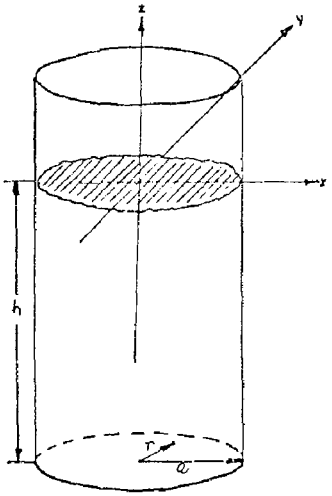

Figure 2. Geometry and Coordinate System, Cylindrical Tank, Bauer Approach

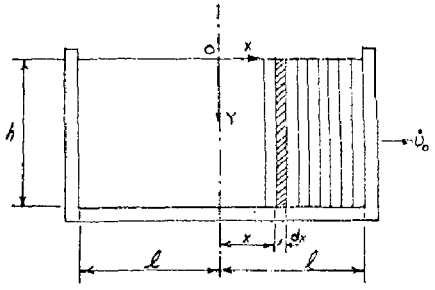

(ℓ = R for cylindrical tank)

(a) Coordinate System for Impulsive Pressure

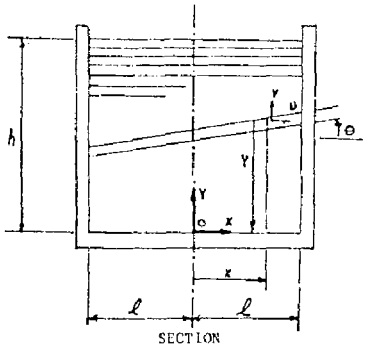

(ℓ = R for cylindrical tanks)

(b) Coordinate System for Convective Pressure

Figure 3. Geometry and Coordinate System, Housner Approach

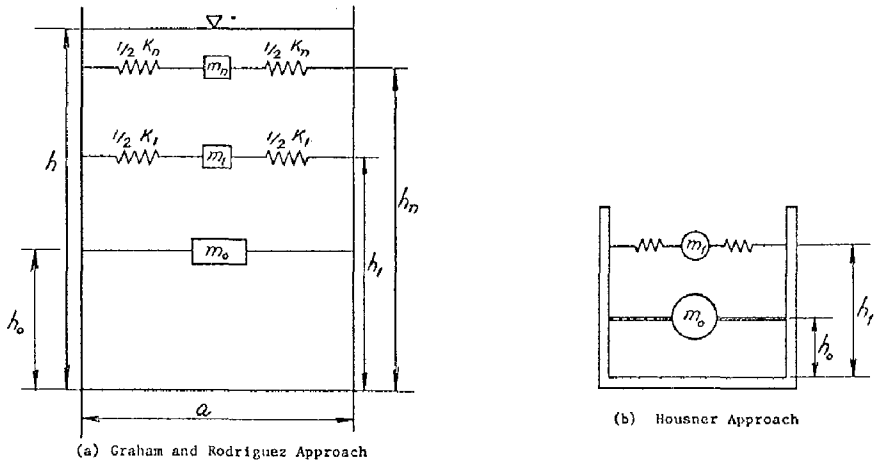

(a) Graham and Rodriguez Approach

(b) Housner Approach

Figure 4. Equivalent Mechanical Models for Rectangular Tanks

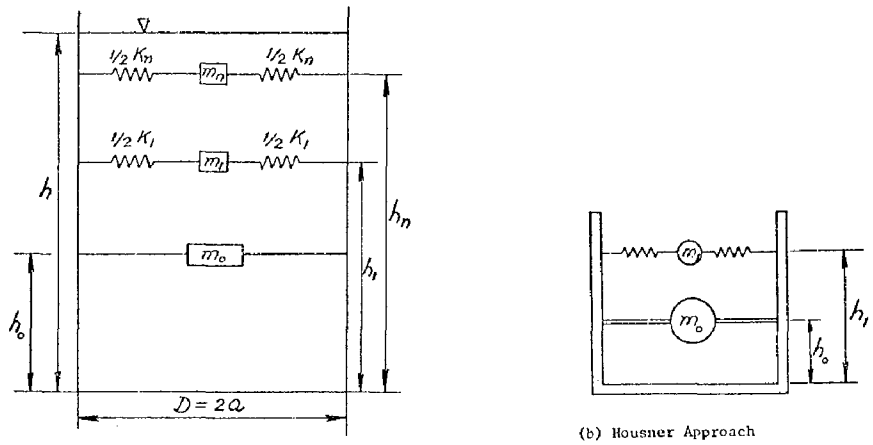

(a) Bauer Approach

(b) Housner Approach

Figure 5. Equivalent Mechanical Models for Cylindrical Tanks

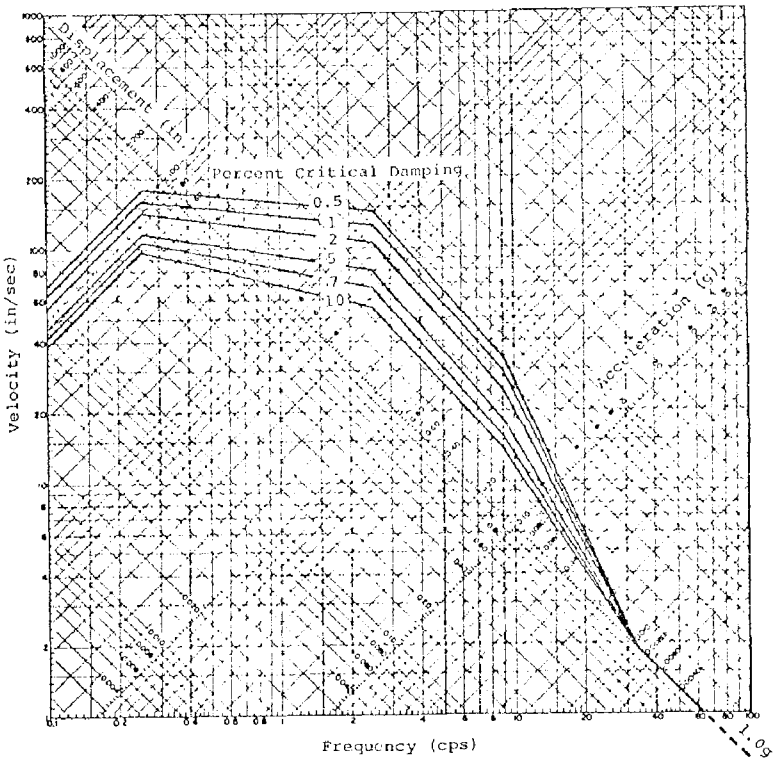

Figure 6. Horizontal Design Spectra For Peak Horizontal Ground Acceleration of 1.0g

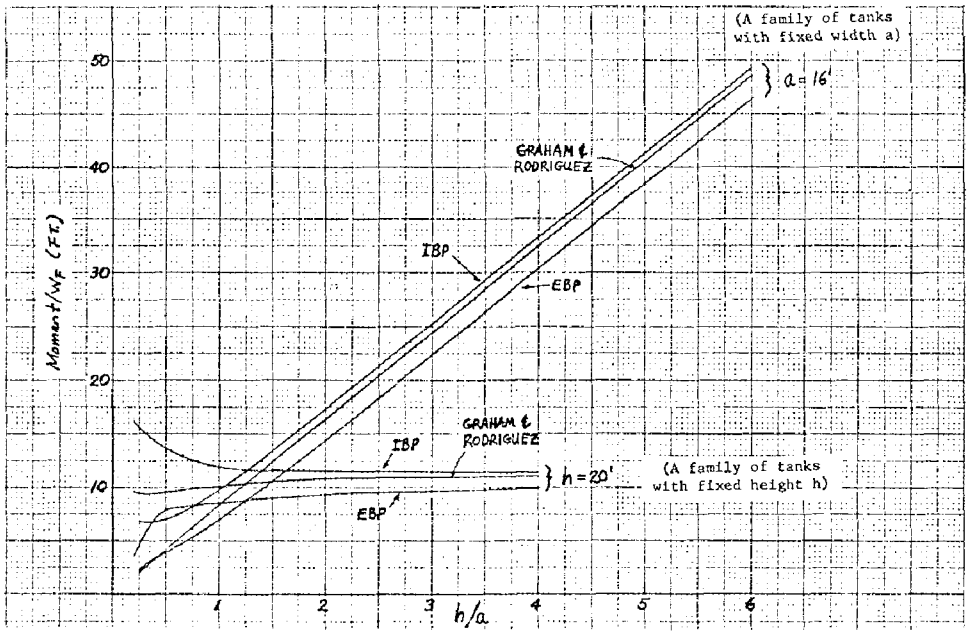

Figure 7. Comparison of Tank Base Moments, Rectangular Tanks

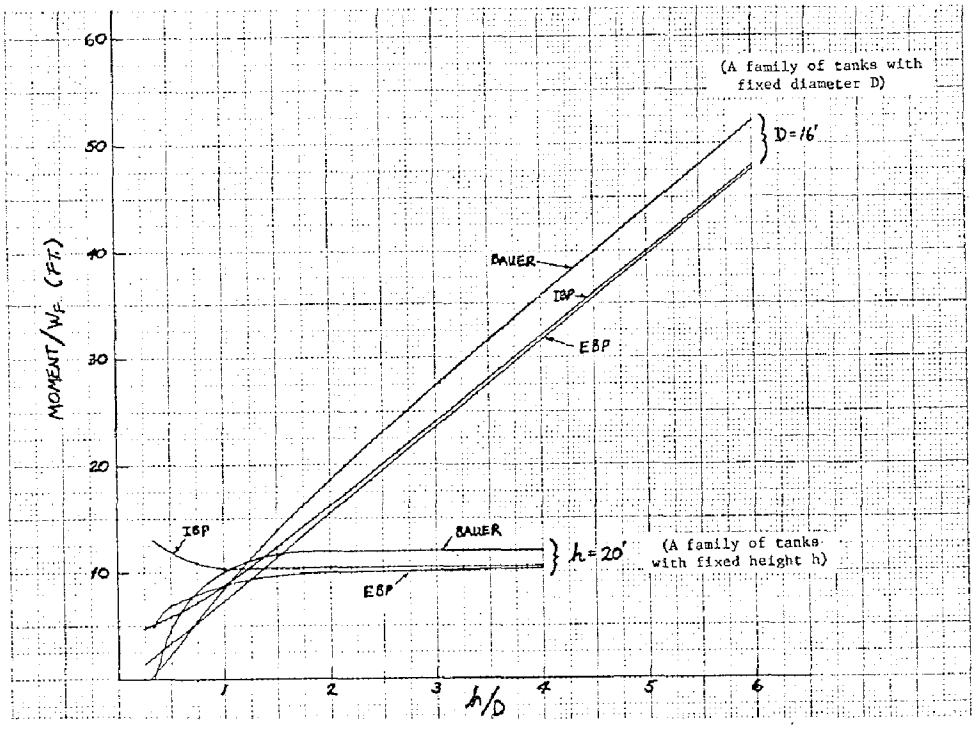

Figure 8. Comparison of Tank Base Moment, Cylindrical Tanks

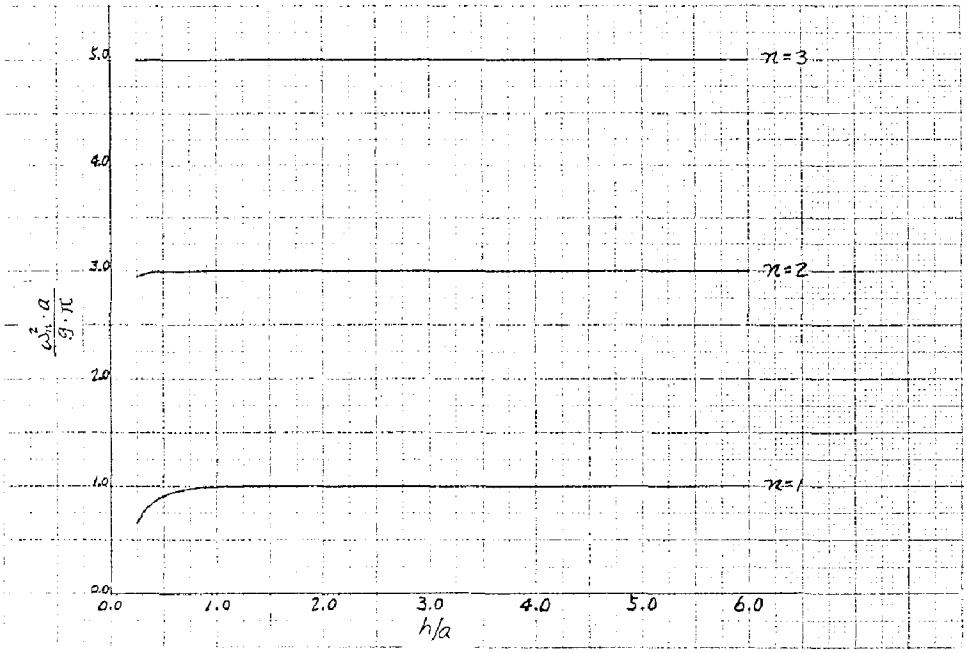

Figure 9. Frequencies of Equivalent Mechanical Mode, Rectangular Tanks

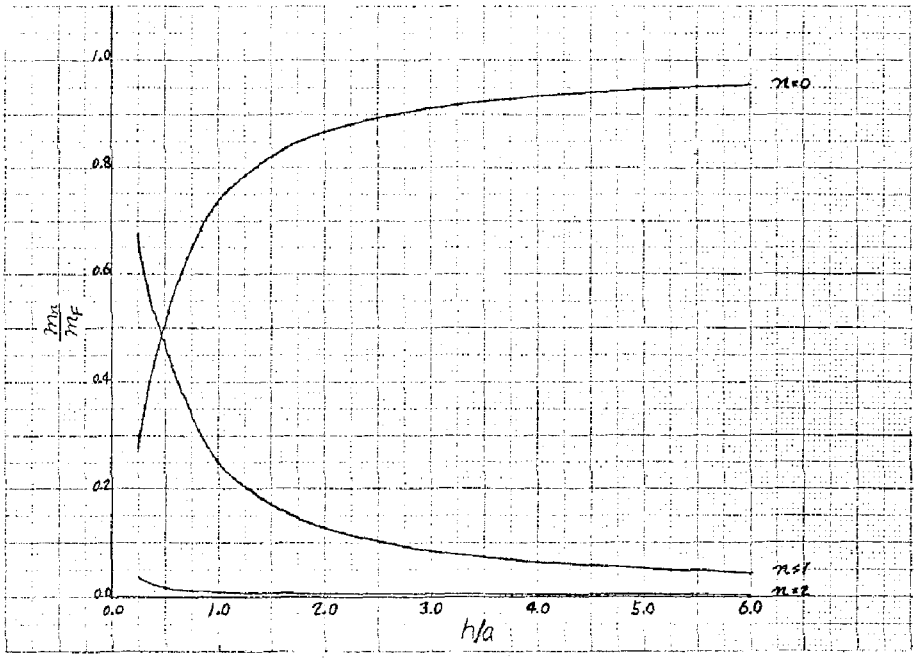

Figure 10. Ratio of Sloshing Masses, Rectangular Tanks

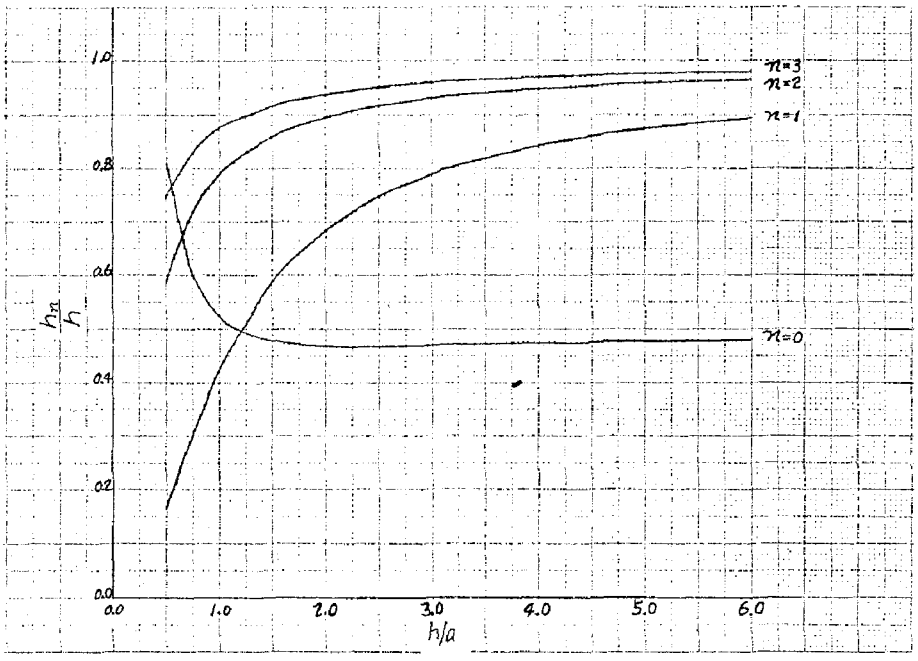

Figure 11. Ratio of Mass Locations, Rectangular Tanks

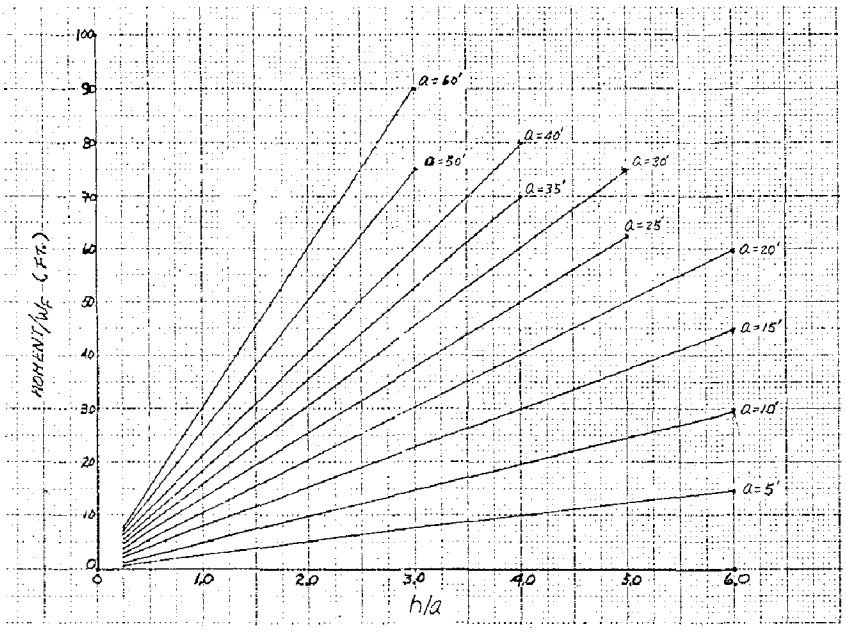

Figure 12. Tank Base Moments, Constant Tank Width, Rectangular Tank

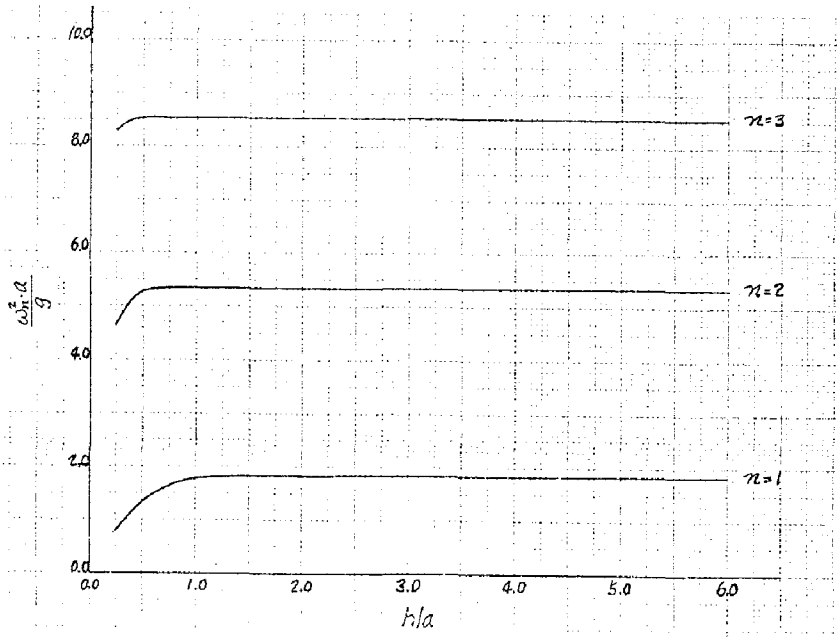

Figure 13. Frequencies of Equivalent Mechanical Model, Cylindrical Tanks

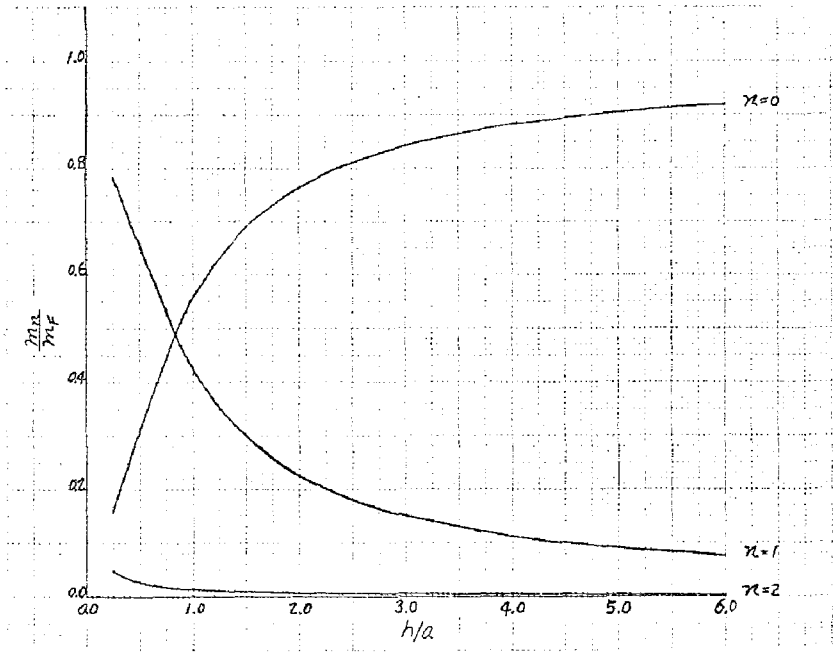

Figure 14. Ratio of Sloshing Masses, Cylindrical Tanks

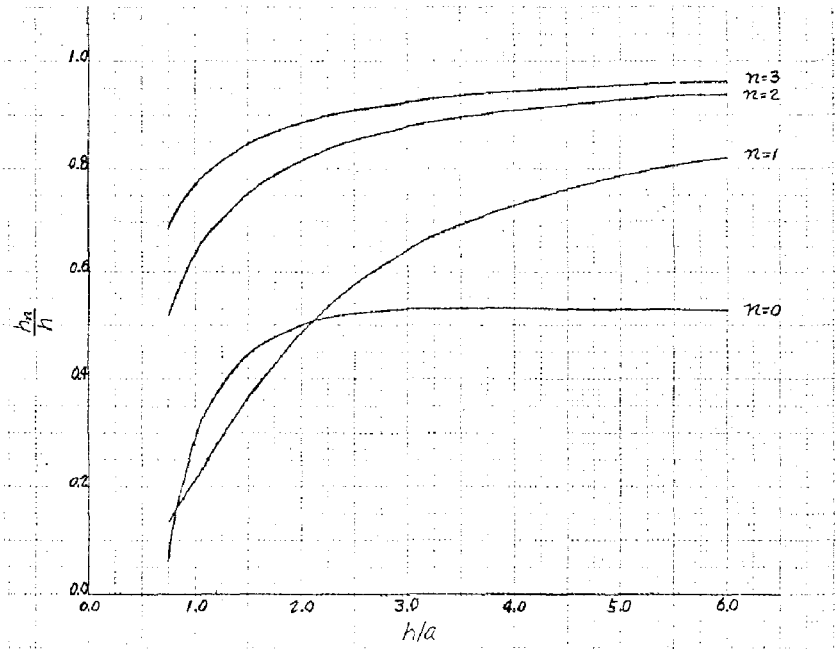

Figure 15. Ratio of Mass Locations, Cylindrical Tanks

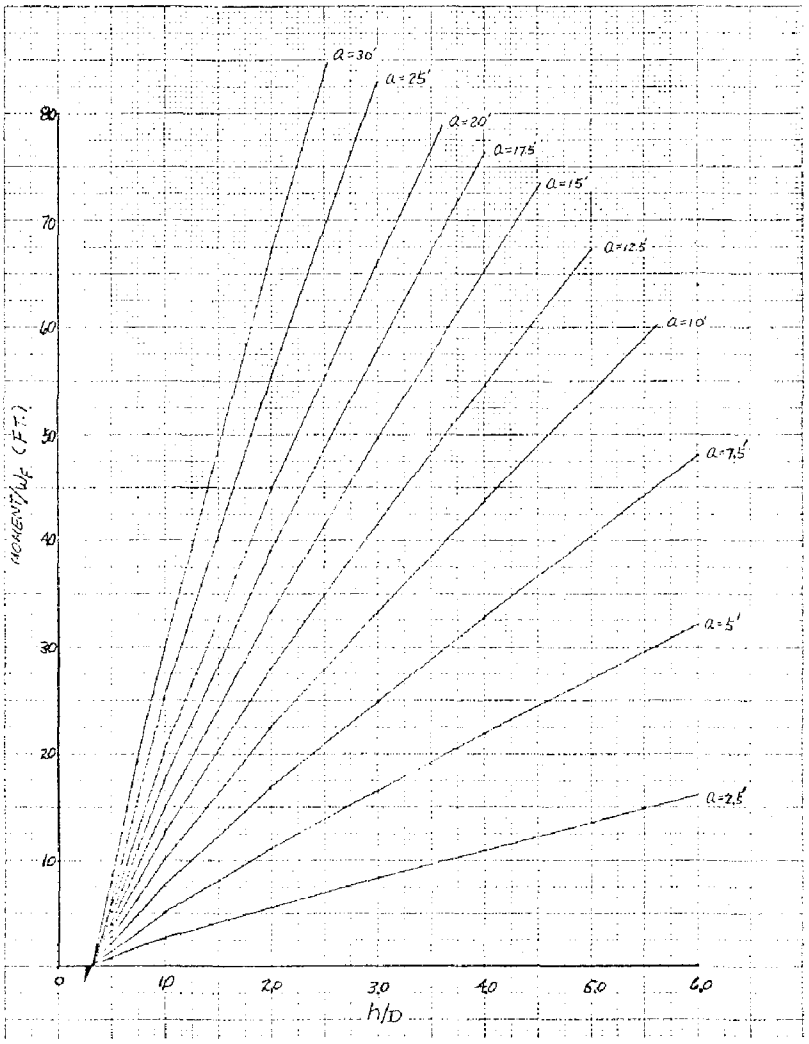

Figure 16. Tank Base Moments, Constant Tank Radius, Cylindrical Tank

INTERNATIONAL SYMPOSIUM ON
EARTHQUAKE STRUCTURAL ENGINEERING
St. Louis, Missouri, USA, August, 1976

ANALYSIS OF NON-UNIFORM COUPLED SHEAR WALLS WITH TWO ROWS OF OPENINGS

A.R.SANTHAKUMAR
Lecturer in Civil Engineering
College of Engineering, Guindy
Madras, India.

SUMMARY

The finite difference method is applied to the solution of coupled shear walls with two or more rows of openings in which properties of beams and walls may vary with height. The method would be useful in analysing shear walls with different boundary conditions, flexible beam wall joints and different pattern of equivalent lateral loads associated with seismic resistant shear wall design. The order of errors introduced on static design quantities is less than 5% for normal coupled shear walls in which the number of storeys is more than six.

INTRODUCTION

In high rise buildings lateral loads resulting from wind and seismic effects are often resisted by a system of shear walls. To evaluate various aspects of behaviour of coupled walls with single row of openings, the laminar analysis has been used (4). In this the beams at each floor level are replaced by a set of infinitesimal elastic laminae of equivalent stiffness. Recently the laminar analysis has been extended to shear walls in which both beam and wall properties vary with height (5). For a set of three symmetrical walls supported on a base structure, which is symmetrical with respect to both geometry and force-deformation characteristics, the analysis may be performed using charts (1). Also, solutions of the coupled differential equations are available for uniform shear walls coupled by two sets of beams (2). The application of laminar analysis for shear walls coupled by two sets of beams is thus restricted to walls which have uniform properties throughtout the height. This situation may not be true even when the walls are uncracked. In tall walls, in addition to variation of beam and wall dimensions, the percentage of reinforcement in the beams may be varied so that the strength of the coupling system corresponds approximately with the elastic laminar shear distribution along the height (3).

In this paper, a finite difference method is applied to the coupled differential equation thereby enabling the solution of coupled shear walls with two or more rows of openings in which properties of beams and walls may vary with height. This method would be useful in analysing shear walls with different boundary

conditions, flexible beam wall joints and different pattern of equivalent lateral loads associated with seismic resistant shear wall design. Finally, a numerical example illustrates the application of the proposed analysis.

GENERAL THEORY

The analysis uses the basic continuous medium theory. As this method has been well documented (1,4,5), only fundamental assumptions and equations as applied to finite difference formulation of the problem are restated here. A system of three coupled shear walls subjected to lateral load distribution and its mathematical model are shown in Figs.1a and 1b respectively. The dimensional properties of a typical storey N for the proto (at level x from top for the model) are shown in Fig.2. The fundamental assumptions of the technique are

a. Axial deformation of the connecting beams are negligible. Thus, the walls deflect equally. The connecting beams in Span A and B deform with a point of centraflexure at their mid-points.

b. The discrete N-th floor connecting beams of moment of inertia I_{bAN}/and I_{bBN} are replaced by uniform continuous medium of equivalent stiffness I_{bAN}/h_N and I_{bBN}/h_N per unit height where h_N is the N-th storey height. The set of discrete shear forces at points of centraflexure in the beams have thus been replaced by corresponding continuous laminar shear distributions of intensity q_{Ax} and q_{Bx} per unit height in each floor. The various wall actions and deformations contributing to the displacement of the mid-point of a typical lamina are shown in Figs.3 and 4 respectively

In order to set up the differential equation of the problem for Spans A and B, the coupled walls are cut along the centres of the laminae (see Fig.2). The displacements at the cut end of the lamina because of actions on the walls (Fig.3), and due to laminar shear forces including shear deformation and flexible beam wall joints (Fig.4) are expressed and combined. Based on the conditions of equilibrium (Fig.3) and compatibility (Fig.4), the following relationships between the external moment M_{Ox} axial forces in the wall 1,2 and 3 (ie. T_{1x}, T_{2x}, and T_{3x}) and the laminar shear forces in Spans A and B (ie. q_{Ax}, and q_{Bx}) at any level are obtained (5).

$$\int_x^H \frac{l_{Ax}\, M_{Ox}\, dx}{E\, I_{ox}} - \int_x^H \frac{l_{Ax}^2\, T_{1x}\, dx}{E\, I_{ox}} - \int_x^H \frac{l_{Ax}\, l_{Bx}\, T_{3x}\, dx}{E\, I_{ox}}$$

$$- \int_x^H \frac{1}{E} \left(\frac{1}{A_{1x}} + \frac{1}{A_{2x}} \right) T_{1x}\, dx + \int_x^H \frac{T_{3x}\, dx}{E\, A_{2x}}$$

$$- \frac{h_x \, l_{sAx}^3}{12 \, E \, I_{Xx}} \, q_{Ax} = 0 \qquad \ldots \qquad (1)$$

and

$$\int_x^H \frac{l_{Bx} \, M_{ox} \, dx}{E \, I_{ox}} - \int_x^H \frac{l_{Bx}^2 \, T_{3x} \, dx}{E \, I_{ox}} - \int_x^H \frac{l_{Bx} \, l_{Ax} \, T_{1x} \, dx}{E \, I_{ox}}$$

$$- \int_x^H \frac{1}{E} \left(\frac{1}{A_{2x}} + \frac{1}{A_{3x}} \right) T_{3x} \, dx + \int_x^H \frac{T_{1x} \, dx}{E \, A_{1x}}$$

$$- \frac{h_x \, l_{sBx}^3}{12E \, I_{Xx}} \, q_{Bx} = 0 \qquad \ldots \qquad (2)$$

Differentiating the above two equations with respect to x leads to the following two coupled equations:

$$\frac{d^2 T_{Ax}}{dx^2} + \frac{d \, \phi_{Ax}}{\phi_{Ax} \, dx} \frac{dT_{Ax}}{dx} - \alpha_{AX}^2 \, T_{Ax} - 4^2_x T_{Bx}$$

$$= \gamma_{Ax} \, M_{ox} \qquad \ldots \qquad (3)$$

and

$$\frac{d^2 T_{Bx}}{dx^2} + \frac{d\phi_B}{\phi_B \, dx} \frac{dT_{Bx}}{dx} - \alpha_{Bx}^2 \, T_{Bx} - 4^2_x T_{Ax}$$

$$= \gamma_{Bx} \, M_{ox} \qquad \ldots \qquad (4)$$

where $\alpha_{Ax}^2 = \left(\frac{1}{A_{1x}} + \frac{1}{A_{2x}} + \frac{l_{Ax}^2}{I_{ox}} \right) \left(\frac{12 \, I_{Xx}}{h_x \, l_{sx}^3} \right)$

$$\gamma_{Ax} = \frac{12 \, l_{Ax} \, I_{Xx}}{I_{ox} \, h_x \, l_{sx}} \; ; \quad \phi_{Ax} = \frac{h_x \, l_{SAx}^3}{12 \, E \, I_{Xx}}$$

$$4_x^2 = \frac{l_{Ax}\, l_{Bx}}{E\, I_{ox}} - \frac{1}{E\, A_{2x}}$$

$$T_{1x} = \int_x^H q_{Ax}\, dx \quad ; \quad T_{3x} = \int_x^H q_{Bx}\, dx$$

THE RECURRENCE EQUATIONS

The equations 3 and 4 involving the variables ϕ_{Ax}, $_{Ax}$, $_{Ax}$, M_{ox}, , , T_{1x} and T_{3x} are transformed into recurrence equations involving unknown axial forces T_{1x} and T_{3x} at discrete nodal points. Reference may be made to Fig.1b with respect to identification of nodal points. The recurrence equations for nodal points 2n-1 and 2n are:

$$\left[1 - \frac{\phi_{A(2n+1)} - \phi_{A(2n-3)}}{4\,\phi_{A(2n-1)}}\right] T_{A(2n-3)} + (0)\, T_{B(2n-2)}$$

$$+ (h_o^2\, A(2n-1) - 2)\, T_{A(2n-1)} + (h_o^2\, B_{(2n)})\, T_{B(2n)}$$

$$+ \left[1 + \frac{\phi_{A(2n+1)} - \phi_{A(2n-3)}}{4\,\phi_{A(2n-1)}}\right] T_{A(2n+1)} = h_o^2\, C_{(2n-1)} \quad \ldots (5)$$

$$\left[1 - \frac{\phi_{B(2n+2)} - \phi_{B(2n-2)}}{4\,\phi_{B(2n)}}\right] T_{B(2n-2)}$$

$$+ (h_o^2\, D_{(2n-1)})\, T_{A(2n-1)} + (h_o^2\, E_{(2n)} - 2)\, T_{B(2n)}$$

$$+ (0)\, T_{A(2n+1)} + \left[1 + \frac{\phi_{B(2n+2)} - \phi_{B(2n-2)}}{4\,\phi_{B(2n)}}\right] T_{B(2n+2)} = h_o^2\, F_{(2n)}$$

$$\ldots \quad (6)$$

where h = distance between the nodal points, the subscripts A and B correspond to the Spans A and B respectively. The bracketed subscripts correspond to the nodal point numbers. In addition, the following notations have been used to condense the equation:

$A_{(2n-1)} = - \alpha^2_{(2n-1)}$ for Span A at (2n-1)

$B_{(2n)} = - \gamma^2$ at (2n) ; $D_{(2n-1)} = - \gamma^2$ at (2n-1)

$C_{(2n-1)} = \gamma_{(2n-1)} M_{o(2n-1)}$ for span A at (2n-1)

$E_{(2n)} = - \alpha^2_{(2n)}$ for Span B at (2n)

$F_{(2n)} = \gamma_{(2n)} M_{o(2n)}$ for Span B at (2n)

The recurrence equation in the operator form is shown in Fig.5.

Application of these operators to all the nodal points, together with the boundary conditions at the top and bottom of the walls give as many linear, algebraic, simultaneous equations as the unknown values of axial force at the nodes. The other static quantities (ie. laminar shears, shear force in the walls etc.) are obtained using the principles of statics.

LOADING AND BOUNDARY CONDITIONS

Any type of load variation could be accommodated. The external bending moment is expressed in terms of the loads at desired level.

The following boundary conditions have been accommodated (5) into the finite difference form:

(a) At the top of walls

(i) free at top
(ii) with rigid diaphragm at top

(b) At the base

(i) restrained at base
(ii) flexible foundation at base
(iii) hinged base
(iv) hinged base on elastic foundation.

In practice, the loading and boundary conditions may occur in any combination. These can be incorporated into the algebraic equations obtained from applying the recurrence operator to the nodes, before solving for the unknown axial forces.

VERSATALITY OF THE ANALYSIS

The total number of independant unknowns for the problem is equal to the number of nodal points. As the nodal points follow a regular pattern, the input data for the shear wall at nodal points are generated for the storeys in which there is no variation in properties with height. This reduces the total input data. The band width formed by the coefficients of the simultaneous difference equations is only 2r + 1 where r is the number of rows of openings. The banded form of the matrix is taken advantage of in reducing the storage requirement.

The analysis presented above could be made use of to allow for the discrete nature of the coupling beams. For this, near zero beam properties may be assigned for the nodes associated with the openings and relevant beam properties for the nodes associated with the beams. A sensitivity analysis was made to assess the order of errors introduced by this approximate method on the static design quantities. The details of this analysis are reported elsewhere (5). The analysis shows that the order of errors introduced on critical design quantities is less than 5% provided that

(a) The number of storeys is more than 6
(b) The stiffness of walls is comparable to the stiffness of beams ie. $\alpha H > 6$
(c) Spacing of the nodal points is less than half the floor height ie. $h_o < 0.5\ h_N$

NUMERICAL EXAMPLE

A ten storey shear core combining two walls was considered. The properties of the structure and loading are assembled in Table 1. In these examples, the properties of the walls have been assumed to vary in each storey. It is unlikely that in a real structure variation of this type would occur. The example is not intended to simulate a prototype structure but to explain the application and approximations involved in the analysis. However, such property changes could occur in a cracked coupled shear wall. The following three analyses were made.

Analysis A: The properties given in Table 1 were used. The shear wall was analysed by the conventional frame analysis which incorporates finite joints, axial deformation of walls and shear deformation of beams.

Analysis B: The properties given in Table 1 were used. The shear wall was analysed using the finite difference approximation developed in this paper.

Analysis C: Average uniform properties were assumed. For this case also, the shear wall was analysed using finite difference approximation.

The results are presented in Fig.6. The total computer time required to analyse this twin core are 2.48 sec., 1.25 sec. and 120 sec. for analysis A, B and C respectively.

CONCLUSIONS

The finite difference technique is a powerful method of analysis for coupled shear wall structures in which properties vary with height. This analysis requires considerably less computer storage and time than frame analysis. The following variables have been accommodated in the finite difference approximation to the laminar analysis:

(a) Variation of properties of members with height
(b) Variation in storey height
(c) Various boundary conditions and loading
(d) Flexible beam wall joints

The sensitivity analysis shows that the errors are within acceptable limits (5%) for shear walls of more than 6 storey height.

BIBLIOGRAPHY

1. Coull, A. and Chantaksinopas, B., "Design Curves for Coupled Shear Walls on Flexible Bases", Proceedings of the Institution of Civil Engineers, Vol.57, Part 2, Dec. 1974, pp.595-618.

2. Eriksson, O., "Analysis of Wind Bracing Walls in Multi-Storey Housing", Ingenioren, International Edition, Vol.5, No.4, 1961, pp 115-124.

3. Paulay, T., "Reinforced Concrete Shear Walls", New Zealand Engineering, Vol.24, No.10, Oct.1969, pp.315-321.

4. Rosman, R., "Approximate Analysis of Shear Walls subjected to Lateral Loads", Journal ACI., Vol.61, June 1964, pp.717-732.

5. Santhakumar, A.R., "The Ductility of Coupled Shear Walls", Ph.D. Thesis, University of Canterbury, Christchurch, New Zealand, pp. 43-66.

NOTATIONS

A_1, A_2, A_3	Area of walls 1,2 and 3 respectively
A_{bA}, A_{bB}	Area of the coupling beams in Spans A and B
d_A, d_B	differential deformation of walls 1-2 and 2-3
d_{mA}, d_{mB}	laminar displacement in spans A and B because of flexural deformations of walls
d_f, d_s, d_j	Deformation in a beam associated with flexure, shear and flexible beam wall joint.
d_{bA}, d_{bB}	laminar deformation ($d_f + d_s + d_j$) for Spans A and B
h_o	distance between nodal points
h, H	Storey height and total height of structure respectively
I_1, I_2, I_3	Moment of Inertias for walls 1,2 and 3
I_{AX}, I_{BX}	Reduced moments of inertia of the lamina taking into account flexural, shear and flexible beam wall joints for spans A and B
I_{bA}, I_{bB}	Moment of inertia of the coupling beam in Spans A and B
l_A, l_B	distance between centre lines of walls for Spans A and B.
l_{sA}, l_{sB}	Clear Spans for coupling beams for spans A and B
M_o	total external moment
M_1, M_2, M_3	final moments in walls 1,2 and 3
M_{10}, M_{20}, M_{30}	Moments shared by walls 1,2 and 3 because of external loading
M_{q1}, M_{q2}, M_{q3}	Moments induced in walls 1,2 and 3 because of laminal shear forces q_A and q_B in spans A and B.
M_{p1}, M_{p2}, M_{p3}	Moments induced in walls 1,2 and 3 because of laminar axial forces p_A and p_B in spans A and B.
P, W and Wl	Point load, triangular load and uniformly distributed load on the shear wall.
T_1, T_2 and T_3	Axial forces in walls 1,2 and 3
V_b	total shear at any level
V_1, V_2, V_3	final shear in walls 1,2 and 3
V_{p1}, V_{p2}, V_{p3}	Shear induced in the walls because of laminar axial forces
V_{10}, V_{20}, V_{30}	Shear shared by walls because of external loading
x, N or n	Subscripts x, N or n represents the value of the corresponding variable at x from top, N-th Storey or n-th node respectively.

TABLE 1 PROPERTIES OF THE TWIN CORE SHEAR WALL

FLOOR	WALL PROPERTIES						BEAM PROPERTIES		FLOOR HEIGHT
	A_1	A_2	A_3	I_1	I_2	I_3	A_A	A_B	h_N
	$\times 10^6$ in^4	$\times 10^6$ in^4	$\times 10^6$ in^4	$\times 10^6$ in^4	$\times 10^6$ in^4	$\times 10^6$ in^4	in^2	in^2	in
10th	3.55	3.65	4.75	3.90	4.50	7.50	794	998	90
9th	3.75	3.85	4.95	4.20	5.00	8.00	794	998	105
8th	3.95	4.05	5.15	4.50	5.50	8.50	794	998	105
7th	4.15	4.25	5.35	4.80	6.00	9.00	842	1055	105
6th	4.35	4.45	5.55	5.10	6.50	9.50	842	1055	105
5th	4.55	4.65	5.75	5.40	7.00	10.00	842	1055	105
4th	4.75	4.85	5.95	5.70	7.50	10.50	987	1240	105
3rd	4.95	5.05	6.15	6.00	8.00	11.00	987	1240	105
2nd	5.35	5.45	6.55	6.30	8.50	11.50	987	1240	120
1st	5.55	5.65	6.75	6.60	9.00	12.00	987	1240	120

Constant Data

Total height of shear wall H = 1065, Overall dimension of shear cores = 22'-0" x 12'-0"
Span l_A = 168.7 in, l_{A1}= 82.2 in, l_{A2}= 86.5 in, Span l_B= 204.4 in, l_{B1}= 91.8 in, l_{B2}= 112.8 in
Beam properties for span A : Beam depth D_A= 24.0 in, Width B_A= 14.0 in, Span l_{SA}= 38 in.
Beam properties for span B : Beam depth D_B= 30.0 in, Width B_B= 14.0 in, Span l_{SB}= 45 in.
Load : Total base shear = 550 Kips
Triangular load W = 400 Kips, uniformly distributed load W_1= 100 Kips, Point load P= 50 Kips.

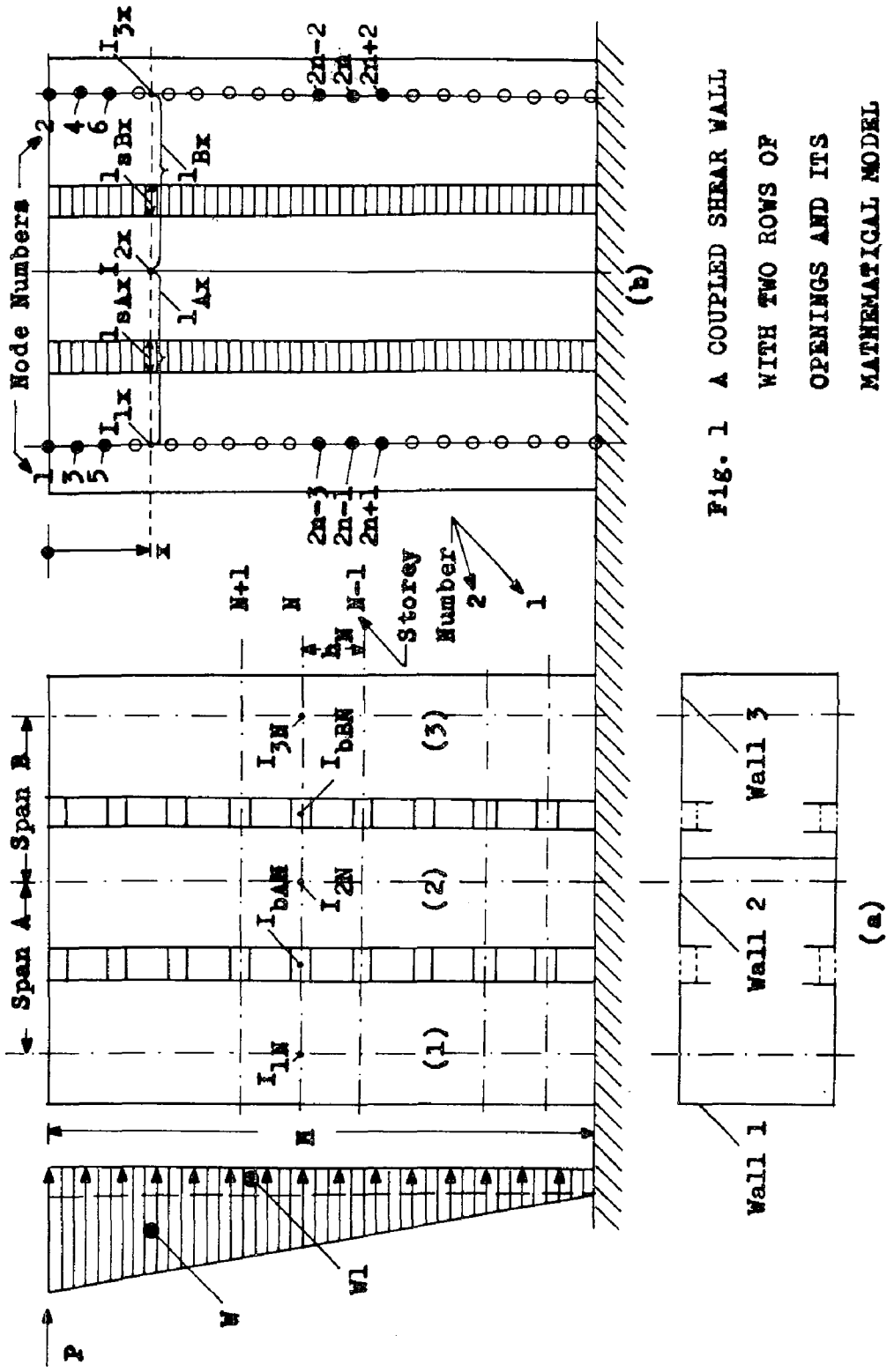

Fig. 1 A COUPLED SHEAR WALL WITH TWO ROWS OF OPENINGS AND ITS MATHEMATICAL MODEL

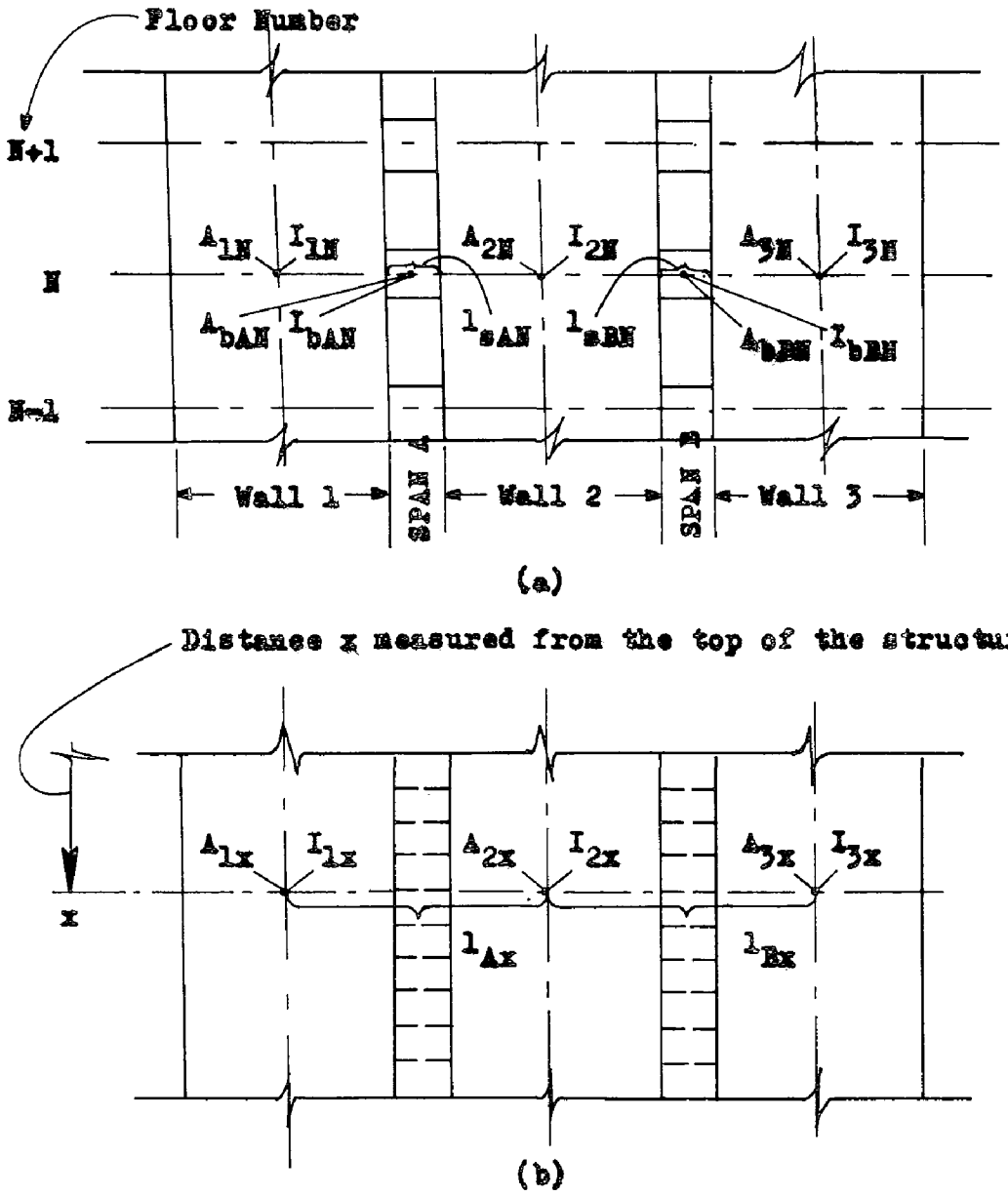

Fig. 2 PROPERTIES OF THE COUPLED SHEAR WALL AND ITS MATHEMATICAL MODEL AT THE N-th FLOOR LEVEL AND AT A DISTANCE x FROM THE TOP OF THE STRUCTURE

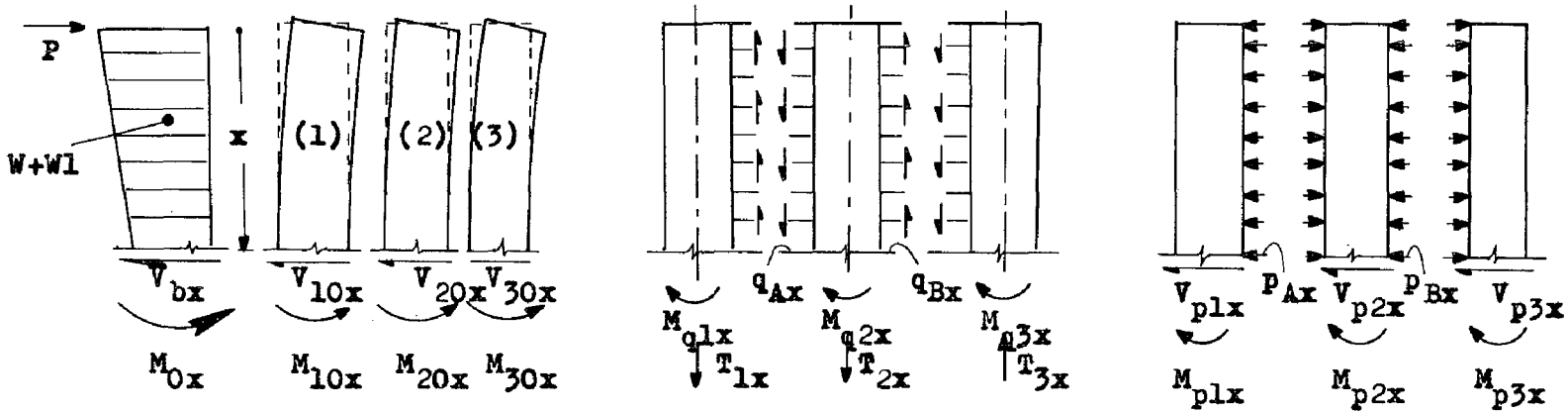

a. External Load

b. Moments and Shears shared by Walls

c. Moments Induced in the Walls due to Laminar Shear

d. Moments Induced in the Walls due to Laminar Axial Force

SHEAR EQUATIONS

$$V_{1x} = V_{10x} + V_{p1x}$$
$$V_{2x} = V_{20x} + V_{p2x}$$
$$V_{3x} = V_{30x} + V_{p3x}$$
$$V_{bx} = V_{1x} + V_{2x} + V_{3x}$$
$$V_{bx} = P + W + Wl$$

MOMENT EQUATIONS

$$M_{1x} = M_{10x} + M_{q1x} + M_{p1x}$$
$$M_{2x} = M_{20x} + M_{q2x} + M_{p2x}$$
$$M_{3x} = M_{30x} + M_{q3x} + M_{p3x}$$
$$M_{0x} = M_{1x} + M_{2x} + M_{3x}$$

AXIAL FORCE EQUATIONS

$$T_{1x} = \int_0^x q_{Ax}\, dx$$
$$T_{3x} = \int_0^x q_{Bx}\, dx$$
$$T_{2x} = T_{3x} - T_{1x}$$

FIG. 3 WALL ACTIONS AND EQUILIBRIUM EQUATIONS

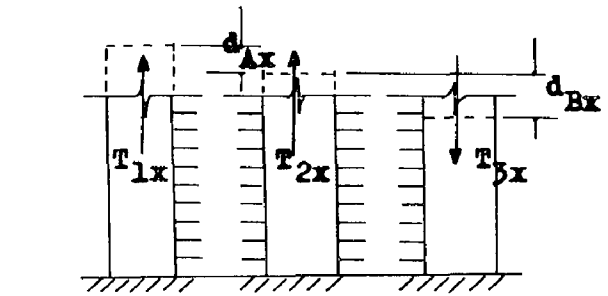

a. Axial Deformation of Walls

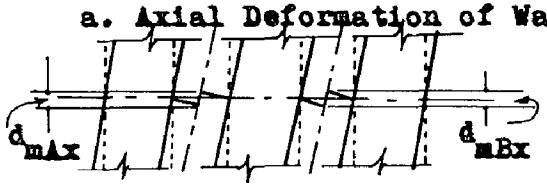

b. Flexural Deformation of Walls

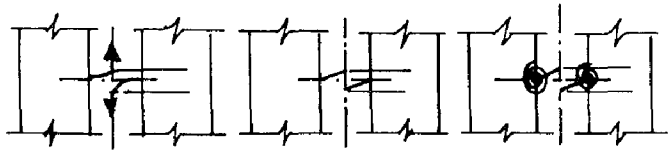

i. Flexure ii. Shear iii. Flexible Joint

c. Deformations in a Typical Beam

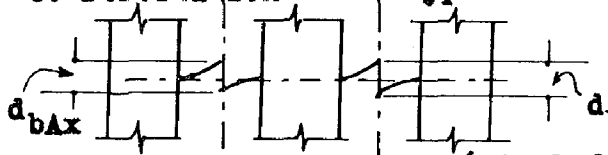

d. Laminar Deformations (includes Flexure Shear and Flexible Beam-Wall Joint Effects)

$d_{Ax} = d_{mAx} - d_{bAx}$ $d_{Bx} = d_{mBx} - d_{bBx}$

FIG. 4 DEFORMATIONS CONTRIBUTING TO THE LAMINAR DISPLACEMENTS

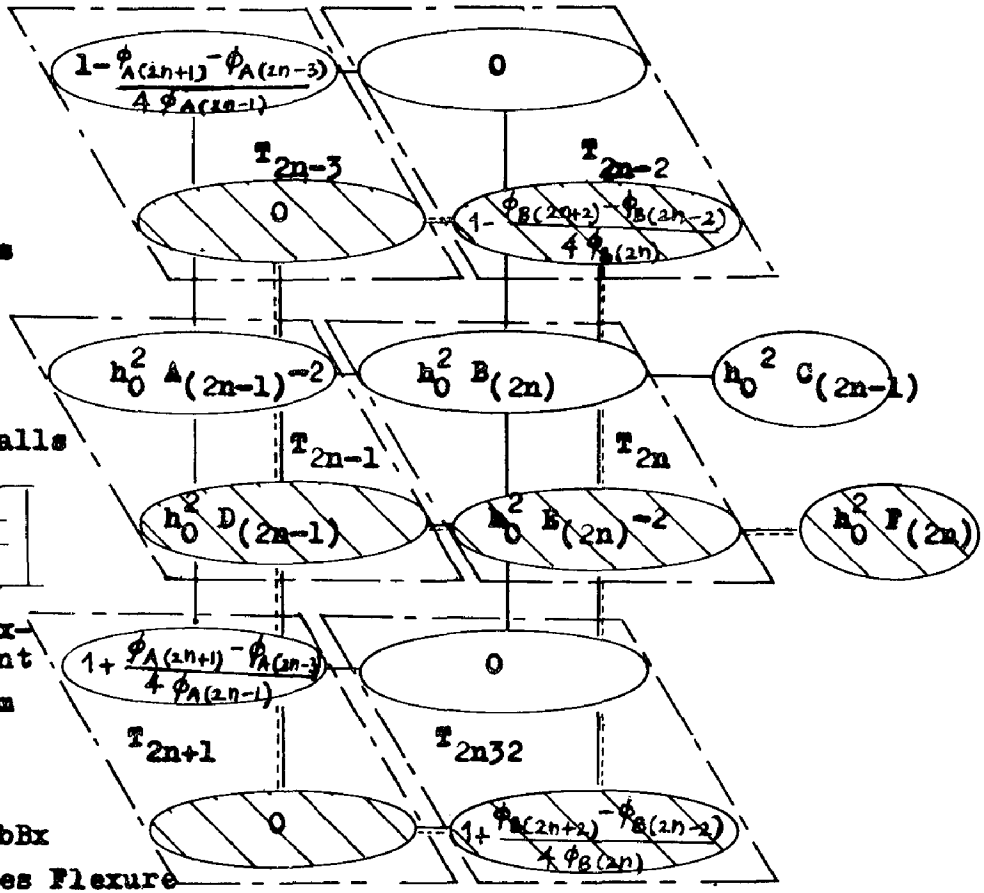

This operator should be applied at the nodes 2n-1 and 2n.

FIG. 5 FINITE DIFFERENCE OPERATOR FOR THE COUPLED DIFFERENTIAL EQUATION

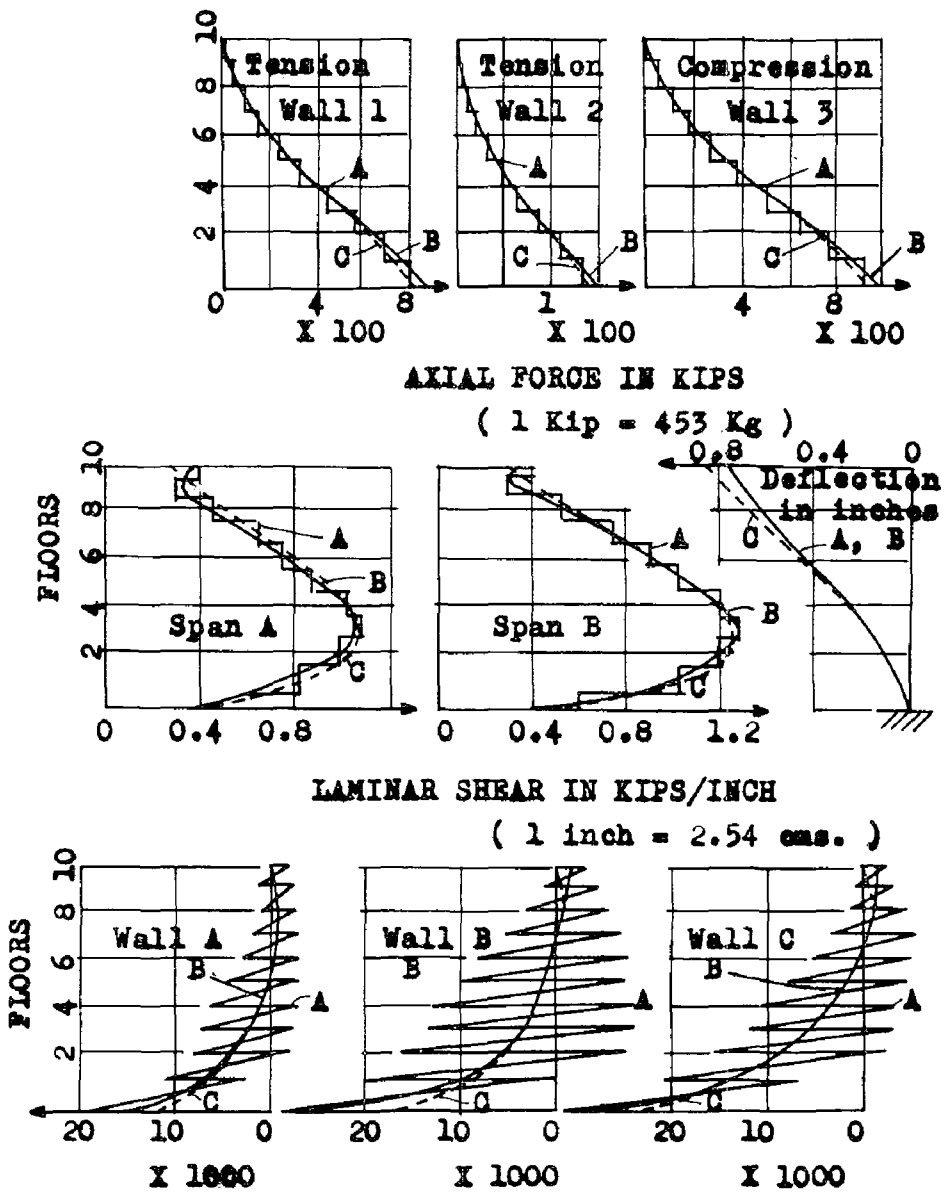

FIG. 6 RESULTS OF THE ANALYSIS OF A 10 STOREY SHEAR WALL WITH TWO ROWS OF OPENINGS

INTERNATIONAL SYMPOSIUM ON
EARTHQUAKE STRUCTURAL ENGINEERING
St. Louis, Missouri, USA, August, 1976

ASEISMIC DESIGN EXAMPLES OF PRESTRESSED CONCRETE WATER TANK

by
AKIO SAKURAI
Chief Research Engineer, Head of Earthquake Engineering
Section No.1, Foundation and Earthquake Engineering Department
Central Research Institute of Electric Power Industry
Abiko City, Chiba, JAPAN

CHIZUKO KURIHARA
Senior Research Engineer, ditto

TAKAHIRO IWATATE
Research Engineer, ditto

SUMMARY

Aseismic designs of prestressed concrete water tank contain interesting problems not only of hydro-elasticity but also of design and construction of thin walled prestressed concrete shell structures. Examples of aseismic design of three prestressed concrete surge tanks of hydro-electric power stations are presented in connection with discussions of virtual mass effect of inner water of flexible tank and discussions of relative merits of stress analysis methods used in these designs. These methods are reviewed by model test and field research on an actual tank during surging tests. Utilization of these examples seems especially appropriate when aseismic designs of thin walled water tank are required.

INTRODUCTION

Yanagimata surge tank of Kyushu Electric Power Co. is the largest prestressed concrete surge tank in operating in Japan (Fig. 1). Two surge tanks of Okuyahagi station of Chubu Electric Power Co. under planning are characterized as the one of tanks will be constructed on a small peak of a ridge (Fig. 2) and the other will be embedded considerably arround the lower part of wall (Fig. 3).

The aseismic designs of these surge tanks raised interesting problems not only of the hydro-elastic vibration of thin walled tank but also of design and construction of prestressed concrete shell structures. Dynamic water pressure or inertia effect so called virtual mass of inner water of a tank during earthquakes become the essential load compared with inertia force of tank body as the same as hydro-static load in usual condition. The virtual mass effect of thin walled tank is differ slightly from the one of rigid tank, because increment of the virtual mass due to deformation of tank wall causes. Then the virtual mass distribution was researched at first by the hydro-elastic theory and a model test which are presented in this paper.

There are many methods offered in order to calculate stresses of cylindrical shell structures and to evaluate responses of that structures during earthquakes. Several methods of them were tried and were inquired in order to select the available procedures of the aseismic design of these structures. The relative merits of these methods used in the analyses were reviewed and the conclusions of the research are presented in this paper.

Constructions of prestressed concrete water tank as well as desings are main concerns to structural engineers in connection with preventable techniques for cracks due to thermal stress, seapage of water through construction joints and stress leakages of prestressing. But contents of this paper are confined within the analytical part of desings and an illustration of arrangements of steel bars and steel wires are only presented.

VIRTUTAL MASS DISTRIBUTION OF A WATER TANK

It is the well-known fact that a object immersed in or in contact with fluid exhibits as if the apparent inertia of the object increase greatly during accelerated motions. This increased inertia is so called the virtual mass or the added mass of fluid. It is noticed that the virtual mass does not adhere fluid substance to the object solidly, then the rigidity of the object does not increase.

The virtual mass distribution $m_v(x_0)$ of a deformable object is given as follows (Ref. 1 and 2);

$$m_v(x_0) = [\rho_0 \phi / f]_{x=x_0}$$

where ρ_0 is a density of fluid, ϕ is a potential function of fluid in a certain boundary conditions, f is a shape of object deformation and x_0 is a vector denoting the boundary surface. The generalized virtual mass Mv is

$$M_v = \rho_0 \int_{S_0} \phi(x_0) f(x_0) dS_0$$

where s_0 denotes the boundary surface.

The exact analytical solution of hydro-elastic vibration is only derived to a problem of cylindrical column standing in a pond or the same problem of cylindrical slender tank under conditions in which water depth is equal to the column height and effects of surface waves are negligible (Ref. 3 and 4). The aproximate solution considered the increment of virtual mass was proposed in Ref. 4 and Ref. 5 and these theories were reviewed by model test (Ref. 4) and vibration tests of actual bridge piers (Ref. 6 and Ref. 7).

The virtual mass distribution $m_v(z, \theta)$ for thin walled water tank in condition of ovaling mode m is given as follows;

$$m_v(z,\theta) = \rho_0 a \cos m\theta \sum_{i=0}^{\infty} \frac{(-1)^i}{\lambda i} I^{(i)}\left(\frac{a}{h}\right) \cdot \cos \lambda i \frac{z}{h} \qquad h$$

$$+ \rho_0 a \cdot \cos m\theta \sum_{i=0}^{\infty} I^{(i)}\left(\frac{a}{h}\right) \int_0^1 f_h(h\xi) \cos \lambda i \xi d\xi \cdot \cos \lambda i \frac{a}{h} \quad (3)$$

$$I^{(i)}\left(\frac{a}{h}\right) = \frac{2}{a/h} \cdot \frac{I_1\left(\lambda_i \frac{a}{h}\right)}{\lambda_i I_0\left(\lambda_i \frac{a}{h}\right) - \frac{h}{a} \cdot I_1\left(\lambda_1 \cdot \frac{a}{h}\right)}$$

$$\lambda_i = \frac{2i+1}{2}\pi$$

where a is an inner radius of tank, h is depth of water, z is a co-ordinate in direction of up ward and z = 0 at the bottom of tank, θ is a co-ordinate in direction of tangential ward and θ = 0 at the direction of vibration, $f(z,\theta)$ is a shape of tank deformation and I_0 , I_1 are the first kind of modified Bessel functions. For the aseismic design of water tank, the case of the first ovaling mode $m = 1$ is generally used.

The first term of Eq. (3) when m = 1 shows the virtual mass distribution for a rigid tank and the second term is the increment of virtual mass distribution induced by the deformation of tank $f(z,\theta)$. The modal shapes of empty tank or of tank with virtual mass distribution for rigid tank instead of $f(z,\theta)$ are available in the approximate calculation. By this treatment, the balance of force at each portion of tank is put out of order slightly, but the total energy balance is in order.

The another dynamic effects of inner water are the one of surface wave or sloshing of inner water. The natural frequencies f_n of sloshing for rigid tank are given as follows;

$$f_n = \frac{1}{2\pi}\sqrt{g\gamma_n \cdot \tanh \gamma_n h} \qquad (4)$$

where is the gravity acceleration and $\gamma_n a$ is given in Table 1. The wave height of sloshing η_0 is given in the next equations;

$$\eta_0 = L \cdot \cos\theta\left[r - \sum_{n=1}^{\infty} An J_1(\gamma_n r) \cdot \cosh \gamma_n h\right] e^{iwt} \qquad (5)$$

$$An = 2a/(\gamma_n^2 a^2 - 1) J_1(\gamma_n a)\left(\cosh\gamma_n h - \frac{g\gamma_n}{W^2} \cdot \sinh\gamma_n h\right)$$

where J_1 is the first kind of Bessel function.

The dynamic effect of inner water for up-down ward vibration must be considered in the aseismic design and is presented in Ref. 2 for compressive fluid. But in these analyses, the static method or the treatment to increase the gravity acceleration was adopted for the simplicity of analysis.

STRESS ANALYSES

In order to calculate the tank stress for static loads in the condition of up surge water level, the following methods were adopted;

Method 1 : analogous method to beam stress analysis on elastic foundation

Method 2 : finite element aproach by thin cylindrical shell element

Method 3 : finite element aproach by triangular element for thick cylindrical shell

The method 1 is given in the following equation neglecting the effect of Poisson's ratio;

$$\frac{d^2}{dz^2}\left(\frac{Et^3}{12}\cdot\frac{d^2f}{dz^2}\right)+\frac{Et}{a^2}\cdot f=P$$

where E is Young's Modulus of tank material, t is thickness of tank wall and P is water pressure.
For tanks with uniform wall thickness,

$$\frac{d^4f}{dz^4}+\frac{12}{a^2t^2}f=\frac{12}{Et^3}P$$

The method 2 was adopted in order to calculate wall stresses neglecting the deformation of tank foundations, because these tanks were planned to construct on firm rock foundations and the preparations of input data for computer by this method were easier than that of the next method 3. The method 3 was used to evaluate the effects of foundation deformation and to estimate the stress concentration near the lower part of tank wall.

For the dynamic stress analyses in condition of high water level, the following methods were adopted;

Method 4 : finite element apraoch by thin cylindrical shell element under non-symmetric loading and static treatment

Method 5 : finite element apraoch by triangular element for thick cylindrical shell under non-symmetric loading and stick treatment

Method 6 : multi-degree- freedom system in which rigidity of tank is estimated by beam theory considering bending and shearing deformations of beam

Method 7 : dynamic analysis using earthquake records by the method 4

Method 8 : combination method by the method 6 and the method 4

The merits of the method 4 and the method 5 are the same as the one of the method 2 and the method 3 above mentioned. The method 6 is the most

handy and tough method of response analysis. The method 7 needs the most high cost to compute, then the method was only used to check the result of final design.

These methods above mentioned are the fundamental knowledge for structural engineers, then the detailed procedures of calculation are neglected in the paper.

RESULTS OF ANALYSES

The method 1 is useful for design analysis under static loading. Then the availability of the method 1 was examined and the comparison of wall stress derived between the method 1 and the method 3 is shown in Fig. 4. The agreement of both methods seems satisfactory.

The natural periods of tanks and of sloshing are shown in Table 2. The periods of sloshing are far apart from the natural periods of tanks. Then the effects of sloshing were discussed separately from the effects of main inertia forces. The natural periods of tanks derived by the method 6 coincide with the one of the method 4 in the various conditions of water level.

The effect of virtual mass increment due to tank deformation was 1.4% increment of the wall stress of the Yanagimata surge tank. Then the virtual mass distribution for rigid tank were used in the following analyses of the Okuyahagi surge tanks.

Fig. 5 shows the wall stress distributions of the Yanagimata surge tank and shows the comparison between the stress derived by the method 4 and the one of the method 5 under the condition of static loading and dynamic loading. The stress distributions derived by the method 5 resemble to the one of the method 4 although the division of triangular element mesh was coarse at the upper portion of the tank. This is because of the major load beeing the hydrostatic load and the assumption of uniform strain of element in the method 5 beeing suitable for this problem especially to the hoop stress.

Fig. 6 shows the stress distribution of the Yanagimata surge tank derived by the method 5 and shows the comparison of wall stresses in the conditions between the dynamic load only and the static load only at the high water level. From this figure, the main stress is the one due to hydro-static load and the percent of stress increment seems equal to the percent of earthquake acceleration to the gravity acceleration or 20%. The effects of dynamic loads to tank stress appear mainly in the vertical stress of wall.

Fig. 7 shows the comparison of the vertical stress of wall derived by the method 7 with the one of the method 6. The result of the method 7 is rather larger than that of the method 6 during the same input record of earthquake. But the difference is small compared with the stress fluctuation due to the used records of earthquake.

In the case of the Yanagimata surge tank, the stresses at the condition of up surging water level covered the stresses during earthquake in which input accelerations were 0.2 g for static analyses and were 0.1 g for dynamic analyses. In the case of the Okuyahagi surge tanks, the stresses of dynamic treatments were largest under the conditions in which the input accelerations were 0.2 g for the static analyses and were 0.15 g for the dynamic analyses. Although the designs of the Okuyahagi surge tanks will follow the results of dynamic treatment by the method 7, the rewrote results for the dynamic input acceleration 0.1 g are presented in the Fig. 7 for the convenience of comparison with the results of the Yanagimata surge tank.

DESIGN

Following these stress analyses above mentioned, prestressing force were decided and the judgment compared with the allowable stresses were carrid out. The result of the Yanagimata surge tank is shown in Table 3. Fig. 8 presents the cross section of the Yanagimata surge tank and illustrate the arrangements of steel bars and steel wires for prestressing.

RESULTS OF TESTS

In order to review the analytical methods, the model test (one fifth scale model) by shaking table and the field research during surging tests on the Yanagimata surge tank were carried out. Following these researches, the next conclusions were derived; The results of model test by shaking table showed that the responses of tank during earthquakes were the one for the ovaling model $m = 1$ as the theory of shell indicated. The vibrations of ovaling mode $m = 2$ of the actual tank of Yanagimata during surging were predominant, and the natural period of the tank varied according to the water level during surging. Fig. 9 shows the relation between the natural frequencies and the water level derived by the surging test and the method 4 for ovaling mode $m = 1$. The same relations obtained by the model test for ovaling mode $m = 2$ are shown in Fig. 10. The figures show the availability of the theory of virtual mass distribution and the methods used in the aseismic desings.

CONCLUSIONS

Following these examples of aseismic design of prestressed concrete water tank, the next conclusions are obtained;

1) The effect of virtual mass increment due to tank deformation to the tank stresses are neglegible.

2) The main stresses are due to hydro-static load. The effects of dynamic loading appear in the vertical stress of wall and the stress increment of that stress due to dynamic loading is comparable to the increment of input acceleration to the gravity accera-tion.

3) The method 6 or the multi-degree-freedom system is available to these problems. If detailed shell stress during earthquakes is needed, the sufficient method 8 or the method conbined the method 6 to the method 4 of thin shell element is recommendable.

4) The adaptation of analytical models was reviewed by the model test and the observation of the actual tank during surging. Utilization of these examples seems especially appropriate when aseismic designs of thin walled water tank are required.

ACKNOWLEDGEMENT

This report work was carried out with the assistance of members of Kyushu Electric Power Co. and Chubu Electric Power Co.. The authors wish to thank them.

REFERENCE

1) Akio Sakurai "Vibrational Problems on Under-Water Structures" Proc. 11th Congress of International Association for Hydraulic Research, Leningrad, Sept. 1965

2) Akio Sakurai "Chapter 4 and Chapter 9 of Vibration Handbook" Edditated by the Japan Society of Civil Engineers, 1964

3) Akio Sakurai "Vibrational Problems of a Flexible Pier Standing in Deep Water" Jurnal of The Civil Engineering, Vol. 16, No. 6, 1961

4) Akio Sakurai "Vibrational Problems on Under-Water Structures (Virtual Mass Distribution, Free Vibration and Forced Vibration)" Technical Report: No. C-63006, Central Research Institute of Electric Power Industry (CRIEPI), 1963

5) Akio Sakurai "Vibrational Problems on Under-Water Structures (An Consideration for Earthquake Response Analysis)" Technical Report: No. C-65061, CRIEPI, 1965

6) Akio Sakurai "Vibrational Problems on Under-Water Structures (Field Measurements and analyses of Flexible Piers of the Ogami Bridge and the Iwase Bridge" Journal of Technical Laboratory, CRIEPI, Vol. 13, No. 3, 1963

7) Akio Sakurai "Vibrational Problems on Under-Water Structures (Energy Losses due to Surface Waves)" Journal of Technical Laboratory, CRIEPI, Vol. 14, No. 2, 1964

8) Shunji Inomata "Design and Construction of Prestressed Concrete" Gihodo, 19

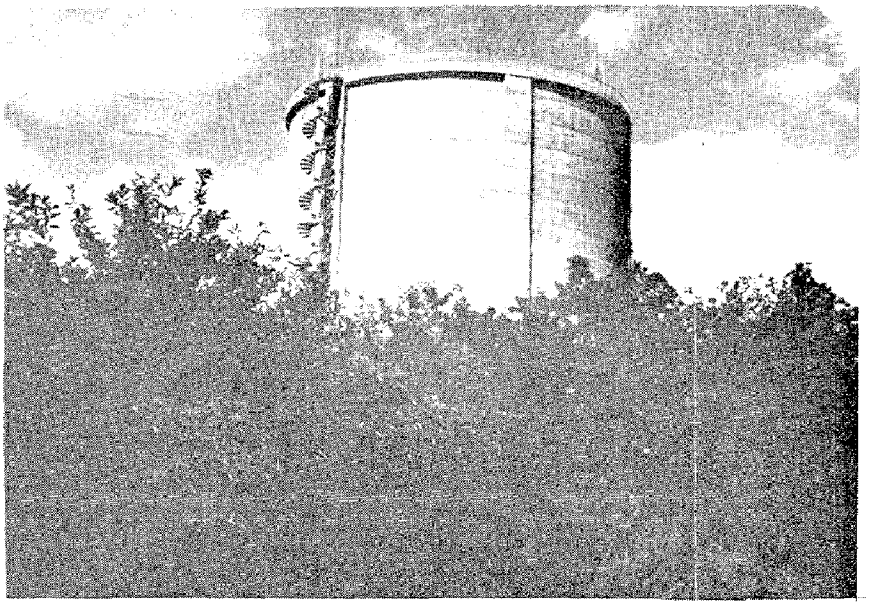

Fig. 1. Side view of the Yanagimata surge tank

Table 1. Value of γ_{na} and $J_1(\gamma_{na})$

n	1	2	3	4	5
γ_{na}	1.841	5.332	8.536	11.71	14.86
$J_1(\gamma_{na})$	0.5817	−0.3461	0.2733	−0.2333	0.2070

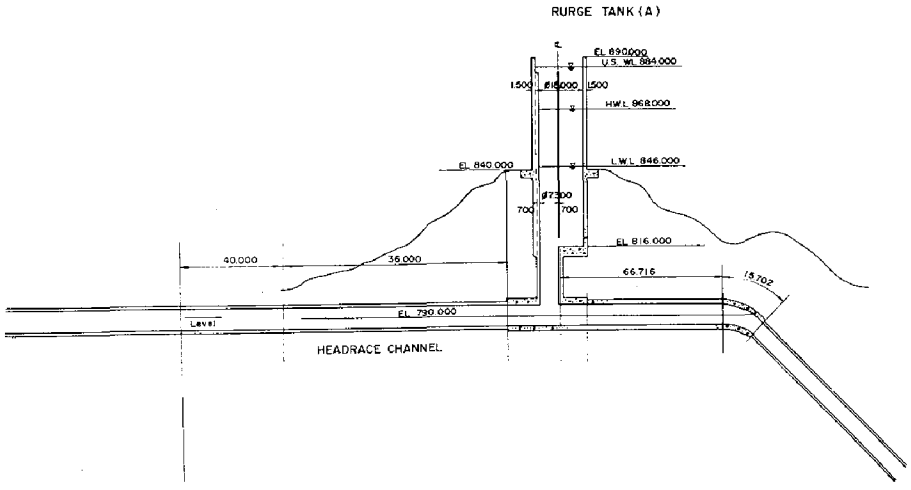

Fig. 2. Surge tank (A) of Okuyahagi station

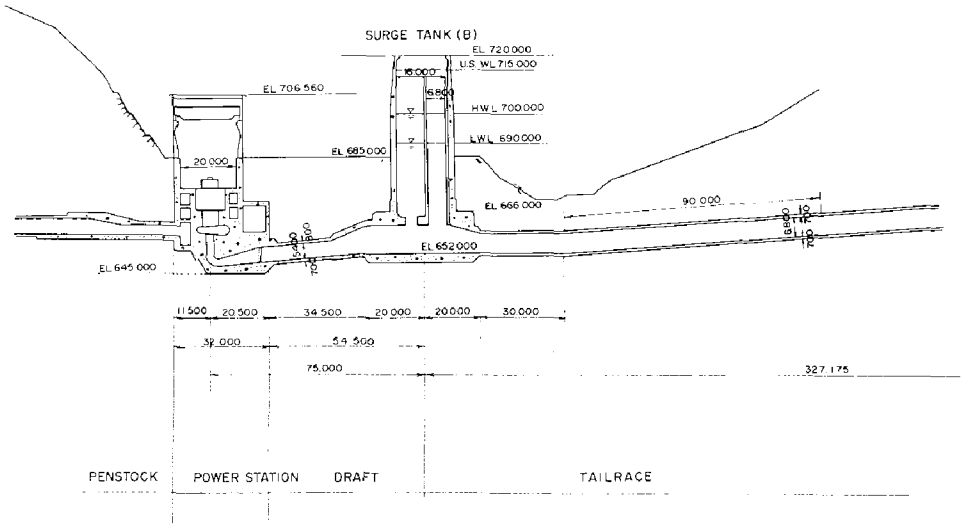

Fig. 3. Surge tank (B) of Okuyahagi station

Method 1	—●— Hoop stress
	—⊖— Normal component of stress in the vertical direction
Method 2	—●— Hoop stress
	—⊖— Normal component of stress in the vertical direction

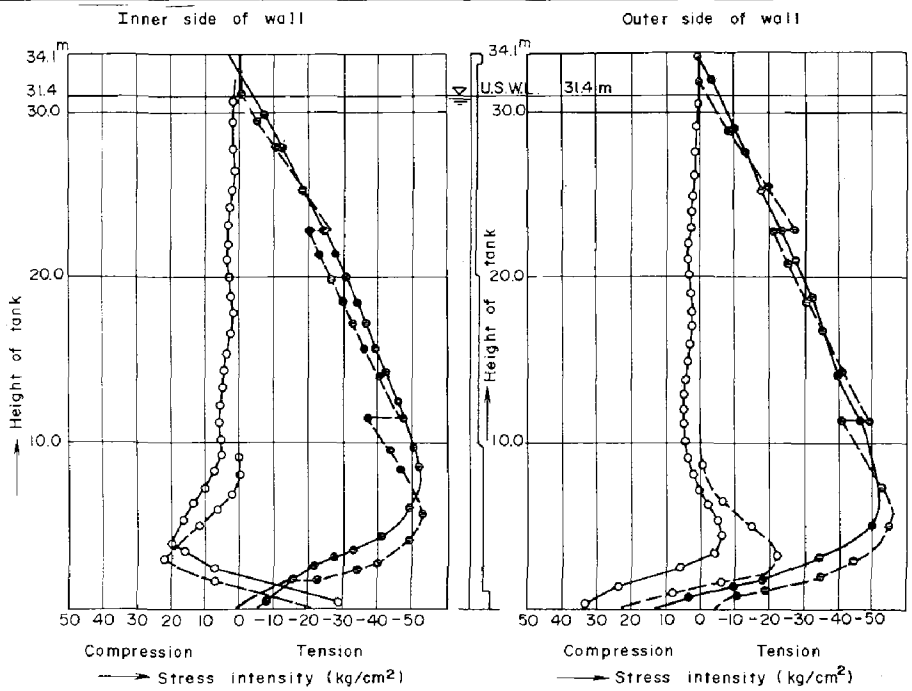

Fig. 4. Longitudinal distribution of stresses
(Hydrostatic load at the up surge water level)

Table 2. The natural periods of tanks and sloshing

Name of Tank	Method	Empty	H.W.L.	U.S.W.L.	Vibration of water surface
YANAGIMATA	Method 4	0.091	0.144	0.226	5.23 (H.W.L.)
	Method 5	0.091	——	——	
	Method 6	0.092	0.138	——	
OKUYAHAGI TANK (A)	Method 4	0.181	0.238		4.44 (H.W.L.)
	Method 5				
	Method 6	0.177	0.202		
OKUYAHAGI TANK (B)	Method 4	0.224	0.310		4.43 (H.W.L.)
	Method 5				
	Method 6	0.220	0.256		

H.W.L. (Hight water level)
U.S.W.L. (Up surge water level)

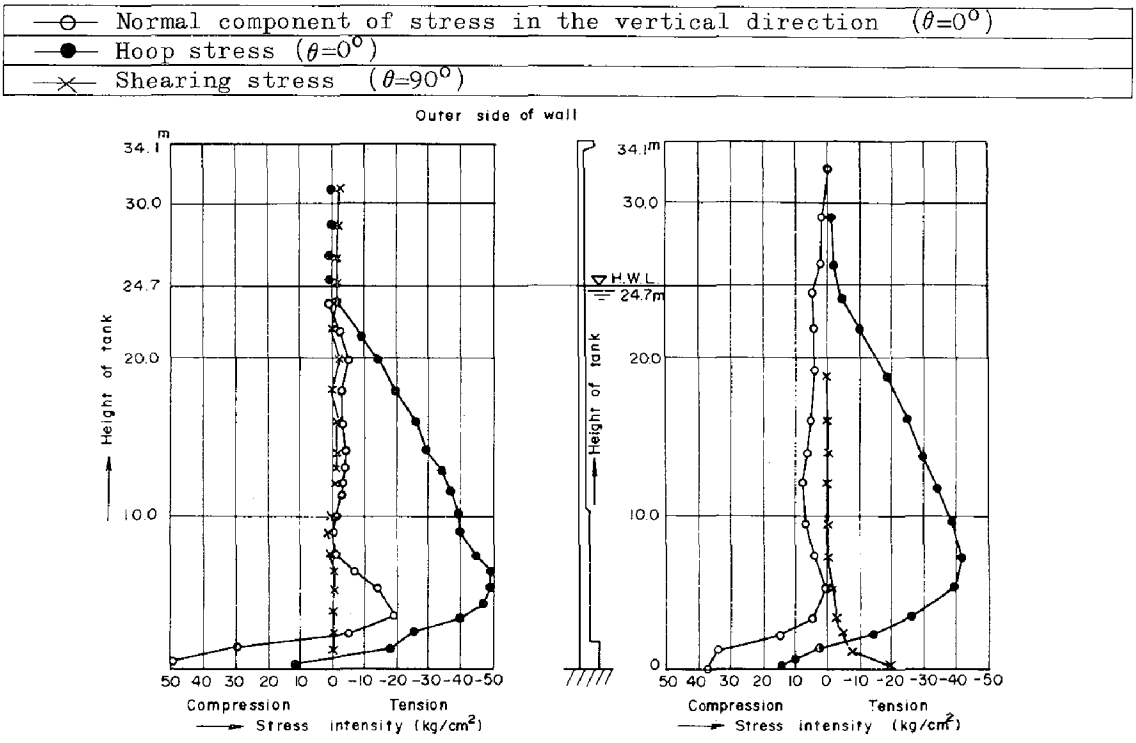

Fig. 5. Longitudinal distribution of stresses (Static loading and dynamic loading at the high water level)

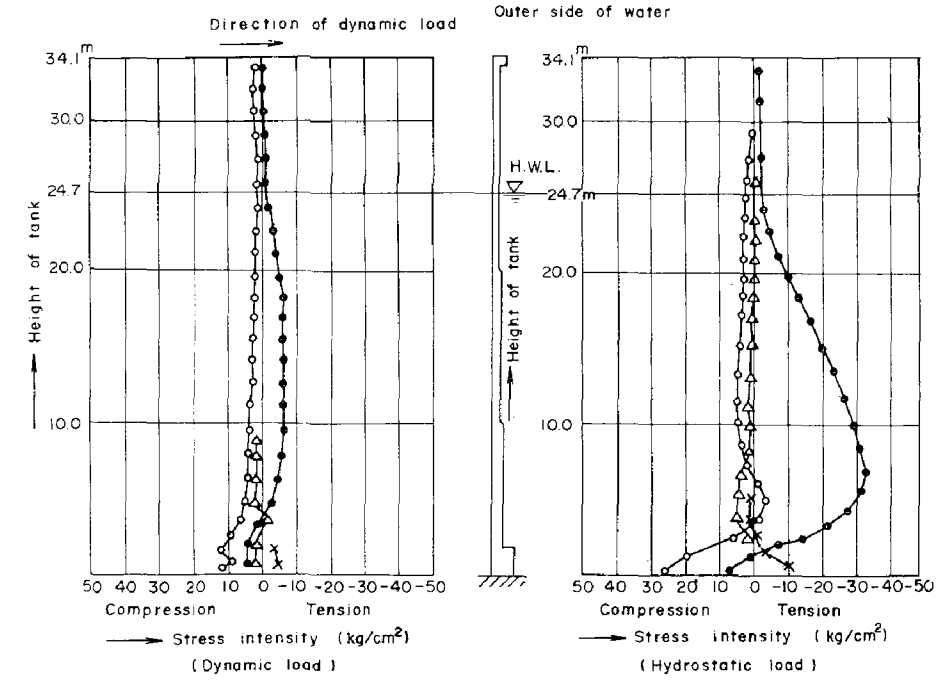

Fig. 6. Longitudinal distribution of stresses at the high water level

———	Method 7 (input acceleration 0.1g ELCENTRO EARTHQUAKE)
— — —	Method 6 (input acceleration 0.1g ELCENTRO EARTHQUAKE)
—·—	Method 6 (input acceleration 0.1g TAFT EARTHQUAKE)
— - - —	Method 5 (input acceleration 0.2g)
— - - - —	Method 4 (input acceleration 0.2g)

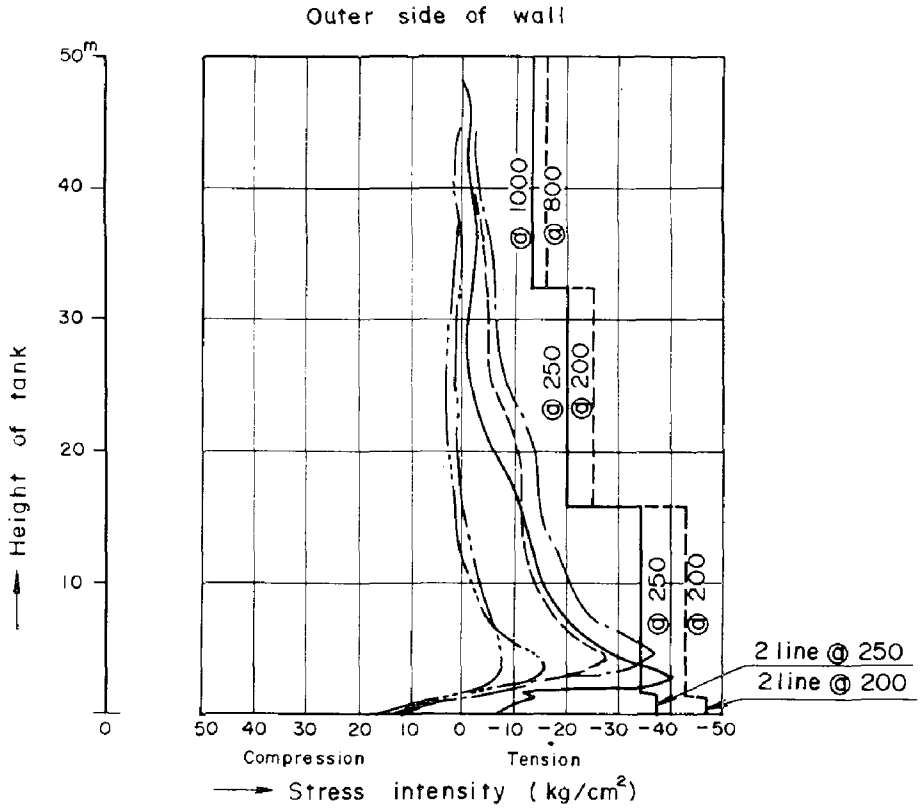

Fig. 7. Longitudinal distribution of normal component stress in the vertical direction (Hydrostatic load and dynamic load) (Surge tank (A) of Okuyahagi station)

Table 3. Total stress intensity of each section of the Yanagimata surge tank (Method 4)

Section	Height from side wall lower edge (m)	Number of steel bar n	Prestressing load $P_P = 48 \times n$ (ton)	Prestressing load $\sigma_P = P_P/A$ (kg/cm²)	Normal component of stress intensity in the vertical direction (kg/cm²)	Total stress intensity (kg/cm²)	Shearing stress intensity (kg/cm²)	Diagonal stress intensity (kg/cm²)	Judgement of stress intensity
1	0	664	30,912	34.2	49.6 −48.5	83.8 −14.3	26.0	7.4	OK
2	2.0	664	30,912	34.2	10.5 −10.0	44.7 24.2	6.7	0.4	OK
3	5.4	160	7,680	15.9	−13.3 11.3	2.6 27.2	0	0	OK
4	10.8	80	3,840	9.6	− 2.7 − 2.1	6.9 7.5	0	0	OK
5	21.6	40	1,923	6.0	− 4.5 − 1.4	1.5 4.6	0	0	OK
Allowable stress intensity						$-25 < \sigma < 200$		$\sigma_1 < 20$	

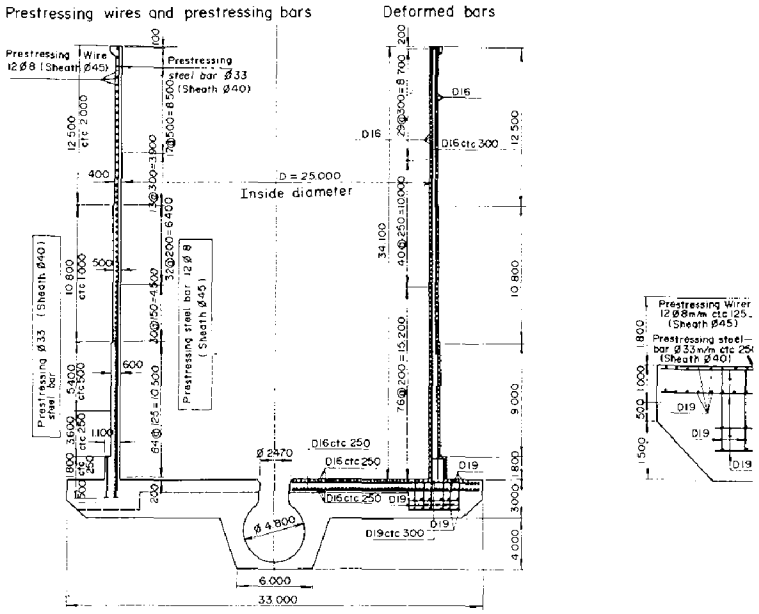

Fig. 8. Cross section and details of reinforcement of the Yanagimata surge tank and its side lower edge

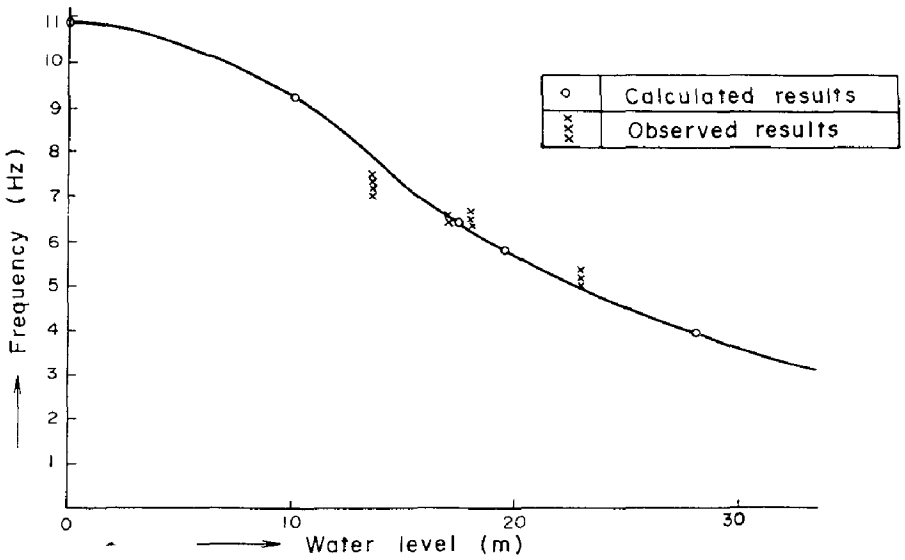

Fig. 9. Natural frequency - water level curve (ovaling mode m=1)

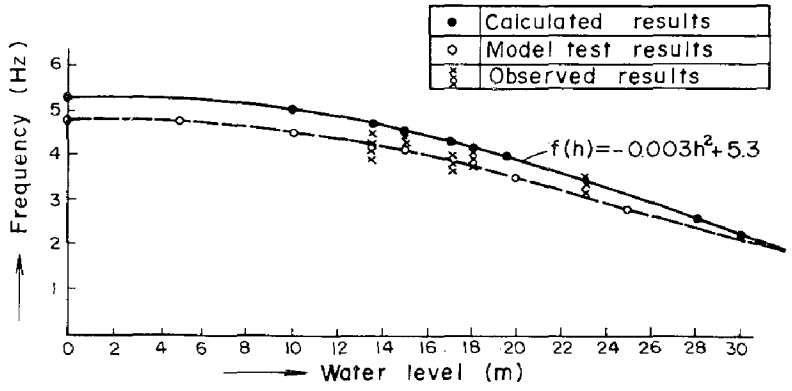

Fig. 10. Natural frequency - water level curve (ovaling mode m=2)

INTERNATIONAL SYMPOSIUM ON
EARTHQUAKE STRUCTURAL ENGINEERING
St. Louis, Missouri, USA, August, 1976

A NEW STRUCTURAL MODEL FOR SHEAR WALLS ANALYSIS

N.UNGUREANU

Dr.Eng.Prof. of
Structural Engineering
Polytechnic Institute of Jassy
Romania

Summary

A new aspect of the analyse of shear-walls, with openings as structural elements, subjected by seismic horizontal loads is presented.

A structural model is proposed, by which the horizontal elements that are coupling the vertical members are equivalently replaced by a continuous connection of variable stiffness according to a periodic law.

The model by which the horizontal coupling elements are replaced by a continuous connection of constant stiffness is much elaborated in the specialized literature. The proposed structural model takes into account, more efficiently, the local effects of the joints between horizontal and vertical elements. For this structural model a differential equation describing the shear-wall deformation is derived.

From the computer analysis of a numerical example of a shear-wall having one row of openings some quantitative and qualitative differences, between the both considered models are emphasized. As it results from some experimental data [2] the proposed model approximates better the actual physical phenomenon.

1. Introduction.

The shear-walls are frequently used as earthquake resistant structures. A complete analysis of the stresses and deformations of shear-walls with openings presents considerable difficulties therefore, for design, some simplified procedures are still used.

In order, to determine the dynamic characteristics of the structure and the seismic forces acting the structural system as well as in order to calculate the stresses induced in structural members, it is necessary to know the shear wall behaviour subjected to the horizontal loadings.

The seismic loads that are continuously distributed along the height of the structure or lumped at the floor level are shared to the structural elements, represented by the shear-walls. For the distribution of the seismic loads on the shear-walls, the commonly used assumptions are adopted, namely the floors are considered absolutely rigid in their plane and hinged at the shear-walls; the height of the stories and the thickness of the wall are supposed to be constant, and the openings along the same vertical to be identical.

For analysing there structures, many methods presently used in current design, have been developed. These methods can be divided in two groups: one includes all the methods, replacing the horizontal elements among the openings (coupling beams) by an equivalent continuous connection with constant density, and the shear-walls in the whole like a cantilever where the vertical elements have in any section the same rotation, their sections remaining plane after deformation; the second group includes the methods in which the shear-wall having openings is idealized as a frame, that frame possessing horizontal beams with rigid segments at the ends.

These two groups of methods give good results in the following practical cases:

- the replacement of horizontal elements among the openings by a continuous uniform connection leads to reasonable results in the case of the shear-walls with one row of symetrical openings, or with many rows of openings having proportional stiffnesses, if the ratio between the opening area $A_o = \ell_1 h_o$ and the area of a horizontal beam $A_b = \ell_1 h_1$ fulfils the condition $A_o/A_b < 3$ and the ratio $\ell_1/h_1 < 3$, ℓ_1 being the horizontal width of the openings, and h_1 the height of a horizontal beam between two openings.

The methods using the idealization of the shear-wall as a frame are indicated when $A_o/A_b > 3$, and $\ell_1/h > 2$, irrespective of the ratio between the rigidities of the vertical elements.

A more appropriate solution can be obtained using finite elements, but for a corresponding precision it is necessary to take into account a very large number of finite elements; this causes a prohibitory increase of the computational amount, especially in the case of the multistoried shear-walls or with many rows of openings.

2. Proposal for a new Structural Model.

The idea to be used herein consists in replacing the discrete connection between vertical elements by a equivalent continuous connection. One starts from the observation that the coupling horizontal elements are influencing the vertical members behaviour on a certain height, their maximum effect being in the axes of the coupling beams (Fig.1). The shear force effect on the deformations of these elements cannot be neglected, and the shear stresses are nonuniformely distributed along the height of the cross-section of horizontal members (Fig.2).

In order to fit closer the actual behaviour, the discrete horizontal connections among openings will be replaced by a continuous connection with variable rigidity k_x having

maximum density in the axis of the horizontal elements and zero in the center of openings. The law which describes such a variation can be, for instance,

$$k_x = a\left(1 + \cos\frac{2\pi x}{h}\right) = \frac{a}{2}\cos^2\frac{\pi x}{h} \qquad (1)$$

and will be called in what follows the function of coupling stiffness. The parameter a can be determined from the condition that the total equivalent coupling stiffness along the height of a story (j - j + 1) to be equal with the stiffness, k, of a horizontal connecting beam,

$$\int_{jh}^{(j+1)h} a\left(1+\cos\frac{2\pi}{h}x\right)dx = k \qquad (2)$$

which gives $a = \frac{k}{h}$ and therefore

$$k_x = \frac{k}{h}\left(1 + \cos\frac{2\pi x}{h}\right) = \frac{k}{2h}\cos^2\frac{\pi x}{h} \qquad (3)$$

In the case of a ground floor with a greater height or of a coupling beam from the top story among some limits one can extend the coupling stiffness function, so that it covers these heights with more than a period.

The actual shear-wall with openings is replaced by the proposed model made of component vertical elements, coupled together by a periodic continuous connection. The continuous equivalent link modelling the coupling replacing the actual horizontal elements discretely disposed, can have various interpretations: it can be considered as being carried out from a very great number of identical laminas, with a variable density, or from a very great number of laminas with a variable sfiffness, or it can be considered as a continuous medium with a Young modulus E, varying after a periodical function (Fig.1 d).

The following remarks are accurate enough for shear-walls provided with one row of symmetrically disposed openings for shear-walls with two rows of symmetrical openings and

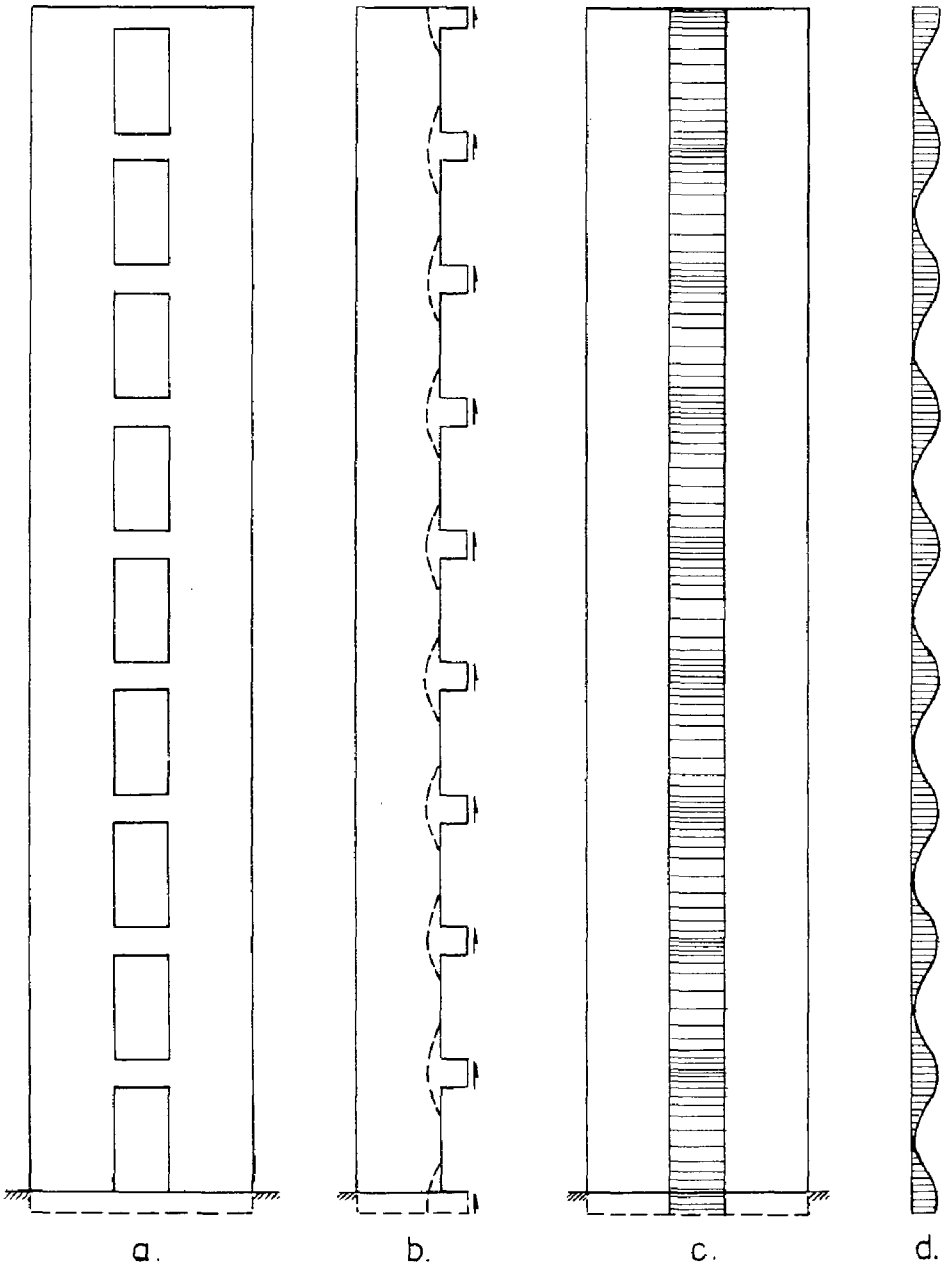

Fig.1. a. Shear wall with openings. b - Effect of joints c. Equivalent model. d. Function of coupling stiffness

having central vertical element stiffness twice greater than the stiffness of a lateral element, also in the case of shear-walls provided with many rows of openings with proportional rigidity of vertical members.

The obtained results could however be applied also to shear-walls with openings slightly asymmetrical and, in some cases, to frames stiffned with shear-walls. At the same time these results can be used for the analysis of structures with a quasirigid central core, formed by the lift tower, stair case, a.s.o. In these cases, when openings are provided on one side, it always appears a geometrical asymmetry, leading to torsion (Fig.3). The torsion centroid will be a variable magnitude along the height of the structure, and the torsional moment will depend besides loading, upon the position of the torsion centroid.

3. The Differential equation of a deformed vertical element.

For the analysis of the assumed model, the assumption that for every separate vertical element is valid the hypothesis of plane sections, is made. The rotations of these elements, considered identical for all vertical members, are taken as unknowns.

In the analysis of displacements into the coupling horizontal beams, the bending moment and the shear force are taken into account, and in the vertical elements only the bending moment effect. Due to the omission of axial forces effect, the total shear force is distributed among the vertical members proportionally to their inertia moments.

Since vertical members in one section have the same rotation, the coupling horizontal elements would have, at the ends, identical rotations and displacements (Fig.4 b).

The conventional stiffness of a horizontal beam taking

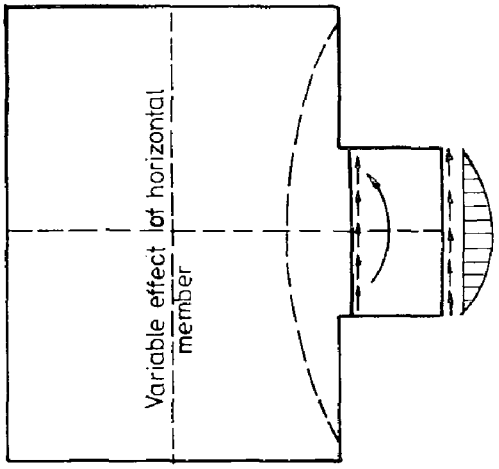

Fig.2. Effect of horizontal members.

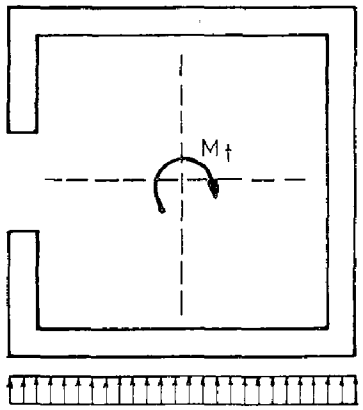

Fig.3 Lift tower (cross section)

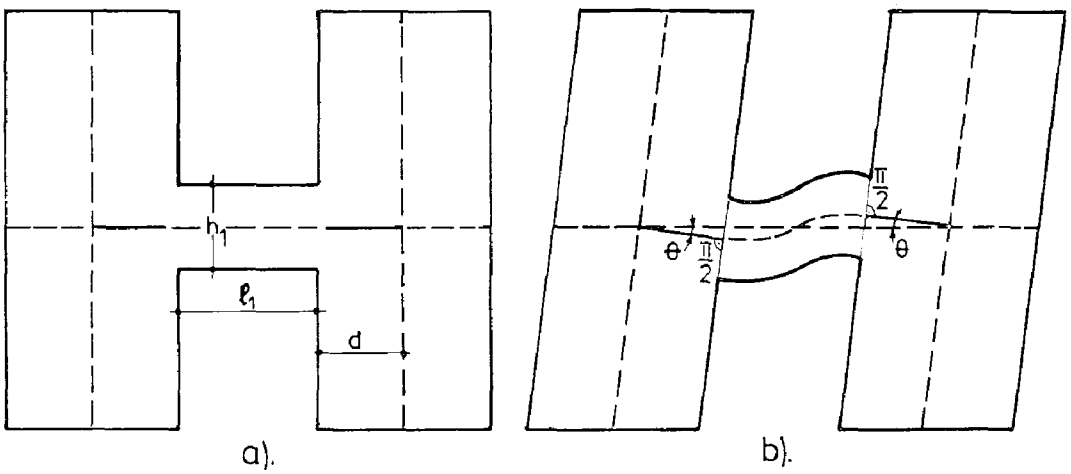

a). b).

Fig.4. A vertical segment of shear walls.
a. Initial segment
b. Deformed segment

also into account the shear force influence, will be the bending moment in the end reactions for a rotation $\theta = 1$ of the shear-wall.

$$k = \frac{6E_1 I_1}{\ell_1} \cdot \frac{1}{1 + 4f} \left(1 + \frac{d}{\ell_1}\right) \tag{4}$$

where d represents the distance from the fix-end point of horizontal elements to the axis of vertical members, and E_1, I_1, ℓ_1 and f refer to the horizontal coupling beams, being: E - the elasticity modulus, I_1 - the inertia moment of the cross-section related to the neutral axis, ℓ_1 - the span, f - a coefficient to be determined by means of the expression

$$f = \frac{3 K_T E_1 I_1}{\ell_1^2 G_1 A_1} \tag{5}$$

In the expression (4), K_T is the shape coefficient of the cross-section, which is 1.2 for the rectangular section, G_1 is the shear modulus and A_1 the cross-section area.

If we take into account (4), the coupling rigidity function k_x will have the form:

$$k_x = \frac{6E_1 I_1}{h \ell_1} \cdot \frac{1}{1+ 4f} \left(1+\frac{d}{\ell_1}\right) \left(1 + \cos \frac{2\pi x}{h}\right) = \tag{6}$$

$$= \frac{6E_1 I_1}{h \ell_1} \cdot \frac{1}{1 + 4f} \left(1 + \frac{d}{\ell_1}\right) \frac{1}{2} \cos^2 \frac{\pi x}{h}$$

If k_x is known, the continuously distributed moments on the edges next to the openings of the vertical members, can be expressed as:

$$m(x) = k_x \cdot \theta(x) = \frac{3E_1 I_1}{h \ell_1} \cdot \frac{1}{1 + 4f} \left(1 + \frac{d}{\ell_1}\right) \cdot \left(1 + \cos \frac{2\pi x}{h}\right) \theta(x) \tag{7}$$

and the density of the distributed forces on the same edge will be.

$$t(x)=\frac{2\,m(x)}{\ell_1}=\frac{6E_1I_1}{h\,\ell_1^2}\cdot\frac{1}{1+4f}\left(1+\frac{d}{\ell_1}\right)\left(1+\cos\frac{2\pi x}{h}\right)\cdot\theta(x) \quad (8)$$

The differential equation of the axis of a deformed vertical member will be written:

$$\frac{d^2u}{dx^2}=-\frac{M(x)}{E\,I}=-\frac{1}{E\,I}\left[M_o+T_o\,x-M_p(x)-\frac{d}{2}\int_o^x t(x)\,d\,x-\int_o^x m(x)\,d\,x\right] \quad (9)$$

where u is the horizontal displacement of the element, E - the modulus of elasticity, I - the inertia moment of the cross-section against the neutral axis, M_o and T_o - the bending moment and the shear force in the bottom section of an element, $M_p(x)$ is the bending moment in section x, given by seismic forces p belonging to a vertical member.

Deriving the both members of equation (9), we obtain

$$\frac{d^3u}{dx^3}=\frac{d^2\theta}{dx^2}=\frac{1}{EI}\left[T_o-T_p(x)-\frac{d}{2}\,t(x)-m(x)\right] \quad (10)$$

where $T_p(x)=\frac{dM_p(x)}{dx}$ is the shear force given by p. Further on if we take into account the relations (7) and (8) the equation (10) becomes

$$\frac{d^2\theta}{dx^2}=-\frac{6E_1I_1}{h\,EI\,\ell_1}\cdot\frac{1}{1+4f}\left(1+\frac{d}{\ell_1}\right)^2\left(1+\cos\frac{2\pi x}{h}\right)\theta=-\frac{T_o-T_p(x)}{EI}=-\frac{T(x)}{EI} \quad (11)$$

If we denote

$$C=\frac{6E_1\,I_1}{h\,EI\,\ell_1}\cdot\frac{1}{1+4f}\left(1+\frac{d}{\ell_1}\right)^2 \quad (12)$$

the equation (11) gets the following simple form

$$\frac{d^2\theta}{dx^2} - C\left(1 + \cos\frac{2\pi x}{h}\right)\theta = -\frac{T(x)}{EI} \qquad (13)$$

or

$$\frac{d^2\theta}{dx^2} - \theta \cdot \frac{C}{2}\cos^2\frac{\pi x}{h} = -\frac{T(x)}{EI} \qquad (14)$$

Integrating the differential equation (13) or (14) we obtain $\theta(x)$, and knowing $\theta(x)$, the stresses in the vertical and horizontal elements can be derived; at the same time the displacements $u(x)$ may also be obtained.

Analytical closed solutions for the differential equations (13) are difficult to obtain, but we can use various numerical methods in order to undertake the analysis by means of the computer. From the numerical methods, one can succesfully use the finite difference method leading to the solution of a system of algebraic equations, or one of the step by step integration numerical methods.

The equation (13) is also valid in the case of shear-walls with many rows of openings, if one considers that one can admit the equality of the rotations θ, in any section, for all vertical members.

Numerical example.

A numerical example has been carried out by means of the computer, for a reinforced concrete shear-wall with one row of symmetrical openings (Fig. 5) in two alternatives of coupling of vertical members a) continuous connection of constant stiffness, b) continuous connection of variable stiffness according to the proposed procedure in this paper. The considered loading was: an uniformely distributed load along the height p = 1o KN/m, and a triangular load with maximum intensity at the upper part p_{max}= loKN/m, which for the more rigid constructions, seems to fit well, to the seismic load distribution.

The geometrical and mechanical characteristics of the shear-wall have been:

- the height of a story: h = 275 cm
- the height of an opening: h_o= 215 cm
- the height of a coupling horizontal element: h_1=6o cm
- the width of the opening: ℓ_1= 1oo cm
- the thikness of the shear-wall: b = 15 cm
- the cross section of a vertical members: 2oo x 15 cm^2
- the modulus of elasticity of the concrete in compression: E = 29oooo daN/cm^2
- the shear modulus of the concrete: G=116ooo daN/cm^2
- the ratio between the compressive modulus of elasticity and the bending modulus of elasticity: 1,6666.

For solving the differential equation, the finite difference methods has been used. Along the height of the 9 -storied shear-wall, 36 dividing points have been taken, that is four points for every story. The bending moment diagrams are presented in figure 5 for a vertical member, namely: for the continuous connection of constant stiffness, in fig. 5b, due to constant intensity loading, and in fig.5 d, due to triangular distributed loading; for the continuous connection of variable stiffness, in fig 5 c for constant intensity loading and in fig. 5 e for triangular loading. The values of the bending moments in the calculated sections for these four variants are given in the table 1.

Conclusions

The assumption that an equivalent continuous connection of variable stiffness, replacing the horizontal coupling elements for the shear-walls with openings can be a better solution than the continuous connection of constant stiffness. Especially for vertical members, the results obtained from this analysis are more appropriate to the physical phenomenon.

From the made numerical example a fact is detaching

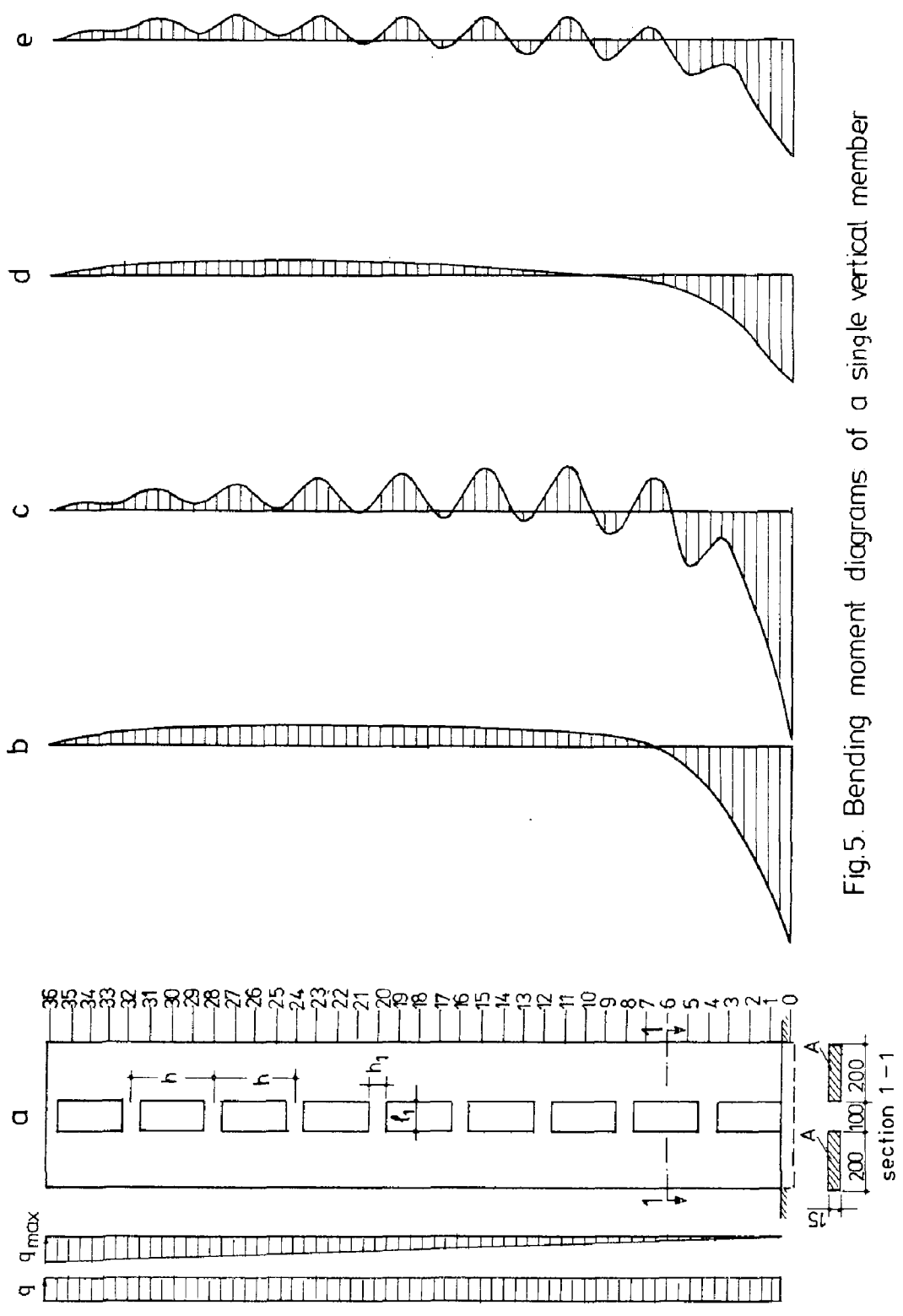

Fig.5. Bending moment diagrams of a single vertical member

Table.1. Bending moment in a vertical member kNm.

Section	Constant load		Triangular load	
	Continuous equivalent horizontal connection			
	Constant stiffness	Periodic stiffness	Constant stiffness	Periodic stiffness
0	-331.122	-483.692	-178.865	-194.803
1	-270.901	-302.307	-148.615	-165.764
2	-173.927	- 166.410	- 99.756	- 95.547
3	- 108.088	- 60.512	- 66.307	- 40.101
4	- 63.389	- 69.527	- 43.319	- 47.570
5	- 33.041	- 93.826	- 27.435	- 62.789
6	- 12.434	- 12.665	- 16.373	- 16.142
7	1.549	61.850	- 8.584	27.271
8	11.045	11.738	- 3.018	- 3.546
9	17.491	- 41.320	1.039	- 35.954
10	21.867	20.796	4.072	3.763
11	24.841	81.343	6.411	42.745
12	26.858	29.419	8.280	9.035
13	28.225	- 22.760	9.831	- 24.881
14	29.154	28.073	11.169	10.744
15	29.784	78.443	12.364	46.161
16	30.206	33.256	13.467	14.827
17	30.490	- 11.607	14.515	- 16.356
18	30.680	29.634	15.328	14.804
19	30.799	70.648	16.104	45.848
20	30.869	34.033	17.037	18.777
21	30.902	- 2.139	17.932	- 8.067
22	30.900	29.863	18.794	18.157
23	30.863	61.675	19.621	44.252
24	30.787	33.939	20.409	20.212
25	30.658	6.629	21.146	0.993
26	30.459	29.415	21.812	21.050
27	30.159	51.940	22.376	40.892
28	29.713	32.706	22.795	25.073
29	29.051	13.711	22.998	9.386
30	28.074	27.023	22.888	22.007
31	26.634	39.713	22.315	34.033
32	24.512	26.867	21.057	23.055
33	21.384	13.374	18.793	11.375
34	16.778	15.964	15.051	14.293
35	2.976	16.251	9.130	14.917
36	0.000	0.000	0.000	0.000

namely the bending moments in the vertical members are differing from each other in either of the considered hypothesis. In the case of the continuous connection of constant stiffness the bending moment diagrams of vertical members are usually rectified, passing from the continuous connection to the discrete one with coupling beams. This correction implies on one hand new errors of approximation and on the other hand, the punctual link does not correspond totally to the realitiy.

The use of a continuous connection of variable stiffness instead of the horizontal coupling elements leads to a bending moment diagram which may be employed without any changes. This latter statement is also confirmed by some experimental data concerning the behaviour of the connection zones among the horizontal and vertical members [2]

References

1. Dhillon, S.R., Analysis of Multistorey Buildings Stiffned by Shear-Walls. Concrete and Constructional Engineering, vol.LXI, 9, 1966.

2. Diaconu, M., Ungureanu, N., Precupanu Dan, Analyse of Stress and Strain States in Shear-Walls with Openings Acted by Seismic Loadings. Polytechnic Institute of Jassy, Research Report, Contract C-68, 1969. (in Rumanian).

3. Diaconu, M., Determination of the Stress State into the Shear-Walls with Openings when Considering the Influence of Shear Force, Construcţii, 23. 12, 1971, 25-36 (in Rumanian).

4. Rosman, R., Approximate Analysis of Shear-Walls Subject to Lateral Loads. Journal of the American Concrete Institute, 6, 1964, 717-733.

5. Ungureanu, N., Amariei, C., The Analysis of Framed-Shear-Walls Structures Proc., 2nd Conference of Technical

Mechanics, Bucureşti, 197o, 65-87 (in Rumanian).

6. Ungureanu, N., On the Analysis of Multistory Buildings at Horizontal Actions, Proc. of The Conference on Earthquake Analysis of Structures, Jassy, Romania, 197o, 697-7o5.

7. Ungureanu, N., Amariei, C., Seismic Analysis of Shear-Walls with Openings Using Transfer Matrix, Proc. of the Conference on Earthquake Analysis of Structures, Jassy, Romania, 197o, 7o6-717.

8. Ungureanu, N., Diaconu, M., Contributions Concernant le Calcul des Murs de Refend et des Portiques aux Charges Horizontales Séismiques, Bul. Stiinţific al Institutului de Construcţii, Bucureşti, XV, Nr.3, 1972, 67-79.

9. Ungureanu, N., Gorbănescu, D., The Design of some Structures of Diaphragms and with Central near Rigid Core, Proc. 7^{th} Conference of Reinforced Concrete Tall Buildings, Jassy, Romania, 1975, 199-21o (in Rumanian).

INTERNATIONAL SYMPOSIUM ON
EARTHQUAKE STRUCTURAL ENGINEERING
St. Louis, Missouri, USA, August, 1976

RESPONSE OF REINFORCED CONCRETE CHIMNEYS TO EARTHQUAKE FORCES

PROFESSOR C.K. RAMESH AND P.V. FADNIS
Indian Institute of Technology, Bombay
Powai, Bombay 400 076, India

INTRODUCTION

Reinforced Concrete Chimneys have not received as much attention as that of building or other tower frames for the evaluation of their response to impulsive lateral forces arising due to ground motions, although many Codes of Practice do provide some guidelines, not always reliable, for estimating these forces and the corresponding displacements of these systems. The present study purports to be a step in this direction in providing some numerical data for a fuller comprehension of the dynamic behaviour of two practical examples of reinforced concrete chimneys (Fig. 1). The analysis is performed using the well known step-by-step numerical integration procedure to a digitised forcing function (Table 3) of an actually recorded accelerogram spectrum. Results have shown the need for a revision of the relevant clauses of a Code of Practice.

ANALYSIS

Besides making the fundamental assumptions of the classical vibration theory, it is also taken for granted that the structural equivalence is fully valid between the given one-dimensional continuum and the assumed lumped-mass-parameter system, whose lateral response to a horizontal north-south component of the input ground motion, is only relevant. The interaction between the foundation and the structure, if any, is neglected while the joint rotation in the structure is considered. For numerical integration the acceleration associated with each degree of freedom of each discretized mass is assumed to vary linearly in a small step interval of time implying thereby quadratic and cubic variations of velocity and displacement, respectively, within the assumed step-interval. Two types of viscous damping mechanisms, one proportional to mass and the other proportional to stiffness, are assumed.

The classical equations of motion, in matrix form, are

$$[M]\left\{\ddot{x}\right\} + [C]\left\{\dot{x}\right\} + [K]\left\{X\right\} = -[M]\left\{\ddot{X}_g\right\} \qquad \ldots(2.1)$$

Adopting an incremental deformation technique, for a small increment t in time, t,

$$[M]\left\{\Delta\ddot{X}\right\} + [C]\left\{\Delta\dot{X}\right\} + [K]\left\{\Delta X\right\} = -[M]\left\{\Delta\ddot{X}_g\right\} \qquad \ldots(2.2)$$

where

$[M]$ = Diagonal mass matrix

$[C]$ = Damping matrix

$[K]$ = Dynamic stiffness matrix

$\Delta\ddot{X}$, $\Delta\dot{X}$, ΔX = Changes in accelerations, velocities and displacements in the time-increment t.

$\Delta\ddot{X}_g$ = Change in ground acceleration in t.

For the analysis of free response of an undamped multi-degree lumped-mass system,

$$[M]\left\{\ddot{X}\right\} + [K]\left\{X\right\} = 0 \qquad \ldots(2.3)$$

This ultimately reduces to a characteristic value problem,

$$[D] - \lambda[I] = 0 \qquad \ldots(2.4)$$

where $[D] = [M]^{-1}[K]$ and the frequency parameter, $\lambda = \omega^2$

For the numerical evaluation for the free response of the two examples on hand (Fig.1), the unsymmetric matrix [D] is reduced, following a conventional procedure, to upper Hessenberg form using similarity transformations; then applying QR transformations and adopting a double shifting technique, an accelerated convergence of the eigenvalues is obtained with the help of a subroutine developed for the purpose.

For the forced response, if conditions of displacement, velocity and acceleration at time t_{m-1} at $(m-1)^{th}$ interval, including the acceleration for the m^{th} interval, $\ddot{X}(t)$, are known, then the velocity and displacement, $\dot{X}_m$ and X_m, respectively, are,

$$\dot{X}_m = \dot{X}_{m-1} + \int_{t_{m-1}}^{t_m} \ddot{X}(t)\,dt \qquad \ldots(2.5)$$

$$X_m = X_{m-1} + \dot{X}_{m-1}(\ t) + \int_{t_{m-1}}^{t_m} \left[\int_{t_{m-1}}^{t_m} \ddot{X}(t)\,dt\right]dt \qquad \ldots(2.6)$$

In the time interval $\Delta t_m (= t_m - t_{m-1})$, the acceleration at any time t, is approximately,

$$\ddot{X}(t) = \ddot{X}_{m-1} + \frac{\ddot{X}_m - \ddot{X}_{m-1}}{\Delta t_m}(t - t_{m-1}) \qquad \ldots(2.7)$$

Then the recurrence formulae for velocity and displacement can be written as

$$\dot{X}_m = \dot{X}_{m-1} + \frac{\Delta t}{2} (\ddot{X}_{m-1} + \ddot{X}_m) \qquad ...(2.8)$$

$$X = X_{m-1} + \dot{X}_{m-1} \Delta t + \frac{\Delta t^2}{6}(2\ddot{X}_{m-1} + \ddot{X}_m) \qquad ...(2.9)$$

In matrix form,

$$\{\dot{X}\}_t = \{\dot{X}\}_{t-\ t} + \frac{\Delta t}{2} \{\ddot{X}\}_{t-\ \Delta t} + \frac{\Delta t}{2} \{\ddot{X}\}_t \qquad ...(2.10)$$

$$\{X\}_t = \{X\}_{t-\Delta t} + \Delta t \{\dot{X}\}_{t-\Delta t} + \frac{\Delta t^2}{3} \{\ddot{X}\}_{t-\Delta t} + \frac{\Delta t^2}{6} \{\ddot{X}\}_t \qquad ...(2.11)$$

Here the subscripts denote the times t and $(t - \Delta t)$ when responses are required of the system. In incremental form,

$$\Delta X = \frac{3}{\Delta t} \{\Delta x\} + \{B\} \qquad ...(2.12)$$

$$\{\Delta \ddot{X}\} = \frac{6}{\Delta t^2} \{\Delta X\} + \{A\} \qquad ...(2.13)$$

where

$$\left.\begin{aligned} \{B\} &= -3 \{\dot{X}\}_{t-\Delta t} - \frac{\Delta t}{2} \{\ddot{X}\}_{t-\Delta t} \\ \{A\} &= -\frac{6}{\Delta t} \{\ddot{X}\}_{t-\Delta t} - 3 \{\ddot{X}\}_{t-\Delta t} \end{aligned}\right\} \qquad ...(2.14)$$

The expressions for $\dot{X}$ and $\ddot{X}$, when substituted in equations (2.2), results in a following form

$$[K^*] \{\Delta X\} = \{\Delta R\} \qquad ...(2.15)$$

where

$$[K^*] = \frac{6}{\Delta t^2}[M] + \frac{3}{\Delta t}[C] + [K]$$

and

$$\{\Delta R\} = -[M]\left\{\Delta \ddot{X}_g\right\} - [M]\{A\} - [C]\{B\} \qquad \ldots(2.16)$$

The numerical process consists of initializing the values of the relative velocity and displacement vectors to zero assuming that the system is initially at rest. The terms of the relative acceleration vector are then found to be equal to the initial acceleration of the ground from equation (2.1), i.e.

$$\left\{\ddot{X}\right\}_o = -\ddot{X}_g\{1\} \qquad \ldots(2.17)$$

The following steps are then executed repeatedly,

$$\{A\} = -\frac{6}{\Delta t}\left\{\dot{X}\right\} - 3\left\{\ddot{X}\right\}$$

$$\{B\} = -3\left\{\dot{X}\right\} - \frac{\Delta t}{2}\left\{\ddot{X}\right\}$$

$$\{\Delta R\} = -[M]\left\{\Delta \ddot{X}_g\right\} - [M]\{A\} - [C]\{B\}$$

$$[K^*] = [K] + \frac{3}{\Delta t}[C] + \frac{6}{\Delta t^2}[M]$$

$$\{\Delta X\} = [K^*]^{-1}\{\Delta R\}$$

$$\{X\} = \{X\} + \{\Delta X\}$$

$$\left\{\dot{X}\right\} = \left\{\dot{X}\right\} + \frac{3}{\Delta t}\{\Delta X\} + \{B\}$$

$$\left\{\ddot{X}\right\} = \left\{\ddot{X}\right\} + \frac{6}{\Delta t^2}\{\Delta X\} + \{A\}$$

The inverse of $[K^*]$ is found on the first pass and is used repeatedly in the subsequent steps.

The procedure is found to be self-starting and also efficient not involving any iteration during a same time step. For a stability of the solution, two different step-intervals are tried to confirm finally that $\Delta t = 1/6$ of

the shortest period of the structure, corresponding to seventeen/thirteen mass-lumpings, is quite satisfactory. The program NUMRINT developed for the purpose, consisting of several subroutines, is found to be sufficiently versatile printing out the member displacements and the member forces in a required format for direct interpretation.

For the forcing function, the digitized, north-south component of the Koyna earthquake (December 1967), having a maximum ground acceleration = 0.63 g, is used for evaluating the dynamic responses of the two examples.

The damping matrix is, following conventional lines, written as

$$[C] = \alpha [M] + \beta [K] \qquad \ldots (2.18)$$

where

$$\alpha + \beta \omega_m^2 = 2 \xi \omega_m \qquad \ldots (2.19)$$

ξ being the ratio of actual damping to critical damping and ω_m is the natural frequency in a m^{th} mode. Knowing ξ for the system it is possible to select the constants α and β to define the damping matrix [C]. The fundamental mode being a predominant mode is adopted along with the second mode to evaluate the values of α and β.

The selection of the step interval or the time-increment, Δt, is dependent on the properties of the structure form of the forcing function, and the numerical procedure used. If the time interval is too small, the truncation and the round off errors will increase making the numerical procedure unstable. On the other hand it should be sufficiently small such that the essential features in the earthquake record are adequately represented. For a proper trade-off therefore, an appropriate time-increment should be chosen for which Newmark (6) has suggested, for a linear acceleration assumption, the step interval to be less than 1/6th to 1/10th of the smallest period. On the other hand Walpole and Shepard(8) have proposed 1/40th of the fundamental period. A period of 1/6th of the shortest period is preferred for the present study as explained earlier.

The two examples (Fig.1) considered for the numerical work refer to two reinforced concrete chimneys, 121.0 m and 100.0 m high, with 6.7 m and 3.0 m base and top diameters, respectively. In the first example the thickness varies uniformly from 45 cm at the bottom to 30 cm at the top. In the second case the thickness varies from 35 cm to 15 cm for a height of 70.0 m from ground, and thereafter a constant thickness of 15 cm is provided. There is in addition a

concrete lining of 30 cm thick provided for the top 4 m portion. The overall stiffness matrix is assembled first, considering three displacements per node, from which a reduced matrix with only single degree of freedom per node is obtained. Using this condensed stiffness matrix and the lumped mass matrix, the free vibration response is evaluated assuming damping to be absent. For the forced response the digitized values of time-acceleration data of the Koyna 1967 earthquake given by Jaikrishna,et al (5) (Table 3) are used in the step-by-step numerical integration procedure from which lateral displacements, velocity, acceleration, shear force and bending moments,are calculated at each node.

CONCLUSIONS

The values of the fundamental period (Tables 1, 2, Fig 2) obtained agree well as expected with I.S. Code (4) confirming the reliability of the code.recommendation. It is generally difficult to ascertain the precise influence of higher modes on the dynamic response characteristics of such slender systems and there are no clear guidelines so far.

For such line-like structures it is evident that the deflection will be a maximum at the free end (Fig.3). It is interesting, however, to note that, for Example II, the deflection at the top is not maximum presumably due to the presence of an additional internal concrete lining (15 cm thick) at the top 4 m portion.

The variation of bending moment with height is shown in Fig.4 and is found to resemble closely with what is reported by Ruman (7), Chandrasekaran (1) etc. The values of the bending moment obtained here are, however, much higher than those obtained from the I.S. Code (4).

The variation of shear force with respect to height is shown in Fig 5. The occurrence of the kinks may be attributed to the lumped mass idealization while the actual structure is a continuous system.

Since detailed calculations for the analysis of these chimneys for equivalent static forces (due to earthquake) are not available, it has not been possible to compare the stresses and deformations obtained from static and dynamic analyses. The study has, however, revealed that large forces and deformations may occur in the system, while the Codes may under-estimate these design considerations. Whether a rigorous analysis is required or not would depend upon the importance and complexity of the structure considered. Besides the problem of uncertainty of the forcing function may also largely vitiate the credibility of rigour in a deterministic study having such uncertain input parameters. Yet for a given forcing function, the forces estimated in the I.S.Code(4)

are far lower than what are likely to be experienced by the structures. There is therefore a case for a more critical reappraisal of the relevant recommendations for evaluating the dynamic forces in such line-like structural systems for a realistic design.

REFERENCES

1. Chandrasekaran, A.R., Vibration of Chimneys, Cement and Concrete Journal, Vol. 10, No.4, January-March 1970, pp 374-381.

2. Dicky and Woodroof, Vibrations of Steel Stacks, ASCE Trans., Vol. 121, 1956, pp. 1054-1086.

3. Housner, G.W., and Keightley, W.O., Vibrations of Linearly Tapered Cantilever Beams, Jr. of the Engg. Mech. Div., Proc. of ASCE, Vol. 88, No. EM2, April 1962, pp. 95-123.

4. I.S. Code of Practice 1893, 1970, Criteria for Earthquake Resistance Design of Structures (Second Revision), I.S.I., New Delhi, 1971.

5. Jaikrishna, Chandrasekaran, A.R., and Saini, S.S., Analysis of Koyna Accelerogram of December 1967, Bulletin of Seismological Society of America, 59, November 1969.

6. Newmark, N.M., A Method of Computation for Structural Dynamics, Jr. of the Engg. Mech. Div., Proc. of ASCE, Vol. , No. EM3, July 1959, pp. 67-94.

7. Ruman, W.S., Earthquake Forces in Reinforced Concrete Chimneys, Jr. of the Struct. Div., Proc. of ASCE, Vol.93, No. ST6, December 1967, pp. 55-70.

8. Walpole, W.R. and Shepard, R., Elasto-Plastic Seismic Response of a Reinforced Concrete Frame, Jr. of the Struct. Div., Proc. of ASCE, Vol. 95, No. ST 10, pp. 2031-2055.

9. Wilson, E.L., and Clough, R.W., Dynamic Response by Step-by-Step Matrix Analysis, Symp. on Use of Computers in Civil Engineering, Lisbon, Portugal, Vol. 2, October 1962, pp. 45.1-45.14.

TABLE 1: FREE VIBRATION RESPONSE OF EXAMPLE I

Mode	Frequency cycles/sec.	Period second/cycle
1	0.342	2.92
2	1.308	0.765
3	3.148	0.318
4	4.890	0.2048
5	9.550	0.1048
6	14.240	0.0703
7	20.000	0.0500
8	26.480	0.0378
9	33.200	0.03012
10	43.10	0.2320
11	51.20	0.0195
12	56.60	0.01765
13	71.60	0.01395
14	82.50	0.0124
15	88.00	0.01138
16	96.15	0.01040
17	110.00	0.00908

According to I.S. Code(4) the value of fundament al period, T = 2.92 sec.

$$\frac{w_2}{w_1} = \frac{1.308}{0.342} = 3.82$$

$$\frac{w_3}{w_1} = \frac{3.148}{0.342} = 9.2$$

TABLE 2: FREE VIBRATION RESPONSE OF EXAMPLE-II

Mode	Frequency cycles/sec.	Period second/cycle
1	0.431	2.32
2	1.654	0.605
3	4.170	0.240
4	8.210	0.1218
5	13.280	0.0754
6	19.700	0.0507
7	27.800	0.036
8	36.840	0.02712
9	46.400	0.02156
10	55.500	0.0180
11	66.200	0.0151
12	70.900	0.0141
13	111.180	0.009

Note: According to I.S. Code(4), the value of fundamental period, T = 2.11 sec.

$$\frac{w_2}{w_1} = \frac{1.654}{0.431} = 3.84$$

$$\frac{w_3}{w_1} = \frac{4.170}{0.431} = 9.68$$

TABLE 3: DIGITISED DATA OF TIME ACCELERATION CURVE FOR N-S COMPONENT OF KOYNA (1967) EARTHQUAKE

Time	Acceleration	Time	Acceleration	Time	Acceleration	Time	Acceleration	Time	Acceleration
0.00000	0.005887	0.02480	0.003967	0.08690	0.022382	0.12670	-0.012866	0.17890	0.006183
0.20370	0.002954	0.26090	0.020049	0.28820	-0.032879	0.33300	0.071826	0.35780	0.013007
0.39760	0.049037	0.41740	0.003290	0.44730	0.022954	0.48210	-0.048929	0.52430	0.009991
0.56900	-0.006291	0.62120	0.029752	0.65100	-0.029061	0.67090	0.029824	0.70570	0.023334
0.72060	0.079596	0.78520	-0.066802	0.82500	0.020884	0.85430	-0.022236	0.88460	0.046470
0.90450	0.013798	0.91940	0.010548	0.93430	-0.015590	0.94930	-0.002490	0.96910	-0.009004
0.98400	0.046602	1.00140	-0.007654	1.02380	-0.012202	1.04370	-0.035066	1.07350	0.043448
1.10830	-0.061142	1.14310	-0.067638	1.17790	0.071047	1.20520	-0.005435	1.22260	-0.007374
1.23010	-0.034833	1.25990	-0.000791	1.29220	-0.008600	1.32200	-0.050292	1.34190	0.038544
1.36920	0.043807	1.39660	-0.073875	1.42370	0.066793	1.49100	-0.041070	1.51340	-0.024696
1.53080	-0.031216	1.55810	0.047289	1.61280	-0.023934	1.64010	-0.006902	1.66250	-0.013418
1.67740	0.001638	1.70220	-0.017955	1.73950	-0.038978	1.76440	0.027885	1.79170	0.120123
1.82900	0.073415	1.85380	-0.021073	1.87370	-0.017784	1.90350	0.165355	1.98800	-0.213868
2.04020	0.015068	2.06260	0.008548	2.08250	0.225030	2.15950	-0.148320	2.18430	0.255200
2.23650	-0.308478	2.25640	-0.288843	2.27380	-0.337877	2.29620	0.026402	2.33600	-0.122025
2.34840	0.191894	2.35080	0.136312	2.37070	0.234423	2.38320	0.206312	2.39810	0.355702
2.44780	-0.275715	2.46520	0.254113	2.48500	-0.354065	2.50990	0.039643	2.53970	-0.497699
2.57850	0.077622	2.59690	0.002427	2.60680	0.541956	2.65150	-0.216616	2.68380	-0.017134
2.73350	-0.100405	2.75340	0.220300	2.76590	-0.308099	2.78330	-0.252501	2.80810	0.275375
2.82300	0.047694	2.84540	-0.026844	2.87020	0.162820	2.90750	-0.190302	2.93730	0.097461
2.95720	-0.075830	2.96960	0.119002	2.98210	-0.052927	3.00190	0.104035	3.02930	0.045284
3.04670	0.195708	3.06660	-0.304566	3.09640	-0.042973	3.12120	-0.101825	3.14610	-0.065852
3.18580	-0.425529	3.21070	0.045340	3.22560	-0.111760	3.25040	0.189074	3.28030	0.025591
3.29270	0.319893	3.30510	0.094285	3.31750	0.123725	3.33490	-0.082257	3.36230	0.127024
3.38710	-0.268556	3.43430	0.228478	3.46660	-0.232560	3.50140	0.104226	3.53380	0.032916
3.54120	0.238323	3.55360	0.221977	3.57350	0.257952	3.59340	-0.239060	3.62320	0.020579
3.64060	-0.013426	3.66300	0.088598	3.68290	-0.016685	3.70770	0.369163	3.72760	0.117389
3.75240	0.375713	3.80210	-0.189960	3.82200	0.101060	3.85180	-0.631380	3.88910	0.332502
3.90150	0.228599	3.92140	0.347625	3.93880	0.202440	3.95620	0.362672	3.98350	-0.012357
4.00590	0.094551	4.03820	-0.010080	4.05560	0.212271	4.12020	-0.327248	4.11010	-0.182912
4.15750	-0.265118	4.18480	0.006281	4.21220	-0.229146	4.23950	0.176316	4.25440	0.012824
4.28670	0.452293	4.31410	-0.039492	4.33890	0.058603	4.35380	-0.029682	4.39860	0.412747

TABLE 3 (contd..)

Time	Acceleration	Time	Acceleration	Time	Acceleration	Time	Acceleration	Time	Acceleration
4.48550	-0.435149	4.53280	-0.046039	4.56750	-0.310900	4.59740	0.117447	4.60730	0.032429
4.63220	0.215539	4.66690	-0.095101	4.69180	-0.000279	4.70920	-0.078758	4.73160	0.222065
4.74150	0.022602	4.75890	0.038948	4.78620	-0.212834	4.81610	-0.078775	4.83100	-0.087934
4.84590	0.056590	4.87320	-0.075517	4.89310	0.055926	4.91790	-0.085336	4.94530	-0.087958
4.96520	0.098427	4.98010	0.146807	5.01240	-0.075550	5.03470	0.035618	5.07200	-0.319473
5.09940	0.065028	5.12170	0.022513	5.14910	0.372379	5.18380	-0.016760	5.20870	0.018644
5.24850	-0.190069	5.27330	0.107478	5.29570	0.002834	5.31800	0.140814	5.34540	-0.019692
5.37270	0.006075	5.39760	0.088761	5.44230	0.061632	5.46170	-0.092061	5.49200	-0.095913
5.52180	-0.157483	5.56660	0.084464	5.58150	-0.026717	5.60380	0.125646	5.63120	-0.010392
5.65600	0.009213	5.67090	0.000704	5.68580	0.185770	5.70320	-0.020240	5.72060	0.130163
5.74050	-0.097428	5.75540	-0.010458	5.78520	-0.141269	5.81510	0.051634	5.83490	-0.007234
5.85230	0.074501	5.88960	-0.084435	5.90450	0.058120	5.91940	-0.035222	5.93930	0.126766
5.96910	-0.040015	5.98900	0.009019	6.00390	-0.026958	6.02130	0.005728	6.03130	-0.053135
6.04620	0.042988	6.05860	-0.020455	6.07600	0.015501	6.08840	-0.066253	6.10330	-0.040104
6.12570	-0.089168	6.15800	0.065800	6.18290	0.008886	6.20270	0.051380	6.22260	-0.017301
6.26240	0.208289	6.29220	0.041503	6.31460	0.235716	6.33690	-0.043546	6.34940	-0.026667
6.35930	-0.066453	6.36670	-0.053380	6.37670	-0.112245	6.39160	-0.050130	6.41400	-0.118815
6.43630	0.065586	6.44880	0.043226	6.45870	0.068183	6.48110	-0.026006	6.49850	-0.017519
6.52580	-0.131987	6.56060	0.072020	6.58540	-0.003207	6.60530	0.093562	6.64010	-0.128818
6.66250	0.008495	6.68480	-0.052333	6.71470	0.060764	6.73700	0.006464	6.76440	0.385741
6.83390	-0.145350	6.85880	-0.057088	6.87370	-0.121192	6.89610	-0.027696	6.92090	-0.154592
6.93530	-0.104907	6.95820	-0.121277	6.97560	-0.014698	6.98800	-0.027790	6.99800	-0.093837
7.00790	0.074208	7.02090	0.123897						

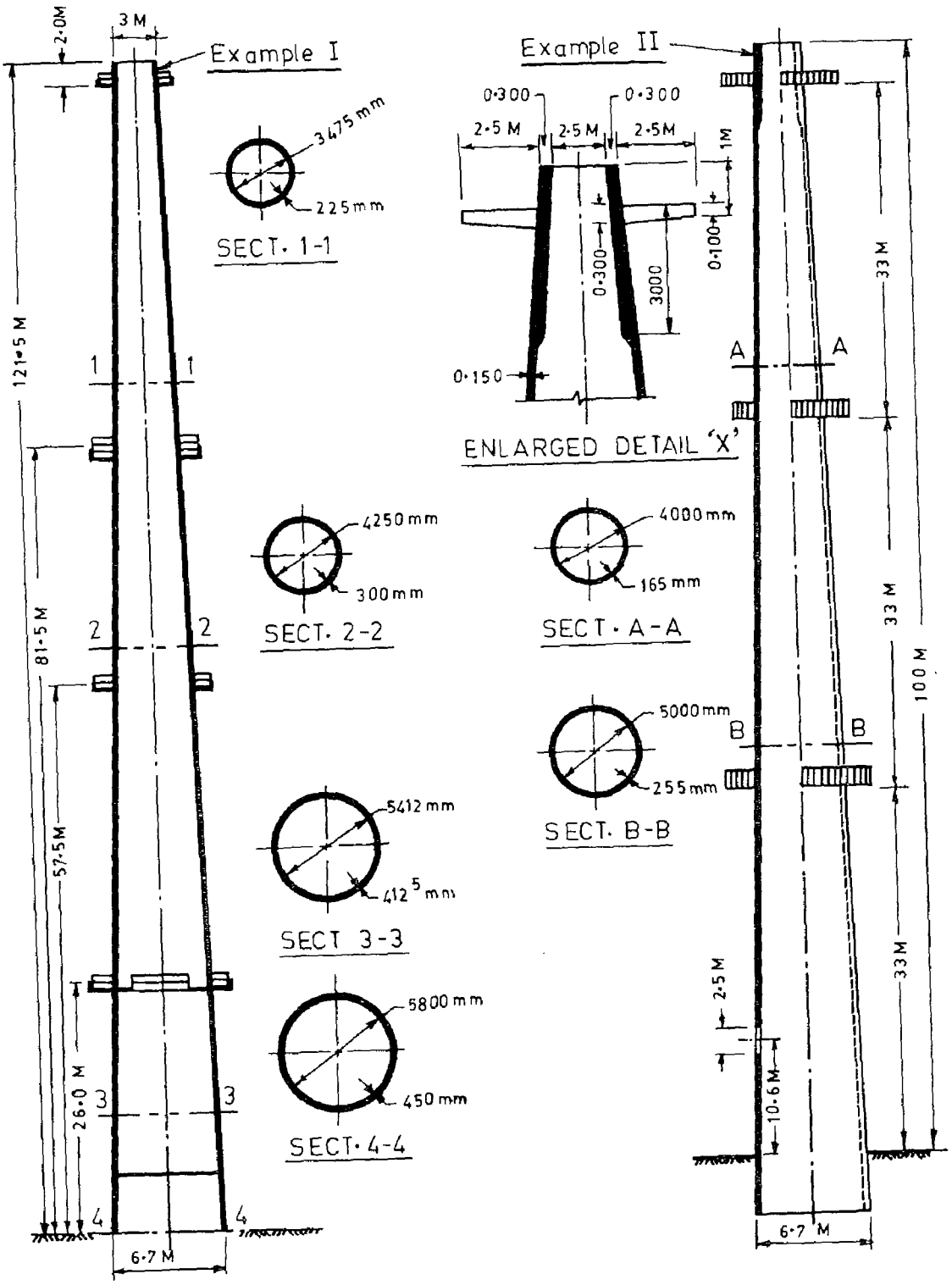

FIG·1 – DETAILS OF EXAMPLE I & II

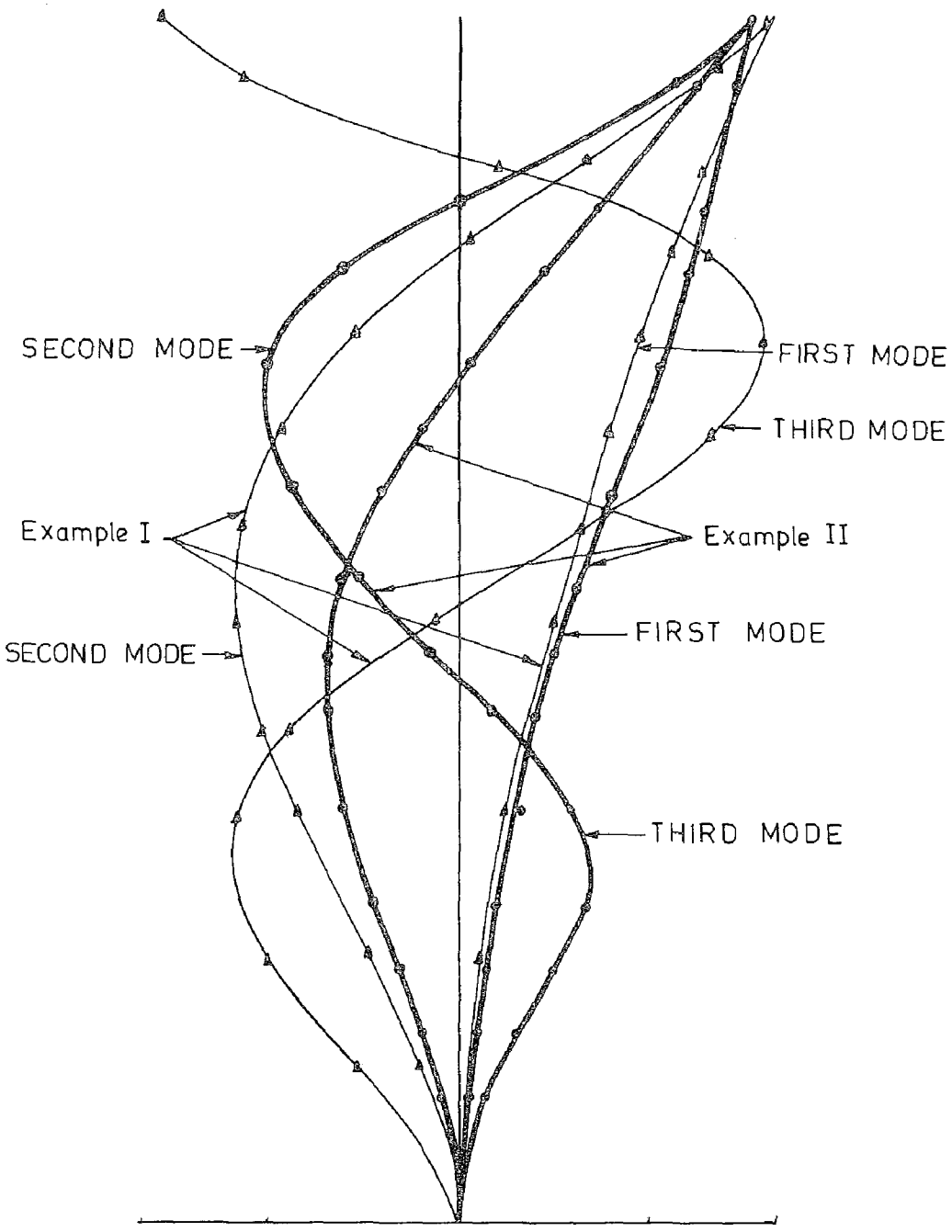

FIG.2-MODE SHAPES FOR EXAMPLE I & II

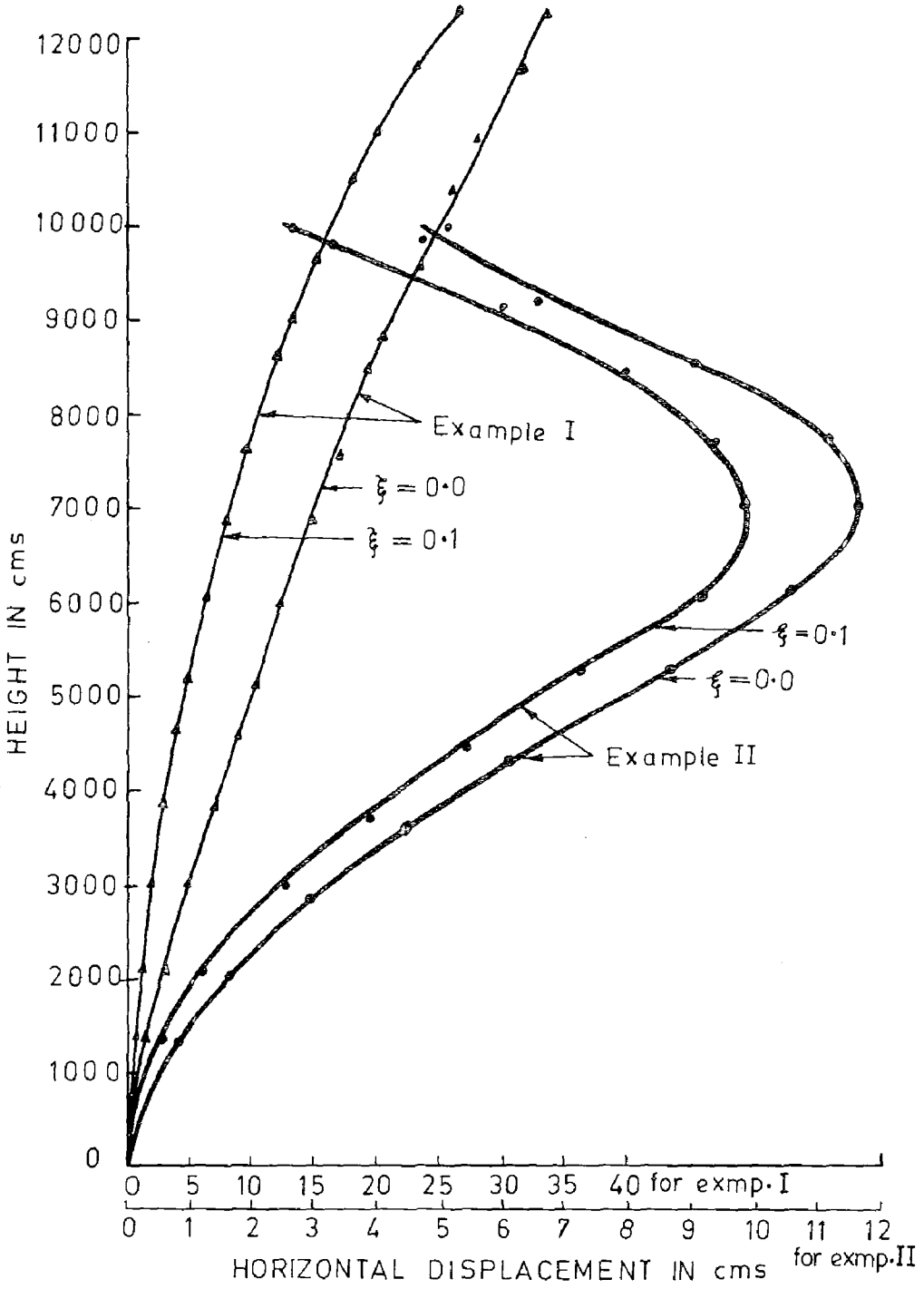

FIG·3- HORIZONTAL DISPLACEMENTS WITH HEIGHT FOR EXAMPLE I & II

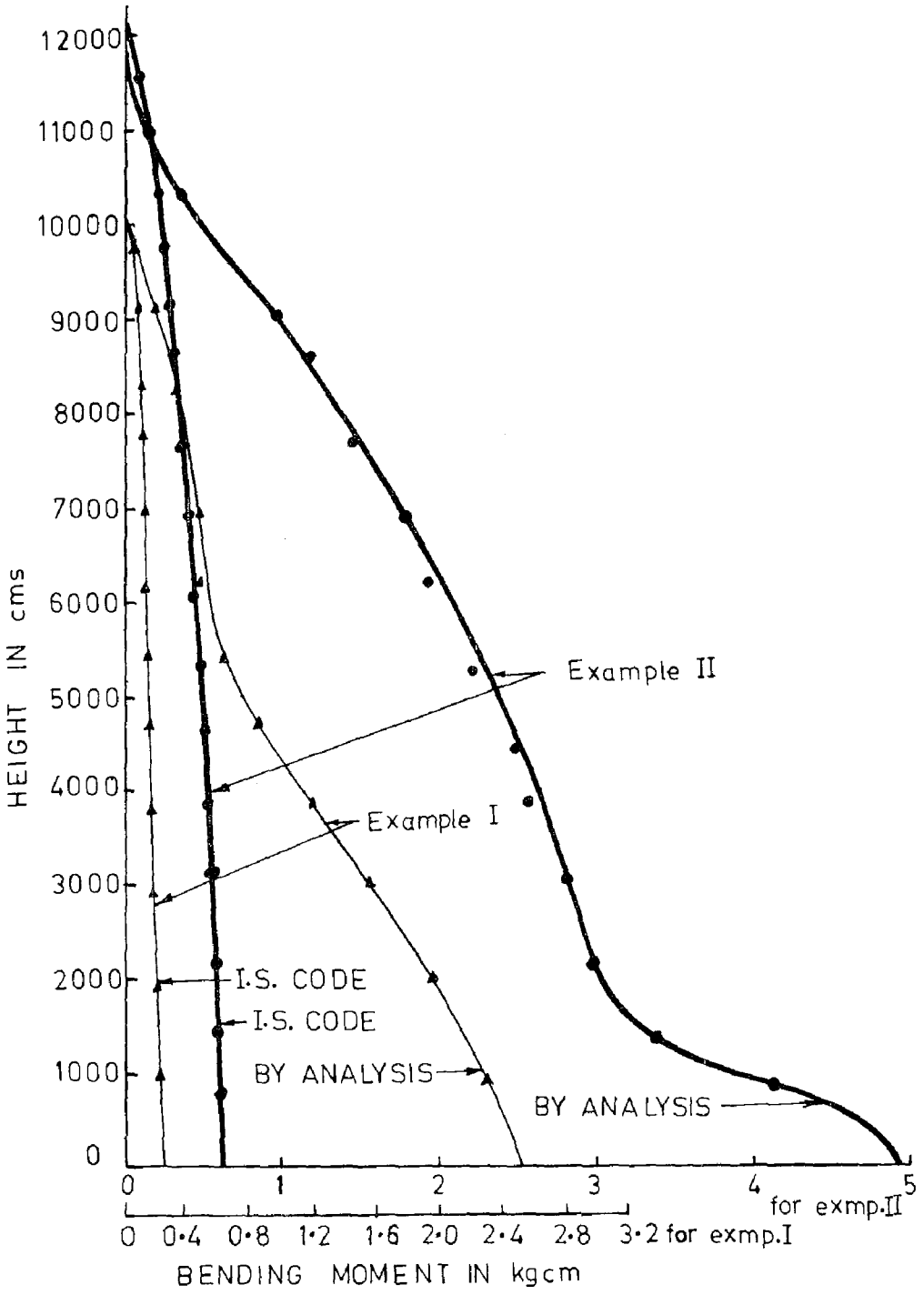

FIG·4 - BENDING MOMENT WITH HEIGHT FOR EXAMPLE I& II

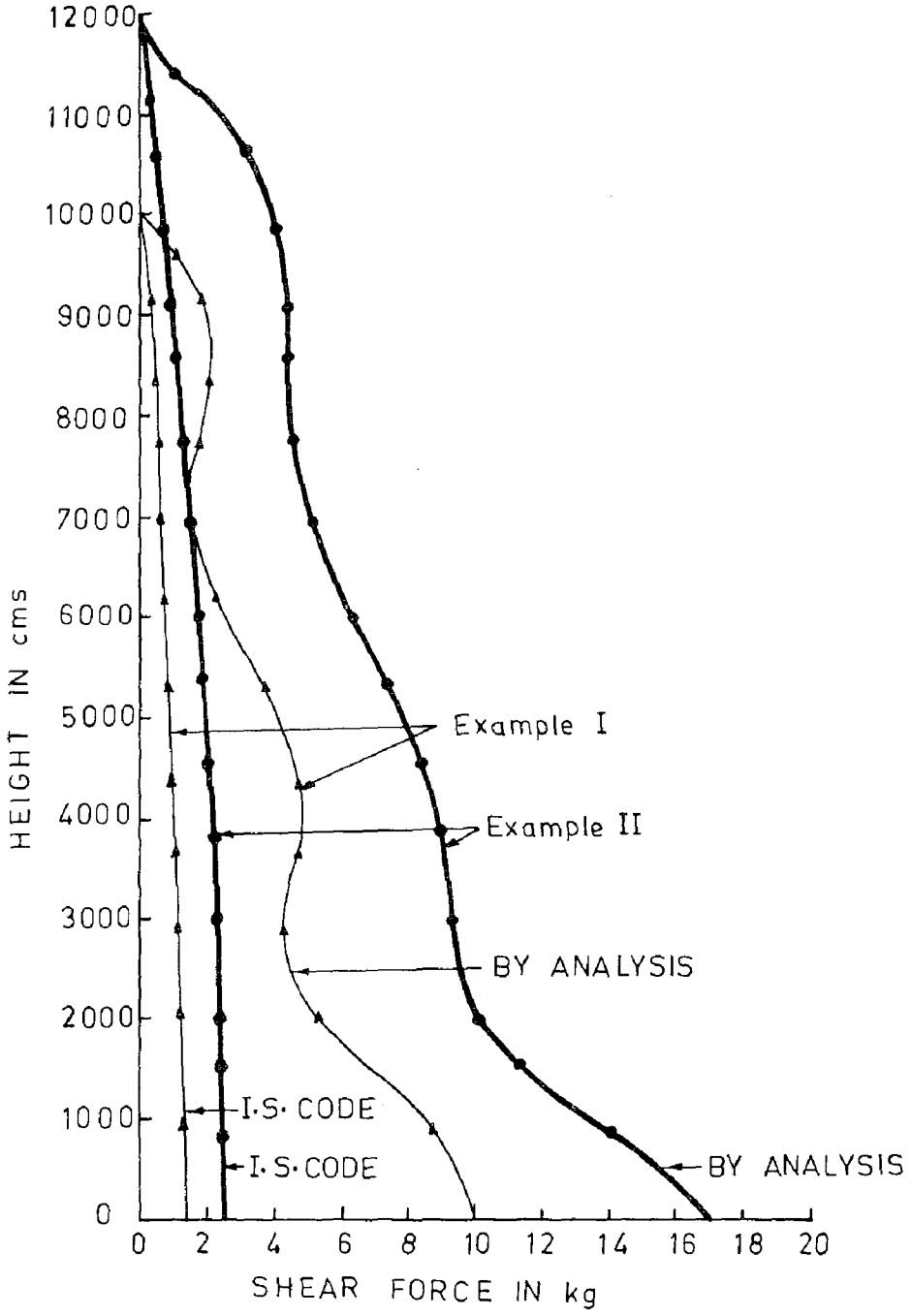

FIG.5—SHEAR FORCE WITH HEIGHT FOR EXAMPLE I & II

SAMPLE OF SYMPOSIUM REVIEW

ENGINEERING News

Lessons from past point to future at earthquake meeting

An international symposium on earthquake structural engineering, held last August in St. Louis, Mo., had as its stated objective to provide a means for interaction and cooperation among practitioners, researchers, educators and other public servants in the field of earthquake structural engineering. Also, it was meant to focus attention on structural design so that it is capable of minimizing the disruptive effects of earthquakes on population centers.

These reporters felt that the symposium went a long way toward meeting its objectives; nearly 200 representatives from 23 different countries (including the USSR) met to present, hear and discuss approximately 90 technical papers. Dr. F.Y. Cheng, University of Missouri-Rolla, directed the symposium. Following are some highlights:

Building codes changed

One result of several recent earthquakes has been a reappraisal of existing building and bridge codes; several (Japan, Turkey, Chile, India, the U.S.) were discussed. Many existing codes have been revised and updated recently in at least two respects: first, the lateral seismic force formula is now a function of a larger number of factors than previously and second, a distinction is made between "simple" structures that can be adequately designed using the equivalent static lateral force and "complex" (long and/or tall) structures which require the use of more detailed, dynamic analysis methods.

In addition to the zone, framing and spectrum factors used to modify the structure dead load in the lateral seismic force formula, new and additional factors include consideration of building occupancy (structure importance factor) and the influence of local soil on structure response (site-structure resonance factor). Changes in the various building codes (including the 1976 UBC) do not represent any surprises to the engineering profession; most were previously recommended in the various engineering studies that follow an earthquake.

In many reinforced concrete buildings in Managua that experienced minor damage to the primary structure the "collapse of partition wall and ceilings" caused a great number of deaths.

Outdated specs

Design code changes have had a direct bearing on existing structures that were designed using outdated specifications, and whose integrity is therefore in question. Although numerous such structures currently exist in various seismically active regions, current codes make no mention of retrofitting and provide no criteria as to how this is to be accomplished should the need arise. In line with this, one of the papers at the symposium covered the subject of retrofitting existing bridges to reduce seismic damage; a number of practical retrofit measures were presented.

Many existing codes have been revised and updated recently in at least two respects: first, the lateral seismic force formula is now a function of a larger number of factors than previously and second, a distinction is made between "simple" structures that can be adequately designed using the equivalent static lateral force and "complex" (long and/or tall) structures, which require the use of more detailed, dynamic analysis methods.

Several papers dealt with discussions of lessons learned from previous earthquakes. The 1972 Managua, Nicaragua earthquake provided some insights into the inadequacy of that city's then existing seismic building code provisions. (It should be pointed out that prior to that earthquake Managua did not have an earthquake-oriented building code.) A review of the response of reinforced concrete structures during the Managua quake recommended that vertical accelerations equal to 80% of the horizontal should be used in the design process. This recommendation is based on accelerogram records with maximum ground acceleration peaks of 0.35g on the horizontal component and 0.28g on the vertical component recorded near the epicenter. The high vertical acceleration is held responsible for the failure of numerous structures in Managua which collapsed due to column failure.

Other major causes of reinforced concrete building collapse included inadequate beam-column connection design, lack of reinforcement anchorage, and inadequate transverse reinforcement of columns. In many buildings that experienced minor damage to the primary structure the "collapse of partition walls and ceilings" caused a large number of deaths.

A new unified approach was presented for designing structures subjected to three components of earthquakes. When the analysis is performed by the response spectrum method, the conventional method gives the maximum probable value of various responses (displacement, force, moment, etc.) which in general do not occur simultaneously. If the design of a structural element or section is based on more than one response, then the maximum probable value of each of them is used as if they were occurring simultaneously—which leads to unnecessary conservatism. Without introducing any new assumptions, the new approach adds the capability of predicting simultaneous variations in various responses. The result is economy with safety.

(CIVIL ENGINEERING thanks A. Longinow and A. K. Gupta, IIT Research Institute, Chicago for reporting on this symposium.)

Audience in one of the conference rooms

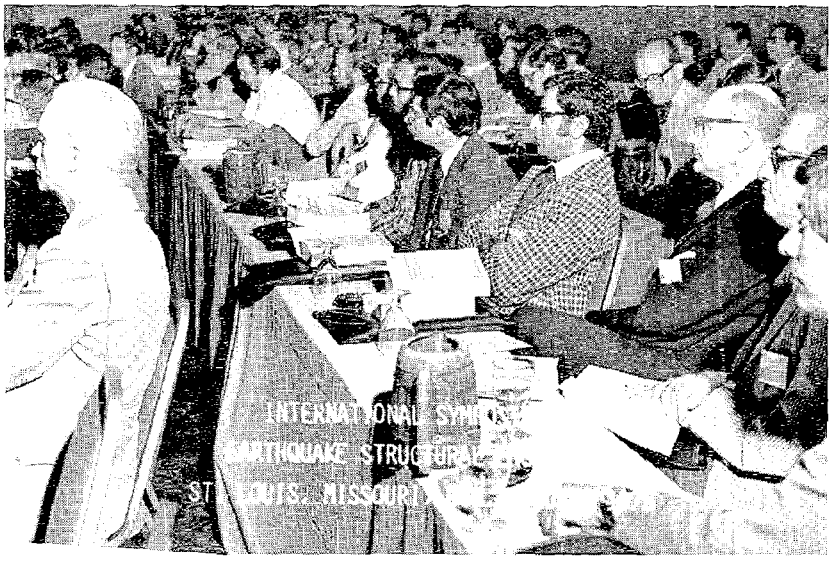

Audience in another conference room

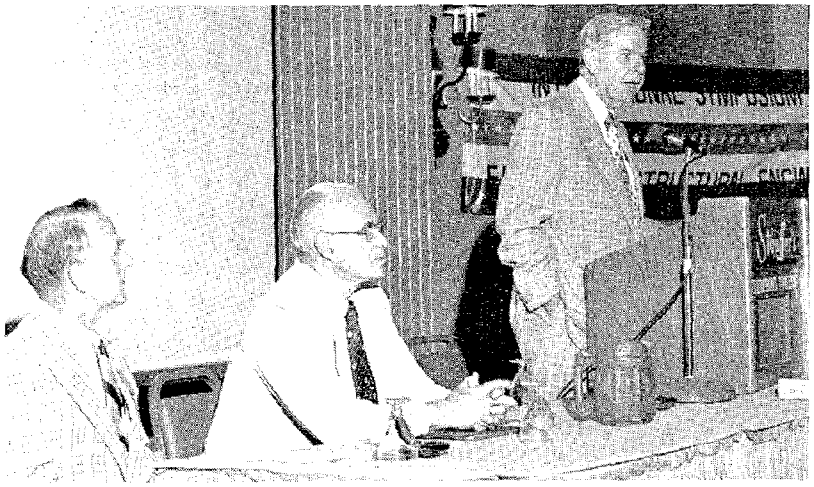

Welcome remarks by Mayor Poelker of St. Louis, Dr. Senne and Dr. Thompson sitting

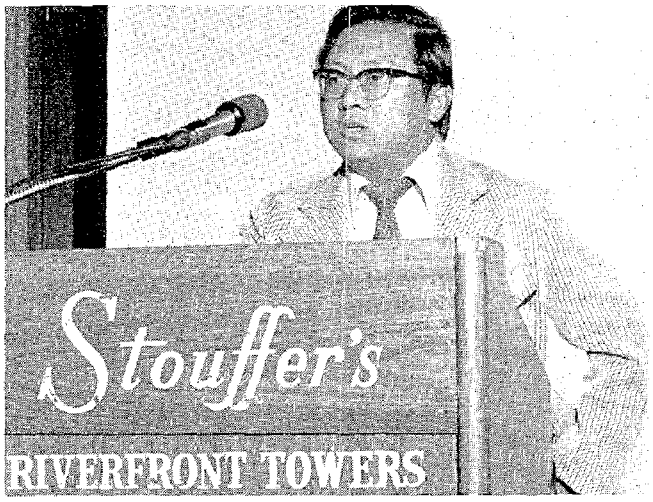

Opening remarks by Dr. S.C. Liu of NSF

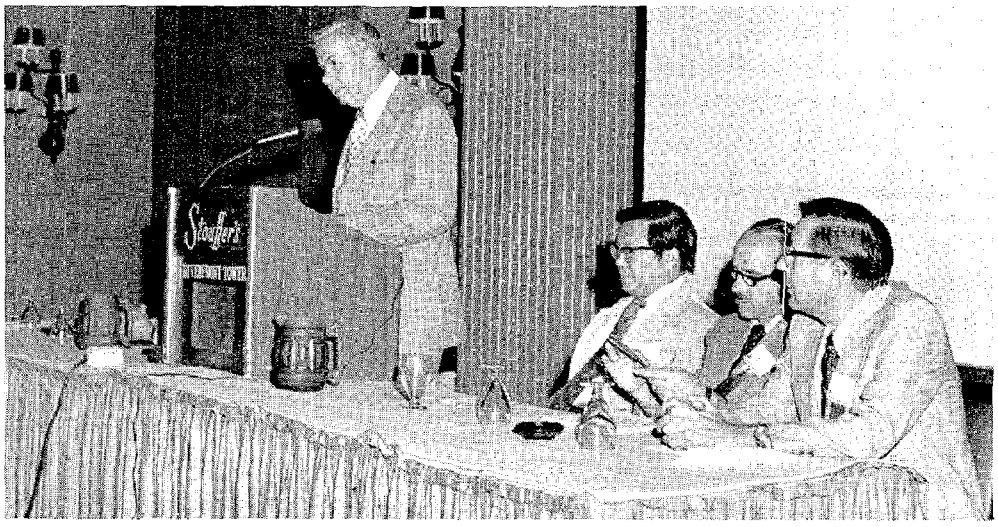

Drs. Nuttli, Galambos, and Liu listening to Mayor Poelker

Some participants at outside of the conference hall.

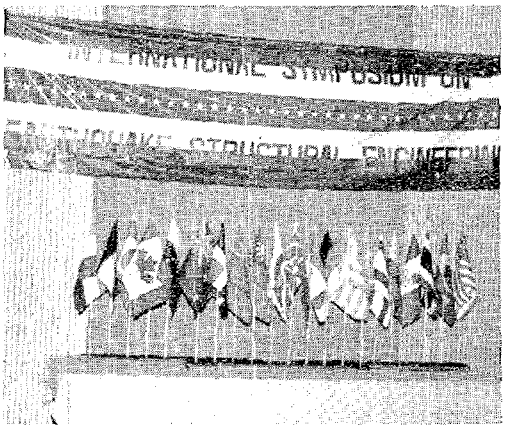

Flags representing various national delegates

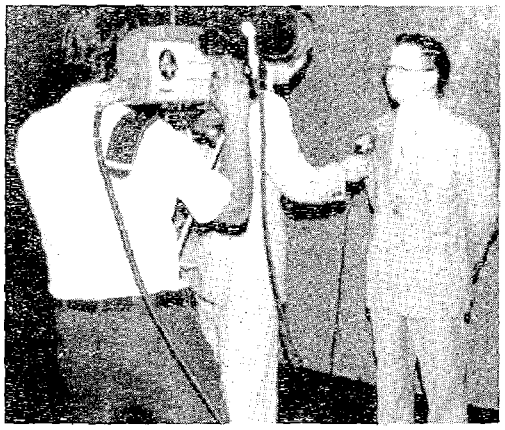

Dr. Cheng on Radio and T.V. interviews

Informal discussion over coffee

Participants getting acquainted at coffee break

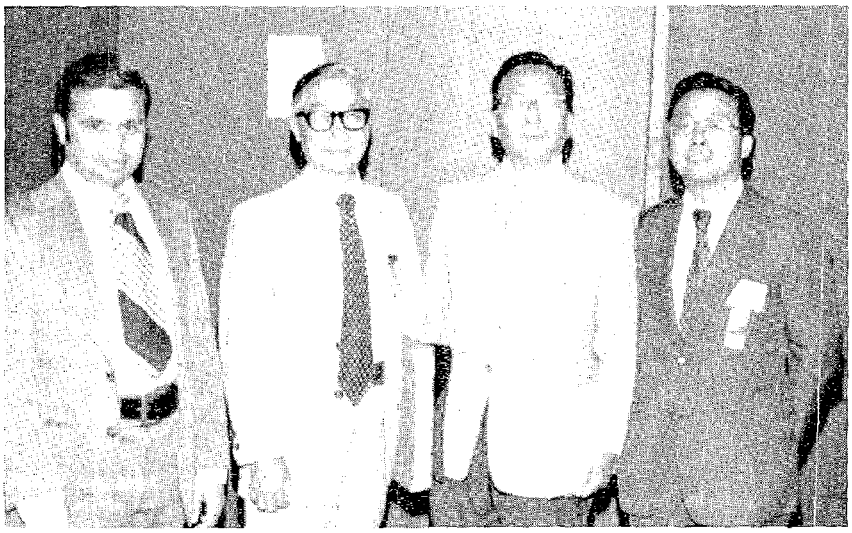

Old friends at the conference

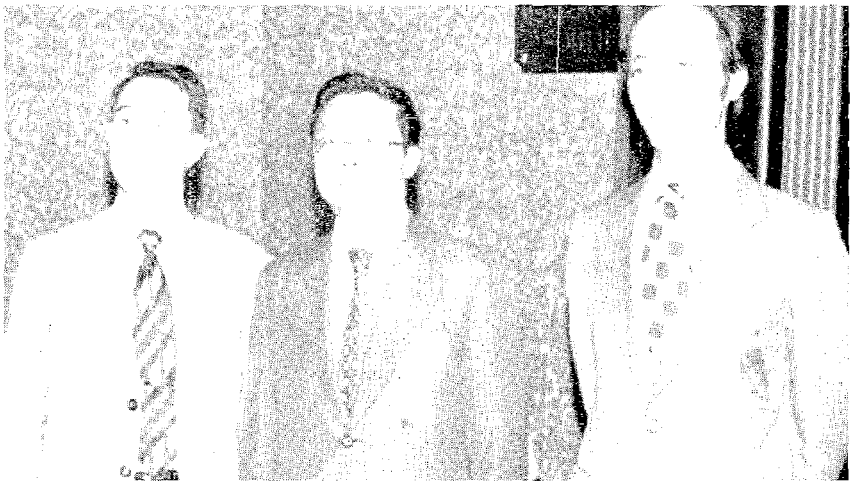

Dr. Cheng with Japanese friends

Ladies activities

Dr. Ang at social hour

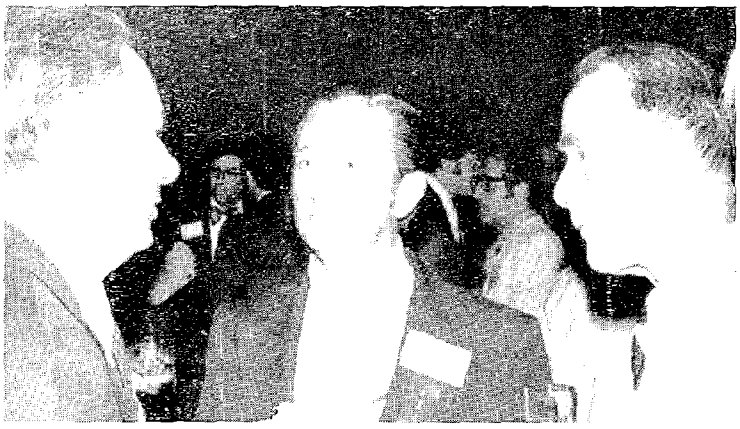

Dr. Senne with his former colleagues

Dr. Bertero exchanging information at social hour

Dr. Roesset and Professor Roberts at banquet

Session chairmen, Drs. Ang, Bertero, Gould, Huang, and Venkayya at banquet

Banquet hall

Dr. Cheng with Soviet delegates on UMR campus--post conference tour